This electronic thesis or dissertation has been downloaded from the King's Research Portal at https://kclpure.kcl.ac.uk/portal/



The random matrix axiverse & axion cosmology in string theory

Stott, Matt

Awarding institution:
King's College London

The copyright of this thesis rests with the author and no quotation from it or information derived from it may be published without proper acknowledgement.

END USER LICENCE AGREEMENT



Unless another licence is stated on the immediately following page this work is licensed

under a Creative Commons Attribution-NonCommercial-NoDerivatives 4.0 International

licence. https://creativecommons.org/licenses/by-nc-nd/4.0/

You are free to copy, distribute and transmit the work

Under the following conditions:

- Attribution: You must attribute the work in the manner specified by the author (but not in any way that suggests that they endorse you or your use of the work).
- Non Commercial: You may not use this work for commercial purposes.
- No Derivative Works - You may not alter, transform, or build upon this work.

Any of these conditions can be waived if you receive permission from the author. Your fair dealings and other rights are in no way affected by the above.

Take down policy

If you believe that this document breaches copyright please contact librarypure@kcl.ac.uk providing details, and we will remove access to the work immediately and investigate your claim.

Download date: 31. Oct. 2023

King's College London

University of London

Faculty of Natural & Mathematical Sciences
Department of Physics
Theoretical Particle Physics & Cosmology Group

A thesis submitted in fulfilment of the requirements for the degree of

Doctor of Philosophy

The Random Matrix Axiverse
&
Axion Cosmology in String Theory



Matthew J. Stott

Supervisor: *Professor Bobby S. Acharya*

Examiners: *Professor Edmund J. Copeland*
Professor David M. C. Marsh

Declaration

I, Matthew J. Stott, declare that this thesis entitled The Random Matrix Axiverse & Axion Cosmology in String Theory and the data presented in it are original and my own work. I hereby declare that this thesis has not been and will not be submitted in whole or in part to another University for the award of any other degree. The work in this thesis was done in collaboration with David J. E. Marsh (Chapter 6 and Chapter 7), Chakrit Pongkitivanichkul, Layne C. Price and Bobby S. Acharya (Chapter 6). References to the work of others have been clearly acknowledged. Quotations from the work of others have been clearly indicated, and attributed to them.

Date:

Signature:



Matthew J. Stott

Copyright © by Matthew J. Stott, 2019. All Rights Reserved.

"*Truth is ever to be found in simplicity, and not in the multiplicity and confusion of things.*"

Sir Issac Newton

"*My goal is simple. It is a complete understanding of the universe, why it is as it is and why it exists at all.*"

Stephen Hawking

"*Physics is really nothing more than a search for ultimate simplicity, but so far all we have is a kind of elegant messiness.*"

Bill Bryson

"*If you realise all the time what's kind of wonderful, that is, if we expand our experience into wilder and wilder regions of experience, every once in a while, we have these integrations when everything's pulled together into a unification, in which it turns out to be simpler than it looked before.*"

Richard P. Feynman

"*Life is really simple, but we insist on making it complicated.*"

Confucius

Abstract

The Random Matrix Axiverse &
Axion Cosmology in String Theory

Consistent frameworks of quantum gravity often predict the existence of large numbers of ultralight pseudoscalar degrees of freedom, forming the phenomenological landscape of the *String Axiverse*. The complexity of the compactified extra-dimensional spacetime manifold and plethoric ensemble of possible vacuum solutions, indicate these fields could possess parameters fixed to cosmologically significant scales in the associated four-dimensional effective field theories, which may span many decades. In the framework of string/M- theory, a systematic construction of the spectrum of these free model variables, the axion decay constant, f_a, and field mass, m_a, when studying explicit realisations of the string axiverse, is an arduous task to perform. The general approach to this problem requires extensive details of all instanton corrections to the model's superpotential, along with a detailed knowledge of the full scalar potential, minimised in the supersymmetric theory. The difficulty of this task scales significantly when considering realistic axion/moduli population numbers. These have often been shown to appear at the order of tens or even hundreds of axionic fields, realised from well defined geometrical constructions and topological features of the model's extra-dimensional manifold.

It is therefore of great interest to consider methods which can alleviate these issues, specifically through a randomised statistical approach, due to the lack of definitive

information we can assert on the higher-dimensional complex space. The link between free probability theory and the asymptotic nature of large random matrices has incorporated itself into various areas associated to multi-axion cosmology. These include models of inflation, quintessence and ensemble sampling of the superpotential Hessian in models of random supergravity. The complexities of these models can be reduced by considering a series of simple yet very powerful nomothetic principles applied to high-dimensional data structures. In this work we introduce a number of random matrix theory inspired models based loosely on axion field alignment considerations for the effective multi-field Lagrangian, as well as a random matrix treatment of the explicit realisation of the string axiverse in M-theory. We detail the forms of their limiting spectral distributions, which take universal forms and provide traceable results based on both central limits theorems and classical ensemble random matrix theory, along with the relevant powerful statements stemming from the field of free probability theory. Using these frameworks we investigate specific configurations of these models based on the initial basis we begin to sample our model, whilst providing simplistic fits to the limiting spectra through considerations for the spectral moments. Such models can be used to test both the presence and viability of axion contributions to the cosmic history, using hierarchical Bayesian inference techniques, along with the possibility of performing an analysis of other phenomenological consequences which may signal the appearance of these fields in our four-dimensional spacetime.

To assess this, we discuss how astrophysical observations for stellar binary and supermassive black hole systems can be used to exclude the existence of axions spanning a large portion of the ultralight mass parameter space, via the superradiance phenomenon. We show how these measurements can be used to constrain properties of the defined and introduced universal statistical distributions, associated to multiple bosonic field theories, covering axion phenomenologies important to the dark sector of cosmological physics and grand unified theories. The presence of multiple fields can enhance the exclusion bounds on both solar and supermassive black holes in

the so called Regge spin plane, as apposed to considering the case of a single field. In this work, we explore for the first time how these measurements can be used to constrain properties of statistical probability measure functions for the masses of multiple bosonic fields. We present an analysis of the statistical likelihoods for each of these models with recorded black hole data spin and mass measurements, in order to provide a picture of the significance of the axion parameter space and its phenomenology in effective theories. Quite generally, in the limit of weak self-interaction, our methodology excludes $\mathcal{N}_{\rm ax} \gtrsim 30$ axion-like fields, associated to a range of mass distribution widths and central values, spanning many orders of magnitude. We demonstrate this for the specific example of axions motivated by string theory and M-theory in the random matrix theory axiverse, where the mass distributions in specific configurations takes universal forms over logarithmic scales.

Finally to conclude, we present an analysis of the background cosmological (quasi-)observables for a selection of the random matrix theory axiverse models, whilst incorporating axion field population numbers, $\mathcal{N}_{\rm ax} \sim \mathcal{O}(10-100)$. This significantly reduces the number of parameters from $2\mathcal{N}_{\rm ax}$ to a small number of statistical *hyper-parameters* related to the matrix parameters which regulate the spectral moments of the parameter distributions. Once again our choice of models in this analysis represents a selection of random matrix models, either motivated purely by statistical considerations, or the structure is specified according to a class of M-theory models and stochastic variables. If the axion masses and (effective) decay constants, lie in specific ranges, then axions contribute to the cosmological dark matter and dark energy densities. We use these models to assess the chance of reproducing suitable dark matter or dark energy cosmologies. Our methodology incorporates the use of both random matrix theory sampling and Bayesian networks. Using Bayesian methods in a a hierarchical model we constrain the hyperparameters of the statistical axion distributions. In some cases the hyperparameters can be related to theoretical aspects of string theory, e.g. constraining the number ratio of axions to moduli, or the typical decay constant scales needed to provide the correct relic

densities today.

Acknowledgments

I would like to begin by thanking King's College London and all the admin, staff and fellow students which have supported, guided and granted me the opportunity to pursue theoretical physics over the past eight years, both as an undergraduate and postgraduate student. Throughout my time at King's I have had the privilege of sharing my time with many kind and motivated individuals. This thesis of course would not be possible without the help, guidance and encouragement from my supervisor Bobby Acharya. I would like to give my sincere thanks to his teaching during my undergraduate days and freedom to conduct fascinating research during my postgraduate ones. I would also like to thank both Professor Ed Copeland and Professor David M.C. Marsh for their insightful inputs and time in reading and examining this thesis.

In particular in the Theoretical Particle Physics & Cosmology Group, I would also like to thank Professor Mairi Sakellariadou, both for her support, guidance and kind words during her supervision of my Masters thesis and as a collaborator on my first publication. Also to Professor Malcolm Fairbairn for his wisdom and support through both my undergraduate and graduate degrees at King's, as well as his input which ultimately pushed me to take up the opportunity to continue down the rabbit hole of theoretical physics. I owe a big thanks my former fellow PhD student and collaborator Chakrit Pongkitivanichkul, for his kind guidance and endless patience during my initial footings into my PhD and all things axions, as well as his support and contributions to the work presented in Chapter 7. Also to Thomas Elghozi, for

his encouragement and guidance during my Masters thesis project with his insights into the world of cosmic strings, along with his persistence and patience to finish our work together.

I owe a huge debt of gratitude to my pseudo-supervisor and now fancy titled collaborator Professor David (Doddy) Marsh, for his endless patience, motivation and general approachable, grounded passion for all things axions. I simply would not have been able to produce the content in this thesis without his encyclopaedic knowledge, generous contributions and creativity in this field. In particular his work which is covered in both Chapter 6 and Chapter 7. I have no doubts what so ever he is destined for a great academic career and many more interesting works in the years to come. Good luck finding *the* or indeed *any* of the axions!

I am thankful to any and all my collaborators and fellow physicists who have given me helpful words, friendly advice and support which has made me feel welcome in this field during my travels. Also to my fellow PhD students and friends at King's over the years who have always brought a friendly and charismatic atmosphere to the Department of Physics. In particular the now Dr. Patrick for joining me from day one of this crazy ride, and beating me to the end for some fancy letters. Thanks for our endless successful procrastination breaks, cinema trips, and general ability to motivate me in the art of looking like I am doing science. Well done for doing a PhD faster than the time it takes receive some post. Also to Priyank in sharing our initial struggles in somehow learning quantum physics, some ridiculous trips and your endless presence in the building over the past eight years, it will not be forgotten.

I would like the thank and acknowledge the generous contributions of the Science and Technology Facilities Council (STFC) for their Doctoral Studentship award which has provided the funding which has made it possible for me to conduct and complete the research presented in this thesis. I would like to also thank the generous contributions of the various grant and funding facilities which have allowed me to travel,

study and present this work at numerous international conferences, meetings and research schools, spanning four continents over the course of my PhD. I have stood in the Korean DMZ, underground in two of the largest particle accelerator laboratories in the world and in the heart of Zululand watching the sun rise and set over the oldest nature reserve in Africa. These are to name a few incredible experiences I have been able to partake in. I would not have expanded my understanding of both physics and what the world has to offer without these opportunities. In particular I would like to thank the Institute of Physics (IOP) Research Student Conference Fund, the IOP C R Barber Trust, the King's College London Postgraduate Conference Fund Grant, the ICHEP 2018 Travel Fund Grant, the SCGSC travel and Participation Fund Grant and the STFC Studentship Travel Grant.

To all my friends and family outside the world of physics I owe you my humble thanks for the many years before this all started, during the process and I am sure after the production of this thesis. I am always grateful to all of you for making my life so colourful outside of physics. To my life long friends for their ever-present ability to help keep me sane and inspired. In particular Chris for many many years of support, adventures, advice, motivation and general grounding in letting me be me. I look forward to continuing to relive our past and seeing what life has in store for many years in the future! Also Alex, for a friendship inspired through sharing our struggle in academia since high school and your help in fooling me I could make it one day. The fact I am writing this dedication in a doctoral thesis in mathematics & theoretical physics is ridiculous. To Anna, I am thankful for your ability to captivate and inspire me to grow in the way that I have over the past years and over the course of this PhD. For putting up with my shortcomings and offering support and good times in return, thank you and of course Dexter as well!

Finally my greatest debt and deepest gratitude goes to my parents, firstly for having the patience to read this thesis (sorry), but mostly for your truly selfless love which has given me all I ever needed in support, guidance and trust, the spirt of your tireless devotion entwined in each and every word which makes this thesis what it

is. From the first school maths problems in the car to the mathematical language of Universe below, every stage has been possible thanks to you. I love you both very much.

M x







Abbreviations

2dFGRS	Two-degree-Field Galaxy Redshift Survey
ΛCDM	Lambda-Cold Dark Matter
ABJ	Adler-Bell-Jackiw
ADMX	Axion Dark Matter eXperiment
AdS	Anti-de Sitter
AGN	Active Galactic Nuclei
ALP	Axion-Like Particle
ALPS	Any Light Particle Search
ATLAS	A Toroidal LHC ApparatuS
BAO	Baryon Acoustic Oscillation
BBH	Binary Black Hole
BBN	Big Bang Nucleosynthesis
BEC	Bose-Einstein condensate
BH	Black Hole
BOSS	Baryon Oscillation Spectroscopic Survey
BPS	Bogomol'nyi-Prasad-Sommerfield
CASPEr	Cosmic Axion Spin Precession Experiment
CCA	Canonical Correlation Analysis
CDF	Cumulative Distribution Function
CDM	Cold Dark Matter
CFT	Conformal Field Theory
CI	Confidence Interval

CKM	Cabibbo-Kobayashi-Maskawa
CLT	Central Limit Theorem
CMB	Cosmic Microwave Background
CMS	Compact Muon Solenoid
COBE	Cosmic Background Explorer
CPL	Chevalliear-Polarski-Linder
CP	Charge-Parity
CS	Chern-Simons
DE	Dark Energy
DFSZ	Dine-Fischler-Srednicki-Zhitnitsky
DGP	Dvali-Gabadadze-Porrati
DM	Dark Matter
DW	Domain Wall
EDM	Electric Dipole Moment
EM	Electromagnetic
EV	Electron-Volt
ESA	European Space Agency
FDM	Fuzzy Dark Matter
FKML	Freimer-Kollia-Mudholkar-Lin
FLRW	Friedman-Lemaître-Robertson-Walker
GLD	Generalised Lambda Distributions
GOE	Gaussian Orthogonal Ensemble
GSE	Gaussian Symplectic Ensemble
GUE	Gaussian Unitary Ensemble
GeV	Giga Electron-Volt
GUT	Grand Unified Theory
GVW	Gukov-Vafa-Witten
GW	Gravitational Wave
HUDF	Hubble Ultra Deep Field

IID	Independent and Identically Distributed
IILM	Interacting Instanton Liquid Model
IMBH	Intermediate Mass Black Hole
IOP	Institute of Physics
IR	Infrared
ISCO	Innermost Stable Circular Orbit
JOE	Jacobi Orthogonal Ensemble
JUE	Jacobi Unitary Ensemble
KDE	Kernel Density Estimation
KK	Kaluza-Klein
KKLT	Kachru-Kallosh-Linde-Trivedi
KeV	Kilo Electron Volt
KNP	Kim-Nilles-Peloso
KSVZ	Kim-Shifman-Vainshtein-Zakharov
L1	Level 1
LOE	Laguerre Orthogonal Ensemble
LIGO	Laser Interferometry Gravitational-Wave Observatory
LDA	Linear Discriminant Analysis
LISA	Laser Interferometer Space Antenna
LSS	Linear Spectral Statistics
LUE	Laguerre Unitary Ensemble
LVS	LARGE Volume Scenario
MACHO	Massive Astrophysical Compact Halo Objects
MCMC	Markov Chain Monte Carlo
MeV	Mega Electron-Volt
NASA	National Aeronautics and Space Administration
NFW	Navarro-Frenk-White
NS	Neveu-Schwarz

ODE	Ordinary Differential Equation
PCA	Principle Component Analysis
PMNS	Pontecorve-Maki-Nakagawa-Sakata
pNGB	Pseudo-Nambu-Goldstone-Boson
PQ	Peccei-Quinn
PQWW	Peccei-Quinn-Weinberg-Wilczek
PVLAS	Polarizzazione del Vuoto con LASer
QCD	Quantum Chromodynamics
QED	Quantum Electrodynamics
QFT	Quantum Field Theory
RAMBO	Robust Associations of Massive Baryonic Object
RMT	Random Matrix Theory
RR	Ramond-Ramond
SIMP	Strongly Interacting Massive Particle
SMBH	Supermassive Black Hole
SUGRA	Supergravity Theory
SUSY	Supersymmetry
Tr	Trace
ULA	Ultra-Light Axion
UV	Ultraviolet
VEV	Vacuum Expectation Value
WGC	Weak Gravity Conjecture
WIMP	Weakly Interacting Massive Particle
WMAP	Wilkinson Microwave Anisotropy Probe

Nomenclature: Physical Constants

The following represent the core and primary physical constants which appear throughout the core structure of this doctoral thesis:

k_{B}	Boltzmann constant ($1.380\ 658 \times 10^{-23}$ JK^{-1})
e	Elementary charge ($1.602\ 176\ 634 \times 10^{-19}$ C)
g_e	Electron g-factor ($-2.002\ 319\ 304\ 362\ 564$)
m_{e}	Electron mass ($9.109\ 383\ 701\ 528 \times 10^{-31}$ Kg)
α	Fine-structure constant ($7.297\ 352\ 569\ 311 \times 10^{-3}$)
G_{N}	Newtons Gravitational Constant (6.67×10^{-11} m^3 s^{-2} Kg^{-1})
π	Pi 3.14159265359...
h	Planck constant ($6.626\ 070\ 150 \times 10^{-34}$ Js)
m_{Pl}	Planck mass $\sqrt{\frac{\hbar c}{G_N}} \simeq 1.220\ 910 \times 10^{19}$ Gev c^{-2})
t_{Pl}	Planck time $\sqrt{\frac{\hbar G_N}{c^5}} \simeq (5.391\ 245\ 600 \times 10^{-44}$ s)
ℓ_{Pl}	Planck length $\sqrt{\frac{\hbar G_N}{c^3}} \simeq (1.616\ 229\ 380 \times 10^{-35}$ m)
m_{P}	Proton mass ($1.672\ 621\ 923\ 700 \times 10^{-27}$ Kg)
$\hbar$	Reduced Planck constant ($1.054\ 572\ 66 \times 10^{-34}$ Js)
M_{Pl}	Reduced Planck mass $\sqrt{\frac{\hbar c}{8\pi G_N}} \simeq (2.435 \times 10^{18}$ Gev c^{-2})
$M_{\odot}$	Solar mass ($1.988\ 470 \times 10^{30}$ Kg)
c	Speed of light ($2.997\ 924\ 58 \times 10^{8}$ ms^{-1})

Nomenclature: Physical Parameters & Mathematical Operations

The following represent the core and primary representations of common parameters or conventions throughout this doctoral thesis. Care should be taken in the context of individual chapters where it is possible to find an overlap or redefined variables with equivalent designations:

μ^{ac}	Absolutely Continuous Measure Function
$\boxplus$	Additive Free Convolution
f_a	Axion Decay Constant
$\mathcal{K}_{ij}$	Axion Kinetic Matrix
m_a	Axion Mass
$\mathcal{M}_{ij}$	Axion Mass Matrix
μ_{ax}	Axion Mass (Superradiance)
M_{BH}	Black Hole Mass
a_*	Black Hole Spin (Dimensionless)
S	Canonical Action
ϕ	Canonical Axion Field
Λ	Cosmological Constant
Ω_{DE}	Cosmic Dark Energy Density Parameter

Ω_{DM}	Cosmic Dark Matter Density Parameter
Ω_i	Cosmic Density Parameter
$a(t)$	Cosmic Scale Factor
$\Gamma^{\alpha}_{\beta\gamma}$	Christoffel Symbol
θ	Dimensionless Axion Field
h	Dimensionless Hubble Parameter
δ	Dirac Delta Function
λ	Eigenvalue
ρ	Energy Density
$T_{\mu\nu}$	Energy Momentum Tensor
$\omega(a)$	Equation of State
$\mathbb{E}(x)$	Expectation
$f(x)$	Function
ℓ_s	Fundamental String Length
$\mathcal{G}(\mu, \sigma)$	Gaussian Distribution
α	Gravitational Fine Structure Constant
$h^{p,q}$	Hodge Number
H_0	Hubble Constant
$\mathcal{H}$	Hypothesis
$\mathbb{I}$	Identity Matrix
∞	Infinity
S_{inst}	Instanton Action
ds^2	Invariant Distance
$\mathcal{L}$	Lagrangian Density
m	Mass
$\mathbb{X}$	(data) Matrix
$\eta_{\mu\nu}$	Minkowski Spacetime Metric
s	Moduli Vacuum Expectation Value
$\boxtimes$	Multiplicative Free Convolution

$\mathcal{N}_{ax}$	Number of Axions
n_{ax}	Number of Axions (Dark Sector Cosmology)
N	Number Density
$\mathcal{O}(x)$	Of the Order
$\partial_\mu \equiv \frac{\partial}{\partial \mu}$	Partial Derivative
$\tilde{M}_{ij}$	Perturbed Axion Mass Matrix
μ^{pm}	Point mass Measure Function
Σ	Population Covariance Matrix
$\mathbb{R}^+$	Positive Real Interval
$V(x)$	Potential
P	Pressure
$P(x)$	Probability Density
μ_λ	Probability Measure Density
$\mathbb{R}$	Real Interval
z	Redshift
z_{eq}	Redshift at Matter-Radiation Equality
$\mathcal{R}$	Ricci Curvature Scalar
$\mathcal{R}_{\mu\nu}$	Ricci Curvature Tensor
x^μ	Spacetime Coordinates
$g^{\mu\nu}$	Spacetime Metric
$\beta_{\mathcal{K},\mathcal{M}}$	Spectral Shaping Parameter
W	Superpotential
Γ_{nlm}	Superradiance Rate
τ_{SR}	Superradiance Timescale
ω_{nlm}	Superradiant Eigenfrequency
T	Temperature
$\dot{x}$	Temporal Derivative
$\mathcal{V}$	Three-Cycle Volume
t	Time

$\mathcal{U}(a, b)$	Uniform Distribution
$\mathbb{U}$	Unitary Rotation
$\mathcal{P}$	Unknown Variable Dimensional Parameter
σ^2	Variance
$\mathcal{W}$	Wishart Distribution
$\mathbb{W}$	Wishart Matrix

Publications

The theoretical material and results covered in this doctoral thesis is based on the following published works:

i.) **M. J. Stott**, D. J. E. Marsh, C. Pongkitivanichkul, L. C. Price and B. S. Acharya, "Spectrum of the axion dark sector," Phys. Rev. D **96** (2017) no.8, 083510 doi:10.1103/PhysRevD.96.083510 [arXiv:1706.03236 [astro-ph.CO]].

ii.) **M. J. Stott** and D. J. E. Marsh, "Black hole spin constraints on the mass spectrum and number of axionlike fields," Phys. Rev. D **98** (2018) no.8, 083006 doi:10.1103/PhysRevD.98.083006 [arXiv:1805.02016 [hep-ph]].

iii.) **M. J. Stott**, "The Spectrum of the Axion Dark Sector, Cosmological Observable and Black Hole Superradiance Constraints," arXiv:1811.05763 [hep-th]. Contribution to the Proceedings of the 39th International Conference on High Energy Physics (ICHEP 2018), 4-11 July 2018, Seoul, Korea

During my doctoral studies I also published the following work which is beyond the scope of the main narrative of this thesis:

iv.) **M. J. Stott**, T. Elghozi and M. Sakellariadou, "Gravitational Wave Bursts from Cosmic String Cusps and Pseudocusps," Phys. Rev. D **96** (2017) no.2, 023533 doi:10.1103/PhysRevD.96.023533 [arXiv:1612.07599 [hep-th]].

International Conferences

The material covered in this doctoral thesis was in part presented during parallel session talks at the following international conferences:

i.) **XXXIX International Conference on High Energy Physics**
4th-11th July 2018, COEX Arena, Seoul, Republic of Korea
28th August 2018 : *"The spectrum of the axion dark sector, cosmological observable and black hole superradiance constraints."*

ii.) **XXII Annual International Conference on Particle Physics and Cosmology**
27th-31st August 2018, Institute of Basic Science and Culture Center, Daejeon, Republic of Korea
5th July 2018 : *"The spectrum of the axion dark sector and black hole spin constraints on the number of axion-like fields."*

iii.) **III International Conference Cosmology on Safari**
3rd-9th March 2019, Hluhluwe, KwaZulu-Natal, South Africa
4th March 2019 *"Constraining cosmological multi-axion models via black hole superradiance."*

iv.) **X International String, Cosmology and Gravity Student Conference**
1st-3rd April 2019, Max-Planck-Institut für Physik, Munich, Germany
2nd April 2019 : *"Multi-axion cosmology and black hole superradiance in the string axiverse."*

v.) **XXII International Conference From the Planck Scale to the Electroweak Scale**

3rd-7th June 2019, Parque de las Ciencias, Granada, Spain

3rd June 2019 : *"Effective ultralight multi-axion string models and constraints via black hole superradiance."*

vi.) **XIX International Conference on String Phenomenology**

24th-28th June 2019, CERN, Geneva, Switzerland

27th June 2019 : *"Effective multi-axion cosmology and constraints from black hole superradiance."*

To Mum & Dad,

for their eternal inspiration,

love and unwavering belief.

Contents

Declaration ii

Abstract iv

Acknowledgments viii

Abbreviations xii

Nomenclature xvi

Nomenclature II xvii

Publications xxi

Conferences xxii

Contents xxv

List of Figures xxxiii

List of Tables lxi

Introduction and Origins 1

Part I. The Standard Model of the Universe 20

1 The Standard Model of Concordance Cosmology 21

1.1 From Cosmogony to Cosmology 21

1.1.1 The Standard Cosmological Principle 21

1.1.2 Epochal Evolution 23

1.2 The Friedman-Lemaître-Robertson-Walker Metric 26

1.3 The Einstein Equations 28

1.3.1 The Field Equations of Matter and Energy 28

1.3.2 The Serendipity of Spacetime 32

1.4 The Friedmann Equations 36

1.4.1 The Expanding Universe 36

1.4.2 The Standard Energy Constituents 40

1.5 The Causality and Kinematics of Spacetime . . . 45
1.6 Beyond the Traditional Paradigms . . . 48
1.6.1 Problems with Concordance Cosmology . . . 48
1.6.2 The Paradigm of Cosmic Inflation . . . 50
1.7 The Matter and Energy Content of the Dark Universe . . . 53
1.7.1 A Historical Perspective of a Dark Universe . . . 53
1.7.2 A Mysterious Matter . . . 54
1.7.3 A Quintessential Quandary . . . 62

2 The Strong CP Problem and the Axion 68
2.1 The Standard Model of Particle Physics . . . 68
2.1.1 A Quantum Theory of Fields . . . 68
2.1.2 Problems with The Standard Model . . . 75
2.2 Quantum Chromodynamics and the $U(1)_{\mathrm{A}}$ Problem . . . 78
2.3 The Strong CP Problem and the Peccei-Quinn Solution . . . 83
2.3.1 An Issue with the QCD Vacuum . . . 83
2.3.2 The QCD Axion . . . 85
2.4 The Standard Model(s) of the QCD Axion . . . 88
2.4.1 Visible Axions . . . 88
2.4.1.1 The Peccei-Quinn-Weinberg-Wilczek Model . . . 88
2.4.2 Invisible Axions . . . 91
2.4.2.1 The Kim-Shifman-Vainshtein-Zakharov Axion Model 91
2.4.2.2 The Dine-Fischler-Srednicki-Zhitnitsky Axion Model 92
2.5 Axion Interactions and Effective Field Theories . . . 94
2.5.1 An Effective Description of the QCD Axion . . . 94
2.5.2 The Effective Axion Potential . . . 96
2.5.3 Standard Model Couplings to the Axion Field . . . 99
2.6 The Cosmological Axion . . . 103
2.6.1 Thermal Axion Relics . . . 103
2.6.2 Vacuum Realignment Axions . . . 105
2.7 Coherent Axion Field Evolution . . . 110
2.7.1 Hubble Friction . . . 110
2.7.2 The Equations of Motion . . . 113
2.8 Dark Axions and Accelerated Expansion . . . 117
2.8.1 The Axion Inflaton . . . 117
2.8.2 A Quintessential Component . . . 120
2.8.3 A Fuzzy Field . . . 124
2.9 Experimental Searches for the Axion Field . . . 127

3 The Landscape of String Theory and The String Axiverse 133
3.1 A Landscape of Landscapes . . . 133
3.1.1 An Outer Dissonance . . . 133
3.1.2 An Inner Harmony . . . 137
3.1.3 String GUTs . . . 141
3.2 Generalities of Moduli . . . 146
3.2.1 Dimensional Reduction . . . 147
3.2.2 Ten-Dimensional Supergravity and Kähler Moduli Stabilisation 150
3.2.2.1 The Kachru-Kallosh-Linde-Trivedi Scenario . . . 153

3.2.2.2 The Large Volume Scenario . . . 155
3.3 The String Axiverse . . . 156
3.3.1 A Plentitude of Pseudoscalars from Topological Complexity . 156
3.3.2 The General Parametric Description of Axion-Like Fields . . 160
3.3.3 The F-theory Landscape . . . 161
3.3.4 The Type IIB Axiverse . . . 162
3.3.5 The M-theory Axiverse . . . 164
3.3.6 The Kreuzer-Skarke Axiverse . . . 168
3.3.6.1 Calabi-Yau Manifolds . . . 168
3.3.6.2 Mirror Symmetry . . . 172
3.3.6.3 From Geometry to Phenomenology . . . 175
3.3.7 Can We Really Have an Axiverse? . . . 177
3.3.7.1 Tachyonic Saxion Masses and AdS Vacua . . . 178
3.3.7.2 An Axiverse Assumption . . . 180

Part II. The Universe and Universality 182

4 Canonical Random Matrix Theory 183
4.1 Elements of Random Matrix Theory . . . 183
4.1.1 Statistical Tools and Assumptions . . . 183
4.1.2 Matrix Theory . . . 186
4.1.3 Fundamentals of Eigendecomposition . . . 188
4.1.4 The Nature of Eigenvalues . . . 191
4.1.4.1 The Orthogonal Polynomial Method . . . 192
4.1.5 Convergence of Limiting Spectral Distributions . . . 196
4.1.6 Classical Random Matrix Theory . . . 197
4.1.6.1 Ensemble Invariance and Physical Systems . . . 198
4.1.6.2 A Minimally Informative Stance . . . 202
4.2 Sample Covariance Matrices and High Dimensional Data . . . 204
4.2.1 Multivariate Statistics and Positive Definite Spectra . . . 204
4.2.1.1 The Sample Covariance Matrix . . . 206
4.2.1.1.1 The High-Dimensional Regime . . . 208
4.2.1.1.2 Data Vectors and Standard Matrix Forms . 209
4.2.2 The Wishart-Laguerre Ensemble . . . 211
4.2.2.1 Laguerre Orthogonal Polynomials . . . 214
4.2.2.2 A General Sample Covariance Matrix . . . 216
4.2.2.2.1 A General Hypothesis and Isometry . . . 218
4.3 Spectral Statistics and Universality . . . 220
4.3.1 The Isotropic Null Formalism . . . 220
4.3.1.1 Bulk Universality and The Marčhenko-Pastur Law . 220
4.3.1.2 Edge Statistics and Extremal Universality of the Spectral Infimum and Supremum . . . 224
4.3.2 The Alternative Formalism . . . 225
4.3.2.1 The Population Covariance Matrix . . . 225
4.3.2.2 Finite Rank Correlations . . . 226
4.3.2.2.1 The Baik-Ben Arous-Péché Phase Transition 228
4.3.2.3 Full Rank Correlations . . . 230

4.3.2.3.1 The Covariance F-Matrix . . . 230
4.3.2.3.2 Correlated Data Observations . . . 231
4.3.2.3.3 Perturbed High-Dimensional Correlated Data Observations . . . 232
4.3.2.3.4 The Inverse Wishart Distribution . . . 233
4.3.2.3.5 The F-matrix Distribution . . . 234
4.4 Free Convolutions of Spectral Measure Densities . . . 237
4.4.1 Asymptotic Freeness and Non-Commutative Probability . . . 237
4.4.1.1 Free Probability Theory . . . 238
4.4.1.2 Probability Spaces and Borel Measures . . . 240
4.4.2 Classically Deformed Models . . . 241
4.4.2.1 Rotation Invariance and Traceability . . . 241
4.4.2.2 Free Convolution Operations . . . 242
4.4.2.3 Limiting Measure Representations of Matrix Ensembles . . . 243
4.4.2.4 The Lebesgue Decomposition Theorem . . . 244

5 The Random Matrix Axiverse 246
5.1 Effective Models of the String Axiverse . . . 246
5.1.1 The Effective Four-Dimensional Multi-Field Action . . . 250
5.1.1.1 Well-Aligned Multi-Field Potentials . . . 250
5.1.1.2 Canonical Normalisation . . . 254
5.1.2 Epistemic Priors on the Axion Parameter Space . . . 257
5.2 The Random Matrix Axiverse . . . 260
5.2.1 Arguments to Explore Modality . . . 260
5.2.2 The Black Boxes of the Axion Cosmology . . . 263
5.2.2.1 Utilising the Spectral Theory of Traditional Ensembles 263
5.2.2.2 Augmenting the Unknown . . . 264
5.2.3 I. Models With Degenerate Mass States *Diagonalised Mass-Eigenstate Basis* . . . 265
5.2.3.1 Degenerate Scalings . . . 265
5.2.3.2 Non-Trivial Metric with a Degenerate Mass Spectrum 266
5.2.4 II. Models With Random Matrix Mass States *Canonically Normalised Kinetic Basis* . . . 267
5.2.4.1 The Marčhenko-Pastur Isotropic Model . . . 267
5.2.4.2 Finite Rank Spiked N-flation Mass Matrix . . . 269
5.2.4.3 Full Rank Perturbed N-flation Mass Matrix . . . 273
5.2.4.3.1 Conjugate Priors . . . 275
5.2.4.3.2 Non-Conjugate Priors . . . 276
5.2.5 III. Kinetically Aligned Mass Spectra *Geometric Lattice Basis* . . . 279
5.2.5.1 The Symmetric Isotropic Case . . . 280
5.2.5.1.1 Unbroken Symmetry ($\beta_{\mathcal{K}} = \beta_{\mathcal{M}}$) . . . 281
5.2.5.1.2 Broken Symmetry ($\beta_{\mathcal{K}} \neq \beta_{\mathcal{M}}$) . . . 282
5.2.5.2 Spiked Kinetic Alignment . . . 282
5.2.5.2.1 Spiked Mass Spectrum . . . 283
5.2.5.2.2 Spiked Decay Spectrum . . . 283
5.2.5.2.3 Double Spiked Point Mass Spectrum . . . 284

5.2.5.3 Correlated Kinetic Alignment . . . 285
5.2.6 Multi-Modality for Extended Sectors of Axion Physics . . . 286
5.2.7 Initial Conditions for the Canonical Fields . . . 288
5.2.7.1 Effective Axion Decay Constants . . . 288
5.2.7.2 Sample Basis Scalings . . . 289
5.2.8 Random Supergravity and the Superpotential Hessian . . . 291
5.2.8.1 The Hessian Matrix . . . 291
5.2.8.2 An Ensemble Approximation to Random Supergravity 292
5.3 The M-theory Stochastic Superpotential . . . 293
5.3.1 The Random Matrix Axiverse in M-theory . . . 294
5.3.1.1 M-theory Moduli Stabilisation . . . 294
5.3.1.2 Diagonal Kähler Metrics . . . 299
5.3.1.2.1 A Model for Dark Radiation . . . 299
5.3.1.2.2 The Spectrum of Decay Constants . . . 301
5.3.1.3 The M-Theory Random Matrix Mass Spectrum . . . 302
5.3.1.3.1 Higher Order Instanton Corrections . . . 302
5.3.1.3.2 The Expanded Effective Superpotential . . . 305
5.3.1.3.3 A Series of Simple Stochastic Variables . . . 308
5.3.1.3.4 Simple Physical Considerations for Spectral Moments . . . 311
5.4 Unimodal Priors for the String Axiverse . . . 314
5.4.1 Algebraic High-Dimensional Matrices . . . 314
5.4.2 Classification of Spectral Moments . . . 316
5.4.2.1 The Pearson Density System . . . 319
5.4.3 Unifying the Model Classes . . . 324
5.4.3.1 Resorting to Normality . . . 325

Part III. Augmenting the Axiverse 328

6 Black Hole Spin Constraints on the Mass Spectrum and Number of Axion-like Fields 329
6.1 Black Hole Superradiance . . . 329
6.1.1 Singularities in Spacetime . . . 329
6.1.1.1 Gravitational Waves and Black Hole Masses . . . 332
6.1.1.2 Black Hole Hair and Spacetime Metrics . . . 334
6.1.1.3 Gravitational Engines as Phenomenological Probes . 335
6.1.2 The Kerr Black Hole Spacetime . . . 339
6.1.2.1 The Rotating Invariant Line Element . . . 339
6.1.2.2 The Ergoregion of the Black Hole Spacetime . . . 341
6.1.3 Axions as Perturbative Catalysts for Superradiant Instabilities 342
6.1.3.1 A Separable Solution . . . 342
6.1.3.2 The Weak-Field Analytical Approximation for Scalar Induced Superradiance . . . 347
6.1.3.3 Numerical Solution in the Strong-Coupling Regime . 352
6.2 The Dynamics of Black Hole Superradiance . . . 355
6.2.1 The Astrophysics of Black Hole Superradiance . . . 358
6.2.1.1 The Gravitational Atom . . . 358

6.2.1.2 The Kinematical Evolution of the Scalar Cloud . . . 359
6.2.2 Multi-Field Superradiant Evolution in the Quasi-Linear Regime 363
6.2.2.1 Dissipative Energy Channels . . . 363
6.2.2.2 Evolution of the Scalar Cloud in the Quasi-Linear Regime . . . 366
6.2.3 The Black Hole Mass-Spin Regge Plane . . . 368
6.2.3.1 Axion Constraints from Astrophysical Black Hole Spin Measurements . . . 368
6.2.3.2 Characteristic Timescales of Black Hole Evolution . . . 370
6.2.4 Spin Measurements of Binary Systems and Active Galactic Nuclei . . . 374
6.2.4.1 Astrophysical Measurements of Black Hole Systems . . . 374
6.2.4.2 A Data Set of Black Hole Candidates . . . 375
6.3 The $\mathcal{N}$-Radiance Regime . . . 375
6.3.1 Axion Self-Interactions and the Bose Supernova Phenomenon . . . 375
6.3.1.1 Additional Dissipative Kinematics . . . 377
6.3.1.2 LMC X-1: A Specific Example . . . 381
6.3.1.3 The Weakly Self-Interacting Regime . . . 383
6.4 Superradiance Constraints on Axion-Like Particles . . . 384
6.4.1 A Single Axion-Like Field . . . 384
6.4.2 Constraints on Axion Masses from Stellar Mass Black Holes . . . 386
6.4.3 Constraints on Axion Masses from Supermassive Black Holes . . . 386
6.4.4 A Degenerate Axion Mass Population . . . 388
6.4.5 Constraints on a Degenerate Population . . . 390
6.4.6 A Non-degenerate Axion Mass Population . . . 393
6.4.6.1 Correlated Eigenstates . . . 393
6.4.6.2 Simplified Factorised Probabilities . . . 397
6.4.6.3 The M-theory Axiverse: the QCD Axion, GUTs, and FDM . . . 398
6.4.7 FDM Probes Via Superradiant Instabilities of M87* . . . 405
6.4.7.1 The Event Horizon Telescope and 21cm Observations . . . 405
6.4.7.2 Constraints on Fuzzy Dark Matter . . . 408
6.5 Discussion and Conclusions on Black Hole Superradiance . . . 410

7 The Spectrum of the Axion Dark Sector 413
7.1 The Dark Universe . . . 413
7.1.1 Axion Cosmologies . . . 414
7.1.2 Late Time Evolution and Initial Model Conditions . . . 416
7.1.3 Bounds on the Axion Masses . . . 419
7.1.4 Axion Field Oscillations . . . 422
7.1.5 Computing the Model Quasi-Observables . . . 423
7.1.6 Epistemic priors on the Dark Axiverse . . . 425
7.2 Constraints on the Random Matrix Axiverse . . . 429
7.2.1 Isometric Y-Matrix Model . . . 431
7.2.1.1 Isometric Y-Matrix Dark Matter . . . 432
7.2.1.2 Isometric Y-Matrix Dark Energy . . . 434
7.2.2 Full Rank Perturbed F-Matrix Model . . . 437

7.2.2.1 Perturbed F-Matrix Dark Matter . . . 437
7.2.2.2 Perturbed F-Matrix Dark Energy . . . 439
7.2.3 Full Rank Perturbed F-Matrix with Rank One Noise Model . 440
7.2.3.1 Full Rank Perturbed F-Matrix with Rank One Noise Dark Matter . . . 443
7.2.3.2 Full Rank Perturbed F-Matrix with Rank One Noise Dark Energy . . . 444
7.2.4 The M-theory Random Matrix Model . . . 446
7.2.4.1 M-theory Random Matrix Dark Matter . . . 446
7.2.4.2 M-theory Random Matrix Dark Energy . . . 448
7.2.4.3 A Finely Tuned M-theory Random Matrix Toy Model 449
7.3 A Bayesian Hierarchical Network of the Axion Dark Sector . . . 452
7.3.1 The Structure of the Network . . . 452
7.3.2 Constraints on the String Axiverse . . . 454
7.3.2.1 Bayesian Isometric Y-Matrix Constraints . . . 455
7.3.2.1.1 Bayesian Isometric Y-Matrix Dark Energy . 455
7.3.2.1.2 Bayesian Isometric Y-Matrix Dark Matter . 456
7.3.2.2 Bayesian Dark Matter from the M-theory Random Matrix Axiverse . . . 459
7.4 Discussion and Conclusions on the Axion Dark Sector . . . 462

Overall Conclusions and Future Directions **468**

A The Expanded Standard Model Lagrangian **483**
A.1 The Equation . . . 483

B Bayesian Statistical Modelling **486**
B.1 Bayes Theorem . . . 486
B.2 Hierarchical Modeling . . . 488
B.3 General Approaches to Variances and Correlations . . . 490
B.3.1 The Separation Strategy . . . 491
B.4 Probability and Measurable Spaces . . . 492

C Matrix Operations **494**
C.1 Matrix Transforms . . . 494

D The Tracy-Widom Limiting Laws **496**
D.1 Extremal Spectral Functions . . . 496

E Combinatorial Sequences and the Fuss-Catalan Distributions **499**
E.1 The Fuss-Catalan Numbers . . . 499
E.2 The Raney Numbers . . . 502

F Elements of Measure Spaces **505**
F.1 Free Operations . . . 505
F.2 Infinite Divisibility . . . 506
F.3 Spectral Noise . . . 507

G Beta Distribution Functions **509**
G.1 Family Parameterisations 509

H Generalised Lambda Distributions **512**
H.1 A Flexible Framework for Spectral Moments 512
H.2 The Freimer-Kollia-Mudholkar-Lin Parameterisation 513

I The Random Matrix Type IIB Superpotential **515**
I.1 The N-flation Matrix Model 515
I.2 A Simplified Superpotential 516

J Superradiance Statistical Model **518**
J.1 Black Hole Mass-Spin Data Coordinates 518
J.2 Effective One-Dimensional Errors 519

K Outlying Cosmologies **522**
K.1 Axionic Cosmic Densities 522

Bibliography **525**

List of Figures

1 Faithful reproduction of Peter Apian's geocentric celestial spheres originally sourced from his Cosmographia [86] (Antwerp, 1539). The iconic celestial spheres often appeared as the foundations of models of fundamental bodies in cosmological models, pioneered by the likes of Plato, Aristotle, Ptolemy and Copernicus. These heavenly bodies were generally considered fixed elements in a series of rotating spheres made of an aetherial, transparent quintessence element, reproducing a natural beauty in the symmetry of geocentricity. Image credit: Celestial Orbs in the Latin Middle Ages, Edward Grant [626]. 3

2 Bohr model of the Hydrogen atom [1057], ^{1}H, representing an electrically neutral atom containing a single, positively charged proton at the centre, along with a single negatively charged electron. The electron sits in one of the designated energy levels, bound to the nucleus by the Coulomb force. The model serves as a first order approximation of the later formulated "true" quantum mechanical description. Traditionally the radius of each orbit goes as n^2, where n represents the principle quantum number. Here we show only the first two electron orbits to the correct scale. The solid black lines represent adsorption series and the dashed lines represent series examples for emission processes. The example electron transition produces the first line of the Balmer series resulting in a proton with a wavelength of 656 nm. 7

3 Symmetric orthographic projection in the Coxeter plane of the E_8 Coxeter group of the Gosset 4_{21} polytope, represented as a two-dimensional skew orthogonal projection inside a Petrie polygon. This particular projection in two-dimensions consists of 6720 edges with an eight-dimensional length $\sqrt{2}$ along with 240 vertices. The Lie group E_8 has dimension 248 and its rank, eight, is the dimension of its maximal torus. Image credit: Author: Jgmoxness, taken from `https://commons.wikimedia.org/wiki/File:E8Petrie.svg`. . . . 12

4 Dynkin diagrams for both the exceptional Lie group E_8 and the Standard Model. The mathematical process of reducing one to the other, represented by the arrow, could hold the key to understanding how our observed spectrum of particles fit in a consistent model of quantum gravity. The byproducts of such a process through compactification of some extra-dimensional spacetime manifold could also provide solutions to some of the largest paradigmatic issues in the Standard Model of Cosmology. Reproduced from figures found in Section 3 of Ref. [1086]. 14

1.1 The Hubble Ultra Deep Field (HUDF), representing an image of some of the oldest visible light seen by mankind. This particular image was taken over eight hundred exposures with the NASA/ESA Hubble Space Telescope, performing four hundred Hubble orbits of Earth in order to finalise the data for this image. The total exposure time was 11.3 days, capturing approximately ten thousand galaxies spanning billions of light years. Image credit: NASA, ESA, S. Beckwith (STScI) and the HUDF Team, `https://hubblesite.org/contents/news-releases/2004/news-2004-07.html`. 24

1.2 Constraints on the curvature of the Universe representing limits for a non-flat universe as a minimal extension to the standard ΛCDM model of cosmology. The dashed lines represent 68% and 95% contour bounds from samples taken using the Planck TT,TE,EE+lowE chains as a function of the total matter and curvature densities, along with limits on the value of H_0. Image credit: Taken from Fig. 29 found in Ref. [40] 31

1.3 Original radial velocity-distance relationship plot for extra-galactic nebulae in a single cluster representing the distinguished work of Edwin Hubble. The original analysis detailed forty six galaxies, which showed the apparent nature of an expanding universe which came to be described by the Hubble-Lemaître Law (Eq. (3)). The slope of best fit represents the Hubble Parameter determined by the Doppler shift of the observed spectra. Image credit: Edwin Hubble, taken from Fig. 1 of Ref. [725]. 32

1.4 The effective relativistic degrees of freedom for both the energy and entropy densities, $g_{*,r}$ and $g_{*,s}$, as a function of temperature beginning at, $T = \mathcal{O}(10^3)$ GeV, evolving assuming the standard evolution of the Standard Model gauge group. The functions separate approximately after $e\pm$ annihilation, when $T_\nu \neq T_\gamma$. The fits are made following the procedure of Ref. [1329] used to approximate the functions given in Eq. (1.73) and Eq. (1.74). The dotted lines (*light blue* (entropy), *dark blue* (energy)) represent the approximate fitted values of $g_{*,r}$ and $g_{*,s}$ at the present time. 37

1.5 Anisotropies of the cosmic microwave background emitted approximately 380,000 years after the Big Bang, as observed by the Planck satellite, a strong indication of the nature of Big Bang cosmology. The Red regions represent densities hotter than the average temperature, the blue regions are cooler, reflecting the apparent density variations present at recombination. The observational aspects of this map represent a vital probe to possible extensions to cosmological physics models. Image credit: ESA and the Planck Collaboration, `http://sci.esa.int/science-e-media/img/61/Planck_CMB_Mollweide_4k.jpg`. 39

1.6 The cosmic energy budget determined by data collected by the Planck collaboration in Eq. (1.80), Eq. (1.81) and Eq. (1.83). The Universe is currently observed to be dominated by two principle dark components which make up $\sim 95\%$ of the total cosmic energy density. The separated wedge component represents the only portion of the observable Universe we can currently account for with the Standard Model of particle physics. 54

1.7 Original superposition of 21 Sc galaxy rotation curves which first appeared in Ref. [1130], detailing the unexpected flattened nature of the curves when extending their analysis far beyond the galactic nucleus. Contributions from a significant hidden unseen "matter" sector were determined to be present in order to explain the observed form of these rotational curves. Image credit: Taken from Fig. 6 found in Ref. [1130]. 59

2.1 The complete framework of the Standard Model of particle physics. Each of the fields represented have been experimentally confirmed and form our best understanding of how matter and the fundamental forces interact. The fermions are comprised of twelve elementary particles of spin $1/2$, in three generations which obey Pauli's exclusion principle. Each particle has its own antiparticle which defines the antimatter content of the Standard Model. The gauge bosons, manifest under the gauge group representation of Eq. (2.1), define the force carriers that mediate the fundamental interactions of the strong, weak, and electromagnetic forces. The Higgs boson is the only fundamental scalar required to describe the elementary-particle masses. Image credit: Taken from `https://commons.wikimedia.org/wiki/File:Standard_Model_of_Elementary_Particles_Anti.svg`. 70

2.2 *Left panel:* Triangle loop interaction diagram for the anomalous axion-gluon-gluon coupling. Each gluon vertex strength is regulated by the strong coupling constant. The axion vertex strength is regulated by the axion-fermion Yukawa coupling. *Right Panel*: Anomalous two-photon vertex interaction which can be used to indicate the stability of the axion field over cosmological time scales. The respective vertex interactions are replaced with charged fermion coupling terms. 87

2.3 The *Mexican hat* symmetry breaking potential of Eq. (2.48), in the complex φ plane. The VEV of the massive radial mode is $f_a/\sqrt{2}$. The axion is apparent as the massless angular phase degree of freedom at the minimum of the potential. The field initially begins at the point denoted by the *green* circle. Once the respective symmetry is spontaneously broken the field moves down its potential to the minimum denoted by the *blue* circle, where is now possesses a continuous shift symmetry. 90

2.4 General form of the standard dilute instanton gas axion potential which forms non-perturbatively, periodic in the initial misalignment angle domain along with associated higher order forms. The three examples presented include the standard axion-cosine potential along with two potentials possessing higher order harmonics. Such potentials are often addressed by considering higher order instanton corrections which allow for features such as the dilution of the axion relic density at rates faster than a standard fluid matter component [774, 1071]. This is shown by the *green* and *yellow* points which represent the same value of θ. 100

2.5 Plots for the example evolution of the cosmological densities, ρ_i in Eq. (1.42) as a function of the cosmic scale factor, a(t), with $\mathcal{N}_{\rm ax} = 10$ axions behaving as the total DM density where the mass eigenstates sampled with a realisation of the isometric S-matrix model in Section 5.2.4.1. *Upper inset*: Enhanced view of the effect of multi-field oscillations on the total axion density, $\rho_{\rm ax}$. *Lower inset*: Comparative matter-radiation equality with crossings of $\rho_m = \rho_b + \rho_{\rm ax}$ and ρ_r at $z_{eq} = 3393$. 109

2.6 Plots for the example evolution of each contribution to the critical density, $\Omega_i = {}^{\rho_i}/_{3H^2}$, as a function of the cosmic scale factor, a(t). This example cosmology represents a realisation of the total DM with axion mass eigenstates sampled using a realisation of the isometric S-matrix model of Section 5.2.4.1, including the remaining Ω_r, Ω_Λ and Ω_b terms. *Inset*: Enhanced view of the effect of multi-field oscillations on the axion density parameter $\Omega_{\rm ax}$ contributing to the critical density. 110

2.7 Evolution of various cosmological axion field quantities using the exact solution of the background evolution of a single axion field determined using the scalar field equations of motion. As the axion field begins to oscillate about its minimum the fields equations of state (*lower left* panel) oscillates between the limits -1 and 1. At this point the field begins to scale as a non-relativistic cold DM component as shown in the *lower right* panel. 115

2.8 Multi-field evolution of the collective equation of state, $\omega_{\rm eff}$, as a function of the cosmic scale factor for three different configurations of multi-axion models with, $\mathcal{N}_{\rm ax} = 5$. Each of the five model masses are scaled in order to reproduce examples realisations with DM dominated, DM/quintessence mixed and quintessence dominated axion cosmologies. 116

2.9 *Left panel*: Temporal evolution of the standard cosmic energy density components, along with two additional ULA fields present in the spectrum. The oscillatory behaviour of the total density is visually observed twice, when the axion masses are sufficient separated so that the heavier fields oscillations are heavily damped at $a\left(t_{\rm osc}^{m_a}\right)$, the time of onset oscillation of the second axion with a reduced mass. The fields initial conditions mean the total contribution to the matter density at the present time is insufficient, avoiding constraints such as those in Ref. [710]. *Right panel*: Schematic representation of late time oscillatory behaviour of the effective equation of state defined in Eq. (2.107) for the two-axion effective matter fluid with features of multi-oscillatory behaviour. 125

2.10 Example Axion-photon interaction via the Primakoff process, present in an external electromagnetic field realised through the two photon coupling to the axion particle, which can be reverted to allow for the conversion to either photons or axions. This is the dominant process in many experimental techniques to search for the axion which arising from the properties of the electromagnetic anomaly. 127

3.1 Propagation of the traditional fundamental components of quantum theories. Relativistic point particles (*left* example) map out their historical trajectories using a world-line which is defined by a single parameter τ often associated to the proper time. The remaining two examples represent the propagation of open and closed fundamental strings, respectively, of finite length ℓ_s, defining the space of the string worldsheet. 134

3.2 The unified space of string theories. Asymptotic expansions around the cusps represent the limits of the weakly coupled superstring theories, which can be studied under the perturbative regime. Currently most of the moduli space associated to the eleven-dimensional quantum theory of M-theory cannot be studied using these limits. The dualities on the outer curves are examples of symmetries used to overcome this issue in order to study the low energy sector using supergravity theories. It is possible that some self-dual point not represented here corresponds to the arbitrary dimensional limit of the true fundamental theory. Whether or not "M" should sit in the centre of this diagram is unclear. This has previously been referred to as *U-theory* [1171] and strongly relates to the notions of string universality. Energy or the distance from the Bogomol'nyi-Prasad-Sommerfield (BPS) limit, increases (decreases) and we move away from (towards) the page. 138

3.3 Approximate Gaussian fits for quantities formed using the topological invariant Hodge numbers, $h^{1,1}$ and $h^{2,1}$. *Left panel*: Ratio of the axion degrees of freedom and the total dimension of the extra-dimensional space defined in Eq. (3.64), represented by the data from the Kreuzer-Skarke list [825] for the distinct Hodge number combinations and approximate density function fit. *Right panel*: Density plot for the Euler characteristic from Eq. (3.61) for Calabi-Yau threefolds along with its approximate density function fit. 158

3.4 Example general Calabi-Yau quintic cross-section, $Z_1^5 + Z_2^5 = 1$. The two-dimensional projectional slice is an embedded surface representing a visualisation of the possible full six-dimensional Calabi-Yau space, $Z_0^5 + Z_1^5 + Z_2^5 + Z_3^5 + Z_4^5 = 0$, which could define the extra-dimensions of spacetime in well-defined superstring compactification models. The structural features of these spaces can have a drastic effect on the particle content in the low-energy four-dimensional theory. 167

3.5 Complete construction of toric hypersurfaces parameterised by $\chi \in [-960, 960]$, using the 30,108 distinct Hodge pairs from the Kreuzer-Skarke dataset of Calabi-Yau hypersurfaces in Gorenstein Fano-toric fourfolds. The coloured surface represents the logarithmic multiplicity of the Euler characteristic and functional height, $y = h^{1,1}+h^{2,1}$ for the 473,800,652 hodge pairs which run over these distinct values peaking with a density $\mathcal{O}(10^6)$ at $h^{1,1} = h^{2,1} = 27$. The *red* dashed line defines the boundaries enforced by the fact that the Hodge numbers are strictly positive. The *black* dashed line is the mirror manifold symmetry boundary. The *grey* solid line is the limits for the Euler characteristic which defines the properties of the manifold. The *light blue* lines represent a *half* mirror symmetry for points which have mirror manifolds about the $\chi = -480$ and $\chi = 480$ axis. The *grey* grid represents symmetry boundaries for features such as $K3$ fibrations [309]. Adapted from the work found in Ref. [309]. 171

4.2 *Left panel:* Density function plots for the Wishart distribution defined in Eq. (4.54) for various values of the parameter representing the functions degrees of freedom. *Right Panel*: Density function plots for the inverse Wishart distribution defined in Eq. (4.97) also for various values of the parameter representing the functions degrees of freedom. 213

5.4 Normalised eigenvalue spectra for the Marčhenko-Pastur RMT model, along with associated probability density functions for the squared axion masses, m_a^2, presented with both linear and logarithmic scales in the *left* and *right panels* respectively. Each panel shows five selected values of the spectrum shaping parameter $\beta_{\mathcal{M}}$, approximately covering its defining interval $\beta_{\mathcal{M}} \in (0, 1]$. *Left panel*: The mass distribution converges to the Marčhenko-Pastur limiting law as $\mathcal{N}_{\rm ax} \to \infty$. Asymptotically the largest eigenvalue, which can fluctuate outside its defined compact interval, is determined by the Tracy-Widom law in Eq. (D.4). *Right panel*: Probability density functions for each of the associated distributions in the *left panel* displayed on a logarithmic mass scale. Inset: As $\beta_{\mathcal{M}}$ increases,1 the positive logarithmic displacement of the upper bound is limited compared to the negative displacement of the lower bound of the distribution. 270

5.5 Normalised eigenvalue spectra for the axion mass matrix defined with spikes from eigenvalues defined in the supercritical regime of the BBP phase transition. *Left panel*: Example mass spectra for the model presented in Section 5.2.4.2 for a range of values of the distribution shaping parameter $\beta_{\mathcal{M}}$. The spiked eigenvalues, $\mu^{\rm pm}_{\rm spike}$, repulsed from the bulk of the spectrum are enhanced by $\mathcal{O}(\mathcal{N}_{\rm ax})$ (*right inset*). The bulk of the spectrum, $\mu^{ac}_{\rm MP}$, is defined by the Marčhenko-Pastur limiting laws (*left inset*). *Right panel*: Example mass spectra for the model presented in Section 5.2.5.2.3 for a range of values of the distribution shaping parameter $\beta_{\mathcal{M}}$. The bulk of the perturbed mass spectrum is defined as $\mu^{\rm ac}_{\rm F}$ found in Eq. (4.101) inheriting two spiked values defined from both the kinetic and mass matrices. In the limit $\beta_{\mathcal{K},\mathcal{M}} = 1$ the total distribution measure becomes an absolutely continuous function with each of the spiked point masses absolved into the bulk support. 274

5.6 Normalised mass spectra for the model presented in Section 5.2.5.1 for a range of values of the distribution shaping parameters $\beta_{\mathcal{K}} = \beta_{\mathcal{M}}$. The multiplicative free convolution of the absolved decay constants with the initial mass matrix causes the sampled spectra to universally converge to a symmetric LSD on logarithmic scales. The mass spectrum measure is defined by the absolutely continuous measure function, $\mu_{\mathrm{F}}^{\mathrm{ac}}$ defined in Eq. (4.101). Each spectra is fitted with a beta distribution function according to the expression found in Eq. (G.6). The $\beta_{\mathcal{M}}$ parameter regulates the limiting distributions kurtosis, acting as a free compression operation, $\boxdot$ (see Section 4.4.2). In the limit $\beta_{\mathcal{M}} \to 0$ the LSD approaches the limiting kurtosis of the infinity divisible bounds for beta distributions, represented by the limit for a semi-circular distribution. 276

5.7 Normalised mass, decay constant and canonical field spectra for the model presented in Section 5.2.5.1, for a single equal value of the distribution shaping parameters $\beta_{\mathcal{K}} = \beta_{\mathcal{M}} = 0.5$. The *upper* panels display model spectra, fitted with beta distribution functions according to the expression found in Eq. (G.6). The vertical *dotted* lines represent the spectral mean, where the *dashed* lines represent a 1σ translation from this value. In the *lower left*, *lower middle* and *left central* panels we display the covariance between each of the simple axion cosmology model parameters. The strongest covariance relationship comes from the decay constants which act as a full rank perturbation to the initial mass matrix ensemble in the geometric lattice basis. The reduced dependance between the other parameters comes from the basis rotations moving into the mass eigenstate basis. The *red dashed* lines represent the two-dimensional peak of the contours in each case. 277

5.8 *Left panel*: Representation of the skew effect apparent when $\beta_{\mathcal{K}} \neq \beta_{\mathcal{M}}$ for arbitrarily normalised eigenvalues defined from matrices in the model presented in Section 5.2.4.1. We demonstrate this using three examples each when $\beta_{\mathcal{K}} < \beta_{\mathcal{M}}$ (*negative skew*) and $\beta_{\mathcal{K}} > \beta_{\mathcal{M}}$ (*positive skew*). Each example has both binned eigenvalue densities from direct sampling along with an approximated beta function fits defined from Eq. (G.6). *Right panel*: Example normalised mass spectra for the model presented in Section 5.2.4.1 for a range of priors on the population covariance matrix. We demonstrate how some standard example models can be well approximated within the bounds of the Beta distribution function of Eq. (G.6) for skewed spectra. Specifically the case of log-uniform priors on the standard deviations using the separation strategy defined in Eq. (B.6) to define the mass matrix population covariance matrix, shows an example where the need for explicit spectral functions may be required. 279

5.10 *Left panel:* Example axion decay constant spectra defined using the Kähler metric defined in Eq. (5.94) which can be modelled by the prior fit in Eq. (5.96) for various values of the minimum and maximum moduli VEVs parameters, $s_{\min}$ and $s_{\max}$. *Right Panel*: Example spectra of the axion decay constant modulus defined using the non-diagonal Kähler metric in Eq. (5.87) formed with uniform priors for the moduli VEVs. The non-centred mean leads to perturbed eigenvalues from the bulk which give a non-positive spectrum for the squared values of the axion decay constants as the matrix is not defined in the form of a sample covariance matrix. 301

5.12 *Left panel:* Example M-theory RMT model eigenvalue spectra representing axion masses, m_a constructed using different variance values, $\sigma_{\tilde{N}}$, when using Gaussian priors defined in Eq. (5.129) on the elements of $\tilde{N}^i_j$ along with Gaussian prior fits. Changing the value of $\sigma_{\tilde{N}}$ has the effect of shifting the mean scale of the spectrum across the ultralight sector. *Right panel:* Example M-theory RMT model eigenvalue spectra representing axion masses, m_a constructed using different mean values, $\bar{\tilde{N}}$ when using Gaussian priors defined in Eq. (5.129) on the elements of $\tilde{N}^i_j$ along with Gaussian prior fits. Decreasing the value of $\bar{\tilde{N}}$ has the effect of both reducing the spread of the spectrum whilst increasing the mean value. 310

5.13 M-theory RMT model eigenvalue spectra representing axion masses, m_a for different values of the spectrum shaping parameter $\beta_{\mathcal{M}}$. The mass spectra converge to an approximate log-normal distribution defined by the function in Eq. (5.132) which have been fitted to each example spectrum in the mass eigenstate basis. Each spectrum is constructed using a fixed value of the average three-cycle volume, $\langle \mathcal{V}_X \rangle = 25$ required for GUT scale unification. The spectra are constructed using 10000 iterations in the case of an axion population size, $\mathcal{N}_{\rm ax} = 10$. 312

5.15 Example mass spectra in M-theory RMT axiverse as found in Fig. 5.14 normalised to shift the mean scale to unity. We demonstrate the nature of universal convergence of the mass spectra in this model to be well described by its first two centralised moments. The logarithm of the spectrum is fitted with a Gaussian density fit (Eq. (5.142)), a Beta distribution function (Eq. (G.6)) and GLD distribution using the method of L-moments (Eq. (H.2)). All of these converge when modelling the peak and tails of the distribution, representing a redundancy in using more complicated distribution families which can model the higher moments. 314

5.17 Hodge fountain for the distributions of the topological invariant Hodge numbers $h^{1,1}$ and $h^{2,1}$ using the Euler number and additive height. The mirror symmetry is realised at Euler number, $\chi = 0$. Each of the banded segments superimposed denotes the manifest forms of the distributions for the spectra of $\log_{10}(m_a)$ using the model in Section 5.2.5 when the distribution symmetry parameters are defined as equal. The selected distributions represent unimodal bounded for the kurtosis of well defined functions. The sum of the shaded regions approximate the total fraction of the spectra which related to symmetric functions about their mean. 321

5.19 Comparative fits for example mass and decay constant spectra using both simplistic priors as well as the GLD determined using various methods. *Left panel*: Normalised mass spectra from the model outlined in Section 5.2.5 for the case where $\beta_{\mathcal{K}} = \beta_{\mathcal{M}} = 1$. The GLD defined by using the method of L-moments (Eq. (H.2)) provides the best fit to the distribution peaks and tails. The worst fit is the Gaussian function (Eq. (5.142)) which provides a good first order approximation but misses several characteristic features of the LSD for the axion masses. *Right panel*: Logarithmic spectra for both the Marčhenko-Pastur density spectra and first order multiplicative convolution of two Marčhenko-Pastur spectra representing the decay constant distributions arbitrarily normalised to two separated scales. Each spectrum is fitted with both a Beta function fit and a GLD function determined by the method of L-moments which to a first order approximation are sufficiently similar. 326

6.1 M87* SMBH at the centre of the Messier 87 galaxy as imaged by the Event Horizon Telescope [48–53]. The BH presents a dark shadow (central spot), which is larger than the BH event horizon, caused by the gravitational warping of light and photon capture at the event horizon. Image credit: Event Horizon Telescope, `https://www.eso.org/public/images/eso1907a/`. 336

6.2 The BH-scalar condensate coupling, $\alpha = \mu_{\rm ax} M_{\rm BH}$. The solid black line represents the unity limit for non-relativistic and relativistic regimes. The dashed line corresponds to $\alpha = 0.5$, the approximate limit in which the analytical approximation for the instability rate is valid. Dotted lines correspond to frequency ranges for monochromatic gravitational wave emission from the scalar cloud accessible to current and future GW observatories [4, 68, 69, 456, 523, 879, 1147]. 337

6.3 Behaviour of a Kerr BH horizons in three-dimensional and two-dimensional Cartesian Kerr-Schild coordinates, for fixed values of the dimensionless spin parameter, a_* approaching the limit for a non-rotating BH. The solid black line represents the ergoregion defined using Eq. (6.12), which is minimally perturbed in the non-relativistic spin limit, $a_* < 1$, where these two regions approach the Schwarzschild solution limit. The dashed blue and cyan lines represent the outer and inner horizons respectively defined using Eq. (6.10). The two hypersurfaces of the event horizon and the ergosphere meet at the co-latitude pole of 0 degrees. The x-axis is the radial distance from the black hole in polar coordinates. 340

6.4 Behaviour of a Kerr BHs defining horizons in three-dimensional space and in the xz-plane for fixed values of the dimensionless spin parameter, a_*, approaching the limit for an extremal BH. The solid *black* line/surface represents the ergoregion defined using Eq. (6.12), the dashed *blue* and *cyan* lines/surfaces represent the outer and inner horizons respectively defined using Eq. (6.10). In the limit that the BH is extreme ($a_* = 1$) the inner and outer horizons coincide. The two hypersurfaces of the event horizon and the ergosphere meet at the co-latitude pole of zero degrees. In the non-relativistic spin region these two regions approach each other in the Schwarzschild limit. The x-axis is the radial distance from the BH in polar coordinates. . . 343

6.5 Imaginary component of the bound-state frequency, $M_{\rm BH}\omega_I$, representing the superradiance instability rate, $\Gamma_{\rm nlm}$, as a function of the dimensionless coupling, $\alpha = \mu_{\rm ax}M_{\rm BH}$. The superradiance rates presented are for each of the orbital/azimuthal quantum numbers, $l = m = 1$ to 5 for various values of the dimensionless BH spin, a_*, approaching the extremal relativistic limit ($a_* = 1$). The functions presented were determined using the weak-field analytical approximations found in Eq. (6.42). 352

6.6 Imaginary component of the bound-state frequency, $M_{\rm BH}\omega_I$ representing the superradiance instability rate, $\Gamma_{\rm nlm}$, as a function of the dimensionless coupling, $\alpha = \mu_{\rm ax}M_{\rm BH}$. The superradiance rates presented are for the fundamental and higher order overtone modes $n = 0$ to 4 for various configurations satisfying either $l = m$ or $l > m$. The red lines correspond to the fundamental overtone modes, $n = 0$ which become subdominant for values of $l = m \geq 4$ (see *inset*). The functions presented were determined using the weak-field analytical approximations found in Eq. (6.42). 353

6.7 Timescale ratios for the superradiance rates determined for an axion with a mass $\mu_{\rm ax} = 10^{-11.5}$ eV. These rates are compared with a typical BH astrophysical timescale, here taken to be $\tau_{\rm Salpeter}$ (Eq. (6.108)). Each cusp represents the analytical limit beyond which Eq. (6.71) is satisfied. The limit to the right of the cusp (soldid line) represents the ratio defining the nature of the timescales where superradiance is apparent. The red volume defines the limit in the two dimensional BH mass-spin parameter space where superradiance occurs within the defined astrophysical timescale used to map the Regge plane isocontour limits, such as those found in Fig. 6.8. 357

6.8 Isocontour exclusion bounds in the BH mass-spin Regge plane for an axion mass, $\mu_{\rm ax} = 10^{-11.5}$ eV, probing the stellar BH parameter space. The limits (*black* outline) for the instability threshold are obtained by fixing the superradiant instability time scales for each value of the orbital/azimuthal quantum numbers, $l = m = 1$ to 5 equal to the timescale of a typical BBH system shown in Eq. (6.106). The extended limits come from considering superradiant instability timescales shorter than $\tau_{\rm Salpeter}$ (*orange*, Eq. (6.108)) and $\tau_{\rm Hubble}$ (*yellow*, Eq. (6.107)). The *red*/*black* data points denote mass and spin estimates of the stellar BHs from X-ray/BBH sources presented in Tabel 6.2. 368

6.9 Isocontour exclusion bounds and calculated total exclusion probabilities in the BH mass-spin Regge plane from superradiant instabilities with a single axion field with a mass, $\mu_{\rm ax}$, spanning the limits in Eq. (6.105). The shaded regions represent instability thresholds shorter than the time scale $\tau_{\rm Salpeter}$ in Eq. (6.108), for each value of the dominant orbital/azimuthal quantum numbers, $l = m = 1$ to 5. The *blue* data points are mass-spin estimates of stellar X-ray and BBH systems. The *orange* points correspond to mass-spin estimates of SMBHs from X-ray reflection spectroscopy. The exclusion probability function (*black* line) is calculated using the statistical model in Appendix J using the BHs compiled in both Table 6.2 and Table 6.3, which is given as a function of the axion mass spanning both the stellar and supermassive regimes. 369

6.11 Contour bounds on the fractional suppression factor of Eq. (6.124) as a function of the axion mass and decay constant highlighting when a bosenova event occurs before the fundamental superradiant mode has extracted the total allowed spin forming a maximally occupied scalar cloud for the case of the stellar mass BH candidate LMC X-1. The QCD axion approximation (*red* dashed line) is determined using Eq. (6.147). 379

6.12 Constraints on the masses of ULAs, $\mu_{\rm ax}$, for singular fields determined by the total probability of exclusion calculated using the methodology in Appendix J via Eq. (J.1). Exclusion bounds are presented in the 68% and 95% CIs as a function of $\mu_{\rm ax}$ with *orange*/*red* lines representing the upper and lower limits of the 68%/95% intervals. These probability limit functions are determined using the BH data given in Table 6.2. 384

6.13 Constraints on the masses of ULAs, $\mu_{\rm ax}$, for singular fields determined by the total probability of exclusion calculated using the methodology in Appendix J via Eq. (J.1). Exclusion bounds are presented in the 68% and 95% CIs as a function of $\mu_{\rm ax}$ with *orange*/*red* lines representing the upper and lower limits of the 68%/95% interval. These probability limit functions are determined using the SMBH data given in Table 6.3. 385

6.15 Isocontour exclusion regions for degenerate mass axion populations with $\mathcal{N}_{\rm ax} = \mathcal{O}(10^0 \to 10^5)$ in the stellar BH parameter-space. The limits for the instability threshold are obtained by fixing the superradiant instability time scales for each value of the orbital/azimuthal quantum numbers, $l = m = 1$ to 5 equal to $\tau_{\rm Salpeter}$ defined in Eq. (6.108) using a fixed axion mass of $\mu_{\rm ax} = 10^{-12.75}$eV. Large values of $\mathcal{N}_{\rm ax}$ effectively correspond to greater superradiance instability timescales considering a single field. The *green* data points are mass-spin estimates of X-ray binary stellar BH candidates. The *blue* data points are primary and secondary sources from BBH coalescence detections at LIGO. 389

6.16 Isocontour exclusion regions for degenerate mass axion populations with $\mathcal{N}_{\rm ax} = \mathcal{O}(10^0 \to 10^5)$ in the stellar BH parameter-space Regge plane. The limits for the instability threshold are obtained by fixing the superradiant instability time scales for each value of the orbital/azimuthal quantum numbers, $l = m = 1$ to 5 equal to $\tau_{\rm Salpeter}$ defined in Eq. (6.108) using a fixed axion mass of $\mu_{\rm ax} = 10^{-18.5}$eV. The *orange* data points are the mass-spin estimates of AGN SMBH candidates detailed in Table 6.3. 390

6.17 Constraints on masses of ULAs, $\mu_{\rm ax}$, via the total exclusion probability in the 68% and 95% CIs for large numbers, $\mathcal{N}_{\rm ax}$, of degenerate fields. *Upper panels:* Dashed red lines represent the shift of the lower bounds in the 95% CI, which decreases as $\mathcal{N}_{\rm ax}$ increases. The exclusion probability functions showing the $\mathcal{N}_{\rm ax}$ type enhancement for the stellar BH data set are calculated using Eq. (6.133). 391

6.18 Constraints on masses of ULAs, $\mu_{\rm ax}$, via the total exclusion probability in the 68% and 95% CIs for large numbers, $\mathcal{N}_{\rm ax}$, of degenerate fields. *Upper panels:* Dashed red lines represent the shift of the lower bounds in the 95% CI, which decreases as $\mathcal{N}_{\rm ax}$ increases. The exclusion probability functions showing the $\mathcal{N}_{\rm ax}$ type enhancement for the SMBH data set are calculated using Eq. (6.133). *Inset:* Oscillatory behaviour of the exclusion probability due to higher values of the orbital/azimuthal quantum numbers passing over low mass SMBHs. 392

6.19 Probability of exclusion represented as a function of the dimensionless variance, σ, defining the mass spectra in the RMT axiverse for $\mathcal{N}_{\rm ax} = (10^0 \to 10^3)$. These constraints are for the scenario in which the mean of the mass spectra is fixed according to Eq. (6.145) in order to maximise the probability of drawing a desired axion mass associated to models of FDM, as detailed in Section 6.4.6.3. In the limit $\sigma \gg 1$ the total probability for $\mathcal{N}_{\rm ax} = 1 \to \infty$ converges to zero as the spread crosses the bounds probable by BH spin measurements. The behaviour in the limit $\sigma \ll 1$ is determined by the accuracy of the available BH mass-spin measurements. 400

6.20 Probability of exclusion as a function of the dimensionless variance, σ defining the mass spectra in the M-theory axiverse for $\mathcal{N}_{\rm ax} = (10^0 \to 10^3)$. *Left panel*: These constraints represent the scenario in which the mean of the mass spectra is fixed according to Eq. (6.143) in order to maximise the probability of drawing a desired axion mass associated to models of GUT in the M-theory axiverse. *Right panel*: These constraints represent the scenario in which the mean of the mass spectra is fixed using Eq. (6.149) in order to maximise the probability of drawing a desired axion mass associated to models of the QCD axion of the Standard Model. In the limit $\sigma \gg 1$ the total probability for $\mathcal{N}_{\rm ax} = 1 \to \infty$ converges to zero as the spread crosses the bounds probable by BH spin measurements. The behaviour in the limit $\sigma \ll 1$ is determined by the accuracy of the available BH mass-spin measurements. 401

6.21 Exclusion bounds for the allowed number of fields, $\mathcal{N}_{\rm ax}$, as a function of the distribution width, σ, represented by 68% (*dotted* line), 95% (*solid* line) and 99.7% (*dashed* line) limits. Each example represents the phenomenological models defined by Eq. (6.143) (GUT), Eq. (6.145) (FDM), and Eq. (6.149) (QCD). Regions above the contours are excluded. The *red* region represents the intersection of the 95% exclusion bounds which excludes $\mathcal{N}_{\rm ax} \gtrsim \mathcal{O}(30)$ for $\sigma \sim \mathcal{O}(1)$ for each of the three examples. 402

6.22 Constraints on the masses of ULAs in the bounds of Eq. (6.105) plus the additional limits from M87* approaching the FDM domain using Eq. (6.155) and Eq. (6.156). The singular field bounds are determined by the total probability of exclusion calculated using the methodology in Appendix J via Eq. (J.1), as in Fig. 6.9. The external lower axis represents the approximate mass bounds of known BHs plus UMBHs, neutron stars (NS) and stellar (S) objects, used to probe specific bosonic field mass bounds. The upper axis represents the generalised volume of the corresponding three-dimensional submanifolds in eleven-dimensional Planck units defined in Eq. (5.104), related to the geometrical axion mass scales of M-theory in the lower axis. The *black dotted* line defines the geometrical axion mass scale and generalised volume associated to gauge coupling unification and the visible sector. Finally the *inset colourbar* represents the associated axion decay constant scale for the QCD axion determined by the relationship to its mass defined in Eq. (6.147). 403

6.23 Constraints on the masses of ultralight FDM axions, $\mu_{\rm ax}^{\rm FDM}$, for singular fields determined by the total probability of exclusion calculated using the methodology in Appendix J via Eq. (J.1). Exclusion bounds are presented in the 68% and 95% CIs as a function of $\mu_{\rm ax}$ with *orange/red* lines representing the upper and lower limits of the 68%/95% intervals. These probability limit functions are determined using the single BH M87* (Fig. 6.1), with the mass and spin of the BH defined using Eq. (6.155) and Eq. (6.156) respectively. The shaded green regions represent example FDM bounds from global 21cm signal observations, defined by the upper (*dotted* line) and lower (*dashed* line) limits of Eq. (6.157). 406

6.24 Constraints on the masses and decay constants (self-coupling) of ultralight FDM axions, $\mu_{\rm ax}^{\rm FDM}$, for singular fields determined by the total probability of exclusion calculated using the methodology in Section 6.3.1.1 and Section 6.3.1.2. The shaded *blue* bounds represent the 68% exclusion bounds, with the *green* and *orange* regions representing the 95% and 99.7% limits respectively for the three heaviest BHs, *Ark 120*, *Fairall 9* and *M87**. The *right axis* represents the limits on the quartic coupling of ULAs, $\lambda \equiv \mu_{\rm ax}^2/f_a^2$. The bounds stop for lower values of f_a where the axion cloud undergoes a bosenova before extracting sufficient spin from the BH. 408

6.25 Summary of results displaying contours for the 95% exclusion regions using a log-normal axion mass distribution, as a function of the width, σ, and number of fields, $\mathcal{N}_{\rm ax}$, for various central mass mean scales, $\bar{\mu}_{\rm ax}$. Regions above the contours are excluded. Certain ranges of σ correspond closely to RMT and M-theory mass spectra, and can also be used to approximate the log-flat or degenerate spectrum. For $1 \lesssim \sigma \lesssim 20$, $\mathcal{N}_{\rm ax} \gtrsim 30$ is excluded for an extremely wide range of central masses. Constraints neglect axion self-interactions and apply approximately in the limit of large decay constants, $f_a \gtrsim 10^{14}$ GeV. . 411

7.8 Density heat maps for the axion DM density parameter, $\Omega_{\rm DM}$ for values of $\beta_{\mathcal{K},\mathcal{M}} \in (0, 1]$ as a function of the remaining model parameters, $n_{\rm ax}$, $k_{\rm max}$ and $m_{\rm max}$. We limit the values of the number of fields in the population to be, $n_{\rm ax} = [1 - 30]$ axions, along with varied limits on both the decay constants parameterised by $k_{\rm max}$ and the masses parameterised by $m_{\rm max}$. Restricting our examples to the case of high decay constants quickly saturates the Universe with DM (*middle* panel). Likewise a spectrum of almost degenerate mass states quickly dominates as DM when the mass scale in increased (*right* panel). We also find a general degeneracy across all mass spectra shapes. 436

7.9 Contour density plots for the axion DE density parameter, $\Omega_{\rm DE}$ in the $\beta_{\mathcal{K},\mathcal{M}}$, $n_{\rm ax} = \mathcal{O}(1 \rightarrow 100)$ plane, demonstrated for different discrete fixed values regulating the upper bound on the axion decay constants, $k_{\rm max}$. High scalings from larger values of $k_{\rm max}$ generally furnish these models with sufficient DE in the bounds defined in Eq. (7.5). When $\beta_{\mathcal{M}}$ approaches the rectangularisation limit of unity a larger number of fields are preferred to counteract the statistical spread of the distribution as shown in *top* panel. 441

7.10 Contour density plots for the axion DE density parameter, $\Omega_{\rm DE}$ in the $\beta_{\mathcal{K},\mathcal{M}}$, $n_{\rm ax} = \mathcal{O}(1 \rightarrow 100)$ plane, demonstrated for different discrete fixed values regulating the upper bound on the axion mass states, $m_{\rm max}$. Axion masses surpassing the limit of M_H quick provide too much DE. When the spectrum sit around or just below this scale once again a larger number are preferred when $\beta_{\mathcal{M}}$ approaches the rectangularisation limit of unity. This is shown in the two *middle* panels sufficiently reproducing values of $\Omega_{\rm DE}$ falling in the bounds of Eq. 7.5. 442

7.11 Probability densities for the fractional percentage of axion DM recovered, measured with the axion DM density parameter, $\Omega_{\rm DM}$ in the M-theory random matrix model presented in both linear and logarithmic scales.. Each example configuration uses the parameter set $\langle \mathcal{V}_X \rangle = \{45, 50, 55, 60\}$, for the average average values for the three-cycle volume. Generally without the use of very narrow priors on the model variables the model produces negligible quantities of axion DM. 447

7.12 Contour density plot for the axion DM density parameter, $\Omega_{\rm DM}$, found by using narrow priors for the moduli VEV, s, and instanton index parameter $\tilde{\bar{N}}$. There is a very minor correlation between the two parameters where inside the transitional region of $\overline{\tilde{N}} \approx 1.02 - 1.06$ which generates DM inside the bound in Eq. (7.3). 448

7.13 Contour density plots for the axion DM parameter, $\Omega_{\rm DM}$ for $\beta_{\mathcal{M}}$ found by using narrow priors on the instanton index parameter $\bar{\tilde{N}}$. The correlation between these parameters is extremely small, with statical fluctuations in the approximate transitional region, $\overline{\tilde{N}} \approx 1.00 - 1.08$, generating DM which falls inside the bounds of Eq. (7.3). 449

7.14 Contour density plot for the axion DE parameter, $\Omega_{\rm DE}$, found by using narrow priors for $\widetilde{N}$ along with an enhancement factor on decay constant, f_a. The parameters are generally well correlated with small regions displaying flections reproducing DE inside the bounds in Eq. (7.5). The axion decay constants are generally required to be enhanced by $\mathcal{O}(10)$ in these limits to produce sufficient DE. 450

7.21 The Vision of the Empyrean: The Empyrean Heaven, representative in the study of ancient cosmogony as the highest heaven occupied by the aether. Classically regarded as a place of divinity, observed in notable works such as Dante's *Paradiso*, the conceptual metaphysical origins used to define the highest heaven translate to our modern understanding and cosmological endeavours regarding the aspiration to quantify the higher dimensions of spacetime. For the theoretical particle cosmologist the metaphorical '*Empyrean*' of UV-completion currently seems to be hidden amongst a colossal phenomenological, geometrical and mathematical landscape. Image credit: Taken from `https://fineartamerica.com/featured/the-vision-of-the-empyrean-gustave-dore.html`. 480

D.1 *Left panel:* Tracy-Widom limiting probability measures defined in Eq. (D.3), Eq. (D.4) and Eq. (D.5) for the normalised singular eigenvalues defining the spectral supremum of each possible choice of real, complex, or quaternion matrix entries for the classical Gaussian ensembles. *Right panel:* Example sample spectra for the largest eigenvalues from 25000 matrix simulations from the GOE ensemble for various values of the dimensionality parameter, β. 497

E.1 Raney density function space defined by Eq. (E.13), with specific limiting density functions generated at the coordinates $(\mathcal{P}, \mathcal{R})$ used to define the Raney numbers in Eq. (E.14). The *green* shaded region relates to the set of non-negative probability measures. The boundary defines the generalisations of the semi-circular distribution. The delta function positioned at $(1, 1)$ (*black* circle) corresponds to the mass distribution in Section 5.2.3 which under the translation $\mathcal{P}+1$ generates the mass spectrum in Section 5.2.4.1 (*blue* circle). The *orange* circle relates to discussions in Section 5.2.4.3.2. Finally the *red* circle could relate to spectral forms associated to shifted distributions of the superpotential Hessian as discussed in Section 5.2.8. Reproduced from Refs. [952, 1047]. 504

J.1 Visual representation of the statistical model methodology using two example stellar BHs, GRO J1655-40 and M33 X-7 (see Table 6.2) with instability bound function for an axion mass, $\mu_{\rm ax} = 10^{-12.75}$ eV. Each data point is shown with 1σ, 2σ and 3σ error contour levels. Effective errors are calculated by projection onto either the x or y axis (crossed points) depending on whether the BH falls inside the instability bounds where $f(x)$ is defined. 520

List of Tables

3.1 Collection of superstring theories and the relevant forms which lead to axion degrees of freedom and associated instantons which generate potentials for the fields. Collected and reproduced from the discussions found in Ref. [657]. 156

6.1 Simple grid parameterisation of possible BH background metric solutions for various configurations of the quantities used to describe a BH under the assumption of the no-hair theorem. The work conducted in this chapter is only concerned with Neutral-Rotating BHs described using the Kerr spacetime. 335

6.2 Stellar BHs used to apply constraints on axion masses and values of $\mathcal{N}_{\rm ax}$ for various model mass spectra. Stellar BHs are selected with reliable mass and spin measurements and associated errors are quoted with their CIs and their corresponding references. Stellar BH measurements are sourced from both X-ray binary systems via X-ray continuum-fitting methods and BBH mergers from detected coalescence events at LIGO. Where two methods have been stated we use averaged posterior values for each. For review material and collections of stellar BHs see Refs. [943, 948, 1289]. 376

6.3 Selected SMBH system candidates used to apply constraints on axion masses and values of $\mathcal{N}_{\rm ax}$ for various model mass spectra. SMBHs are selected with reliable mass and spin measurements along with associated errors are quoted with their both their CIs and corresponding references. SMBH systems all are observed AGN using X-ray reflection spectroscopy. Where two methods have been stated we have used averaged posterior values for each. For review material and collections of compiled AGN data see Refs. [280, 1100–1102, 1289]. 377

7.1 The full range of parameters used in the study in this chapter, including the cosmological input parameters along with the model dependant RMT parameters and theoretical M-theory stochastic variable parameters. Our cosmological density and parameter data comes from the *Planck 2015 TT+lowP* likelihood's found in Ref. [37] with our CMB temperature defined using COBE data in Ref. [541]. 426



Now the moving cloud of lepidoptera

Forever the circumgyrating light of mysteries

Now the crust of the Earth and the Dominion

Forever the food of the Soul and the quintessence

Now the Moon's incurable swarthiness

Forever the Galaxy's golden blue scintillation

Now the amalgam of peoples and the black Number

Forever the statue of Justice and the great Eye

To Axion Esti

(Worthy, It Is)

Odysseus Elytis

Introduction and Origins

> "*There is no law of physics that does not lend itself to most economical derivation from a symmetry principle. However, a symmetry principle hides from view any sight of the deeper structure that underpins that law and therefore also prevents any immediate sight of how in each case that mutability comes about.*"
>
> Foundational Problems in the Special Sciences.
>
> John Wheeler

Space and Time

Many of the most elementary questions first proposed by humanity, conveying our intrigue in the finer details surrounding our origins, quickly found themselves challenging the metaphysical characteristics of the heavens. We have come a great distance certainly, since the various ages where our understanding of the foundations of the Universe were inherently derived from numerous philosophical doctrines. In *De Caelo et Mundo*, Aristotle's chief cosmological treatise, dated 350 BC, we are encouraged to adopt the reference frame of a temporally infinite, eternal steady state, unique[1] in existence, confined only to a spatially finite setting [92, 627]. Much like its ancient dogmatic counterpart, *creatio ex nihilo*, greek natural philosophic arguments drove the narrative of our role in what seemed to be a concept so vast, humanity surely could not possibly understand both how it came to be, and would come to

[1] A point still debated today, closely tied to the study of eternal inflation [649, 681, 1296] and anthropic considerations [867, 1157, 1229].

pass. The transition from the common conceptions of an eternal cosmos, into the study of cosmogony minus the overarching framework of theogony, began to shape the way fundamental physics, as well as distinct mathematical reasoning, would change the landscape of all fundamental science. Over two millennia later, the fundamental postulates of Newtonian mechanics formulated in the *Philosop Naturalis Principia Mathematica* [360, 978], detailed the revolutionary formalities of gravitational kinematics, both defining and cementing astronomy and the motions of the observed heavily bodies as a core branch of mathematical physics. The conceptualisation of *universality* beautifully encoded in the simplistic expression representing the classical universal force of gravity,

$$F = \frac{G_{\rm N} m_1 m_2}{r^2} \ , \tag{1}$$

for two massive bodies, m_1 and m_2 separated by a distance r. Newton's gravitational proportionality constant $G_{\rm N}$, is defined in Eq. (1.9). An overarching philosophical backbone had remained resolute between the two time periods of these defining works. In the century following Newton's seminal work, various vastly celebrated works such as *Die kritik der reinen Vernunft* [768], Immanuel Kant's précis on the scope of metaphysical arguments, began to suggest a full adoption of a Newtonian universe was an intellectuals just cause, asserting a very different picture from the classical, ontological trajectory of thinking. These works were representative of the changing ethos of the leading intellectual conglomerate, the theoretical seesaw now more evenly weighted between the divinity of the primordial chaos and the notions of scientific analysis and reasoning. Many brilliant works surrounding observational astronomy began to both open up and drive the very natural desire for more robust inductive physical arguments over the following two centuries, which would ultimately be used to revolutionise our reasoning behind the structure and inherent nature of the Universe, deterring from those with a more deductive, logical basis and philosophical grounding.



Figure 1: Faithful reproduction of Peter Apian's geocentric celestial spheres originally sourced from his Cosmographia [86] (Antwerp, 1539). The iconic celestial spheres often appeared as the foundations of models of fundamental bodies in cosmological models, pioneered by the likes of Plato, Aristotle, Ptolemy and Copernicus. These heavenly bodies were generally considered fixed elements in a series of rotating spheres made of an aetherial, transparent quintessence element, reproducing a natural beauty in the symmetry of geocentricity. Image credit: Celestial Orbs in the Latin Middle Ages, Edward Grant [626].

Olbers' paradox, the abstruse question as to why the Universe appears so *dark* in the night sky, an example of the initial footings into considering solutions requiring a spatially and temporally finite model of the Universe. This question would ironically come to haunt theorists much later for very different reasons when moving into the age of astrophysical cosmology after successfully mapping the energy content of the observable universe. The era and understanding of modern cosmology began with the insights and revolutionary arguments of Albert Einstein. His defining work on the nature of spacetime succeeding his already striking presentation of the mass-energy equivalence principle [510], summed up in arguably one of the most famous

equations in any field of study,

$$E = mc^2 \ . \tag{2}$$

This mass (m), energy (E) equivalence serving as a vital revolutionary insight and grounding into what we now understand as the field of relativistic quantum field theory [1340–1342]. The theory of general relativity [513] was a captivating revolution in our conceptualisation and understanding of gravity, a grandiose expression in the ability to define results in the most complex of landscapes through a series of relatively simple mathematical formulations. It quickly became apparent the richness of Einstein's mathematical equations proposed interesting solutions to the temporal nature of the Universe, along with its geometrical structure. These solutions would prove to be the focal point of many important features in cosmology, which today remain key elements which must be incorporated into any realistic cosmological model. Two of the most fascinating solutions concerned themselves with the strong-field limit of Einstein's equations and the evolutionary nature of the Universe. The first relates to the explicit solutions of Einstein's equations formulated by Karl Schwarzschild [1163], his metric solution to the spacetime surrounding spherically symmetric, non-rotating objects with zero charge, eventually leading to the formal definition of the mathematical curiosities known as black holes (BHs) [334]. These astrophysical wonders were later championed by the likes of Stephen Hawking and Rodger Penrose [683] as very generic predictions for cosmological scenarios, and remain today a vital probe of unchartered physics [106, 539, 584, 745, 878, 892, 894, 927]. In order to conform to the general consensus of thinking, Einstein later added the *kosmologische Gleid* (see Eq. (1.41)), his now posthumously celebrated addition of a cosmological constant counter term, included to ensure his equations would reproduce a static universe.

The second solution of interest, was realised over a series of seminal works in the 1920's, forming the basis of what is referred to today as the standard cosmological model. The first half of the decade saw the establishment of the Friedman equations

[565], subsequently corroborated in the second half through the independent results of Georges Lemaître [845]. The work of Howard Robertson and Arthur Walker in the following decade unified the Friedmann-Robertson-Lemaître-Walker (FRLW) [846, 1114–1116, 1316] metric, which certified the dynamics of the Universe over cosmological scales under the description of the general theory of relativity, which was ultimately forced to obey a modern interpretation of the The *Copernican Principle*. The Copernican Principle states that as observers of the Universe we are not privileged in our position situated on Earth or more generally in the Solar System. The modern adaptation of this notion is known as the *Cosmological Principle*, the conjecture that the field equations must correspond to a homogeneous and isotropic universe. A seminal point in the development of this Standard Model of Cosmology came with Edwin Hubble's understanding of the redshift-distance correlation and recessional nature of galaxies expressed with a simple relation known as, the Hubble-Lemaître Law [725],

$$v = H_0 d \ , \tag{3}$$

where H_0 denotes Hubble's constant as defined in Eq. (1.86). The remaining two values are the recessional velocity v and proper distance d. This work formalising the independent findings of Georges Lemaître [844] and Vesto Melvin Slipher. Slipher performed the first measurements of the radial velocities for galaxies [1195, 1197] which lead to our current understanding today of an expanding universe, amongst numerous other seminal observational works. The initial calculation for the value of the Hubble constant, H_0, representing the ratio of the recession velocity to distance of the observed objects, returned a value of $H_0 \sim 500\,\mathrm{kms}^{-1}\,\mathrm{Mpc}^{-1}$. This value is approximately an order of magnitude out from the current best measurements [40] (see Eq. (1.86), but clearly showed the first convincing evidence the Universe was indeed expanding[2]. Following this extraordinary discovery attempts were made to under-

[2]Supposedly after these results were published Einstein later referred to the addition of his cosmological constant term as the '*biggest blunder*' of his career. Given the erudition of Einstein, it came as no surprise his greatest mistake in his eyes would turn out to be a stroke of genius with the discovery of the nature of the Universes acceleration some years later.

stand how the composition of the chemical elements [61] would be realised within this framework, eventually leading to the vital prediction the Universe previously contained a radiation dominated epoch [60]. This rapidly developing framework soon came to be referenced as the Big Bang[3] model of cosmology.

Shortly after what seemed to be a great period of discovery and standardisation as to how to model our Universe, big issues began to arise. It was soon discovered the Universe contained a mysterious *dark matter* (DM) component, understood through the kinematics of galaxies, specifically initially through their perplexing rotational velocity curves [252, 560, 1129, 1130]. This extended matter component was required to ensure the rapidly developing observational techniques and gathered data could be accounted for using the known laws of gravitation. The magnitude of this matter, now a staple of any cosmological analysis, has been further clarified through extended probes such as gravitational lensing [1097, 1250], general cosmological structure formation [59] and features of the cosmic microwave background (CMB) [603]. These have all subsequently offered a wealth of convincing evidence for DM over a range of different scales. One of the most important observational discoveries of the 20^{th} century was actually a decisively fortunate accident [1048], enlightening us to the presence of the CMB, the previously predicted radiation background, observed as a strikingly perfect blackbody, offering decisive evidence for the Big Bang scenario. Since its discovery it has undergone a dynamic and intensive analysis, now offering a vitally important indication of how to shape and probe allowed extensions to cosmological models, stemming from more exotic constructions in fundamental physics, which must conform or not significantly perturb the conjectured evolution of primordial physics during this epoch.

Meanwhile on the quantum mechanical frontier, the formulation of field theories building on the physics and mathematics behind relativistic waves, began to holistically describe the various matter constituents under the elegance of gauge theory.

[3]This term was coined by Fred Hoyle, an advocate of steady-state cosmology [717], during a radio broadcast, in an attempt to undermine the principles behind the singular nature of the universe in its initial state for the up and coming models of an expanding universe.

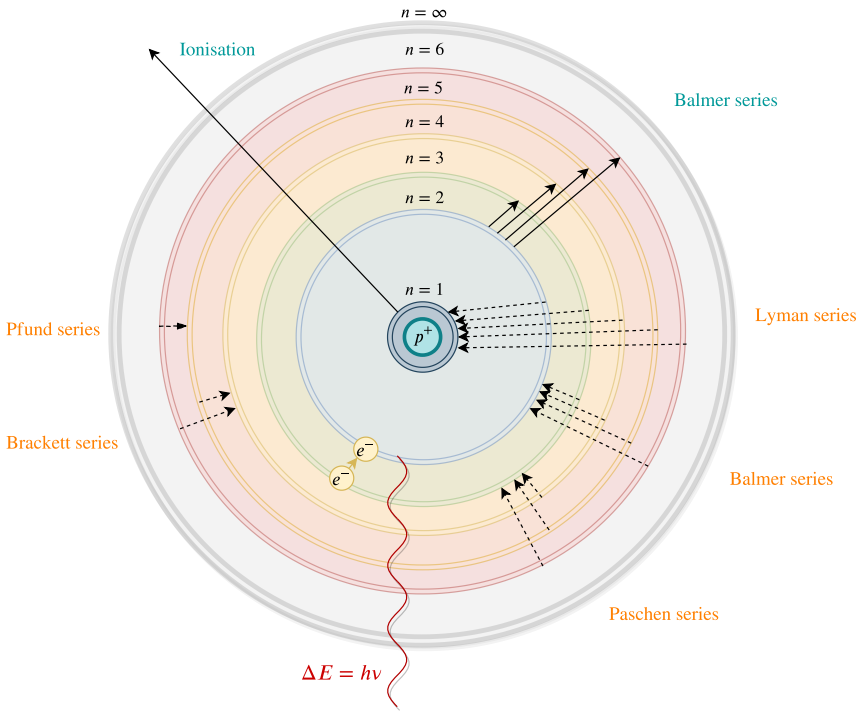


Figure 2: Bohr model of the Hydrogen atom [1057], ^{1}H, representing an electrically neutral atom containing a single, positively charged proton at the centre, along with a single negatively charged electron. The electron sits in one of the designated energy levels, bound to the nucleus by the Coulomb force. The model serves as a first order approximation of the later formulated "true" quantum mechanical description. Traditionally the radius of each orbit goes as n^2, where n represents the principle quantum number. Here we show only the first two electron orbits to the correct scale. The solid black lines represent adsorption series and the dashed lines represent series examples for emission processes. The example electron transition produces the first line of the Balmer series resulting in a proton with a wavelength of 656 nm.

These models presented an invariance over particular Lie groups, specifically making use of Lie algebras under certain representations, reaffirming the importance of symmetry arguments in a mathematical universe. Standing on the esteemed theoretical shoulders of the eminent founders of quantum theory operating in the 1920's and 1930's [249, 250, 411, 540, 695, 696, 1026, 1027, 1158, 1159], a new generation of theorists began the aspiring task of unifying the fundamental forces of nature. Pioneers such as Abdus Salam [612, 1141, 1142], t'Hooft [1233, 1234, 1237, 1239], Feynman [535, 537, 538], Gell-Man [592–594], Weinberg [607, 608, 1332, 1333], Higgs [703–705], Glashow [416, 606], Yukawa [1383], along with many other distinguished

physicists, over a series of elegant and captivating works, mainly confined to the 1960's and 1970's, established and defined the Standard Model of particle physics as a fully renormalisable quantum field theory. The model possesses a gauge symmetry, characterised by a non-abelian symmetry group, representing three of the fundamental forces of nature, an incredibly promising gauntlet thrown down to the task of completing the elusive picture of everything. The decades which followed the formulation of the Standard Model and its representation were proliferated with experimental discoveries in fundamental physics, furnishing theory and evidence with a comforting sense of unity and direction [6, 14, 120, 122, 398, 1050, 1098], the experimental frontiers crescendo recently coming with the discovery of the Higgs Boson [3, 336].

Although it appeared that both naturalistic beauty and physical order was staring theorist's in the face, complete gauge unification and harmony with cosmological physics and relativity via ultraviolet (UV)-completion proved an enigmatic pursuit. Of course, much like the parallel field of cosmology, particle physics faced many issues regarding its paradigmatic structuring and how these linked to previous experimental endeavours. Absent of any obvious DM candidate, its arbitrary nature and complicated number of parameters did little to reassure many in the community that the model was sitting at the level of a beautiful formulation to the effective level, ultimately representing a largely incomplete framework. How *natural* this theory is in the context of grand unification motivated extensions to particle physics models in the form of supersymmetric field theories. These field theories offered a new formulation of spacetime and the conjectured fundamental fields, one of the most successful theoretical results coming from the ability to define an attractive relationship between the bosonic and fermionic states of the Standard Model, through the internal symmetries of microscopic phenomena. These mathematically robust field theories, alongside the mysterious emerging field of string theory, quickly asserted that maybe the picture wasn't just incomplete, it was actually operating on an entirely different scale and dimension.

Returning to cosmology, the CMB anisotropies, or small temperature fluctuations about the black body peak were first detailed by COBE in Ref. [541] (see Fig. 1.5). The physics of these temperature fluctuations and density perturbations are now a very well understood phenomena, representing the origins of the so called *golden age* of cosmology, which soon became a fully incorporated feature of Big Bang cosmology, providing theoretical motivations for the seeds of large scale cosmological structure and ultimately, life. Cosmic inflation [647, 864] was proposed as a phase of quasi-exponential spacetime expansion, conjectured to have taken place in the very early universe to withdraw some of the standard model of cosmologies shortcomings with the observed anisotropies amongst other poignant issues. The quantum nature of this period is of great interest to both cosmologies and particle physics today due to the energy scales involved. Armed with the ability to eliminate competing theories, Big Bang cosmology slowly morphed into a model accounting for first order observational fits, known as the concordance model of cosmology or Lambda Cold Dark Matter (ΛCDM) model. Following the initial results of COBE, the angular power spectrum for the CMB was precisely mapped, further supporting the magnitude of the distributions of DM and dark energy (DE) [40, 709]. The first term referenced in this paragon model stemming from observation evidence, is incorporated from the experimental results of supernovae Ia measurements from the Supernova Cosmology Project and High-Z Supernova Search Team surveys, affirming that the comic expansion is accelerating [1051, 1108]. The apparent cosmic expansion now synonymous with the general reference of a non-zero cosmological constant or DE component for the Universe, possessing a negative equation of state.

Around the same time that cosmology was forced to fully adopt the unexpected enigma of accelerated expansion, the Standard Model of particle physics also received a very unique consensus placed on one of its constituents [574, 663]. The discovery of a non-zero mass and conformation [357] of the nature of atmospheric neutrino oscillation [891, 1068, 1069] for each of the Standard Model neutrinos, an almost certain sign that extended physics was operating outside the bounds of

the traditional Gauge group structure which had been adopted over the previous decades. This discovery would give suggestions on the directions extended models could take, which is briefly highlighted below. If the previous age was golden, we now find ourselves in the age of precision, recently captivated by the direct detection of gravitational waves [9], coming a century after Einstein informed the world of their theoretical motivations. The recent image of the supermassive BH M87* [48–53] (see Fig. 6.1) in the supergiant elliptical galaxy, *Messier 87*, a wondrous achievement demonstrating the first visual conformation of the singular and mysterious nature of spacetime. The emerging region of the observational spectrum which will support these future endeavours is the field of gravitational wave astronomy. Much like its historical predecessors it aims to bring clarity to the most extreme solutions of Einstein's field equations, opening up new observational windows for key processes such as cosmic inflation and astrophysical object merges/dynamics.

By the turn of the 21$^{\text{st}}$ century, cosmology and particle physics ultimately found themselves united and intertwined in a confounding ambiguity, the theoretical cracks formed from the 20th centuries observational endeavours in exploring our physical universe, defining the problematic paradigms of fundamental physics which drive many theoretical physicists today. Drawing together what appeared to be significant, but fractured pieces of the overall puzzle from the numerous works highlighted above, has now lead to a huge investment in extending these well defined solutions to incorporate elements from a more fundamental domain. Kindred in spirit to how Einstein changed everything with our understanding of space and time, along with the force of gravity, is the modern task of quantising this aforementioned fundamental force within a framework of elementary particle physics. *Superstring theories* are the leading theories which aim to replicate these ambitious goals through considerations of the spacetime of a fundamental string, whilst accounting for the supersymmetric and gauge symmetries it is required to exhibit. The dynamics of classical string theory initially showed that these one-dimensional objects could reproduce a conformally invariant two-dimensional quantum field theory that is consistently

renormalisable. Building on this excitement, superstring theories went through two primary revolutions, each of which distinctly morphing its plausibility as a fundamental theory to reconcile the quantum nature of all the fundamental forces. The hidden six/seven extra dimensions these theories tax us with generally live on some compact manifold with a size of the order the Planck length,

$$l_{\rm Pl} = \sqrt{\frac{\hbar G_{\rm N}}{c^3}} \approx 1.617 \times 10^{-35} \text{ m} \ , \tag{4}$$

a seemingly discouraging roadblock in the general scientific practise of preaching theory and practising proof. Operating a general direct probe at these scales is currently far beyond the realms of mans greatest achievements to date. This does not however, limit the scope of both our potential understanding of this space, nor the ability to look for signals representing a smoking gun of distinct features these models must incorporate, to an impossible task. It is the echos from the primordial chaos manifest as phenomenological ripples in our four-dimensional spacetime which may prove vital in the meantime when building our understanding of physics on the smallest scales.

Symmetry has long been the mathematical chisel to physical ignorance when defining models representing elements or features of the natural world. The utilisation of Lie algebras, which have provided so much historical success in the fundamental ground work of field theories, continue to offer a wealth of catalytic theoretical sparks through the utilisation of more extensive groups. In particular two of the exceptional algebras, G_2 and E_8, may offer the key to unlocking the mysterious nature of spacetime [1086, 1376]. This exceptional Lie group is formally characterised as the automorphism group of the octonions as a normed algebra. It has rank 2 with dimension 14 and two fundamental representations (dimension 7 and 14). The smallest of the exceptional algebras is fundamental in M-theory model constructions, as highlighted in both Section 3.3.5 and Section 5.3.

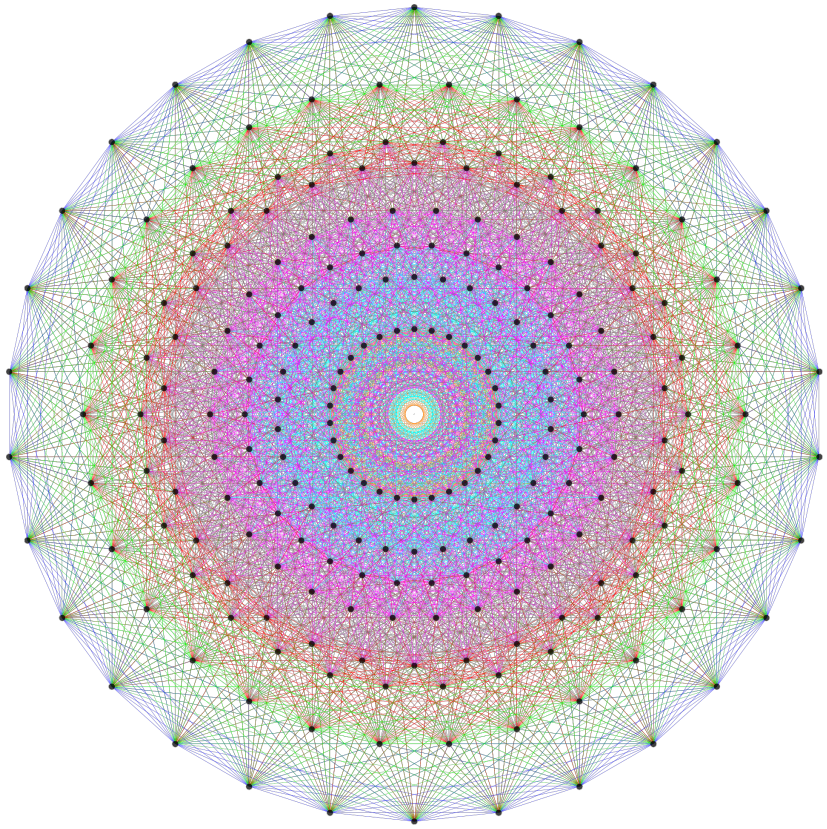


Figure 3: Symmetric orthographic projection in the Coxeter plane of the E_8 Coxeter group of the Gosset 4_{21} polytope, represented as a two-dimensional skew orthogonal projection inside a Petrie polygon. This particular projection in two-dimensions consists of 6720 edges with an eight-dimensional length $\sqrt{2}$ along with 240 vertices. The Lie group E_8 has dimension 248 and its rank, eight, is the dimension of its maximal torus. Image credit: Author: Jgmoxness, taken from `https://commons.wikimedia.org/wiki/File:E8Petrie.svg`.

The exceptional group E_8 also presents a tantalising offering, both[4] on the grounds of consistent superstring theory models and the ability to neatly embed the charges of both the quarks and leptons, encompassed in the representation of the Standard Model gauge group, as shown in Fig. 4, originating from a more fundamental standpoint. The story loosely follows [1086] (which we quote here only for context) from the ability to initially embed the Standard Model representation neatly into an $SU(5)$ representation [597] i.e. $SU(5) \supset SU(3) \otimes SU(2) \otimes U(1)$. The previously mentioned discovery of neutrino masses suggest the existence of a suitable Dirac

[4]There are other fascinating unified field theories incorporating E_8 such as *An Exceptionally Simple Theory of Everything* [869] used to describe all known fundamental interactions.

partner. The $SU(5)$ group would now naturally fit in the fundamental spinor representation of $SO(10)$ [568], i.e. $SO(10) \supset SU(5) \otimes U(1)$. Extending this by a singular rank, we encounter the complex representation of the exceptional Lie group E_6. This is understood as, $E_6 \supset SO(10) \otimes U(1)$ [646]. The final stage of this symmetry hierarchy concerns the fundamental complex representations with no anomalies [1086], resulting in the set structure, $E_8 \supset E_7 \otimes SU(2) \supset E_6 \otimes U(1)$. In the case of string theory briefly covered in Section 3.1.1, the specific case of the heterotic string [636] strongly motivates the appearance of the E_8 group, naturally realised through the form of a ten-dimensional spacetime. Of course the previous point on embedding the Standard Model along with the neat properties of preserving supersymmetry when compactifiying the extra six-dimensional manifold, make this solution particularly appealing.

In Fig. 3 we show a symmetric orthographic projection in a Coxeter plane of the E_8 coxeter group. Although this representation is a beautiful snapshot of the complexity features of superstring theories could be required to tackle, we can draw a symbolic comparison with both Fig. 1 and Fig. 2. The history of our endeavours have always been motivated by the ability to identify the most eloquent and simplest approaches. Indeed although Fig. 1, Fig. 2 and Fig. 3 share an endearing pictorial resemblance, their historical significance is more profound. Contrasting our initial fascination with the symmetries of objects believed to be a conception mirrored in the structures of nature, to the mathematical rigour and beauty in defining results in hugely complex frameworks, each figure represents the trajectory in the evolution of our understanding, moving from the largest to the smallest scales. The constant evolution of modelling, which has radically changed through our successive successful ability to probe scales ranging in many orders of magnitude, now puts us in a landscape which, although potentially simplified through symmetrical formalities, is ultimately far more complex than anything humanity has encountered before, in the context of some consistent model for the dynamics of the fundamental domain. We must now seek to understand if the mathematical symmetries, such as those

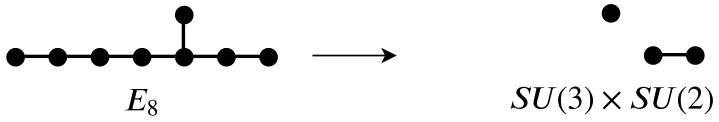


Figure 4: Dynkin diagrams for both the exceptional Lie group E_8 and the Standard Model. The mathematical process of reducing one to the other, represented by the arrow, could hold the key to understanding how our observed spectrum of particles fit in a consistent model of quantum gravity. The byproducts of such a process through compactification of some extra-dimensional spacetime manifold could also provide solutions to some of the largest paradigmatic issues in the Standard Model of Cosmology. Reproduced from figures found in Section 3 of Ref. [1086].

represented in Fig. 3, offer a physical manifestation or maybe need a significant refinement, such as our intuitive but ultimately naive theoretical footings represented in Fig. 2.

The scope and potential pay off of this landscape has catapulted it to the forefront of particle, cosmological and phenomenological research today. In particular, a focus often placed on the possible benefits found in the extra-dimensional sector operating on the smallest scales related to the mentioned symmetry constructions. Theorists currently often rely on the ability to draw up models based on conjectured principles in this landscape, such as the existence of an extended sector of scalar fields. One of these and the elementary focus of this thesis comes from the ever-present nature of moduli, or more specially the fundamental prediction of ultralight scalar degrees of freedom which have both Standard Model motivations as solutions to issues regarding the vacuum structure of quantum chromodynamics (QCD) and as intrinsic signatures of extra-dimensional physics, known collectively as the field of *axion* physics.

Outline of the Thesis

The role and importance of ultralight scalar particles which are continually present in models approaching the task of grand unification cannot be understated in terms of both their prospective phenomenological flexibility and ability to infer theoretical model validity through observational evidence. This is often realised via their ability to potentially constrain significant and tricky to probe sectors of cosmological physics. The structural organisation of this thesis is as follows. In Chapter 1 we introduce the standard model of cosmology and the concepts of isotropy and homogeneity, which can be used to model the evolution of scalar field components in a simplistic manner, evolving as background densities on a geometrically flat, expanding spacetime, due to numerous seminal works over the 20th century. We will also comment on several of the large scale issues facing our understanding of cosmological physics, in particular the dark sector of cosmology and the potential challenges facing models in this sector. Following the discussions of large scale dynamics, Chapter 2 introduces and details elements of the Standard Model of particle physics, in particular its constituents and current theoretical limitations. We shall also highlight some of the pervasive issues facing its historical formulation and the possible required extensions present in the literature, which seek to best realise a consistent framework capable of matching various key observational and experimental results. In particular a focus is placed on that of the *strong CP problem* of the Standard Model, concerning CP invariance and the topological complexities of the QCD vacuum. This concern, motivates the introduction of a theoretically uncomfortable, θ parameter into the effective field theory. A possible and very well motivated solution of this issue defines the theoretical foundations and historical emergence of the *axion* field, its inception quickly becoming the dominant mechanism to dynamically evolve the troublesome topological term in the Standard Model Lagrangian, stemming from the QCD vacuum. It is likely the QCD axion is ultralight, possessing a distinct cosmological significance which may address several of the uncertain paradigms of dark

sector physics. In the final chapter of Part I we selectively comment on elements of superstring theory compactification models which often lead to the appearance of ultralight degrees of freedom with properties analogous to the physics of the QCD axion, stemming from high-dimensional gauge symmetries. The results stated in this chapter are done so without derivation, provided only to give context to the nature and complexity of axion fields in extended models of fundamental physics. These axion-like fields have a distinct independence in their fundamental defining parameters, realised as intrinsic scalar degrees of freedom associated to higher dimensional forms, and therefore have a large degree of cosmological flexibility. They generally act as a generic, ubiquitous prediction in all low energy four-dimensional sectors of supergravity theories. This string conjecture scenario is often referred to as the *string axiverse*. We will introduce the basic properties of the string axiverse and highlight features of explicit models in both Type IIB superstring theory and M-theory. The features of these models of the string axiverse heavily rely on our understanding of moduli stabilisation techniques and the geometry of the extra-dimensional spacetime, which define the features and scales of the axion fields in the low energy limit of the effective theory.

Subsequently in Part II we begin in Chapter 4 by highlighting the statistical methods we use to alleviate the complexities in this landscape from the high-dimensionality of the problem. These are concerned with canonical random matrix theory, used to model high-dimensional statistical data. These methods can be used to draw possible inferences from a vastly complex space in the large $\mathcal{N}$ limit of large random data matrices. We first introduce the general topic and basic theory surrounding random matrices, a focus placed on the key seminal formulation of the invariant Gaussian and Wishart-Laguerre ensembles. Next considering a focus on the Wishart-Laguerre ensemble, we explore the principles of universality via the convergence of spectral measures which provide limiting distributions for a large number of classes of high-dimensional random matrices, in particular sample covariance matrices often used to model measure spaces on the real positive definite domain. We focus on the nature of

maximally random ensembles and the position of minimal information in our effective equations, which can be perturbed by both full rank and finite rank operations. Using features of free probability theory we cover selected powerful results associated to free random variables and the analysis of models of perturbed high-dimensional matrices, formed in principle from invariant ensembles. We show how general convolution operations are used to ensure probability measure functions can be traced and assigned in each basis of the multi-field effective description, guaranteeing regularity with a positive definite spectrum for the physical model parameters. All of the theoretical concepts covered in this chapter are highlighted to demonstrate the ability and motivations behind assigning a set of simplistic statistical priors on the axion parameter space. In Chapter 5 we follow up the theoretical concepts covered in the previous chapter, in order to present selected models in the random matrix axiverse, where we show how the principle results of the theory of random sample covariance matrices can be applied in the context of effective field theories for the case of many axion fields. We first introduce the standard multi-scalar effective field theory equations for the multi-axion framework where we work in the simplified basis in which the multi-field potential is well aligned to allow for a trivial expansion about the minimum. This fixes the effective equations to be concerned with two statistical matrix arguments to leading order, which are susceptible to the methods covered in the previous chapter. We introduce both our models of the random matrix axiverse and their limiting measure decompositions, along with a special random matrix model of the G_2 compactified M-theory axiverse, making use of the model parameters as a series of stochastic variables, each with some assigned prior representing theoretical uncertainty in the model. We conclude with discussions on how these models can be considered using simplified priors from the universal nature of the spectra on logarithmic scales, in order to capture a significant portion of model behaviour in a statistically simplistic manner.

The final part (Part III) of this thesis is dedicated to the phenomenological results published in Refs. [1219, 1221], making use of the random matrix models covered

in Part II, a specific focused is placed on the topics of BH superradiance and the dark sector of axion physics. In Chapter 6 we explore how it is possible to constrain the number of axion-like particles, with parameters determined by simple statistical priors, fixed at scales susceptible to the Penrose process, via the use of spin measurements for astrophysical BHs. Using these astrophysical observations of rapidly spinning BHs, which span the approximate range, $5M_{\odot} \lesssim M_{\rm BH} \lesssim 10^{8}M_{\odot}$, it is possible to exclude the existence of certain massive bosons. In this work, based on Ref. [1219] we explore how these measurements can be used to constrain properties of the discussed statistical distributions for the masses of multiple bosonic fields. We place upper and lower bounds on the fields masses in the weakly interacting limit for multiple fields before discussing constraints on $\mathcal{N}_{\rm ax}$ for certain scenarios of interest. These are realised approximately as mass distributions in GUT models such as M-theory or models for DM, including particular phenomenological fields. In the final chapter of this thesis, based on the work covered in Ref. [1221], we present further results, this time concerned with dark sector cosmology. By sampling the axion fields in the introduced effective models, we investigate a population of axion fields with masses, m_a, and (effective) decay constants, f_a, which lie in specific ranges relevant for contributions to the cosmological DM and DE densities. We compute the background cosmological (quasi-)observables for models with a large number of axion fields, $\mathcal{N}_{\rm ax} \sim (10-100)$, using a number of distributions, both those motivated purely by statistical considerations and when the structure is specified according to a class of M-theory models. Using Bayesian methods, specifically a Bayesian hierarchical network analysis, we are able to constrain the hyperparameters of the distributions. We then conclude the thesis with a discussion regarding all the topics covered in each of the chapters, along with thoughts regarding possible future directions. Under the principles of concordance cosmology it is clear our picture of the Universe requires a significant extended sector of physics in order to unravel some of the biggest mysteries facing the unification of the smallest and largest physical scales. Where exactly this sector is defined is still a huge enigma, requiring a very

detailed analysis of previous results to unravel where this mysterious physics could be located.

"*Something deeply hidden had to be behind things.*"

Albert Einstein

Autobiographical Notes



Part I

The Standard Model of the Universe

Chapter 1

The Standard Model of Concordance Cosmology

> "*Philosophy is written in that great book which ever is before our eyes – I mean the universe – but we cannot understand it if we do not first learn the language and grasp the symbols in which it is written. The book is written in mathematical language, and the symbols are triangles, circles and other geometrical figures, without whose help it is impossible to comprehend a single word of it; without which one wanders in vain through a dark labyrinth.*"
>
> Il Saggiatore
>
> Galileo Galilei, (October 1623)

1.1 From Cosmogony to Cosmology

1.1.1 The Standard Cosmological Principle

Cosmology in its essence holds a rich philosophical history, both grandiose in its ambitions and meticulous in its stubborn efforts to unify prodigious experimental data with the elegant, beautifully simplistic rigorous mathematical formulation. It can

not however, despite its successes, escape the reality (at least up to certain energy scales) that it contains an erroneous sector, theoretically and fundamentally disconnected in several key areas from the vibrant and luminous spectrum of the Standard Model of particle physics defining a vital, but currently detached, component of the elusive theory of everything. It is this mandate in the theoretical and experimental communities that forces the search for intrinsic theories at the smallest scales outside of the known and well defined forces of nature in order to give reason and momentum to problems on the grandest proportions, before we can declare some sense of command over the tentative philosophical origins of what cosmology truly tries to divulge. At the core of cosmological theory lies the so called *Cosmological Principle*, the assumption that the universe is both homogenous and isotropic when viewed on sufficiently large scales. This notion can be viewed in Fig. 1.5, displaying the temperature map of the CMB [447, 1048], as measured by the Planck space observatory, representing the largest observable scales currently probed by humanity. The temperature anisotropies in this map are of some of the earliest electromagnetic radiation present in our observable universe, showing temperature fluctuations of density deviations at the level of $\sim 10^{-5}$ [414]. This picture represents the pioneering conformation that matter and light both originally behaved as a radiation like fluid, in a thermal equilibrium best described by Planckian blackbody. This universal understanding cemented the idea that the Universe started in a hot, dense initial state and subsequently expanded whilst cooling, the so called *big bang model* of cosmology. The modern and standardised fully adopted model for mapping our cosmological evolution is the ΛCDM model or the model of *concordance* cosmology. The model incorporates Einstein's theory of General Relativity partnered with a minimum parameterisation of the two unknown but well measured energy quantities in the cosmological dark sector. The term concordance is a reference to practical disregard of the true nature of the theoretically unknown, used to define a baseline for analysis of the expected evolution of measured properties and components. These consist of the existence of the CMB and large scale structure.

The abundance of light nuclei such as hydrogen, deuterium, helium, and lithium (H, D, ^{3}He, ^{4}He, ^{7}Li) and the seemingly accelerating state the universe finds itself in. The theoretical pillars of the model consist of general relativity, representing a valid description of gravity, the nature that a majority of the matter content of the universe consists of an additional non-relativistic component to the observed baryonic matter, these possible cold particles can be approximated as only interacting through gravity. The final component, the unwanted gift of Einstein, a cosmological constant term. This simple but devilish mystery to his vacuum solutions represents the more prevalent form of energy we observe today. It is expected then that to a minimal level any extended physics should reproduce the results of ΛCDM to a satisfactory agreement.

1.1.2 Epochal Evolution

The thermal evolution of the Standard Model of Cosmology can be briefly recapitulated using a series of epochal states of evolution. The initial stages of the Universe currently present a range of conflicting theories surrounding the undertaking of grand unification, with a few pillars of conjecture to normalise discussions. It is generally expected gravity became a classical theory with fixed dimensions in space and time shortly after the Planck time, $t \sim 10^{-35}$ s and $\rho \sim (10^{17}\text{GeV})^4$. Before this, quantum corrections to general relativity are expected to render the theory invalid. Shortly after it was believed that there was a a phase of cosmic inflation (see Section 1.6) related to models of grand unification and symmetry breaking of high dimensional gauge theories at around $t \sim 10^{-32}$ s or $\rho \sim (10^{16}\text{GeV})^4$ [987]. The final stage of cosmic ambiguity is the epoch of reheating [812, 813], where the hypothetical oscillating inflaton field decays into the thermal bath of Standard Model matter fields, transitioning into the hot Universe. The primordial plasma at this point contains all the Standard Model particles such as quarks, leptons and the Higgs boson. A little better understood are the phases of symmetry breaking which

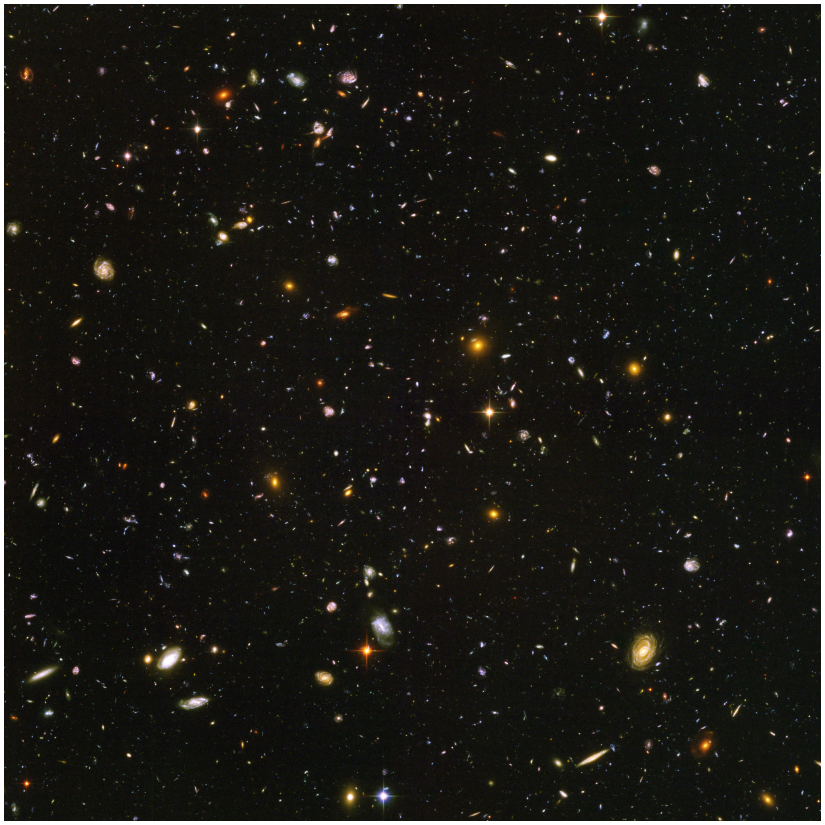


Figure 1.1: The Hubble Ultra Deep Field (HUDF), representing an image of some of the oldest visible light seen by mankind. This particular image was taken over eight hundred exposures with the NASA/ESA Hubble Space Telescope, performing four hundred Hubble orbits of Earth in order to finalise the data for this image. The total exposure time was 11.3 days, capturing approximately ten thousand galaxies spanning billions of light years. Image credit: NASA, ESA, S. Beckwith (STScI) and the HUDF Team, `https://hubblesite.org/contents/news-releases/2004/news-2004-07.html`.

generate the states of matter we observe today, at the current temperature of the Universe. Electroweak symmetry breaking occurs at $t \sim 10^{-6}$ s or $\rho \sim (100\text{GeV})^4$, where the Higgs mechanism generates masses for the vector gauge bosons and breaks the full symmetry to a lower gauge group structure. Next chiral symmetry breaking, colour confinement and the defining of the QCD vacuum occurs at approximately $t \sim 10^{-4}$ s or $\rho \sim (100\text{MeV})^4$, confining the quarks into the hadronic states of matter as either color-singlet-quark-triplet or color-singlet-quark-antiquark states. At this point the true power of the Standard Model kicks in with a series of thermodynamical transitions to non-equilibrium dynamics, constituting the observational

pillars of the standard cosmology. Firstly *big bang nucleosynthesis* (BBN) [61, 585] occurs, generating the light nuclei elements such as hydrogen, helium and lithium via the process of incorporating neutrons inside the relevant nuclei. This period is traditionally parameterised by the photon-Baryon ration, η_B. This occurs approximately at $t = \mathcal{O}(1-100)$ s, $T = (10^9 - 10^{10})$ K, or $\rho \sim ((0.1 - 1)\,\mathrm{MeV})^4$. At around $t = \mathcal{O}(10^4)$ yrs, $T = (\mathcal{O}10^4)$ K, or $\rho \sim (\mathcal{O}(1)\ \mathrm{eV})^4$, matter radiation occurs, where the dominant fluid component switches. Finally at $t = \mathcal{O}(10^5)$ yrs, $T = 2500$ K, or $\rho \sim (\mathcal{O}(1)\ \mathrm{eV})^4$ the *recombination* of atoms leaves the photons decoupled, where they are free to propagate and free-stream along geodesics. Observing the CMB today indicates the nature of how the Universe must have evolved. Finally the tiny anisotropies as initially detailed by The Cosmic Background Explorer (COBE) [1202] which are imprinted in the matter distribution, are greatly amplified, acting as the sources responsible for the formation of stars, galaxies, clusters, and all large scale structures we observe today in our Universe.

The persistent endeavour to understand these stages of universal transformation lead us to question what is the nature of space and time and what model takes the simplest form, which allows us to describe the four-dimensional geometrical landscape which humanity calls its home. It turns out there is a topological simplicity to the Universe we ceaselessly look out into, a humbling fraction of which is displayed in Fig. 1.1. Enlightenment can be found in both the past and present nature of the universe due to a series of extensive pioneering theories and demonstrations of erudition over the 20^{th} century. A suitable starting point to understand the various properties of the cosmos and its inhabitant *quanta* are the assumptions of homogeneity and isotropy of spacetime itself.

1.2 The Friedman-Lemaître-Robertson-Walker Metric

The most general standard background we can consider conforming to the cosmological principle for an expanding, homogeneous and isotropic universe are described by the functions of the Friedman-Lemaître Robertson-Walker (FLRW) metric. The features of the cosmological principle are suitably encoded in the form of a coordinate system which in cartesian coordinates does not depend on its position. The general spacetime coordinates are expressed in the standard vectorial form,

$$x^{\mu} = (x^0, x^i) \ . \tag{1.1}$$

The zeroth index represents the temporal component, $x^0 = t$ and the remaining three indices, $x^i; i = 1, 2, 3$ run over the three spatial components. The simplest parameterisation of a general coordinate reference frame for the invariant distance between two points is,

$$ds^2 \equiv g_{\mu\nu} dx^{\mu} dx^{\nu} \ , \tag{1.2}$$

invoking the usual summation notation over any repeated indices with a spacetime metric denoted, $g_{\mu\nu}$. In any geometrical coordinate system, the value of ds^2 represents the squared invariant distance, where the properties of the spacetime are then understood via the representational form of the spacetime metric, $g_{\mu\nu}$. In order to describe our observed four-dimensional universe, $g_{\mu\nu}$ in Eq. 1.2 must be a 4×4 tensor, possessing the features of the standard cosmological principle. Specifically the FLRW metric must possess vanishing off-diagonal terms, $\mu \neq \nu$, to account for invariance over our choice of direction and the conjecture of isotopy. Homogeneity then enforces the metric must have independence over the spatial components. The

flat or Euclidean spacetime FLRW metric can be expressed as,

$$g_{\mu\nu} = \begin{pmatrix} -1 & 0 & 0 & 0 \\ 0 & a^2(t) & 0 & 0 \\ 0 & 0 & a^2(t) & 0 \\ 0 & 0 & 0 & a^2(t) \end{pmatrix} , \tag{1.3}$$

where $a(t)$ represents the cosmic scale factor and can be neatly written in the form of the compact invariant line element,

$$ds^2 = -dt^2 + a^2(t)\delta_{ij}dx^i dx^j \ , \tag{1.4}$$

where δ_{ij} represents the Euclidean-space Kronecker delta operator. Locally a spacetime observer is governed by the physics of *special relativity*, where the spacetime metric, $g_{\mu\nu}$, is replaced with the local approximation of Minkowski spacetime with a metric signature, $\eta_{\mu\nu} = \text{diag}(-1, +1, +1, +1)$. Geometrically, we could consider the case in which the global picture of the Universe may not be perfectly flat, possessing a curvature factor. It is then convenient to introduce a new parameterisation of the spacetime distance, of the form,

$$ds^2 = -dt^2 + a^2(t)d\Sigma^2 \ . \tag{1.5}$$

The three-dimensional space interval $d\Sigma^2$, is a time independent function in uniformly curved space, which can be expressed in terms of hyperspherical coordinates,

$$d\Sigma^2 = dr^2 + S_k^2(r)d\Omega^2 \ , \tag{1.6}$$

where $d\Omega^2 = d\theta^2 + \sin^2\theta d\phi^2$, and the Gaussian curvature, k, are defined by the bounds,

$$S_k(r) = \begin{cases} |k|^{-1/2} \sin(|k|^{1/2} r) & \text{for } k > 0 \ , \\ r & \text{for } k = 0 \ , \\ |k|^{-1/2} \sinh(|k|^{1/2} r) & \text{for } k < 0 \ . \end{cases} \tag{1.7}$$

The spacetime metric is now parameterised in terms of both the cosmic scale factor and a normalisation with respect to the spatial three-dimensional curvature, for each of the topologically distinct spacetimes, conforming to elliptical ($k > 0$), hyperbolic ($k < 0$) and Euclidean ($k = 0$) three-dimensional spaces. The metric gives us a geometrical blueprint to the nature of both the local and global spacetime of a given model of the Universe.

1.3 The Einstein Equations

1.3.1 The Field Equations of Matter and Energy

At the turn of the 20$^{\text{th}}$ century, the work of leading mathematicians and theoretical physicists began to unravel the morphology behind our understanding of space and time. The renowned Einstein field equations formulated in his 1915 seminal paper, characterise the relationship between local spacetime curvature and the local energy and momentum distribution, encapsulated in the stress energy or energy-momentum tensor, $T_{\mu\nu}$. These two tensors come about by defining the action for both gravity and the dynamics of the spacetime metric along with the action for matter on the given spacetime. The first of these is the Einstein-Hilbert action for canonical matter,

$$S_{\text{Grav}} = \frac{1}{2\kappa} \int d^4x \mathcal{R} \sqrt{-g} \ , \tag{1.8}$$

where $g = \det(g_{\mu\nu})$ is the metric determinant, $\mathcal{R}$ is the Ricci scalar and $\kappa \equiv 8\pi G_{\rm N} = {}^{8\pi}/_{m_{\rm Pl}^2} = {}^{1}/_{M_{\rm Pl}^2}$, defined using Newton's gravitational constant,

$$G_{\rm N} \simeq 6.67 \times 10^{-11}\ {\rm m}^3\ {\rm s}^{-2}\ {\rm Kg}^{-1}, \tag{1.9}$$

and $m_{\rm Pl}$ is the Planck mass. The reduced Planck mass, $M_{\rm Pl}$ is defined as,

$$M_{\rm Pl} \simeq 2.4 \times 10^{18}\ {\rm GeV}\ . \tag{1.10}$$

Our global understanding of the content matter-energy for a fixed point in spacetime, with a spacetime coordinate of the form in Eq. (1.1), comes from the geometrical properties of the Einstein tensor, $G_{\mu\nu}$, which is used to define the Einstein field equations by varying the Einstein-Hilbert action with respect to the metric, $g_{\mu\nu}$,

$$G_{\mu\nu} + \Lambda g_{\mu\nu} \equiv \frac{2\kappa}{\sqrt{-g}}\frac{\partial S_{\rm Grav}}{\partial g_{\mu\nu}} = R_{\mu\nu} - \frac{1}{2}\mathcal{R}g_{\mu\nu} + \Lambda g_{\mu\nu}\ , \tag{1.11}$$

where,

$$R_{\mu\nu} = R^{\beta}_{\mu\nu\beta}\ , \tag{1.12}$$

is the Ricci curvature tensor defined from the Riemann curvature tensor and Λ, a cosmological constant. Let us also introduce the standard form of the canonical action for matter,

$$S_{\rm m} = \int d^4x \mathcal{L}_{\rm m}\sqrt{-g}\ , \tag{1.13}$$

with $\mathcal{L}_{\rm m}$ the four dimensional matter Lagrangian. Under variation of the metric, $g_{\mu\nu}$, we can define the energy-momentum tensor,

$$T_{\mu\nu} \equiv -\frac{2}{\sqrt{-g}}\frac{\partial S_{\rm m}}{\partial g_{\mu\nu}} = g_{\mu\nu}\mathcal{L}_{\rm m} - 2\frac{\delta\mathcal{L}_{\rm m}}{\delta g^{\mu\nu}}\ , \tag{1.14}$$

which reveals the famous Einstein field equations of the form,

$$G_{\mu\nu} \equiv R_{\mu\nu} - \frac{1}{2}\mathcal{R}g_{\mu\nu} + \Lambda g_{\mu\nu} = 8\pi G_{\rm N} T_{\mu\nu}\ . \tag{1.15}$$

The Ricci curvature tensor encapsulates the magnitude of convergence or divergence of matter over time, expressed via the various *Christoffel symbols*, $\Gamma^{\mu}_{\alpha\beta}$,

$$R_{\mu\nu} = \Gamma^{\alpha}_{\mu\nu,\alpha} - \Gamma^{\alpha}_{\mu\alpha,\nu} + \Gamma^{\alpha}_{\beta\alpha}\Gamma^{\beta}_{\mu\nu} - \Gamma^{\alpha}_{\beta\nu}\Gamma^{\beta}_{\mu\alpha} \ . \tag{1.16}$$

The Christoffel symbols relate to the partial derivates of the metric at a spacetime point (i.e. $\partial_\beta g_{\alpha\nu} = {}^{\partial g_{\alpha\nu}}/_{\partial x^\mu}$), describing the metric connection for a physical model where,

$$\Gamma^{\mu}_{\alpha\beta} = \frac{g^{\mu\nu}}{2}(\partial_\beta g_{\alpha\nu} + \partial_\alpha g_{\beta\nu} - \partial_\nu g_{\alpha\beta}) \ . \tag{1.17}$$

Taking the trace of the Ricci tensor with respect to the spacetime metric defined in Eq. (1.16) gives the *Ricci Scalar*,

$$\mathcal{R} \equiv R^{\mu}_{\mu} = g^{\mu\nu}R_{\mu\nu} \ , \tag{1.18}$$

which is a scalar measure of the geometrical features of the spacetime manifold, for a fixed spacetime point and the simplest scalar quantity defined from the curvature of a general Riemannian manifold. For the general FLRW metric in Eq. (1.5), the complete non-vanishing set of Christoffel symbols are,

$$\Gamma^{0}_{11} = \frac{a\dot{a}}{1-kr^2} \ , \qquad \Gamma^{0}_{22} = a\dot{a}r^2 \ , \qquad \Gamma^{0}_{33} = a\dot{a}r^2\sin^2\theta \ , \tag{1.19}$$

$$\Gamma^{1}_{11} = \frac{kr}{1-kr^2} \ , \qquad \Gamma^{1}_{22} = -r\left(1-kr^2\right) \ , \qquad \Gamma^{1}_{33} = -r\left(1-kr^2\right)\sin^2\theta \ , \tag{1.20}$$

$$\Gamma^{1}_{01} = \Gamma^{2}_{02} = \Gamma^{3}_{03} = \frac{\dot{a}}{a} \ , \qquad \Gamma^{2}_{12} = \Gamma^{3}_{13} = \frac{1}{r} \ , \qquad \Gamma^{3}_{23} = \cot\theta \ , \tag{1.21}$$

$$\Gamma^{2}_{33} = -\sin\theta\cos\theta \ , \tag{1.22}$$

where each of the indices, $\{0,1,2,3\}$, correspond to the set of coordinate parameters $\{t, r, \theta, \phi\}$. The Ricci tensor contains the following non-zero components along its

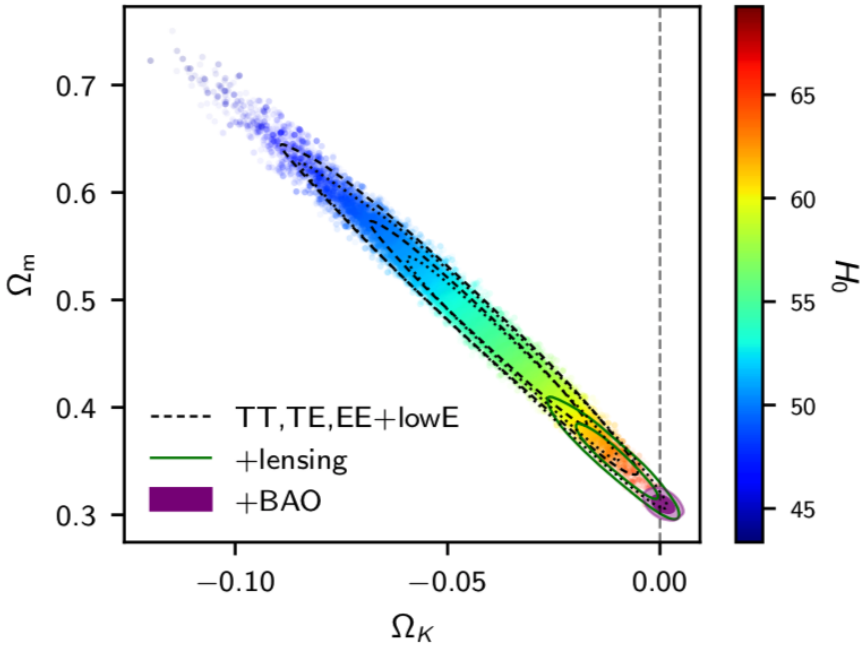


Figure 1.2: Constraints on the curvature of the Universe representing limits for a non-flat universe as a minimal extension to the standard ΛCDM model of cosmology. The dashed lines represent 68% and 95% contour bounds from samples taken using the Planck TT,TE,EE+lowE chains as a function of the total matter and curvature densities, along with limits on the value of H_0. Image credit: Taken from Fig. 29 found in Ref. [40]

diagonal,

$$R_{00} = -3\frac{\ddot{a}}{a} \ , \qquad R_{11} = \frac{a\ddot{a} + 2\dot{a}^2 + 2k}{1 - kr^2} \ , \tag{1.23}$$

$$R_{22} = r^2\left(a\ddot{a} + 2\dot{a}^2 + 2k\right) \ , \qquad R_{33} = r^2\left(a\ddot{a} + 2\dot{a}^2 + 2k\right)\sin^2\theta \ . \tag{1.24}$$

Under a contraction of the FLRW spacetime metric with the Ricci tensor we can define the following form for the Ricci scalar,

$$\mathcal{R} = 6\left[\left(\frac{\dot{a}}{a}\right)^2 + \left(\frac{\ddot{a}}{a}\right) + \left(\frac{k}{a^2}\right)\right] \ . \tag{1.25}$$

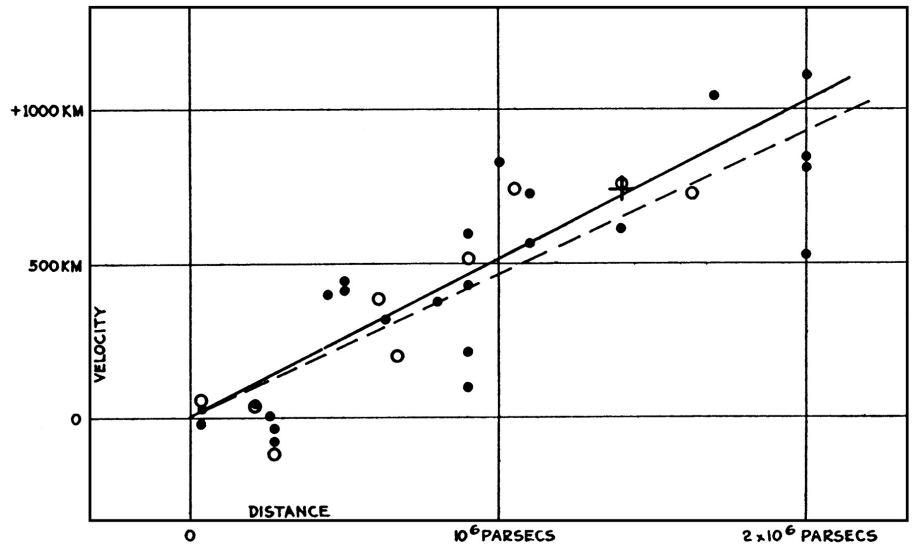


Figure 1.3: Original radial velocity-distance relationship plot for extra-galactic nebulae in a single cluster representing the distinguished work of Edwin Hubble. The original analysis detailed forty six galaxies, which showed the apparent nature of an expanding universe which came to be described by the Hubble-Lemaître Law (Eq. (3)). The slope of best fit represents the Hubble Parameter determined by the Doppler shift of the observed spectra. Image credit: Edwin Hubble, taken from Fig. 1 of Ref. [725].

Excluding the addition of the cosmological constant in Eq. (1.15), the remaining non-vanishing components of the Einstein tensor are,

$$G_{00} = 3\left[\left(\frac{\dot{a}}{a}\right)^2 + \left(\frac{k}{a^2}\right)\right] \ , \tag{1.26}$$

$$G_{11} = -\left[\left(\frac{\dot{a}}{a}\right)^2 + 2\left(\frac{\ddot{a}}{a}\right) + \left(\frac{k}{a^2}\right)\right]\frac{a^2}{1-kr^2} \ , \tag{1.27}$$

$$G_{22} = -\left[\left(\frac{\dot{a}}{a}\right)^2 + 2\left(\frac{\ddot{a}}{a}\right) + \left(\frac{k}{a^2}\right)\right]a^2 r^2 \ , \tag{1.28}$$

$$G_{33} = -\left[\left(\frac{\dot{a}}{a}\right)^2 + 2\left(\frac{\ddot{a}}{a}\right) + \left(\frac{k}{a^2}\right)\right]a^2 r^2 \sin^2\theta \ . \tag{1.29}$$

1.3.2 The Serendipity of Spacetime

The global geometrical structure of the Universe actually proposes a *double edged sword* of sorts in regards to a theoretical treatment of the concordance model of

cosmology. The ability to treat the Universe as effectively flat ($k \simeq 0$), is the first key point in terms of understanding the principle conjecture required to simplify how we model the evolution and features of matter and energy density components defining the Universe today. This issue is a cosmological fine tuning problem, which goes under the name of the *cosmological flatness problem*. Specifically this issue relates to the nature of the initial conditions required in order to realise the present day observational data, suggesting the value of k is only a very minor deviation from unity which indicates our universe is spatially flat to the best part in 10^{-2} [40]. The standard approach in order to realise an attractor solution which predicts a more natural realisation of a flat universe is the introduction of a period of spacetime expansion known as cosmic inflation. Figure 1.2 shows the current constraints from *Planck* data for the exclusion bounds at 68% and 95% confidence intervals (CIs) taking into account TT, TE, EE+lowE, lensing and baryon acoustic oscillation (BAO) data. The full joint constraints combine to provide a picture very consistent with a flat universe today. We have very strong observational evidence to believe that we can take the value of k to be zero at the effective level of our cosmological theory. Assuming then that our Universe is topologically flat with a spacetime metric described by a FLRW Universe, using the metric of the form in Eq. 1.3, and inserting $k = 0$ into Eq. (1.19), Eq. (1.20), Eq. (1.21) and Eq. (1.22), the Christoffel symbols can be further factorised using the symmetries of a geometrically flat Universe,

$$\Gamma^0_{0\mu} = \Gamma^0_{\mu 0} = 0 \ , \qquad \Gamma^0_{0\mu} = \delta_{ij}\dot{a}a \ , \tag{1.30}$$

$$\Gamma^i_{0j} = \Gamma^i_{j0} = \delta_{ij}\frac{\dot{a}}{a} \ , \qquad \Gamma^i_{\alpha\beta} = 0 \ , \tag{1.31}$$

which leads to the definition of the following components of the Ricci tensor,

$$R_{00} = -3\frac{\dot{a}}{a} \ , \tag{1.32}$$

$$R_{ij} = \delta_{ij}\left(2\dot{a}^2 + a\ddot{a}\right) \ . \tag{1.33}$$

Finally we can define the simplified Ricci scalar as,

$$\mathcal{R} = 6\left(\frac{\ddot{a}}{a} + \frac{\dot{a}^2}{a^2}\right) \ . \tag{1.34}$$

Let us return now to the issue of matter in the Universe. For each species of test particle described by a perfect isotropic fluid, its evolution is governed by our understanding of its motion over a straight line in the context of a non-trivial metric. This standardised trajectory is known as geodesic motion, which is formulated via the geodesic equation,

$$\frac{d^2x^\mu}{d\lambda^2} = -\Gamma^\mu_{\alpha\beta}\frac{dx^\alpha}{d\lambda}\frac{dx^\beta}{d\lambda} \ , \tag{1.35}$$

for a given scalar monotonically increasing variable λ, which describes the geodesic position. The final terms in Eq. (1.35) correspond to the four-velocity with respect to this variable, along the particles path. In the limit of a non-relativistic test particle, with a significantly weak gravitational potential, the geodesic equation recovers the principles of Newtonian mechanics,

$$\frac{d^2\vec{x}}{dt^2} = -\vec{\nabla}\phi \ , \tag{1.36}$$

where $\vec{\nabla}$ is the gradient operator. The stress-energy tensor in Eq. (1.15) for a perfect isotropic fluid in thermal equilibrium with energy density, ρ and pressure, P is formulated as,

$$T^{\mu\nu} = (\rho + P)\, U^\mu U^\nu + P g^{\mu\nu} \ , \tag{1.37}$$

with is conserved in an expanding universe. The Bianchi identities enforce the covariant derivative must vanish,

$$D_\mu T^\mu_\nu \equiv \partial_\mu T^\mu_\nu + \Gamma^\mu_{\alpha\mu}T^{\alpha\nu} - \Gamma^\alpha_{\mu\nu}T^\mu_\alpha = 0 \ . \tag{1.38}$$

In an inertial frame, i.e. $U_\mu = {}^{dx_\mu}/_{dt} = (1, \vec{0})$, comoving with the perfect fluid in homogenous and isotropic space, the stress-energy tensor has the reduced form of a

diagonal matrix,

$$T^{\mu}_{\nu} = \begin{pmatrix} \rho & 0 & 0 & 0 \\ 0 & -P & 0 & 0 \\ 0 & 0 & -P & 0 \\ 0 & 0 & 0 & -P \end{pmatrix} , \tag{1.39}$$

which encodes the requirements of the cosmological principle for the constituent matter components of the Universe. A rather interesting feature of the stress-energy tensor in this form is the emergence of a vacuum energy component, ensuring the presence of a cosmological constant. Locally the vacuum energy should be Lorentz invariant, which when subsequently generalised to general coordinates yields,

$$T^{\rm vac}_{\mu\nu} = -\rho_{\rm vac} g_{\mu\nu} \ . \tag{1.40}$$

When this is expressed in terms of the Einstein field equations we find,

$$\Lambda = 8\pi G_{\rm N} \rho_{\rm vac} = -P_{\rm vac} \ . \tag{1.41}$$

The cosmological constant can now be understood in terms of a *DE fluid*, which we will address later in more detail in Section 1.7.3. Decomposing into temporal and spatial components yields expressions for the energy density and the pressure of matter respectively. The temporal component of the conservation relation, $\nabla_{\mu} T^{\mu\nu} = 0$, defines the continuity equation,

$$\dot{\rho}_{\rm tot} + 3\frac{\dot{a}}{a}\left(\rho_{tot} + p_{\rm tot}\right) = 0 \ . \tag{1.42}$$

The continuity equation stems from the principles of thermodynamics where, $dU = -pdV$ with $U = \rho V$ and $V = a^3$, ensures we have an adiabatic expansion of the Universe. The main components of the Universe consist of a dust like non-relativistic matter fluid (ρ_m and p_m), a radiation energy component (ρ_p and p_r) and an effective cosmological constant fluid or vacuum energy component ($\rho_{\Lambda} = {}^{\Lambda}/_{8\pi G_{\rm N}}$). A common

dimensionless parameterisation of the diagonal components of the stress-energy tensor for a perfect fluid is given by the standard equation of state, governing the relationship between the density and pressure,

$$\omega_i = \frac{p_i}{\rho_i} \ , \tag{1.43}$$

where the index i runs over each cosmological fluid. The equation of state for pressureless dust, relativistic species and vacuum energy with negative pressure are respectively,

$$\omega_m \simeq 0 \ , \tag{1.44}$$

$$\omega_r = \frac{1}{3} \ , \tag{1.45}$$

$$\omega_\Lambda = -1 \ . \tag{1.46}$$

The equation of state defines the following form of the continuity equation,

$$\dot{\rho} + 3\frac{\dot{a}}{a}\left(1+\omega\right)\rho = 0 \ . \tag{1.47}$$

It is now possible to understand the evolutionary nature of each constituent fluid density by defining their phases of epochal evolution using time-dependent solutions to the defined Einstein equations.

1.4 The Friedmann Equations

1.4.1 The Expanding Universe

The metric tensor we have introduced, $g_{\mu\nu}$, is a measure of the geometric and causal structure of spacetime. We must now take into account that we will consider the case of an expanding universe and so must understand the nature of the cosmic scale factor, $a(t)$, i.e. the time dependent nature of the solutions for the the spatial

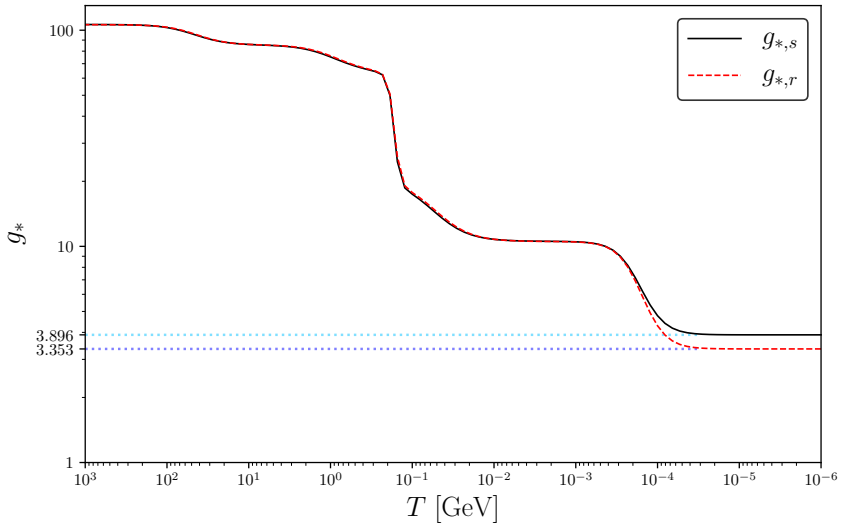


Figure 1.4: The effective relativistic degrees of freedom for both the energy and entropy densities, $g_{*,r}$ and $g_{*,s}$, as a function of temperature beginning at, $T = \mathcal{O}(10^3)$ GeV, evolving assuming the standard evolution of the Standard Model gauge group. The functions separate approximately after $e\pm$ annihilation, when $T_\nu \neq T_\gamma$. The fits are made following the procedure of Ref. [1329] used to approximate the functions given in Eq. (1.73) and Eq. (1.74). The dotted lines (*light blue* (entropy), *dark blue* (energy)) represent the approximate fitted values of $g_{*,r}$ and $g_{*,s}$ at the present time.

curvature and the homogeneous energy density present in the Universe. To do this we turn back to the non-zero components ($\mu = \nu = 0$) of the Einstein field equations in Eq. (1.15). The first of these is given by the temporal (G_{00}) component of Eq. (1.30),

$$G_{00} \equiv 3\left[\left(\frac{\dot{a}}{a}\right)^2 + \left(\frac{k}{a^2}\right)\right] = 8\pi G_{\rm N}\left(\rho + \rho_\Lambda\right) \ , \tag{1.48}$$

which is rearranged to define the first of the Friedmann equations,

$$\frac{\dot{a}^2(t)}{a^2(t)} = \frac{8\pi G_{\rm N}}{3}\rho - \frac{k}{a^2} - \frac{\Lambda}{3} \ . \tag{1.49}$$

We have at this stage reintroduced a dependance on the spatial curvature, whilst also formally defining the Hubble parameter,

$$H(t) \equiv \frac{\dot{a(t)}}{a(t)} \ , \tag{1.50}$$

a measure of the history of the cosmic expansion. In a similar fashion the remaining diagonal components of the Einstein field equations reveal further information regarding the evolution of the cosmic expansion,

$$G_{ii} \equiv \left[2\left(\frac{\ddot{a}}{a}\right) + \left(\frac{\dot{a}}{a}\right)^2 + \left(\frac{k}{a^2}\right) \right] = 8\pi G_{\rm N}\left(\rho + P\right) \ , \tag{1.51}$$

which after rearrangement give the *acceleration* or *Raychaudhuri* equation,

$$\frac{\ddot{a}(t)}{a(t)} = -\frac{4\pi G_{\rm N}}{3}(\rho + 3p) + \frac{\Lambda}{3} \ . \tag{1.52}$$

The cosmic deceleration parameter is defined as,

$$q = -\frac{\ddot{a}}{a}\frac{1}{H_0^2} \ , \tag{1.53}$$

which can also be expressed as,

$$q = \frac{\Omega_{\rm tot}}{2}\left(1 + 3\omega_{\rm tot}\right) \ , \tag{1.54}$$

where $\Omega_{\rm tot}$ is the total dimensionless density as defined in Eq. (1.64). If the cosmological constant, Λ, or some cosmic fluid with an equation of state matching its behaviour i.e. $\omega < 1/3$, the deceleration parameter becomes negative, representing the presence of an accelerating expansion of the Universe. The total equation of state is simply the following linear summation,

$$\omega_{\rm tot} \equiv \frac{\sum_i P_i}{\sum_i \rho_i} \ . \tag{1.55}$$

This summation over the values of ρ_i and P_i represents the total energy density and total pressure of the fluid system components comprising the Universe. The nature of Eq. (1.52) tells us that the expansion is both adiabatic whilst ensuring that the total entropy is conserved. Using Eq. (1.49) and Eq. (1.52) the Bianchi identities return us to the stage where we can derive the continuity equation, for a system

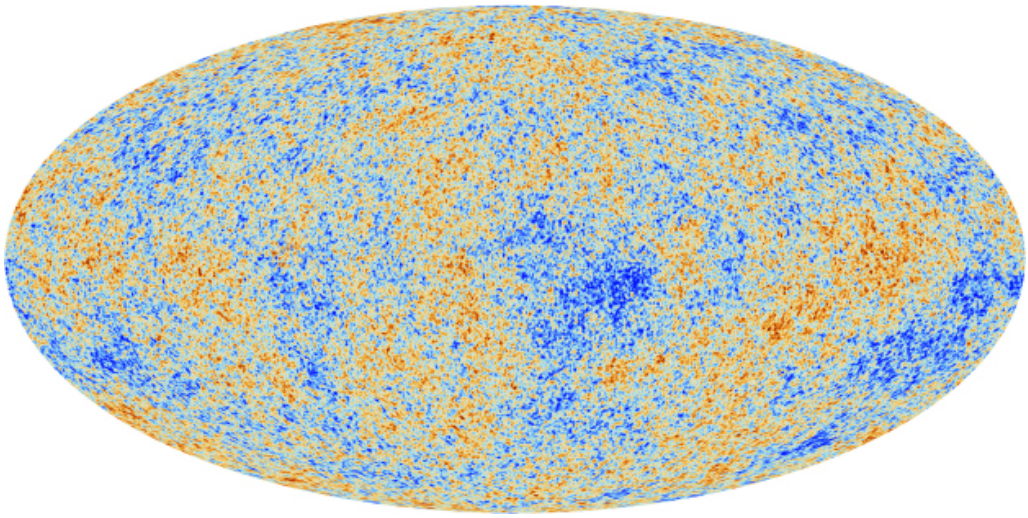


Figure 1.5: Anisotropies of the cosmic microwave background emitted approximately 380,000 years after the Big Bang, as observed by the Planck satellite, a strong indication of the nature of Big Bang cosmology. The Red regions represent densities hotter than the average temperature, the blue regions are cooler, reflecting the apparent density variations present at recombination. The observational aspects of this map represent a vital probe to possible extensions to cosmological physics models. Image credit: ESA and the Planck Collaboration, `http://sci.esa.int/science-e-media/img/61/Planck_CMB_Mollweide_4k.jpg`.

containing the complete spectrum of fluid components in the Universe, as defined in Eq. (1.42). It is also possible to define the evolutional properties of the cosmic scale factor and fluid densities via the equation of state (Eq. (1.43)), continuity equation (Eq. (1.42)) and Friedmann equation (Eq. (1.49)). This understanding of the evolution takes the form,

$$\rho_{i,t} = \rho_{i,0} \left(\frac{a}{a_0} \right)^{-3(1+\omega_i)} , \tag{1.56}$$

where the zero subscript defines the value at the present time and the subscript, i, runs over each energy density component. Correspondingly for the cosmic scale factor we have,

$$a(t) = a_0 \left(\frac{t}{t_0} \right)^{\frac{2}{3(1+\omega)}} . \tag{1.57}$$

with an initial time, t_0 and time, t. By replacing the values defined in Eq. (1.44), Eq. (1.45) and Eq. (1.46) into Eq. (1.56), we retrieve the standard scale dependance

for the cosmic densities, where for dust like components we have, $\rho_m \propto a(t)^{-3}$ and for radiation components, $\rho_r \propto a(t)^{-4}$. Performing the relevant integration gives the complete set of dominant component evolutions,

$$\alpha(t) \propto \begin{cases} t^{\frac{2}{3(1+\omega)}} & \omega \neq -1 \ , \\ e^{Ht} & \omega = -1 \ . \end{cases} \tag{1.58}$$

Defining the epochs of matter and radiation domination where $\rho_{tot} \approx \rho_m$ and $\rho_{tot} \approx \rho_r$, respectively allows us to determine the dynamical time dependance of the cosmic scale factor for each period,

$$\text{Radiation domination} - a \propto t^{\frac{1}{2}} \text{ and } H(t) \propto \frac{1}{2t} \ , \tag{1.59}$$

$$\text{Matter domination} - a \propto t^{\frac{2}{3}} \text{ and } H(t) \propto \frac{2}{3t} \ , \tag{1.60}$$

where finally for a dark-energy-dominated universe we have,

$$\text{DE domination} - a \propto e^{\sqrt{\frac{\Lambda}{3}}t} \text{ and } H(t) \propto \sqrt{\frac{\Lambda}{3}} \ . \tag{1.61}$$

The exponential dependance in this relationship leaves the spacetime geometry identical to a de Sitter Universe.

1.4.2 The Standard Energy Constituents

A common nomenclature in cosmological literature is the expression of the cosmological fluid densities with respect to the critical density parameter. Throughout this work we will now assume the background evolution is defined on a spatially flat universe, that is the normalised spatial curvature appearing in Eq, (1.7) is set to, $k = 0$. As such it is possible to define the critical energy density using the

Friedmann equations (Eq. (1.49) and Eq. (1.52)),

$$\rho_{\rm crit} \equiv \frac{3H(t)^2}{8\pi G_{\rm N}} \ , \tag{1.62}$$

$$\rho_{\rm crit,0} \equiv \frac{3H_0(t)^2}{8\pi G_{\rm N}} \simeq 1.88 \times 10^{-29} h^2 \ {\rm g \ cm^{-3}} \ . \tag{1.63}$$

Using $\rho_{\rm crit}$ we can define each of the dimensional cosmic density parameters as,

$$\Omega_i = \frac{\rho_i}{\rho_{\rm crit}} \ , \tag{1.64}$$

where the index i again runs over each component evolving on the spacetime background. We can also define the quantities,

$$\rho_k \equiv -\frac{3k}{8\pi G_{\rm N} a^2} \ , \tag{1.65}$$

$$\rho_\lambda \equiv \frac{\Lambda}{8\pi G_{\rm N}} \ , \tag{1.66}$$

and,

$$\Omega_{\rm tot}(t) = \Sigma_{i\neq k}\Omega_i = 1 - \Omega_k \ \equiv 1 \ , \tag{1.67}$$

for a spatially flat Universe. The total contributions from radiation today in the summation are suppressed with respect to dust like components and consists of contributions from photons and neutrinos, as for standard ΛCDM considerations we should not traditionally expect to receive any significant contributions from hot DM. The equilibrium thermodynamics of the relativistic energy densities can be understood via the quantities,

$$\rho_\gamma = \frac{\pi^2}{15} T_\gamma^4 \ , \tag{1.68}$$

$$\rho_\nu = N_{\rm eff} \frac{7\pi^2}{120} T_\nu^4 \ , \tag{1.69}$$

where $N_{\rm eff} \simeq 3.046$ [898], represents the effective number of relativistic species and T_γ and T_ν are the photon and neutrino temperatures respectively. These quantities

define the total radiation energy density in terms of the total relativistic degrees of freedom,

$$\rho_r = \sum_i \rho_i = \rho_\gamma + \rho_\nu = \frac{\pi^2}{15} T_\gamma^4 \left[1 + \frac{7}{8} \left(\frac{4}{11} N_{\rm eff} \right)^{4/3} \right] \ . \tag{1.70}$$

The total relativistic energy density well after the phase of electron-positron annihilation is expressed as,

$$\rho_r = N_{\rm eff} \frac{7}{8} \left(\frac{4}{11} \right)^{4/3} \rho_\gamma \ \equiv \frac{\pi^2}{30} g_*(T) T^4 \approx 8.09 \times 10^{-34} \text{g cm}^{-3} \ , \tag{1.71}$$

today, where the value of $7/8$ accounts for the variations in Fermi and Bose statistics. Correspondingly the total system entropy is,

$$s = \sum_i s_i = \frac{2\pi^2}{45} g_{*,s}(T) T^3 \ . \tag{1.72}$$

The complete picture of the entropy and radiation density is approximated by counting the relativistic degrees of freedom. When the temperature of the primordial plasma drops below the mass of a particular field, the particle's contribution to both the entropy and radiation density drops out. An accurate expression for the effective contributions to the total energy density and pressure of all species, expressed using the photon temperature and g_*, representing the total number of effectively massless degrees of freedom, i.e. $m_i \ll T$ Ref. [1329] is,

$$g_{*,r}(T) = \sum_i \left(\frac{T_i}{T} \right)^4 \frac{15 g_i}{\pi^4} \int_0^\infty dx \frac{\sqrt{x^2 + y_i^2}}{\exp \sqrt{x^2 + y_i^2} + (-1)^{Q_i^f}} \ , \tag{1.73}$$

$$g_{*,s}(T) = \sum_i \left(\frac{T_i}{T} \right)^3 \frac{45 g_i}{4\pi^4} \int_0^\infty dx \frac{x^2 \sqrt{x^2 + y_i^2}}{\exp \sqrt{x^2 + y_i^2} + (-1)^{Q_i^f}} \left(1 + \frac{1}{3} \frac{x^2}{x^2 + y_i^2} \right) \ . \tag{1.74}$$

Here $Q^f = 1$ for fermionic degrees of freedom, $Q^f = 0$ for bosonic degrees of freedom, $g_{*,r}$ is the effective degrees of freedom for the density and $g_{*,s}$ represents the effective degrees of freedom for the entropy. The value of T represents the temperature of the plasma and T_i the temperature of each species where $y_i = {}^{m_i}/_{T_i}$. The separation of

these two functions occurs at neutrino decoupling, after $e\pm$ annihilation at the time when $T_\nu \neq T_\gamma$. In the standard thermal history $g_{*,s} \simeq g_{*,r}$, with possible variations occurring at defining periods such as during the QCD phase transition. In Fig. 1.4 we show fits for the effective degrees of freedom $g_{*,R}$ and $g_{*,S}$, using the functional fit procedure found in Ref. [1329]. The case of non-relativistic species is somewhat easier to track. The quantity Ω_m represents a summation over the total matter density in the Universe, comprising of the baryonic, Ω_b and DM, $\Omega_{\rm DM}$ components respectively,

$$\Omega_m = \Omega_b + \Omega_{\rm DM} \ . \tag{1.75}$$

The Friedmann equation can also be re-expressed in terms of the dimensionless density parameters,

$$\Omega_{\rm tot}(t) = \Omega_r(t) + \Omega_m(t) + \Omega_\Lambda(t) + \Omega_k(t) \ , \tag{1.76}$$

representing the form of the total summation where we exclude any external degrees of freedom from physics beyond the standard model. Suitably Eq. (1.49) parameterised with respect to the composition of the Universe today is,

$$\frac{H^2(t)}{H_0^2(t)} = \Omega_{r,0}a^{-4} + \Omega_{m,0}a^{-3} + \Omega_{\Lambda,0} + \Omega_{k,0}a^{-2} \ . \tag{1.77}$$

The final component, $\Omega_k = 1 - \Omega_{\rm tot}$ drops out for a spatially flat universe, recovering Euclidean expressions when $\Omega_k \to 0$. Observationally the spatial hypersurfaces are heavily constrained using both Planck lensing and BAO data [40],

$$\Omega_{k,0} = 0.0007 \pm 0.0019 \ , \tag{1.78}$$

which sufficiently breaks the geometric degeneracy so we can safely assume the flat nature of the Universe. We can then suitably truncate $\Omega_k(t)$ out of Eq. (1.76) and Eq. (1.77), fully adopting the issues of the flatness problem. This then defines the

simplistic density relation,

$$\Omega_{\rm tot}(t) = \Omega_r(t) + \Omega_m(t) + \Omega_\Lambda(t) = 1 \ , \tag{1.79}$$

where the values of the density parameters have been normalised against the critical density. The current best estimates of these time dependent functions determined by the Planck collaboration [40], defines the values of the following cosmological parameters,

$$\Omega_{b,0}h^2 = 0.02242 \pm 0.00014 \ , \tag{1.80}$$

$$\Omega_{\rm DM,0}h^2 = 0.11933 \pm 0.00091 \ , \tag{1.81}$$

$$\Omega_m h^2 = 0.1430 \pm 0.0011 \ , \tag{1.82}$$

$$\Omega_{\Lambda,0} = 0.6889 \pm 0.0056 \ , \tag{1.83}$$

all of which are quoted using the TT,TE,EE+lowE+lensing+BAO 68% CI data. The radiation density is defined to be,

$$\Omega_r h^2 = 4.31 \times 10^{-5} \ , \tag{1.84}$$

found using the fits for the relativistic degrees of freedom in Eq. (1.71), whilst assuming the photon temperature today is,

$$T_0 \simeq 2.75K \ . \tag{1.85}$$

The value of the Hubble parameter today is quoted as,

$$H_0 = 100 \times h \text{ Km s}^{-1}\text{Mpc}^{-1} = 67.37 \pm 0.54 \text{ Km s}^{-1}\text{Mpc}^{-1}. \tag{1.86}$$

Each of the values in Eq. (1.80), Eq. (1.81), Eq. (1.82) and Eq. (1.83), represent the 68% CI from the baseline TT, TE, EE+lowE+lensing data. We normalise both $\Omega_{\rm tot}$ and the cosmic scale factor $a(t)$ to unity at t_0, which we define as the current time.

1.5 The Causality and Kinematics of Spacetime

The nature of measuring time and tracking the evolution of distance in the Universe is understandably no easy task. A fundamental measure assigned to track such a procedure is the definition of the comoving distance. In order to build a picture of distances in a homogeneous and isotropic universe we use a redefinition of the spacetime coordinates, where we focus on the case of radiation emitted at a source and observed after a finite period of propagation. Due to the expansion of the universe any incident electromagnetic radiation is redshifted away, where there is an enhancement to the observed wavelengths ($\lambda_{\rm obs}$) when compared to the original value emitted at the source ($\lambda_{\rm emit}$). This notion defines the cosmological redshift,

$$z \equiv \frac{\lambda_{\rm obs} - \lambda_{\rm emit}}{\lambda_{\rm emit}} \ . \tag{1.87}$$

The cosmological redshift parameter can be defined as an expression of the ratio of detected lights wavelength to the emitted wavelength,

$$1 + z \equiv \frac{\lambda_{\rm obs}}{\lambda_{\rm emit}} = \frac{\delta t_0}{\delta t_e} = \frac{a(t_0)}{a(t)} \ , \tag{1.88}$$

where the numerator in the final term is normalised to unity today to give, $1/a(t)$. It is possible to redefine the the first of the Friedmann equations using the relationship for the cosmological redshift into the form,

$$\dot{a}^2 = H_0^2 \left[\sum_i \Omega_i(t_0) a^{-(1+3\omega_i)} + (1 - \Omega(t_0)) \right] \ . \tag{1.89}$$

Performing the relevant integration leads to an estimation of the age of the Universe,

$$t = \frac{1}{H_0} \int_z^\infty \frac{dz(1+z)^{-2}}{\left(\Sigma_i \Omega_i(t_0)(1+z)^{(1+3\omega_i)} + 1 - \Omega_0\right)^{1/2}} \ . \tag{1.90}$$

If we begin at $t = 0$ representing a point like singularity as our initial conditions, the age of the universe is approximated to be,

$$t_{\rm Univ} \approx 13.796 \text{ Gyrs} \ . \tag{1.91}$$

The causal horizon can be defined as the region of spacetime connected to a point translated into other region by causal physical processes. The limit of this horizon can be fixed by the propagation of light where the massless waves travel on geodesics, $ds^2 = 0$. Using the spherical coordinates and addressing the radial direction defines the comoving distance,

$$\frac{dt}{a(t)} \equiv d\chi = \pm \frac{dr}{\sqrt{1 - kr^2}} \ , \tag{1.92}$$

where $\chi(r)$ is defined as the comoving coordinate and the $\pm$ solutions relate to a propagation towards and away from the observer. These coordinates leads to a reparameterisation of the FLRW metric, where it can now be conveniently expressed in the form,

$$ds^2 = -dt^2 + a^2(t) \left\{ d\chi^2 + f_k^2(\chi) \left(d\theta^2 + \sin^2 \theta \theta d\phi^2 \right) \right\} \ , \tag{1.93}$$

where the principle of homogeneity always allows us to renormalise our reference frame to $r = 0$. The curvature relation of the positional function is defined as,

$$f_k(\chi) = \begin{cases} \sin \chi(r) \ , & k = +1 \ , \\ \chi(r) \ , & k = 0 \ , \\ \sinh \chi(r) & k = -1 \ . \end{cases} \tag{1.94}$$

The conformal time is defined as,

$$\tau(a) \equiv \int_{t_{\rm emit}}^{t_0} = \frac{dt}{a(t)} = \int_{a(t_{\rm emit})}^{a(t_0)} \frac{da}{a^2(t) H(a)} = \int_0^{z(t_{\rm emit})} \frac{dz}{H(z)} \ , \tag{1.95}$$

which represents the maximum distance for the propagation of information in the comoving distance, defining the disconnection limits of regions of causal connection. It is common practise to quantify distances in terms of *standard candles* defined at some comoving distance coordinate, χ. Initially the luminosity passing through a spherical shell of radius defined at a distance d_L emitting at an intrinsic luminosity, L, is,

$$\mathcal{F} = \frac{L}{4\pi d_L^2(a)} \ . \tag{1.96}$$

This flux can be redefined in terms of the comoving coordinate to account for the expansion of the Universe by accounting for the physical distance relation for the shell corresponding to the comoving distance,

$$\mathcal{F} = \frac{La^2}{4\pi\chi^2(a)} \ , \tag{1.97}$$

which now relates to the luminosity distance,

$$d_L(a) = \frac{\chi(a)}{a} \equiv \chi(z)(1+z) \ . \tag{1.98}$$

We can also define the angular distance which relates the intrinsic size of an object to its angular presence in the sky,

$$\theta \equiv \frac{D}{d_A(a)} \ , \tag{1.99}$$

with D the luminosity distance. In the case of a flat universe ($k = 0$) we recover the simple relationship between the angular distance and the comoving coordinate,

$$d_A \equiv a\chi(a) \ . \tag{1.100}$$

Finally we can express the matter and radiation densities in terms of the cosmological redshift,

$$\rho_m = \rho_{m,0} \left(1+z\right)^3 \ , \tag{1.101}$$

$$\rho_r = \rho_{r,0} \left(1+z\right)^4 \ , \tag{1.102}$$

the case of equality between the matter and radiation domination epochs defines the value of redshift equality,

$$1 + z_{eq} \equiv \frac{\rho_{m,0}}{\rho_{r,0}} \simeq 3387 \ , \tag{1.103}$$

according to the best fit measures on the cosmological parameters presented in Eq. (1.82) and Eq. (1.84).

1.6 Beyond the Traditional Paradigms

1.6.1 Problems with Concordance Cosmology

Despite the extremely successful framework above allowing for both an understanding of spatial distance and the temporal evolution of matter, the simple model of a cosmological constant and a CDM component do not provide the necessary theoretical ground work for homogeneity and isotropy in the Universe. There are several key observation contradictions to what the Standard Model of Cosmology predicts, such as:

- *The Spatial Flatness Problem* - The initial epochs of the Universe require a large amount of fine tuning in order generate a value of $\Omega_{\rm tot}$ of order unity today [40]. This apparent spatial flatness will shift from unity as the Universe expands if $\ddot{a} < 0$. The fine tuning can be as extreme as $|\Omega_{\rm tot} - 1| < \mathcal{O}(10^{-64})$ at the Planck epoch [1113], which represents the stability precision required

to ensure the Universe doesn't over-close or accelerate too quickly to deny the possibility of large scale structure formation.

- *The Cosmic Horizon Problem* - The total particle horizon at decoupling corresponds to the spacetime regions where observed photons in the CMB, present at the time of decoupling, could have causal contact. Taking the ratio for this limit and the particle horizon today, shows the causality regions are in fact very small, restricted to minor angular distances in the observable sky. We know however, that observed photons do thermalise at the same temperatures all across the visible sky. This discrepancy in the nature of CMB photon temperatures is known as the cosmic horizon problem.

- *The Absence of Magnetic Monopoles* - The early phase transition periods of the Universe generate many relics in particle physics theories [489, 650, 786]. These possible relics often have the potential to spoil required observations due to the dissipative nature of matter content over the expected dominant radiation contribution [1075]. A large problem arises for point topological defects, which are expected to dominate the matter content in hot Big Bang models. Such relics have yet to be observed. These magnetic monopoles seem to require extended physics in order to generate a negligible relic density that would remain unobservable today.

- *Large Scale Structure* - The ability to formulate a mechanism which accounts for the large scale structure in the universe is impossible to realise in the Standard Model of cosmology when considering the nature of the present primordial fluctuations [1209, 1271]. A reconciliation of the scales required and the nature of the evolution of the Hubble radius seem to require a catalyst for dynamics beyond simple Big Bang Cosmology concerns.

1.6.2 The Paradigm of Cosmic Inflation

The inflationary paradigm is an accelerated period of exponential expansion hypothesised to address the core problems detailed above, where we have,

$$a(t) \sim e^{Ht}, \tag{1.104}$$

occurring approximately, $10^{-36}\text{s} - 10^{-33}\text{s}$ after the initial singularity. The initial formulations of inflationary dynamics in the cosmic setting described de-Sitter inflation by using a first-order transition to the true vacuum [647, 1148]. It soon became apparent that issues surrounding inhomogeneity and bubble collisions required models of slow-roll inflation and second-order phase transitions to the true vacuum [55, 864]. Modifications to these models were presented to fix fine-tuning problems by requiring enough time is spent in the false vacuum, known as *chaotic inflation* [865]. Acceleration occurs ($\ddot{a} > 0$), when the fluid responsible for its dynamics presents a negative pressure, i.e. $\rho + 3P < 0$. The hypothetical field often introduced in order to drive this accelerated period is known as the *inflaton*. The scalar dynamics of the inflaton require the general relations,

$$3H\dot{\phi} \approx -V(\phi) \ , \tag{1.105}$$

$$H^2 \approx \frac{1}{3M_{\rm Pl}^2} V(\phi) \ , \tag{1.106}$$

which are often collectively referred to as the *slow roll conditions*, with field potential $V(\phi)$. The quantum fluctuations of the inflation field could provide a vital solution to the evolutionary nature of the matter content in the Universe today. These fluctuations are typically frozen during the cosmic acceleration, when the fields scale leaves the Hubble radius, where the perturbations offer a possible explanation to the seeds of large-scale structure formation. Likewise a readjustment to the trajectory of the Hubble radius can allow for a phase expansion which causes unwanted topological relics to be red-shifted away during inflation, solving for example the

standard Monopole problem. This is only sufficient of course, given unwanted particles do not now enter the spectrum during the phase of reheating which follows. If the reheating temperature is accounted for in such a way to ensure the avoidance of unwanted energy transfer into radiation, spoiling the balance of phases such as nucleosynthesis, then the issues of any unobserved relic abundance totally vanishes.

The standard measure of inflationary models is given by the slow roll parameters, used to formally define the slow roll conditions found in Eq. (1.105) and Eq. (1.106) which measure the ability to sufficiently inflate the Universe. The slow roll parameters for cosmic inflation are,

$$\epsilon = \frac{M_{\rm Pl}^2}{16\pi}\left(\frac{V'}{V}\right)^2 \ , \tag{1.107}$$

$$\eta = \frac{M_{\rm Pl}^2}{8\pi}\left(\frac{V''}{V}\right) \ , \tag{1.108}$$

with V' and V'' the first and second derivatives of the fields potential. We require, $\epsilon \ll 1$ and $|\eta| \ll 1$, in order for the potential to dominate its kinetic function thereby allowing for subsequent reheating. When both ϵ and η become $\mathcal{O}(1)$ the period of cosmic inflation ends. The amount of inflation a model can generate is normally expressed in terms of the number of *e-folds*,

$$N_{\rm fold} \equiv \ln\left(\frac{a_{\rm fin}}{a_{\rm ini}}\right) = \int_{t_{\rm ini}}^{t_{\rm fin}} H dt \ . \tag{1.109}$$

In order to address both the horizon and flatness fine tuning problems the ratio between the initial and final phases of inflation defines the ratio between the initial ($\Omega_{\rm ini}$) and final ($\Omega_{\rm fin}$) dimensionless density quantities,

$$\frac{|\Omega_{\rm fin} - 1|}{|\Omega_{\rm ini} - 1|} \simeq \left(\frac{a_{\rm ini}}{a_{\rm fin}}\right)^2 = e^{-2N_{\rm fold}} \ , \tag{1.110}$$

assuming that the value of H is relatively constant during inflation itself. In order to ensure that $|\Omega_{\rm ini} - 1| \simeq \mathcal{O}(1)$ we require $N_{\rm fold} \gtrsim 70$, give or take $\mathcal{O}(10)$ depending on the specifics of the model, in order to find a satisfactory solution to the issues

surrounding the cosmic horizon which also results in a spatially flat universe.

There are copious methods of incorporating a period of inflation into the evolution of the Universe [883]. These are broadly classified as *large* field inflation models ($\Delta\phi \gg M_{\rm Pl}$), *small field* ($\Delta\phi \ll M_{\rm Pl}$) inflation models and Modular ($\Delta\phi \sim M_{\rm Pl}$) inflation models. Classic models include Eternal inflation [648, 1296] and eternal chaotic inflation [863]. Many variants and clever emulators of the original proposal consist of R^2 [888], new [1172], chaotic, extended inflation [816, 834], power-law [876], classical hybrid inflation [866], natural [562], supernatural [1088], extranatural [98], D-term [222], F-term [904], oscillating [486], trace-anomaly driven [684] and Standard Model Higgs inflation [216] to name a few. Further examples take advantage of multiple fields such as models of assisted inflation with multiple fields [860] and multi-component chaotic inflation [170, 885, 1145, 1146, 1212]. String theory generally also offers a vast landscape to construct models of inflation [176, 757, 760]. In particular inflation in brane world cosmology [488, 1083], warped brane inflation [177], relativistic brane inflation [1186], D-brane inflation in an unwarped compactifications [402, 403, 691, 719, 720], matrix inflation [113, 114] and modular inflation [151, 223, 227, 835, 862, 1119], again a minor sample of the theoretical landscape. The most relevant to discussions in subsequent chapters are models of axion inflation [353, 457, 499, 561, 761, 1010], which we shall expand on in Section 2.8.1. It seems that the dynamics of the Universe over large scales do certainly require additional modifications to explain these paramount issues without help from the well documented luminous matter candidates. It is also clear there are many consistent ways in which to tackle such problems.

1.7 The Matter and Energy Content of the Dark Universe

1.7.1 A Historical Perspective of a Dark Universe

A glaringly obvious omission from any cosmological model is the true understanding behind the theoretical origins of approximately 95% of the energy density present in the Universe today, as demonstrated in the typically obliged representation of Fig. 1.6, the so called dominating *dark* sector of cosmology. The simplest parameterisation of Big Bang cosmology which is used to account for this dark sector as we have covered, is the concordance model of cosmology or ΛCDM. The origins of concordance cosmology stem from the desire to unify baryonic matter to a mysterious dark sector, whose density dominates over the constant components of the low energy sector of particle physics which we can formulate from the Standard Model. The initial origins of the term "*dark*" being used to describe a component of our Universe, evasive to standard observational or experimental rigour, can be traced as far back as several decades before the turn of the 20$^{\text{th}}$ century. Although blissfully unaware at the true puzzle behind the monolithic door of cosmology they found themselves at, the reference to "*dark nebulae*", "*dark clouds*" and even "*dark masses*" providing a captivating insight into how the foundations of the scientific community sensed that the astronomical picture of our surroundings were far from complete. Perhaps the most famous pioneer in this sector pertaining to the infamous galactic rotational curves was Swiss-American astronomer *Fritz Zwicky* and his comments on the Coma Cluster, a preface to the seminal pillars in observational astronomy which would eventually highlight the presence of a vast mysterious sector of physics. The 20$^{\text{th}}$ century saw an explosion of work regarding the inherent observational consistency that both the presence of non-luminous unaccounted for matter and later vacuum energy were not just present but indeed an extensive issue [713, 726, 877, 1000, 1196]. It eventually took until the turn of the century for

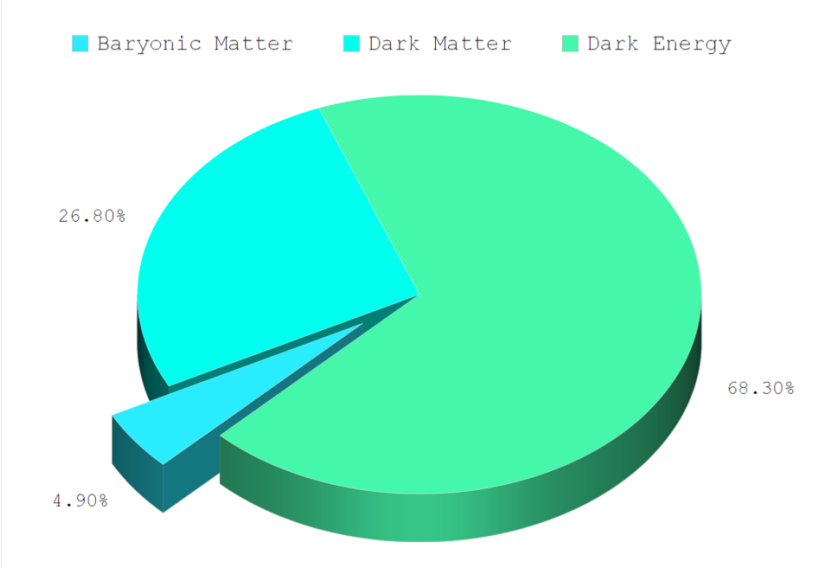


Figure 1.6: The cosmic energy budget determined by data collected by the Planck collaboration in Eq. (1.80), Eq. (1.81) and Eq. (1.83). The Universe is currently observed to be dominated by two principle dark components which make up $\sim 95\%$ of the total cosmic energy density. The separated wedge component represents the only portion of the observable Universe we can currently account for with the Standard Model of particle physics.

the standardised conventions and complexities to make themselves known with the discovery of anisotropies in the CMB [542] along with the first direct detections of an accelerating Universe [1051, 1108]. These sectors commonly treated as a divided issues inherit many challenging factors in order to reproduce the formulations from the standard approaches to cosmological models, the origins of which remain a vast mystery today.

1.7.2 A Mysterious Matter

The realisation that baryonic matter with the familiar picture of empirical science via the manipulation of protons and neutrons was not the dominant form of matter density in the Universe was a pivotal turning point in 20^{th} century science. The abundance of this mysterious matter is significant, it's measured density approximately five times our own ordinary matter, enforcing it must be considered as a staple necessity in realistic cosmological models [212, 396, 426, 587]. There are

several standard properties DM must possess stemming from astrophysical observations, which must be incorporated into minimal DM models. Firstly it can not be made from Standard Model particles, as these generally possess unwanted charges and couplings. For example possible candidates such as the Higgs and Z bosons both have short lifetimes and neutrinos are considered too light. Its interactions with Baryons must be heavily suppressed to account for the absence of observational signatures such as baryon-DM galactic disks and modifications to the CMB from the baryon-photon fluid. It should also be weakly self-interacting to avoid complications with halo-dark-matter structure, as to avoid the *gravothermal catastrophe* [881]. Finally of course it must be dark, coupling very minimally to photons in order to avoid constraints from the dimming of spectra from astrophysical sources. The clarity behind DM and its historical inception comes from its primary gravitational coupling. The first footings into what we now define as the DM problem came from particular works, such as Jacobus Kapteyn study of the kinetic theories of gases and their relationship with observed velocity dispersions of the stars [775]. Further work continued with one of his students, Jan Oort, who continued the pressing idea of analysing stellar kinematics in the context of estimating the matter content [1000]. Both pieces of work revealed a non-negligible component, which must be accounted for to produce the observed and documented dynamics. Edwin Hubble and his groundbreaking work on galactic redshifts [725] later motivated Fritz Zwicky to address the velocities of galaxies inside selected galaxy clusters. His results were salient in nature, using the virial theorem to predict that the *Coma cluster* should be ~ 400 times larger than what luminous matter observations were initially indicating [1398]. These were the initial footings into the physics of dark halos, galactic rotational curves and the conclusion of general DM domination we take as fundamental gospel today.

For any massive body where we can neglect the possibility of collisions in a stable orbit, we can first define using a spherical matter distribution, the relationship

between the density of matter $\rho(r)$ and its gravitational potential $\Phi(r)$ as,

$$\Delta\Phi(r) = 4\pi G_{\rm N}\rho(r) \ , \tag{1.111}$$

where $\Delta \equiv \nabla^2$ is the Laplacian operator. Using the Poisson equation above and standard Newtonian Gravity the motion of the bodies in a circular orbit is,

$$v_{\rm rot}(r) = \sqrt{\frac{G_{\rm N}M(r)}{r}} \ , \tag{1.112}$$

for an enclosed mass, M,

$$M(r) = \int_0^r \rho(r')d^3r' \ , \tag{1.113}$$

and radial distance, r. The rotational velocity for the mass of the body should follow Keplars law of proportionality,

$$V(r) \propto r^{-1/2} \ , \tag{1.114}$$

representing the velocity profiles of galaxies and the expected distributions of luminous matter. Some decades after the initial speculations of Jacobus Kapteyn, Jan Oort and Fritz Zwicky, Vera Rubin [1128] and others used doppler shift measurements of distant galaxies to show the velocity profile actually remains constant at increasing radius. These flat rotational curve profiles suggest a contribution to the matter density outside of the luminous matter core which scales with the radius of the profile [171, 253, 254, 560, 1130, 1397]. This apparent DM component is understood purely from the astrophysical nature and properties of its gravitational interactions with visible baryonic matter. An example of this is shown in Fig. 1.7 from the seminal work which presented the data for 21 Sc rotational curves detailing the flattened nature of the rotational curves when extending far beyond the galactic nucleus [1130]. Further work continued [509, 1007] which highlighted that this problem could extend beyond the initially considered scales, rotational curves still acting as inference methods for mass measurements today with the help of dark halo

models [373].

A more modern understanding and further examples providing indications of DM come from, gravitational microlensing and measurements in observational cosmology such as BAOs and the matter power spectrum [169, 392]. The primordial baryon acoustic waves in the baryon-photon plasma generate overdensities which tie together the physics of baryonic matter and DM. Various surveys (2dFGRS [361], Sloan Digital Sky Survey III [54] and BOSS [410]) have shown that perturbative theories of gravity, used in order to describe power spectrum oscillations must contain a DM component. Other methods include looking at the Lyman-α emission lines and the nature of the Lyman-α forest [404, 700]. Direct signal indications of the presence of DM have been made in recent years [359] through lensing techniques. Lensing is typically factorised into two regimes. Strong lensing occurs when gravity is sufficient enough to generate several geodesic paths for the light to reach the observer. This phenomena can lead to the presence of Einstein rings, the appearance, density and distributions of which help map the nature of the DM [855],

$$\theta_{\rm Ein} \simeq \sqrt{\frac{4G_{\rm N}Md_{\rm os}}{d_{\rm o}d_{\rm s}}} \ , \tag{1.115}$$

where $d_{\rm os}$ is angular diameter distance between the lens and the source, $d_{\rm o}$ is the angular diameter distance to the lens and $d_{\rm s}$ is the angular diameter distance to the source. The weak lensing regime [731, 925] makes inferences based on the bending of light and minor distortions through measurements of galaxy shear. These can be used to infer the general large scale baryonic to DM ratios. Lensing can provide interesting constraints on the particle nature of DM, which is well demonstrated through observations of the *Bullet Cluster* [1089], limiting the DM particle self-interaction cross section to, $^{\sigma}/_{m_\chi} < 0.7{\rm cm}^2{\rm g}^{-1}$ for a particle of mass, m_χ.

Often many of the traditional methods used to model DM invoke various forms of a density profile for the distribution of the missing matter. In particular N-body simulations try to incorporate the DM as an important component in structure for-

mation where they apply semi-analytical methods to galaxy formation with complete hydrodynamical simulations, including other details such as supernovae explosion dynamics. Classical approaches for DM halos with large sizes use the model of the Navarro-Frenk-White (NFW) profile [972] for the density of dark matter as a function of radius,

$$\rho_{\rm NFW}(r) = \frac{\rho_0}{\left(\frac{r}{r_s}\right)\left[1+\left(\frac{r}{r_s}\right)\right]^2} \ , \tag{1.116}$$

which is divergent in the limit, $r \to 0$. The values of $\rho_0 = \rho_{\rm crit}\Omega_0 h^2$ and $r_s = {}^{r_v}/_{\mathcal{C}}$ represent the characteristic density and scale radius of the profile, both parameters which vary between halos. The scale radius r_s, is defined via the virial radius, r_v and a concentration parameter, $\mathcal{C}$. Further well known example profiles consist of, the Einasto profile [508] and Burkert profile [298]. Switching to the particle nature of DM, models are conventionally categorised as either *cold* [90, 960, 973, 1331], *warm* [242] or *hot* [669, 804, 1156] which were initially introduced in order to define the nature of DM at the time of decoupling. Hot DM arises in particle physics models where the DM candidate has sufficiently high thermal velocities. Models of DM with negligible thermal velocities compared to the expansion of the Hubble flow are primarily considered leading candidates due to numerous observational features and the ability to avoid complications in during the early formation of the Universe. So what exactly is the true nature and origins of a possible DM candidate? The standard approach of assuming a CDM component may present issues with higher relic densities than required or greater predicted substructure on small scales than what is observed. Primarily the literature and historical documentation of recent studies into the properties of DM concerns itself with either weakly interacting massive particles (WIMPs) or massive astrophysical compact halo objects (MACHOs) (sometimes referred to as robust association of massive baryonic objects (RAMBOs) [959]) with highly suppressed luminous emissions [270]. MACHOs focus on the dark nature of DM, where it could in fact be represented by familiar cosmological objects, possibly identified by lensing analysis. There are strong constraints on the

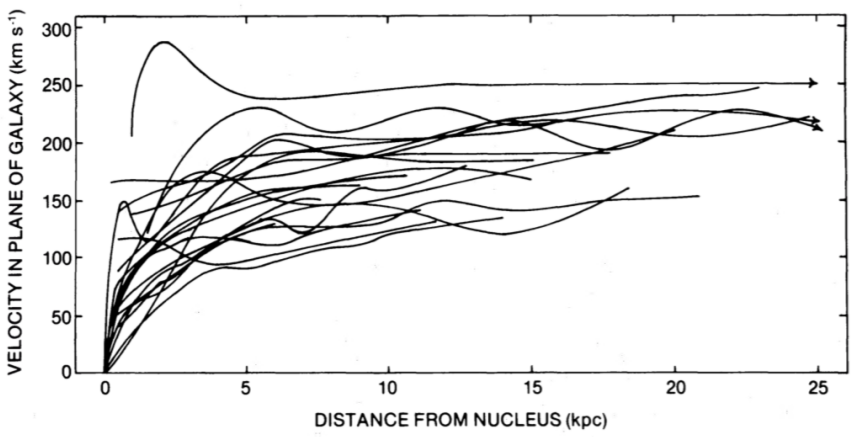


Figure 1.7: Original superposition of 21 Sc galaxy rotation curves which first appeared in Ref. [1130], detailing the unexpected flattened nature of the curves when extending their analysis far beyond the galactic nucleus. Contributions from a significant hidden unseen "matter" sector were determined to be present in order to explain the observed form of these rotational curves. Image credit: Taken from Fig. 6 found in Ref. [1130].

contributions these can make, with microlensing surveys [56, 182] showing a limited number of events [1260]. Whilst potentially accounting for a large quantity of unaccounted for baryonic density, it is well known the possible contributions to DM are therefore minimal, requiring additional external contributions [576, 577]. Understanding these contributions is mainly important in the context of the dynamics and structure of galactic disks. Possible sources are, faint stars and stellar remnants (i.e. brown dwarfs located suitably far into the dark halo) [937, 982, 1387], cold gas clouds and molecular hydrogen [698, 1055], hot intergalactic gas representing the filamentary web which connects the dark halos of groups of galaxies and clusters [979]. Baryonic objects such as brown dwarfs, BHs, and neutron stars are also fairly strongly excluded to exist in galactic halos, suggesting these certainly can't explain previous measurements of halo masses. The treatments of BBN in general also rule out other forms of baryonic matter accounting for a substantial portion of the DM. We must then turn outside of traditional baryonic forms of matter and look more closely at at more exotic models which produce massive relics. WIMPs serve as one of the traditional leading candidates to act as the DM particle, where their

attractive motivations come from their tantalising link between the ability to realise a suitable cosmological relic density of CDM and the possible interaction strength in the electroweak sector.

The WIMP paradigm represents a collection of realisations based upon cosmological implications along with statistical mechanics embedded in particle and nuclear physics. The relic density of WIMP DM can be parameterised as [135],

$$\Omega_\chi h^2 \simeq \frac{s_0 h^2}{\rho_{\rm DM}} \left(\frac{45}{\pi^2 g_*}\right)^{1/2} \frac{1}{x_f M_{\rm Pl}} \frac{1}{\langle \sigma_{\rm ann} v \rangle} \ , \tag{1.117}$$

where the denominator is regulated by the thermally averaged WIMP self-annihilation cross section. The value of s_0 denotes the present day entropy density of the Universe, g_* the number of relativistic degrees of freedom at freeze-out and $x_f \equiv {}^{T_{\rm fr}}/_{m_X} \sim 25^{-1}$, the freeze-out temperature normalised to the particles mass, m_X. By modelling the number of relativistic degrees of freedom at freeze-out and entering known values for the remaining parameters [995], defines the normalised density relation in terms of the thermally averaged WIMP annihilation cross section, $\sigma_{\rm ann}$ and the WIMP relative velocity, v,

$$\Omega_\chi h^2 \simeq \frac{0.12}{\left\langle \frac{\sigma_{\rm ann} v}{10^{-36}{\rm cm}^2 0.1c} \right\rangle} \ , \tag{1.118}$$

demonstrating that a cross section of weak scale strength, with some WIMP candidate possessing typical velocities at freeze out, generates the correct relic density of DM we expect today. This thermal *miracle* is the stark realisation that the DM particle could simply be generated from new electroweak physics occurring at the Fermi scale, i.e. $\sigma \sim G_F^2 T^2$ where $G_F \simeq 1.1663787 \times 10^{-5}$ GeV$^{-2}(\hbar c)^3$ [1243] is the Fermi constant and T represents the typical freeze out temperature, whilst implying the field mass should also be of the same order. Despite this there are a number of issues with WIMP candidates such as the validity of the mass scale, the true relic abundance of DM with specific candidates, the true nature of couplings and relationship with new physics appearing around and above the Higgs scale, and of

course arguably the only required issue to understand, a distinct continuous lack of any experimental signal [1120]. There are many WIMP candidates [1120] such as the lightest neutralino [517, 611], two Higgs doublet models [269], little Higgs [95–97, 1154] and sneutrinos [653, 737], some practically ruled out, others still offering an interesting possibility to using familiar physics to solve this cosmological dilemma. The above issues have lead many to now consider this general sector of research as a possible mathematical misnomer, superfluous to further investment, extending searches far beyond Standard Model motivated candidates.

There are a myriad [135] of excellent candidates which attempt to provide theoretical solutions to account for the total DM density whilst tackling the problematic nuances along the way. Specific examples include: warm DM [241], mixed DM [857], self-interacting DM [43, 1053, 1207, 1278, 1319], self-annihilating or decaying DM [384, 771], fuzzy dark matter (FDM) [722], modified Newtonian dynamics [187, 935, 945], strongly interacting massive particles (SIMPs), saxion DM [782], gravitino DM [192, 246, 573, 1214], non-topological solitons or Q-balls [828–830], Chaplygin gas [201, 220, 221], axino DM [345, 382, 383], majorons [205], branons or brane world DM [330], sterile neutrinos [7, 264], minimal DM [354, 355], primordial BHs as the DM [311, 320, 1011], wimpzillas [348, 817, 831], mirror matter [548, 956, 993] or exotic types of matter present in a hypothetical hidden sector or mirror world [204], Kaluza-Klein (KK) particles [338, 1173, 1174] and finally pseudo-Nambu Goldstone boson (pNGB) or axion DM [482] to name but a few. Despite all these possible confusions it could certainly be argued that this is not the most perplexing issue still evading theorists and experimentalists in terms of observationally observed and undefined energy. Although more traditionally considered as separate problems, the vacuum energy of the Universe could potentially be understood through models which may actually have a close relation to some of the best DM candidates using the physics of fundamental scalar fields.

1.7.3 A Quintessential Quandary

The standard cosmological model is an extremely successful framework to describe the nature of the core features we observe in our cosmological evolution. In particular, the previously mentioned nature and features of the CMB, the formation of galactic and large scale structure, the abundances of light atomic structures and the incorporation of a universe undergoing an accelerated expansion. This last feature is theoretically plagued with two of the most troublesome questions regarding model construction beyond standard ΛCDM concerns. The aims of UV completion and the incorporation of physics to account for the almost certainly confirmed observation that our universe is accelerating, must answer two pressing issues:

- *The cosmological constant problem* - One of the largest issues at the heart of unification between a relativistic quantum field theory (QFT) and observational cosmology. This famous discrepancy spanning approximately one hundred and twenty orders of magnitude is an unavoidable enigma which can be understood on the basis of two very different scales. The cosmological constant introduced by Einstein into his field equations for an expanding Universe predicts a gravitational contribution to the vacuum fluctuations. The observed value of the cosmological constant is measured to be of the order, $\Lambda_{\text{obs}} \sim 10^{-120} M_{\text{Pl}}^4$. On the other hand, QFT tells us that the matter components of the Universe are quantised, possessing a continual non-vanishing energy density even when under its vacuum state description. The form of the stress energy tensor is $\langle T_{\mu\nu} \rangle = -\langle \rho \rangle g_{\mu\nu}$ where $\langle \rho \rangle$ is understood as a summation over the zero-point energies for a collection of independent harmonic oscillators, up to some cutoff scale on the theory. Even up to scales $\Lambda_{\text{Cut}} \sim \mathcal{O}(1)$ TeV, which the Standard Model has been tested to extensively, the theoretical value of the cosmological constant is, $\Lambda_{\text{Theory}} \sim 10^{-60} M_{\text{Pl}}^4$. The possible scale of this issue is approximated using the infamous catastrophic theoretical and observational vacuum energy ratio when the cut off scale is

taken to the Planck scale, revealing the full one hundred and twenty orders of magnitude separation in the two values.

- *The coincidence problem* - The ratio of the energy density of DM and DE at the current time as inferred from observational measurements is, $\rho_{m,0}/\rho_{\Lambda,0} \sim \mathcal{O}(1)$, which suggests fine tuning is required for the model to reproduce the data. This fine tuning would rectify the uncomfortable notion that the cubic inverse scaling power law for matter matches the constant evolution of the cosmological constant in the current epoch. Why exactly this period of physics is occurring at our time of observation is a mystery potentially understood as either coincidental or something more fundamental, either of which propose interesting questions regarding the dynamics of DE.

Historically there are several distinct signatures that provide evidence for the nature of the present epochs expansion rate. Various contributions consist of, Type-1a Supernovae acting as standard candles [806, 1051, 1108], which can be calibrated to provide quality distance measurements irregardless of the surrounding complications of the host galaxy. The temperature anisotropies of the CMB can be used in order to measure and place independent constraints on the properties of the cosmic densities, implies that it is dominated by acoustic peaks from sound waves in the photon-baryon fluid. The positional structure of these peaks is a strong indicator of the properties of cosmic expansion. The characteristics of the CMB photons which are susceptible to distortions in the CMB spectrum through inverse Compton scatterings, where such known signatures are described using the Integrated Sachs-Wolfe effect, occurring over large angular scales [1135, 1166]. Measurements of the matter power spectrum and the presence of BAOs acting as a *standard ruler* [362, 479, 1377], related to over densities or clustering of baryonic matter at specific length scales, can generate measurements to be made and compared with the theoretical estimates on three-dimensional position measurements of galaxies and sound horizon scales of large scale structure. Weak gravitational lensing can be used to determine the nature of DM and how its clustering is effected by the presence of

DE, through estimates on the distributions on distant objects and the geometrical nature of the spacetime manifold [690, 1179]. Measurements and analysis of the *cosmic shear* of galaxies, through weak lensing effects indicate the Universe is now in a phase of cosmic acceleration. These methods can also be applied to numerous other cosmological energy sources, white dwarfs [528], clusters of galaxies [59, 654, 1325] and expansion dynamics [559, 1382] etc.

Like most issues, some of which we have covered that refuse to enlighten theorists with an obvious conclusion, the two issues above have a wide array of proposed novel solutions which attempt to bring together the problematic nature of vacuum energy into a singular defined solution [375, 1275, 1343], utilising dynamical/geometrical extensions beyond the cosmological constant model [514]. Some examples consist of holographic models of DE, which aim to use the principles of holography and dimensional analysis [1226, 1238] in order to parameterise the DE density using an infrared cutoff length scale [1327]. Various models consist of, original holographic DE [851], new agegraphic [1180] and Ricci DE [1389]. Modifications to gravity at large distances and Einstein's tensor in his field equations [358, 413, 1203, 1274] with examples including the Dvali-Gabadadze-Porrati (DGP) model [490], the α DE extension to this [487], double coupled massive gravity [694] and vacuum metamorphosis [304, 1015, 1016]. Popular models often materialise as general minimal models incorporating additional matter fields. The simplest and leading theory in terms of phenomenological models is the *quintaessentia* inspired model of dynamical quintessence [166, 276, 277, 534, 566, 858, 1094, 1137, 1138, 1194, 1284, 1346, 1395]. Other examples of scalar-field/matter theory applied as minimal extensions are *k-essence* models [42, 102, 415], ghost condensation [99, 1058], kinetic gravity braiding [422, 807, 980, 1082] and the Chaplygin gas model [200, 756, 764], normally formulated using D-brane theories. Other states of matter can also act as the quintessence field [852] such as vector fields [101], fermionic spinor fields [1105, 1276, 1370], p-form fields [400, 815] and fields with exotic nature [243, 421, 942].

The general quintessence model can be understood using the action of a canonical

scalar field, minimally coupled to gravity, its potential defined in such as way to allow for a successful mimicking of the cosmological constant on large scales. The evolution of this dynamical DE is slow enough to give rise to a negative pressure, hence a solution to both accelerated expansion and apparent late time domination by the mysterious energy. The quintessence action for non-relativistic matter acting as a barotropic perfect fluid is,

$$S_{\rm Quin} = \int d^4x\sqrt{-g}\left[\frac{1}{2}M_{\rm Pl}^2\mathcal{R} - \frac{1}{2}g^{\mu\nu}\partial_\mu\phi\partial_\nu\phi - V(\phi)\right] + S_{\rm m} \ , \tag{1.119}$$

with $S_{\rm m}$ is canonical action for matter (Eq. (1.13)). In a flat FLRW universe the field in usually constructed using a sum of a homogeneous component and a small perturbation, which for the purposes of reproducing an effective cosmological constant on large scales, allows for a removal of the inhomogeneous piece present in the equations of motion. The dynamical evolution of the field is normally understood in two main classes, denoted as thawing or freezing models [301]. We now recover the scalar dynamics covered in Section 2.7 where the equations of motion for the quintessence field follow the continuity equation found in Eq. (1.42). The equation of state for the additional matter must follow, $p_\phi < -\rho_\phi/3$, for late time acceleration as well as the general slow roll condition $\dot{\phi} \ll V(\phi)$, for the kinetic field component. These conditions fix the scale of potential where we require the approximate scale proportionality, $H \sim \sqrt{\partial^2 V/\partial\phi^2}$. The new scalar field mass must then be proportional to the Hubble scale today,

$$m_\phi \leq H_0 \approx 10^{-33} \text{ eV} \ . \tag{1.120}$$

The equation of state for DE is often re-parameterised, i.e. Chevalliear-Polarski-Linder (CPL) parameterisation [340, 868] or Wang parameterisation [1328] etc. in order to adopt a functional form to track its evolution [375, 868]. An example common general expression is a scale factor dependent equation of state of the form

[340, 868],

$$\omega(a) = \omega_0 + \omega_a (1 - a) \ , \tag{1.121}$$

where ω_0 represents the equation of state and ω_a its derivative with respect to the logarithm of the cosmic scale factor at present time. Such models allow for the exploration of possible tensions with the standard ΛCDM model using specific model parameter measurements. This form of $\omega(a)$ also allows for the re-parameterisation of the Hubble parameter,

$$H^2(a) = H_0^2 \left[\Omega_m a^{-3} + \Omega_r a^{-4} + \Omega_\Lambda a^{-3(1+\omega_0+\omega_a)} e^{-3\omega_a(1-a)}\right] \ . \tag{1.122}$$

The determination of $\omega(a)$ will shed a light on whether our Universe is currently being accelerated by a quintessence field or other options such as phantom energy [303] or quintom cosmology [299]. With $\omega_a = 0$ fixed, the current value today is currently constrained to,

$$\omega(a) = -1.028 \pm 0.03242 \quad (68\% \text{ CI}) \ , \tag{1.123}$$

from the Planck TT,TE,EE+lowE+lensing+SNe+BAO data [40]. Allowing w_a to vary leads to slightly different bounds on the value of H_0,

$$H_0 = (68.35 \pm 0.82) \text{ kms}^{-1}\text{Mpc}^{-1} \ , \tag{1.124}$$

$$H_0 = (68.34 \pm 0.83) \text{ kms}^{-1}\text{Mpc}^{-1} \ , \tag{1.125}$$

where ω_a is not allowed and allowed to vary respectively. Current observations fail to enlighten us to the nature of the DE we could be dealing with, leaving concordance cosmology as a suitable first order model. The coincidence side of the problem is normally treated with so called tracker solutions [124, 302, 374, 534, 668, 1124, 1136, 1218, 1395].

Dynamical models of DE can also act as mechanisms to alleviate tensions in other

areas in cosmological models. So called *early DE* models [474, 712], provide non-negligible contributions from DE at early times, i.e. $m_\phi \gtrsim H_0$. The value of H_0 in Eq. (1.86) has a potential discrepancy referred to as the *Hubble tension* or H_0-*tension*. This recent statistically significant tension has manifest itself through an analysis of values of the Hubble expansion rate today from both supernovae data and CMB observations. Supernovae data has been found and continues to show evidence of preferring larger values of H_0. For example recent local supernovae measurements calibrated using Cepheid star variables in host galaxies has returned the value [1107],

$$H_0^{\rm Local} = (74.03 \pm 1.42)\ {\rm kms}^{-1}{\rm Mpc}^{-1}\ . \tag{1.126}$$

Comparing the value in Eq. (1.126) to those inferred from Planck CMB and ΛCDM presents a discrepancy at the level of 4.4σ [1107]. There are also many other techniques or measurements which have reenforced this issue, with approximate data combinations now returning discrepancies with the early Universe results found in Eq. (1.86) ranging from $\gtrsim 4\sigma \sim 6\sigma$. See Refs. [1106, 1295] or the discussions in Refs. [224, 248, 1110–1112] for a summary of the current status of the Hubble tension along with an analysis of the significance of these values and the methods used to acquire them. Naturally there have been several different approaches deployed in order to offer a possible resolution to this issue. Examples include models of dark radiation [207] and early DE [1072]. These measurements are essentially independent constructs yet they almost agree. Whether this deviation is emergent from troublesome systematics or a hint at something deeper in the physics is yet to be clarified, offering an interesting topic of debate in the era of precision cosmology over the forthcoming years.

Chapter 2

The Strong CP Problem and the Axion

> "*There must be a beginning of any great matter, but the continuing unto the end until it be thoroughly finished yields the true glory.*"
>
> Letter to Sir Francis Walsingham
> Sir Francis Drake (May 1587)

2.1 The Standard Model of Particle Physics

2.1.1 A Quantum Theory of Fields

The Standard Model of particle physics [15, 958, 1052] represents one of the greatest accomplishments of fundamental physics to date, the theoretical apogee representing a spectacular revolution in our understanding of nature across the 20^{th} century, forming the mathematical framework of the fundamental forces among the experimentally verified defining constituents of matter. Subdivided into two defining categories, the first class of components of the Standard Model, defines the fermionic sector of particles with fractional spin, organised into three families which are are further sub-dived into leptons and quarks. Quarks come in six different flavours,

u, d, s, c, b and t[1] with fractional charges, $Q = {}^{2}/_{3}, -{}^{1}/_{3}, -{}^{1}/_{3}, {}^{2}/_{3}, -{}^{1}/_{3}$ and ${}^{2}/_{3}$, in units of the elementary charge e, respectively. The known leptons are the electron, e^{-}, muon, μ^{-}, and tau, τ^{-}, which are each partnered with the corresponding neutrinos, ν_e, ν_μ and ν_τ respectively. The observed matter particles formed from quarks represent colourless composite structures, incorporating either two or three quark combinations. The baryons are made from three quarks such as the neutron, $n \sim ddu$ and the mesons are formed from quark, anti-quark pairs such as the neutral pion, $\pi^0 \sim u\bar{u}/d\bar{d}$. The second class of components are the elementary vector gauge bosons of spin, $s = 1$, each of which are associated to the generators of their respective gauge representation groups. The complete Standard Model is built as a quantum field theory based on the specific gauge symmetry group,

$$G = SU(3)_{\mathrm{C}} \otimes SU(2)_{\mathrm{L}} \otimes U(1)_{\mathrm{Y}} \ , \tag{2.1}$$

where $SU(3)_{\mathrm{C}}$ is the symmetry group representing the colour interactions. The gauge bosons for colour interactions are the eight massless gluons, g_i, where $i = 1 \ldots 8$. The remaining $SU(2)_{\mathrm{L}} \otimes U(1)_{\mathrm{Y}}$ symmetry represents the electroweak interactions, a subgroup of which forms the group of the unified electromagnetic interactions, $U(1)_{\mathrm{em}}$. The perturbative theory of the electromagnetic quantum vacuum is known as quantum electrodynamics (QED) [536]. The four vector gauge bosons of $SU(2)_{\mathrm{L}} \otimes U(1)_{\mathrm{Y}}$ are the photon, γ and weak gauge bosons, $W^{\pm}$ and Z^0. Like the colour charge mediators, the photon is massless, however the weak gauge bosons are experimentally observed as massive, self-interacting particles. The significance of this property in the low energy spectrum represents the fact that $SU(2)_{\mathrm{L}} \otimes U(1)_{\mathrm{Y}}$ is in fact not a true symmetry of the vacuum. The Standard Model group structure in Eq. (2.1) is required to be spontaneously broken down to a further group, which by construction is a true symmetry of the vacuum,

$$SU(3)_{\mathrm{C}} \otimes SU(2)_{\mathrm{L}} \otimes U(1)_{\mathrm{Y}} \rightarrow SU(3)_{\mathrm{C}} \otimes U(1)_{\mathrm{em}} \ , \tag{2.2}$$

[1] up, down, strange, charm, bottom and top

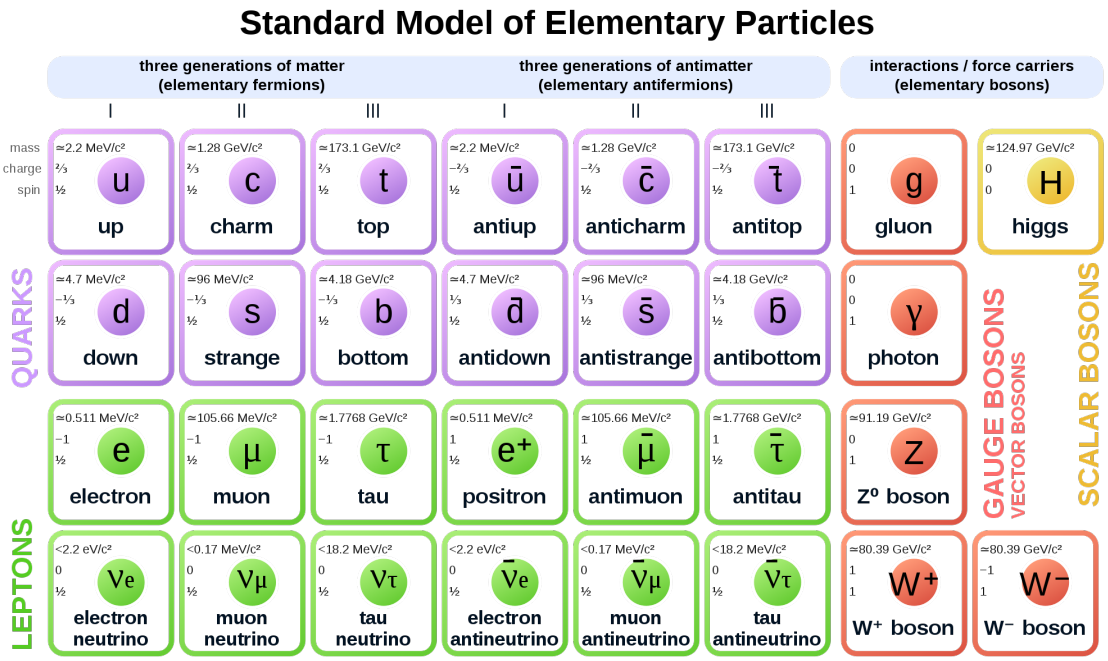


Figure 2.1: The complete framework of the Standard Model of particle physics. Each of the fields represented have been experimentally confirmed and form our best understanding of how matter and the fundamental forces interact. The fermions are comprised of twelve elementary particles of spin $1/2$, in three generations which obey Pauli's exclusion principle. Each particle has its own antiparticle which defines the antimatter content of the Standard Model. The gauge bosons, manifest under the gauge group representation of Eq. (2.1), define the force carriers that mediate the fundamental interactions of the strong, weak, and electromagnetic forces. The Higgs boson is the only fundamental scalar required to describe the elementary-particle masses. Image credit: Taken from `https://commons.wikimedia.org/wiki/File:Standard_Model_of_Elementary_Particles_Anti.svg`.

a theoretical exercise implemented by the well-known *Brout-Englert-Higgs-Guralnik-Hagen-Kibble mechanism* [292, 521, 643, 644, 704]. Initially the vector gauge bosons are massless, coupling to both themselves and the massless fermions in the theory. The non-abelian Glashow-Weinberg-Salam theory of the electroweak sector postulates the addition of scalar bosons with gauge invariant couplings to each of the vector bosons and fermions incorporated. The self-coupling interactions of the newly introduced scalar define its potential to be in the form found in Eq. (2.52). The simplest example of these models introduces a single complex Higgs multiplet, which transforms as a doublet under weak $SU(2)$ gauge symmetry. Once the new

field gains a non-zero vacuum expectation value (VEV) the symmetry is spontaneously broken, due to the form of the potential. The relevant transformations which leave the field at its minimum invariant are associated to electric charge, i.e. electromagnetism remains a symmetry property of the vacuum when the additional scalar field obtains a VEV. The four scalar degrees of freedom from the introduced complex Higgs doublet factorise out of the physical theory, three of which are the massless Goldstone bosons, absorbed and assigned to the longitudinal polarisation components of the massive vector bosons. The remaining neutral component is associated to a physical scalar field known as the *Higgs boson*, the recently discovered final piece of the fundamental jigsaw displayed in Fig 2.1 [3, 336]. The fields renormalisable interactions are deemed such that the Higgs field acquires a VEV which fixes the scale of electroweak symmetry breaking, $v \approx 246$ GeV. The fermions receive their masses through Yukawa type interactions of the form,

$$\mathcal{L}_{\text{Yukawa}} = f_e^* \bar{l}_L \phi e_R + f_u^* \bar{q}_L \tilde{\phi} u_R + f_d^* \bar{q}_L \phi d_R + h.c. \; . \tag{2.3}$$

The first terms consists of most general gauge-invariant renormalisable Lagrangian terms involving the Higgs doublet and leptons for a single generation. The value of f_e^* represents a dimensionless coupling constant[2], e_R an $SU(2)_L$ singlet and $\bar{l}_L$ an $SU(2)_L$ anti-doublet fermion field. The second and third relate to the up and down quarks respectively. In these terms $\bar{q}_L$ represents an $SU(2)_L$ quark doublet with u_R and d_R the up and down quark singlets respectively. Finally ϕ represents the an $SU(2)_L$ doublet for the Higgs field which in unitary gauge takes the form,

$$\phi = \begin{pmatrix} 0 \\ (v+h)/\sqrt{2} \end{pmatrix} \tag{2.4}$$

[2]The coupling constant is in general complex but its phase can be absorbed into a physically consistent redefinition of the phase for the right-handed electron field in order to consider a real valued variable.

with dimensionless constant λ, where h is a field of mass, $m_h = \sqrt{2\lambda v^2}$ and the value of v is defined above from the scale of electroweak symmetry breaking. The conjugate Higgs doublet is denoted by $\tilde{\phi}$ given by,

$$\tilde{\phi} \equiv i\sigma^2\phi^* = i \begin{pmatrix} 0 & -i \\ i & 0 \end{pmatrix} \begin{pmatrix} \phi^- \\ \phi^{0*} \end{pmatrix} = \begin{pmatrix} \phi^{0*} \\ -\phi^- \end{pmatrix} \ . \tag{2.5}$$

After consideration of the Higgs doublet representation at the potential minima take the form,

$$\mathcal{L}_{\text{Yukawa}} = \frac{f_e v}{\sqrt{2}} \left(\bar{e}_L e_R + \bar{e}_R e_L\right) + \frac{f_u v}{\sqrt{2}} \left(\bar{u}_L u_R + \bar{u}_R u_L\right) + \frac{f_d v}{\sqrt{2}} \left(\bar{d}_L d_R + \bar{d}_R d_L\right) \ , \tag{2.6}$$

where the relevant mass terms for the fermions can now be identified as,

$$m_i = -\frac{f_i v}{\sqrt{2}}; \quad i = e, u, d \ . \tag{2.7}$$

The points above represent a minor snapshot of a remarkable collective piece of work, responsible for many outstandingly accurate predictions across the field of modern particle physics. Of particular note are precision tests of QED and results for the fine structure constant and the anomalous magnetic moment of the electron [83–85, 667]. After spontaneous symmetry breaking occurs (see Fig 2.3) the factorised Standard Model Lagrangian takes the general factorised form,

$$\mathcal{L}_{\text{SM}} = \mathcal{L}_{\text{Gauge}} + \mathcal{L}_{\text{Yukawa}} + \mathcal{L}_{\text{Higgs}} + \mathcal{L}_{\text{Fermion}} \ , \tag{2.8}$$

determined by the standard approach of modelling the electroweak gauge sector in a consistent renormalisable field-theory capable of reproducing all current experimental data.

The complete picture of the Standard Model interactions explained above in Eq. (2.8) can be expressed in the grandiose, completely expanded form of the Standard Model Lagrangian density found in Eq. (A.1) of Appendix A. This collection of terms rep-

resent both a beauty in our ability to write down an effective description of many of the phenomena we observe, but does however still form a stark reminder that our current best understanding of fundamental physics from a completionist point of view, houses a rather large number of free parameters formed from the complex products of essentially arbitrary gauge sub-groups. This unsatisfactory aesthetic offers no pleasing clarification for the values these parameters should take and the measured hierarchy between them. There is also no routed understanding in this equation as to why the heavier fermionic families exist in the manner they do, along with the three-generational groupings and the apparent deviations in their Cabibbo-Kobayashi-Maskawa (CKM) mass matrix mixings etc. There is no defining reason as to why the structure of these particular facets, i.e. charge quantisation of the specific multiples of the fermionic sectors families, lead us to the electrical neutrality of atoms. The fermion masses generated via interactions of the form in Eq. (2.6) and associated dimensionless couplings, possess a logarithmic sensitivity to a scale in which any new physics, Λ is deemed relevant. The observed Higgs boson of the Standard Model (which we now refer to with the H notation) as a scalar component of the theory has a quadratic sensitivity to this hypothetical parametrically higher scale, the observable mass squared term taking the following form,

$$m_{\mathrm{H}}^2 = m_{\mathrm{H},0}^2 + \frac{kg^2\Lambda^2}{16\pi^2} \approx \sqrt{\frac{\lambda}{2}}v \ , \tag{2.9}$$

where g is the electroweak coupling constant, k is a constant of $\mathcal{O}(1)$ variation, λ is the Higgs self coupling strength and $m_{\mathrm{H},0}^2$ is the true fundamental parameter of the theory referred to as the tree-level bare mass. The value of the final term has been previously defined in the discussions surrounding Eq. (2.6). If Λ is in fact significantly larger than the electroweak scale, associated to the observable Higgs, then the theory must also possess unnatural cancellations to counter significant corrections from the quadratically-divergent corrections stemming from higher order loop diagrams. It is at least expected the integrals should be cut-off at the scales which re-introduce gravity, i.e. the Planck scale, naively fixing $m_{\mathrm{H}} \sim \mathcal{O}(\Lambda) \sim$

$\mathcal{O}(M_{\rm Pl})$. The ability to allow for a stabilisation of the electroweak scale and observed Higgs mass with expected fundamental scales of the theory, often gives rise to models which inject new physics occurring just above the electroweak scale, collectively known as *supersymmetric* theories [919], which originally appeared in attempts to generalise the Poincaré algebra to mix representations with different spin [613, 1314, 1345]. These theories introduce a new boson-fermion symmetry. Formally in a relativistic field theory we must introduce graded Lie algebras, which are formalised by the representation of the Super-Poincaré Lie algebra possessing supersymmetry generators of the general form,

$$\bar{Q}\,|Boson\rangle \sim |Fermion\rangle\,; \quad Q\,|Fermion\rangle \sim |Boson\rangle \ , \tag{2.10}$$

where Q and $\bar{Q}$ represent Weyl spinors related by the ani-commutation relation $\{Q_\alpha, \bar{Q}_{\dot{\beta}}\} = 2(\sigma^\mu)_{\alpha\dot{\beta}} P_\mu$. Here P_μ represents a Poincaré operator and $\sigma^\mu = \{\mathbf{1}, \sigma\}$ the four vector of Pauli matrices. Precise measurements of the gauge unification coupling constants in Eq. (2.1) numerically predict the running of the renormalisation group equations do not unify by several deviations of σ. Supersymmetric generalisations of this exercise with sufficiently low scales, $\mathcal{O}(1)$ TeV, do however make unification a possible reality. Currently any signs of supersymmetry are evasive in ongoing efforts to identify any trace of signals for new underlying physics and may be the defining prerogative of future incarnations of high-energy colliders [516, 899].

Returning to the Standard Model, the theoretical formulation of the Higgs boson scattered amongst the terms of Eq. (A.1) and its eventual discovery finalised the shape this completed framework should take, representing both a necessary, and striking solution to understanding the mechanics behind the electroweak sector. Its discovery by both the ATLAS and CMS collaborations experimentally reinforced the scale of the issue at hand, detailed in Eq. (2.9), which is often formally referred to as the *hierarchy problem* of the Standard Model. Supersymmetric theories offer protection of the low energy theory against radiative corrections due to the pres-

ence of contributions from the newly introduced super-partner particles in the loop integrals.

2.1.2 Problems with The Standard Model

Despite its prestigious successes within the field of particle physics the Standard Model along with numerous validations of its predictions, made under its gauge field representation, there are number of further intimidating issues yet to be suitably addressed. An obvious additional aspiration is the ability to provide a natural candidate for the DM particle in cosmological models and an explanation of the myserteous nature of DE. It is clear even only from the hierarchy problem alone that the Standard Model requires a significant expansion to incorporate the new physics required to correctly understand the deeper routes and theoretical questions surrounding the origins of mass generation. Further specific examples of major empirical and cosmological issues/tensions consist of:

- *The nature of neutrinos.* The construction of the Standard Model leaves neutrinos under their chiral representation both massless and left-handed. Observations of neutrino flavour oscillations [575] conclude that these particles should possess a theoretical mechanism to produce massive states, with their masses related by unitary mixing of the Pontecorve-Maki-Nakagawa-Sakata (PMNS) matrix. The true understanding of neutrinos often spans to physics beyond the Standard Model, a primary example is the mysterious nature of right-handed neutrinos of opposite chirality. These are expected to be represented as singlets under all gauge interactions and potentially completely understood using sterile neutrino models [264, 478].

- *Muon anomalous magnetic moment* - The briefly mentioned successes of the Standard Model to explain the anomalous magnetic moment of the electron actually relates to one of obvious tensions of the Standard Model when looking at the properties of the Muon. Unlike the electron, the calculation of the

anomalous magnetic moment of the Muon presents a theoretical prediction of $0.5 \times (g_\mu - 2) = 0.00116591803(69)$ [1021] and an experimental result of $0.5 \times (g_\mu - 2) = 0.00116592091(9)$ [957]. This difference represents a deviation of more than 4σ, a result which could suggest a hint for new physics required to explain the variations in the loop integrals.

- *Inflation* - The inflationary paradigm [647] was introduced to understand the apparent origins of matter in the observable Universe, a solution to the horizon and flatness problems. During an extreme phase of acceleration, primordial density perturbations are stretched from sub-Hubble to super-Hubble length scales. Observationally this approach is supported by precision measurements of perturbations in the CMB. We have already commented on the only natural candidate in the Standard Model to represent the inflation field, the Higgs boson. It is often a complicated procedure to embed this idea successfully and so the introduction of additional scalars represent the standard approach to model construction.

- *Matter-Antimatter asymmetry* - The baryon asymmetry of the Universe is defined as the difference between the number of baryons and anti-baryons, divided by their sum or entropy just before antiprotons disappeared from the primordial plasma. The value of the asymmetry is parameterised in terms of the ratio,

$$\eta_{\rm mat} = \frac{n_{\rm B}}{n_\gamma} \equiv \eta_{\rm anti-mat} \simeq 10^{-10} \ , \tag{2.11}$$

where $n_{\rm B}$ and n_γ represent the number density of baryons and the cosmic background radiation photons respectively. This quantity well measured by both data from the cosmic background anisotropy determined by the Wilkinson-Microwave-Anisotropy-Probe (WMAP) [1208] and BBN physics [1215]. This value suggests that the current significant matter-antimatter asymmetry was actually much smaller in the past. In 1967 Andrei Sakharov defined the conditions used to quantify how to generate the asymmetry we measure, something

which may be understood in terms of microphysical laws:

1. *The theory must violate fermion number.*
2. *The laws of nature must violate C and CP symmetries.*
3. *The fermion number violating processes must be out of equilibrium in the Universe.*

Both the Standard Model of particle physics and cosmology do actually successfully predict the Sakharov conditions to be satisfied [832]. The Baryon number is violated by sphaleron processes and the non-equilibrium condition apparent due to the expansion of the Universe. The final condition and a key area of focus in this thesis concerns the violation of P and CP symmetries, violated by the weak interactions and quark Yukawa couplings [346, 1369]. However, the magnitude of the CP-violating Kobayashi-Maskawa phase with the measured mass of the Higgs particle lead to the conclusion it is extremely difficult to realise successful baryogenesis within the current form of the Standard Model. Measurements of CP violation are also still too small. The ability to fully explain the origins of the primordial matter-antimatter asymmetry is still a defiant mystery.

The overriding message from the details above is we still require our understanding to evolve significantly before a more unified picture becomes experimentally perceptible. Theoretical physics provides many exciting and sometimes divisive options to explore these directions in the meantime. These novel and seemingly required extensions to the Standard Model can also often provide a coupled solution to the issues detailed above, reintroducing the comforting feeling of naturalness, albeit it is often required to move into a vastly more complicated landscape beforehand (general supersymmetric GUT extensions). One final problem inherent to the Standard Model and a further example of a fine-tuning problem is known as the *strong CP problem*. Its favoured solution offers a captivating frontier in both fundamental particle physics and cosmology. Its historical origins come from a more detailed look at

the complexities involved in the colour interactions and the gauge group structure in Eq. (2.2), which serves as the theoretical catalyst for the work presented in this thesis.

2.2 Quantum Chromodynamics and the $U(1)_A$ Problem

One of aforementioned fundamental forces of nature, the strong interactions of particle physics, is a *non-abelian* gauge theory used to describe all known nuclear phenomena. The theory formulated to understand these interactions is formally known as Quantum Chromodynamics (QCD) and as a QFT, possess many features qualitatively different as to using a classical field theory approach. The bare non-Abelian gauge theory QCD Lagrangian for N quark flavours, ψ_r^a with masses m_r is,

$$\tilde{\mathcal{L}}_{\text{QCD}} = -\frac{1}{4} G^a_{\mu\nu} G^{a,\mu\nu} + \sum_{r=1}^{N} \bar{\psi}^a_r \left(i \not{D}^b_a - m_r \delta^b_a \right) \psi_{rb} \ , \tag{2.12}$$

with covariant derivative, $\not{D}^b_a = \gamma_\mu \left(\partial_\mu \delta^b_a + i g_s \frac{1}{2} \lambda^i_{ab} A^\mu_i \right)$ and $SU(3)$ gauge group generators λ^i_{ab}. The index r runs over all the quark flavour species of the theory. The gluon field strength tensor is defined as,

$$G^a_{\mu\nu} \equiv \partial_\mu A^a_\nu - \partial_\nu A^a_\mu - g_s f_{abc} A^b_\mu A^c_\nu \ , \tag{2.13}$$

where f_{abc} are the $SU(3)$ structure constants and A^a_ν, the gluon field strength. The initial foundations of the axion field, which has become a dynamic and prevailing feature of many theoretical extensions to the Standard Model, stem from the consistent structural complexities of Eq. (2.12) and the elegant solution proposed to understand the so called *strong CP problem* it inherits. Before we address this we need to understand a troubling aesthetic question of the theory regarding *why the structure of the QCD vacuum doesn't appear to break charge-parity (CP) symmetry.*

The roots of the answer to this question begin with the symmetry properties of the theory of QCD via the experimentally apparent hadronic spectrum of quark condensates. Initially it was pointed out that in the massless limit for the quark masses the Lagrangian in Eq. (2.12) possesses a global chiral $U(1)_{\mathrm{V}} \otimes U(1)_{\mathrm{A}}$ symmetry in which the fields transform under the following rotation,

$$\psi \to e^{i\alpha} \otimes 1_3 \psi \ , \tag{2.14}$$

for singlet vector transformations and,

$$\psi \to e^{i\alpha\gamma^5} \otimes 1_3 \psi \ , \tag{2.15}$$

for singlet axial transformations, where α is a real number and γ^5 is a product over the four gamma matrices, $\gamma^5 = i\gamma^0\gamma^1\gamma^2\gamma^3$. The vector symmetry of the model is invariant as it is non-chiral and not broken by the condensate. This symmetry corresponds to baryon number conservation via Noether's theorem. Experimentally we know, that in the limit of vanishing quark masses this is not a realisation of nature, i.e. the three lightest quarks, u, d and s can be considered under the more general group, $U(N_f)_{\mathrm{V}} \otimes U(N_f)_{\mathrm{A}}$, where $N_f = 3$ represents the number of flavours we are considering. There are then, nine conserved axial currents which break the vacuum of the general symmetry group. The axial part of this general group structure is in fact spontaneously broken into the further decomposed group structure, $SU(N_f)_{\mathrm{V}} \otimes U(1)_{\mathrm{A}}$. Using Goldstone's theorem, spontaneous symmetry breaking leaves us with a spectrum of massive Goldstone bosons. Experimentally these bosons are realised in nature as the octet set of light, but explicitly non-zero mass pseudo-Nambu-Goldstone bosons (pNGB). These are the three pions π^0, $\pi^{\pm}$, the four kaons K^0, $\bar{K}^0$, $K^{\pm}$ and the eta meson η. At this point, theory and experimental evidence seemingly diverge, where the required realisation of the diagonal $U(3)_{\mathrm{V}}$, cannot be accounted for via the spontaneous breakdown of the $U(1)_{\mathrm{A}}$ symmetry. To account for this we would require a further breakdown corresponding

to a ninth *light* pNGB, which to date has no experimental candidate to match this required feature of the theory. The closest candidate is the η' meson which has the approximate mass, $m_{\eta'} \approx 960$ MeV. The bound on the $U(1)_{\rm A}$ boson however is fixed by the mass of the pion m_π, to the limit,

$$m_{U(1)_{\rm A}} \lesssim \sqrt{3} m_\pi \ , \tag{2.16}$$

which rules out a clear and simplistic understanding for the fundamental nature of this region of the spectrum. This comprehension determines the symmetry issue reducible only in the massless limit unless new physics is introduced to account for this deviation from our theoretical expectations. The absence of a valid candidate for the $U(1)_{\rm A}$ Goldstone boson or the discrepancy between its expected mass is known as the $U(1)_{\rm A}$ problem [1334]. This troublesome $U(1)_{\rm A}$ current has an anomalous divergence at the quantum level, where its solution must be forged from a deeper understanding of the QCD vacuum structure and a treatment of its chiral anomaly [38]. The presence of this anomaly means that the divergence of the axial current is non-vanishing. The symmetry breaking can actually be realised not through quantum symmetries of the QCD gauge theory but from Adler-Bell-Jackiw (ABJ) anomalies [1236]. The presence of the chiral anomaly means that the divergence of the remaining axial current is non-vanishing from quantum corrections of triangle graph configurations,

$$\partial_\mu J_5^\mu = \frac{\mathcal{C} g_s^2}{32\pi^2} G^a_{\mu\nu} \tilde{G}_a^{\mu\nu} \ , \tag{2.17}$$

up to some numerical constant $\mathcal{C}$ and gauge coupling constant term g_s. The term furthest to the right in Eq. (2.17) is the Hodge dual of the gauge field strength tensor,

$$\tilde{G}_a^{\mu\nu} = \frac{1}{2} \epsilon^{\mu\nu\alpha\beta} G_{\alpha\beta a} \ , \tag{2.18}$$

where $\epsilon^{\mu\nu\alpha\beta}$ is the completely anti-symmetric Levi-Civita tensor [1341]. Using this notation is it possible to express the four dimensional operator for the strength

tensor contracted with its dual as a total divergence,

$$G^a_{\mu\nu}\tilde{G}^{\mu\nu}_a = \partial^\mu K_\mu \ , \tag{2.19}$$

which for the study of QCD is given by the Chern-Simons (CS) current [158, 795, 1033],

$$K^\mu = \frac{1}{16\pi^2}\epsilon_{\mu\nu\alpha\beta}\left(G^a_\nu \partial_\alpha G^a_\beta + \frac{f_{abc}}{3}G^a_\nu G^b_\alpha G^c_\beta\right) \ . \tag{2.20}$$

Performing an integration over this total derivative reveals a key feature of the more complicated vacuum structure of QCD. Fixing the boundary conditions, $G^\mu_a = 0$, at spatial infinity, this surface integral is non-vanishing for certain gauge conditions [188], where the gauge field takes a general form,

$$G_\mu = if(r)g^{-1}(x)\partial_\mu g(x) \ , \tag{2.21}$$

$$f(r) = \frac{r^2}{r^2+\rho^2} \ , \tag{2.22}$$

with $g(x)$ deemed a pure gauge transformation and ρ the size of the instanton. The classical gluon field theory of QCD now presents a series of instanton solutions which satisfy the anti-duality condition,

$$G^a_{\mu\nu} = \tilde{G}^a_{\mu\nu} \ . \tag{2.23}$$

The integer index emitted is known as the topological charge of the gauge field configuration or *Pontryagin number*, used to distinguish between different homotopy classes,

$$n = \frac{1}{16\pi^2}\int d^4x \mathrm{Tr}\ G\tilde{G} = \frac{1}{32\pi^2}\int d^4x\ G^a_{\mu\nu}\tilde{G}^{\mu\nu}_a \ , \tag{2.24}$$

where Tr denotes the trace over gluon field strength tensor contraction with its dual. Any classical solutions are defined to fall within the set,

$$n = -\infty, \ldots, -1,\ 0,\ 1, \ldots, \infty \ . \tag{2.25}$$

Perturbative field theory has trivial topology and so zero topological charge. The $|n\rangle$ states are not physical states, these are vacua belonging to different topological equivalence classes where physical solutions are realised by a superposition of the eigenstates of these vacuum solutions. Each value of n relates to the winding number of the $U(1)_{\mathrm{A}}$ symmetry and is used to parameterise a linear combination of $|n\rangle$ vacuum solutions, the so called, *theta vacua*,

$$|\theta\rangle = \sum_{n=-\infty}^{+\infty} e^{i\theta n} |n\rangle \, . \tag{2.26}$$

The parameter θ in QCD is a vacuum angle, an arbitrary phase which is periodic in the interval of a unit circle,

$$\theta \in [0, 2\pi] \ . \tag{2.27}$$

Formally the instanton solutions are non-vanishing configurations of topologically non-trivial solutions to the classical field theory equations in four-dimensional Euclidean space. These solutions are a description of transitions between different vacuum states, where the more complex vacuum structure has consequences on the effective action of the theory. An expression of the vacuum to vacuum transition amplitude using the path integral formulation reveals the following sum over the difference in index, ξ, of the winding number vacua,

$${}_{+}\langle\theta|\theta\rangle_{-} = \sum_{\xi} \int \delta G e^{iS_{\mathrm{eff}}[G]} \delta \left[\nu - \frac{g_s^2}{32\pi^2} \int d^4x G^a_{\mu\nu} \tilde{G}^{\mu\nu}_a \right] \ , \tag{2.28}$$

which can be re-expressed by introducing a topological term into the effective action,

$$S_{\mathrm{eff}}[G] = S_{\mathrm{QCD}}[G] + \frac{\theta g_s^2}{32\pi^2} \int d^4x G^a_{\mu\nu} \tilde{G}^{\mu\nu}_a \ , \tag{2.29}$$

where $S_{\mathrm{QCD}}[G]$ represents the original action formed from Eq. (2.12). This translates as a redefinition to the effective Lagrangian density,

$$\mathcal{L}_{\mathrm{QCD}} = \mathcal{L}_{\mathrm{QCD},0} + \mathcal{L}_{\theta} = \mathcal{L}_{\mathrm{QCD},0} + \frac{\theta g_s^2}{32\pi^2} G^a_{\mu\nu} \tilde{G}^{\mu\nu}_a, \tag{2.30}$$

where $\mathcal{L}_{\text{QCD},0}$ is the bare theory Lagrangian (see Eq. (2.12)). The incorporation of this topological term is indeed a novel solution to the $U(1)_{\text{A}}$ axial problem, however the newly introduced θ parameter certainly cannot be glossed over in the perturbative theory. Details are still required for its presence to be accounted for from a fundamental standpoint. This transition is comprehended as moving to an initial problem of naturalness and fine tuning, referenced as the *strong CP problem* of the Standard Model.

2.3 The Strong CP Problem and the Peccei-Quinn Solution

2.3.1 An Issue with the QCD Vacuum

If the newly introduced θ term of QCD is to tune the physical spectrum of the Standard Model it must be pointed out that by definition it is invariant under charge conjugation but does violate time and parity reversal symmetry, stemming from $\vec{E}_a \cdot \vec{B}_a$ interactions of the colour fields. This term is then fully understood to violate CP invariance, revealing the origins to the name of the problem at hand. The magnitude of this issue is realised by the extremely strong bound placed on the neutron electric dipole moment (EDM). There have been many different methods aiming to refine the calculation used to measure this value however a conservative limit on the EDM of the neutron is [389],

$$d_n \approx 3.6 \times 10^{-16}\ \theta\ e\ \text{cm}\ , \tag{2.31}$$

where e is the absolute value of the electron charge. The permanent static dipole moment is constrained to a result which details the extent of the fine tuning required [143],

$$|d_n| < 2.9 \times 10^{-26}\ e\ \text{cm}\ , \tag{2.32}$$

at the 90% CI. This is understood via the following relationship for the θ parameter,

$$d_n \simeq \frac{e\theta m_q}{m_{\mathrm{N}}^2} \ , \tag{2.33}$$

where m_{N} is the mass of the neutron and m_q is a mass expression in terms of the up and down quark mass parameters,

$$m_q = \frac{m_u m_d}{m_u + m_d} \ . \tag{2.34}$$

These relationships define the current bound on θ to be,

$$|\theta| \lesssim 10^{-10} \ . \tag{2.35}$$

This constraint is actually made worse when we account for a further term of CP violation coming from the structure of the QCD vacuum. Aside from strong interactions if we consider interactions in the electroweak sector, we must account for leading order corrections to the θ parameter. Spontaneous symmetry breaking of the electroweak gauge symmetry provides a mass term for the quarks of the Standard Model, who's values are encoded in a mass matrix, $\mathcal{M}_{\mathrm{Quark}}$, residing in the Standard Model Lagrangian. Following this phase of symmetry breaking, the basis of the mass matrix is in general both non-hermitian and non-diagonal, requiring a unitary transformation to the chiral quark fields to move into a physical basis, thereby defining the mass eigenstates. These transformations incorporate a chiral $U(1)_{\mathrm{A}}$ transformation, which also acts as a rotation of the θ vacua via the properties of the axial anomaly, inducing non-invariance at the quantum level. The coefficient in Eq. (2.30) must then be redefined as,

$$\bar{\theta} = \theta + \theta_{\mathrm{Weak}} = \theta + \arg(\det(\mathcal{M}_{\mathrm{Quark}})) \ . \tag{2.36}$$

This reparameterisation is the *true* Strong CP problem of the Standard Model, our lack of understanding as to why we should have no *a priori* basis in which

to understand a cancellation of the original topological QCD vacuum term and the associated properties of the electroweak and strong gauge sectors. The next question we must then ask is, *how can we naturally realise such a cancellation?*. There are several methods which can be applied in order to solve the strong CP problem. Broadly speaking these can be categorised into three different schemes inside a framework of naturalness, the salient issue being addressed suitably. The first, briefly touched on previously, observes that if the up quark is massless then the Lagrangian in Eq. (2.30) allows for the simple transformation,

$$\mathcal{L}_{\rm QCD} \to \mathcal{L}_{\rm QCD,0} \ , \tag{2.37}$$

via a chiral rotation of the quark fields, which naturally removes the θ term and fixes the issue rather straightforwardly. This possibility has however been strictly ruled out via measurements of a non-zero value of the up quark mass. The second model involves a form of θ renormalisation in the Standard Model via approaching the source of CP violation as mainly an issue with $\theta_{\rm Weak}$. These class of models are known as Barr-Nelson CP violating models [164, 165, 975]. In such a framework the value of $\theta_{\rm Weak}$ is reduced to zero at the tree level under certain considerations for CKM mixing and the magnitude of the phase in the quark mass matrix. The non-zero value of $\theta_{\rm Weak}$ is then restored via higher loop corrections only.

2.3.2 The QCD Axion

Possibly the most celebrated and elegant solution to the Strong CP problem comes from the work of Roberto Peccei and Helen Quinn, who introduced a further $U(1)$ global chiral symmetry invariance to the full Standard Model Lagrangian. We shall refer to this symmetry now as the Peccei-Quinn symmetry denoted as, $U(1)_{\rm PQ}$. This newly introduced symmetry which still suffers from the chiral anomaly, elevates the $\bar{\theta}$ parameter from the static vacuum angle to a dynamical field. This symmetry is not a natural product of the Standard Model and so requires either a significant extension

to the theory with physics beyond the Standard Model or minimal implementation via adjustments to the standard spectrum of particle physics such as Higgs sector physics. The pNGB produced from the spontaneous symmetry breaking of the $U(1)_{\rm PQ}$ symmetry is known as the *axion*. The axion field, $a(x)$ transforms under the PQ symmetry transformation,

$$a(x) \xrightarrow[U(1)_{\rm PQ}]{} a(x) + \alpha f_a \ , \tag{2.38}$$

with α a phase parameter. The newly introduced parameter f_a, is an order parameter associated to the symmetry breaking scale of the $U(1)_{\rm PQ}$ symmetry, known as the *axion decay constant* (up to colour anomaly number normalisation concerns). After symmetry breaking has occurred the axion field ($a \equiv a(x)$) possesses a Lagrangian of the form,

$$\mathcal{L}_a = -\frac{1}{2}\partial^\mu a \partial_\mu a + \frac{aN}{f_a}\frac{g_s^2}{32\pi^2}G^a_{\mu\nu}\tilde{G}^{\mu\nu}_a \ , \tag{2.39}$$

where N is the PQ colour anomaly, defined as a sum over the PQ-charged species in the fermionic sector defined in Eq. (2.72). The form of Eq. (2.39) suppresses any higher order derivative couplings interaction terms to other Standard Model matter fields, which are contained in $\mathcal{L}_{\rm SM}$, where the new form for the QCD Lagrangian is,

$$\mathcal{L}_{\rm QCD} = \mathcal{L}_{\rm QCD,0} + \mathcal{L}_{\bar{\theta}} + \mathcal{L}_a \ , \tag{2.40}$$

$$= \mathcal{L}_{\rm QCD,0} + \frac{\theta g_s^2}{32\pi^2}G^a_{\mu\nu}\tilde{G}^{\mu\nu}_a - \frac{1}{2}\partial^\mu a \partial_\mu a + \frac{aN}{f_a}\frac{g_s^2}{32\pi^2}G^a_{\mu\nu}\tilde{G}^{\mu\nu}_a \ . \tag{2.41}$$

As the axions $U(1)_{\rm PQ}$ symmetry is susceptible to the colour anomaly the field couples to gluons, via triangle loop interactions, as demonstrated in the interaction vertex shown in the *left panel* of Fig. 2.2. We still must understand the nature of the dynamics as to how the θ term is effectively removed. Analysing the effective potential of the axion field we see that the minimum lies at,

$$\langle a(x) + {}^{f_a\bar{\theta}}/_{N}\rangle = 0 \ , \tag{2.42}$$

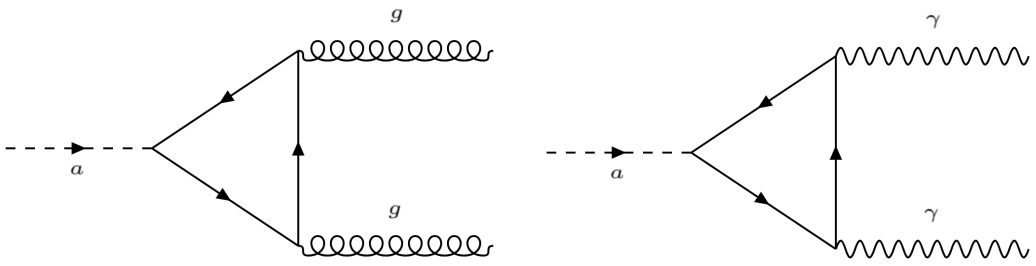


Figure 2.2: *Left panel:* Triangle loop interaction diagram for the anomalous axion-gluon-gluon coupling. Each gluon vertex strength is regulated by the strong coupling constant. The axion vertex strength is regulated by the axion-fermion Yukawa coupling. *Right Panel*: Anomalous two-photon vertex interaction which can be used to indicate the stability of the axion field over cosmological time scales. The respective vertex interactions are replaced with charged fermion coupling terms.

which can also be expressed as,

$$\left\langle \frac{\partial V_{\text{eff}}}{\partial a} \right\rangle = -\frac{N}{f_a}\frac{g_s^2}{32\pi^2}\left\langle G^a_{\mu\nu}\tilde{G}^{\mu\nu}_a \right\rangle\Big|_{\langle a\rangle = -f_a\bar{\theta}/N} = 0 \ , \tag{2.43}$$

where $\langle a\rangle = \langle 0|a|0\rangle$ is the axion field VEV. We now arrive at one of the most important features of the axion field, its periodicity (see Eq. (2.38)). The periodicity of $\bar{\theta}$ means that $\langle a\rangle$ has a periodicity naturally realised in n, $\langle a\rangle = 2\pi n f_a$. This ability to shift the axion field value can be defined by the *axion misalignment angle*,

$$\theta = \bar{\theta} + \frac{aN}{f_a} \ . \tag{2.44}$$

Finally defining the physical axion field as, $a_{\text{phys}} = a - \langle a\rangle$, which can be inserted into Eq. (2.41), we rather neatly remove the CP violating term present in the Lagrangian. The spontaneous symmetry breaking of the newly introduced anomalous $U(1)_{\text{PQ}}$ global symmetry has introduced a new dynamical parameter understood as *pseudoscalar* field which, under dynamical evolution to its CP conserving potential minimum can replace CP violating interaction terms by ensuring we have, $\bar{\theta} = 0$ in our effective description. The introduction of the axion is a novel solution to the strong CP problem, however formalising its embedding among the historical matter fields is a little more troublesome.

2.4 The Standard Model(s) of the QCD Axion

The introduction of the $U(1)_{\rm PQ}$ symmetry in order to solve the strong CP problem has so far replaced a theoretical exercise in model consistency with experimental conclusions, with a further problem, similar in principle. The anomalous nature of the symmetry generates a potential for the axion field, which is periodic in the vacuum angle and as we have seen in Eq. (2.42), which is used to solve the presence of any CP violating interaction terms in our effective Standard Model Lagrangian. Expanding this solution to the potential reveals a mass for axion as shown in Eq. (2.43), so the solution is actually a massive pseudoscalar boson apparent in the spectrum. Obviously then we must address, *how do we naturally realise this newly introduced symmetry in the context of either new sectors or modifications to existing physics* and *what are the couplings and scales associated to this new field.* Frankly expressed, *where is it?*

2.4.1 Visible Axions

2.4.1.1 The Peccei-Quinn-Weinberg-Wilczek Model

Historically there have been several consistent frameworks drawn up very soon after the theoretical inception of the axion into the literature, now serving as pedagogical examples, each of which predicting several different aspects in order to understand the axions place in the context of the Standard Model. The first model is known as the *visible axion model* and although it is ruled out through experimentation, it still serves as a good insight into issues regarding embedding the axion consistently in models of particle physics and the energy scales required to avoid collider constraints. See Refs. [91, 305, 437, 438, 604, 1126] for other frameworks incorporating the axion into grand unified theories (GUTs) slightly outside the following historical, traditional concerns. The axion can be considered as a phase degree of freedom to

an introduced complex scalar field,

$$\varphi(x) = \eta(x) \exp\left(\frac{ia(x)}{f_a}\right) \ , \tag{2.45}$$

where the axion field is the angular degree of freedom or the phase of φ. The radial component of φ initially obtains a VEV, $\langle\eta\rangle = {}^{f_a}/\sqrt{2}$. This field is heavy, naturally regulated by the high scales of any PQ symmetry breaking. The original axion model was formed by Peccei, Quinn, Weinberg and Wilczek, by introducing the required chiral symmetry through two Higgs doublets, H_u and H_d, which are used to generate masses for the up and down quarks. This *visible* axion model is often referred to as the PQWW axion [1035, 1036, 1335, 1353]. The primary reason this model fails to hold up is the required scale of the fields VEV and its relationship with the electroweak sector. Symmetry restrictions enforce a single Higgs doublet is not invariant under the required transformations for the required $U(1)_{\rm PQ}$ symmetry. This does change however if we account for the presence of two Higgs doublets [1035]. Using these Higgs doublets we can express the relevant terms in the Yukawa sector as,

$$\mathcal{L}_{\rm Yukawa} = \lambda_u \bar{q}_L H_u u_R + \lambda_d \bar{q}_L H_d d_R + \text{H.c.} \ , \tag{2.46}$$

where q are the left and right handed quark doublets, which are invariant under the following chiral rotations,

$$q_l \to e^{i\alpha} q_L, \quad q_R \to e^{-i\alpha} q_R, \quad H_u \to e^{2i\alpha} H_u, \quad H_d \to e^{-2i\alpha} H_d \ . \tag{2.47}$$

It is required the full Lagrangian possesses the global symmetry who's chiral rotations shift the angular part of the complex scalar in Eq. (2.45), which in this case is a common phase field between the Higgs doublets, by some constant value. The new complex scalar is coupled to the Standard Models fields via Yukawa terms like those in Eq. (2.46). Due to these connections the spontaneous symmetry breaking of the global $U(1)_{\rm PQ}$ symmetry occurs at the electroweak symmetry breaking scale,

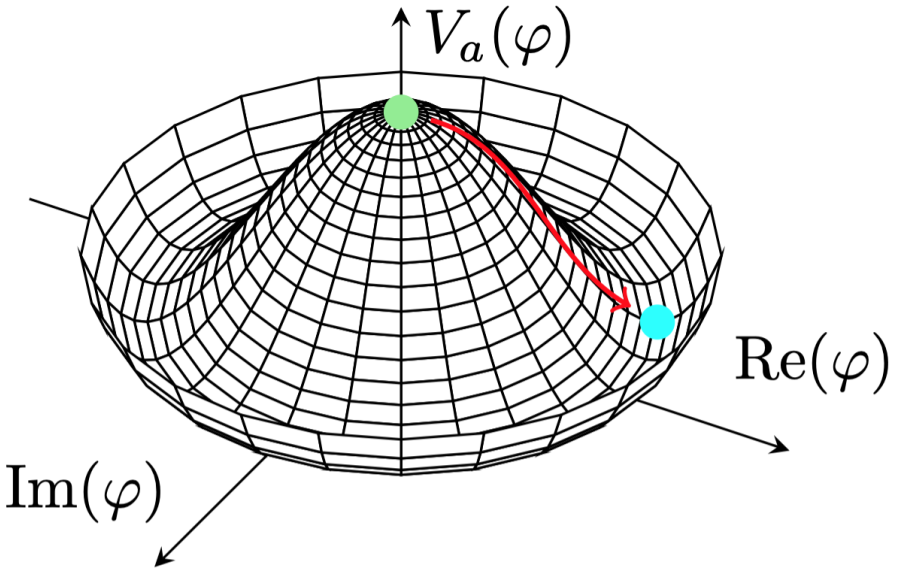


Figure 2.3: The *Mexican hat* symmetry breaking potential of Eq. (2.48), in the complex φ plane. The VEV of the massive radial mode is $f_a/\sqrt{2}$. The axion is apparent as the massless angular phase degree of freedom at the minimum of the potential. The field initially begins at the point denoted by the *green* circle. Once the respective symmetry is spontaneously broken the field moves down its potential to the minimum denoted by the *blue* circle, where is now possesses a continuous shift symmetry.

i.e. $v_{\mathrm{EW}} = \sqrt{v_u^2 + v_d^2} \approx 246$ GeV, where the phase field possess the famous *Mexican hat* symmetry breaking potential,

$$V_a(\varphi) = \lambda \left(|\varphi| - \frac{f_a^2}{2} \right)^2 , \tag{2.48}$$

as visualised in Fig. 2.3. The radial model of the potential obtains a VEV due to the non-zero VEVs of each Higgs doublet. It soon became apparent these scales are problematic though, and the model was quickly eliminated [473, 794] as a possible candidate to realise the axion field. Specifically they are excluded by beam dump experiments [790] and collider exclusions [466, 949]. The required solution to these exclusion issues is that the symmetry breaking scale or axion decay constant f_a, must be significantly increased in order to avoid these types of constraints. Visible axions can also impose very interesting features in regards to the wider picture of particle physics, namely providing solutions to explain the anomalous magnetic

moment of the muon [175, 335, 906] and factors of electroweak symmetry breaking such as solutions to the hierarchy problem via the *relaxion* [543, 624]. Axion particles with symmetry breaking scales around the electroweak scale are relatively unimportant for cosmological physics. When, however we impose the general understanding needed to avoid the exclusions of the visible axion model with higher symmetry breaking scales (and in turn suppressed Standard Model couplings) for the introduced global chiral symmetry, we enter the realm of the *ultralight* axion which is potentially of great importance to the standard model of cosmology. These are generally known as *invisible* axion models.

2.4.2 Invisible Axions

2.4.2.1 The Kim-Shifman-Vainshtein-Zakharov Axion Model

The first invisible axion model is referred to as the KSVZ axion after its introduction in the work by, Kim, Shifman, Vainshtein and Zakharov [789, 1182]. This model contains a general freedom from couplings to Standard Model matter fields and so are also sometimes referred to as *hadronic* axions (apart from the regular anomalous QCD gluon coupling and higher order loop couplings to photons), but this comes at a cost, the incorporation of a heavy quark doublet. Theoretically the origins of such a field are not so clear, once again potentially shifting the model completion issues from one sector to another. The PQ scalar field, φ, now becomes a Standard Model singlet. The heavy quark doublet field, Q possesses a discrete R symmetry in order to avoid the presence of any bare mass terms [788]. The relevant KSVZ Lagrangian Yukawa terms are,

$$\mathcal{L}_{\text{KSVZ,Yukawa}} = -\lambda_Q \varphi \bar{Q}_L Q_R + \text{h.c.} \,, \tag{2.49}$$

with Yukawa coupling, λ_Q. The quark field is invariant under the global PQ symmetry, leaving the model Lagrangian invariant at the classical level. For scales lower than the axion decay constant, symmetry breaking occurs and the radial part of

the complex scalar freezes out, leaving just the remaining phase free to evolve dynamically for the scalar singlet. As with the previous model, the chiral rotational invariance of the Lagrangian shifts the axion field. The spontaneous symmetry breaking of the PQ symmetry gives a large effective mass term to the heavy quark, $m_Q \sim \lambda_Q f_a$. As we require $f_a \gg v_{\rm EW}$ the effective mass must in fact be very large. At tree level there are no couplings to the Standard Model quarks, where we only need to account for gluon couplings via chiral rotations at high energies, along with couplings to photons via the heavy quarks couplings to the electroweak gauge bosons. The effective Lagrangian after any chiral rotations of the heavy quark fields, which are integrated out (after suppressing couplings to photons) becomes,

$$\mathcal{L}_{\rm KSVZ} = -\frac{1}{4}G^a_{\mu\nu}G^{\mu\nu}_a + \left(\bar{\theta} - \frac{a}{f_a}\right)\frac{g}{8\pi}G^a_{\mu\nu}\tilde{G}^{\mu\nu}_a + \frac{1}{2}\partial_\mu a \partial^\mu a \ . \tag{2.50}$$

The standard canonical choice for photon couplings comes from loop contributions of the EM anomaly, where Q fields are assumed to be uncharged. This means the coupling actually arises as the longitudinal mode of the Z-boson [793]. In this model the colour anomaly term N, which is also equivalent to the domain wall number $N_{\rm DW}$ (see Section 2.6.2) [791, 1183], is fixed to $N = N_{\rm DW} = 1$, corresponding to a single axion minimum.

2.4.2.2 The Dine-Fischler-Srednicki-Zhitnitsky Axion Model

A further consistent framework drawn up as a minimal model approach to realising an invisible axion field is the Dine-Fischler-Srednicki-Zhitnitsky (DFSZ) axion [459, 1392]. Again the Standard Model Lagrangian must be invariant under the new Global PQ symmetry where the axion field is coupled via the Higgs sector. In this model the Standard Model fermions are charged under the PQ symmetry which alleviates the issue of including heavy quarks present for the KSVZ axion. Like the previous PQWW model we require two Higgs doublets which must couple to light quarks but this time we include the axion as a Standard Model singlet, although

models do exist with three doublets etc., along with so called *non-universal* DFSZ models (see Ref. [438]). The relevant Yukawa coupling terms in the model are,

$$\mathcal{L}_{\text{Yukawa}} = \lambda_u \bar{Q}_L H_u u_R + \lambda_d \bar{Q}_L H_d d_R + \text{h.c.} \ , \tag{2.51}$$

where the axion scalar singlet, denoted ϕ couples to the two doublets in the Higgs sector with the most general scalar Higgs potential [459],

$$\begin{aligned} V(H_u, H_d, \phi) = {} & \Xi_u \left(|H_u^2| - v_u^2 \right)^2 + \Xi_d \left(|H_d|^2 - v_d^2 \right)^2 \\ & + \Xi \left(|\phi|^2 - v_\phi \right)^2 + \left(\mathcal{A}|H_u|^2 + \mathcal{B}|H_d|^2 \right) |\phi|^2 \\ & + \mathcal{C} \left(H_u^i \epsilon_{ij} H_d^j \phi^2 + \text{H.c.} \right) + \mathcal{D}|H_u^i \epsilon_{ij} H_d^j|^2 + \mathcal{E}|H_u^* H_d|^2 \ . \end{aligned} \tag{2.52}$$

The completely antisymmetric tensor of $SU(2)$ gauge theory is ϵ_{ij} and the values of Ξ_u, Ξ_d, Ξ and $\mathcal{A}$,$\mathcal{B}, \mathcal{C}, \mathcal{D}, \mathcal{E}$ all represent dimensionless constants of the theory. The potential is fully invariant under the following chiral rotations,

$$H_u \to H_u e^{i\alpha_u}, \quad H_d \to H_d e^{i\beta_d}, \quad \phi \to \phi e^{\frac{i}{2}(\alpha_u - \beta_d)} \ , \tag{2.53}$$

with α_u and β_d both phase parameters for the up and down Higgs doublets respectively. Repeating the procedure, once we break the PQ symmetry with a potential of the form defined in Eq. (2.48), the radial component of the scalar field freezes and we are left with the axionic angular phase degree of freedom. The parameters in the Higgs potential in Eq. (2.52) must be specially selected in such a way that the Higgs fields will remain light, reproducing the standard experimentally observed 125 GeV Higgs Boson [3, 336] of the Standard Model with the phenomenologically required scale, v_{EW}. This represents an element of tuning present in the model. Once electroweak symmetry breaking occurs the the Higgs is replaced by its VEV in Eq. (2.51), which induces axial current coupling between the Standard Model fermions so that we have tree-level couplings between the axion in the model, with the requirement that the individual VEV scales associated to the Higgs doublets

follow,

$$\sqrt{2}\,\langle\phi\rangle = f_\phi \gg \sqrt{(f_u^2 + f_d^2)} \equiv f_a \ . \tag{2.54}$$

The Higgs doublets each contain four degrees of freedom. As is standard practise, the redundant massless degrees of freedom below the electroweak phase transition are accounted for in the unitary gauge. The remaining degree of freedom mixes with the axion phase via the last term in Eq. (2.52) such that the electroweak sector is modified with an extra axial Higgs field from standard considerations analogous to supersymmetric Higgs models. As all the Standard Model quarks are charged under the PQ symmetry in this model, the value of the colour anomaly is higher, $N = 6$.

2.5 Axion Interactions and Effective Field Theories

2.5.1 An Effective Description of the QCD Axion

The standard models of the QCD axion in Section 2.4 generally represent a detailed embedding of the field in some grand unified framework, those of which account for the appearance of the axion in the low energy spectrum as a solution to the strong CP problem. The axions global symmetry generates specific model dependant interactions in each of these cases. It is beneficial therefore, to make a series of model independent statements which, ultimately in turn, can be further generalised to particles enjoying the same symmetry properties, through investigating the fields mixings induced via the topological QCD term responsible for the anomalous coupling to gluons. Below the QCD confinement scale, the gluons and quarks of the theory must be integrated out, where QCD takes on the form of an effective chiral theory. This point should be stressed, non-perturbative physics is a complex landscape, stemming from the non-trivial nature of the QCD vacuum and the topological features which manifest themselves as factors in the effective low-energy sector. This

is a model dependant statement and we have seen previously how the value of N for the colour anomaly in the normalisation of the potential in Eq. (2.68), is fixed depending on explicit models of the axion. This number actually has a further intuitive purpose. The axion field is an angular variable which as we have mentioned possesses a shift symmetry like that found in Eq. (2.38), which acts on the interval $[0, 2\pi n f_a]$, where n is an integer periodicity term. The value of N can always be normalised to take integer values which in the context of the axion potential, represents the number of vacua in the shift symmetric interval [1210]. Values of $N \equiv N_{\rm DW} > 1$ are sources for long-lived string wall configurations, where the decay products of topological defects act as sources for axion particle generation.

The orthonormal combination which is responsible for the solution of the strong CP problem via a shift to the minimum energy of the potential mixes with the remaining scalar mesons in the spectrum in order to generate a mass. The induced transitions to quark states and therefore to the neutral pion, π_0. The small axion mass then holds the approximate mass scale relationship with the mass (m_π) and decay constant (f_π) of the neutral pion,

$$m_a f_a \approx m_\pi f_\pi \ , \tag{2.55}$$

$$m_a \propto f_a^{-1} \ . \tag{2.56}$$

Vafa and Witten showed that the instanton potential is always minimised at the CP conserving limit [1288]. This mixing of the axion with the neutral pseudoscalar meson forms a rich model-independent phenomenology we can explore without the need to limit ourselves to a specific class of model. We can therefore study the form of the effective potential in order to draw conclusions about the QCD axion. A more precise understanding of the potential comes from first order considerations in chiral perturbation theory defining the effective *chiral potential*, expressed as a function of the masses of the lightest quarks, the neutral pion mass and the fields symmetry

breaking scale,

$$V(a) = -m_\pi^2 f_\pi^2 \sqrt{1 - \frac{4 m_u m d}{\left(m_u + m_d\right)^2} \sin^2\left(\frac{a}{2 f_a}\right)} \,. \tag{2.57}$$

After the QCD phase transition the quark bilinears can be used to determine an effective QCD axion mass proportionality relationship, by expanding the potential to quadratic order [1335],

$$m_a = \frac{m_u m_d}{\left(m_u + m_d\right)^2} \frac{m_\pi^2 f_\pi^2}{f_a^2} \approx 6 \times 10^{-6} \text{ eV} \left(\frac{10^{12}\text{GeV}}{{}^{f_a}/_{N_{\text{DW}}}}\right) \,, \tag{2.58}$$

found using the values, $m_\pi \simeq 135$ MeV, $f_\pi \simeq 92$ MeV and the ratio of the lightest quark masses, approximated as ${}^{m_u}/_{m_d} \approx 0.56$ [588, 849], although this can posses some freedom [503].

2.5.2 The Effective Axion Potential

A phenomenologically beneficial form of the effective potential which is both more tractable and susceptible to an analytic expansion, can be realised from Eq. (2.43) at its CP conserving minimum, $\langle a \rangle = 0$ when we allow for the adoption of a semi-classical approximation [441, 1362]. Any possibility of a general explicit analytical treatment is generally ruled out due to the presence of strong QCD coupling effects. The spacetime integral of the anomalous coupling does however only require a consideration of instanton field configurations and the nature of the Pontryagin index at spacial infinity related to the winding number of the gluon field. Therefore, the effective potential can be defined by integrating out the gluon field of the path integral, usually expressed in Euclidean spacetime in the following form,

$$\mathcal{Z} = e^{\left[-\int d^4x V(a)\right]} = \int \mathcal{D}A_a e^{-S[A_a] - i\theta \int d^4x \left[\frac{\alpha}{8\pi} G^a_{\mu\nu} \tilde{G}^{\mu\nu}_a\right]} \,. \tag{2.59}$$

An effective approximation must be made for an analytical treatment of the potential, which comes from the ability to saturate the path integral in the effective potential description with considerations made to important features of the problem, namely the instantons present from the coupling to the topological charge [1329]. This is done under the so called *dilute instanton gas approximation* [306, 307, 635, 1281], using an ensemble of non-interacting instantons where the path integral in the effective potential factorises into single constituent contributions. At zero temperature [1235], it has been shown under this approximation the effective potential must be periodic due to the topological nature of the QCD path integral exponent,

$$V(a) = -2 \int d\rho n(\rho) \cos\left(\frac{a}{f_a}\right) . \tag{2.60}$$

Combining the form of the potential in Eq. (2.60) with Eq. (2.64) leads to the standard expression of the periodic axion field potential known as the *instanton potential*, demonstrated as the *black* line in Fig. 2.4,

$$V(a) = f_a^2 m_a^2(T) \left[1 - \cos\left(\frac{N_{\mathrm{DW}} a}{f_a^2}\right)\right] , \tag{2.61}$$

which in terms of the complex scalar in Eq. (2.45) and the potential in Fig. 2.3 is,

$$V(\varphi) = \frac{\lambda}{4}\left(|\varphi|^2 - f_a^2\right)^2 + f_\pi^2 m_\pi^2 \frac{|\varphi|}{f_a}\left(1 - \cos\theta\right) . \tag{2.62}$$

This is the residual potential of spontaneous PQ symmetry breaking, which after factorisation of the radial mode in Eq. (2.62) leaves the most general, model independent configuration for the axion field. Expanding either general forms for the effective potential in Eq. (2.57) or Eq. (2.61) around the origin up to quartic interaction terms, yields the simple algebraic series form for the potential,

$$V(a) = V_0 + \frac{1}{2} m_a^2 a^2 + \frac{\lambda_a}{4!} a^4 + \dots . \tag{2.63}$$

This is the standard approach taken to axion phenomenology in a cosmological setting, where the most general simplified case consists of an axion field described by a potential with quadratic minimum and periodicity of 2π. The potential in Eq. (2.61) need not be to unitary power at leading order. It is possible to find periodic potentials of higher harmonics via higher order instanton corrections to the effective potential. The potentials in Fig. 2.4 represent general forms of the axion potential up to third order exponents in the periodic domain for the field. Potentials of higher order approach the minimum of the potential faster when perturbed from their initial position, which corresponds to accelerated dilution of the axion relic density in a cosmological setting. The axion mass can be found under a redefinition of the vacuum,

$$m_a^2 \equiv \left.\frac{\partial^2 V(a)}{\partial a^2}\right|_{a=0} = \frac{\chi(T)}{f_a^2} \equiv \lim_{\mathcal{V}\to\infty} \frac{\langle Q^2\rangle_T|_{\theta=0}}{f_a^2 \mathcal{V}} \ , \tag{2.64}$$

$$\sim \frac{\Lambda_{\rm QCD}^4}{f_a^2} \ , \tag{2.65}$$

where $\chi(T) \equiv f_a^2 m_a^2(T)$ is the topological susceptibility factor as a function of temperature with the defining energy scale for QCD, $\Lambda_{\rm QCD}$. The values of Q and $\mathcal{V}$ represent the topological charge and a four volume normalisation factor respectively. The terms in Eq. (2.65) are representative of the dimensionality of the problem. At high energies the topological susceptibility is heavily suppressed where its dependance can be neglected and at zero temperature its value saturates to, $\Lambda_{\rm QCD} = \chi^{1/4}(0) \approx 75$ MeV [631], leading to the zero temperature formalities in Eq. (2.58). We must be careful however when approaching the QCD confinement scale. For high temperatures, perturbative simplifications still remain valid solutions, i.e. the topological susceptibility is sufficiently suppressed as long as a temperature dependant correction factor is included in the form of a power-law [635],

$$m_a^2(T) = \alpha \frac{\Lambda_{\rm QCD}^3 m_u}{f_a^2} \left(\frac{T}{\Lambda_{\rm QCD}}\right)^{-n} \quad \text{for } T \gtrsim 1\text{GeV} \ , \tag{2.66}$$

where the values for n and α come from the fits of calculations computed non-perturbatively on the lattice, e.g. see Ref. [1329] and must be matched to results in the zero temperature limit. In the intimidate regime however the complicated nature and dynamics of the QCD plasma calls for lattice simulations to maintain sufficient consistency, given the high non-linearity. We must account for the instantons interactions, replacing the dilute gas approximation with the *interacting instanton liquid model* (IILM) [557, 635, 1329].

2.5.3 Standard Model Couplings to the Axion Field

Although it is commonly accepted that the full potential should contain many more additional complex terms [572, 580, 581, 655, 656], it is understood that the first order periodic form for the effective potential should capture the dynamics of the axion fields to an excellent approximation [792]. In this context, it is common place for most predictions to be entirely based on the semi-classical expansion of the Euclidean path integral in the limit of temperature QCD under the assumption of validity of a dilute gas of non-interacting instantons with no considerations made for the higher moments of the topological charge distributions. Under this general cognisance the form of the axion potential can be determined by following the work in Ref. [159, 1335], leading to a general form of the axion effective Lagrangian, which was initially studied using algebraic techniques under consideration of the effective field theory. In between the epochs of the electroweak scale, $E_{\rm EW} \sim O(100)$ GeV and the QCD confinement transition, $\Lambda_{\rm QCD} \sim O(100)$ MeV, the Lagrangian for the effective theory including the axion to first order is factorised according to CP conserving and CP-violating integration terms [598],

$$\mathcal{L}_{\rm eff} = \frac{1}{2}\partial_\mu a \partial^\mu a - \frac{g}{8\pi} G^a_{\mu\nu}\tilde{G}^{\mu\nu}_a - \frac{g_{a\gamma}}{4} a F_{\mu\nu}\tilde{F}^{\mu\nu} - \frac{\partial_\mu a}{2f_a}\sum_f C_f \bar{\psi}_f \gamma_5 \gamma^\mu \psi_f \ , \qquad (2.67)$$

with the Maxwell stress tensor $F_{\mu\nu}$, and its respective dual, $\tilde{F}^{\mu\nu}$. The final term in this expression represents the model dependent derivative couplings to chiral

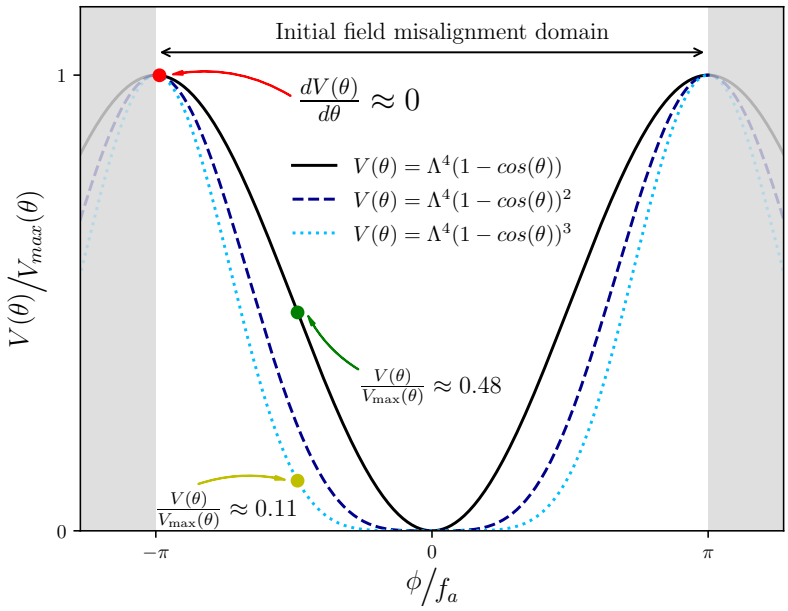


Figure 2.4: General form of the standard dilute instanton gas axion potential which forms non-perturbatively, periodic in the initial misalignment angle domain along with associated higher order forms. The three examples presented include the standard axion-cosine potential along with two potentials possessing higher order harmonics. Such potentials are often addressed by considering higher order instanton corrections which allow for features such as the dilution of the axion relic density at rates faster than a standard fluid matter component [774, 1071]. This is shown by the *green* and *yellow* points which represent the same value of θ.

currents of the massive Standard Model fermion fields. The index f runs over the fermions of the Standard Model and the values of $g_{a\gamma\gamma}$ and C_f represent the axion-photon and axion-fermion coupling constants respectively. The ratio of E/N is a model dependant component (DFSZ = $8/3$ [788] and KSVZ = 0 [1392] etc) and in general, allowed to vary forming a banded range in axion-mass and decay constant space [339, 769, 793]. Once the potential is minimised at its CP conserving value via the dynamical relaxation of the QCD θ term the Lagrangian takes the reduced form,

$$\mathcal{L}_a = \frac{1}{2}\partial_\mu a \partial^\mu a - m_a^2 f_a^2 \left[1 - \cos\left(\frac{aN}{f_a}\right)\right] - \frac{g_{a\gamma}}{4} a F_{\mu\nu}\tilde{F}^{\mu\nu} - \mathcal{L}_{a\mathrm{SM}} \ , \tag{2.68}$$

the final term represents the remaining axion-Standard Model interactions. The presence of these axial currents deems the interactions of the axions with standard model constituents as spin-dependant, acting only between spin-polarised sources. The significance of this statement is that ultralight scalar axion particle is not susceptible to long range scalar forces and problems with fifth force constraints present in other models incorporating additional scalars [911], an vitally important feature in cosmological models.

The second from last term determines a generic interaction vital in the search for the axion via the study of *axion electrodynamics* representing the anomalous axion-photon coupling [823, 854, 1300, 1305, 1354],

$$\mathcal{L}_{a\gamma} = \frac{g_{a\gamma}}{4} a F_{\mu\nu} \tilde{F}^{\mu\nu} = -g_{\alpha\gamma} a \mathbf{E} \cdot \mathbf{B} \ , \tag{2.69}$$

with electric field, $\mathbf{E}$ and magnetic field, $\mathbf{B}$. Axions will transform into photos and vice versa via the presence of an external $\mathbf{B}$ field. The model dependant corrections stemming from the axion mass are negligible to leading order, so the only model dependant concerns lie in the anomaly coefficients. This decay mode is the dominant channel unless the axion mass follows, $m_a \gtrsim 2m_e$. The coupling constant for the interaction in the *right panel* of Fig 2.2, which receives contributions via the EM anomaly, is parameterised using the fine structure constant α,

$$\begin{aligned} g_{a\gamma} &= \frac{\alpha}{2\pi f_a} \left(\frac{E}{N} - \frac{2}{3} \frac{4 + {}^{m_u}\!/_{m_d}}{1 + {}^{m_u}\!/_{m_d}} \right) \\ &= \frac{\alpha}{2\pi} \left(\frac{E}{N} - \frac{2}{3} \frac{4 + {}^{m_u}\!/_{m_d}}{1 + {}^{m_u}\!/_{m_d}} \right) \frac{1 + {}^{m_u}\!/_{m_d}}{\sqrt{{}^{m_u}\!/_{m_d}}} \frac{m_a}{m_\pi f_\pi} \equiv \frac{\alpha}{2\pi f_a} C_\gamma \ , \end{aligned} \tag{2.70}$$

where $\alpha \approx 137^{-1}$ is the fine structure constant, C_γ is a specific constant relating to the axion-photon interaction, with E and N the electromagnetic and colour anomaly for the axial current of the axion field [41, 1084, 1210]. This ratio is determined to

the grand unified model considered and are expressed via the linearised sums,

$$E \equiv 2\sum_{f} Q_{f,\mathrm{PQ}} Q_{f,\mathrm{EM}}^{2} V_{f} \equiv 2\mathrm{Tr} Q_{\mathrm{PQ}} Q_{\mathrm{EM}}^{2} \ , \tag{2.71}$$

$$N \equiv \mathrm{Tr} Q_{\mathrm{PQ}} \ , \tag{2.72}$$

for each of the PQ (Q_{PQ}) and EM (Q_{EM}) charges, where V_f is determined by whether the fermion in the triangle loop interactions is a charged lepton singlet or a quark triplet [1084]. The dimensionful couplings all possess the f_a^{-1} suppression factor, categorising the axion as weakly coupled, capable of avoiding detection through such channels given the magnitude of suppression. Finally the two-photon coupling does highlight an additional important feature of the axion in generic models. For a KSVZ axion, the decay rate in the photon channel is expressed as [793, 1084],

$$\Gamma_{a\to\gamma\gamma} = \frac{g_{a\gamma}^{2}}{64\pi} \approx 1.1 \times 10^{-24} s^{-1} \left(\frac{m_a}{\mathrm{eV}}\right)^{5} \ , \tag{2.73}$$

which, analogous to pion decays, details the axions lifetime dependance on the fields mass to the fifth power. If the axion is then assumed to be at least, $m_a \lesssim 1\mathrm{eV}$, then axion particles are stable over cosmological timescales. The standard phenomenological concerns of the axion are broadly related to those of weakly coupled pNGBs with global symmetries spontaneous broken at large energy scales. These extremely stable fields which are disconnected from the PQ mechanism and the distinct PQ symmetry breaking will not realise their scales from QCD physics, relaying only on other non-trivial effects in order to break the general symmetries. These types of additional scalar are often referred to as *axion-like particles* (ALPs). The stability, symmetries and couplings of the generic axion define this field as a possible solution to the strong CP problem, whilst also acting as a versatile utility capable of slotting into paradigm solutions required in standard models of cosmology. These features define the phenomenological landscape of the *cosmological axion field*.

2.6 The Cosmological Axion

We now move away from the focus considering the axion as a specific issue surrounding particle physics and focus on the general understanding which we can draw from the simplified effective potential in Eq. (2.68). Assuming the concluding points of the previous section, if the axion field does exist then it has significantly suppressed couplings to the other matter fields, regulated by some high energy scale, it is stable on cosmological timescales and possesses a parametrically light mass. All of these features actually lead the axion to be understood as not just a novel solution to issues surrounding Standard Model unification but as something of great interest in the standard approach to the picture of cosmology too. Interest in an *invisible* axion, which can contribute significantly to the cosmic energy density budget, provide extremely interesting solutions within a range of physical models. The production of axions can be factorised into two principle categories, thermal and non-thermal or cold. Our main area of focus will be non-thermal production mechanisms, where we specifically focus on axions generated specifically though the dominant mechanism of *vacuum realignment*.

2.6.1 Thermal Axion Relics

In the evolution of the early Universe, thermal axions can originate alongside various other exotics and the Standard Model matter fields [620, 926, 1143]. In general this thermal population is usually considered in the context of models for the QCD axion due to the general nature of symmetry breaking scales in models containing axion-like fields and the explicit nature of the expected couplings from Standard Model gauge theories. Axions, which possess couplings to the Standard Model, are created and annihilated via their contact and interactions with the primordial plasma. This density produced from the Standard Model interactions in the plasma decouples when the pion scattering rate, $\pi + \pi \to \pi + a$, drops below the rate of the Hubble flow. At this point the interactions *freeze out*. The relic density is then determined

by the temperature of this decoupling process, $T_{\rm D}$ [911]. Even axions not in contact and in thermal equilibrium with the primordial plasma, due to the scales of inflation can be produced by scattering processes. The general number density of thermal axions, n_a, is controlled and regulated by the Boltzmann equation,

$$\frac{{\rm d}n_a}{{\rm d}t} + 3H(t)n_a + \sum_i n_i \left\langle \sigma_i v \right\rangle \left(n_a - n_{a,{\rm eq}}\right) = 0 \ , \tag{2.74}$$

for particle species, n_i where $n_{a,{\rm eq}}$ represents the number density of axions in thermal equilibrium assuming a negligible chemical potential,

$$n_{a,{\rm eq}} = \frac{\zeta(3)}{\pi^2} T^3 \ , \tag{2.75}$$

where $\zeta(x)$ is the Riemann zeta function of argument x. It is considered safe to exclude index values $i = a$, as the axion self-interactions are suppressed by factors of f_a^4 in the quartic interactions of the effective Lagrangian defined in Eq. (2.63). The total rate of interactions between axions and the other particle species is dependent on the temperature of the thermal plasma. The sum over $\langle \sigma v \rangle$ represents the rate of axion creation and annihilation as the flux-averaged cross-section,

$$\Gamma_{\rm ann} = \sum_i n_i \left\langle \sigma_i v \right\rangle \ . \tag{2.76}$$

This average can be found by determining the momentum, the matrix element for the relevant interaction process and the associated distribution functions. Currently the thermal axion number density today can be expressed relative to the photon number density n_γ, as,

$$n_a = \frac{n_\gamma}{2} \frac{g_{\star S}\left(T_0\right)}{g_{\star S}\left(T_{\rm D}\right)} \ , \tag{2.77}$$

determined by the conservation of comoving entropy and expressed using the the dilution factor following from the energy density in a comoving volume, with T_0 the CMB temperature today. The values of $g_{\star S}$ can be determined using Eq. (1.74). When $T_{\rm D} > m_a$, considering standard thermal histories, the axions are relativistic

and contribute to the effective relativistic degrees of freedom $N_{\rm eff}$, shifting the value by $\Delta N_{\rm eff} \approx 0.0264 {}^{n_a}/_{n_{a,\rm eq}} \approx 10$ [911]. Thermal axions can therefore be cosmologically categorised similar to massive neutrinos, whereby they contribute to the overall hot DM density. The upper bound on thermal axion masses are restricted by CMB constraints on these hot DM models [88, 439, 440], which follow the loose bound,

$$m_a < \mathcal{O}(1) \text{ eV} \ . \tag{2.78}$$

It is possible to enhance these limits under the adoption of non-thermal histories [633]. Axions with lower decay constant scales are required in order to enhance the significance of the contributions made from thermal sources, i.e. $f_a \lesssim 10^9$ GeV [1282] for the QCD axion. Populations of thermal axions can also be removed from the thermal spectrum under periods of inflation when some models require extra methods in order to re-establish such a population. It should also be stated that in general case of ALPs, particularly in string models, their couplings to QCD are far less than the case of the QCD axion. We shall assume going forward any thermal population of axions is significantly diluted today, focusing only on the case of cold production mechanisms.

2.6.2 Vacuum Realignment Axions

The simple principle of vacuum realignment or misalignment production of axions can be understood by a field in the early Universe, which may take any random initial state or amplitude. This misalignment methodology may serve as a description for the production of the total required relic density of a cold DM fluid component. Vacuum realignment is also very relevant for models of axion quintessence and inflationary models with an axion serving as the inflaton field. The magnitude of misalignment corresponds to the degree in which the field is displaced from its potential minima. At some point in time in the fields evolution, it is allowed to evolve dynamically, rolling towards its potential minimum with a velocity sufficient

to induce an oscillatory period about the minimum. In the simplest case these oscillations are coherent, where the field is approximated under the simple system description of a harmonic oscillator. The cosmological stability of these quanta determines they evolve as an effective cold DM fluid on cosmological timescales. Vacuum realignment is a reference to the dynamical relaxation of this initial value to the potential minimum. For the axion field, causality dictates how we understand the evolutionary properties of field. The chronological order of the epoch of cosmic inflation and the spontaneous breaking of PQ symmetry, determine homogeneity of the cosmological field. When symmetry breaking occurs the initial field values, θ_i, generate casually disconnected regions inherent with topological defects. This can be understood in terms of the temperature of PQ symmetry breaking, $T_{\rm PQ}$ and some critical temperature, $T_{\rm IN}$, related to scales present in inflationary models. If,

$$T_{\rm PQ} > T_{\rm IN} \approx f_a \ , \tag{2.79}$$

cosmic inflation is believed to have occurred before or during the complete phase of symmetry breaking where any initial defects are diluted away. We must also assume that any PQ symmetries are not restored after cosmic inflation has finished. The casual regions of θ are now stretched, homogenising a single uniform value of the initial field over our Hubble volume. Our understanding of θ then, as a random variable, is a uniform vacuum potentially taking any random initial phase value from the unit circle. In model construction terms the *anthropic window* for axion relic densities comes from considering a tuning to the range of initial values '*our*' axion can take. The most dominant mode is the zero-moment mode, when the PQ scales are beyond the inflationary scales of concern. We will see that zero momentum modes produce a simplified description of the fields evolution as a damped harmonic oscillator, representing the dominant contributing factor for a population of cold axions. On scales larger than the axion coherence length, the field will behave as a collection of cold collisionless particles. The field produces wavelike effects on scales

of order the *De Broglie* wavelength,

$$\lambda_{\rm ax} \sim \frac{2\pi}{p_{\rm ax}} \ , \tag{2.80}$$

with a relativistic momentum for the axion, $p_{\rm ax}$. This gives rise to fascinating phenomena such as the formation of *axion stars*, localised and coherently oscillating solutions of the axion classical equations of motion [405, 699, 1185, 1350]. A particular feature of cold axion dynamics we shall return to in Chapter 7.

We can understand a general lower bound on the axion decay constant, f_a, by considering the Gibbons-Hawking temperature [911] $T_{\rm GH}$, defined using the Hubble rate when the pivot scale of primordial initial conditions became larger than the horizon,

$$T_{\rm GH} = \frac{H_I}{2\pi} \ , \tag{2.81}$$

where H_I is the inflationary Hubble scale. Bounds on the tensor-to-scalar ratio, along with measurements of the CMB scalar amplitude are used to place an estimated limit on the lowest relevant temperature for which inflation is exhausted. Using the requirements in Eq. (2.79) and Eq. (2.81) this fixes the general bound,

$$f_a \lesssim \frac{H_I}{2\pi} \ , \tag{2.82}$$

which in turn translates across to give an approximate upper limit for the axion decay constant [911],

$$f_a \gtrsim 8.2 \times 10^{12} \text{ GeV} \ . \tag{2.83}$$

This also relates to the reheating temperature, $T_{\rm RH}$ [349],

$$f_a \sim T_{\rm IN} \approx \sqrt[4]{T_{\rm RH}^2 H_I M_{\rm Pl}} \ , \tag{2.84}$$

which determines the scales where PQ symmetry is not restored once broken. If symmetry breaking occurs beyond the scales of Eq. (2.83) then topological de-

fects are present and must be accounted for. Topological defects are important structures which occur during symmetry breaking phase transitions of the early Universe. These can include topological features of the vacuum manifold such as one-dimensional cosmic (super)strings, which can form a cosmic string network which may have observational signatures via gravitational wave burst emissions [376, 397, 708, 787, 1139, 1140, 1220, 1286, 1297]. Other higher dimensional variants of these solitonic solutions to the Kibble-Zurek mechanism are two-dimensional domain walls and three-dimensional textures. Relevant to the case of axion production are the presence of axion-strings [406] and domain walls [814], when the symmetry breaking scales are sufficiently low. These strings can interact as they enter the cosmic horizon, whereby they form loops and junctions, entering into a scaling solution. These loops can decay into axions, contributing to the total axion energy density. These decays are in general dominated by low frequency modes, where these particles are cold and so could represent a portion of the CDM.

We have briefly touched on the nature of the periodic, dimensionless axion field in Eq. (2.44). The number of distinct minima is regulated by $N_{\rm DW}$, the domain wall number. If this value exceeds $N_{\rm DW} > 1$ then the axion may posses a domain wall problem [1385], under the selection of different minima in causally disconnected regions. There are a number of solutions to this, the most obvious solution when $N_{\rm DW} > 1$ is to enforce PQ symmetry breaking before or during inflation as we have covered. Other novel solutions to this situation consist of a small explicit breaking of the PQ symmetry [1183].

The topological mechanisms in general maintain a large number of added complexities in order to study the full inhomogeneous evolution of the PQ field, certainly in the case of incorporating multiple fields. We will then from now on assume that any PQ symmetry breaking occurs above the bound in Eq. (2.83), the axion field fluctuating adiabatically with a single value of the initial vacuum misalignment which determines any contributions to the axion energy density. We will also assume the scales are sufficiently high enough for any ultralight fields to fix $N_{\rm DW} = 1$, factoris-

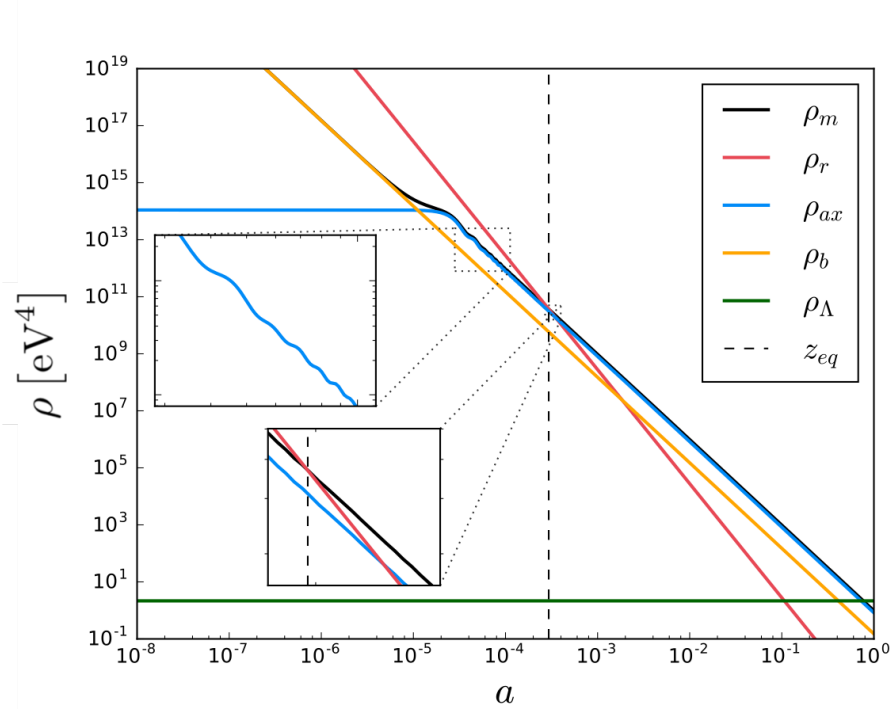


Figure 2.5: Plots for the example evolution of the cosmological densities, ρ_i in Eq. (1.42) as a function of the cosmic scale factor, a(t), with $\mathcal{N}_{\rm ax} = 10$ axions behaving as the total DM density where the mass eigenstates sampled with a realisation of the isometric S-matrix model in Section 5.2.4.1. *Upper inset*: Enhanced view of the effect of multi-field oscillations on the total axion density, $\rho_{\rm ax}$. *Lower inset*: Comparative matter-radiation equality with crossings of $\rho_m = \rho_b + \rho_{\rm ax}$ and ρ_r at $z_{eq} = 3393$.

ing its presence out of any future discussions. For the considered energy scales, the effects of cosmological axions can be easily accounted for using the salient features of the fields cosmology, which is determined by the simple three-dimensional parameter space,

$$\vec{\mathcal{X}} = \{\theta, f_a, m_a\} \ . \tag{2.85}$$

The determination of the spectrum of the scalings in $\vec{\mathcal{X}}$ will be the focus of Chapter 5, where we now discuss their importance for the evolutionary properties of the fields oscillatory behaviour.

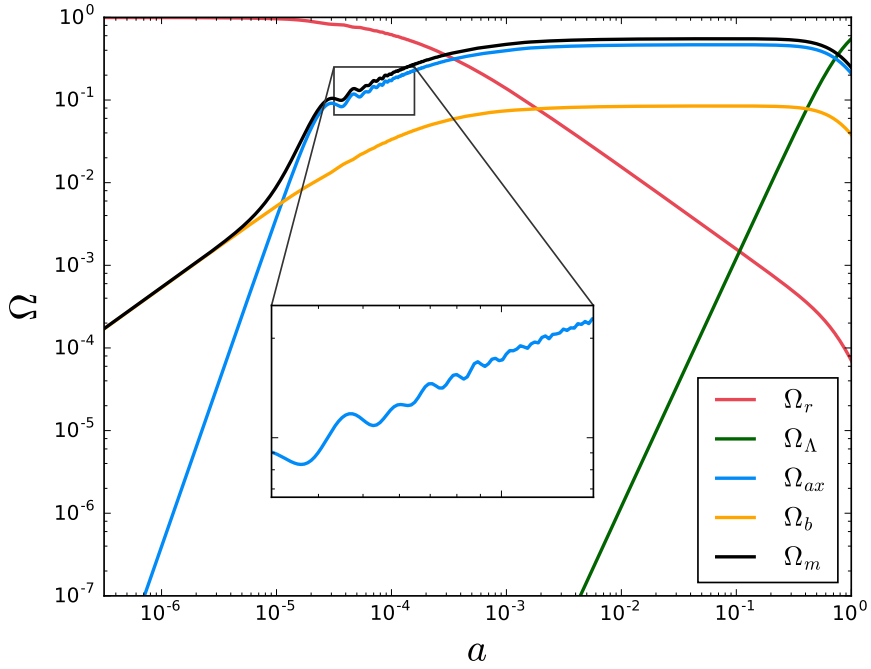


Figure 2.6: Plots for the example evolution of each contribution to the critical density, $\Omega_i = \rho_i/3H^2$, as a function of the cosmic scale factor, a(t). This example cosmology represents a realisation of the total DM with axion mass eigenstates sampled using a realisation of the isometric S-matrix model of Section 5.2.4.1, including the remaining Ω_r, Ω_Λ and Ω_b terms. *Inset*: Enhanced view of the effect of multi-field oscillations on the axion density parameter $\Omega_{\rm ax}$ contributing to the critical density.

2.7 Coherent Axion Field Evolution

2.7.1 Hubble Friction

The background determining the evolution of the axion fields is assumed to be that of a flat FLRW universe, introduced and discussed in Section 1.2. It is assumed the field is a homogeneous component of the model, its expectation value only a function of time, where the evolutionary equations for the axion field follow from the canonical action for matter,

$$S_{\rm ax} = \int \mathrm{d}^4x\sqrt{-g}\mathcal{L}_{\rm ax}\,, \tag{2.86}$$

with g the FLRW metric determinant and $\mathcal{L}_{\rm ax}$ some four dimensional effective Lagrangian for the axion field. The equations of motion for the homogeneous component, or *zero mode* of the axion field, now denoted ϕ, are given by the homogeneous Klein-Gordon equation by varying the canonical action in Eq. (2.86) with respect to the cosmic scale factor and some potential V,

$$\ddot{\phi}_i + 3H(t)\dot{\phi}_i + \frac{\partial V}{\partial \phi} = 0\,, \tag{2.87}$$

where we have enforced the freedom to suppress gradient effects and terms relating the decay of the field due to its stability over cosmological timescales. Assuming the field is suitably described by the instanton potential in Eq. (2.61), we can Taylor expand to give an approximation of the final derivative term in Eq. (2.87),

$$V(\phi) = \Lambda^4 \left(1 - \cos\left(\frac{\phi}{f_a}\right)\right) \approx \frac{1}{2} m_a^2 \phi^2\ . \tag{2.88}$$

The quadratic form of the fields potential, leads to the field equations of a damped harmonic oscillator,

$$\ddot{\phi}_i + 3H(t)\dot{\phi}_i + m_{a,i}^2 \phi_i = 0\,, \tag{2.89}$$

where the over-dot denotes a derivative with respect to the cosmic time. The evolution of Eq. (2.89) is epochal, due to the time dependance of the damping term. When the age of the Universe is of order $t \lesssim {}^1\!/_{m_a}$, so that $H(t) \gtrsim m_a$, the field has had insufficient time to oscillate and is over-damped, fixed at its initial value taken before inflation occurred via *Hubble friction*. At this stage the field slowly rolls down its potential, $\dot{\phi}_i \approx 0$, with an almost constant equation of state, $w_a \approx -1$. As the Universe expands the following condition is satisfied,

$$m_a \simeq 3H(t_{\rm osc})\ . \tag{2.90}$$

The value of $t_{\rm osc}$ represents the cosmic time in which the axion field begins to oscillate about the minimum of its potential. The axion field is now underdamped

oscillating with a frequency $f \approx m_a^{-1}$, and an amplitude determined by its initial fields misalignment angle where the mass remains an adiabatic invariant. Example plots for the oscillatory evolution of the axion parameters acting as a damped harmonic oscillator are shown in Fig. 2.7. At this point in time the number of axions in a comoving volume is fixed. On time scales $t \ll H^{-1}$, the energy density is fixed to $\rho_{\max} = {}^1\!/_2 m_a^2 \phi_{\max}^2$ where the field takes on the ansatz solution $\phi = \phi_{\max} \cos(m_a t)$, where $\phi_{\max}$ is a slowly varying function. Using the WKB approximation, the pressure in the axion energy momentum tensor is expressed to leading order as,

$$P = \rho_{\max} - 2V(\phi) = \frac{1}{2} m_a^2 \phi_{\max}^2 \cos(2mt) \ . \tag{2.91}$$

The pressure is oscillatory, and when considered over short enough timescales it contributes to an equation of state of state which is a non-trivial and is a strongly time dependent function. However when analysed over timescales, $t^{-1} \gtrsim m_a$, the pressure averages to zero,

$$\langle P_a \rangle = 0 \ . \tag{2.92}$$

When the time scale passes $t = t_{\rm osc} \sim H^{-1}$, the axion energy density begins to dilute, the scaling found from the ansatz field solution which gives $\phi_{\max} \propto a^{3/2}$ leading to,

$$\rho_a \propto a(t)^{-3}. \tag{2.93}$$

The explicit homogeneous energy-density and pressure of the axion zero mode are,

$$\rho_a = \frac{1}{2}\dot{\phi} + V(\phi) \ , \tag{2.94}$$

$$P_a = \frac{1}{2}\dot{\phi} - V(\phi) \ , \tag{2.95}$$

where $V(\phi)$ follows the approximation found in Eq. (2.88). The equation of state of the axion field to leading order is given by the ratio of the homogenous pressure

and density functions which when time averaged gives,

$$\omega_a = \frac{\langle P_a \rangle}{\langle \rho_a \rangle} \simeq 0 \ , \tag{2.96}$$

detailing the behaviour of the zero-momentum mode axion field as non-relativistic matter, entering the scaling regime applicable to act as a cold DM component. The power law scaling on the time-dependant cosmic scale factor in the matter and radiation dominated phases of the Universe found in Eq. (2.89) has the exact analytical solution [911],

$$\phi = a^{-3/2} \left(t/t_i \right) \left[\mathcal{U}_1 J_n(m_a t) + \mathcal{U}_2 Y_n(m_a t) \right] \ . \tag{2.97}$$

The constants $\mathcal{U}_1$ and $\mathcal{U}_2$ are determined the initial conditions. The functions J_n and Y_n are Bessel functions of the first and second kind, where the subscript $n = (3p-1)/2$, which is a function of p, is determined by the exponent factor of the fluid power law in Eq. (1.57).

2.7.2 The Equations of Motion

When the axion field comes to dominate the comic energy density, the solution must be solved numerically. The initial conditions of Eq. (2.97) are defined when the equation of motion is over-damped,

$$\phi(t_i) = f_a \theta_a \ , \tag{2.98}$$

$$\dot{\phi}(t_i) = 0 \ . \tag{2.99}$$

Recalling the Friedmann constraint on the Hubble parameter in Eq. (1.77), the Hubble equation can be expressed incorporating the axion fluid density defined in

Eq. (2.94), into the cosmic budget via,

$$H = \sqrt{\frac{1}{3M_{\rm Pl}}\left(\frac{\rho_{m,0}}{a(t)^3} + \frac{\rho_{r,0}}{a(t)^4} + \rho_\Lambda + \rho_a\right)} \ , \tag{2.100}$$

$$= H_0\sqrt{\Omega_m(a(t)) + \Omega_r(a(t)) + \Omega_\Lambda(a(t)) + \Omega_a(a(t))} \ , \tag{2.101}$$

where $\rho_{\rm crit}$, used to define the second expression, is defined in Eq. (1.62) and $\Omega_a(a(t))$ is introduced as the total dimensionless density for the axion. The values of $\rho_{m,0}$ and $\rho_{r,0}$ are the usual observed matter and radiation density constants at the current time. Combining Eq. (2.101) with the Klein-Gordon equation of motion, reveals the following first and second order differential equations defining the complete evolution of the field,

$$\dot{a}(t) = \frac{1}{\sqrt{3}M_{\rm Pl}}\sqrt{\left(\frac{\rho_{m,0}}{a(t)} + \frac{\rho_{m,0}}{a(t)^2} + \rho_\Lambda a(t)^2 + \rho_a a(t)^2\right)} \ , \tag{2.102}$$

$$\ddot{\phi} = -\frac{\sqrt{3}}{M_{\rm Pl}}\left(\sqrt{\frac{\rho_{m,0}}{a(t)^3} + \frac{\rho_{r,0}}{a(t)^4} + \rho_\Lambda + \rho_a}\right)\dot{\phi} - m_a^2\phi \ . \tag{2.103}$$

Depending on the tuning of the axion parameters we can realise this newly introduced field as a field which can satisfy either,

$$\Omega_a \equiv \Omega_{\rm CDM} \approx 0.26 \ , \tag{2.104}$$

$$\Omega_a \equiv \Omega_\Lambda \approx 0.69 \ , \tag{2.105}$$

which serves as the focus of discussions in Chapter 7, for the cosmological axion dark sector of physics.

In the case of multiple fields when more than one axion enters the cosmic horizon, the equations must be linearised to run over a further index j, to account for $j = 1, \ldots, \mathcal{N}_{\rm ax}$ fields contributing to the total energy density, expressed via the simple summation,

$$3H^2M_{\rm Pl}^2 = \sum_{i,j}\rho_{i,j} \ , \tag{2.106}$$

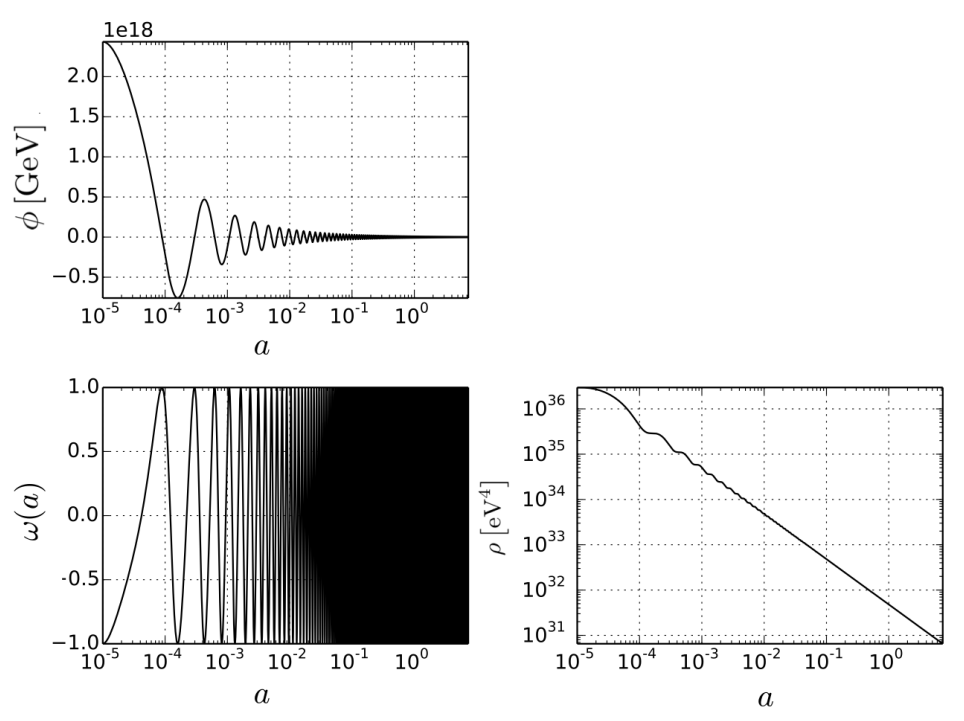


Figure 2.7: Evolution of various cosmological axion field quantities using the exact solution of the background evolution of a single axion field determined using the scalar field equations of motion. As the axion field begins to oscillate about its minimum the fields equations of state (*lower left* panel) oscillates between the limits -1 and 1. At this point the field begins to scale as a non-relativistic cold DM component as shown in the *lower right* panel.

where the sum over i extends over all axions, ordinary matter, DM, radiation, and the cosmological constant. For all i not representing an axionic contribution each further index j is zero for all $i \neq j$. We solve the axion field equations in cosmic time, and use the Friedmann constraint to find $a(t)$, which determines the evolution of the standard fluid components via their equation of state. The combined effective equation of state for the axions used to determine the cosmic acceleration parameter, $\ddot{a}$, is defined by the summation,

$$w_{\text{eff}}(a) = \frac{P_a}{\rho_a} = \frac{\frac{1}{2}\sum_i^{\mathcal{N}_{\text{ax}}} \dot{\phi}_i^2 - V(\phi)}{\frac{1}{2}\sum_i^{\mathcal{N}_{\text{ax}}} \dot{\phi}_i^2 + V(\phi)} \ . \tag{2.107}$$

This represents the full temporal evolution of the effective equation of state from a linear mixture of multiple components. In Fig. 2.5 we detail an example evolution of

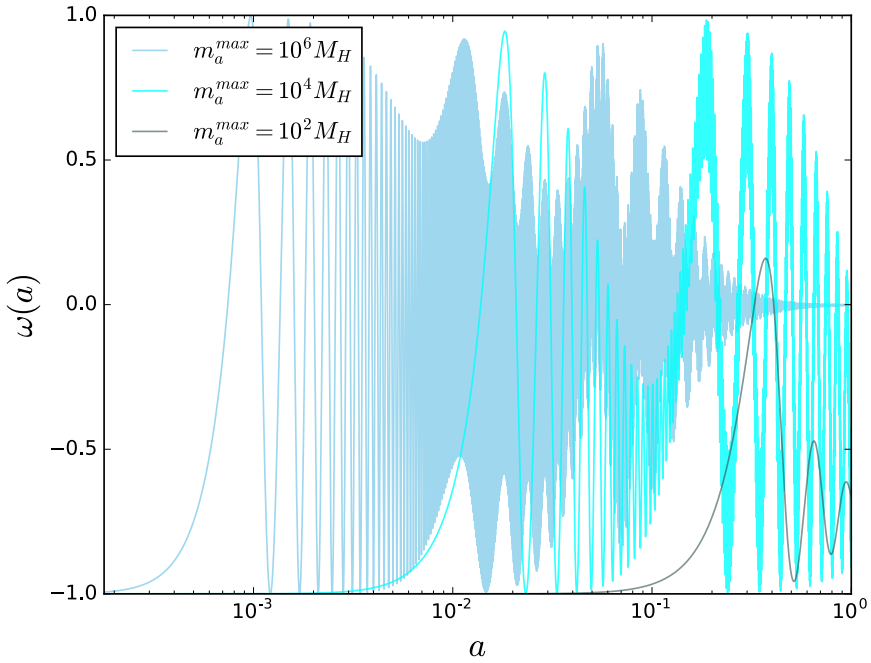


Figure 2.8: Multi-field evolution of the collective equation of state, $\omega_{\rm eff}$, as a function of the cosmic scale factor for three different configurations of multi-axion models with, $\mathcal{N}_{\rm ax} = 5$. Each of the five model masses are scaled in order to reproduce examples realisations with DM dominated, DM/quintessence mixed and quintessence dominated axion cosmologies.

the components of the energy density through numerical integration of the equations of motion for $\mathcal{N}_{\rm ax} = 10$ fields, as well as the remaining standard ΛCDM parameters. The evolution of the corresponding critical density parameters are plotted in Fig. 2.6. We also present a comparative plot for the total equation of state for axion fields distributed about selected mass scales in Fig 2.8. The highest, middle and lowest scales represent collective field behaviour suitable for DM, constrained late-time DM and quintessence configurations respectively. At any given time, fields with $H \gtrsim m_{a,i}$ will behave as a contribution to the total effective DE density, $\Omega_{\rm DE}$ and fields with $H \lesssim m_{a,i}$ behave as contribution to the total DM density, $\Omega_{\rm DM}$. We classify axions as either DM or DE components of the energy density of the Universe according to the descriptions found in Section 1.4. We use this to determine the total sums, $\Omega_m = \Omega_b + \Omega_{\rm DM}$ and $\Omega_{\rm DE,tot} = \Omega_\Lambda + \Omega_{\rm DE}$, which we will introduce in Chapter 7. The evolution of ρ_m with redshift determines the redshift of matter radiation equality,

$z_{\rm eq}$.

2.8 Dark Axions and Accelerated Expansion

2.8.1 The Axion Inflaton

Although not a focus of the work in this thesis, we shall quickly review here the ability of the axion to represent a natural candidate to drive the hypothesised period of inflationary expansion in the very early Universe. The scales considered for these models are in principle disconnected from the concerns we have with the ultralight sector of cosmology, but the dynamics and model construction are very much relatable. The axion-inflaton potential must be extremely flat, to sufficiently drive the expansion. This requirement is parameterised in terms of the fields slow roll conditions, defined in Eq. (2.113) and Eq. (2.114). It is generally expected that the axion acting as the inflaton should decay, rejecting the hypothesis that this field can also be the DM, DE or QCD model counterparts. As is standard practise with inflationary models the axion potential can be constrained using the tilt, $n_{\rm s}$ and the tensor to scalar ratio, $r_{\rm T}$ parameters. It is expected that the primordial power spectra are described using power laws.

The simplest form the axion-inflaton potential can take is that of *natural* inflation [562], using a standard single field slow roll model. In order to embed the axion in models of natural inflation requires a general theoretically unsettling phenomenology requiring, $f_a \gg M_{\rm Pl}$ [154]. Higher order instantons can induce higher harmonics and corrections to the canonical potential, but this is expected with an amplitude that is sufficiently suppressed to leading order in the non-perturbative scales in which it appears. We do however generally expect large field excursions inhibit an instability in the perturbative control of the potential, particularly dangerous are the quantum mechanical corrections of quantum gravity [882]. There are several methods often used to circumvent these issues arising for the case of a single canonically

normalised field. Examples consist of enforcing the axion shift symmetry is broken in a controlled manner, either explicitly or spontaneously. Generating enhanced dynamics through multi-component spectra, dynamics from couplings to other fields and extra-dimensional operators etc. When the shift symmetries are not explicitly broken, the axion potential is constant at all orders in perturbation theory.

A primary example of modifications to the axion inflation model in order to generate the large field displacements is the model of axion monodromy [366, 544, 931, 1187]. These models modulates the power law spectra with periodic features, attempting to unify the principle of chaotic and natural inflation. In the context of string theory monodromy occurs when the axion field is wound around a particular location in moduli space, in order to explicitly break the periodicity of the fields potential and extend the field range of individual axions to distances exceeding the Planck scale. The general monodromy potential takes the form [911],

$$V(\phi) = \mu^{4-p}\phi^p + \Lambda_a^4 \left[1 - \cos\left(\frac{\phi}{f_a}\right)\right] \ , \tag{2.108}$$

with p some numerical value. When the field excursions are large, the potential averages out to be described by the power law proportionality relationship, $V \propto \phi^p$. On small scales the potential is modulated using the standard axion instanton cosine piece. This modulation procedure leads to oscillatory features of primordial curvature perturbations [544]. Further expected results predict resonant non-Gaussianity and unique signals in primordial correlators. Features which may be detectable in future experiments. Inflation can be *assisted* by the presence of multiple fields. The Kim-Nilles-Peloso (KNP) alignment model [798] first considered the case of two fields using natural inflation to account for possible dynamics of the effective potential when rotating through the fields. Each field possesses associated symmetry breaking scales from non-perturbative physics of varying degree. The considered

potential with two interacting axion fields is,

$$V(\rho,\theta) = \Lambda_1^4\left[1-\cos\left(\frac{\rho}{f_1}+\frac{\theta}{g_1}\right)\right]+\Lambda_2^4\left[1-\cos\left(\frac{\rho}{f_2}+\frac{\theta}{g_2}\right)\right] \ . \tag{2.109}$$

In this expression the values of $f_{1,2}$ and $g_{1,2}$ represent the fundamental axion decay constants and θ and ρ are the initial dimensionless values taken by the fields. Under the approximate relation, ${}^{f_1}\!/_{f_2} \simeq {}^{g_1}\!/_{g_2}$ it is possible for the linear combination of axions to present a combination where one field substantially lighter. Inflation is then driven by the lighter combination entering the spectrum, where the heavier field has settled to its minimum. A further two component axion model of inflation is the *Dantes inferno* model [206], where a two-field potential displays a stable trench for a linear combination which slowly rolls dynamically, rendering the resultant physics essentially identical to single-field chaotic inflation.

It is also possible to generate effective trans-Planckian decay constants using the phenomenological predictions of many-field axion models. The N-flation model incorporates $\mathcal{N}_{\rm ax}$ axions with identical potentials for the canonically normalised fields,

$$V\left(\phi_n\right) = \sum_{n=1}^{\mathcal{N}_{\rm ax}} \Lambda_n^4 \cos\left(\frac{\phi_n}{f_n}\right) + c \ . \tag{2.110}$$

Each axion is defined to only allow for sub-Planckian displacements from its potential minima, $\Delta \equiv \phi_n - \phi_n^0 \sim f_a \ll M_{\rm Pl}$. When accounting for the total displacement of the N-dimensional effective potential, the maximum is given by the diagonal of a hypercube (see Fig. 5.1 and Fig. 5.2 and relevant discussions). The so called N-flation type enhancement projects the total displacement to be of the order $|\Delta\phi_n| \sim \sqrt{\mathcal{N}_{\rm ax}} f_a$, which for large enough values of $\mathcal{N}_{\rm ax}$ can transcend the Planckian theoretical barrier. It is then this collective effect which acts as the effective inflaton field. The general effective potential can find a *flat direction* though alignment when there is enough degeneracy between the decay constants, each of which strictly obey the weak gravity conjecture (WGC). The form of the N-flation model will be a primary focus in the effective models of the ultra-light dark sector we will introduce in Chapter 5

and has features easily translatable to the needs of quintessence cosmology.

2.8.2 A Quintessential Component

The apparent natural occurrence of ALPs in numerous high energy physics models had lead many to consider these fields as an attractive solution to help solve one of the greatest issues in theoretical physics to date [300, 1041, 1109, 1137]. The identification of axions as a possible clarification on issues surrounding the cosmological constant, now identified as the mysterious dominant DE component of the Universe, quickly became a desirable model as it offered a potential rectification to both components of the origins of such uncertain physics, i.e. its natural realised presence, whilst addressing the cosmic coincidence problem. Axion models for DE are often analogous to inflationary models with one key differential feature, the energy scale required for the field potential is deemed to be much smaller than the supersymmetry breaking scale of the embedded GUT. The origins of such schools of thought protrude from anthropic tuning [1339] in the string landscape [260, 293, 1229]. The *quintessence* scenario postulates that the current acceleration of the Universe is driven by the potential energy of scalar field displaced from the minimum of its potential [1275], the string landscape provides a suitable background to realise this proposal, the axion an obvious candidate. Examples of quintessence models include *tracker/freezing* models, which suggest functional forms to the quintessence potential tuned to reproduce the measured behaviour of dominant energy density component at late times in the cosmic history, via so called tracker solutions which fix the equation of state as constant during the matter era [302, 1094, 1347]. Other models which require exceptionally flat potentials are often referred to as *thawing models*, which if motivated by an axion-like field [322, 567, 707], inherit the required properties from the protective shift symmetries the axion enjoys to all orders or perturbation theory. The canonical axion potential can give sizeable contributions to a negative energy density factor of the vacuum energy, potentially alleviating

the requirements of external sources in the model to contribute. Generic late-time potentials predict the DE axion mass must be ultralight,

$$m_{a,\text{quin}} \simeq \frac{\Lambda_a^2}{f_a} \equiv H_0 \sim 10^{-33} \text{ eV} \ , \tag{2.111}$$

to ensure the required dynamic shallowness of the potential, with H_0 the present-day Hubble rate. The scale of the dynamically generated potential can be approximated as,

$$\Lambda_a^4 \simeq \overbrace{10^{-130} \ M_{\text{Pl}}^4}^{\text{Observational}} \ll \overbrace{M_{\text{Pl}}^4}^{\text{Theoretical}} \quad . \tag{2.112}$$

There is a general degeneracy between the initial field displacement and the requirements for large decay constants, which can be constrained by cosmological measurements [1198]. In order for the axion to play a suitable role in quintessence models it must vary sufficiently slowly on cosmological scales, defining the general slow role conditions for the potential,

$$\left(\frac{V''}{V}\right) M_{\text{Pl}} \leq 1 \ , \tag{2.113}$$

$$\left(\frac{V'}{V}\right)^2 M_{\text{Pl}} \leq 1 \ , \tag{2.114}$$

where the form of the instantonic periodic potential suggests that ${}^{V''}\!/_{V} \sim ({}^{V'}\!/_{V})^2 \sim {}^{1}\!/_{f_a^2}$, so that in general we require,

$$f_a \gtrsim M_{\text{Pl}} \ . \tag{2.115}$$

This is a notable issue for axion quintessence models where the inclusion of *an* axion field with a trans-Planckian decay constant in a simple sense violates the *WGC*, determining gravity as the weakest force [100]. Tensions from standard swampland conjecture with the WGC however fix the general bound on the decay constant as,

$$\alpha f_a \lesssim M_{\text{Pl}} \ , \tag{2.116}$$

where $\alpha \leq 1$ is a suppression factor specific to the model considered. In string theory the suppression factor is generally related to $S_{\rm inst}$ (the action of the string instanton that generates the axion potential) as considered in Ref. [1230], the size of the instanton action over the corresponding cycles responsible for the axion. In order to generate a suitable axion potential for successful quintessence requires,

$$S_{\rm inst} \sim 200 - 300 \ , \tag{2.117}$$

which for multi-field style quintessence fixes,

$$\mathcal{N}_{\rm ax} \gtrsim S_{\rm inst}^2 \sim 10^4 \ . \tag{2.118}$$

Currently there have been numerous ways in which the expansive string landscape has been able to tread carefully around the wall of the WGC and UV physics. These are often enforced dynamically with the use of clever N-flation [172, 353, 457] type enhancements to the vacuum energy through the presence of multiple ultralight scalars which become dynamical at late times. These models often incorporate the *alignment* mechanism [762, 798], a topic that will be covered in more detail in Section 5.1.1.1. These ensure higher order corrections to the field potential, with higher harmonics in the expansion over the instanton contributions, do not spoil the required flatness. The window in which these fields can enter the cosmic horizon defines the nature of their evolution through various constraints. For *early DE* the critical scale defines the mass of the axion,

$$m_{a,\rm quin} \sim H_c \sim H_0 \sim 10^{-27} \text{ eV} \ , \tag{2.119}$$

which falls in the parameter space of potential ultralight DM. This region is problematic due to cosmological observations and strongly constrained by cosmological observations of the CMB and galaxy data [70, 710]. Such models have interesting features such as the ability to help alleviate the Hubble tension [1072, 1201].

If the decay constant is assumed to follow and conform to Eq. (2.116), then we can consider the maximum value of the field decay constants to be of the order, $f_{a,\max} \sim M_{\rm Pl} \sim 10^{18}$ GeV. For *late-time* DE this can be achieved by ensuring the initial displacement of the axion misalignment angle is maximised, $\theta \sim \pi$, in turn maximising the potential required to sufficiently mimic the behaviour of DE. If a singular axion is present in the particle spectrum then this method would only appear to translate one fine tuning problem to another, the cosmological constant with the fields initial displacement whilst also failing to enlighten us further on the subtleties of the coincidence issue. Often then to relieve these two tensions naturally it is proposed that the so called historical singular quintessence field [210, 211, 323, 1386] is found either within or assisted by an ensemble of ALPs in order to enforce a reasonable statistical degree to the serendipity of the solution. This scenario is indeed well motivated in the string landscape and something that will be discussed in Section 3.3. Originally this idea gained traction from the myriad of string vacua often found in the string landscape. Assuming the Universe is governed by some string vacuum which finds its place amongst vast number of the possible vacua (i.e. 10^{500}) then both the coincidence problem and statistical grievances of late time acceleration are potentially solved in the framework of the *string axiverse*. In Ref. [765] it was argued that a ensemble of axion fields with sub-Planckian decay constants in the spectrum could result in sufficient conditions to account for DE, their mass hierarchy used account for a reasonable solution to the *coincidence* of the problem by proposing an axion field should become dynamical approximately once per decade, i.e. the instanton action changes $\mathcal{O}(10)$ per field and is found using the proposed axion mass function,

$$m_a = \frac{\Lambda_a^2}{f_a} \simeq H_0 \frac{\mu_{12}^2}{\alpha_{0.1}} e^{-\frac{(\beta_a - 223.1)}{2}} \ . \tag{2.120}$$

The values of β_a and μ_{12} are $\mathcal{O}(1)$ dimensionless constants used to tune the scales of the theory. The value of $\alpha_{0.1}$ is a reference to fixing the approximate decay constant scales to $f_a \sim 0.1 M_{\rm Pl} \simeq 10^{17}$ GeV. Under certain considerations with fixed decay scales, it was found it only requires 24 axions to generate a 1% chance

or obtaining sufficient DE, where the 24^{th} axion is the quintessence field. The symmetry breaking scales in this model are bounded under problematic UV physics limits and the fine-tuning is restricted, however there is a phenomenological trade off. The approximate equidistant logarithmic steps each field mass takes in Eq. (2.120) places some of the first 23 fields in constrained problematic regions of the parameter space (see Fig. 5.3). These constraints can be avoided if the fields are allowed to dissipate sufficiently quickly, which can be achieved if their potentials take the form of the higher harmonics in Fig. 2.4 [765, 1071]. We will argue in Section 5.2.1 these issues can be avoided whilst realising a large number of fields in the spectrum via motivations of modality in the mass function and separated scales for clusters of fields determined by universal laws, as opposed to point measure masses.

2.8.3 A Fuzzy Field

It is known cold DM models with a vanishing equation of state are the general leading frameworks to account for the mysterious majority of unaccounted for matter content in the Universe. Axions in principle satisfy two criterion which make them excellent alternative solutions to the problem of DM identification, arising from weakly coupled string models. If the axion relic population is formed pre/during inflation via the misalignment mechanism[3] then it is non-relativistic, with potentially sufficient quantities to reproduce the complete DM density required. They are also effectively collisionless, only relying on long range gravitational interactions [13, 458, 1074]. The original models of the axion covered in Section 2.4.2 provide the possibility that if the axion mass simply obeys, $m_a \gtrsim 10^{-27}$ eV, then the axion energy-density dilutes equivalent to non-relativistic particles after matter-radiation equality, ensuring their candidacy to provide the full DM density of the Universe. Ultralight axionic DM which approaches the scales of early DE is heavily constrained

[3]We can focus our general arguments on realignment production as there is always a contribution to the DM density from this mechanism. Although other mechanisms exist as discussed in Section 2.6, these are often model dependent and can have effects on the tensor modes on the CMB, requiring a suppression to the magnitude of their contributions. See Ref. [453] for details.

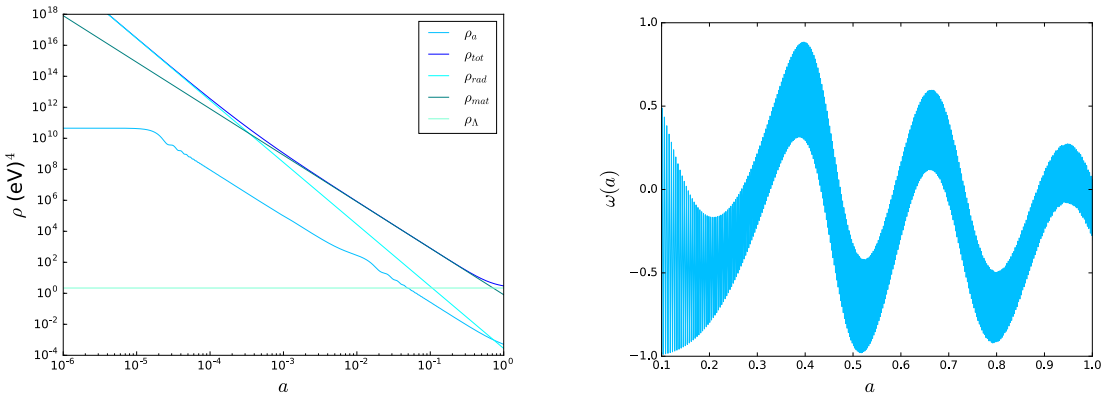


Figure 2.9: *Left panel*: Temporal evolution of the standard cosmic energy density components, along with two additional ULA fields present in the spectrum. The oscillatory behaviour of the total density is visually observed twice, when the axion masses are sufficient separated so that the heavier fields oscillations are heavily damped at $a\,(t^{m_a}_{\rm osc})$, the time of onset oscillation of the second axion with a reduced mass. The fields initial conditions mean the total contribution to the matter density at the present time is insufficient, avoiding constraints such as those in Ref. [710]. *Right panel*: Schematic representation of late time oscillatory behaviour of the effective equation of state defined in Eq. (2.107) for the two-axion effective matter fluid with features of multi-oscillatory behaviour.

via acoustic peaks of the CMB and shapes of the amplitudes of the matter power-spectrum [710]. An example field evolution of a two-component axion cosmic density is shown in the *left panel* of Fig 2.9 which avoids such constraints, highlighting its ability to only contribute a minor fraction of the total DM today. The right panel of Fig 2.9 shows the two-component oscillations of the effective equation of state when each field has a significant hierarchy between the masses. To highlight the strengths general ultralight pseudoscalars have as a DM candidate we will focus on a leading model incorporating an ultralight axion (ULA) field as an alternative approach to the issues of DM. There are numerous small-scale problems with galaxy formation in concordance cosmology. These consist of the missing satellites problem [805, 853, 1199], the Too-Big-To-Fail Problem [265, 266, 1014, 1117], the Core-Cusp problem [251, 545, 913, 1393], and the Plane Satellites Problem [964] to name a few. The true nature to how these issues arise is currently unclear but the exotic nature of DM on small scales is a troublesome part of the problem that must be

understood.

A modification to the standard models of the cold and collisionless axion field to address these issues is known as *fuzzy DM* (FDM) or wave DM [70, 615, 722, 1040, 1078, 1152, 1190]. FDM postulates the scalar-particles are initially in a Bose-Einstein condensate (BEC) which yields kiloparsec scale de Broglie wavelength properties for the DM field. This allows for the field to support the cores of galaxies via their exerted quantum pressure. The free parameter of the model is the axion field mass, m_a. The limiting window which could potentially simultaneously solve the Missing Satellites Problem, the Core-Cusp Problem, and perhaps the related Too-Big-To-Fail Problem is then of great interest. These models are often seen as much more beneficial compared to say warm DM as these have non-negligible free-streaming properties which in turn suppresses structure formation on small scales.

The ultralight dark scalar particles are required to fall inside the approximate mass window,

$$10^{-22}\ \text{eV} \lesssim m_{\text{FDM}} \lesssim 10^{-21}\ \text{eV}\ . \tag{2.121}$$

The FDM mass is often then parameterised as,

$$m_{22} \equiv {}^{m_{\text{FDM}}}\!/_{10^{-22}}\ \text{eV}\ , \tag{2.122}$$

where the approximate time the scalar field approximates to CDM is [974],

$$t_{\text{osc}} \sim \left(10^{-22}\ m_{22}\ \text{ev}\right)^{-1} \simeq 0.2 m_{22}^{-1}\ \text{yr}\ . \tag{2.123}$$

When the scalar mass is $m_a \gtrsim 10^{-20}$ eV the Jeans scale acts as the geometric mean between the dynamical scale and the Compton scale,

$$r_{\text{jeans}} = \frac{2\pi}{k_{\text{jeans}}} = \pi^{3/4} \left(G\rho\right)^{-1/4} m_{22}^{-1/2}\ , \tag{2.124}$$

and is suppressed significantly such that FDM becomes indistinguishable to CDM

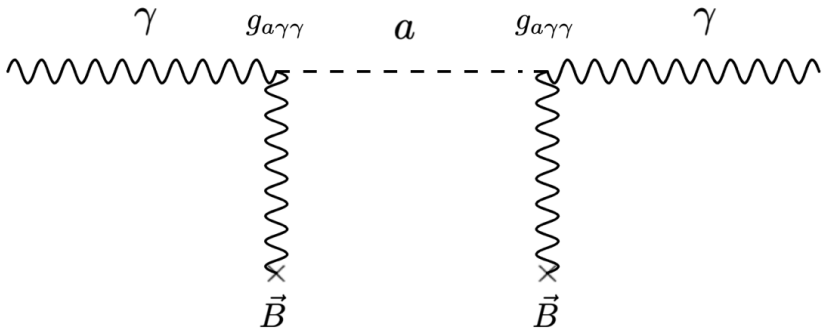


Figure 2.10: Example Axion-photon interaction via the Primakoff process, present in an external electromagnetic field realised through the two photon coupling to the axion particle, which can be reverted to allow for the conversion to either photons or axions. This is the dominant process in many experimental techniques to search for the axion which arising from the properties of the electromagnetic anomaly.

models, where $k_{\rm jeans}$ is the Jeans wave number [722]. This fixes an approximate demarkation boundary between CMD and FDM axion cosmologies. The relic density of the FDM axion with initial field value $\phi^{\rm ini}$, is parameterised as [453, 808],

$$\Omega_{\rm FDM} \simeq 0.16\sqrt{m_{22}} \left(\frac{\phi^{\rm ini}}{10^{17}\ {\rm GeV}}\right)^2 \ln^{3/2}\left[\frac{e}{1-(\phi^{\rm ini}/\pi f_a)}\right] \ , \tag{2.125}$$

where the logarithmic correction is required for anharmonic effects. It is not hard to find limits in which $\Omega_{\rm FDM} = \Omega_{\rm DM}$ as motivated by both particle physics and cosmological observations. Fields possessing high scale decay constants with masses of order, $m_a \simeq m_{22}$ are of particular interest for our analysis. In particular we will discuss constraints on the mass bound in Eq. (2.121) in the context of the 21cm signal and BH constraints with the recently imaged supermassive BH (SMBH) M87* and a spectrum of fields in Section 6.4.7.

2.9 Experimental Searches for the Axion Field

Given the wide landscape of axion masses and associated energy scales quoted in countless models, a small number we have touched on above, many have sought

to develop practical and cleaver solutions in order to search for indications of a signal representative of the possible presence of an axion-like field in the low energy spectrum. Although ALPs have remained elusive so far, substantial effort has been made to exclude and limit the axion parameter windows, where these inferences can be used to drive how to construct and shape future models. The family of *invisible axions* in Section 2.4.2 proposed the first insight as to how consistent models of the axion offered a pretty vexatious freedom in the sheer extent of the fields feasible mass range. We have already commented on how beam dump experiments quickly ruled out [790] any considerations for the original visible axion model of Section 2.4. The general assumption that the axion decay constant scale should be raised and fixed towards more fundamental scales naturally manifests issues surrounding the now significantly suppressed couplings to probeable matter contents of the Standard Model, greatly increasing the difficulty of the task at hand. For example, for the case of the QCD axion the couplings expressed as a function of the inverse energy of the axion field scale, f_a^{-1} are [739],

$$g_{af} \equiv \frac{C_{af} m_f}{f_a} = 1.75 \times 10^{-13} C_{af} \frac{m_f}{\text{GeV}} \frac{m_a}{\mu\text{eV}} \ , \tag{2.126}$$

$$g_{a\gamma} \equiv \frac{\alpha}{2\pi} \frac{C_{a\gamma}}{f_a} = 2.0 \times 10^{-16} C_{a\gamma} \frac{m_a}{\mu\text{eV}} \text{GeV}^{-1} \ , \tag{2.127}$$

$$g_{a\gamma n} \equiv \frac{C_{a\gamma n}}{m_n f_a} = 6.4 \times 10^{-16} \frac{m_a}{\mu\text{eV}} \text{GeV}^{-2} \ . \tag{2.128}$$

Axion experimental searches rely on these couplings which are often as general as possible to account for the ability to search for both the QCD axion and ALPs arising in extended theories such as general string compactification models. Various observational sources have been used to constrain these couplings [739], i.e. neutron star cooling [1167] and SN1987A ν-pulse duration [621] etc. The one-to-one correspondence of the QCD axion decay constant to its mass when realising the new axion symmetry forms a single function line in the axions two-dimensional parameter space. For ALP concerns it is often argued there is an independence between these two parameters, where the field couplings and its mass are relatively

free to be tuned, turning the functional parameter line into a parameter window. For an extensive overview of current searches for ALPs and the QCD axion see Refs. [623, 739, 911]. There are recent interesting suggestions that the boundaries between searches for the QCD axion and purely derivative couplings of spin-0 fields, could in fact very much be the same endeavour [289]. The couplings and symmetries of the QCD axion and ALPs ensure there are several key physical processes which can be measured. Below we detail a selection of the experimental methods used to look for the axion which is certainly far from an exhaustive list, but highlights the diversity and intriguing nature of the approaches taken thus far:

- *Axionic DM direct detections using haloscopes* - One of the classical experiments in order to approach the difficult task of detecting such weakly coupled and ultralight fields [1184]. Currently the most promising active experiment looking for signs of DM is the Axion DM eXperiment (ADMX) [118]. If the axion is the DM particle, then when it enters the microwave cavity with an applied magnetic field, it interacts using the photon coupling to produce a signal which can be measured. The structure of the cavity is tuned so to enhance this process ensuring resonant conversion rates. ADMX is tuned to look for axions with masses, $m_a \approx 10^{-6}$ eV. Future upgrades to ADMX and similar experiments will start to rule our larger portions of the axion mass space in the classical QCD axion window with $f_a \approx 10^{12}$ GeV.

- *Black hole superradiance* - The primary focus of Chapter 6, BH superradiance offers strong constraints though the fields gravitational couplings for ALPs with a Compton wavelength comparable to the Kerr radii of both stellar and supermassive BHs. Principally a model independent process, this interaction in principle does not rely on couplings to Standard Model matter fields or the cosmological energy density, as these quasi-stable bound states can form from quantum fluctuations of the vacuum. The scalar cloud which forms may also offer interesting dynamics to source monochromatic gravitational waves which could be detectable by future detectors. We will cover the fundamentals of this

subject along with a discussion of obtained results in more detail in Section 6.2 and Section 6.4 respectively.

- *Solar axions* - Axions possess a two photon vertex which can lead to the production of photons in an external electric or magnetic field though the so called *Primakoff process* [123, 448], as shown in Fig. 2.10, which was initially detailed in terms of pion physics [1081]. The solar playground of our sun may give indications to the presence of axions due to the electromagnetic fields in the interior of the stellar plasma, which can generate a solar-axion flux measurable on the earth. Contributions can also occur from other ionised sources. The approximate differential flux from solar ALPs is [623],

$$\frac{d\Phi_a}{dE} = 6.02 \times 10^{10} \left(\frac{g_{a\gamma}}{10^{-10}\text{GeV}^{-1}}\right)^2 E^{2.481} e^{-E/1.205} \frac{1}{\text{cm}^2 \text{ s keV}} , \tag{2.129}$$

where E denotes the energy in keV. In the context of the QCD, many of the approaches taken are currently not satisfactory in order to probe the model parameter space.

- *Light shining through a wall* - One of the more captivating methods of detection based on its apparent simplicity and 'pure' laboratory setting [39, 89, 215, 1096]. When a laser is shinned at a surface or 'wall' this represents a production region in which a magnetic field is applied, so that axion conversion occurs and the particles are free to travel through the experimental wall. The process can be reverted on the other side in order to convert the axions back into photons, which come with an associated probability of conversion [911],

$$P(\gamma \to a) = \frac{4 g_{a\gamma}^2 B^2 \omega^2}{m_a^4} \sin^2\left(\frac{m_a^2 L}{4\omega}\right) , \tag{2.130}$$

where ω denotes the energy of the photons and B a coherent magnetic field of length L. Using this current constraints are not as exciting as those imposed from astrophysical sources giving the current strongest bounds [911], $g_{a\gamma} \lesssim$

7×10^{-8} GeV^{-1} ($m_a \lesssim 10^{-3}$eV) [507], which may be enhanced with future experiments [136, 314], with Any Light Particle Search II (ALPS-II) sensitivity expected to hit $g_{a\gamma} < 2 \times 10^{-11}$.

- *Vacuum birefringence and dichroism* - The vacuum of of a static B-field is birefringent and dichroic [697, 732, 1184] due to Primakoff interactions between axions and photons mediated by virtual electron loops [890]. Magnetic fields induce vacuum birefringence where any incident electromagnetic radiation with parallel or perpendicular polarisation modes perpendicular to the B-field posses a different refractive index, stemming from the one-loop QED corrections to the field equations. The dichroism amplitude is given by [911, 1384],

$$\varepsilon = \sin 2\theta \left(\frac{BLg_{a\gamma}}{4}\right)^2 \left[\frac{\sin\left(m_a^2 L/4\omega\right)}{m_a^2 L/4\omega}\right]^2 , \tag{2.131}$$

  where θ is the angle between the magnetic field and the remaining parameters are defined according to those found in Eq. (2.130). By assessing evidence of any polarisation rotation, constraints can be translated to axion couplings and masses. Currently results have proved to be inconclusive, initial Polarizzazione del Vuoto con LASer (PVLAS) signatures deemed to posses no relation to solutions of the strong CP problem or galactic DM.

The methods above represent just a snapshot of the task at hand in either determining the nature of the current hypothetical QCD axion or any signs of possible existence for similar ALPs. Other methods include, the Cosmic Axion Spin Precession Experiment (CASPEr) [294], which proposes an interesting concept to revert away from traditional reliance of the two-photon vertex, underground ion detectors [103], spin dependant fifth force experiments [900], polarisation experiments [430, 1242], Primakoff-Bragg in crystals [740] and Pick up coil and LC circuits [759]. In fact if we dig deeper into unification territory at the must fundamental scales, models actually show almost surely under the assumption of their validity, the QCD axion is most likely not a degenerate state of scalar ultralight matter we should expect to find.

The problem of understanding this space seemingly gets significantly more complex when we consider the fact these fields are often realised as multifarious constituents of a much larger and more complex framework, related to the size and structure of the extra-dimensional spacetime manifolds found in the world of string theory and the extensive landscape of possible vacua forming the string axiverse scenario.

Chapter 3

The Landscape of String Theory and The String Axiverse

> "*The best that most of us can hope to achieve in physics is simply to misunderstand at a deeper level.*"
>
> To Jagdish Mehra, in Berkeley, California
>
> Wolfgang Pauli (May 1958)

3.1 A Landscape of Landscapes

3.1.1 An Outer Dissonance

There are a number of compelling models or frameworks proposed to tackle forming a theory of quantum gravity. One of the main features they all share is that their current appearance in the literature is far from close to being complete. The two theoretical pillars in this endeavour are superstring theories [184, 235, 387, 461, 625, 629, 800, 1063–1065, 1262, 1344, 1366, 1399] and loop quantum gravity [115, 116, 245, 824, 1121–1123, 1258, 1259]. Some major and some minor offshoots are causal-set spacetime [247], asymptotic safety [1240, 1336], shape dynamics [156], superfluid vacuum theory [1191–1193], twistor theory [1043, 1045] and E_8 theory

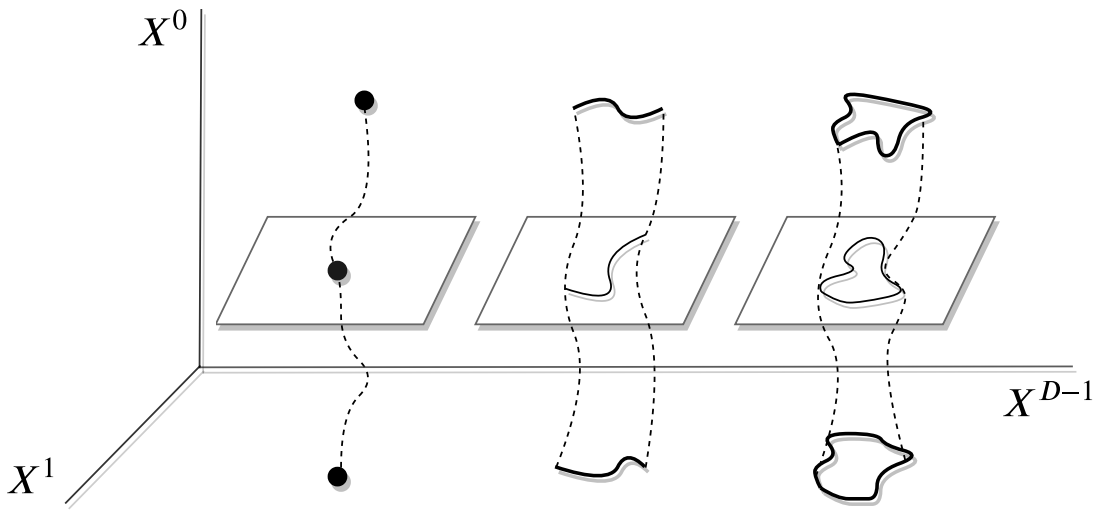


Figure 3.1: Propagation of the traditional fundamental components of quantum theories. Relativistic point particles (*left* example) map out their historical trajectories using a world-line which is defined by a single parameter τ often associated to the proper time. The remaining two examples represent the propagation of open and closed fundamental strings, respectively, of finite length ℓ_s, defining the space of the string worldsheet.

[869]. Perhaps the metaphorical torch barer of these models based on its potentially rich particle content, generated from the elementary vibrational modes of fundamental one-dimensional extended objects, is the broad framework of *string theory*. These objects are parameterised with a one dimensional spatial direction, σ, which propagates in time, τ, both of which define the functions $X^\mu(\sigma,\tau)$ which map out the strings worldsheet, with coordinates (σ,τ). The string worldsheet action determining the evolution of an initial configuration to a final state for a free propagating string, is a sum over string worldsheets, where the action contains terms proportional to,

$$S \supset \int d\sigma d\tau \partial_\alpha X^\mu \partial_\alpha X^\nu G_{\mu\nu}(X) \ , \tag{3.1}$$

where the index i runs over both the temporal and spatial coordinates and $G_{\mu\nu}(X)$ is the spacetime metric. It is possible to define two types of propagating string, those of *open strings* and *closed strings*. Each of these propagate in an open interval and a closed circle respectively, as shown in Fig. 3.1, possessing a different number

of degrees of freedom from their different respective boundary conditions, along with the nature of their left and right moving modes. Originally formulated with the study of scattering amplitudes associated to hadronic bound states in the 1960's [1290, 1299], these studies eventually lead to the conceptual formulation of fundamental relativistic strings from the works of Susskind, Nambu and Nielsen [570, 1224, 1225]. If such models were to connect with the rapidly forming Standard Model of particle physics, parity violation had to be accounted for. This process tends to see the introduction of gauge anomalies which raise complications in constructing a well-defined quantum theory. Initially quantum anomaly considerations for a well defined quantum theory, along with gauge symmetry formalities in order to quantise these strings, offered two very surprising results. The first was an analysis of the string world-sheet action showed the arguments of standard quantisation remained invalid, unless the spacetime considered was in twenty six dimensions [875], containing a particle spectrum hard to control in terms of tachyonic states. These models of the *bosonic string* are now firmly ruled out for numerous obvious physical reasons but they did lay the groundwork for a series of far more interesting *superstring theories*, with the incorporation of the supersymmetry algebra. In this case the string worldsheet now inherits anti-commuting fermionic coordinates representing spacetime vectors of fermionic spinors. The general action now contains terms for the superstring which compared to Eq. (3.1) for the bosonic string are proportional to,

$$S \supset \int d\sigma d\tau \left(\partial_\alpha X^\mu \partial_\alpha X^\mu + \bar{\psi}^\mu \rho^\alpha \partial_\alpha \psi_\alpha \right) \ , \tag{3.2}$$

where ρ^α are two-dimensional Dirac matrices with indices, $\alpha = \{0, 1\}$, with ψ^μ and $\bar{\psi}^\mu$ representing left-moving and right-moving fermionic coordinates respectively. The general introduction of a supersymmetric spacetime, with fermionic degrees of freedom on the string worldsheet, offered a number of comforting and exciting prospects to the particle spectrum. Firstly the number of dimensions is rather dramatically reduced to a much more congenial ten. Secondly the tachyonic states present in bosonic quantisation are removed via the new supersymmetric symme-

try and familiar zero-point energy cancellations. Furthermore issues regarding free closed superstring quantisation and the apparent massless spin-2 states actually developed a courteous relationship with the unwanted massless spin-1 open string counterpart. It quickly became accepted closed and open strings were in fact descriptions of gravity and gauge theory interactions, all that theorists would need in principle to form the basis of a quantum theory of all the fundamental forces of nature. The spin-2 component, which can now be associated with the graviton via quantisation of the closed string, also generates a further degree of freedom known to as the dilaton. This scalar component is part of the *moduli* sector in string theories, which in principle can take an arbitrary value for its VEV and dynamically determines the values of the string coupling constant, g_s. Understanding the properties of a theories moduli represent one of the most important issues in superstring model constructions today.

The second striking result from the process of removing anomalies which are not dependant on the physics in the UV sector, is how anomaly freedom leads to five distinct consistent superstring theories. These can be roughly categorised according to the incorporation of open and closed strings which are historically defined as *Type I* and *Type II* models respectively. Type I is often reserved to reference theories with both open and closed string excitations about the vacuum. Type II superstring theories historically contain only oriented closed strings, where it was later realised these theories could include open string using structures known as *D-branes*. In both the Type I and Type II cases their low energy limits reduce to Type I and Type II supergravity theories respectively. In the critical ten-dimensional limit anomaly-free supergravity theories were found in several perturbative limits based on different gauge group structures. Type IIA by definition is free of anomalies due to its non-chiral formulation. In the case of Type IIB theories its resulting supergravity limit was found to be anomaly-free by using non-trivial cancellations from various anomalous contributions [67]. In a similar nature, model consistency was found in the Type I case when theories were coupled to super Yang-Mills theories. In Ref. [628] it was

shown that anomaly-free field theories existed with the special gauge group configurations, $SO(32)$ and the exceptional gauge group $E_8 \times E_8$, where all gauge and gravitational anomalies rather nicely cancel. Shortly after these results, the formulation of the Heterotic string [636] was discovered using the twenty six dimensional bosonic string for the left-movers and the ten-dimensional superstring for the right movers. This made it possible to build in the distinct gauge groups of dimension 496 and rank 16 which enjoy a $\mathcal{N} = 1$ supersymmetry in ten-dimensions. There were by the end of the *first superstring revolution* five-well defined UV-finite perturbative field theories satisfying all the general requirements such as unitarity and causality etc. A focus was then placed on the anomaly freedom coming from restrictions on the gauge groups themselves, rather than traditional concerns of representation limits in four-dimensional field theory and the Standard Model. Although the shape of this framework still contained seemingly arbitrary features, the discovery of string dualities and the ability to relate all five superstring theories to one another and a common vacua of a more fundamental theory, provided a very positive, refreshing outlook and focus adopted over the *second superstring revolution*.

3.1.2 An Inner Harmony

The second superstring revolution brought about a transition of sorts from natural pessimism which began to manifest itself at the end of the first revolution, to eager optimism in the use of string theory as a viable physical model, the inertia of which is very much apparent today. This was understood by the formation and conceptualisation of the string landscape and the understanding that a vast number of four-dimensional theories were actually related. The primary catalyst for this and a vital theoretical discovery in the historical construction of superstring theories are the remarkably unique duality conjectures. These conjectures, at the rudimentary level, offer a teasing insight into how we might reach the non-perturbative sector of superstring theories, representing a very deep connection between our current

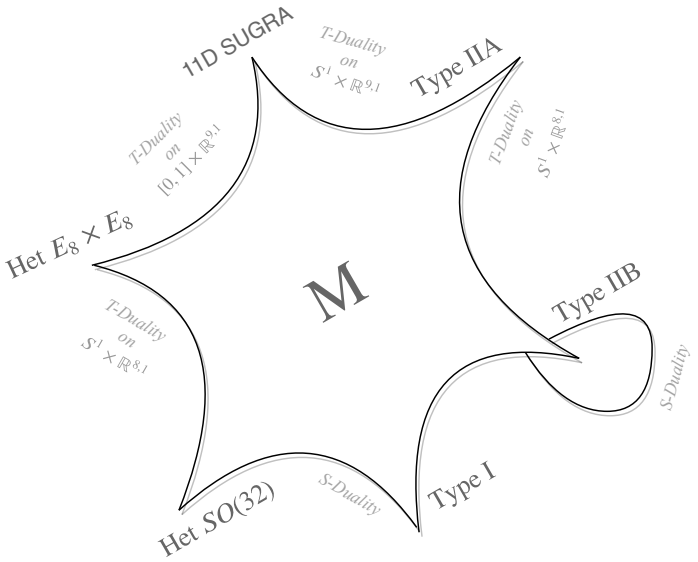


Figure 3.2: The unified space of string theories. Asymptotic expansions around the cusps represent the limits of the weakly coupled superstring theories, which can be studied under the perturbative regime. Currently most of the moduli space associated to the eleven-dimensional quantum theory of M-theory cannot be studied using these limits. The dualities on the outer curves are examples of symmetries used to overcome this issue in order to study the low energy sector using supergravity theories. It is possible that some self-dual point not represented here corresponds to the arbitrary dimensional limit of the true fundamental theory. Whether or not "M" should sit in the centre of this diagram is unclear. This has previously been referred to as *U-theory* [1171] and strongly relates to the notions of string universality. Energy or the distance from the Bogomol'nyi-Prasad-Sommerfield (BPS) limit, increases (decreases) and we move away from (towards) the page.

consistent field theories. These conjectures are understood as a series of equivalence symmetries, which have to date been well tested. They still however, due to the impracticalities of the non-perturbative limits in this sector, remain a fundamental belief in the structure of the string landscape, which have lead to many interesting extensions to the original models. The two principle dualities are the *target space duality* or *T-duality* [65, 605] and the *strong-weak duality* or *S-duality* [1168]. Consider two arbitrary superstring theories $\mathcal{A}$ and $\mathcal{B}$. When theory $\mathcal{A}$ holds an equivalence on a space with large volume to theory $\mathcal{B}$ compactified on a space with small volume, these two theories possess a T-duality symmetry, which can be

expressed perturbatively. This duality relates two string theories when we consider one of the spatial dimensions as S^1. If each theory $\mathcal{A}$ and $\mathcal{B}$ have a ten-dimensional geometry $R^9 \times S^1$ their relationship can be expressed as,

$$R_1 R_2 = \alpha' \ , \tag{3.3}$$

where R_1 and R_2 are the circle radii in each theory and $\alpha' = \ell_s^2$ is the Regge slope parameter related to the fundamental string length. This defines the general T-dual relationship,

$$R \to \frac{\alpha'}{R} \ , \tag{3.4}$$

where KK excitations in one string theory are interpreted as a winding-mode excitations in another. T-duality symmetry relates both the Het $E_8 \times E_8$ and Het $SO(32)$ theories as well as Type IIA and Type IIB theories, defining relationships between two limiting points or cusps in a continuous moduli space of many quantum vacua as shown in Fig. 3.2. The discovery of T-duality was also vital in later discoveries such as orientifold constructions, key components in understanding the low energy spectra in particular superstring theories. The second principle duality, S-duality can be expressed as the quantum mechanical equivalence of two theories via the following simple relationship,

$$g = \tilde{g}^{-1} \ , \tag{3.5}$$

where a weakly coupled theory (g) is related to a strongly coupled one ($\tilde{g}$). The ability to perturbatively expand g ensures non-perturbative information can be obtained about the theory described by $\tilde{g}$. S-duality relates Type I theories to the Het $SO(32)$ as well as Type IIB theories to themselves. This provides information on the strong coupling regimes for each of these three theories. The unification of these two dualities is often referred to as *unification duality* or *U-duality* [729, 950, 992]. When theory $\mathcal{A}$ is compactified on a space of either large or small volume and it holds equivalence to theory $\mathcal{B}$ at strong or weak coupling respectively, then $\mathcal{A}$ is the U-dual of $\mathcal{B}$. These studies lead to a further mathematical symmetry, known as *mir-*

ror symmetry which has lead to a series of extremely powerful physical statements in what initially appeared to be a vastly complex geometrical space (see Fig. 3.5). This symmetry is now best understood with its foundations related to T-duality [1223] and will be briefly touched on in Section 3.3.6. The nuances of how these dualities act on each of the weakly coupled limits, which can be thought of as mapping one point in the moduli space to another, combined with the inclusion of D-branes, lead to a very interesting result. It was determined that in the case of the Type IIA superstring and the $E_8 \times E_8$ heterotic string an eleventh dimension with a size of the order, $g_s \ell_s$ is revealed in the limit of strong coupling [729, 1264]. This mutual limit and non-perturbative extension of superstring theory, defines the branch of study known as *M-theory* [715, 1162, 1365], often used to refer to a consistent quantum theory of gravity in eleven dimensions. In the weakly coupled limit M-theory reduces to a theory representing the limiting critical dimension of supergravity determined by supersymmetry. Unlike the previously defined ten-dimensional theories, M-theory has no dilaton and therefore no perturbative expansion. In the limit of decompactification, it is a theory constructed using two-dimensional extended objects referred to as membranes as opposed to one-dimensional strings. The traditional dilaton in the weakly coupled limits is a scalar mode of the eleven-dimensional metric, detailing M-theory as a more fundamental formulation. A particular use of our understanding of these dualities in an attempt to define results in the non-perturbative regime is *M(atrix)-theory* [152, 1227, 1251], which defines a quantum theory of membranes in eleven dimensions.

Of course all of these beautiful symmetry properties, from a physicists perspective, only have significant value if they can fully connect to the experimental landscape of four-dimensional physics. Chiral fermions arise naturally from theories with $\mathcal{N} = 0$ and $\mathcal{N} = 1$ supersymmetry, so this is often deemed a preferential starting point to aim for. In a general sense there has been real traction to believe these theories act as a very natural candidate to understand many of the mysteries coming from the Standard Model. Even within these consistent theories there are several pervasive

issues for phenomenologists. An obvious one is the space of vacua is extremely large. The famous quoted number of possible flux vacua [112, 260, 428],

$$N_{\text{flux}} \sim \mathcal{O}(10^{500}) \ , \tag{3.6}$$

a number on the surface, which seems to rule out any practical methods of scanning or exploring the possible total space. At this current stage in the evolution of these theories, a fascinating and very necessary task which presents itself is the exploration and contemplation of string theoretic features which are common in what appears to be all current consistent formulated string models, or rephrased, common in entire classes of compactification methods. Possible inferences can then be drawn from these underlying symmetry concepts or features. These theoretical features could lead to what is one of a number of possible *smoking guns* to the presence of superstrings. The process of connecting the critical higher dimensional spaces to the four-dimensional universe predict the appearance of generic signatures, such as fundamental scalars which act like the axion of the Standard Model found in the discussions of Section 2.4. How exactly these manifest themselves is understood in how we stabilise the scalar moduli. It should be noted in the following sections a substantial number of formulae are quoted without derivation or explicit construction, as this is beyond the scope of this thesis. They are therefore included only to provide some context to the complexities behind the nature of axions apparent in four-dimensional extensions to the Standard Model of particle physics.

3.1.3 String GUTs

Although string theory in principle provides us everything we need to describe the world we observe, gravitational interactions, non-abelian gauge groups and chiral matter etc. the task of cementing these features in a more fundamental GUT theory representation stemming from a string model is a tricky task. The general consideration and excitement surrounding GUT models embedded in some string framework

has seen the construction of many techniques aiming to arrive at the Standard Model and unify these two visions. From the ground up, a pillar of this endeavour concerns the incorporation of the important feature that the gauge coupling constants of Eq. (2.1) appear to unify in the minimal supersymmetric extension of the Standard Model (MSSM) [455, 1337]. It would then appear we are on the right track by considering the familiar matter content of the Standard Model to be part of a more simple group (for example $SU(5)$ or $SO(10)$). As discussed in Section 2.1 the Standard Model of Particle Physics contains a large number of free parameters. The ability to reduce this number is a natural feature of GUTs through the incorporation of a relationship between the matter fields and interactions at some high energy scale, i.e. $M_{\rm MSSM} \simeq 2 \times 10^{16}$ GeV. For a GUT construction the desire of unifying the three Standard Model gauge couplings will occur when they meet at a common value, $\alpha_{\rm GUT} = g^2/4\pi$ at the relevant fundamental scale. The value of g represents the gauge coupling constant of the gauge unification group. In the context of string theory, given the vast space the theoretical landscape offers, suitable *phenomenological guidelines* (gauge coupling unification, proton decay, the chiral spectrum, Yukawa couplings and neutrino masses etc.) are often considered as solid aims to guide the search for '*realistic*' string models. This represents just one example of a suitable strategy deployed to deal with the vast numbers of four-dimensional vacua. In its minimal implementation unification offers a number of set backs. One key example being $SU(5)$ GUT extensions incorporating a standard Higgs sector and the apparent tensions between the bounds on proton decay [837, 983]. Given the various extended freedoms we may encounter in the landscape, string theoretic models may well hold the key to unlocking these issues from details stemming from the top down approach to unification [79, 181, 255, 841, 971]. It is therefore of great importance to understand how unification may be realised in string theory where these principles motivate the exploration of a subset of vacua in the landscape. Of course traditional supersymmetric GUTs are not a unique path to unification although it does appear the most natural, other examples and extension [449] also include

heavy string threshold corrections [337, 450, 451, 465, 772, 928, 929, 984, 1059], strong-coupling effects [1367], non-standard hypercharge normalisations [452, 733], extended MSSM matter [450, 451] to name a few.

Historically a significant part of the formulation of GUTs with string theory belongs to the heterotic String and the ability to naturally realise GUT subgroups with a promising spectrum at the perturbative level. We have already touched on an example of this group structure in the introduction, namely $E8 \supset E_6 \supset SO(10) \supset SU(5) \supset SU(3) \otimes SU(2) \otimes U(1)$ (see also Fig. 3 and surrounding discussions). Ever since the first string revolution there have been a many string model constructions which have demonstrated the ability to provide a total number of three generations. This work nicely built on many of the successes which provided the ground work for realistic string frameworks, producing grand unified theories combined with quantum gravity, such as the insights of Green-Schwarz anomaly cancellation in Ref. [1363]. The subsequent construction of the $E_8 \times E_8$ heterotic string [636] signalled a defining point in the practically of approaching a string description of GUTs. The model used the compactification of a Calabi-Yau manifold, specifically with the unique supersymmetric background where only the internal metric is non-trivial [308]. The primary motivations behind this work coming from the attractive feature that groups one would typically associate to GUTs, such as those quoted above, naturally embed themselves in one of the E_8 factors and the naturally high string scales in these models. Subsequent to these models, heterotic string solutions on six-dimensional orbifold spaces were considered with some considerable success. One early example of a *benchmark* model can be found in Refs. [735, 738], making use of the $\mathbb{Z}_3$ orbifold and Wilson lines, due to the naturally ability to find multiples of three families [73–75, 471, 622]. Later attempts were also made in the context of the internal degrees of freedom of free fermions [81, 779] or bosons on a covariant lattice [848] formulating consistent four-dimensional heterotic string vacua.

One broad categorisation of these higher dimensional models are those with either *local* or *non-local* GUT symmetry breaking. Local unification concerns itself

with consistent (global) string models in which the gauge symmetries are enhanced at special points in extra-dimensional space. An example of local GUT symmetry breaking can be found in traditional orbifold compactifications [230, 326, 327, 344, 461, 462, 547, 735, 738, 841–843, 985] of the heterotic string [637, 638]. Orbifold compactification of the heterotic string is a process which takes advantage of the simplicity of torus compactification and the relevant presence of realistic gauge groups and the resultant spectrum in four-dimensions. Example Non-local GUT breaking can be found in models explored through Calabi-Yau compactifications [72–74, 256, 275, 634]. Many subsequent models which stemmed from the original formulation of the heterotic string often contain extended content such as vector-like pairs, exotics or unconstrained moduli. See Ref. [629] for a review of GUT frameworks arising from these compactification models. These issues are an example of one possible signal that a deeper exploration amongst the web of dualities of string theory may be required for consistency.

Many modern approaches have considered Type II frameworks which switch up the paradigm with the use of D-branes [234–236, 475, 880, 986]. The most relevant details for D-branes being that they can produce the required gauge symmetries in Type II models exactly where gauge groups cannot appear otherwise. In Type II constructions, non-abelian gauge structure is found by embedding stacks of D-branes on a Calabi-Yau three-fold [385, 386]. In terms of realising the MSSM, a minimal model takes the form of a Calabi-Yau three-fold, taken to be an orbifold where the Standard Model gauge structure can be identified through a stack of three D-branes ('*baryonic*'), intersecting a stack of two D-branes ('*left*' - for left-chiral quarks and leptons) finally intersecting several single D-branes (one '*leptonic*' and one '*right*' for right-chiral fields). The resulting four-dimensional gauge sector is of the form $SU(3)\otimes SU(2)\otimes U(1)\otimes U(1)$. The required symmetries are manifest from independent oriented open strings that can be attached to a D-brane or to a stack of superposed D-branes. For a review of Type II constructions and the useful features of D-branes see Ref. [234, 237, 889]. See Refs.[71, 328, 609, 610] for discussions of

Type IIA models and Refs. [71, 238, 391, 903] for discussions around Type IIB. For Type IIA and Type IIB theories, GUTs can also arise from the compactification of M-theory or F-theory on Calabi-Yau fourfolds respectively.

In the context of F-theory, a minimal approach to local models concerns itself with a stack of seven-branes wrapping a del Pezzo 8-surface equipped with the desired gauge group SU(5) (or some larger applicable group) [180, 181]. Under this representation, localised on curves where the GUT brane intersects other branes we find features such as the three generations of chiral matter or the Higgs field. See Ref. [240] for a non-local approach realised on a Calabi-Yau four-fold. One consideration in F-theory which differs from other approaches, in the context of the rigidity of the framework, is the nature of how to break the GUT group. For example the use of a del Pezzo surface restricts the applicability of Wilson line breaking. One example alternative to this is making use of gauge field fluxes [181]. For a review of F-theory approaches see Ref. [180, 181, 239, 469, 470, 685, 905, 908, 1330]. See also Refs. [329, 368, 546, 692, 736, 777, 847, 907, 908, 1249] for particular considerations on certain phenomenological guidelines as mentioned above.

It has been shown in numerous works that M-theory compactified on a manifold of G_2 holonomy reduces nicely to four-dimensional models with supersymmetry. For general considerations in these models the presence of Yang-Mills fields and chiral fermions occur from the exploration of particular singularities in the extra-dimensional space [23, 25]. More specifically the Yang-Mills fields are localised along three-dimensional subspaces of the seven-dimensional manifold in the presence of an orbifold singularity. The chiral fermions in these models are coupled to the Yang-Mills fields and appear at localised points at which there is a conical singularity. See Refs [20, 22, 23, 27–29, 31, 119] for an extensive review of these points and a more complete look at the M-theory framework in which realistic four-dimensional vacua can arise.

The G_2-MSSM [22, 29] represents a framework which considers the general known

properties of G_2 compactifications of M-theory in order to explore numerous details in the context of string phenomenology. In particular success has been found in areas such as, radiative electroweak symmetry breaking [28], baryogenesis [767], inflation [766] and investigations of Yukawa couplings [614]. These models offer several novel features in regards to their phenomenological viability with unification such as a possible resolution [35] to the *double triplet splitting problem* [734] or a solution [32] to the μ problem [797]. In terms of unification and extended groups examples MSSM type models in the low energy limits of M-theory with GUTs based on $SO(10)$ were considered in Refs. [35, 36]. These models utilised discrete symmetry and Wilson lines [1368] to prevent proton decay whilst ensuring the required gauge unification. Assuming an MSSM visible sector below the unification scale, the unified gauge coupling can be parametrised by the volume of the seven dimensional internal space (Eq. (5.78)) or suitably the three cycle volume supporting the visible sector (see Eq. (5.127) and surrounding discussions). The Yukawa couplings are determined by membrane instantons which relate to singularities in which the chiral superfields are supported. We will cover some features of these models in more depth in both Section 3.3.5 and Section 5.3. The examples mentioned above are of course far from an exhaustive list of the spaces in the string landscape and techniques used where comfort has been found in regards to the possibility of unification.

3.2 Generalities of Moduli

The striking feature of superstring models and their low energy supergravity limits for phenomenologists and cosmologists is the obvious appearance and requirement to account for the extra-dimensional spacetime, present for consistency in quantisation. The standard caveat of string model building is that we must account for, and suitably stabilise, the model moduli when compacting the extra-dimensions. As we have seen grand unified supersymmetric models for mathematical consistency currently require at least a ten/eleven dimensional spacetime, in which the extra

six/seven dimensions must be compact and suitably small to maintain consistency in the limit of the four-dimensional observational universe we inhabit. This process manifests the appearance of scalar moduli which can have a drastic effect on both model viability and phenomenological predications.

3.2.1 Dimensional Reduction

In order to understand the principles behind what is ultimately a very complicated picture let us begin with the general principle of bosonic field theories with extra dimensions and the defining precursor of string compactification using the generalities of KK reduction [763, 802, 803]. The theoretical origins of five-dimensional theories initially came on the back of extensions to general relativity and attempts to unify the gravitational force and electromagnetism. The general action of a real massless scalar field ϕ, in five dimensions is,

$$S = \int d^5x \partial_{\mathrm{M}}\phi\partial^{\mathrm{M}}\phi \ , \tag{3.7}$$

using the standard conventions ∂^{M}, with Minkowski field space metric, $\eta_{\mathrm{MN}} = \partial_{\mathrm{MN}} = \mathrm{diag}(-,+,\ldots,+)$, $\mathrm{M},\mathrm{N} = 0,\ldots,4$. The flat space metric is such that the five-dimensional space $\mathcal{M}^5$ has a product form,

$$\mathcal{M}^5 = \mathcal{M}_4 \times \mathrm{S}_1 \ , \tag{3.8}$$

where $\mathcal{M}_4$ is four-dimensional Minkowski space and S_1 represents a circle of radius R. The background metric solutions then take the form,

$$\eta_{\alpha\beta}(\vec{x},\vec{y}) = \begin{pmatrix} \eta_{\mu\nu}(\vec{x}) & 0 \\ 0 & \eta_{mn}(\vec{y}) \end{pmatrix} \ , \tag{3.9}$$

with $\eta_{mn}(\vec{y})$ the newly introduced metric on the compact space, with the full coordinate decomposition, $x_{\mathrm{M}} = (x_\mu, y)$, where $\mu = 0,1,2,3$ and $y \in [0, 2\pi R]$. The

value of R represents the radius of the compact dimension. The field can be decomposed using these coordinates due to its periodicity, $\varphi(x_\mu, y) = \varphi(x_\mu, y + 2\pi R)$, as a generalisation of a Fourier expansion on a circle,

$$\varphi(x, y) = \frac{1}{\sqrt{2\pi R}} \sum_{n=-\infty}^{\infty} \varphi_n(x) e^{\frac{iny}{R}} \ , \tag{3.10}$$

where the quantities, $R_n(y)$, represent the orthonormalised eigenfunctions of the Laplacian ∂_y on S_1. The decomposed action is now,

$$S = \int d^4x \int_0^{2\pi R} dy \partial_\mu \varphi \partial^\mu \varphi + \partial_y \varphi \partial^y \varphi \ , \tag{3.11}$$

where the field satisfies the five-dimensional equations of motion defined using the five-dimensional Laplacian operator,

$$\Box_5 \varphi = 0 \ , \tag{3.12}$$

$$\partial_\mu \partial^\mu \varphi + \partial_y^2 \varphi = 0 \ . \tag{3.13}$$

Substituting in the Fourier expansion of Eq. (3.10) into the equations of motion yields,

$$\partial_\mu \partial^\mu \varphi_n - \frac{n^2}{R^2} \varphi_n = 0 \ , \tag{3.14}$$

which represents a four-dimensional scalar field $\varphi(x)$, with a mass n/R. Combining the orthonormal eigenfunctions with the decomposed action of Eq. (3.11) along with an integration over the extra radial dimension gives the new form of the action,

$$S = \sum_{n=-\infty}^{\infty} \int d^4x \left(\partial_\mu \varphi_n \partial^\mu \varphi_n^* + \frac{n^2}{R^2} \varphi_n \varphi_n^* \right) \ . \tag{3.15}$$

This reveals the nature of compactification, where in four dimensions there is now a single massless scalar plus an infinite tower of massive scalars each with a mass, n/R. The VEV of the field is the radius and a free parameter of the background, where the background solutions are required to produce Ricci flat metrics. When

the field, $\phi(x_\mu, y)$ has a five-dimensional mass m_0^2, the four-dimensional KK degrees of freedom have a mass, $m_n^2 = m_0^2 + {}^{n^2}/_{R^2}$. This can easily be generalised to a torus in higher dimensions where we now have, $m^2_{n_5,n_6,\ldots} = m_0^2 + {}^{n_5^2}/_{R_5^2} + {}^{n_6^2}/_{R_6^2} + \ldots$. The values of R_6 etc. are the radii of the higher dimensional compact dimensions. Generally we are interested in a reduction of the extra-dimensional space in the limit $R \to 0$, where it is small enough such that it cannot be probed, meaning the four-dimensional effective description does not see the compact space. In this limit the zero-mode φ_0 often remains light and φ_n when $n \neq 0$ are heavy degrees of freedom we integrate out of the spectrum.

Suppose now we consider the metric itself as a dynamical field then KK compactification can be expressed starting with the five-dimensional Einstein-Hilbert action,

$$S = M_5^3 \int d^5x \sqrt{-G} R_{5\mathrm{D}} \ , \tag{3.16}$$

where $G = \det(G_{\mathrm{MN}})$ and $R_{5\mathrm{D}}$ is the five-dimensional Ricci scalar. A Fourier expansion of the metric field gives,

$$G_{\mathrm{MN}} = \frac{1}{\sqrt{2\pi R}} \sum G^n_{\mathrm{MN}}(x) e^{\frac{iny}{R}} \ , \tag{3.17}$$

where performing the same process as before with the metric field expansion and the five-dimensional Einstein-Hilbert action reveals a spectrum for the massless sector, with the graviton, $g_{\mu\nu}$ partnered with a vector field, A_μ and scalar S from the zero-mode component of the metric [802]. These general additional scalar fields can be viewed as the presence of extra-dimensional gravitons, massless modes which always appear in compactification models when perturbing around the leading order linearised equations. It is clear then, that in general this process gives rise to both problematic components such as massless moduli generally forbidden due to the nature of long range forces. It can also furnish our theory nicely with suitable candidates representing fields expected to appear in the low energy sector, taking phenomenological concerns into account. We seek a solution of the lower-dimensional

equations of motion which also serve as a solution to the full higher-dimensional counterparts. Using these general ingredients the minimal ten-dimensional superstring models offer a rich low energy effective description where KK reduction is applicable in certain regions of the moduli space of consistent vacua.

3.2.2 Ten-Dimensional Supergravity and Kähler Moduli Stabilisation

There are numerous consistent compactification models which work in the critical ten/eleven-dimensional limit required for superstring theories. Some examples are M-theory on G_2 [25, 481, 1013], Non-Kähler [183, 571, 1222] or heterotic string compactifications [308, 1222, 1364]. In the case of a ten-dimensional theory, let us briefly focus on a snapshot representation of the principle features of the well structured case of flux vacua in Type II theories. Once again, the equations quoted in this section are done so without derivation, presented only to provide a ten-dimensional context to the four-dimensional theory addressed in this thesis. In the simplest case we now want to address,

$$\mathcal{M}_{10} = \mathcal{M}_4 \times K_6 \ , \tag{3.18}$$

where $\mathcal{M}_4$ is a four-dimensional Minkowski space and K_6 is a compact space admitting a Ricci-flat metric. Compactified Type IIB superstring theories preserve $\mathcal{N} = 2$ supersymmetry where it is required to introduce external objects such as orientifold planes and D-branes to break down the theory to the case of a $\mathcal{N} = 1$ [235], four-dimensional theory. In the limit of supergravity any interactions of the relevant modes are described by a low-energy effective Lagrangian which is formed using KK reduction of the ten-dimensional Lagrangian. The Type IIB classical effective supergravity action is divided up as follows [602, 784],

$$S^{(10)}_{\rm IIB} = S_{\rm Bulk} + S_{\rm CS} + S_{\rm Source} \ , \tag{3.19}$$

where each component is defined in the string frame. The decomposed factors S_{Bulk}, S_{CS} and S_{Source} are explicitly defined to leading order in α' as,

$$S_{\text{Bulk}} = \frac{1}{(2\pi)^7\alpha'^4}\int d^{10}x\sqrt{-g}\left[e^{-2\phi}\left(\mathcal{R}+4(\nabla\phi)\right)-\frac{F_1^2}{2}-\frac{1}{2\cdot 3!}G_3\cdot\bar{G}_3-\frac{\tilde{F}_5^2}{4\cdot 5!}\right] , \tag{3.20}$$

$$S_{\text{CS}} = \frac{1}{4i(2\pi)^7\alpha'^4}\int e^{\phi}C_4\wedge G_3\wedge\bar{G}_3 , \tag{3.21}$$

$$S_{\text{Source}} = \sum_{\text{Sources}}\left(-\int_{\mathbb{R}^4\times\Sigma} d^{p+1}\xi T_p e^{-\phi}\sqrt{-g}+\mu_p\int_{\mathbb{R}^4\times\Sigma}C_{p+1}\right) , \tag{3.22}$$

with the form fields C_n, and field strengths $F_{n+1}\equiv dC_n$. The term $\mathcal{R}$ represents the Ricci scalar and $G_3 = F_3 - \phi H_3$ ($H_3\equiv dB_2$) in the CS action is the field strength formed from the Ramond-Ramond (RR) and Neveu-Schwarz (NS) three-form field strengths. The final term represents the possibility of including localised sources in the background such as the D3/D7-branes and orientifold planes used to regulate the level of supersymmetry and the resulting spectrum. The values of T_p and μ_p represent the tension and charge of the Dp-brane respectively. The term ϕ defines the *axion-dilaton* field,

$$\phi = C_0 + ie^{-S} , \tag{3.23}$$

with S the Dilaton and C_0 the axion. Finally the five-form field which satisfies the self-duality condition with the Bianchi identity is defined as, $\tilde{F}_5 = F_5 - \frac{1}{2}C_2\wedge H_3 + \frac{1}{2}B_2\wedge F_3$. We can consider the warped compactifcation metric ansatz for a Calabi-Yau to leading order in α', for solutions of the form, $\mathcal{M}^{\alpha}\times\mathcal{C}^{(11/10-\alpha)}$ analogous to that of Eq. (3.18), for a six dimensional compact manifold, where in the presence of fluxes we have,

$$ds_{10}^2 = \sum_{m,n=0}^{9} G_{mn}dx^m dx^n = e^{2a(y)}\eta_{\mu\nu}dx^\mu dx^\nu + e^{-2a(y)}g_{\alpha\beta}dy^\alpha dy^\beta , \tag{3.24}$$

using four-dimensional coordinates x^μ and compact manifold coordinates, y^α. The nature of these warped solutions on a compact manifold determines various con-

straints for the valid flux/brane configurations to consider [417, 893]. The value of $a(y)$ represents a warp factor related to the scale of the four-dimensional Minkowski space. The axion/dilaton can vary over the compact manifold, $\phi = \phi(y)$. When compactifiying the extra dimensions on a Calabi-Yau to a four-dimensional theory, the naturally arising supergravity theory is parameterised by a Kähler potential, K, a superpotential, W, and gauge kinetic function, F. A Kähler modulus is understood as the radial modulus in a four-dimensional superfield, ρ. The tree-level Kähler potential after dimensional reduction of the ten-dimensional action is,

$$K = \underbrace{-3\ln\left[(\rho+\bar{\rho})\right]}_{\text{Radius}} \overbrace{- \ln\left[\left(\phi+\bar{\phi}\right)\right] - \ln\left[-i\int_{\mathcal{M}}\Omega\wedge\bar{\Omega}\right]}^{\text{Dilaton and complex structure moduli}} , \tag{3.25}$$

where Ω is the holomorphic (3,0) form. The present fluxes generate a superpotential of the Gukov-Vafa-Witten (GVW) form [642],

$$W = \int_{\mathcal{M}} \Omega \wedge G_3 \ , \tag{3.26}$$

independent of the Kähler moduli but dependant on the complex structure moduli. Similar physical scenarios arise and can be defined with F-theory compactified on an elliptically fibered Calabi-Yau four-fold [1170]. In principle when K and W are well defined, the moduli potential can be calculated at the minima, where they are stabilised. There are both perturbative and non-perturbative corrections to the effective supergravity action. In the case of $\mathcal{N} = 1$ supersymmetric compactifications the ten-dimensional effective supergravity action is perturbatively corrected by a series of higher-derivative terms,

$$S = S_{(0)} + \alpha'^3 S_{(3)} + \ldots \alpha'^n S_{(n)} + \ldots \ , \tag{3.27}$$

where the α' correctional terms have absolved factors of string loop corrections suppressed by powers of g_s. The nature of these corrections will become important in defining the spectrum of axions. The $\mathcal{N} = 1$ supergravity scalar potential is

defined as,

$$V = e^K \left(\sum_{a,b} g^{a\bar{b}} D_a W \overline{D_b W} - 3|W|^2 \right) \ , \tag{3.28}$$

with Kähler potential K, where the values of both a and b run over all the moduli and $D_i W = \partial W_i + (\partial_i K) W$. In a very general $\mathcal{N} = 1$ compactification sense these components (Eq. (3.25), Eq. (5.101) and Eq. (3.28)) define the ability to compute the spectrum of axions. The process must consider all leading order corrections to the superpotential in Eq. (5.101), whilst then computing the full scalar potential in Eq. (3.28), which must finally be minimised to define metastable de Sitter vacua [657]. In the case of large Hodge numbers this quickly becomes a systematically devilish task. Specifically returning to the case of Type IIB flux compactifications, the scalar potential emits a *no-scale* structure [388, 518], where the full tree-level flux potential is,

$$V_{\rm ns} = e^K \left(\sum_{i,j} g^{i\bar{j}} D_i W \overline{D_j W} \right) \ , \tag{3.29}$$

where we have performed a sum over the Kähler moduli to cancel the $3|W|^2$ term in Eq. (3.28). The indices i and j now run over the dilaton and complex structure moduli. These two terms can now be defined in a supersymmetric minimum by solving the requirement, $D_a W = 0$. We must still account for the nature of the volume modulus, where it is currently understood to be a flat direction. The two principle moduli stabilisation methods deployed in order to obtain realistic stabilised vacua from the Type IIB superstring setting are the two flux compactification model procedures of Kachru-Kallosh-Linde-Trivedi (KKLT) compactification and the *LARGE Volume Scenario* (LVS).

3.2.2.1 The Kachru-Kallosh-Linde-Trivedi Scenario

The KKLT scenario [758] proposes that all the Kähler moduli are stabilised by solving $D_{T_i} W = 0$, considering the nature of non-perturbative corrections to the superpotential. It is possible to retrieve deSitter vacua in this framework with

the incorporation of a small number of anti-D3-branes [625]. The simplest set up considers a Calabi-Yau with a single Kähler modulus,

$$T \equiv \tau + i\theta \ , \tag{3.30}$$

with τ a Kähler moduli and θ its associated pseudoscalar partner. The Kähler potential and superpotential are of the standard form,

$$K = -2\ln\mathcal{V} = -3\ln(T + \bar{T}) \ , \tag{3.31}$$

$$W = W_0 + Ae^{-aT} \ , \tag{3.32}$$

where a is a numerical coefficient (e.g. brane instantons ($a = 2\pi$) or gaugino condensation ($a = 2\pi N^{-1}$)). The parameter $\mathcal{V}$ represents the volume of the Calabi-Yau in string units. The value of $|W_0|$ is fine-tuned to extremely small values in order to neglect perturbative corrections to the Kähler potential. The minimisation of the induced scalar potential defines the nature of the stable vacuum for the τ and θ degrees of freedom. KKLT is often considered a toy configuration at the level of a conceptual understanding of compactifications of Type IIB Calabi-Yau orientifolds. Relevant to the physics of effective field theory axions, this method has problematic concerns when realising the traditional axiverse scenario as the Kähler moduli are fixed by assuming that the superpotential has non-perturbative contributions for each Kähler modulus. In this case each axion field in the low energy theory is realised as a state which inherits a mass of order the Kähler moduli,

$$m_\theta \simeq m_\tau \simeq m_{3/2} \simeq \frac{|W_0|}{\mathcal{V}} M_{\rm Pl} \ , \tag{3.33}$$

fixed at the scales of the models gravitino mass ($m_{3/2}$), with moduli stabilisation occurring by only superpotential effects. The mass in the effective action is associated to the single non-perturbative effect relating to the cycle of the single modulus. In general we would wish to form schemes which generate basic stabilisation require-

ments, i.e. QCD axion and ultralight DM fields, suitable supersymmetry breaking terms and heavy moduli fully stabilised.

3.2.2.2 The Large Volume Scenario

The LVS [144, 369] allows for the stabilisation of the overall volume of the compactification at some exponentially large value, making use of both perturbative and non-perturbative terms. Unlike the previous compactification the LVS is realised in its simplest form with a Calabi-Yau orientifold, this time with two Kähler moduli, τ_b and τ_s [353],

$$\mathcal{V} = \tau_b^{3/2} - \tau_s^{3/2} \ . \tag{3.34}$$

As apposed to the flux superpotential in KKLT in Section 3.2.2.1, $|W_0|$ is order unity, where perturbative corrections now must be considered for moduli stabilisation. Considering only the leading order α' correction, the Kähler potential is defined as,

$$\overbrace{-2\ln(\mathcal{V})}^{\text{KKLT}} \rightarrow \underbrace{-2\ln\left(\mathcal{V} + \frac{\xi}{g_s^{3/2}}\right) \simeq -2\ln\mathcal{V} - \frac{\xi}{g_s^{3/2}\mathcal{V}}}_{\text{LVS}} \ . \tag{3.35}$$

The term ξ is proportional to the Euler characteristic in Eq. (3.61) and g_s is now a parameter to be fixed by the fluxes. The scalar potential is greatly simplified in the limit, $\tau_b \gg \tau_s$. In this example one of the axions, related to τ_s, obtains a mass the same order as that found in the simple KKLT example found in Eq. (3.33). The remaining large modulus τ_b, is fixed according to balancing the leading order α' correctional effects. The associated remaining axion only generates its potential through sub-leading terms in the non-perturbative superpotential of the order,

$$m_{\theta_b} \simeq \sqrt{|W_0|} M_{\rm Pl} e^{-\frac{a_b}{2}\mathcal{V}^{2/3}} \ , \tag{3.36}$$

generating a parametrically lighter degree of freedom in the low energy spectrum. We will see how these concepts give rise to a natural realisation of the axiverse, when

Table 3.1: Collection of superstring theories and the relevant forms which lead to axion degrees of freedom and associated instantons which generate potentials for the fields. Collected and reproduced from the discussions found in Ref. [657].

Axionic Forms		
String Model	**Forms**	**Euclidean instantons**
M-theory	C_3	M2 Brane instantons
F-theory and Type IIB	B_2 and C_0, C_2, C_4, B_2.	Worldsheet instantons, ED(-1), ED1, and ED3-instantons.
Type IIA	C_1, C_3, C_5 and B_2	Worldsheet instantons, ED0, ED2 and ED4-instantons.
Heterotic	B_2	String worldsheet instantons

this process is generalised to the case of including many moduli in Section 3.3.4.

3.3 The String Axiverse

3.3.1 A Plentitude of Pseudoscalars from Topological Complexity

The general process of dimensional reduction covered in Section 3.2.1 can be extended to the case of generic compactification models related to the traditional weakly coupled string models which form the web in Fig. 3.2. Taking a step back, there are several ways we can approach the issue of dealing with a landscape of models which arise, when approaching the limits of quantum gravity. Consistency arguments such as BH thermodynamics and causality have historically motivated what this landscape could look like. General conjecture offers a much looser approach to the high energy framework, however their strengths and features are not often a well defined topic. This approach does often lead to many benefits in terms of assessing likelihoods in cosmology and general phenomenology though. Finally we can expand our understanding of the four-dimensional space and effective field theories which arise in the weakly coupled limits of well defined string vacua through enumeration. One such conjecture which has emerged much to the delight of phenomenologists is

the particle treasure chest scenario of the *string axiverse* [107, 1231]. The massless spectrum of any string model seems to suggest the dimensional reduction of the extra-dimensional spacetime manifold, $\mathcal{M}_{6/7}$, emits a spectrum of antisymmetric forms which appear as ALPs in the four-dimensional effective theory [107, 1231]. These fields possess shift symmetries from the higher dimensional gauge symmetries, rendering them as phenomenological counterparts to the original axion field introduced in Section 2.3. They are generally manifest as the imaginary components of a complex modulus scalar field, used to regulate characteristics such as the size of the extra-dimensions or low-dimensional gauge couplings etc. The nature of this plethoric spectrum of fields is represented by the potential topological complexity the extra-dimensional compact space can inherit. This freedom and uncertainty gives a very general prediction that there exists a family of fields in any string model with masses that span a huge number of decades, right down to the Hubble scale today. This represents one of the most important features of string theory in regards to the identification of a possible low energy signature representing its existence, and has evolved to become a vital field of study in general high-energy physics today. The number of these fields is fixed by the topology of the extra-dimensional compact space, parameterised by its Betti numbers, a value strictly determined by topological considerations. This value tends to be of the order,

$$\mathcal{N}_{\rm ax} \sim \mathcal{O}(10) - \mathcal{O}(100) \ , \tag{3.37}$$

in generic Calabi-Yau models (see Fig. 3.5) and could even be much higher (see Section 3.3.3). The number of fields which survive the compactification process right down to the effective theory is of course a very specific model feature. For example the orientifold projection first mentioned in Section 3.1.2, used to define a chiral $\mathcal{N} = 1$ theory in Type II theories, will project out some of these degrees of freedom, but this does not generally tend to change the order of magnitude of the ALPs in the existent axiverse.

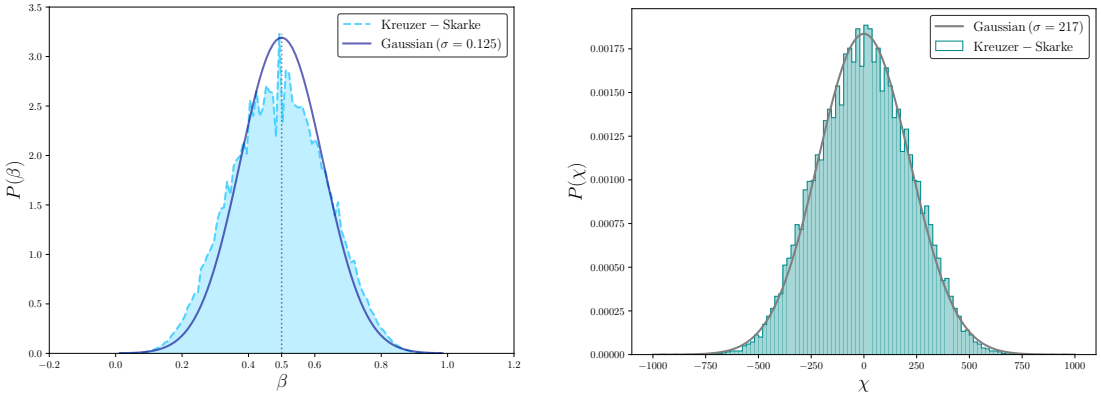


Figure 3.3: Approximate Gaussian fits for quantities formed using the topological invariant Hodge numbers, $h^{1,1}$ and $h^{2,1}$. *Left panel*: Ratio of the axion degrees of freedom and the total dimension of the extra-dimensional space defined in Eq. (3.64), represented by the data from the Kreuzer-Skarke list [825] for the distinct Hodge number combinations and approximate density function fit. *Right panel*: Density plot for the Euler characteristic from Eq. (3.61) for Calabi-Yau threefolds along with its approximate density function fit.

As these ubiquitous PQ symmetries analogous to the familiar Standard Model axion, do naturally arise in string models in a multifarious fashion, it is common practise to reproduce string modes which can behave like the phenomenologically desired axion fields in the low energy effective action. Following the discussions found in Refs. [657, 911] we can summarise the general four-dimensional compactified axiverse as follows. The arbitrary D-dimensional effective quantum field theory supergravity action with $D > 4$ contains terms of the form,

$$S \supset \int d^D x \, \sqrt{-g_D} \, d\mathcal{C}_p \wedge \star d\mathcal{C}_p \, , \tag{3.38}$$

where $\mathcal{C}_p$ represents the p-form gauge field and $\sqrt{g_D}$ is the D-dimensional metric determinant. The field strength $\mathcal{F}_{p+1} = d\mathcal{C}_p$, has an equation of motion, $d\mathcal{F} = 0$ and transforms under the gauge symmetry as,

$$\mathcal{C}_p \to \mathcal{C}_p + d\Lambda_{p-1} \, , \tag{3.39}$$

with Λ a $(p-1)$-form. Consider the familiar general compactification ansatz in

which the D-dimensional manifold $\mathcal{X}_D$, is expressed as,

$$\mathcal{X}_D = X_4 \times \mathcal{M}_{D-4} \ , \tag{3.40}$$

where X_4 represents the required (3+1)-dimensional non-compact manifold. We can dimensionally reduce the effective action in Eq. (3.38) for a smooth $(D-4)$-dimensional manifold, $\mathcal{M}_{D-4}$. This is done by accounting for the fact that the p-form gauge field $\mathcal{C}_p$, can be written as a sum of non-trivial harmonic p-forms on $\mathcal{M}_{D-4}$, forming a complete basis,

$$\mathcal{C}_p = \sum_i^{b_p} a_i(x)\omega_{p,i}(y) \ , \tag{3.41}$$

the sum running over the p^{th} Betti number b_p (see Section 3.3.6.1), with $\omega_{p,i} \in H^p(X,\mathbb{Z})$. The coordinates x act on the non-compact (3+1) dimensions and the coordinates y act on the compact space of $\mathcal{M}_{D-4}$. The 4-dimensional fields, $a_i(x)$ are the axion fields. These pseudo-scalars remain apparent in the dimensionally reduced form of the action, possessing continuous shift symmetries manifest from the higher-dimensional gauge symmetry in Eq. (3.39). Formally the axion fields are related to the p-form gauge field, $\mathcal{C}_p$ via the integral,

$$a_i = \int_{\mathcal{B}_{p,i}} \mathcal{C}_p \ , \tag{3.42}$$

where $\mathcal{B}_{p,i}$ the i^{th} closed basis of p-cycles on $\mathcal{M}_{D-4}$. The basis sum runs over the total number of harmonic p-forms determined by the topology of the manifold structure. This number is evaluated by the number of homologically non-equivalent p-cycles expressed as the p^{th} Betti number, b_i. We can generally define,

$$\mathcal{N}_{\text{ax}} \equiv b_i(\mathcal{M}_{D-4}) \ . \tag{3.43}$$

When considering the standard landscape of string theory in the (3+1) low energy

limit, with $\mathcal{N} = 1$ supersymmetry the complex manifold $\mathcal{M}_6$ is that of Calabi-Yau. The KK reduction process shown in Section 3.2.1 of Eq. (3.38) gives a massless spectrum which later defines a spectrum of axion decay constants and masses from the full details of the moduli stabilisation as the Universe evolves.

3.3.2 The General Parametric Description of Axion-Like Fields

The general parametric dependance on the two defining string axion parameters can be summarised as:

- *The axion decay constant* - f_a - The process of KK reduction kinematically mixes the axions where they couple to the moduli through the Kähler metric. General considerations include factors such as the volume and warp factor of the internal space, along with mixings with other model remnants and defining model scales, i.e. supersymmetry breaking scales. The decay constants appear as a linearly suppressed factor of fundamental scales, using properties of the associated cycles,

$$f_a \sim \frac{M_{\rm Pl}}{S} \lesssim M_{\rm Pl} \ , \tag{3.44}$$

  where S represents the volume of the cycle. The value of f_a is generally expected to be the order of the GUT scale in string models [1231].

- *The axion mass* - m_a - As compared to its modulus counterpart, the axion has a familiar shift symmetry, its potential generated from non-perturbative physics. Spontaneous symmetry breaking of global $U(1)_{\rm PQ}$ symmetries by numerous instantons sources such as flux, worldsheet, brane, QCD or EW sectors etc. lead to the understanding that axion masses should mimic the following general relationship,

$$m_a^2 \sim \frac{\mu^4}{f_a^2} e^{-S_{\rm inst}} \ , \tag{3.45}$$

where $S_{\rm inst}$ is the action over the corresponding cycles. The parameter, μ, represents a hard non-perturbative physics scale, generally expected to be of the order,

$$\mu \simeq \sqrt{m_{\rm SUSY} M_{\rm Pl}} \, . \tag{3.46}$$

The axion masses scale exponentially with the volume of the cycle determined by the action of the cycle, leading to the expectation of homogeneity of the axion field masses over logarithmic scales.

This process is a simple representation of the standard blueprint applied to realise both the number of ALPs and their approximate scalings, where the quantity $\mathcal{C}_p$ in Eq. (3.41) representing closed string axions, can be identified in a number of ways as shown in Table 3.1, along with the various instanton solutions present in each theory which can be used to generate the fields potential. The axiverse represents a principle conjecture of all four-dimensional effective field theories in weakly coupled string limits. There has been various successful demonstrations of how it is possible to suitably stabilise the moduli for cosmological concerns whilst producing a hierarchical spectrum of pseudo-scalars one can associate to the string axiverse scenario, with special efforts made to incorporate a candidate for the QCD axion. These have been formulated in both the background of Type IIB and M-theory, defining explicit model class realisations of the string axiverse.

3.3.3 The F-theory Landscape

Much like the theories of Type IIA and Het $E_8 \times E_8$, possessing a T-duality symmetry with a more fundamental eleven-dimensional theory, Type IIB also possess an interesting symmetry relation which relates to a higher dimensional framework. The Type IIB superstring theory possesses a $SL(2, \mathbb{Z})$ symmetry which is a modular group of a torus. F-theory [962, 1287] is a non-perturbative geometric reformulation of Type IIB models, which is understood using a duality relation with M-theory. F-theory has found various success in model construction [180, 181, 469, 686]. In the

case of a four-dimensional theory the space is unsurprisingly very large. In Ref. [660] the geometrical ensemble studied was a collection of $4/3 \times 2.96 \times 10^{755}$ six-manifolds, acting as the extra dimensions of spacetime. For the case of axions arising from the reduction of the form, C_4, is has been shown that typical configurations often give, $h^{1,1} \simeq \mathcal{O}(1000)$ [660, 1252, 1253]. It has been suggested that F-theory itself has weakly coupled limits [1169, 1170], where the statistical appearance of when these weakly coupled limits appear, in such vast ensembles, still offers a series of interesting open-ended questions [661]. For the case of a string axiverse this framework does offer interesting theoretical suggestions that an *ignorant* sampling of the space in an effective model could motivate the inclusion of $\mathcal{O}(1000)$ axion fields.

3.3.4 The Type IIB Axiverse

Continuing from the points in Section 3.2.2.2, the LVS compactification process has been used to form an explicit model of the string axiverse realised in Type IIB models utilising Calabi-Yau manifolds [144, 369]. The LVS Type IIB axiverse [351, 352] produces a series of closed string axions which stem from the orientifold compactification, which come to be realised as a logarithmically hierarchical set of states in the low energy field theory. In the natural regime $W_0 \sim \mathcal{O}(1)$, a single Kähler modulus, the del Pezzo divisor, is fixed by non-perturbative effects. All remaining moduli are generally expected to be stabilised perturbatively through correctional α' or g_s effects. The general scalar potential is defined using several contributions, each which scale differently according to the overall exponentially large volume,

$$V = V_D + V_F^{\text{tree}} + V_F^{\text{np}} + V_F^{\text{p}} \,, \tag{3.47}$$

representing a sum of the D-term potential (V_D), tree-level F-term scalar potential (V_F^{tree}), non-perturbative scalar potential (V_F^{np}) and perturbative potential (V_F^{p}). The leading order effect for the expansion in inverse powers of the volume is the D-term potential, minimised when $V_D = 0$. In order to ensure the overall volume, $\mathcal{V}$

remains exponentially large, the minimisation condition, whilst also considering the nature of visible sector, i.e. required couplings, forces the LVS axiverse to contain, $\mathcal{N}_{\rm ax} \geq 2$. The term $V_F^{\rm p}$ is the source of the LVS axiverse, generating a series of exponentially suppressed ALP states. The α' corrections give rise to terms which dominate over any g_s corrections where the remaining $\mathcal{N}_{\rm ax} - 1$ flat directions are lifted at sub-leading order. Terms similar to the final summation in Eq. (3.53) constitutes a potential for the axions c_i, through minor non-perturbative effects of the form [351],

$$V_{W_{\rm np}}(c_i) \simeq -\sum_{i=1}^{\mathcal{N}_{\rm ax}} e^{-n_i a_i \tau_i} \frac{n_i a_i \tau_i W_0}{\mathcal{V}^2} \cos(n_i a_i c_i) \ , \tag{3.48}$$

where again the prefactor terms a and n are determined by the relations $a = {}^{n}\!/_{2\pi}$, with $n = 1$ for an E3-instantons and $n = N$ for gaugino condensation on N D7-branes [351]. Axions can also generate a potential via non-perturbative corrections to the Kähler potential [364], which takes a similar general form,

$$V_{K_{\rm np}}(c_i) \simeq \frac{W_0^2}{\mathcal{V}^3} \sum_{i=1}^{\mathcal{N}_{\rm ax}} e^{-n_i a_i \tau_i} \cos(n_i a_i c_i) \ . \tag{3.49}$$

Considering an axion mass generated by a single Kähler potential contribution gives the natural mass hierarchy [351, 364],

$$m_a \lesssim m_{3/2} e^{-\pi \alpha_{\rm QCD}^{-1}} \lesssim \mathcal{O}(10^{-11}) \text{ eV} \ , \tag{3.50}$$

under considerations for chirality and the relevant instanton contributions when the gravitino mass is of the order, $m_{3/2} \sim 100$ TeV, signalling the general expectation of ULA fields in the spectrum. This represents the suppression on the other axion masses with respect to the QCD axion, which generates fields which sit inside an ultralight axiverse. The simplest realisations of the LVS axiverse includes two fields, one of which is realised as a candidate for the QCD axion along with a generic ALP counterpart. The number of fields in these models is related to the topology of the

internal manifold which are all closed string axions living in the bulk. A general model with a large value of $h^{1,1}$ will naturally realise a large number of ultralight fields which is also related to the degree of supersymmetry at the effective level of the theory. For Type IIB flux compactifications where the axions are manifest as KK zero modes of the RR antisymmetric tensor fields C_2 and C_4 [351, 632, 752]. The effective action for the axion fields is [351],

$$\begin{aligned}\mathcal{L} \supset & -\frac{e^{\Phi}}{4\mathcal{V}^2}\left(dc^a + \frac{e^{-\Phi}}{2\pi}M_{\rm Pl}A_i r^{ia}\right)\mathcal{K}^{ab}\wedge\star\left(dc^b + \frac{e^{-\Phi}}{2\pi}M_{\rm Pl}A_i r^{jb}\right) \\ & + \frac{2\pi M_{\rm Pl}^2}{\mathcal{V}^2(2\pi)^3}e^{-\Phi}A_iA_j r^{ia}r^{jb}\mathcal{K}^{ab} - \left(dc_\alpha + \frac{M_{\rm Pl}}{\pi}A_i q_{i\alpha}\right)\frac{\mathcal{K}_{\alpha\beta}}{8}\wedge\star\left(dc_\beta + \frac{M_{\rm Pl}}{\pi}A_j q_{j\beta}\right) \\ & + \frac{M_{\rm Pl}^2}{2(2\pi)^2}A_iA_j q_{i\alpha}\mathcal{K}_{\alpha\beta}q_{j\beta} + \frac{1}{4\pi M_{\rm Pl}}\left(r^{i\alpha}c_\alpha + q_{ia}c^a\right)\mathrm{tr}(F\wedge F) - \frac{r^{i\alpha}\tau_\alpha}{4\pi M_{\rm Pl}}\mathrm{tr}(F_i\wedge\star F_i)\ ,\end{aligned} \tag{3.51}$$

which we quote without derivation to highlight the complications which come from modelling an effective theory of this form. The values of c^a and c_α represent the axion-like pseudo-scalars of the theory. The quantities A_i are the massive anomalous $U(1)$ gauge bosons which can eat some of the axions. See Eq. (2.1) of Ref. [351] and surrounding discussions for definitions of the remaining parameters.

3.3.5 The M-theory Axiverse

M-theory is a vast endeavour which attempts to unify current consistent superstring theories into one consistent language, as an eleven-dimensional quantum theory. Traditionally studies are often focused around particular (9+1) dimensional limits M-theory reduces to, given the ambiguity which can easily be encountered in terms of compactification. These limits are represented by the apparent dualities used to make inferences in such a complex space. Unlike the ten-dimensional weakly coupled theories M-theory does not possess a defined coupling constant to generate calculations beyond its low energy limit. M-theory is principally constructed as an eleven-dimensional theory which reduces to our familiar four, whilst preserving

$\mathcal{N} = 1$ supersymmetry using a seven dimensional metric which is understood with a holonomy group equal to the exceptional Lie group G_2 [33]. These manifolds tend to emit our desired particle content under specific configurations and considerations of present singularities. For example chiral fermions charged under a non-abelian gauge symmetry, arise in four-dimensions when special considerations are made for the orbifold singular nature of the seven-manifold [25, 119]. Currently a more holistic classification of the natural outputs in these types of manifolds is an extremely difficult task. Although it is strongly suspected compactified versions of these geometrical structures do exist with the full required phenomenological content, i.e. conjectured using the T-Dualities between heterotic $E_8 \times E_8$ and Type IIA [23] (see Fig. (3.2)) which represent particular limits where we could realise consistent structure. It is currently safe to say a general analysis of the full phenomenological landscape is no easy feat, although much can be understood in the context of KK reduction of the low energy limit of M-theory, namely eleven-dimensional supergravity. In this limit the supergravity theory of M-theory possesses a metric, a three-form gauge field and a gravitino. Of course as always, the moduli must be suitably accounted for and stabilised. For particle content consistency it is preferential for this to be done without fluxes, a topic that we expanded on in Section 5.3. All the moduli in these models are massless fluctuations of the extra-dimensional manifold. The harmonic fluctuations of the three-form gauge fields along the G_2 compactified manifold represent the axionic content of the theory. These are required to live in complex chiral supermultiplets, partnering to the real scalar moduli under supersymmetry considerations. Understanding the nature of these complex scalar fields representative of the constituents of the chiral superfields is how we can realise the string axiverse in an M-theory framework. This is done by assessing the relation between the VEV scales of the moduli, the extra dimensional volumes and gauge couplings of the matter content.

As we just mentioned an explicit realisation of the string axiverse using M-theory involves the interesting proposition that full model consistency requires the use of

leading order moduli stabilisation with an absence of fluxes [31]. The nature of the axion spectrum is determined when moduli stabilisation occurs at a sufficiently large mass to avoid BBN constraints. Much like the Type IIB axiverse in Section 3.3.4 the moduli are stabilised using a combination of Kähler potential and superpotential effects. The axions arise from a reduction of the three-form in eleven dimensions to the required four, where the higher dimensional gauge symmetries reduce to the axion shift symmetries. Chiral superfields are formed from modes stemming from the dimensional reduction of the metric, which also possess relevant shift symmetries,

$$\Phi_i \to \Phi_i + c_i \ . \tag{3.52}$$

These qualitative results transform across to the scenario where the tree-level superpotential is tuned to be $W_0 = 0$, such as generic Type IIB concerns, where a single non-perturbative effect can be shown to generate a stable minimum for all the Kähler moduli. The stabilisation of all the moduli relates to the nature of one axion, the imaginary degree of freedom of the ample divisor expected to exhibit specific characteristics, lifted to become a massive state in the effective theory. The remaining $h^{1,1} - 1$ contributions to the axiverse spectrum later develop a suitable potential via higher order instanton corrections of the form,

$$W = W_0 + Ae^{-aT_{\rm am}} + \sum_{i=1}^{h^{1,1}-1} A_i e^{-n_i a_i T_i} \ , \tag{3.53}$$

where $T_{\rm am}$ represents the ample divisor modulus, the T_i represent a combination of moduli orthogonal to $T_{\rm am}$ and W_0 is fixed by different concerns in Type IIB and M-theory scenarios with numerical constants A_i. The stabilisation of axions in these scenarios involves a general exponential suppression compared to $m_{3/2}$, unlike the issues encountered in more general KKLT models. The stabilised axions are now distributed according to approximate equidistant separations on logarithmic scales. Unlike the Calabi-Yau threefolds we will cover below G_2 manifolds have an added complexity due to their topological practicalities in terms of defining a suitable met-

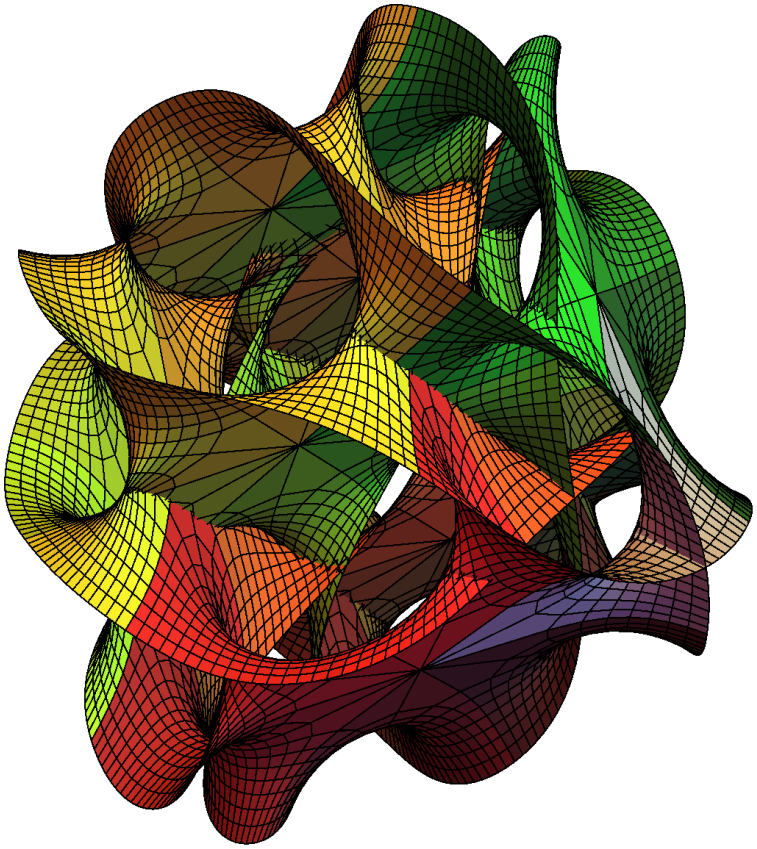


Figure 3.4: Example general Calabi-Yau quintic cross-section, $Z_1^5 + Z_2^5 = 1$. The two-dimensional projectional slice is an embedded surface representing a visualisation of the possible full six-dimensional Calabi-Yau space, $Z_0^5+Z_1^5+Z_2^5+Z_3^5+Z_4^5 = 0$, which could define the extra-dimensions of spacetime in well-defined superstring compactification models. The structural features of these spaces can have a drastic effect on the particle content in the low-energy four-dimensional theory.

ric [33, 1013]. There are various construction attempts made to understand the likely degrees of freedom we could find in the four-dimensional space such as those detailed in Ref. [657]. Generally these surround twisted connected sum constructions of G_2 manifolds [271–274, 379, 658, 822]. It has been shown these ensembles often lead to $b_3 \simeq \mathcal{O}(30)$ [379, 657], suggesting numerous axions are generally present in the low energy descriptions of compactified seven-manifolds. We will leave the remaining subtleties of the formation of an ultralight axiverse spectrum in this landscape to the discussions in Section 5.3.1.

3.3.6 The Kreuzer-Skarke Axiverse

3.3.6.1 Calabi-Yau Manifolds

A very detailed example of how enumeration methods can be applied to effective field theories, which could arise from concerns surrounding string geometries, is detailed in the Kreuzer-Skarke Axiverse [427]. A Calabi-Yau manifold $\mathcal{Z}$, can be defined as a complex manifold admitting a Kähler metric with vanishing Ricci curvature, and can generally be defined in two categories, compact and non-compact. They serve as generalisations of K3 surfaces in any number of complex dimensions. Specifically in the context of superstring theory these complex manifold spaces are required to possess a complex dimension, $d_c = 3$. These are referred to as Calabi-Yau threefolds. See Fig. (3.4) for a two-dimensional slice representation of a generic six-dimensional Calabi-Yau quintic manifold. The points discussed below are extensively covered in Ref. [688]. The tools used to study the cohomology groups of a smooth manifolds geometry such as a compact Riemannian or Kähler manifold comes under the umbrella of Hodge theory. The condition that imposes vanishing curvature is known as the Calabi-Yau condition, where the metric of the Kähler form is Ricci flat,

$$R_{ij} = 0 \ . \tag{3.54}$$

Using an amalgamation of the aforementioned condition, Hodge theory and Poincaré duality allows us to express the hodge diamond representation of the Hodge numbers of $\mathcal{Z}$, assuming it is simply connected. The Hodge numbers are represented by,

$h^{p,q}(\mathcal{Z})$ with $p,q = 1,2,3$, and are arranged as,

$$\begin{array}{ccccccc} & & & h^{0,0} & & & \\ & & h^{1,0} & & h^{0,1} & & \\ & h^{2,0} & & h^{1,1} & & h^{0,2} & \\ h^{3,0} & & h^{2,1} & & h^{1,2} & & h^{0,3} \\ & h^{2,0} & & h^{1,1} & & h^{0,2} & \\ & & h^{1,0} & & h^{0,1} & & \\ & & & h^{0,0} & & & \end{array} \ . \tag{3.55}$$

Specifically the complex conjugate shows that, $h^{p,q} = h^{q,p}$ and Poincaré duality defines the relation, $h^{p,q} = h^{n-p,n-q}$. The Betti numbers of a Kähler n-fold $\mathcal{Z}$ are defined by the Hodge sum [688],

$$b_k = \sum_{\substack{p,q=0 \\ p+q=k}}^{n} h^{p,q}(\mathcal{Z}); \quad k = 0,\ldots,n \ . \tag{3.56}$$

There are several simplifications which can be made to the initial diamond form in Eq. (3.55) in order to determine the relevant degrees of freedom for Calabi-Yau threefolds. When $\mathcal{Z}$ is compact and connected we have, $b_0 = 0$ defining $h^{0,0} = 1$. If the connection is simple then this also reduces $h^{1,0}$ and $h^{0,1}$ to $h^{1,0} = h^{0,1} = 0$. This can be taken a step further with the unique non-vanishing holomorphic n-form which defines $h^{n,0} = h^{0,n} = 1$, with Poincaré duality finally defining, $h^{p,0} = h^{n-p,0}$. Taking all these equivalence simplifications into account the reduced Hodge diamond

now becomes,

$$\begin{array}{ccccccc} & & & 1 & & & \\ & & 0 & & 0 & & \\ & 0 & & h^{1,1} & & 0 & \\ 1 & & h^{2,1} & & h^{1,2} & & 1 \\ & 0 & & h^{1,1} & & 0 & \\ & & 0 & & 0 & & \\ & & & 1 & & & \end{array} . \tag{3.57}$$

The threefold Hodge diamond is now fully defined by the non-trivial Betti numbers, $b^2 = h^{1,1},\ b^3 = 2 + 2h^{2,1}$ and $b^4 = h^{1,1}$ which detail how these manifolds can be fully understood using only two degrees of freedom. These are the Kähler parameters, $h^{1,1}(\mathcal{Z})$ and complex structure parameters $h^{2,1}(\mathcal{Z})$, which define the dimensions of the associated cohomology groups. The Euler number, which can be used to understand the topological structure of a Riemann surface, represents a single integer for Calabi-Yau threefolds defined using an alternating sum of Betti numbers,

$$\chi(\mathcal{Z}) = \sum_{i=0}^{\dim_{\mathbb{R}}(\mathcal{Z})} (-1)^i b^i \ . \tag{3.58}$$

When combined with the simplified Hodge diamond in Eq. (3.57) the summation reduces to,

$$\chi(\mathcal{Z}) = b^0 - b^1 + b^2 - b^3 + b^4 - b^5 + b^6 \ , \tag{3.59}$$

$$= 1 - 0 + h^{1,1} - (2 + 2h^{2,1}) + h^{1,1} - 0 + 1 \ , \tag{3.60}$$

$$= 2\left(h^{1,1} - h^{2,1}\right) \ , \tag{3.61}$$

representing the free parameters of the metric. The lower bound on the complex deformation parameter, $h^{2,1} = 0$ defines a rigid manifold. The value of $h^{1,1}$ is always assumed to be at least unity to ensure the manifold can be defined as Kähler.

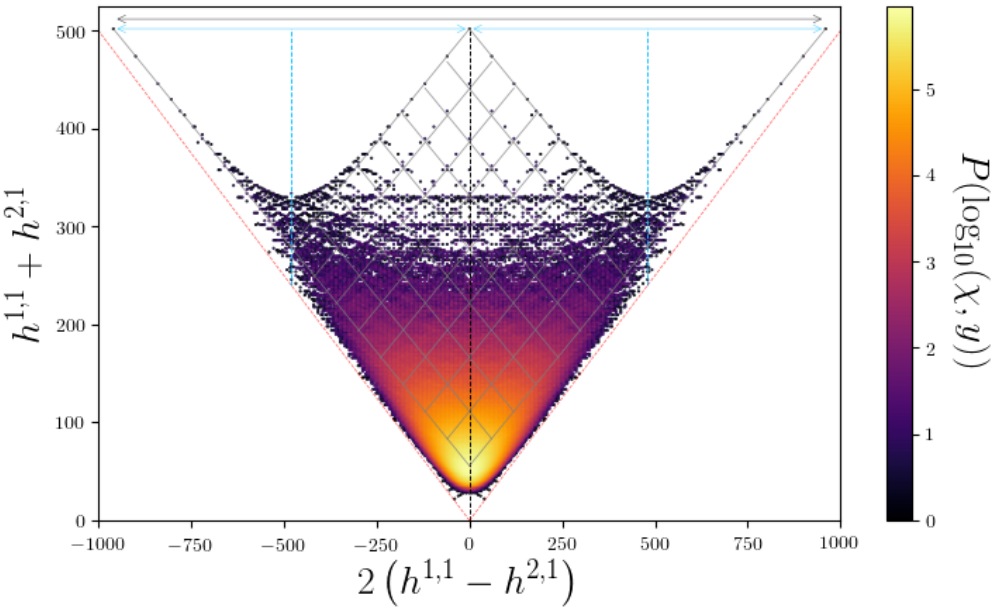


Figure 3.5: Complete construction of toric hypersurfaces parameterised by $\chi \in [-960, 960]$, using the 30,108 distinct Hodge pairs from the Kreuzer-Skarke dataset of Calabi-Yau hypersurfaces in Gorenstein Fano-toric fourfolds. The coloured surface represents the logarithmic multiplicity of the Euler characteristic and functional height, $y = h^{1,1} + h^{2,1}$ for the 473,800,652 hodge pairs which run over these distinct values peaking with a density $\mathcal{O}(10^6)$ at $h^{1,1} = h^{2,1} = 27$. The *red* dashed line defines the boundaries enforced by the fact that the Hodge numbers are strictly positive. The *black* dashed line is the mirror manifold symmetry boundary. The *grey* solid line is the limits for the Euler characteristic which defines the properties of the manifold. The *light blue* lines represent a *half* mirror symmetry for points which have mirror manifolds about the $\chi = -480$ and $\chi = 480$ axis. The *grey* grid represents symmetry boundaries for features such as $K3$ fibrations [309]. Adapted from the work found in Ref. [309].

Calabi-Yau manifolds in general come in families whereby a deformation of a given Calabi-Yau manifold structure through a change of parameters can be made without a violation of the Calabi-Yau condition. The Calabi-Yau families are parameterised in terms of the above mentioned Kähler parameters and complex deformation parameters. The first of these specifies relative sizes, for example the areas of the embedded holomorphic curves. The second determines the nature of the complex structure. The value of the Kähler parameters defines the number of axionic degrees of freedom we could expect to find in the low energy phenomenology of supergrav-

ity theories arising from these compact spaces. Under the general process of KK reduction, as discussed in Section 3.2.1, these metric deformations become four-dimensional scalar fields that define the moduli of the model.

3.3.6.2 Mirror Symmetry

A core and fundamental principle of the symmetry classes present in the construction of string models and an example of the previously mentioned string dualities, is the beautifully manifest mirror symmetry for Calabi-Yau threefolds. As displayed in Fig. 3.5, for any Calabi-Yau manifold $\mathfrak{Z}$ there exists a further Calabi-Yau manifold, $\tilde{\mathfrak{Z}}$ whereby any model $\mathfrak{A}$ embedded on $\mathfrak{Z}$ holds equivalence to any model, $\mathfrak{B}$ embedded on $\tilde{\mathfrak{Z}}$. This relation between model parameters is known as a mirror map, expressed by the Hodge symmetry condition,

$$h^{1,1}(\mathfrak{Z}) = h^{2,1}(\tilde{\mathfrak{Z}}) \ . \tag{3.62}$$

Visually Eq. (3.62) is represented by the appropriate reflection transformation defined over the *black* dashed line in Fig. 3.5, which relates the transformed Hodge diamonds. In the context of superstring theories, topologically distinct Calabi-Yau threefolds are partnered up in mirror pairs which relate Type IIA and Type IIB theories. The massless spectrum in Type IIA theories contains $h^{1,1}$ vector multiplets, $h^{2,1}$ hypermultiplets and one tensor multiplet [645]. For Type IIB this is reversed where we now have one $h^{2,1}$ vector multiplet, $h^{1,1}$ hypermultiplets and one tensor multiplet. This suggests the four-dimensional effective theories share the relation,

$$\mathcal{L}^{(\mathrm{IIA})}(\mathcal{Z}) = \mathcal{L}^{(\mathrm{IIB})}(\tilde{\mathcal{Z}}) \ , \tag{3.63}$$

where we have assumed a disregard for any possible complications stemming from the inclusion of fluxes which can change the nature of the effective field theory. These points represent just a small insight into how geometrical features can used

to simplify and express the properties of complex spaces, relating to the vacua of different theories associated to the extra dimensions of spacetime. In Ref. [499] a random matrix approach is taken to express a spectrum of axions in the context of multi-field inflation, where the masses are regulated using the topological invariants associated to Type IIB theories. Specifically the Hodge numbers, h^{11} and $h^{2,1}$, define the number of axions and the total dimension of the moduli space, understood via the parameterisation,

$$\beta = \frac{h^{1,1}}{h^{1,1} + h^{2,1} + 1} \ . \tag{3.64}$$

This ratio represents the nature of the number of axionic degrees of freedom present in different manifold structures. One of the most striking demonstrations of the interplay between geometrical data and theoretical physics is presented in the vast database of categorised Calabi-Yau threefolds, found in the Kreuzer-Skarke database of four-dimensional reflexive polytopes [64, 825]. The topological information in this database can be manipulated to construct and build an understanding of string models in a cosmological/phenomenological context. In the nomenclature of toric geometry, the Calabi-Yau data in the database is categorised according to the topological invariant Hodge numbers, second Chern class and intersection numbers. Despite the potential complexity a complete analysis of the extra dimensional space could yield, compactification models on Calabi-Yau hypersurfaces benefit greatly from Yau's theorem and the extensive nature of the Kreuzer-Skarke database. The database contains a total of $473,800,776$ polytopes, denoted by Δ° where performing a fine, regular, star triangulation (FRST) of any of these polytopes defines a toric variety. The Hodge numbers themselves can be expressed in terms of the polytope data [689, 825],

$$h^{1,1}(\mathcal{Z}) = \ell(\Delta^\circ) - \sum_{\text{codim}\theta^\circ=1} \ell^\star(\theta^\circ) + \sum_{\text{codim}\theta^\circ=2} \ell^*(\theta^\circ)\ell^\star(\theta) - 5 \ , \tag{3.65}$$

$$h^{2,1}(\mathcal{Z}) = \ell(\Delta) - \sum_{\text{codim}\theta=1} \ell^\star(\theta) + \sum_{\text{codim}\theta=2} \ell^*(\theta)\ell^\star(\theta^\circ) - 5 \ , \tag{3.66}$$

which displays the the polar duality, $\Delta \leftrightarrow \Delta^\circ$ for the ambient toric variety. In these expressions the terms θ and θ° represent the faces of specified codimension of the polytope Δ and its dual Δ°, respectively. Finally $\ell()$ represents the number of integer points of the polytope while $\ell^\star()$ is the number of interior integer points [689]. The anticanonical hypersurafaces which arise as smooth Calabi-Yau threefolds, present a total of 30,108 distinct Hodge pairs, $(h^{1,1}, h^{2,1})$, for the possible combinations of $h^{1,1}$ and $h^{2,1}$, defining the distinct values of the Euler characteristic. The Hodge numbers are independent of triangulations, so future extensions to the full list of Calabi-Yau hypersurfaces for all possible triangulations will not alter these defining features. The Euler number is fixed within the bounds, $\chi \in [-960, 960]$, which represents an interesting and currently undefined limitation set on the magnitude of the Hodge numbers we could wish to consider when building an axiverse. In Fig. (3.5) we display the apparent fractal nature of manifest symmetries found by plotting the Euler number against the Hodge summation, $h^{1,1} + h^{2,1}$. The mirror line symmetry centred around zero is an obvious feature of this plot. The Hodge numbers peak at the most occupied mirror symmetric point, $(h^{1,1} = 27, h^{2,1} = 27)$ with a multiplicity of 910,113, which we can associate to the typical number of axions we could expect. The general density of these points gives us a good reference point to the number of axions we might expect in some general string compactification model, which we will assume is roughly of the order,

$$\mathcal{N}_{\rm ax} \equiv h^{1,1} \simeq \mathcal{O}(30) \ . \tag{3.67}$$

Rather interestingly the Euler number is approximately Gaussian distributed (see the *right panel* of Fig. 3.3 and discussions in Ref. [444]) and well modelled in certain contexts by modified pseudo-Voigt/Planckian distributions [689]. The total dimension of the moduli space expressed in Eq. (3.64) can also be extracted using the Kreuzer-Skarke list and the distinct Hodge number combinations. This parameter also approaches a Gaussian like curve as displayed in the *left panel* of Fig. 3.3. These two examples represent the ability to replace (at least as a very approximate

assumption) geometrical topological parameters with simplified priors represented by unimodal functions. The polar duality in Eq. (3.65) and Eq. (3.66) is an incredible numerical realisation of the conjectured mirror symmetry in string theory models through the study of Calabi-Yau manifolds and their interchangeable features with respect to the associated reflexive polytope and its dual polytope. There are in fact many patterns or apparent symmetries which can greatly simplify the process of analysis when considering the way the topological invariants are distributed. For extended details see discussions in Refs. [309, 372, 645, 687, 688, 724].

3.3.6.3 From Geometry to Phenomenology

In Ref. [427] an analysis was considered using a subset of threefolds determined by triangulating polytopes for various values of $h^{1,1}$. A general focus was placed on the study of ensembles with a large values of $h^{1,1}$ in the context of axion cosmology. This analysis determined a series of interesting results in terms of how the geometrical features for the complex manifolds both relate and define a possible spectrum of ultralight fields. Of course these results represent an indication of possible model behaviour for isolated Type IIB compactification models on an orientifold of a hypersurface X, due to the limited nature of the sampling process, which does not rule out configurations completely. For geometries where $h^{1,1} > 22$, their initial results indicate that each geometry reproduces a series of ultralight states, representative of an axiverse, where the lightest field is hyperlight and essentially a massless quantity. In fact for configurations where $h^{1,1} \gg 1$[1] it was shown that in the regime of control of the α' expansion, the effective field theories tend to manifest a large number of fields which are very light, possibly falling in regions of great interest in models of ULA cosmology. The kinetic matrix eigenvalues, associated to defining the axion fundamental domain were also found to be small, in turn defining the effective axion decay constants as small, generally confined to sub-Planckian ranges. Previous literature has already shown the domain is sub-Planckian for all geometries with $h^{1,1} \leq 4$

[1]See Ref. [64] for details on the $h^{1,1} \leq 6$ domain.

[874]. In Ref. [427] this was extended to geometries with a large number of axions where it was found a limited number of configurations could potentially realise a trans-Planckian fundamental domains, which would be of great interest to model frameworks such as cosmic inflation. Models with large $h^{1,1}$ tend to show promise in finding fields which may appear in problematic and constrained regions of the axion parameter space. Specifically in the regime of control of the α' expansion, a three-fold hypersurface, along with sub-varieties can inherit very large volumes in string units. Although the complete picture of moduli stabilisation would be required to rule these out, along with a detailed focus on the regime of control of the α' expansion, these results do offer a fascinating prospect for future studies. Namely the consideration of specific phenomenological model features such as the independent axion gravitational coupling determining the nature of the superradiance process covered in Chapter 6, which could begin to rule out geometrical parameters for the extra-dimensional space directly.

It is currently, for the case of a general assessment of cosmological parameters and phenomena, too difficult to perform explicit string calculations to sample complete geometrical spaces in order to understand the overall properties of axiverse phenomenology. A minimalist approach is to consider the effective field theory of the Standard Model coupled to an extended sector symmetry or symmetries representing the axion field(s). These arguments now rely more simply on the parameters of the effective theory, which can be inspired or fully motivated by considerations made from the string models discussed above. Such methods often call upon randomised landscapes and the powerful mathematical phenomena of *universality* in order make sense of the dimensionality of the problem. With a reduction of the models information it is possible to generate results which could lead to inferences relevant for shaping future explicit model constructions.

3.3.7 Can We Really Have an Axiverse?

Given the assumption of the axiverse in the context of phenomenology, it's important to pause briefly to assess further details regarding the ability to realise this scenario in the surroundings of the wider string landscape. There may be few or indeed no light axionic degrees of freedom remaining once physical constraints are placed on models, e.g. moduli stabilisation mechanisms and other requirements for the resultant vacua. This may therefore bring into question the plausibility of details surrounding the assumptions made for the incorporation of light axions. In Section 3.3.4 and Section 3.3.5 we briefly covered the basic features of the string axiverse realised in both Type IIB and M-theory models respectively. These both provide two suitable frameworks in which a hierarchy of axion mass scales are well realised. Although these represent a '*proof of concept*' of finding an axiverse in the string landscape, it is important to consider an example of *when can't we realise the string axiverse?*

Issues surrounding the viability of light axions associated to supersymmetric moduli configurations which generically result in AdS vacua in the context of the string landscape [758] will be discussed. Indeed it has been shown that the presence of tachyons are generic for constructions attempting to stabilise the moduli supersymmetrically while preserving unfixed axions [364]. For any supersymmetric compactification solution the axions are partnered up with their scalar counter parts, the *saxions*. In this context the phenomenological features of ultralight solutions such as the QCD axion therefore heavily depend on the features and details of the stabilisation details of this scalar partner. The statement that supersymmetric solutions for any $U(1)_{\rm PQ}$-invariant effective supergravity framework lead to a tachyonic saxion mass is a powerful one. Solutions to this tension can be found in areas such as the required uplifting the potential undergoes in order arrive at a phenomenologically viable dS/Minkowski vacuum [758] (see discussions below in Section 3.3.7.2). To understand this example we will quickly review the *no-go* theorem of supersymmetric

moduli stabilisation with axions defined to be unfixed, applicable to general string compactification models, found in Section 3.3 of Ref. [364]. See also the relevant discussions in Refs. [341, 351, 460, 702, 781].

3.3.7.1 Tachyonic Saxion Masses and AdS Vacua

As detailed in Ref. [364] consider the framework of an arbitrary $\mathcal{N} = 1$ supergravity theory with two classes of moduli denoted by Φ_α and $T_\beta = \tau_\beta + ic_\beta$. The string-theoretic axions are identified as the imaginary component of T_β, indicated by c_β. The Kähler potential and the superpotential are a function of the moduli fields of the form, $K(\Phi_\alpha, T_\beta + \bar{T_\beta})$ and $W(\Phi_\alpha, T_\beta)$ respectively. We are concerned with details of the saxion masses ($\tau_\beta \equiv \mathrm{Re}(T_\beta)$) in the supersymmetric vacuum and the possible presence of light axions. In the supersymmetric vacuum, with stabilised moduli, we have the solutions, $D_{\Phi_\alpha} W = 0$ and $D_{T_\beta} W = 0$ for all values which run over the indices α and β. The chiral superfields can be re-expressed in a basis maintaining any required holomorphic properties such that there exists a superfield whose imaginary component is an axion unfixed by the solutions of the supersymmetric vacuum [364]. We will denote this axion, $c_\Upsilon \equiv \mathrm{Im}(T_\Upsilon)$.

As the solutions to the F-term equations are independent of c_Υ, the unfixed axion is a flat direction of the potential in Eq. (3.28) at the supersymmetric locus. The potential at the supersymmetric locus is defined as, $V = -3e^K |W|^2$. The axion c_Υ does not appear in the Kähler potential and as a flat-direction indicates that $|W|$ is independent of c_Υ, and therefore W can also be considered so[2]. Holomorphy dictates that the superpotential also has no explicit dependence on its saxion partner and therefore the modulus superfield, T_Υ. This leads to the realisation that, $\partial_{T_\Upsilon} W \equiv 0$ which also recalling that $D_{T_\Upsilon} W = 0$ leads to the following conclusion that we must consider either one of the two conditions $\partial_{T_\Upsilon} K = 0$ or $W = 0$ at the supersym-

[2]As pointed out in Ref. [364] there is an exception to this assumption. If the axion c_Υ represents an overall phase i.e. $W = e^{-aT_\Upsilon}$ then the assumption breaks down. This is however expected to be an exceptional case.

metric locus. Focusing on the case of $\partial_{T_\Upsilon} K = 0$ for motivations of genericity[3], the scalar potential in Eq. (3.28) can be investigated whilst using the previously stated conditions. The first derivative is given as [364],

$$\partial_{\tau_\Upsilon} V = e^K \mathcal{K}^{i\bar{j}} \left(\partial_{\tau_\Upsilon} \left(\partial_i K \right) W \left(D_{\bar{j}} \overline{W} \right) + D_i W \partial_{\tau_\Upsilon} \left(D_{\bar{j}} \overline{W} \right) \right) \ , \tag{3.68}$$

which is found by expanding $D_i W$ and using $\partial_{\tau_\Upsilon} W \equiv 0$. Eq. (3.68) contains only the terms which will provide non-vanishing contributions to the second derivative at the supersymmetric locus. Evaluating the second derivative of the potential gives details of the mass of the saxion of interest which is determined by the expression [364],

$$\partial_{\tau_\Upsilon} \partial_{\tau_\Upsilon} V = e^K \mathcal{K}^{i\bar{j}} \left(2 \partial_{\tau_\Upsilon} \left(\partial_i K \right) \partial_{\tau_\Upsilon} \left(\partial_{\bar{j}} K \right) W \overline{W} \right) - 3 \left(\partial_{\tau_\Upsilon} \partial_{\tau_\Upsilon} K \right) e^K W \overline{W} \ . \tag{3.69}$$

Utilising both that $\mathcal{K}_{i\bar{j}} = \mathcal{K}_{ij}$ and $\tau_\Upsilon = {}^1\!/_2 \left(T_\Upsilon + \overline{T}_\Upsilon \right)$ which defines the relationship, $\partial_{\tau_\Upsilon} K \left(T + \overline{T} \right) = 2 \partial_{T_\Upsilon} K \left(T + \overline{T} \right)$, leads to a simplified expression for the second derivative of the potential,

$$\partial_{\tau_\Upsilon} \partial_{\tau_\Upsilon} V = 4 e^K W \overline{W} \left(2 \mathcal{K}^{i\bar{j}} \mathcal{K}_{i\Upsilon} \mathcal{K}_{\Upsilon\bar{j}} - 3 \mathcal{K}_{\Upsilon\bar{\Upsilon}} \right) = -4 e^K W \overline{W} \mathcal{K}_{\Upsilon\bar{\Upsilon}} \leq 0 \ . \tag{3.70}$$

Recalling that $\mathcal{K}_{i\bar{j}}$ is a metric the quantity $\mathcal{K}_{\Upsilon\bar{\Upsilon}}$ is strictly positive definite leading to the conclusion that the τ_Υ direction is indeed tachyonic. The above gives a no-go theorem for the ability to realise a naturally suppressed mass for c_Υ required to explore phenomenological and cosmological solutions such as the QCD axion or quintessence. The arguments above imply that the supersymmetric locus is always tachyonic, with one tachyon for every massless axion. In this sense the appearance of undesirable tachyonic saxions would seem a generic prediction in these models of the AdS vacuum whilst seeking the axiverse. Specifically that there does not exist any

[3]As detailed in Ref. [364] even in the case that the superpotential vanished it is expected to obtain non-perturbative corrections to result in a non-vanishing potential. Given it follows that $\partial_{\tau_\Upsilon} \partial_{\tau_\Upsilon} V = 0$ the massless modulus τ_Υ would leads to issues such as fifth forces as yet unobserved.

supersymmetric minimum of the F-term potential consistent with stabilised moduli and unfixed axions one would desire for an axiverse scenario.

3.3.7.2 An Axiverse Assumption

While we have detailed in previous sections that axions appear to be a ubiquitous feature of critical string theories, the details of their survival within a framework of some low energy four-dimensional effective field theory can ultimately prove a very complex issue. In the case of incorporating many axions we have seen in Section 3.3.7.1 there may be many tachyons present, one for each massless axion field. A general conclusion then from the above points is the implication that light axions such as the QCD axion or light DM fields prefer non-supersymmetric moduli stabilisation. As pointed out in Ref [364] there are a number of loopholes to the arguments in Section 3.3.7.1 we could consider. These include the true nature of the Kähler potential in the non-perturbative limit and the subsequent dependency on the axion. The interplay of the D-term potential and the ability to consider the supersymmetric locus as a true minimum of the full potential. Alternatively the application of stability and the possible ability to ignore wether the locus is an actual minimum of the potential and details surrounding the Breitenlohner-Freedman bound [278]. A number of solutions have also been proposed in order to find stable vacuum with non-tachyonic saxions and a positive definitive mass matrix as required by realistic models. For example the utilisation of an uplifting potential induced by supersymmetry breaking brane stabilised at the end of warped throat [342, 343, 758] as detailed in Ref. [341].

One can then consider the assumption of an axiverse as both a limitation placed on the compactification scenario from the general underlying theory which motivates it and the total space of the string landscape we are operating in. That is the ad hoc assumption, we are only focused on the portion of the landscape in which sampling the axion parameter space of an axiverse is well motivated in the low

energy effective field theory. One of the most important problems in string theory is the ability to make direct and consistent contact with low-energy phenomenology we adopt in some effective theory as an extension to the Standard Model. The key takeaway is that ultralight fields are not features we can blindly associate to the vacuum. We can retain however the statement they are well motivated and will do so for the remained of this thesis. There has been good progress in defining both consistent masses for axions and moduli. A good example is the toy model presented in Appendix B of Ref. [31]. Given the current state of the field of axion cosmology and its place in the wider framework of string theory we can at best conjecture that the moduli are suitably stabilised. This leads to the conclusion that the study of axions whose masses are logarithmically hierarchical into an ultralight sector a well motivated endeavour. We will assume throughout any effective theories stem only from either the general framework of an Axiverse [107, 1230, 1231] or explicit works such as those in Refs. [21, 22, 27, 28, 31] which cover aspects of microscopic models. Our main focus will predominantly be on considering a random distribution of both decay constants, allowing for kinetic mixing of the axions and dynamical mass scales via the use of random matrices. These assumptions will allow us to study the dynamics of the axions.



Part II

The Universe and Universality

Chapter 4

Canonical Random Matrix Theory

> "*My colleagues in elementary particle theory in many lands are driven by the usual insatiable curiosity of the scientist, and our work is a delightful game. I am frequently astonished that it so often results in correct predictions of experimental results. How can it be that writing down a few simple and elegant formulae, like short poems governed by strict rules such as those of the sonnet or the waka, can predict universal regularities of Nature?*"
>
> Nobel Banquet Speech
>
> Murray Gell-Mann (December 1969)

4.1 Elements of Random Matrix Theory

4.1.1 Statistical Tools and Assumptions

The following sections in this chapter will detail some of the very well researched RMT machinery which allows us to make simplified statements or assumptions on a potentially extremely complex space to study or sample from. Our use of RMT will only be applied to a simplified treatment of a general two-derivative effective Lagrangian for a spectrum of ultralight fields which is well motivated in the context

of string models. We will be specifically interested in the case of random matrix ensembles which produce positive definite spectra in order to sample the dimensionful parameters at some phenomenological scale of interest, their values determined by a distribution of eigenvalues. The '*landscape*' of possible potentials incorporating a large number of scalar degrees of freedom resulting in masses spanning many scales (i.e. the Axiverse scenario [107]) is a very different space compared to the solutions we may find in the '*string landscape*' as highlighted in Section 3.3.7, representing the landscape provided to us by string theory. Our choice to sample based on the ad hoc assumption of an axiverse defines a starting point in our choice of modelling and represents just a part of the overall space we could choose to operate in. It does not therefore account for solutions or models, which factoring physical criteria (i.e. details of moduli stabilisation or supersymmetric concerns) suggest a possible absence of hierarchically light axions as highlighted by the example no-go theorem in Section 3.3.7. Our models and subsequent results are therefore to be interpreted as only relevant to the fraction of the string landscape in which an axiverse of scales seems to be a possible feature, and not the general axion parameter space as a whole. As a result we expect a significant space of string models and therefore string cosmology/phenomenology which cant be explored with the approaches we will take and ultimately our conclusions.

We also do not currently have a reason to believe statistical RMT models offer an accurate representation of actual string data from the top down. Therefore such approximations can be very restrictive and certainly in the context of the string landscape will fail to incorporate much of the possible rich structure which can be found there. The use of data vectors will take us far from physically realistic models and details of any microscopic parameters. However we can argue that as an initial investigation of part of what could be an important feature of the string landscape (ultralight sector cosmology), we can still retain some (albeit potentially limited) of the fundamental features of a model at the effective level that allow us to gain an understanding of some of the landscape's properties through our choice of ensembles

classes.

Using this incentive previous results have been determined applying both more detailed and simple matrix models with random potentials in the study of cosmological issues. This predominantly to-date has involved several or many scalar fields tackling the problem of inflationary modelling. Some other examples include random multi-field models such as those in Refs. [5, 347, 501, 502, 918] or approximations made to random supergravities (see Section 5.2.8 and references therein). For studies of multiple scalar fields or axions specifically, closer to the work in this thesis, parameter ensembles have also been considered which feature models with strictly positive spectra and sample covariance matrices. These are loosely inspired by explicit compactifications of string theory, in order to investigate simple axion cosmologies (Eq. (2.85)) and can found within the following works. Firstly utilising the assumption that the mass distribution depends only on the basic structure of the mass matrix itself, with the spectrum well-approximated by a Wishart matrix, (see Section 4.3.1.1 and Appendix I) can be found in Refs. [128, 173, 176, 268, 347, 353, 499, 501, 799, 1079, 1080]. For details of non-trivial kinetic matrices, charge matrices and a look at the fundamental domain of the axion field space using canonical ensembles of positive definite random matrices see Refs. [126, 128–133, 133, 134, 533, 693].

We will follow these motivations along with some elements of the examples listed above in order to investigate a simple picture of part of the multiple axion field landscape, the key difference from some of these works being the scale of the problem. Our approach considers modelling both the axion kinetic mixing and mass matrices simultaneously where we focus on the case of taking the quadratic approximation to the potential. That is we are assuming any higher order terms can be neglected, so that what are really cosine functions under the dilute gas approximation for the axion potential can be approximated to the case of $\mathcal{N}_{\rm ax}$ massive uncoupled fields. The applicability of this analysis is prompted by the general expectation these parameters (Eq. (2.85)) should present a non-trivial spectrum, which could span many orders of

magnitude. We then wish to assess this through a statistical analysis, absent of any specific information for the microscopic parameters of some theory which they find their motivations. Using the general case of random potentials highlighted above as an example one may choose to assume that the landscape consists of a sufficient number of largely uncorrelated terms that it can be treated probabilistically. This does not how ever suggest the string landscape itself is arbitrary, an important distinction.

The benchmark models we consider in a minimal framework become beneficial when considering an analysis of the case when $\mathcal{N}_{\rm ax} \gtrsim \mathcal{O}(10) - \mathcal{O}(100)$. Our models of the axiverse using the statistical tools below whilst incorporating a large number of fields have considerations and assumptions placed on their masses, decay constants and interactions, following the ad hoc assumption of an axiverse scenario as detailed in Ref. [107] and Section 3.3. A primary assumption we are making is therefore that our field masses can span many scales (i.e. M_H - $M_{\rm Pl}$) with a specific focus placed on the ultralight sector (See both Section 5.1.2 (Eq. (5.32) and Eq. (5.33)) and Section 7.1.3 for the mass ranges we consider). Likewise we will make the assumption the axion decay constants may also span many decades, as discussed in both Section 2.6.2 and Section 5.1.2 (Eq. (5.30) and Eq. (5.31)). In general we will ignore interactions between the fields (as is often seen in the literature) although we will touch on elements of this in Section 6.3 in regards to BH superradiance. The interpretation of the results and analyses in both Chapter 6 and Chapter 7 therefore apply only for the case of a general axion parameter space sampled using the matrix theory covered in this chapter. The following sections present the theoretical elements which allow us to understand spectral features of our models in each basis in which we sample.

4.1.2 Matrix Theory

We will begin by focusing on the study of a subset of the general linear group, $GL(\mathcal{N}, \mathbb{R})$ for all $\mathcal{N} \times \mathcal{N}$ non-singular real matrices, as well as the matrix groups

which act on that subset such as the orthogonal, $O(\mathcal{N})$ group, in order to define solutions to systems of randomised linear equations. The applications of RMT are numerous, making use of many of the available ensemble forms to structure the analysis of random operators [1298], counting devices [442], ensemble functional analysis and relevant for our interests for sampling physical dimensionful model parameters, data driven concerns surrounding sample covariance matrices [137, 1060] with high dimensional data analysis [755]. The standard and extensive literature on the compelling subjects surrounding random matrices and their striking results can be found in the monographic works and discussions in Refs. [138, 641, 939, 1279]. As a mathematical tool, RMT provides a very flexible and powerful framework in which to manipulate and move around large data sets associated to complex models and systems, often allowing for the extraction of conclusions based on introduced global symmetries. At the heart of this framework, often relied upon for many forms of analysis or methodologies used to gain insight into physical systems, is the beautiful theoretical aphorism of *universality*. The topic of RMT has a lavish and diverse narrative in the literature, several key landmark works injected into the landscape of mathematics during its booming phase of development, now represent staple configurations of analysis. The defining formulation of the invariant Haar measure over the classical groups, a theoretical underpinning of the many novel representations and modern disciplines of RMT today [443, 730]. Some decades after these studies, random matrices initially appeared in the work of John Wishart [1360], with his efforts to generalise the two parameter family of continuous gamma probability distributions to multiple dimensions, along with the work of Hsu [721] as far back as the 1930's. This aforementioned family formulation is known as the Wishart distribution, defining a series of probability distributions over the symmetric, nonnegative-definite matrix-valued random variables. The asymptotic formalism for random matrix ensembles came some twenty years later however, with the work of Wigner in regards to his research surrounding nuclear physics, where he postulated apparent associations between the spacings of lines in the spectrum of heavy

atomic nuclei and the eigenvalues of random matrices [1351, 1352, 1360].

Random matrix theory (RMT) is often broadly classified as the analysis and decomposition of eigenvalues (also often referred to as latent or characteristic roots) and eigenvectors of high-dimensional matrices distributed according to a defined statistical distribution. A symmetric random matrix can be classified as positive definite if and only if its eigenvalues are strictly all positive, negative definite if and only if its eigenvalues are all negative, and positive semi-definite if and only if all its eigenvalues are strictly non-negative. It is common to work in the regime where the size of the random matrix is taken to infinity which, given the defining results of numerous studies, has been shown to provide excellent accurate descriptions of the finite dimensional domain. Let us define this now as:

- **Analysis in the large $\mathcal{N}$ limit:** The study of the universal laws of convergence, central limit theorems (CLTs) and asymptotic statistics (for example limiting density functions) which arise when the dimension of the matrix is taken to the limit $\mathcal{N} \to \infty$.

4.1.3 Fundamentals of Eigendecomposition

The primary matrix decomposition we will concern ourselves throughout this thesis is the *spectral decomposition* or *eigendecomposition* of a matrix, which for any Hermitian matrix can be defined by a real diagonal matrix Λ,

$$\mathbb{M} = \mathbb{U}\Lambda\mathbb{U}^{-1} \ , \tag{4.1}$$

which possesses diagonal entries defined by the matrix eigenvalues, uniquely determined by $\mathbb{M}$. The Jacobian decomposition is defined as,

$$d^{\beta}(\mathbb{M}) = \prod_{1 \leq i < j \leq \mathcal{N}} |\lambda_i - \lambda_j|^{\beta} \prod_{k=1}^{\mathcal{N}} d\lambda_k d\mu(\mathbb{U}) \ , \tag{4.2}$$

where $d\mu(\mathbb{U}) = [\mathbb{U}^{-1}d\mathbb{U}]$ is the Haar measure. The specific form for the Jacobian can be defined by the choice of matrix ensemble, which produces a marginal distribution of the joint probability distribution. The invariance of the measure on $\mathbb{M}$ directly stems from the invariance of the Haar measure. For any matrix $\mathbb{M} \equiv \mathbb{M}(\mathcal{N})$, its ensemble can be understood through a probability distribution function that depends on the statistical nature of the entries forming the matrix elements. If we must insist on statistical independence for the matrix entries, often prescribed for analytical simplification, along with general basis transformation invariance, then general arguments taking a non-biased approach determine we must focus on the general results associated to ensembles related to the classical Gaussian ensembles, as often such features cannot be generalised to other random matrix ensembles consisting of real symmetric matrices. Formally our matrix ensemble distribution must retain the following symmetry arguments,

$$P(\mathbb{M}) \propto \prod_{i=1}^{\mathcal{N}} f_i(\mathbb{M}_{ii}) d\mathbb{M}_{ij} \prod_{i<j} f_{ij}\left(\mathbb{M}_{ij}\right) d\mathbb{M}_{ij} \ , \tag{4.3}$$

$$P(\mathbb{M}) = P(\mathbb{U}\mathbb{M}\mathbb{U}^{-1}) \ , \tag{4.4}$$

for the Gaussian functions, f_i and f_{ij}, where Eq. (4.4) is a consequence of the properties of the trace in the exponent of Eq. (4.5). By ensuring this choice in regard to the probability distribution of the matrix ensemble, we can now integrate over the relevant parameters related to the ensemble eigenvectors in order to determine an expression for the joint symmetrised probability density of the eigenvalues of $\mathbb{M}$ [748, 939],

$$P_{\mathcal{N},\tilde{\beta}}(\lambda) d^{\mathcal{N}}\lambda = \frac{1}{\hat{Z}_{\mathcal{N},\tilde{\beta}}} e^{-\xi \sum^{\mathcal{N}_{i=1}} V_{\mathcal{N},\tilde{\beta}}} \prod_{1\leq i<j\leq \mathcal{N}} |\lambda_i - \lambda_j|^{\tilde{\beta}} d\lambda_1 \ldots d\lambda_{\mathcal{N}} \ . \tag{4.5}$$

where ξ is is a constant determined by the choice of $\tilde{\beta}$ (see discussions in Section 4.1.4.1) and $\hat{Z}_{\mathcal{N},\tilde{\beta}}$ a normalisation constant. The presence of the Vandermonde determinant, $\prod_{1\leq i<j\leq \mathcal{N}} |\lambda_i - \lambda_j|^{\tilde{\beta}}$ is a consequence of a change of variables for the

eigenvalues and is significant as its square represents the statistical nature that there is a natural *eigenvalue repulsion* inherent to the distribution. The special form of this repulsive term, allows us to study such ensembles using orthogonal polynomials (see Section 4.1.4.1). The spectral behaviour of the characteristic roots from these relevant polynomials are generally factorised into two regions:

- **The global macroscopic regime**: *Probability measure space and linear formulations for the empirical spectral measures concerned with the bulk statistics, CLTs and limiting laws which demonstrate convergence over the entire set of ensemble eigenvalues.*
- **The local microscopic regime**: *Repulsive behaviour between the spacing of individual eigenvalues, along with statistical fluctuations at spectral radii of both the infimum and supremum at the relevant hard and soft edges via the determination of data correlations.*

Traditionally the limiting spectral density laws for the global space are represented by a deterministic measure density up to some scale associated to the eigenvalue spacing, normally of the order of the bulk spectrum normalisation factor, $O(\mathcal{N}^{-1})$. In the large $\mathcal{N}$ limit the normalisation factor saturates, placing a mass of $\mathcal{N}^{-1}$ on each random eigenvalue when sampling the ensemble. When sampling our model we therefore normally assume a given statistical model is ignorant to the scale of the physical problem we are attempting to solve, requiring normalisation to the limiting forms of the universal spectra according to the spacing in the bulk of the spectrum in the large $\mathcal{N}$ limit. This leaves a natural factorisation of the model scale and the global and local asymptotics coming from the random matrix.

Matrix models in theoretical physics have found traction regarding many fascinating fields of study. Close relations to string theory span as far back as the 1970's [281] (see Ref.[525] for classified examples of RMT usage). Further interesting insights have been drawn up regarding the study of eigenvalue repulsion and the holographic behaviour of matrix BHs [153, 1067, 1228], or the study of wrapped D-branes coordi-

nates [1066], study of moduli spaces [257, 524, 821], F-terms [454] and matrix valued scalar inflation [113], a small subsample of the complete analytical space. M-theory has also seen results derived from the conjecture that there exists a correspondence between uncompactified M-theory and the large $\mathcal{N}$ limit of supersymmetric quantum mechanics for D0 branes [152].

4.1.4 The Nature of Eigenvalues

Only if the diagonal elements of Λ in Eq. (4.1) are independent, identically distributed (IID) random variables, does the joint eigenvalue density take a factorisable form,

$$\rho_{\mathcal{N}}(\lambda_1, ..., \lambda_{\mathcal{N}}) = P(\lambda_1) \dots P(\lambda_{\mathcal{N}}) \ . \tag{4.6}$$

The applicability of Eq. (4.6) is therefore only valid if we wish to model variables usually determined by the spectrum of the matrices in a simplistic manor, not the spectrum of a matrices themselves. Take for example the axiverse solution we will discuss in Section 5.1.2. Taking a simplistic prior on the field parameters, f_a and m_a represents an approach of minimal information inspired by the possible landscape of solutions, motivating the type of prior in Eq. (4.6). The statistical independence in this simplistic model will never hold however when considering the eigenvalues of a random matrix representation for the axion parameter space, which we may encounter in some effective theory, for example a random matrix representing the unknown axion mass matrix. The joint eigenvalue density of a general class of invariant random matrix models (such as those determined using Eq. (4.2)) we may wish to use will take the following generic form,

$$\rho_{\mathcal{N}}\left(\lambda_1, ..., \lambda_{\mathcal{N}}\right) = \mathcal{C} \prod_{1 \leq i < j \leq \mathcal{N}} |\lambda_i - \lambda_j| \prod_{i=1}^{\mathcal{N}} e^{-V} \ , \tag{4.7}$$

where $\mathcal{C}$ represents a normalisation constant and V a polynomial. See Eq. (4.5) and surrounding discussions for details on the structure of this density function. The

probability for each eigenvalue is a more complicated picture due to the natural correlations between the eigenvalues. See Section 4 of Ref. [599] and Chapters 3, 4 and 5 of Ref. [939] for detailed discussions on topics such as correlation functions, cluster functions and gap probabilities which contribute to a correct understanding the true relationships between individual eigenvalues in classical matrix ensembles.

4.1.4.1 The Orthogonal Polynomial Method

There are various solutions and algebraic methods used in both the finite $\mathcal{N}$ and large $\mathcal{N}$ limits [525, 939], devised to evaluate the limiting behaviours of ensemble eigenvalues. Examples are the Stieltjes method [939], saddle point analysis [281], loop equations [944], superintegrals [651] and orthogonal polynomials [214]. Focusing on this last example, it is worth highlighting the use of this systematic procedure as it often plays a vital role in the analysis of limiting results of classic ensembles. For a detailed account of the complete procedure we only briefly highlight below of one of the most commonly used ansatz when investigating a distribution of eigenvalues see Refs. [46, 231, 423, 579, 811, 939, 1356]. A key feature of invariant ensembles is the ability to express the joint density of $\mathcal{N}$ eigenvalues as an expression incorporating a $\mathcal{N} \times \mathcal{N}$ determinant. An example of this is shown in the density function in Eq. (4.5). This relationship allows for the extraction of the limiting eigenvalue behaviour through the study of the asymptotics of orthogonal polynomials. Consider a generic Hermitian matrix model described by a partition function whose eigenvalues are described by a gas of $\mathcal{N}$ equally charged particles in the real domain. Their interactions are determined by a log potential and are confined by some polynomial potential of degree ν,

$$Z_{\mathcal{N}} = \int d^{\mathcal{N}}x e^{\left[-\mathcal{N}^2\{\mathcal{N}^{-1}\sum_k v(x_k) - \mathcal{N}^{-2}\sum_{i\neq j}\log|x_i - x_j|\}\right]} . \tag{4.8}$$

The powerful methods behind orthogonal polynomials are used to formally define exact solutions to Hermitian matrices of the form defined in Eq. (4.8), for all values

of $\mathcal{N}$, efficiently in terms of a kernel.

To begin we must focus on the properties of the Vandermonde determinant found in the exponential of Eq. (4.8). The statistical probability that individual eigenvalues are close is very small due to this term. The Gaussian orthogonal ensembles which relate to Eq. (4.8) are more formally referenced as *Hermite* ensembles due to their relation with the Hermite polynomials. These incorporate the Gaussian orthogonal ensemble (GOE), Gaussian unitary ensemble (GUE) and Gaussian symplectic ensemble (GSE). This categorisation was formalised back in 1962 when Freeman Dyson published a series of seminal works [493–495, 497, 497] which accrued in Ref. [492], where he proposed a symmetry classification of these invariant ensembles by introducing the Dyson index $\tilde{\beta}$. This parameter categorises the different possible real, complex, or quaternion entries, formulating the classical *threefold way*.

For any monic polynomial (a single-variable polynomial with a leading coefficient equal to 1), $p_k(x) = x^k + \ldots$, using elementary column operations on the Vandermonde determinant we can define,

$$\det \begin{bmatrix} 1 & x_1 & \ldots & x_1^{\mathcal{N}-1} \\ 1 & x_2 & \ldots & x_2^{\mathcal{N}-1} \\ \vdots & \vdots & & \vdots \\ 1 & x_{\mathcal{N}} & \ldots & x_{\mathcal{N}}^{\mathcal{N}-1} \end{bmatrix} = \det \begin{bmatrix} p_0(x_1) & p_1(x_1) & \ldots & p_{\mathcal{N}-1}(x_1) \\ p_0(x_2) & p_1(x_1) & \ldots & p_{\mathcal{N}-1}(x_2) \\ \vdots & \vdots & & \vdots \\ p_0(x_{\mathcal{N}}) & p_1(x_{\mathcal{N}}) & \ldots & p_{\mathcal{N}-1}(x_{\mathcal{N}}) \end{bmatrix} , \tag{4.9}$$

where the value of k represents a finite sequence and we have replaced the monomials in the left hand expression with polynomial functions. There are many '*classical*' orthogonal polynomials which represent our choice of basis (Jacobi polynomials, Laguerre polynomials or Hermite polynomials etc.) each required to follow the general condition,

$$\int_a^b p_j(x) p_i(x) w(x) dx = c_i c_j \delta_{ij} \ , \tag{4.10}$$

where $w(x)$ represents a *weight function* over the interval $[a, b]$, with constants c_i and c_j. The remaining terms $p_j(x)$, represents our selected series of orthogonal polyno-

mials of degree j. The canonical orthogonal ensembles weight functions are $|x|^a e^{-x^2}$, $x^a e^{-x}$ and $x^a(1-x)^b$ for the Hermite, Laguerre and Jacobi ensembles respectively. The system of $\mathcal{N}$ eigenvalues of interest may be considered as $\mathcal{N}$ fluctuating particles (Coulomb gas analogy). As the $\tilde{\beta}$ parameter in Eq. (4.5) tends to ∞, these particle positions behave as multivariate normals with variance $\mathcal{O}(1/\tilde{\beta})$, their variance and means located at roots of the respective orthogonal polynomials [483, 484]. A useful feature from the orthogonality of the chosen polynomials is that they must also satisfy a three-term recurrence relation, of the form,

$$xp_k(x) = p_{k+1}(x) + S_k p_k(x) + R_k p_{k-1}(x) \ , \tag{4.11}$$

where S_k and R_k are real constants. This is a simple recursive system of linear equations which leads to important features regarding the spectral information of the matrix ensemble. It is convenient to normalise the polynomials rather than work with the monic orthogonal polynomials to produce an orthonormal set of functions on the support of the relevant weight, $\phi_j(x) \equiv p_j(x)\sqrt{w(x)}$. These expressions satisfy the basis condition, $\int \phi_i(x)\phi_j(x)dx = \delta_{ij}$. These normalised polynomials define the reproducing kernel, a vital component in a general analysis of invariant matrix ensemble eigenvalue behaviour,

$$K_{\mathcal{N}}(x,y) = \sum_{k=0}^{\mathcal{N}-1} \phi_k(x)\phi_k(y) \ . \tag{4.12}$$

The reproducing kernels are defined as self-reproducing from our choice of an orthonormal set, and abide by the following self-replication condition,

$$\int K_{\mathcal{N}}(x,y)K_{\mathcal{N}}(y,z)d\mu(y) = K_{\mathcal{N}}(x,z) \ , \tag{4.13}$$

for each value of $\mathcal{N}$. The kernel in Eq. 4.12 can be expressed in terms of both $\phi_{\mathcal{N}-1}$ and $\phi_{\mathcal{N}}$ as a result of the Christoffel-Darboux formula [811, 939]. This informs us that the study the large $\mathcal{N}$ behaviour of these kernels is encoded in the study of just

two polynomials. Using Dyson's lemma [496] and Eq. (4.13) (see also [44, 45]) we learn that the marginal distributions for the eigenvalues can be represented in the form of a determinant constructed from the same kernel. This tells us the whole statistical information is contained in our definition of $K_{\mathcal{N}}(x, y)$. Specific investigated examples include the probability density of bulk and extremal eigenvalues (Eq. 4.15), correlation functions, cluster functions, gap probabilities (see Section 6.4.6.1 ($\acute{P}$)), Janossy densities and spacing distributions, all of which can be expressed in terms of a kernel in the form in Eq. (4.12). Three extremely common examples of kernels in RMT are the Airy kernel [262, 551, 1265], sine kernel [493, 968, 1018] and Bessel kernel [551, 968, 1267]. These each correspond to scaling at the *soft edge* of the GUE, scaling in the spectral *bulk* of the GUE, and scaling at the *hard edge* of the LUE/JUE respectively.

The fundamental Dyson representation for the join density and $\mathcal{N}$-point correlation function,

$$R_k\left(x_1, \ldots, x_k\right) = \frac{\mathcal{N}}{(\mathcal{N}-k)!} \int P_{\mathcal{N}}\left(x_1, \ldots, x_{\mathcal{N}}\right) \prod_{i=k+1}^{\mathcal{N}} d^2 x_i \ , \tag{4.14}$$

are respectively re-expressed as [939],

$$P(x_1, \ldots, x_{\mathcal{N}}) = \frac{1}{\mathcal{N}} \det\left(K_{\mathcal{N}}(x_p, x_q)_{1 \leq p,q \leq \mathcal{N}}\right) \ , \tag{4.15}$$

$$R_k\left(x_1, \ldots, x_k\right) = \det(K_{\mathcal{N}}(x_i, x_j))_{i,j=1}^{k} \ . \tag{4.16}$$

The $\mathcal{N}$-point correlation function is associated to the probability density that $\mathcal{N}$ of the eigenvalues, irrespective of order, lie in infinitesimal neighbourhoods, $x_1, \ldots, x_{\mathcal{N}}$. It is representative of a marginal distribution on the set of $\mathcal{N} \leq k$ eigenvalues. The kernels which arise from the use of orthogonal polynomials therefore give rise to explicit formulae for the spectral quantities of interest. The asymptotic behaviour of of these kernels dictate our understanding of the statistics of the eigenvalues of unitary ensembles in the large $\mathcal{N}$ limit and give us a heuristical understanding of

universality in random ensembles.

4.1.5 Convergence of Limiting Spectral Distributions

One example of universality is often found with a consideration of the marginal eigenvalue distribution, found by integrating the joint and unordered eigenvalue distribution over each latent root aside from the one of interest. This is also understood as placing a probability measure on the matrix, $\mathbb{M}$ and subsequently its eigenvalues, which once evaluated represents the nature of a randomised eigenvalues for a random matrix, i.e. a member of the chosen ensemble. When this is averaged over the defined probability measure, the limiting eigenvalue distribution is found. This function represented in a form which characterises the distribution of eigenvalues, is known as the empirical spectral distribution (ESD),

$$\mu_{\mathcal{N}}^{\mathbb{M}} = \frac{1}{\mathcal{N}} \sum_{i=1}^{\mathcal{N}} \delta_x \left(x - \lambda_i \right) \ , \tag{4.17}$$

where δ_x represents a Dirac delta measure at x, leading to the ordered set of eigenvalues of $\mathbb{M}$,

$$\lambda_1 \leq \lambda_2 \leq \cdots \leq \lambda_{\mathcal{N}-1} \leq \lambda_{\mathcal{N}-1} \ . \tag{4.18}$$

If $\lambda_i \neq \lambda_j$ for all j where $j \neq i$ then the spectrum distribution is *simple*. Perhaps one of the most powerful ideas stemming from the properties of the eigenvalue spectrum is the principles of *convergence of measure*, ergodicity or self-averaging the spectrum demonstrates in the large $\mathcal{N}$ limit. The statistical features of the invariant ensembles we have mentioned have flourished since their initial appearance, where often a focus is placed on the level densities, spacing distributions and spectra of eigenvalue extrema found in these models. As a defining feature present in many ensembles of random matrices, the ESD will converge to a unique and deterministic form as $\mathcal{N} \to \infty$. This function is known as the spectrums *limiting spectral density* (LSD) which is understood as $\mu^{\mathbb{M}}$ converging weakly on $\mathbb{R}$ either almost surely or with a

given probability, to some non-random probability distribution function, $\mu_{\mathcal{N}}^{\mathbb{M}}$. The deterministic probability measures converge in the weak* topology on a given space, Ω with an associated algebra to a defined measure, μ where such convergence holds if, $\mu_{\mathcal{N}}^{\mathbb{M}} \to \mu^{\mathbb{M}}$ if and only if $||\mu_{\mathcal{N}}^{\mathbb{M}} - \mu^{\mathbb{M}}||_{\infty} \to 0$ along with the general limits,

$$\mu_{\mathcal{N}}^{\mathbb{M}} \xrightarrow[\mathcal{N}\to\infty]{\text{Weak}} \mu^{\mathbb{M}}, \qquad \forall \in \mathcal{C}_c(\mathbb{R}), \qquad \lim_{\mathcal{N}\to\infty} \int \mu_{\mathcal{N}}^{\mathbb{M}} \mathrm{d}\mu_{\mathcal{N}}^{\mathbb{M}} = \int \mu^{\mathbb{M}} \mathrm{d}\mu^{\mathbb{M}} \, , \tag{4.19}$$

for the continuous bounded function set, $\mathcal{C}_c(\mathbb{R})$. The LSD can be expressed via the self-averaging properties of the ESD found by averaging over our choice of matrix ensemble, with an average eigenvalue density,

$$\mu^{(\mathbb{M})} = \lim_{\mathcal{N}\to\infty} \mu_{\mathcal{N}}^{\mathbb{M}}(x) = \mathbb{E}\left\{ \frac{1}{\mathcal{N}} \sum_{i=1}^{\mathcal{N}} \delta_x \left(x - \lambda_i\right) \right\} = \int \frac{1}{\mathcal{N}} \sum_{i=1}^{\mathcal{N}} \delta_x \left(x - \lambda_i\right) d\mu_{\mathcal{N}}^{\mathbb{M}} \, . \tag{4.20}$$

The above points represent mathematical formalities generally beyond the scope of the topics in this thesis. The principle of weak convergence a formality which allows us the ability for us to fix statistical priors and suitable function approximations to limiting measures in our analysis.

4.1.6 Classical Random Matrix Theory

In order to introduce the familiar matrix ensembles we will begin with a particular special class of matrix ensemble concerns those invariant under group basis automorphisms, formally defined by a Radon-Nikodym density of the form,

$$P_{\mathcal{N},\tilde{\beta}}(\mathbb{M}) d_{\tilde{\beta}}\mathbb{M} = \frac{1}{Z_{\mathcal{N},\tilde{\beta}}} e^{-\mathrm{Tr}\left[V_{\mathcal{N},\tilde{\beta}}(\mathbb{M})\right]} d_{\tilde{\beta}}\mathbb{M} \, , \tag{4.21}$$

with respect to a flat Lebesgue measure on the space of algebraically independent entries, where $Z_{\mathcal{N},\tilde{\beta}}$ is a normalisation constant, present to ensure we maintain the correct probabilistic normalisation, $\int d\mu(\mathbb{M}) = 1$. The subscript, $\tilde{\beta} = 1, 2$ and 4 represents the orthogonal, unitary and symplectic ensembles for the $\mathcal{N} \times \mathcal{N}$ real

symmetric, $\mathcal{N} \times \mathcal{N}$ real Hermitian and $2\mathcal{N} \times 2\mathcal{N}$ Hermitian self-dual matrices respectively. The exponent in Eq. (4.21) is an arbitrary real function of the matrix, $V_{\mathcal{N},\tilde{\beta}}(\mathbb{M})$, which is also referred to as the potential of the invariant ensemble. When $V_{\mathcal{N},\tilde{\beta}}(\mathbb{M})$ is degree two, i.e. $V_{\mathcal{N},\tilde{\beta}}(x) \propto x^2$ we retrieve the classical case relating to the famous Gaussian ensembles. These ensembles are often referenced in the literature as defining an ensemble class with invariant trace. Gaussian ensembles are unique as they represent both a family of invariant ensembles, which also belong in the ensemble of matrices defined with IID entries. These are paradigmatic ensembles, with a natural realisation in many models of physical systems used to describe the universal laws of physics.

4.1.6.1 Ensemble Invariance and Physical Systems

One of the first defining presentations of the insights these ensembles bring with an understanding of eigenvalue spacings, serving as a test for the conjecture of universality in a naturalistic study, was Wigners' motivations to study generic models representing the spectral fluctuation properties of complex many-body systems in nuclear physics. Specifically he focused on the general properties of the energy levels of atomic nuclei with the use of a random Hamiltonian, H. The real or complex Wigner ensemble consists of general $\mathcal{N} \times \mathcal{N}$ self-adjoint matrices with normalised variance. The entries have an imposed symmetry constraint, $h_{ij} = \bar{h}_{ji}$. A Wigner matrix is defined as a matrix with the form,

$$\mathbb{W}_{\text{Wig}} = \frac{1}{\sqrt{\mathcal{N}}}\mathbb{H}_{\mathcal{N}} \ , \tag{4.22}$$

with centred real or complex random variable entries, $\mathbb{E}h_{ij} = 0$ and $i, j = 1, 2, \ldots, \mathcal{N}$. Wigner proved that the weak limiting empirical density of the eigenvalues converges

to the now renowned semicircle distribution,

$$\mu_{\rm SC} \equiv f\left(\lambda\right) = \begin{cases} \frac{1}{2\pi}\sqrt{4-\lambda^2} & \text{if } |\lambda| \leq 2 \ , \\ 0 & \text{if } |\lambda| \geq 2 \ , \end{cases} \tag{4.23}$$

the famous CLT canonical density for scalar probability theory (see Fig. 4.1). Rather interestingly these distributions have also been manipulated and embedded in the context of representing the limiting spectra in flux compactification models, using shifted Wigner spectra in order to greatly simplify the treatment of the study of vacua utilising random ensembles of supergravity theories [125, 127, 429, 909]. Similar example ensembles also appear such as the Altland-Zirnbauer CI ensemble [63] when modelling non-supersymmetric flux vacua [429, 909]. The use of these minimal information randomised landscapes has also found significant traction as a tool in inflationary multi-field cosmology [564, 1039]. The *black* dotted line in Fig. 4.1 defines the empirical eigenvalue limiting law often referred to as the *Wigner sea*. The density points outside this region represent the local fluctuations of the spectrum in the finite limit over a scale of width $\mathcal{N}^{-1/6}$. The limiting density function of these fluctuations is determined by the Tracy-Widom distributions introduced in Appendix D. Each of the coloured lines represent the density functions of fluctuated spectra for different values of the smallest eigenvalue in the spectrum. In the context of random vacua, the function corresponding to $\lambda_{\rm min} = 0$ (*blue* line), is representative of a specific example where we realise an eigenvalue spectra detailing a *metastable* vacuum configuration, formed from probability relations of fluctuations to atypical configurations. The probability function for these fluctuations as a function of the smallest eigenvalue is,

$$P(\lambda)_{\lambda_{\rm min}} = \frac{1}{6\sqrt{3}\pi}\left(3\lambda - \lambda_{\rm min} + \sqrt{12+\lambda_{\rm min}^2}\right)\sqrt{\frac{-3\lambda+\lambda_{\rm min}+2\sqrt{12+\lambda_{\rm min}^2}}{\lambda-\lambda_{\rm min}}} \ , \tag{4.24}$$

which recovers the famous semicircular law of Eq. (4.23) in the limit $\lambda_{\rm min} = -2$. As

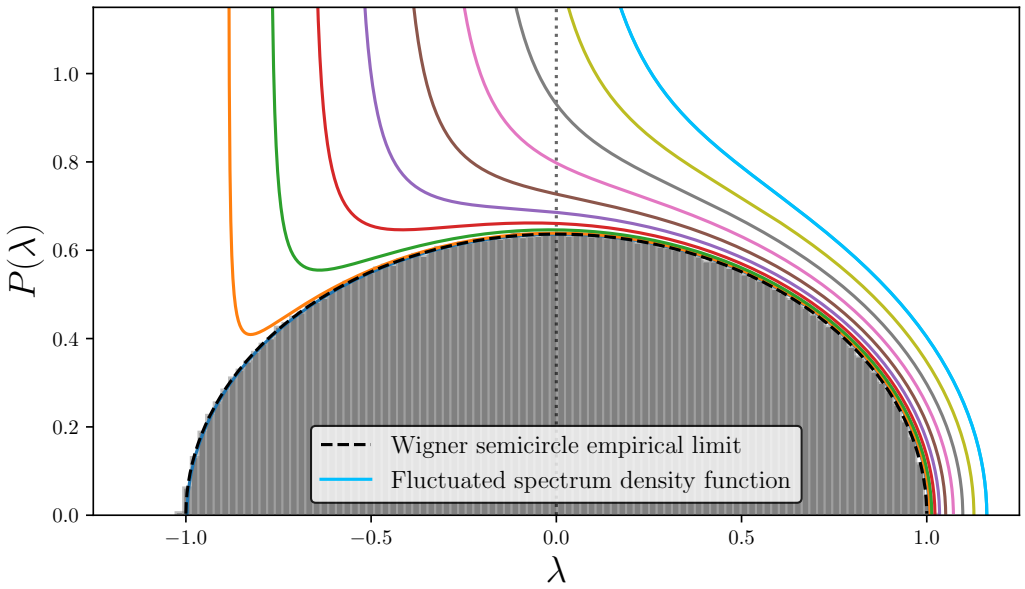


Figure 4.1: Normalised eigenvalue spectrum of the GOE ensemble for classical random Gaussian matrices [505, 939], represented by both numerical samples and the empirical spectral Wigner semicircle density limiting law defined in Eq. (4.23) [1352]. Each coloured density function in regards to the probability of large fluctuations of extreme eigenvalues is defined using Eq. (4.24), which is found in Ref. [418] and detailed in Ref. [1039], for different specific bounds placed on the infimum eigenvalue. The final function (*blue* line) represents the atypical fluctuated spectrum in which the complete set of eigenvalues are defined on the real positive interval.

detailed in Ref. [1039] the probability of realising such fluctuations is computed by integration of the probability density function,

$$P(\lambda > \lambda_{\min}) = \int_{\lambda_{\min}}^{+\infty} dP \ , \tag{4.25}$$

where the saddle point evaluation of Ref. [418] leads to the probability function,

$$P = e^{-\beta N^2 \Phi(\lambda_{\min})} \ , \tag{4.26}$$

with a rate,

$$\begin{aligned} \Phi(\lambda_{\min}) = &\frac{1}{432}\left[72\lambda_{\min}^2 - \lambda_{\min}^4 + \left(30\lambda_{\min} + \lambda_{\min}^3\right)\sqrt{12+\lambda_{\min}^2}\right] \\ &+ \frac{1}{432}\left[108\ln(36) - 216\ln\left(-\lambda_{\min} + \sqrt{12+\lambda_{\min}^2}\right)\right] \ , \end{aligned} \tag{4.27}$$

which represents a specific example of landscape statistics in order to define the required density of states. Such simple landscapes represent potentially vast possible field space regions, defined by the theory. These models are in principle used to model the energy landscape of random potentials and such concern themselves with the statistical nature of stable vacuum considerations. For example in the case of the Hessian modelled in the landscape of Gaussian random fields the saddle point approximation [399] can be used to assess the form of the statistical functions for critical points [1371]. The form of these functions detail the potentially non-trivial and exponential suppression to realise the desirable atypical eigenvalue alignment required for metastable vacua of critical points. Statistically this represents a vast suppression against realising solutions given by the universal lampposts of RMT. See Section 5.2.8 for a more detailed discussion on these topics.

The properties of the individual eigenvalues Wigner had poured his focus into reaped a novel result, his prediction, the fluctuations of the gaps are universal, distributed according to a law referred to as the *Wigner surmise*. His sentiments on the significance of this result translated through his words on the subject:

> "*Perhaps I am now too courageous when I try to guess the distribution of the distances between successive levels (of energies of heavy nuclei). Theoretically, the situation is quite simple if one attacks the problem in a simpleminded fashion. The question is simply what are the distances of the characteristic values of a symmetric matrix with random coefficients.*"

As it turns out, Wigners' law was incorrect, the true solution later formulated by Gaudin [589], following the recently developed orthogonal polynomial methods of M. L. Mehta [938]. Wigner had however at the very least, set a gratifying precedent, successfully testing the conjecture that complicated quantum systems were well modelled by universal forms, with dependancies seemingly only placed on the symmetry classes of the physical system, with the ability to integrate out other detailed structures. Must like the models of other physical systems such as random

supergravity (Section 5.2.8) the key aspects of the universal limits were inevitability perturbed by various forms of required correctional terms representing a level of quasi-universality of the systems description.

4.1.6.2 A Minimally Informative Stance

An interesting perspective on the use of these invariant ensembles in model building with RMT is the principle that they can be understood at a fairly fundamental level as a model of *'minimal information'*, through Shannon's information theory [1178]. To give an insight as to why we might wish to use such ensembles when leaning on features of universality, we can look at the stance taken by Roger Balian [145, 291], some time shortly after the decisive work of Wigner-Dyson-Mehta. It quickly became apparent that particular canonical matrix ensembles, i.e. those of Eq. (4.21) can be reformulated by minimising the information content of the probability distribution which defines the ensemble, once symmetry considerations have been taken into account. Alternatively this is viewed as maximising the entropy of the system, factorising the remaining system properties to be assumed as *maximally random*. Consider the case of discrete events where the information for a set of probabilities is defined as,

$$I\left[P\right] \equiv \sum_{i=1}^{\mathcal{N}} P_i \log P_i \ , \tag{4.28}$$

which is generalised for the case of continua,

$$I\left[P\left(\mathbb{M}\right)\right] \equiv \int d\mathbb{M} P\left(\mathbb{M}\right) \log P\left(\mathbb{M}\right) \ , \tag{4.29}$$

up to normalisation factors. We wish to select the probability distribution $P\left(\mathbb{M}\right)$, which is constrained to satisfy certain properties that de-biases our approach, minimising the information and maximising the entropy functions on the matrix space,

which takes the form [291],

$$S \equiv -\int \ldots \int D\left(\mathbb{M}\right) \log\left[D\left(\mathbb{M}\right)\right] d\mathbb{M} \ , \tag{4.30}$$

for fixed requirements placed on the conditions and symmetries of the problem. The standard procedure now involves fixing conditions such as the expectation of the lowest order traces which are required to conform to defined prescribed values [579],

$$\mathbb{E}\left[\mathrm{Tr}\mathbb{M}\right] = \mathcal{A} \ , \tag{4.31}$$

$$\mathbb{E}\left[\mathrm{Tr}\mathbb{M}^2\right] = \mathcal{B} \ . \tag{4.32}$$

These constraints are placed into the minimisation by using forms for Lagrange multipliers, ν_1 and ν_2, where the function,

$$I\left[P\left(\mathbb{M}\right)\right] = -\int d\mu\left(\mathbb{M}\right) P\left(\mathbb{M}\right)\left[\log P\left(\mathbb{M}\right) - \nu_1 \mathrm{Tr}\mathbb{M} - \nu_2 \mathrm{Tr}\mathbb{M}^2\right] \ , \tag{4.33}$$

is now minimised. Allowing for a variation of Eq. (4.33) with respect to $\delta P(\mathbb{M})$ gives the expression,

$$\delta I\left[P\left(\mathbb{M}\right)\right] = -\int d\mu\left(\mathbb{M}\right) \delta P\left(\mathbb{M}\right)\left[1 + \log P\left(\mathbb{M}\right) - \nu_1 \mathrm{Tr}\mathbb{M} - \nu_2 \mathrm{Tr}\mathbb{M}^2\right] = 0 \ , \tag{4.34}$$

which must take the proportional solution,

$$P(\mathbb{M}) \propto e^{\left(\nu_1 \mathrm{Tr}\mathbb{M} + \nu_2 \mathrm{Tr}\mathbb{M}^2\right)} \ , \tag{4.35}$$

which is nothing more than a Gaussian form for the distribution placed on the matrix elements. Defining the probability distribution for the matrix $\mathbb{M}$, allows us to now focus on the nature of the joint eigenvalue distribution. The required Gaussian matrix distribution for the elements is obtained by maximising the Boltzmann-Gibbs-Shannon entropy with considerations for the expectation values in Eq. (4.31)

and Eq. (4.32). This represents an extremely strong link between the nature of Gaussian statistics and the eigenvalues of a large class of random matrix models, when the requirements on the trace are fixed. See Refs.[16–19, 213, 1263] for construction of random matrix ensembles by using the same approach this time with the Tsallis' non-extensive entropy [1272, 1273], a generalisation of Boltzmann-Gibbs entropy statistics.

4.2 Sample Covariance Matrices and High Dimensional Data

4.2.1 Multivariate Statistics and Positive Definite Spectra

Parametric statistics is now a mainstay in the modern climate of data analysis, utilised in models in many fields requiring more and more elements in their fundamental domains. Many of these have a natural desire for more and more powerful inference methods to evaluate the deterministic and potentially unknown model parameters. These natural concerns are often centred around possible conclusions we can draw from our model via the use of a subset of statistical principles, multivariate statistics, which concerns itself primarily with vector valued data. Beyond the classical contemplations of the 20^{th} century, random matrices have seen a vast resurgence due to the modern practicalities of examining high-dimensional data sets. It is indeed common to encounter the asymptotics of large $\mathcal{N}$ and $\mathcal{P}$ synonymous with the theoretical manifestations of limiting distributions formulated some decades previous. The so called *large* $\mathcal{P}$-*large* $\mathcal{N}$ setting is the current prime landscape for informative discussions of high-dimensional data. Of course in this day and age it is expected much of the data found in the modern world should concern itself with multicomponent vectors of random data, or data sets consisting of multiple if not numerous variables. How these data sets or variables relate to each other has a long history

spanning back to the seminal works of Karl Pearson and even as far back as the work of Carl Friedrich Gauss. The understanding that it is possible to encompass such theoretical uncertainty in a simplified model revolutionised the approaches made toward highly complex and initially assumed to be analytically untouchable, physical systems, where predictive conclusions were eventually formed on the grounds of symmetries and universality. Given the recent evolution of computational capacities and algorithms, such as machine learning methods and the powerful theoretical foundations to generate model reference frames, it is no surprise innovative model applications requiring the analysis and statistical formulations of random matrix arguments, representing high-dimensional data structures are numerous in the fields of theoretical physics [436], telecommunications [1280], number theory [371], quantum mechanics [58, 259, 641, 1291], condensed matter physics [185], information theory [145, 930, 966] and quantitive finance [258, 370, 640, 836, 836, 895, 1009, 1062, 1285], representing a taste of the reach this branch of mathematics has.

Typically sampled data sets can be factorised into two contributing components, *signal* and *noise*. Sampled data can be compared against the universal cornerstone laws relevant for high dimensional data structures which have driven much of the research in the field over the past many decades, in order to declare whether one observes correlations between data vectors for model variables. These conclusions stem from the nature of singular values and deviations from the RMT predictions often associated to local spacing and bulk singular value statistics, such as the celebrated *quarter* and *semi*circle laws [1351, 1352, 1360] or Marčhenko-Pastur law [901, 1360]. Lets us flip this procedure on its head and now suppose the deterministic generation of model data under a frequentist style framework is in general, beyond either analytical or computational practicalities, such as requiring solutions to vast systems of explicit linear equations. These powerful laws of statistical convergence can also be viewed from a different stance in regards to model evaluation and the school of statistics we use to formulate our conclusions. Replacing the deterministic data sets from directly sampled inputs, we now call upon the Bayesian type approach

discussed in Appendix B, introducing an estimator quantity for the data, where the uncertainty of the data inputs is translated across from theoretical uncertainty present in model, now turning to the study of priors and parameterisation of measure spaces. This theme of universal asymptotic behaviour ever present in our discussions so far is indeed analogous to that found in classical probability theory. A standard example is the sum of independent standard normal random variables producing a normalised sum, which is understood as a further independent standard normal random variable. A common use for multivariate random variables is to define a series of data vectors which categorise a series of unknown values under the pretence of a lack of sufficient information or imperfect knowledge of an overall model. These data vectors form the structure of a sample covariance matrix.

4.2.1.1 The Sample Covariance Matrix

The question we should now address is how we understand the universal nature of RMT in the context of the priors we place on our ensemble and how both *signal* and *noise* elements are represented in terms of data vectors. Let us begin with the random variable X, where we define X to be absolutely integrable if $\mathbb{E}|X| < \infty$ and almost surely finite if $|X| < \infty$. The expectation of a given quantity is denoted by $\mathbb{E}$, where we can express the first raw and second centralised moments of our random variable respectively as,

$$\mu_x = \mathbb{E}[X] \ , \tag{4.36}$$

$$\sigma_X = \sqrt{\mathbb{E}[(X - \mu_X)^2]} \ . \tag{4.37}$$

Now, by introducing a further random variable Y, we can define the integral definitions of both the covariance and correlation between two variables,

$$\Sigma_{X,Y} = \mathbb{E}[(X - \mu_X)(Y - \mu_Y)] \ , \tag{4.38}$$

$$\rho_{X,Y} = \frac{\Sigma_{X,Y}}{\sigma_X \sigma_Y} \ . \tag{4.39}$$

Elevating this statistical standardisation, to a system incorporating many correlated random variables for model data sets forms the notion of a covariance matrix, used to regulate covariates between elements of higher dimensional structures,

$$S_{ij} = \mathbb{E}[(X_i - \mu_{X_i})(X_j - \mu_{X_j})] \ , \tag{4.40}$$

which is defined in the positive semi-definite subset of all $(\mathcal{P} \times \mathcal{P})$-matrices,

$$S \in \mathbb{R}^{\mathcal{P}\times\mathcal{P}} : \ x^{\mathrm{T}} S x \geq 0, \ \forall x \in \mathbb{R}^{\mathcal{P}} \ . \tag{4.41}$$

The conventional approach to making an estimation of the population covariance replaces the matrix in Eq. (4.40) with the sample covariance matrix, now making use of sample estimates. The unbiased-maximum-likelihood-based estimator of a population covariance matrix is expressed via the relationship,

$$\hat{S}_{ij} = \frac{1}{\mathcal{N}-1} \sum_{i=1}^{\mathcal{N}} \left(X_{iy} - \bar{X}_i\right) \left(X_{jy} - \bar{X}_j\right) \ , \tag{4.42}$$

$$\bar{X}_i = \frac{1}{\mathcal{N}} \sum_{\alpha=1}^{\mathcal{N}} X_{i\alpha} \ , \tag{4.43}$$

where $\bar{X}_i$ is the sample mean, acting as a common estimator for the covariance matrix, $\hat{S}_{ij}$. Matrices defined in this way offer many beneficial features such as orthonormal eigenvectors, non-negative definitive eigenvalues and symmetricity. Sample covariance matrices serve to provide initial estimates of relationships between random variables and to provide sample estimates used in model construction. Sample covariance matrices will act as our primary mathematical tools in order to alleviate the complexity of the string landscape, encoding the theoretical uncertainly of a large number of unknown contributions to the effective theory in a series of data parameter vectors, with a given statistical distribution prior fixed primarily using the requirement of minimal information. Consider a collection of data samples, $x_1, ..., x_{\mathcal{N}} \in \mathbb{R}^{\mathcal{P}}$ which for a defined number of degrees of freedom forms the

data array understood as a $\mathcal{N} \times \mathcal{P}$ dimensional matrix,

$$\mathbb{X}_{\mathcal{N}} \equiv (x_{ij})_{1 \leq i \leq \mathcal{P}, 1 \leq j \leq \mathcal{N}} \in \mathbb{R}^{\mathcal{N} \times \mathcal{P}} \, , \tag{4.44}$$

$$\mathbb{X}_{\mathcal{N},\mathcal{P}} = (x_{ij})_{\mathcal{N},\mathcal{P}} = \begin{bmatrix} x_{11} & x_{12} & \dots & \dots & \dots & x_{1\mathcal{P}} \\ x_{21} & \vdots & \vdots & \vdots & \vdots & x_{2\mathcal{P}} \\ \vdots & \vdots & \vdots & \vdots & \vdots & \vdots \\ \vdots & \vdots & \vdots & \vdots & \vdots & x_{\mathcal{N}-1\mathcal{P}} \\ x_{\mathcal{N}1} & x_{\mathcal{N}2} & \dots & \dots & x_{\mathcal{N}\mathcal{P}-1} & x_{\mathcal{N}\mathcal{P}} \end{bmatrix} \, , \tag{4.45}$$

where the index denotes the primary dimension of interest for the sample statistic in the data frame. The dimensions of the matrix in Eq. (4.44) represent defined statistical features, which shape the combinatorics of the data set, normally associated to the following parameters of interest,

- $\mathcal{N}$ - The number of observations or samples.
- $\mathcal{P}$ - The number of unknown random variables relevant to the reduced dimensional description of the model.

These correspond to the size of the rows and columns respectively. The sample results are stored in the rectangular matrix formed of empirical data. Each sample, i then has statistical data in the $p-$vector, x_i and so on. The dimensionality or concentration of the data matrix is understood via the *rectangularity* ratio of these two dimensions,

$$\beta = \frac{\mathcal{N}}{\mathcal{P}}. \tag{4.46}$$

When the value of β converges to a constant value, then we are operating in the framework of large-dimensional asymptotics or *the high-dimensional regime*.

4.2.1.1.1 The High-Dimensional Regime

When the dimension of $\mathcal{P}$ is fixed and the sample size $\mathcal{N} \to \infty$, the problem reduces to the limits of classical multivariate asymptotic theory for each random variable. At

this point the sample covariance matrix converges to use the population covariance matrix as the standard estimator. As the value of β approaches large $\mathcal{N}$ limits we enter into various regimes which account for the validity of our statistical estimation. The realm of large $\mathcal{N}$-large $\mathcal{P}$ asymptotics predict fundamental differences from the classical counterpart by leaving empirical estimators of covariance unreliable. Each of the regimes of interest are:

- **Classical regime**: $\mathcal{P} \gg \mathcal{N}$: As the dimensionality of the random variable vectors tends to infinity with a fixed sample size, the sample covariance estimation is no longer valid and breaks down.
- **High-dimensional regime**: $\mathcal{P}, \mathcal{N} \to \infty, {}^{\mathcal{N}}/_{\mathcal{P}} \to \beta$. *The non classical criterion*: There exists well defined constants, c_1 and c_2 such that in the large $\mathcal{N}$ limit, $0 < c_1 \leq \beta \leq c_2 < \infty$ for the general regime of analysis using large dimensional random sample covariance matrices.

We will always be interested in and operate in the high-dimensional regime, ensuring both c_1 and c_2 are suitably well defined values between 0 and 1 to ensure the spectrum is non-singular. Let us more formally define the structure of a general data matrix used to sample a simple description of a high dimensional model and explore how universal features arise.

4.2.1.1.2 Data Vectors and Standard Matrix Forms

The principle foundations to measure convergent or universal behaviour comes from considerations made to the moments of the statistical entries used to generate the random data vectors. Under the assumption that the limiting laws for large numbers hold, then in the limit where $\mathcal{P} \gg \mathcal{N}$, the eigenvalues of the sample covariance matrix tend to non-degeneracy at unity. In this setting we can define the following standard form of the random symmetric positive definite sample covariance matrix estimator,

$$\mathbb{Y}_{ij} = \frac{1}{\mathcal{P}} \sum_{i=1}^{\mathcal{P}} X_i X_i^{\mathrm{T}} \equiv \frac{1}{\mathcal{P}} \mathbb{X}\mathbb{X}^{\mathrm{T}} \ , \tag{4.47}$$

where the generic form of sub-matrices we will use to construct $\mathbb{Y}_{ij}$ are defined in Eq. (4.44). The normalisation shift compared to Eq. (4.42) represents an estimation of the mean using the maximum likelihood before calculating the maximum likelihood estimate of the covariance. The mean vector, sometimes referred to as the *centroid*, is a quantity which is assumed to be undefined and therefore factorised out of the covariance estimation. The model scales are accounted for externally, where we are only interested in the remaining statistical dispersions estimated using the standard variance-covariance estimator in Eq. (4.47). Models of this form often take advantage of very powerful statistical laws concerning the convergence of random variables such as the previously mentioned *law of large numbers*. For any sequence of independent real valued random variables drawn from a common statistical distribution, their summation $\sum_{i=1}^{\mathcal{N}} x_i$ will converge to the following expression, representing the *strong* criterion of the law,

$$\sum_{i=1}^{\mathcal{N}} x_i \sim \mathcal{N} \int x dF(x) \ , \tag{4.48}$$

provided that $\int |x| dF(x)$ is finite. When the sample covariance matrix is a high-dimensional matrix the requirement to define a suitable measure of correlations between random data vectors defines the *population* spectral measure,

$$\mu_{\mathcal{P}}^{(\Sigma)}(x) = \frac{1}{\mathcal{P}} \sum_{i=1}^{\mathcal{P}} \delta_{\sigma_i}(x) \ , \tag{4.49}$$

where δ_{σ_i} represents a point mass of weight unity at each population covariance eigenvalue, σ_i. In the limit of the null formalism defined below the population spectral measure is simply a point mass at unity, where $\mu_{\mathcal{P}}^{(\Sigma)}(x) = \delta_1$. The nature of rates of convergence are normally found using the Stieltjes transform introduced in Eq. (C.1).

Model sampling using matrices of the form in Eq. (4.47) represents a standard simplification one can bring to the description of a physical problem via the incorporation

of random variables or vector quantities which are used to represent the underlying properties of that system. This is done with the use of multivariate random variables to define a series of data vectors which categorise a series of unknown values under the pretence of a lack of sufficient information or imperfect knowledge of the overall model, in order to approximate explicit deterministic values of interest. The relationship between a model and observed data can often lead to significantly complicated mathematics in order to drive constraints whereby we must call upon the notions of ensemble statistical inference in order to develop our understanding. We restrict ourselves to sample covariance matrices of the general form, $\mathbb{M} = \mathcal{P}^{-1}\mathbb{X}\mathbb{X}^{\mathrm{T}}$ which posses the desired ensemble symmetry properties (Eq. (4.3) and Eq. (4.4)). This defines our RMT statistical baseline, which using the aspirations of sample covariance and minimal information (see Section 4.1.6.2) concerns matrix elements drawn using normal multivariate distributions and matrices residing in the Wishart-Laguerre ensemble.

4.2.2 The Wishart-Laguerre Ensemble

In the statistical landscape, the RMT analogue of the Pearson estimator defines the Wishart-Laguerre ensemble. The Wishart-Laguerre ensemble represents a *standard* method when estimating in the domain of *big data*. Traditionally physics has seen many examples concerning themselves with invariant ensembles such as the Wigner ensemble we previously commented on in Section 4.1.6.1. In the so called *Kolmogorov regime*[1] the Wishart-Laguerre ensemble also offers many powerful universal results, some shared and some vitally different from its paramount field defining counterpart, the Wigner ensemble. The finite moment convergence condition corresponds to the limitation placed on the matrix ensemble, stating the random variables, x_{ij} are jointly IID and obey the following moment limits. Firstly

[1]The Kolmogorov condition, named after Andrey Kolmogorov is a further term reserved for the previously defined high-dimensional regime, the conditions that the ratio $\mathcal{N}/\mathcal{P}$ is suitably convergent to some constant value.

the variables are centred, i.e. have zero mean with unitary variance and also up to some order exponent, obey the following general supremum condition [1246–1248],

$$\sup_{i,j} \mathbb{E}[x_{i,j}]^{\Delta} \leq C \ , \tag{4.50}$$

for a given constant C, independent of the dimension of the matrix. At this stage we need not distinguish between continuous or discrete distributions although we shall naturally assume any prior distribution for the data elements comes from a continuous function. This is indeed a very powerful statement on the sampling potential of our random variables. This independence placed on the distribution for the random data vectors requires we only need to consider the expectation of the moments follow finite constraints up to a given order, in order to define the required local and global statistics in the high-dimensional regime. Traditionally most models of statistical theory concern themselves with normal or multi-normal models. The simplest multivariate prior or selection for a statistical distribution, Ω, for the entries of the $p-$data vectors in Eq. (4.45) is the centred standard normal distribution, $\mathcal{N}(\mu, \sigma^2 = 1)$, where $\mu \in \mathbb{R}$ and $\sigma^2 > 0$ defined by the density function,

$$f(x) = \frac{1}{\sqrt{2\pi\sigma^2}} e^{\left(-\frac{(x-\mu)^2}{2\sigma^2}\right)} \ , \tag{4.51}$$

encoding the theoretical uncertainty of the model into a multivariate normal linear model. In a multidimensional sense the generated entries are understood as a sampling from a $p-$dimensional normal distribution, with unitary covariance between random vectors,

$$\Omega = \mathcal{N}(0, \Sigma \propto \mathbb{I}) \ . \tag{4.52}$$

The sum of squares of independent univariate Gaussian random variables, such as those drawn from Eq. (4.51), is chi-squared distributed. The multivariate generalisation of this is the sum of outer products of $p-$dimensional Gaussian random variables which is Wishart distributed. We will for the time being denote a random matrix which contains IID entries with $\mathbb{W}$ inside a defined class or family of

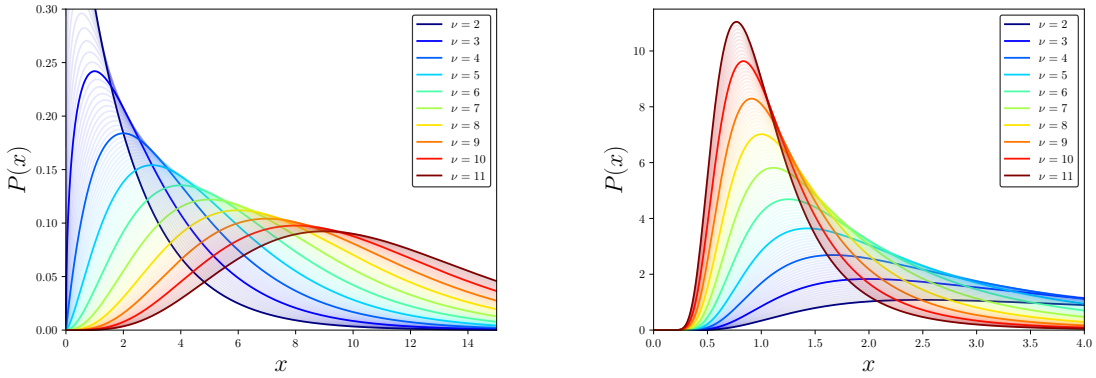


Figure 4.2: *Left panel:* Density function plots for the Wishart distribution defined in Eq. (4.54) for various values of the parameter representing the functions degrees of freedom. *Right Panel*: Density function plots for the inverse Wishart distribution defined in Eq. (4.97) also for various values of the parameter representing the functions degrees of freedom.

$\mathcal{P}-$variate sample covariance matrices,

$$\mathbb{W} \sim \mathcal{W}_{\mathcal{N}}(\Sigma, \mathcal{P}) \ . \tag{4.53}$$

Explicitly if this family of random matrices utilises real valued sampling, we define the real-Wishart ensemble for symmetric positive definite matrices. This ensemble is understood by the following naturally arising probability distribution function, vital for inference in multivariate data analysis [138, 939],

$$f(\mathbb{W}) = \frac{1}{2^{\mathcal{N}\mathcal{P}/2}\Gamma_{\mathcal{N}}\left(\frac{\mathcal{P}}{2}\right)|\Sigma|^{\mathcal{P}/2}}|\mathbb{W}|^{(\mathcal{P}-\mathcal{N}-1)/2}\exp\left[-1/2\ \mathrm{Tr}\left(\Sigma^{-1}\mathbb{W}\right)\right], \tag{4.54}$$

where $\Gamma_{\mathcal{N}}$ is the multivariate gamma function and $\mathcal{P}$ represents the degrees of freedom. In the *left panel* of Fig. 4.2 we demonstrate the Wishart distribution for various different degrees of freedom, denoted by ν. The Wishart distribution is a multivariate generalisation of the Gamma distribution when the degrees of freedom are real valued, and the chi-square (χ^2) distribution when the degrees of freedom are integer valued. We shall refer to the case when $\Sigma = \mathbb{I}$ in Eq. (4.53) as the standard Wishart distribution. Analogous to the standardisation of the normal distribution

to exhibit a centralised first moment and unitary variance, the Wishart distribution can be centralised according to the assumption of identity covariance. This will be explicitly detailed under two formalisms later.

4.2.2.1 Laguerre Orthogonal Polynomials

Continuing from Section 4.1.4.1 the explicit spectral statistics of the Wishart-Laguerre ensemble can be determined using Laguerre polynomials. These functions therefore have an extremely useful relationship to the limiting spectral distributions found in the context of multivariate statistics and sample covariance matrices. Formally the Laguerre polynomials $L_n^a(x)$, can be defined by the relationship [550, 555],

$$n!L_n^a(x) = e^x x^{-a} \frac{d^n}{dx^n} \left(e^{-x} x^{n+a} \right) \ . \tag{4.55}$$

We can rewrite the expression in Eq. (4.10) in order to define the ensembles orthogonal relationship using the relevant classical weight function class for the Laguerre polynomials [46],

$$\int_0^\infty L_n^\alpha(x) L_m^\alpha(x) x^\alpha e^{-x} dx = \frac{\Gamma(\alpha + n + 1))}{\Gamma(n+1)} \delta_{m,n} \ . \tag{4.56}$$

The Laguerre polynomials L_n^α, are orthogonal on the interval $[0, \infty)$ with respect to the Gamma density $x^\alpha e^{-x}$, (when $\alpha > -1$). The Gamma density function is found in eigenvalue density of the Wishart-Laguerre ensemble analogous to how the Gaussian density function occurring in an analysis of the GUE and GOE eigenvalue densities occurs. The joint probability density for the eigenvalues of product matrices in the form, $\mathbb{X}^\dagger \mathbb{X}$ (where the elements are assumed to be IID random variables) takes the form [231, 425],

$$P(\lambda_1, \ldots, \lambda_{\mathcal{N}}) = K_{\mathcal{N}} e^{-\tilde{\beta}\sigma} \sum_{i=1}^{\mathcal{N}} \lambda_i^{\frac{\tilde{\beta}}{2}(1+\mathcal{P}-\mathcal{N})-1} \prod_{j<k} |\lambda_j - \lambda_k|^{\tilde{\beta}} \ . \tag{4.57}$$

The parameter σ is for the variance of the matrix entry distribution. The reproducing kernel $K_{\mathcal{N}}$ in Eq. (4.57) represents our incorporation of Laguerre polynomials into the analysis of the spectral features of the matrix ensemble. Using the general methodology found in Section 4.1.4.1 we can compute probabilities for spectral features of Wishart-Laguerre matrices. The asymptotic density of the scaled zeroes which directly relate to the eigenvalues of Eq. (4.57) (normalised to ensure they do not diverge to infinity), are defined by the limiting relationship [550],

$$\lim_{\mathcal{N}\to\infty} = \frac{1}{\mathcal{N}} \sum_{i=1}^{\mathcal{N}} \left(\frac{x_{i,\mathcal{N}}}{\mathcal{N}} \right) = \frac{1}{2\pi} \int_0^4 f(x) \sqrt{\frac{4-x}{x}} dx \ , \tag{4.58}$$

for every continuous function $f(x)$, defined on the interval, $[0, 4]$. See Refs. [432, 526, 826] for various proofs for the the asymptotic distributions of the zeros of Laguerre polynomials with varying parameters. The right hand side of this expression is what we will understand as the Marčhenko-Pastur limiting density function (Eq. 4.67), as discussed in Section 4.3.1.1. This family of classical orthogonal polynomials (along with the other classic families) has one of few integral representations, a feature often exploited when discussing their properties. The Laguerre polynomials are extremely useful in understanding various macroscopic and microscopic universal features of classics sample covariance matrices residing in the Wishart-Laguerre ensemble. Exploiting the asymptotic behaviour of the corresponding orthogonal polynomials also provides us with information on the larger class of these matrices associated with the same orthogonal polynomials [556, 586].

To be a little more specific to the real ensembles ($\tilde{\beta} = 1$) we will encounter in Section 4.2.2.1 and use in Section 5.2.4.1 (which we only quote for consistency) for finite values of $\mathcal{P}$ and arbitrary values of $\mathcal{P} - \mathcal{N} \geq 1$ (see Eq. (4.54)) information in regards to the spectral density and correlation functions of the real Wishart-Laguerre ensemble are defined by a Pfaffian determinant for a kernel incorporating skew-orthogonal polynomials [1292–1294, 1357]. These are what can be expressed in terms of the previously discussed Laguerre polynomials in Eq. (4.55).

4.2.2.2 A General Sample Covariance Matrix

It should be noted that under the conditions of the dimensionality criterion we ensure is fixed throughout ($\mathcal{P} \geq \mathcal{N}$), the limiting spectra of $\mathbb{X}\mathbb{X}^{\mathrm{T}}$ and $\mathbb{X}^{\mathrm{T}}\mathbb{X}$ differ by only their singular eigenvalues, so that in the limit of non-singular sample covariance matrices this product is interchangeable and the spectrum commutes. In a Bayesian sense the function in Eq. (4.54) is defined as the conjugate prior of the inverse covariance-matrix of a multivariate-normal random-vector. Wishart matrices often represent the prior precision matrix of multivariate Gaussian data sets. This problem can be reparameterised by using a Wishart distribution as the conjugate prior of the inverse covariance-matrix for a series of multivariate normal random vectors. We can define a further, more general factorisation of the standard sample covariance matrix form in Eq. (4.47), which now takes the form [138],

$$\mathbb{W}_{\mathcal{N}} = \mathcal{P}^{-1}\Sigma_{\mathcal{P}}^{1/2}\mathbb{X}_{\mathcal{N}}\mathbb{X}_{\mathcal{N}}^{\mathrm{T}}\Sigma_{\mathcal{P}}^{1/2} \ . \tag{4.59}$$

As referenced previously we maintain the normalisation factor, $\mathcal{P}^{-1}$, as a replacement for $\mathcal{P}-1$ in Eq. (4.42), where the sample covariance is the maximum likelihood under normality but no longer unbiased. Alternatively one can define the sample set of observations using the form in Eq. (4.59), $W_j = \Sigma_{\mathcal{P}}^{1/2}X_j$ for the $\mathcal{N} \times \mathcal{P}$ set $\{X_1, \ldots, X_{\mathcal{N}}\} \equiv \{x_{ij}\}_{1 \leq i \leq \mathcal{N}, 1 \leq j \leq \mathcal{P}}$. The divisor normalisation factor in Eq. (4.59) represents a scaling term on the eigenvalues and eigenvectors, where our sample eigenvalues of course remain unaffected by such normalisation, which does not depend on the nature of rank deficiency. If the rank of the sample covariance matrix is $\mathcal{R}$, then it must hold that for a data matrix, X that $\mathcal{R} \leq \min(\mathcal{N}, \mathcal{P})$. If the number of variables is assumed to be larger than the number of samples then rank is at most equal to the sample size of the covariance matrix, i.e. $\mathcal{R} \leq \mathcal{N} < \mathcal{P}$. The remaining terms in Eq. (4.59) are present to account for the factorised components of the population covariance matrix, $\Sigma_{\mathcal{P}}$. The spectral decomposition of $\mathbb{W}$ is defined via the

unitary conjugation of the eigenvector matrix,

$$\mathbb{W} = \mathbb{U}^{\mathrm{T}}\Lambda\mathbb{U} \ , \tag{4.60}$$

where $\Lambda = \mathrm{diag}(\lambda)$ and $\mathbb{U}$ is a matrix in the group of orthogonal matrices, $O(\mathcal{N})$, defining the vector set of sample Wishart eigenvalues of $\mathbb{W}$,

$$\{\lambda_{\mathcal{N}}\} = \lambda_1^{(\mathbb{W})} \geq \ldots \geq \lambda_{\mathcal{N}}^{(\mathbb{W})} \ . \tag{4.61}$$

Equivalently the population eigenvalues of the covariance matrix, $\Sigma_{\mathcal{P}}$ are defined in the vector set,

$$\{\sigma_{\mathcal{P}}\} = \sigma_1^{(\Sigma)} \geq \ldots \geq \sigma_{\mathcal{P}}^{(\Sigma)} \ . \tag{4.62}$$

Performing an orthogonal transformation on $\mathbb{W}$ yields a transformed distribution for the Wishart matrix,

$$\mathbb{U}\mathbb{W}\mathbb{U}^{\mathrm{T}} \sim \mathcal{W}(\mathcal{P}, \mathbb{U}\Sigma\mathbb{U}^{\mathrm{T}}) \ , \tag{4.63}$$

highlighting the orthogonal invariance of the standard Wishart distribution under the null formalism ($\Sigma = \mathbb{I}$). This can be extended for any decomposed non-singular matrix, $\Sigma = \mathbb{A}\mathbb{A}^{\mathrm{T}}$,

$$\mathbb{W} \equiv \mathbb{A}\mathbb{W}_{\mathbb{I}}\mathbb{A}^{\mathrm{T}} \sim \mathcal{W}(\mathcal{P}, \Sigma) \ , \tag{4.64}$$

where $\mathbb{W}_{\mathbb{I}}$ represented matrix distributed according to the standard wishart distribution, transformed under a decomposed non-singular matrix rotation. This point is something which will prove extremely important later when we account for limits of perturbed cases using free probability theory (see Section 4.4). Assuming the covariates of the matrix are defined and non-singular any Wishart matrix is susceptible to a spectral decomposition, defining the similarity relation, $\mathbb{A} = \mathbb{V}\Lambda^{1/2}$ via the product of the associated eigenvector matrix, and matrix square root of the positive eigenvalues.

4.2.2.2.1 A General Hypothesis and Isometry

For the uncorrelated *null* case which occurs when $\Sigma_{\mathbb{W}} = \mathbb{I}$, the empirical spectral distribution of $\mathbb{W}$ almost surely converges in the weak* topology, towards a non-negative and continuous probability measure on the half-real interval, $[0, \infty)$. In the classical regime where $\mathcal{P}$ remains fixed, as the sample size $\mathcal{N} \to \infty$, the sample covariance matrix remains a consistent estimator [225, 1374]. In the high-dimensional regime however this convention breaks down and we must refer to hypothesis tests as a standard measure of covariance. We will now begin the process of standardising our analysis in terms of the forms of the components in Eq. (4.59), indicating how these relate to general multivariate normal models. We have two areas we must hypothesise in order build a multivariate random matrix. The first are the assumptions made on the distribution moments for the entries of the $\mathcal{P}-$random data matrices. The second is the initial level of control we enforce over the covariates of the random data vectors.

Abstractly speaking we will adopt the nomenclature of statistical hypothesis testing, in order to build and suitably contrast the frameworks of our random matrix models. We must state we have adopted this convention in accordance with statistical practises only and not to infer any physical meaning of covariance in terms of any underlying theory we are attempting to represent. The second consideration regarding a prior on the covariates or hierarchies between model variables can be classified as taking either the *null* or *alternative* cases. When taking the null hypothesis, which corresponds to the notions of isotropy, which we denote with $\mathcal{H}_0$, the population covariance matrix is defined as, $\Sigma \propto \mathbb{I}$ residing in a subset of classes of alternative hypotheses, $\mathcal{H}_A$ where, $\mathcal{H}_0 \in \mathcal{H}_A$. Any matrix constructed under this hypothesis is distributed according to the standard Wishart distribution, sometimes referred to as a *white* or *uncorrelated* Wishart matrix. In the context of large sample covariance matrices the *null* hypothesis represents the statement that there are no correlations between the $\mathcal{P}$-variables we are making uncertain statements for. The

analytical tractability of the measure density in the limit of large random matrices under the null hypothesises can be directly linked to the perturbative structure and nature of element correlation (specifically a lack of) for the sample parameter space. Considering the law of large numbers and the Cramér-Wold theorem with deviations from the *null* case represent the presence of true information in the system and the introduction of noise. Let us formally define each of the standard hypotheses associated to the covariance formalism for a given sample matrix which constructs two common testing grounds, namely the proportionality or equality of the population covariance matrix to a known matrix form:

> **The Null Formalism**: For a given empirical problem incorporating large sample covariance matrices, let us define the invertible covariance matrix Σ_0 under the hypothesis, $\mathcal{H}_0 : \Sigma = \Sigma_0$, where $\Sigma_0 \propto \mathbb{I}$. This hypothesis represents the nature of sphericity and that the observations are cross-sectionally uncorrelated and have homoscedastic variance.
>
> **The Alternative Formalism**: For a given empirical problem incorporating large sample covariance matrices let us define the invertible covariance matrix Σ_0 under the hypothesis, $\mathcal{H}_A : \Sigma = \Sigma_0$, where $\Sigma_0 \propto\!\!\!\!/\ \mathbb{I}$. This hypothesis corresponds to additive or multiplicative perturbations to the covariance matrix of either singular, finite or full rank.

Our simplest starting point will make the initial assumption of zero correlation between the random vectors. A model which rejects the *null* formalism would suggest the introduction of correlated entries and ultimately any eigenvalue which jumps from the expected measure support in the limit $\mathcal{N} \to \infty$ holds a strong correlation to the eigenvalues of the bulk in the local regime.

4.3 Spectral Statistics and Universality

4.3.1 The Isotropic Null Formalism

The cornerstone matrix model of RMT introduced in the previous section will act as the general baseline and reference point for any of our random matrix models, a bench mark for a statistical analysis in the multivariate landscape. The null hypothesis for the sample covariance matrix in Eq. (4.59) fixes the covariance matrix to its isotropic limit, $\Sigma \propto \mathbb{I}$, where we can define the general matrix form,

$$\mathbb{Y} = \mathcal{P}^{-1}\mathbb{X}\mathbb{I}\mathbb{X}^{\mathrm{T}} \ . \tag{4.65}$$

We will refer to a data matrix of this form as a Y-matrix. The limiting spectral distribution and bulk statistics for these matrices represent one of the defining results of RMT and a principle feature of multivariate models developed over the course of the 20^{th} century. Under the assumption that the covariance matrix takes the form of a scale matrix, then it has been shown the limiting spectrum of singular values converges almost surely when the dimensionality constant in Eq. (4.46) approaches a constant in the large $\mathcal{N}$ limit. This universal behaviour also holds in the statistics of the local extrema, which serve as a testing ground for a rejection of the null hypothesis. An emerging signal subspace via higher variances of the standard noise variables constitutes statistical fluctuations outside the limiting spectra present under the assumption of null covariance. This is understood via the union intersection principle [217, 1022, 1125].

4.3.1.1 Bulk Universality and The Marčhenko-Pastur Law

In many models the eigenvalues of matrices represent critical elements of the theory. The large $\mathcal{N}$ limit has given very useful qualitative and quantitative results which can guide both the the classification of model structure or provide a source of complexity

alleviation in scenarios where the theoretical uncertainty is high. One of the most celebrated limiting features of RMT concerns the spectral analysis and empirical limits of sample covariance matrices under the *null* formalism, with matrix entries assumed to be IID random variables with mean zero and finite variance. In the limit that $\mathcal{N}$ grows sufficiently large at a comparable rate to $\mathcal{P}$ inside the fixed bounds,

$$\frac{\mathcal{N}}{\mathcal{P}} \to \beta \in (0, \infty) \ , \tag{4.66}$$

then with unity probability the ESD of Eq. (4.65) converges in the weak* topology with respect to Lebesgue measure such that $\mu^{\mathbb{Y}} = f_{\text{MP}}$. The function f_{MP} is the LSD function represented by the Marčhenko-Pastur distribution law [901],

$$f_{\text{MP}}(\lambda) = (1 - \beta)\, \delta_0 + \frac{1}{2\pi\beta\lambda\sigma^2_{\text{MP}}} \sqrt{(\lambda_+ - \lambda)\,(\lambda - \lambda_-)} 1_{\gamma_- \leq \lambda \leq \gamma_+} \ , \tag{4.67}$$

where 1 is an indicator function on the interval $[\gamma_-; \gamma_+]$. When $\beta \geq 1$ the spectrum of $\mathbb{Y}$ has $\mathcal{N} - \mathcal{P}$ zero eigenvalues. This is shown in the density function of Eq. (4.67) where we find a point mass at 0, along with a density function, each weighted by $1 - 1/\beta$ and $1/\beta$ respectively. When $\beta \geq 1$ and $\mathcal{N} = \beta\mathcal{P}$ then we have a fractional split of $1 - 1/\beta$ zero and $1/\beta$ non-zero eigenvalues in the spectrum. The parameter σ^2 represents the model scaling term associated to the distribution variance, used to shift the spectrum from its standard normalised window. When we restrict ourselves to consider the following interval,

$$\frac{\mathcal{N}}{\mathcal{P}} \xrightarrow{\mathcal{N} \to \infty} \beta \in (0, 1] \ , \tag{4.68}$$

the point mass at zero drops out and we are left with just the spectral bulk determined by the Marčhenko-Pastur density, representing the limits to formulate a strictly positive definite spectrum from a non-singular matrix. The rate of convergence for the ESD function towards Eq. (4.67) is equivalent to the semi-circle limiting distribution of the Wigner ensemble, which when sampled using canonical

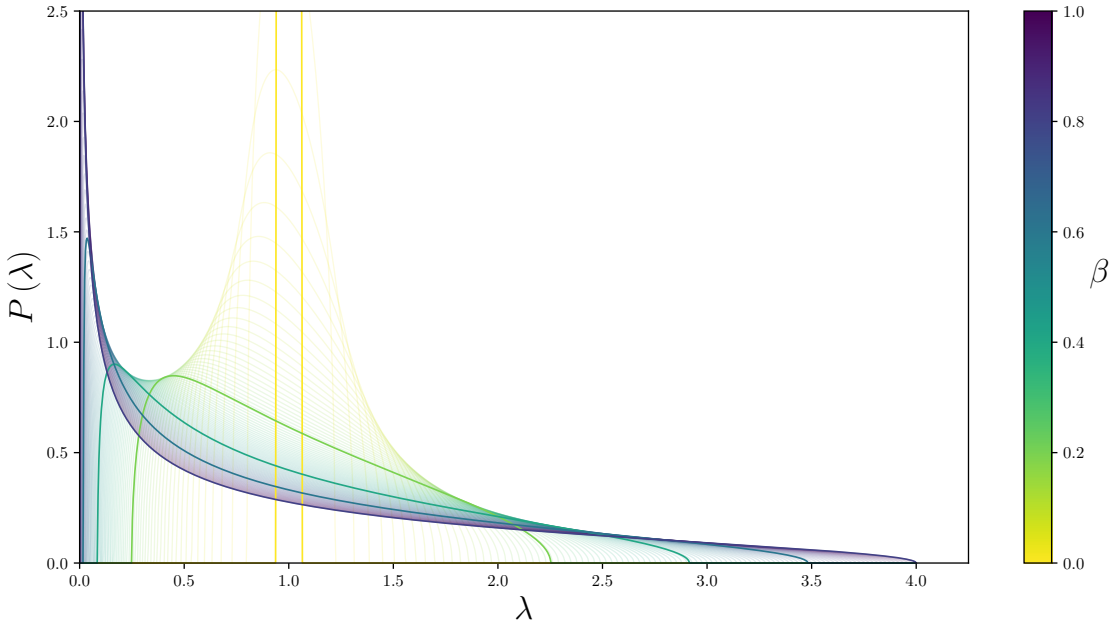


Figure 4.3: Marčhenko-Pastur density functions representing the limiting spectral distributions of the isometric Y-matrix as defined by the function in Eq. (4.67). The functions are defined with the distribution shaping parameter, β, inside the interval $\beta \in (0, 1]$, which gives Lebesgue absolutely continuous measures over the bounds $\lambda \in (0, 4]$, apart from in the limit $\beta = 1$ where a point mass appears at $\lambda = 0$.

Gaussian ensembles is $\mathcal{N}^{-2/5}$ [141]. The values of λ_+ and λ_- denote the supremum and infimum eigenvalues of the standard uncorrelated sample covariance matrix set, fixing the spectral radii. These limits were defined in the large $\mathcal{N}$ limit for the largest scaled eigenvalue [1375], which converges almost surely to the boundaries of the support defined to be,

$$\lambda_+ = \sigma^2_{\text{MP}} \left(1 + \sqrt{\beta}\right)^2 \ , \tag{4.69}$$

and when $\beta \leq 1$ the smallest scaled eigenvalue [141] also converges to,

$$\lambda_- = \sigma^2_{\text{MP}} \left(1 - \sqrt{\beta}\right)^2 \ , \tag{4.70}$$

such that each eigenvalue falls in the support bounds,

$$\lambda_- \leq \lambda_i \leq \lambda_+ \ , \tag{4.71}$$

for all $i = 1, 2, \ldots, \mathcal{N}$. In the special limit $\beta = 1$ the upper edge eigenvalue saturates to, $\lambda_+ = 4$ defining,

$$\frac{df_{\mathrm{MP}(\lambda)}}{d\lambda} = \frac{1}{2\pi\lambda}\sqrt{(4-\lambda)\,\lambda}1_{0\leq\lambda\leq 4} \ , \tag{4.72}$$

which is a representation of the semicircle distribution under the general mapping $\lambda \to \lambda^2$. When ${}^{\mathcal{P}}/_{\mathcal{N}} \to 0$, the ESD of the covariance matrix, $W_{\mathcal{N}} = \sqrt{{}^{\mathcal{N}}/_{\mathcal{P}}}\,(S_{\mathcal{N}} - \sigma^2\mathbb{I}_{\mathcal{P}})$ converges almost surely to the limiting Wigner semicircle law with scale index variable, σ^2. The normalised semicircular distribution is a translated large $\mathcal{N}$ limit defined on the real domain, $\mathbb{R}_+$. The n^{th} moment of the Marčhenko-Pastur density is defined as,

$$\int x^n f_\beta(\lambda)d\lambda = \sum_{i=0}^{n} \frac{\begin{pmatrix} n-1 \\ i \end{pmatrix}\begin{pmatrix} n \\ i \end{pmatrix}}{(i+1)} \ . \tag{4.73}$$

The associated first raw and second centralised moments are,

$$\text{Mean}: \quad \sigma^2_{\mathrm{MP}} = \int \lambda \ d\mu_{\mathrm{MP}}(\lambda) \ , \tag{4.74}$$

$$\text{Variance}: \quad \frac{\sigma^4_{\mathrm{MP}}}{\gamma} = \int \lambda^2 \ d\mu_{\mathrm{MP}}(\lambda) - \left(\int \lambda \ d\mu_{\mathrm{MP}}(\lambda)\right)^2 \ . \tag{4.75}$$

We can also define the eigenvalue density of an isotropic inverse Wishart matrix or inverse Y-matrix via the Marčhenko-Pastur law in Eq. (4.67), formed using Eq. (4.97),

$$f(\nu) = \frac{\zeta}{\nu^2\pi}\sqrt{(\nu_+ - \nu)}(\nu - \nu_-) \ , \tag{4.76}$$

using the change of variables $\nu = ((1-\beta)\,\lambda)^{-1}$. The upper and lower bounds are now defined as,

$$\nu_\pm = \left(\zeta + 1 \pm \sqrt{2\zeta + 1}\right) = \frac{(1-\beta)}{\lambda_\pm} \ , \tag{4.77}$$

with the dimensionality relation taking on the translated form,

$$\beta = \frac{1}{2\zeta + 1} \in (0, 1] \ , \tag{4.78}$$

which shows the ability to interchange the use of both Wishart and inverse Wishart matrices in many different types of invariant modelling.

4.3.1.2 Edge Statistics and Extremal Universality of the Spectral Infimum and Supremum

The predictive nature of the eigenvalue statistics for large random matrices is a vital tool often used in high dimensional data analysis. As we have previously reviewed these universal features come with the benefits of independence of the underlying distributions for the random variable vector quantities used to construct the high dimensional data set. It is of course of great interest therefore, to seek under what conditions it is to be expected that eigenvalues could be found outside of such convergent limits for the bulk statistics and the categorisation of whether these are an artefact of finite dimensionality or present in the large $\mathcal{N}$ limit of the theory. This local universality can be classified at each of the two spectral edges. More formally singular values which reside outside the bounds of a LSD probability measure are usually concerned with two types of statistics. Firstly the presence of perturbations to the population covariance matrix from the null formalism and secondly the statistical properties of *finite* $\mathcal{N}$ realisations for the sample set. let us focus on the second of these two points.

- **Soft-edge universality:** The soft edge of the limiting spectral distribution is defined as the supremum limit of the spectral radii. As the eigenvalue density is non-zero for finite perturbations from this value in the finite limit, this is referred to as the soft edge.

- **Hard-edge universality:** The hard edge of the limiting spectral distribution is defined as the infimum eigenvalue boundary, fixed by the model. For the Laguerre ensembles the neighbourhood of the origin for the positive definite Hermitian matrices fixes the hard edge to the value zero.

For an example see Appendix D for the famous Tracy-Widom limiting laws. These

are powerful universal laws, which demonstrate convergence in the local statistics of the eigenspace under the assumption of identity population covariance. When Σ is not a multiple of the identity, the local statistics become factorised into regimes which were first considered in Ref. [754]. Stemming from motivations of principle component analysis (PCA), the behaviour of large sample covariance matrices were studied under conditions representing the presence of trends in the correlations of the population covariance matrix. These models have later become defined as *spiked population models*, representing the case of matrices which have undergone a finite rank perturbation from the null case in the high dimensionality limit, a specific case of perturbative matrix dynamics.

4.3.2 The Alternative Formalism

4.3.2.1 The Population Covariance Matrix

The form of the covariance matrix in both Eq. (4.47) and Eq. (4.65) represents the isometric limit of the general normalised variance-covariance matrix introduced in Eq. (4.59), which under a similarity transformation and commutativity we can re-express as,

$$\mathbb{Y}_{ij} = \frac{1}{\mathcal{P}} \mathbb{X}_{ik} \Sigma_{kl} \mathbb{X}_{lj}^{\mathrm{T}} \ , \tag{4.79}$$

where Σ_{kl} is the $\mathcal{P} \times \mathcal{P}$ population covariance matrix, its spectral measure defined in Eq. (4.49). The null hypothesis formalism of Section 4.3.1 represents the simplest composition of *Wishart-like* matrices we can use to sample the parameters of our model. Deviations from this formalism can sometimes require sophisticated approaches such as forming spectral expressions determined by zonal polynomials [701, 747–749], whose explicit forms are often not known in a more general setting. If we wish to de-bias the sample eigenvalues, it is normally required to estimate the so-called population spectral distribution, a probability measure that characterises the population eigenvalues of the covariance matrix. This is certainly a well motivated

general stance to take. Often the assumptions of *zero-information* and *pure-noise* residing in the bulk represents an impractical approach for model construction of complex systems. This indicates the current need and general trend in the literature to model a population covariance estimator, its significance to indicate the possible magnitude and rank of correlations, not an explicit definition, given this ambiguity.

4.3.2.2 Finite Rank Correlations

A logical starting point in understanding the nature of how our model could diverge from the results of classical universal ensembles, is the study of the introduction of idiosyncratic noise in the form of finite rank perturbations, where we will briefly review the theoretical concepts behind the seminal work of Jinho Baik, Gérard Ben Arous and Sandrine Péché. This work highlighted the presence of a *phase transition phenomena*, suitably referenced as the Baik-Ben Arous-Péché (BBP) phase transition. If the true population covariance matrix, Σ in Eq. (4.79), consists of a singular perturbed value and $\mathcal{P}-1$ eigenvalues at unity then these matrices represent ensemble distributions inherent with *signal* and *noise*, defined as *rank one spiked* Wishart models [142, 232, 233, 954, 1321]. These models were initially studied in Ref. [753], formally introduced by Johnstone in Ref. [754] and extensively expanded on in Ref [1038]. They represent the initial presence of strong correlations in the prior understanding of the test model. In a general sense these models are Hermitian matrices with a spiked external source, where the real Wishart-Laguerre ensemble is a special example of the potential $V(x) = {}^{x}/_{2} - \frac{\mathcal{N}-\mathcal{P}-1}{2\mathcal{P}}\log(x)$ defined in Eq. (4.21). Focusing on the case of a single stray eigenvalue away from the limiting bulk of the distribution, means we must consider the limiting laws of the largest and smallest extremal eigenvalues for random sample covariance matrices in the spectrum. It follows from the Bai-Yin theorem [140, 141] that for a given matrix comprised of isotropic random vectors with IID components, Z_{ij} with zero mean,

unit variance and finite fourth moment,

$$\mathbb{E}(Z_{11}) = 0, \quad \mathbb{E}(|Z_{11}|^2) = 1, \text{ and } \mathbb{E}(|Z_{11}|^4) < \infty \ , \tag{4.80}$$

the distribution of the largest eigenvalue converges almost surely in the large $\mathcal{N}$ limit to,

$$\lambda_{\max} = \begin{cases} \left(1+\sqrt{\beta}\right)^2 , & \vartheta_{\max} \leq 1+\sqrt{\beta} \ , \\ \sigma_1 + \frac{c\sigma_1}{\sigma_1 - 1}, & \vartheta_{\max} \geq 1+\sqrt{\beta} \ . \end{cases} \tag{4.81}$$

The limiting spectral distribution remains valid even if the first centralised moment of the statistical distribution used for the entries is non-zero. However in the case where the Bai-Yin theorem breaks down we now find a susceptibility for finite rank perturbations in the local regime at the soft spectral edge of the bulk. Intuitively this can be seen as perturbing a model additively by a rank one matrix of growing norm, forming additive noise around the rank one matrix. This behaviour can be induced by using a uniform prior, which importantly is a non-centred function, on the elements of our sample covariance matrix, $Y_{ij} \in \mathcal{U}[a,b]$ where $a+b \neq 0$. In the case of singular rank deformation this is equivalent to defining the population covariance for the data set of independent vectors as,

$$\Sigma_{\mathcal{P}} = \mathrm{diag}(\overbrace{1+\theta}^{\lambda_{\max}}, \underbrace{1, \ldots, 1}_{\lambda_{\text{bulk}}}) \ . \tag{4.82}$$

For all sample eigenvalues with associated unitary population covariance, the spectral properties are confined to the bulk formed from both the hard and soft edges of the limited probability measure. See Ref. [553] for discussions of the presence of spikes in the context of the joint probability density function of the ensembles eigenvalues. This phenomena was initially considered for the quarternionic Wishart case in Ref. [1320] and described in detail for the real case in Ref. [953, 954].

4.3.2.2.1 The Baik-Ben Arous-Péché Phase Transition

The limiting spectral features of these models has been thoroughly investigated since their inception into the literature. The value of θ in Eq. (4.82) defines the bounds of three distinct regimes based on eigenvalue criticality:

- *The subcritical regime* - When the eigenvalue perturbation falls inside the limits, $-1 < \theta < \gamma^{-1}$ the perturbation is not sufficiently strong enough to form a spike in the LSD, where the largest eigenvalue sits inside the bulk. As shown in Ref. [530] the LSD remains the same as the null isotropic case for matrices in the LOE.

- *The critical regime* - Inside the regime where $1 - \beta\vartheta = \mathcal{O}\left(\mathcal{P}^{-1/3}\right)$, the perturbation is just sufficient to form a spike on the limiting edge of the bulk. Studies of the statistical fluctuations of these spikes in the case of real analysis can be found in both Ref. [954] and Ref. [232].

- *The supercritical regime* - If $\vartheta > 1$ then the perturbation is strong enough to form a spike in the LSD where the largest eigenvalue is placed beyond the soft edge of the spectrum bulk. The asymptotic properties of the formed spike were considered in Ref. [1023] and generalised in Ref. ([1322]). In the regime the largest sample covariance eigenvalue, $\lambda_{\max}$ converges to $\lambda_{\max} \to \vartheta\left(1 + {}^{\beta}/_{\vartheta - 1}\right)$.

To summarise, for any eigenvalues sufficiently close to unity, then the associated sample eigenvalues behave approximately in same way as if the true covariance were the identity. Beyond this threshold the original work also demonstrated the scaling was also shown to deviate. Eigenvalues remaining in the bulk scale as $\mathcal{N}^{2/3}$ and those repulsed outside scale as $\mathcal{N}^{1/2}$. In the non-large $\mathcal{N}$ limit estimates can be made for the criticality bounds for as expressed by the inequality,

$$\left(1 - c^{-}\sqrt{{}^{\mathcal{N}}/_{\mathcal{P}}}\right)^{2} \leq \lambda_{\min}(\mathbb{W}) \leq \lambda\left(\mathbb{W}\right) \leq \lambda_{\max}(\mathbb{W}) \leq \left(1 + c^{+}\sqrt{{}^{\mathcal{N}}/_{\mathcal{P}}}\right) \ , \tag{4.83}$$

where $c^{\pm} > 0$ are model constants. The properties of the largest finite eigenvalues

for real wishart matrices are understood in terms of these constants. See Ref. [356] for discussions of eigenvalue correlation kernels defined from criticality regimes for finite perturbations.

In general the observed data is represented as a series of vectors, $Y_i = X_i + \epsilon_i$ where $X_i \in \mathbb{R}^p$, representing the information plus noise understanding of these models. In much of the literature the data contained in X_i is defined as representing an unobserved signal where a linear perturbation of the transformation vector ϵ_i, represents model noise. A signifiant amount of work has been conducted regarding the high-dimensional asymptotics of these models. In the regime of identity covariance incorporating Gaussianity, the limits were detailed in Ref. [754]. For real spiked Wishart matrices let us denote the population eigenvalues as, $\vartheta_i \equiv 1 + \theta_i$ for the sample eigenvalue spikes or signal components. These have been shown to fluctuate asymptotically as a Gaussian, which is repulsed $\mathcal{O}(\mathcal{N})$ from the bulk. Consider $\vartheta_{\max} > 1 + \sqrt{\beta}$ with unitary multiplicity, then in the large $\mathcal{N}$ limit [77, 1023],

$$\sqrt{\mathcal{N}}\left(\lambda_{\max} - \eta_{\max}\right) \to \mathcal{N}(0, \sigma^2(\vartheta_{\max})) \ , \tag{4.84}$$

where,

$$\eta(\vartheta) = \vartheta\left(1 + \frac{\beta}{(\vartheta - 1)}\right) \ , \tag{4.85}$$

and,

$$\sigma^2(\vartheta) = \frac{2\vartheta\eta(\vartheta)}{1 + \vartheta\beta\int x(\eta(\vartheta) - x)^{-2} dF_\beta(x)} = \frac{2\vartheta\eta(\vartheta)}{1 + \frac{\vartheta\beta}{(\vartheta-1)^2-\beta}} = 2\vartheta^2\left(1 - \frac{\beta}{(\vartheta-1)^2}\right) \ , \tag{4.86}$$

representing Gaussian fluctuations of the supremum. Counting the number of spikes has important consequences in general statistics, i.e. the number of factors in factor models [997, 998] or the number of signals in signal processing [967]. When the rank of the perturbation is low the spectrum remains recognisable due to Weyl's interlacement property of eigenvalues. If however we associate this spiked phase transition process to every eigenvalue, possibly through fixed assumptions placed on

model correlations, then the symmetry classifications break down fully where the system has undergone a full rank perturbation.

4.3.2.3 Full Rank Correlations

4.3.2.3.1 The Covariance *F*-Matrix

If we take the matrix considered in the previous section, $\Sigma_{\mathcal{P}}$, and decrease the triviality of its rank then we can readdress the problem of eigenvalue transitions as a more general matrix perturbation issue. Consider the general perturbation matrix $\mathbb{P}$, which we assume is full rank. Also consider a statistically independent random matrix, $\mathbb{X}$. The most general case of matrix products, $\mathbb{PX}$ will typically reproduce a non-Hermitian matrix, with complex eigenvalues. Under the similarity relation, we can express the matrix product of self-adjoint matrices in the form,

$$\mathbb{PX} = \sqrt{\mathbb{P}}\mathbb{X}\sqrt{\mathbb{P}} = \sqrt{\mathbb{X}}\mathbb{P}\sqrt{\mathbb{X}} \, , \tag{4.87}$$

as they posses the same moments where the square-root operation represents the Hermitian matrix square-root. It is possible to define a Hermitian matrix required to ensure a positive spectrum eigenvalues using the above relation, supported only on the positive real axis where we now have, $\sqrt{\mathbb{P}} = U^{\mathrm{T}}\mathrm{diag}(\sqrt{\lambda_1}, \ldots, \sqrt{\lambda_{\mathrm{N}}})U$. The characteristic polynomial is preserved under invariant transformations whereby the characteristic roots or eigenvalues are identical preserving an identical spectrum. The matrix $\mathbb{X}$ can be identified as our initial data matrix and $\mathbb{P}$ its externally defined perturbative counterpart. If both $\mathbb{X}$ and $\mathbb{P}$ are positive definite then $\mathbb{Y}_{\mathrm{N}}$ is congruent to $\mathbb{X}$ and must also be positive definite, have positive eigenvalues and can be well defined in its eigendecomposition basis by Sylvester's law of inertia. If these two matrices also commute, the limiting spectra is simply defined as the convolution of their measures but this assumption may not always be valid. If the matrix product components are invariant then the resultant matrix is also invariant.

There are numerous methods dispatched in order the formulate the LSD of structures such as those found in Eq. (4.87) incorporating the general case with possible non-commutativity in the large $\mathcal{N}$ limit. Perhaps the most powerful of these is the field of *free probability theory* introduced by Voiculescu [1205, 1307–1309, 1312], which is comprehensively covered in the monograph of Ref [393]. We will address this topic in Section 4.4 and the power these methods have to incorporate non-commutative operations.

4.3.2.3.2 Correlated Data Observations

Suppose now that the matrix $\mathbb{X}$ is a correlated or non-isotropic Wishart matrix and $\mathbb{P} \equiv \Sigma_{\mathcal{P}}$, a deterministic positive definite Hermitian matrix, we recover the sample covariance matrix in Eq. (4.79) often motivated for linear models in multivariate statistics,

$$\mathbb{Y} = \mathcal{P}^{-1}\mathbb{P}^{1/2}\mathbb{X}\mathbb{X}^{\mathrm{T}}\mathbb{P}^{1/2} \ , \tag{4.88}$$

$$\equiv \mathcal{P}^{-1}\mathbb{X}\Sigma\mathbb{X}^{\mathrm{T}} \ . \tag{4.89}$$

In the limit $\mathbb{P} = \mathrm{diag}(t_i)$, $\mathbb{Y}$ reduces to a generalisation of the standard sample covariance matrix or *gram* matrix [652], $\mathbb{Y} = \mathbb{Z}\mathbb{Z}$, where the elements of $\mathbb{Z} = \mathbb{P}\mathbb{X}$ must be independent by definition, modelling the empirical covariance of a sample of $\mathcal{N}$ independent observations. The BBP phase transition phenomena in Section (4.3.2.2) concerned itself with finite rank perturbations of the form,

$$\mathbb{Y} = \sqrt{B}\mathbb{W}\sqrt{B} \ , \tag{4.90}$$

where $\mathbb{W}$ was represented by a matrix in the LUE ensemble and $\mathbb{B}$ is a diagonal matrix with a finite number of elements or spikes which deviate from unity. Beyond the regime of the rank one spiked models initially introduced into the literature, it was shown the same phase transition also occurs in unitarily invariant models with

higher rank perturbations, defining the *unitary multiplicative perturbation ensemble*,

$$\mathbb{F} = \sqrt{\mathbb{P}}U^{*}\mathbb{Y}U\sqrt{\mathbb{P}} \ . \tag{4.91}$$

Here $\mathbb{Y}$ is defined according to the isotropic principle of Eq. (4.65) with the required unitary invariance over Haar-distributed random matrix conjugations ensured by our use of a Wishart sample covariance matrix. If $\mathbb{Y}$ is defined according to Eq. (4.90), then this defines the *finitely deformed unitary multiplicative perturbation ensemble*,

$$\mathbb{F}_{\epsilon} = \sqrt{\mathbb{P}}U^{*}(\mathbb{Y} + \epsilon\mathbb{I})U\sqrt{\mathbb{P}} \equiv \mathbb{F} + \epsilon\mathbb{P} \ , \tag{4.92}$$

where the LSD is formed with both a spectral bulk and a series of spikes determined by the multiplicative convolution of the eigenspaces, as addressed in Section 4.4. It is also possible to define the perturbation $\mathbb{P}$ to possess spikes itself.

4.3.2.3.3 Perturbed High-Dimensional Correlated Data Observations

It is clear there are general additive and multiplicative forms a perturbed matrix can take just considering the form of $\mathbb{F}$ and $\mathbb{F}_{\epsilon}$ above. In order to encode this total behaviour we can first consider the most general form a high-dimensional sample covariance matrix could take, found by expanding and decomposing the form in Eq. (4.79) to [515, 1025, 1390],

$$S_{\mathcal{N}} = \frac{1}{\mathcal{P}}\mathbb{Z}Z^{\mathrm{T}} = \frac{1}{\mathcal{P}}\mathbb{P}^{1/2}\mathbb{X}\Sigma_{\mathcal{P}}\mathbb{X}^{\mathrm{T}}\mathbb{P}^{1/2} \ . \tag{4.93}$$

This represents the most general form for the empirical covariance matrix, constructed with the perturbed correlated data observations, $\mathbb{Z} = \mathbb{P}^{1/2}\mathbb{X}\Sigma^{1/2}$, the inherent form of the data which incorporates both cross-correlations and auto-covariance between variables and an external perturbative deformation source. If $\mathbb{P}$ is a strictly non-negative definite perturbation then the matrices in Eq. (4.93) generalise matrices of the form in Eq. (4.88), where there are statistical correlations between the

row and column vectors of the initial data matrix. If $\mathbb{P}$ and Σ are symmetric non-negative definite Hermitian matrices, i.e. $\mathbb{P}$ possesses a unique positive-definite root, then the eigenvalues of Eq. (4.93) are then same as,

$$S_{\mathcal{N}} = \frac{1}{\mathcal{P}} \mathbb{P}_{\mathcal{N}} \mathbb{X} \Sigma_{\mathcal{P}} \mathbb{X}^{\mathrm{T}} \ , \tag{4.94}$$

which is understood via the similarity transformation relationship,

$$\mathbb{P}\Sigma = \mathbb{P}^{1/2} \Sigma \mathbb{P}^{1/2} = \mathbb{P}^{-1/2} \left(\mathbb{P}\Sigma \right) \mathbb{P}^{1/2} \ , \tag{4.95}$$

presuming the commutativity between $\mathbb{P}^{1/2}$ and $\mathbb{X}$ holds. Specifically these relationships help us relate the equivalent nature of general unitarily invariant models and perturbed correlated models. Said alternatively there is an equivalence relationship between considering the final form of the sample covariance matrix as either a problem regarding correlation priors or a matrix perturbation problem after initial declaration. There is a caveat to the decompositional form of Eq. (4.93). A general detailed approach and precise understanding of the properties of such distributions is a challenging task and not fully explored in the literature. The full impact on the posterior inference for such models has been explored in the contexts of structured ensembles of composite systems via various probabilistic techniques such as planar diagrams, free probability and comparisons of hypergeometric function via functional transformation techniques [148, 197, 296, 554, 965, 1047, 1400].

4.3.2.3.4 The Inverse Wishart Distribution

The standard approach to modelling covariance estimation for sample covariance matrices is to use an inverse Wishart distribution prior, the proper conjugate prior for an unknown multivariate normal covariance matrix [596], due to its analytical convenience and tractability. This is defined as,

$$\mathbb{W}_{\mathrm{IW}} \sim \mathcal{W}^{-1}(\Psi, \nu) \ , \tag{4.96}$$

for a general matrix $\mathbb{X}$ whose inverse, $\mathbb{X}^{-1}$ is Wishart distributed. The degree of freedom parameter, ν is regarded as the prior sample size. The probability density function of the inverse Wishart prior is shown in the *right panel* of Fig. 4.2 and is defined by the function [161, 939, 1279],

$$f\left(\mathbb{W}_{\text{IW}}\right) = \mathcal{C}|\Sigma|^{\frac{-(\nu+p+1)}{2}} e^{\left[-\text{Tr}\left(\Sigma\Psi^{-1}\right)/2\right]} \ . \tag{4.97}$$

Often chosen to simplify posterior results, this function's conjugacy properties mean its combination with the likelihood function results in a posterior function in the same family of distributions. The inverse Wishart prior is the multivariate generalisation of the inverse Gamma distribution, however analogous to its univariate counterpart it has been show to be problematic for a number of reasons. The use of an inverse Wishart prior is fully parameterised by the scale hyperparameter matrix and a single degree of freedom hyperparameter, that only allow for a singular specification in the overall degree of confidence in all the elements of the hyperparameter scale matrix. As the inverse of any inverse Wishart distributed matrix has a strictly non-negative definite posterior mode, the diagonal elements must all possess the same number of degrees of freedom and as such all the components of $\mathbb{X}$ depend on each other. This dependance can lead to the inverse Wishart prior to be considered as a potentially highly informative procedure, where large correlation coefficients correspond to large marginal variances. It is therefore not desirable to include unitarity in control for all of the precision elements for the covariance matrix, with possible dependencies between the correlations and the variances [1261].

4.3.2.3.5 The *F*-matrix Distribution

We now adopt the formalities of the multivariate analysis of variance (MANOVA) to define the form of the classical sample matrix under the least informative approach incorporating covariance priors. The matrix ensemble of the *Fisher* matrix or simply F-matrix is distributed according to a multivariate F-distribution, also referred to as

Snedecors' F distribution or the *Fisher-Snedecor distribution*s [664, 963, 1024, 1326]. The probability density function for the scaled matrix-F function is [963],

$$f(\Sigma;\nu,\delta,\Lambda) = \frac{\Gamma_k\left(\frac{\nu+\delta+k-1}{2}\right)}{\Gamma_k\left(\frac{\nu}{2}\right)\Gamma_k\left(\frac{\delta+k-1}{2}\right)|\Lambda|^{\frac{\nu}{2}}}|\Sigma|^{\frac{\nu-k-1}{2}}|\mathbb{I}_k+\Sigma\Lambda^{-1}|^{-\frac{\nu+\delta+k-1}{2}} \ , \tag{4.98}$$

which satisfies the required reciprocity condition, where Λ is defined as a positive definite scale matrix, with associated degrees of freedom, $\nu > k-1$ and $\delta > 0$. When the scale matrix reduces to the identity we recover the standard form of the distribution proposed in Ref. [409], whilst for $k = 1$ the standard representation of the univariate case. Perhaps more edifying for model classification is the ability to represent the matrix-variate F distribution as a *Wishart-mixture* of functions (and suitably inverse Wishart mixture) [963],

$$f(\Sigma;\nu,\delta,\Lambda) = \int \mathcal{W}\left(\Sigma;\nu,\Psi^{-1}\right) \times \mathcal{W}\left(\Psi;\delta+k-1,\Lambda\right) d\Psi \ , \tag{4.99}$$

for a $\mathcal{P}\times\mathcal{P}$ positive definite random matrix. Often used in many statistical inference models [856, 920, 1165]. The F-matrix also represents the product of a sample covariance matrix of independent data ($\mathbb{E}X_{ij} = 0, \mathbb{E}Y_{ij} = 0$ and $\mathbb{E}|X_{ij}|^2 = 1, \mathbb{E}|Y_{ij}|^2 = 1$) with the inverse of an independent covariance matrix possessing independent data for its covariance. It is a common intrinsic prior used to test covariance estimation for multivariate normal data and is broadly defined as non-informative, i.e. the parameters of Eq. (4.98) can be tuned to extract a minimally informative prior ($\nu = k, \delta = 1$) in Eq. (4.99). In a Bayesian sense this represents the generalised way to sample eigenvalues incorporating the default prior for covariance. Although a sample covariance matrix distributed according to the F-distribution is often a non-naturally arising form for a covariance matrix, is does possess a key trait. The LSD of a matrix distributed according to Eq. (4.98) is the same as a sample covariance matrix of the form [139],

$$\mathbb{F} = \mathbb{Y}_1\mathbb{Y}_2^{-1} = \left(M^{-1}\mathbb{X}\mathbb{X}^{\mathrm{T}}\right)\left(N^{-1}\mathbb{L}\mathbb{L}^{\mathrm{T}}\right)^{-1} \ . \tag{4.100}$$

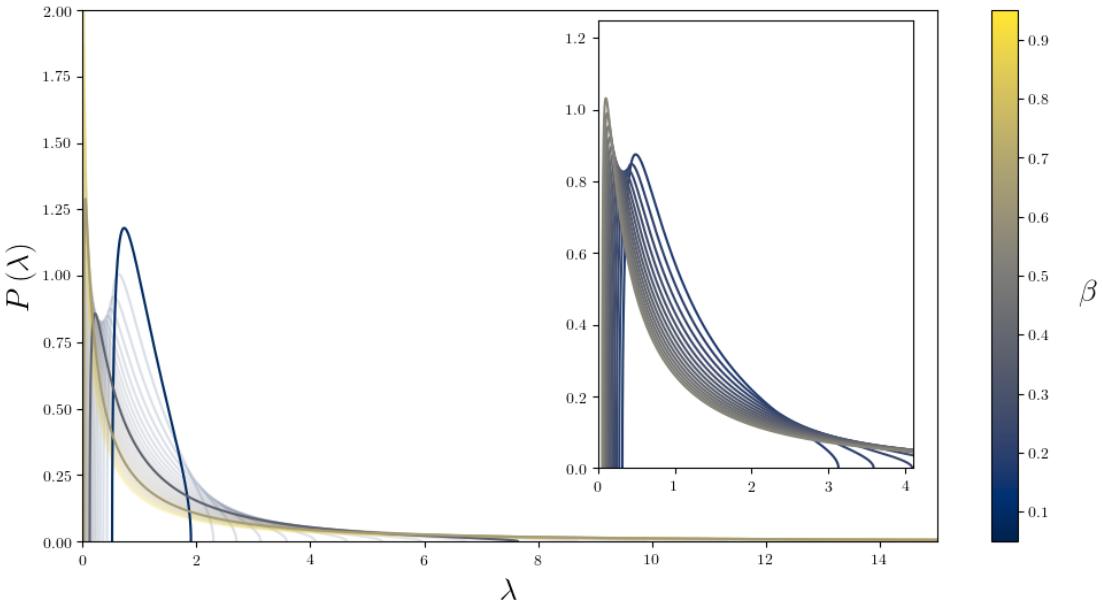


Figure 4.4: Matrix-F density functions defined in Eq. (4.98), representing the limiting spectral distributions of the F-matrix defined in Eq. (4.100), formed using an inverse Wishart prior for the population covariance. The functions are defined with the distribution shaping parameter for each matrix equated such that, $\beta = \beta'$, and are defined inside the interval $\beta \in (0, 1]$ returning Lebesgue absolutely continuous measures. *Inset:* Range of values of β which result in measures defined inside the bounds found for the case of an isometric Wishart matrix. In general the addition of covariance increases the bounds of the resulting spectrum.

It was originally shown that the empirical distribution function of the eigenvalues of Eq. (4.100) converges in probability in the large $\mathcal{N}$ limit to a non random probability measure density function. The limiting form of the non-random density function for values of $\beta, \beta' \in (0, 1]$ was found to be [1188],

$$f_{\beta}(\lambda) = (1 - \beta') \sqrt{(\lambda - \lambda_{-})(\lambda_{+} - \lambda)} \, , \tag{4.101}$$

which possesses a support on a closed interval on $\mathbb{R}^{+}$ between the spectral radii fixed by the infimum and supremum supports,

$$\lambda_{+} = \left(\frac{1 + \sqrt{1 - (1 - \beta)(1 - \beta')}}{1 - \beta'} \right)^{2} \, , \tag{4.102}$$

$$\lambda_{-} = \left(\frac{1 - \sqrt{1 - (1-\beta)(1-\beta')}}{1-\beta'} \right)^2 , \tag{4.103}$$

the density of which falling to zero outside this support. The CLTs of the linearised spectral statistics were determined in Refs.[139, 1391]. See Ref. [665] for a general approach using these models. In the context of MANOVA the eigenvalues of matrices of the form in Eq. (4.100) are in a one-to-one correspondence with *matrix variate beta* or *double Wishart* ensembles [139, 1024]. The largest eigenvalues have determined results for data with zero mean [664],

$$\lim_{\mathcal{P}\to\infty} P\left(\frac{N/M}{\sigma} \leq s \right) = F_1(s) , \tag{4.104}$$

which remains the functional form found in the *left panel* of Fig. (D.1) when, $\beta \leq 1$, an example indication of extremal local spectra universality of correlated or perturbed models.

4.4 Free Convolutions of Spectral Measure Densities

4.4.1 Asymptotic Freeness and Non-Commutative Probability

As we have touched on traditional random matrix methods often take advantage of the so called Coulomb gas methodologies in order to evaluate general spectral linear statistics. This analogy is present for invariant ensembles, the rotational invariance leading to the eigenvalues and eigenvectors of large-dimensional random matrices to present a unique statistical independence. Traditionally the probability measure placed on the matrix ensemble represents a canonical distribution of a system of identical particles. Under this procedure the normalisation constant such as those

found in Eq. (4.21), takes the form of a positional partition function. This picture is very useful and intuitive in order to build a picture of invariant ensembles and pair repulsion. When however, a noise source is introduced to the invariant ensemble these methods break down for an analysis of the resultant spectrum. There are three principle classes of model we can define based on matrix perturbation theory. That of the baseline unperturbed case for isometric uncorrelated matrices, those of finite rank perturbation and finally matrices subject to a full rank perturbation. A neat and extremely powerful way to classify these models is in terms of a series of convolution operations associated to the properties of free random variables and free subordination functions. These operations relate to defined probability measures on the positive real line $\mathbb{R}^+$, which allow us to compute and infer a series of basic characteristics for the empirical spectral densities of large and potentially complicated random matrices.

4.4.1.1 Free Probability Theory

Free probability theory is a non-commutative generalisation of the spaces we will be operating in, the physical realisation and application of its mathematics embedded strongly within RMT. Originally introduced to consider special classes of Von Neumann algebras, the study of free probability relates to a series of non-commutative operators which principally rely on the notion of *freeness*. The concepts of free independence were first discussed by Voiculescu in Ref. [1308], where its powerful associations and applicability to RMT were later introduced in Ref. [1310]. The discovered link between rotationally invariant ensembles which asymptotically satisfy the freeness criterion provides, a very enlightening analysis of both global and local behaviour of eigenvalues and eigenmeasure spaces of polynomials in asymptotically free random matrices. The simplified main principle is the consideration of two eigenspaces, corresponding to deterministic matrices in randomly chosen relative basis, where the notion of a random matrix structure is replaced with a series of operations which are in free relation. Two random independent self-adjoint matrices

are asymptotically free if the spectral density of each matrix converges almost surely in the large $\mathcal{N}$ limit, where importantly one of the matrices must also be invariant under a rotational change of basis, their eigenbasis related by an random rotation. Consider the normalised ensemble trace operation for all polynomial sequences,

$$\zeta(\mathbb{M}) = \frac{1}{\mathcal{N}}\mathrm{Tr}\mathbb{M} \ , \tag{4.105}$$

which defines a measure of the the sequence of moments and therefore effectively the LSD for the ensemble. Traditional approximations for convolution operations are given using either combinatorial theory [1204] for the moments up to a defined order or free subordination methods, on the basis of practicality in analytically manipulation and numerical implementation [191, 219, 1311, 1313]. In order to simplify our analysis we restrict ourself to introducing the basics of asymptotic freeness, with a specific focus on the operations placed on measure functions we can suitably assign as limiting probability measures we can understand in a Bayesian sense as prior functions. For the case of two independent self-adjoint matrices, $\mathbb{M}_1$ and $\mathbb{M}_2$ freeness is realised for the values of, $\epsilon_1 \dots \epsilon_z$ and $\varepsilon_1 \dots \varepsilon_z$, where $z \in \mathbb{N}^+$, when,

$$\zeta(\mathbb{M}_1^{\epsilon_1}\mathbb{M}_2^{\varepsilon_1}\mathbb{M}_1^{\epsilon_2}\mathbb{M}_2^{\varepsilon_2}\dots\mathbb{M}_1^{\epsilon_z}\mathbb{M}_2^{\varepsilon_z}) = \zeta(\mathbb{M}_1^{\epsilon_1})\zeta(\mathbb{M}_2^{\varepsilon_1})\zeta(\mathbb{M}_1^{\epsilon_2})\zeta(\mathbb{M}_2^{\varepsilon_2})\dots\zeta(\mathbb{M}_1^{\epsilon_z})\zeta(\mathbb{M}_2^{\varepsilon_z}) \ , \tag{4.106}$$

given $\zeta(\mathbb{M}_1) = \zeta(\mathbb{M}_2) = 0$. This property is often considered as the statistical analogue of the moment factorisation property, often vital in estimating statistical properties of measure approximations. It is usually common practise to consider perturbed models where the noisy component of the model is defined by a suitable invariant ensemble, the addition of a signal a fixed choice of prior or deterministic matrix.

4.4.1.2 Probability Spaces and Borel Measures

Recall from Appendix B (which we again quote as points beyond the scope of this thesis for context) that a general probability measure space can be understood under the triplet representation, (Ω, σ, P). The parameter σ represents the sigma-algebra for the subsets of Ω and P is a probability measure on (Ω, σ). Our random matrix, $\mathbb{M}$, represents the measurable map when moving from (Ω, σ), to the complete set of all $\mathcal{N} \times \mathcal{N}$ matrices [444]. Consider $\mathcal{B}$ to be the class of all Borel probability measures on the real line, $\mathbb{R}$. The relevant subclass of measures we will focus on defines the subclass, $\mathcal{B}^+$ which comprises of all probability measures suitably bounded on the positive real interval, $\mathbb{R}^+$ fully analytic in the bounds, $[0, \infty)$. Let us reintroduce and also define two Borel measures, μ and ν which correspond to the LSD of both the initially defined space and its perturbing source term. Both models of finite and full rank perturbations can be considered as limits of information plus noise type matrices, the principles of these models covered in Section 4.3.2.2 for the rank one perturbed case. It is well known that free convolution of two admissible measures, will in general produce an invertible measure which we will now explore. For the case of two generic measures the asymptotics are not so clear. If our two measures μ and ν are defined as general there free multiplicative convolution often can only be understood in terms of details revolving around their S-transforms. Strictly speaking its explicit formulation is defined using inverse mapping of the Cauchy-Stieltjes transform. It is certainly possible to draw conclusions in more generic frameworks, see techniques discussed in Ref. [1311] for example. These often require a much more detailed analysis with incorporation of subordination functions, curtailing the brevity we require for a more simplistic randomised analysis of the positive define space for the field parameters.

4.4.2 Classically Deformed Models

4.4.2.1 Rotation Invariance and Traceability

We are generally not too concerned at this point about the specifics revolving around the forms of the limiting distributions and their explicit spectral representations formed under convolution operations. We will mainly focus on the convergent stability of the spectrum itself, where we require an understanding of the general resulting nature of a spectral measure description, the localisation of eigenvalues and the fluctuations of extremal limits. Any probability measures we consider are well defined with compacted support on the positive real line. The results of free probability theory give us a good understanding on the limiting spectrum in the large $\mathcal{N}$ limit for specific classical cases of deformed models using traditional isometric positive definite sample covariance matrices. Let us formally introduce the three classical cases of deformed ensemble for isotropic models, as detailed extensively in Refs. [313, 1255], invariant under a sequence of unitary operations, formed with their distribution normalised under the Haar measure on the unitary group $U(N)$:

- *Additive perturbation model* - Consider the case of two deterministic matrices, $\mathbb{X}$ and $\mathbb{P}$, each with compactly supported limiting eigenvalue distributions denoted, μ and ν respectively. The additively perturbed model is defined as [1255],

$$\mathbb{M} = \mathbb{X} + \mathbb{U}^* \mathbb{P} \mathbb{U} \ , \tag{4.107}$$

  where $\mathbb{U}$ is a Haar-distributed unitary random matrix. This model relates to the transformation operation for free random variables, $R_{\mathbb{M}} = R_\mu + R_\nu$ and key transformations, $R_\mu(y) = G_\mu^{-1}(y) - 1/y$, where $G_\mu(z)$ represents the Cauchy transform of Eq. (C.1) of the measure μ on the real line. Although not a focus in this thesis, these models have been used in the context of scalar physics in models of random supergravity (see Section 5.2.8).

- *Multiplicative perturbation model* - Consider the case of two normalised matrices, $\mathbb{X}$ and $\mathbb{P}$, defined to be non-negative definite, each with compactly supported limiting eigenvalue distributions denoted, μ and ν respectively. The multiplicatively perturbed model is defined as [1255],

$$\mathbb{M} = \mathbb{P}^{1/2}\mathbb{U}^{*}\mathbb{X}\mathbb{U}\mathbb{P}^{1/2} \equiv \mathbb{P}\mathbb{U}^{*}\mathbb{X}\mathbb{U}, \tag{4.108}$$

  where $\mathbb{U}$ is a Haar-distributed unitary random matrix. Any examples we consider are related to both perturbations of non-negative unitary matrices. This model relates to the transformation operation for free random variables, $S_{\mathbb{M}}(z) = S_{\mu}(z)S_{\nu}(z)$ and key transformations, $T_{\mu}(z) = \int \frac{xd\mu(x)}{z-x}$, $S_{\mu}(y) = {}^{1+y}/_{y} \cdot {}^{1}/_{T_{\mu}^{-1}(y)}$.

- *Information plus noise model* - Relevant for discussions in Section 4.3.2.2. Consider the case of two independent rectangular matrices of dimension $\mathcal{N}\times\mathcal{P}$, $\mathbb{X}$ and $\mathbb{P}$. The information plus-noise type matrix takes the form [477],

$$\mathbb{M} = \mathcal{P}^{-1}\left(\mathbb{X} + \sigma\mathbb{P}\right)\left(\mathbb{X} + \sigma\mathbb{P}\right)^{*} \ . \tag{4.109}$$

  These matrices represent a series of data vectors $x + \sigma p$, where x carries the information of the system and p represents a perturbative vector of additive noise, its strength regulated by σ.

It is known that $\mathbb{U}^{*}\mathbb{X}\mathbb{U}$ and $\mathbb{P}$ are asymptotically free when both $\mathbb{X}$ and $\mathbb{P}$ are Hermitian matrices, $\mathbb{U}$ is a Haar matrix independent of both and each possess compactly supported eigenvalue distributions.

4.4.2.2 Free Convolution Operations

We can then make general statements on the LSD of $\mathbb{M}$, the resultant matrix in each of the perturbed models above by considering the the probability measures for the original matrix and the perturbative matrix as a series of relevant operations

between their asymptotically limiting measures. For an extensive review of these topics and the liming features of perturbed matrix spectra and operations we again refer to Refs. [313, 1255]. The primary operations on the eigenspaces are defined as,

- $\boxplus$ - *Additive free convolution*: For two compactly supported Borel measures, μ and ν on $\mathbb{R}$, the additive free convolution is denoted as $\mu \boxplus \nu$, where $\phi_{\mu \boxplus \nu}(z) = \phi_{\mu}(z) + \phi_{\nu}(z)$. The induced measure is defined as the sum of two free random variables.

- $\boxtimes$ - *Multiplicative free convolution*: For two compactly supported Borel measures, μ and ν on $\mathbb{R}^{+}$, the multiplicative free convolution is denoted as $\mu \boxtimes \nu$. The matrix perturbation product associated to these two measures is self-adjoint where its resultant free probability measure depends only on the individual Borel measure spaces. The free multiplicative convolution operation on $\mathcal{B}^{+}$ is both associative and commutative.

These operations serve as natural analogues of classical convolutions found in free probability theory representing the distributions of either traceable additive or multiplicative perturbations [202, 1308, 1309].

4.4.2.3 Limiting Measure Representations of Matrix Ensembles

Using the operations above there have been many free probabilistic interpretations of the LSD for each class of perturbed matrix model mentioned. It has been shown the concepts on universality remain valid in this sector where the behaviour of free self-adjoint random variables allow us to trace the generic behaviour of compactly supported measure spaces, associated to well known distribution functions. Consider the three example perturbed matrix models above consisting of large self-adjoint random matrices, $\mathbb{X}$ and $\mathbb{P}$. When the matrices are in generic position we can first recall the limiting form from the almost sure convergence for the eigenvalue distribution attributed to additive and multiplicative perturbations. Convergence of measure for the general BBP phase transition phenomena has been demonstrated for deformed

Wigner type matrices [198], sample covariance matrices [198] and information plus noise type matrices [199]. In the context of free probability we maintain the weak* measure convergence defined in Eq. (4.20), which for the specific deformed model cases gives the following universal results,

- Isotropic Wigner type matrices:

$$\mu_{\mathbb{M}} = \mu_{\mathrm{SC}} \boxtimes \nu \ . \tag{4.110}$$

- Isotropic Wishart covariance matrices:

$$\mu_{\mathbb{M}} = \mu_{\mathrm{MP}} \boxtimes \nu \ . \tag{4.111}$$

- Information plus noise type matrices:

$$\mu_{\mathbb{M}} = \left(\sqrt{\mu_{\mathrm{MP}}} \boxplus_{\beta} \nu\right)^2 \ . \tag{4.112}$$

The operator, $\boxplus_{\beta}$ represents the ability to generalise the primary operations above to include the rectangularity parameter, β. Free rectangular convolution in general is a much more complicated picture in terms of formulating explicit results, often operating in regimes with measures supported on multiple intervals. The non commutative probability framework of rectangular free additive convolution, $\boxplus_{\beta}$, was the focus of study in Refs. [189, 194, 196]. It is also possible to consider free rectangular infinite divisibility for rectangular free convolution with the ratio parameter, β.

4.4.2.4 The Lebesgue Decomposition Theorem

In order to collect and summarise the results detailed above it is perhaps best to consider the ability to decompose the structure of $\mu_{\mathbb{M}}$ in each model. For any Borel

probability measure μ, defined on the real interval, $[0, \infty)$, we can define its *Lebesgue decomposition* as [190, 750],

$$\mu = \mu^{\text{pm}} + \mu^{\text{sc}} + \mu^{\text{ac}} \ , \tag{4.113}$$

where the linearised terms, μ^{pm}, μ^{sc} and μ^{ac} represent the point mass, singular continuous, and absolutely continuous components of the measure function respectively. It has been shown when the operand measure is that of Marchenko-Pastur the defined absolutely continuous probability measure in this case is always an analytic function on the real positive interval [476]. For the case where we have the presence of spikes such as the rank one perturbative case covered in Section 4.3.2.2 the addition of correlated signal presents a single outlier, the location of which is represented by the perturbed point mass measure, μ^{pm}. The eigenvector of this singular point possesses a square projection in the direction of the spike given by the mass of the atom. We can of course also present the case of finite perturbative terms which fall inside the sub-critical regimes which interlace themselves into the absolutely continuous measure function. We have reviewed here just the basics of a series of powerful statements regarding the continuity and bounded nature of the density of states using convolution operations.

Chapter 5

The Random Matrix Axiverse

> "*In desperation I asked Fermi whether he was not impressed by the agreement between our calculated numbers and his measured numbers. He replied, "How many arbitrary parameters did you use for your calculations?" I thought for a moment about our cut-off procedures and said, "***Four***." He said, "I remember my friend Johnny von Neumann used to say, with four parameters I can fit an elephant, and with* **five** *I can make him wiggle his trunk." With that, the conversation was over."*
>
> A meeting with Enrico Fermi [491]
>
> Freeman John Dyson

5.1 Effective Models of the String Axiverse

Each of the models presented in this chapter can be categorised according to how we assert a simplistic treatment of the high dimensional effective axion parameter space, ensuring they are formed on the grounds that they are suitable to be embedded in some hierarchical framework, such as those introduced in Appendix B.2. Each model represents a simple effective statistical model of a low energy effective phenomenology determined by a general two-derivative theory description for the ultra-light bosons. These are motivated by those which appear in many flux compactification

models such as those detailed in Refs. [129, 427, 429, 475, 659, 660, 873, 874, 909]. We will consider three classes of model. Each of these consider minimal information placed on our understanding of the underlying physics or geometrical space. That is we make many assumptions in terms of the microphysical parameters begging with the ad hoc solution of an axiverse scenario and a positive spectrum of fields present is the four-dimensional limit of the theory. The motivations and representation of each model are in concordance with previous simplified models of the axiverse and their respective dimension or (hyper)parameterisation:

> **Class I** - Section 5.1.2 - *Epistemic priors on the independent parameter space based solely on the general theoretic conjecture of the string axiverse.*
>
> **Class II** - Section 5.2 - *The statistical RMT axiverse with measure spaces defined using free probability convolution operations associated to the arguments of the expanded effective potential in the multi-field action.*
>
> **Class III** - Section 5.3 - *Random matrix treatment of the explicit model of the string axiverse in M-theory on manifolds of G_2 holonomy, using the expanded effective superpotential. The physical model parameters are treated as stochastic variables with some theoretical uncertainty motivated by phenomenological concerns.*

In order to cope with the high dimensionality of any multivariate distributions coming from the form of the simplified multi-field action, we can make best use of the symmetries in conventional matrix ensemble classes, to generate statistical prior distributions, stemming from empirical sample covariance matrices in order to visualise key aspects of these distributions. Adopting a focus on so-called non-informative priors we form a series of *reference models* to be used as standardised points of comparison, when performing more comprehensive approaches. These models are in a physical sense formulated using parsimonious modelling, utilising fundamental matrix models in multivariate statistics, coarse-graining a part of the landscape to search for universal features with minimal information. Again we stress the use of

such models are very simplistic in the context of the rich landscape of more explicit models. The primary features of each model we consider will be some distinct, singular mean phenomenological scale, where statistical draws are made about. Aside from possible extended point masses, each distribution is by construction unimodal, where we can generalise the discussions in the following sections in the future for multimodal functions with a hierarchy of scales. We will address this possibility in Section 5.2.6.

Our first class of model represents a statistical straw man, where we only need to consider how we normalise the prior bounds placed on the simple cosmological axion parameter space. The second and third model classes introduce the high-dimensional nature of the problem using the most general case of the effective field action defined in Eq. (5.6), along with the universal convergence and unique modes of the parameter spectra which arise in these limits. Each Class II model is concerned with compound matrix distributions and Bayesian predictions using Borel measures on $\mathbb{R}^+$ for general multivariate linear models as a proxy for the unknown dimensionful parameters. Broadly speaking in the context of the physical considerations for the the fields, the matrix arguments of Eq. (5.12) are replaced with the following factorised sample covariance matrices,

$$\mathcal{K}_{ij} = \frac{1}{\mathcal{P}} \mathbb{X} \overbrace{\Sigma_{\mathcal{P}}}^{\substack{\text{Field alignment} \\ \text{coefficients}}} \underbrace{\mathbb{X}^{\mathrm{T}}}_{\substack{\text{Decay constant} \\ \text{data vectors}}} , \tag{5.1}$$

$$\tilde{\mathcal{M}}_{ij} = \frac{1}{\mathcal{P}} \underbrace{\mathbb{P}_{\mathcal{N}}^{1/2}}_{\substack{\text{Canonical} \\ \text{normalisation} \\ \text{perturbation}}} \mathbb{X} \overbrace{\Sigma_{\mathcal{P}}}^{\substack{\text{Mass state} \\ \text{correlation indices}}} \underbrace{\mathbb{X}^{\mathrm{T}}}_{\substack{\text{Mass state} \\ \text{data vectors}}} \mathbb{P}_{\mathcal{N}}^{1/2} . \tag{5.2}$$

Each of these data sets represent a measure space, where by ensuring rotational invariance for the ensemble representing the initial decay constant and mass state data vectors, fixes a traceable nature to the induced probability measures for both $\mathcal{K}_{ij}$ and $\mathcal{M}_{ij}$ in any basis. The matrices must be normalised to a defining scale. For

the axion mass eigenstates, we can choose for this to follow on of three standard general ultralight sector scale hierarchies, taking motivations from phenomenological concerns in string inspired models. These are fixed according to the infimum and supremum of the eigenvalue set,

$$m_a^{\rm min} \lesssim m_a^{\rm max} \lesssim H_0 < M_{\rm mod} < M_{\rm KK} < M_{\rm s} < M_{\rm Pl} \ , \tag{5.3}$$

$$H_0 \lesssim m_a^{\rm min} \lesssim m_a^{\rm max} < M_{\rm mod} < M_{\rm KK} < M_{\rm s} < M_{\rm Pl} \ , \tag{5.4}$$

$$m_a^{\rm min} \lesssim H_0 \lesssim m_a^{\rm max} < M_{\rm mod} < M_{\rm KK} < M_{\rm s} < M_{\rm Pl} \ . \tag{5.5}$$

Each of the expressions above is motivated by the general assumption that all the moduli are stabilised in such a way to avoid the cosmological moduli problem (see discussions in Section 5.3). We also assume a sufficiently separated hierarchy for the ultralight tower of mass states which are either bounded by the lightest modulus and the Hubble scale today (Eq. (1.86)) or the lightest modulus mass and unbounded from below. This represents the general understanding that ULAs could behave as either DE, DM or both, from a single spectrum of fields.

There are of course many considerations to be made in a complete multi-field analysis of ALPs and their possible phenomenology, especially those which seek to model directly the nature of the possible vacua in the landscape. In this thesis we will only limit our attention to the parameter space of a set of very simple example models consisting of fields retaining discrete shift symmetries. As stated above and in the discussions at the start of Chapter 4, in this chapter we only consider a very limited case of sampling from distributions utilising specific elements of RMT, taking into account features and motivations such as the phenomenological scales of interest and the dimension of the '*black box*' data vectors which we use to define the parameters of the axion fields. It must therefore be stressed that the use of data vectors take our analysis far from the physically realistic models which often inspire this type study and is certainly not a general approach to the use of RMT in the field of axion cosmology. We are in principle allowing for many assumptions placed on the

underlying physics in our approach, primarily to retain statistical traceability and simplicity in our approach. The following sections are therefore concerned with a simple statistical analysis of the multi-field space applied in the context of simple models of BH superradiance (Chapter 6) or axion DM and DE (Chapter 7). The models in this chapter are inspired by the treatment and approaches made with multiple scalars highlighted at the start of Chapter 4 [1]. This analysis does not therefore provide insight directly into how random matrix modelling of the axiverse may in fact be related to the actual microscopic physical parameters in string models and the nature of the string landscape directly. This work is a fascinating ongoing sector of research which has already seen some interesting initial results (for example see Section 5.2.8 and references therein).

5.1.1 The Effective Four-Dimensional Multi-Field Action

5.1.1.1 Well-Aligned Multi-Field Potentials

Continuing the topics covered in Section 2.5, we can consider an extension of the effective equations to incorporate the case of multiple fields. Truncating any sub-leading source terms, the most general multi-field effective action for the axion fields below any fundamental, KK, PQ symmetry breaking, moduli stabilisation or non-perturbative physics scales, along with a suppression of derivative coupling terms to any Standard Model matter fields is,

$$\mathcal{L} = -M_{\rm Pl}^2 \mathcal{K}_{ij} \partial_\mu \theta_i \partial^\mu \theta_j - \sum_{n=1}^{\mathcal{N}_{inst}} \Lambda_n^4 U_n \left(\mathcal{Q}_{i,n} \theta_i + \delta_n \right) \ , \tag{5.6}$$

where θ_i are the dimensionless axion fields, $\mathcal{K}_{ij}$ is a kinetic field space metric with mass dimension two, U_n is the n^{th} general periodic instanton potential coupled to the anomaly coefficients lattice charge matrix $\mathcal{Q}$, with δ_n representing the CP phases. Conforming to the standard phenomenological approach used to study the effective

[1] For accessibility the relevant similar approaches can be found in Refs. [126, 128–134, 173, 176, 268, 347, 353, 499, 501, 533, 693, 799, 1079, 1080].

axion, the leading non-perturbative periodic potential, U, takes the form of the general dilute gas instanton potential which we recall here for convenience,

$$U_n = [1 - \cos(\theta)] \ , \tag{5.7}$$

first introduced in Ref. [1035] considering leading order Yukawa couplings for the complex scalar charged with global $U(1)_{\rm PQ}$ symmetry. In order to avoid the generalities of analytical complexity which arise due to the form of the potential when both $\mathcal{N}_{\rm ax}, \mathcal{N}_{\rm inst} \gg 1$, we assume the simplest *fundamental domain* for the dimensionless fields in Eq. (5.7), parameterised by a single potential argument. The periodicities of the dimensionless fields form a hypercube fundamental domain with sides of length, 2π in $\mathbb{R}^{\mathcal{N}_{\rm ax}}$. By considering the most simplified periodic domain for the dimensionless fields, fixes the $\mathcal{N}_{\rm ax}$ axionic continuous shift symmetries of a general multi-field effective potential to be broken down to discrete symmetries, by only $\mathcal{N}_{\rm inst} = \mathcal{N}_{\rm ax}$ leading order non-perturbative effects. The intersection of the $2\mathcal{N}_{\rm inst}$ hyperplane to constrain the domain is trivial, fixing the fundamental dimensionless field domain to be,

$$-\pi \leq \theta^i \leq \pi \ . \tag{5.8}$$

See Ref. [131] for an extensive review of potentials beyond this simplified approach utilising general multi-axion theories with considerations made for the more general case of $\mathcal{N}_{\rm inst} \geq \mathcal{N}_{\rm ax}$. In order to realise Eq. (5.8), we assume generalities allow us to consider the case where the exact axion shift symmetries effectively cancel the presence of the CP phases. We must also enforce the null hypothesis on the rational anomaly coefficients, i.e. assume an initial trivial form inside the potential argument, $\mathcal{Q} = \mathbb{I}$, or that the decomposition of the lattice charge matrix must adhere to the relationship, $\mathcal{Q}\mathcal{K}\mathcal{Q} = \mathbb{I}$, an approximation made in numerous multi-field axion models [128, 131, 499]. Under this consideration the potential can now be expressed in the following simplified form in Planck units,

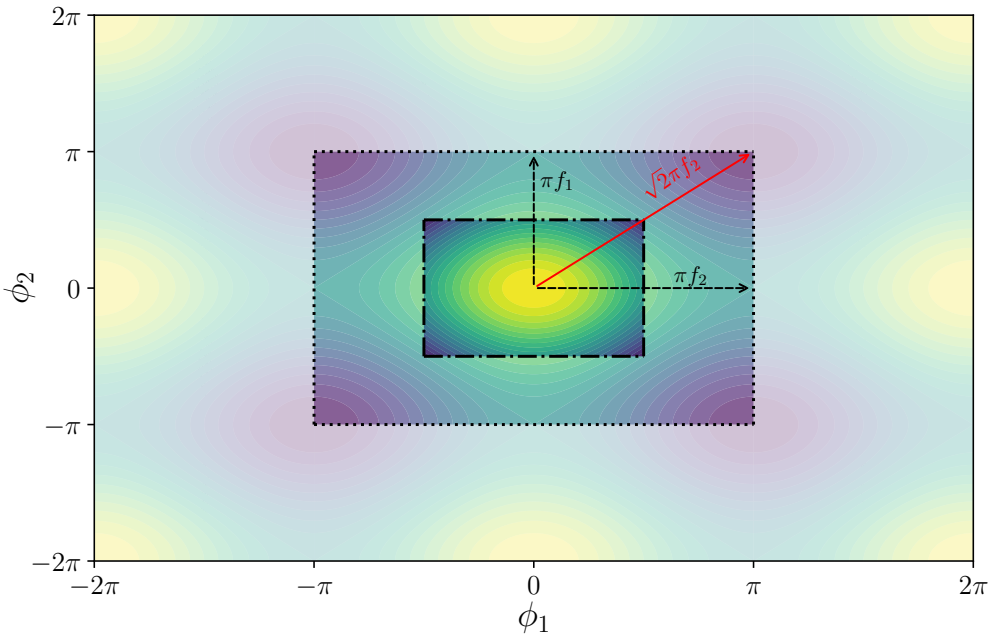


Figure 5.1: Fundamental domain for canonical fields in the two-axion N-flation model where each field possesses a well-aligned potential. Both fields are defined in the periodic boundary $\phi \in [-\pi, \pi]$, which is represented by the dotted *black* line limit. The *black* vectors represent the individual maximum displacements which can sum to the maximal Pythagorean *red* vector in the two dimensional potential. The inner region enclosed by the *black* dot-dashed boundary represents the quadratic domain where the potential can be well approximated by a second order expansion as detailed in Ref. [131].

$$\mathcal{L} = -\mathcal{K}_{ij}\partial_\mu\theta_i\partial^\mu\theta_j - \sum_{n=1}^{\mathcal{N}_{\rm ax}} \Lambda_n^4 \left(1 - \cos\left(\theta_n\right)\right) \ , \tag{5.9}$$

assuming the unitary nature of the non-perturbative source terms for each axion field, along with an absence of further higher order corrections. We will refer to this basis as the *geometric lattice basis* for well-aligned potentials. See the excellent discussions in Refs. [129–134, 874] for extensive details on axion field alignment in a more general setting. Although far from a veracious account of the space defining the possible axion fields potential, considering the case of well-aligned theories represents a good trade off with the systematics of the effective description when allowing for the possibility of including many fields, as opposed to providing a qualitative description of the likely very complex form of the true potential for multiple axions.

The alignment properties of Eq. (5.9) define the potential for the fields in canonical coordinates as the simple linearised sum,

$$V = \sum_{i}^{\mathcal{N}_{\rm ax}} V_i \left(\phi_i\right) . \tag{5.10}$$

When $\mathcal{N}_{\rm inst} \geq \mathcal{N}_{\rm ax} \geq 1$ we can assume all the axions in the spectrum possess non-zero masses, generated from non-perturbative contributions to the potential, where our alignment assumptions fix $\mathcal{N}_{\rm inst} = \mathcal{N}_{\rm ax} \geq 1$. Assuming the potential is suitably minimised, whereby each field is fixed close to its local minima, we can expand about the potential minimum, where the quadratic term approximation of Eq. (5.9) is valid (see Fig. 5.1 and Fig. 5.2). The potential is now understood as a linear summation of mass eigenstates to leading order,

$$V_{\phi_i} \simeq \sum_{i=1}^{\mathcal{N}_{\rm ax}} \frac{1}{2} m_i^2 \phi_i^2 \ , \tag{5.11}$$

where $m_i^2 > 0$ and each axion is the i^{th} mass eigenstate of the mass hierarchy set, $m_1^2 \leq m_2^2 \leq \cdots \leq m_{\mathcal{N}_{\rm ax}}^2$, encoded as the eigenvalues of the axion mass matrix counter-term, $\mathcal{M}_{ij}$. Considering the minimal number of terms from a truncation of the expanded potential where we begin in the geometrical basis where the kinetic terms are sampled under the assumption of initial field independence, defines the simplest general multi-field equation ansatz we could assume,

$$\mathcal{L} = -\mathcal{K}_{ij} \partial_\mu \theta_i \partial^\mu \theta_j - \mathcal{M}_{ij} \theta_i \theta_j \, . \tag{5.12}$$

This expression is formed solely from the simplified bare quantities of the general non-canonically normalised Lagrangian. In order then to define the axion cosmology we must understand how a hierarchy of mass eigenstates are defined in accordance to effective statistical theories by considering the priors placed on the kinetic and potential terms in Eq. (5.12), in the geometric lattice basis. Our approach is then only concerned with the axion potential aligned in such a way the problem can

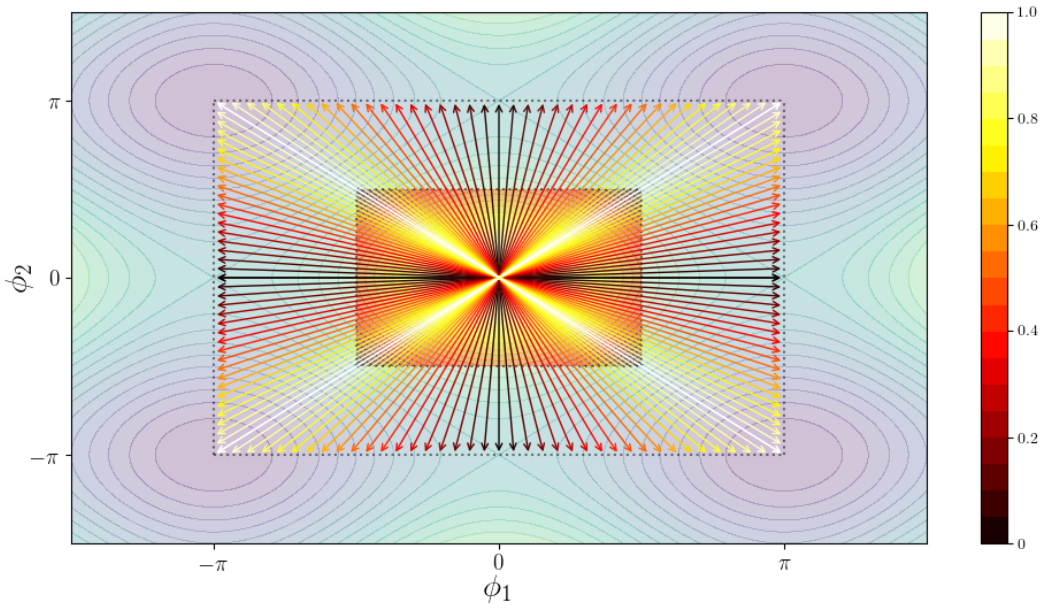


Figure 5.2: Enhanced view of the fundamental domain of the canonical fields in the two-axion N-flation model with well aligned potentials. Each of the fields are defined in the periodic boundary $\phi \in [-\pi, \pi]$ outlined by the dotted *black* line. The colour scale represents the magnitude (1 is maximal and 0 is minimal) of enhancement utilising two fields. This is maximal along the pythagorean sum between the two-dimensional fields potential and minimal when the potentials are orthogonal. The inner region enclosed by the *black* dot-dashed boundary represents the quadratic domain where the potential can be well approximated by a second order expansion as shown in Ref. [131].

be considered as an outright statistical analysis of two random matrix arguments, which must then be simultaneously diagonalised.

5.1.1.2 Canonical Normalisation

In order to fully define a simple set of canonical fields, we must first diagonalise and canonically normalise the axion field space kinetic matrix with a unitary congruence transformation, $\mathbb{U}_{ij}$,

$$\mathcal{K}_{ij} = \mathbb{U}^T_{ik}\text{diag}(\mathcal{K}_{kl})\mathbb{U}_{lj} = \frac{1}{2}\mathbb{U}^T\text{diag}(f_a)\text{diag}(f_a)\mathbb{U}\,. \tag{5.13}$$

After this transformation the vector of axion decay constants, f_a, can be defined in Planck units as the normalised eigenvalues of the diagonal field space metric,

$$\vec{f_a} = \sqrt{2\text{eig}\left(\mathcal{K}_{ij}\right)} \ . \tag{5.14}$$

Absolving this vector of decay constants into the dimensionless misaligned fields, transforms them into canonical coordinates in the kinetic basis. The canonical fields in this basis are,

$$\tilde{\phi}_i = M_{pl}\text{diag}(f_a)\mathbb{U}_{ij}\theta_j \ . \tag{5.15}$$

The effective field Lagrangian in the kinetic basis is now expressed with canonically normalised kinetic terms,

$$\mathcal{L} = -\frac{1}{2}\delta_{ij}\partial_\mu\tilde{\phi}_i\partial^\mu\tilde{\phi}_j - \frac{1}{2}\tilde{\phi}_i\tilde{\mathcal{M}}_{ij}\tilde{\phi}_j \ , \tag{5.16}$$

where the perturbed axion mass matrix in this basis is now defined as,

$$\tilde{\mathcal{M}}_{ij} = 2\text{diag}(1/f_a)\mathbb{U}\mathcal{M}\mathbb{U}^T\text{diag}(1/f_a) \ . \tag{5.17}$$

The kinetic terms are unitarily invariant, proportional to the identity matrix, where we are free to diagonalise the perturbed mass matrix with a subsequent unitary congruence transformation, $\mathbb{V}_{ij}$. The rotated, perturbed mass matrix now takes the form,

$$\tilde{\mathcal{M}}_{ij} = \mathbb{V}^T\text{diag}(m_a)\text{diag}(m_a)\mathbb{V} \ , \tag{5.18}$$

defining a vector of mass eigenstates,

$$\vec{m_a} = \sqrt{\text{eig}\left(\tilde{\mathcal{M}}_{ij}\right)} \, . \tag{5.19}$$

The canonical fields in the mass eigenstate basis are,

$$\phi_i = \mathbb{V}\tilde{\phi}_i = M_{pl}\mathbb{V}\text{diag}(f_a)\mathbb{U}\theta_i \ , \tag{5.20}$$

with the effective Lagrangian now in the simple diagonalised form,

$$\mathcal{L} = -\frac{1}{2}\partial_\mu\phi_i\partial^\mu\phi_i - \frac{1}{2}\text{diag}(m_a^2)\phi_i\phi_i\,. \tag{5.21}$$

The steps above represent a simple general procedure of canonical field normalisation used to determine the spectra in each effective model. The diagonalisation of both $\mathcal{K}_{ij}$ and $\mathcal{M}_{ij}$ represent basis rotations where the parameters can be suitably sampled, loosely based on the principles of axion field alignment and the convergence of universal forms for the parameter distributions. These basis rotations from canonical normalisation can be related to a series of full rank perturbation operations performed on the initial matrix parameter spectra we define in our choice of model. There are three distinct basis we can initialise our analysis based on the steps above:

- *Geometric lattice basis* - The initial basis which defines the effective two-derivative axion field Lagrangian in its most simple general form, containing both a non-trivial mixing of the kinetic terms along with a non-diagonal mass matrix, which is in general not trivially aligned with the field space metric. In this basis the initial Lagrangian is defined in the form found in Eq. (5.12).

- *Canonically normalised kinetic basis* - The basis in which the axion effective Lagrangian contains canonically normalised kinetic terms with a trivial field space metric, proportional to the identity, but possesses a non-diagonal mass matrix. In this basis the Lagrangian is defined in the form found in Eq. (5.16).

- *Diagonalised mass-eigenstate basis* - The sample basis for the mass-eigenstates for each of the axion fields where the axion mass matrix is now in its eigendecomposition basis. In this basis the Lagrangian is defined in the form found in Eq. (5.21).

Each model we introduce will be referenced in terms of the distributions for the elements in the geometric lattice basis and how the sample distribution changes

for the mass eigenstates as we rotate through each subsequent basis. To visualise the general features of the limiting spectra we perform the following parameter normalisations,

$$f_a^2 \to \log_{10}\left(f_a^2\right) \ , \tag{5.22}$$

$$m_a^2 \to \log_{10}\left(m_a^2\right) \ , \tag{5.23}$$

$$\phi \to \log_{10}(\phi) \ , \tag{5.24}$$

akin to the common parameterisation practise for priors found when modelling simple models of the string axiverse. This coordinate transformation will later help reduce the number of moments we must account for by producing a skew-symmetry under certain considerations for the initial form of each matrix.

5.1.2 Epistemic Priors on the Axion Parameter Space

As is often custom in simplistic models of the phenomenological axiverse found in Ref. [107], the axion decay constants and masses are drawn from log-flat priors, under the motivations of scale invariance on the positive, real, *physical* and dimensionful parameters [1306] determined by $\mathcal{K}_{ij}$ and $\mathcal{M}_{ij}$. Very simplistic arguments follow that both the axion masses (See discussions in Section 3.3.2) and decay constants are expected to span several decades [154, 367, 714]. We use a log-flat prior on both of these unknown dimensionful quantities as a '*maximally ignorant*' baseline approach to an ad hoc axiverse solution assumption. The uniform distribution is unnormalised, only defined as a proper prior for our considerations once the end points of the distribution are fixed by controlling limits. These of course can naturally be extended to include some degree of variation with the use of a hyperparameter. By definition this breaks the scale invariance of our prior, however we retain motivations for bounded limits in concordance with the literature. The values,

$$\text{eig}(\mathcal{K}_{ij}) \equiv f_{a,i}^2 \, , \tag{5.25}$$

$$\text{eig}(\mathcal{M}_{ij}) \equiv m_{a,i}^2 \,, \tag{5.26}$$

represent the elements of the diagonalised kinetic and mass matrix respectively, we could find in a matrix approach to a non-trivial spectrum for these parameters. Without any deterministic or explicit definition placed on the parameters of the underlying physical theory the point of least information concerns itself with a general scale invariance placed on the simple axion cosmology parameter space. This *zeroth order* approximation and statistical straw man seeks to factor in the wealth of possible models which may realise an axion field at many different energy scales, from the assumption that string compactification models generally give rises to vast numbers of moduli which span many decades due to the the plethoric properties of the landscape [107, 1231]. This is achieved by a simultaneous sampling of the parameter space in the mass eigenstate basis where, by definition, the parameters are strictly uncorrelated. The non-canonically normalised parameter space is a hypercube, which for the simplified axion cosmology with $n = 3$ parameters gives a non-informative prior cube for the dimensionless fields. The normalised side lengths are then fixed by assumptions determined by string model motivations. We sample each parameter in the simple axion cosmology using the model priors,

$$\log_{10}\left(\text{eig}\left(\mathcal{K}_{ij}\right)\right) \in \mathcal{U}[k_{\text{min}}, k_{\text{max}}] \,, \tag{5.27}$$

$$\log_{10}\left(\text{eig}\left(\mathcal{M}_{ij}\right)\right) \in \mathcal{U}[m_{\text{min}}, m_{\text{max}}] \,, \tag{5.28}$$

$$\theta_i \in \mathcal{U}[-\pi, \pi] \,. \tag{5.29}$$

The uniform distributions are initially unnormalised, in a Bayesian sense acting analogous to taking a Jeffery's prior. The limits k_{min} and k_{max} are associated with lower and upper bounds on CP symmetry breaking scales, with m_{min} and m_{max} bounds on scales for non-perturbative scales which break the high-dimensional gauge symmetries. The limits can be normalised to either the full space or sub-normalised for considerations of dealing with particular phenomenologies, i.e. DM cosmologies

or quintessence fields. The upper limit for $f_a^{\max}$ is motivated by the WGC and limits on non-effective trans-Planckian displacements of an axion field. For an effective field theory description, shift symmetries with large periodicities encounter issues in regards to stability in the UV sector of the theory, although effective displacement from alignment could raise the value of $f_a^{\max}$ we wish to model or allow for. It is often well motivated to assume then that,

$$\log_{10}\left(f_a^{\max}\right) \sim 0 \ , \tag{5.30}$$

in Planck units to avoid the inclusion of too many scales which don't adhere to current understanding of string vacua, which exhibit parametric control in the effective limits of the theory. The lower bound on $\log_{10}(f_a^{\min})$ we could wish to account for generally comes from cosmological constraints, such as stellar object cooling bounds [459, 789, 1181, 1306, 1392], fixing the approximate lower bound,

$$\log_{10}(f_a^{\min}) \gtrsim -9 \ , \tag{5.31}$$

in Planck units. The values for both $m_a^{\min}$ and $m_a^{\max}$ are fixed purely by cosmological model concerns. The value of $m_a^{\min}$ should be conservative, accounting for the fact the spectrum could contain fields which have not begun oscillating about their potential. This fixes $m_a^{\min}$ to follow the approximate bound,

$$m_a^{\min} \sim \alpha H_0 \sim \alpha 10^{-33} \text{ eV} \ , \tag{5.32}$$

where $\alpha \leq 1$ is a $\mathcal{O}(\mathcal{N}_{\text{ax}}^{-1})$ suppression factor and H_0 the is Hubble scale today. The upper bound $m_a^{\max}$ is a relatively free parameter, although as we are primarily concerned with the ultralight sector we shall ensure this follows,

$$\log_{10}\left(m_a^{\max} \text{ eV}^{-1}\right) \ll 0 \ . \tag{5.33}$$

The initial field misalignment follows standard practice, drawn from the unit circle for PQ symmetry breaking. These general phenomenological limits above will also be followed when fixing the scales of the matrices in our models of the effective RMT axiverse.

5.2 The Random Matrix Axiverse

5.2.1 Arguments to Explore Modality

Any string or M-theory model that seeks to realises one of the phenomenological axion models of interest, (QCD axion, FDM, or GUTs etc.) could contain a distribution of masses fixed according to some defining value. Even a small spread over logarithmic distances could lead to strong constraints on the model from numerous forms of constraints both theoretical and observational. Consider the following toy model conforming, to standard string axiverse conjecture of using the epistemic priors outlined in Section 5.1.2. As it was previously discussed in Section 3.3, Ref. [107] introduces the idea that the axion masses are well motivated to follow a log-flat distribution from the Planck scale to the Hubble scale, covering potentially approximately sixty orders of magnitude. Take one set of the numerous astrophysical bounds placed on axions, such as the BH superradiance constraints covered in Section 6.4.1. These constraints currently conservatively cover at least four orders of magnitude, as detailed using the methods covered in Appendix J, which already imposes an interesting tension to this form of modelling. Assuming independent and identically distributed draws from the epistemic prior in Eq. (5.28), this naive model of the axiverse is excluded with a very simple probability,

$$P_{\rm ex} = 1 - (56/60)^{\mathcal{N}_{\rm ax}} \ , \tag{5.34}$$

which is greater than the 95% CI if $\mathcal{N}_{\rm ax} \geq 44$. Clearly, a model with such an uninformative prior on the axion mass is excluded by BH superradiance alone, for a large number of fields *a priori*. The exclusion is a function of the upper and lower bounds on the mass spectrum, or the relevant scales of the theory associated to non-perturbative physics. The constraint gets considerably stronger if the upper bound is below the Planck scale, and vanishes if the distribution does not extend below about $\mathcal{O}\left(10^{-11}\right)$ eV, for these particular constraints. Such a truncated spectrum, on the other hand, cannot realise many of the models of interest to cosmologists.

Consider also the specific model of quintessence covered in Section 2.8.2, used to identify a suitable quintessence field candidate, utilising an axion spectrum comprised of $\mathcal{N}_{\rm ax} = 24$ fields. Assuming the mass states are equidistantly separated on logarithmic scales, as detailed in Ref. [765], driven by the exponential sensitivity of the instanton action over the corresponding cycles, the axion states must '*step*' through the entire ultralight sector towards the Hubble scale today. If no means are deployed to dissipate the energy density of these fields, or additional mechanisms incorporated to alleviate the relevant constraints, then the model is very quickly ruled out by BH constraints along with other ultralight limits such as those detailed in Ref. [710]. For example using Eq. (2.120) to define our axion mass scales up to $m_a^{24} \approx M_H$, the middle axion is defined at approximately the order of the upper bound limits coming from stellar mass BH superradiance constraints. As shown in Fig. 5.3 this simple model of the axiverse produces a number of problematic and potentially strongly constrained masses when attempting to realise a suitable DE axion candidate. Even just considering bounds from stellar mass BHs, supermassive BHs and late time DM fields this model produces at least six fields falling inside constrained contours as shown in Fig. 5.3. Considering many string models generally predict $\mathcal{N}_{\rm ax} \gg 24$, it is clear that modal prior functions on the axion mass space offer the ability to potentially realise multi-field dynamics incorporating large numbers of fields in the ultralight sector, whilst potentially avoiding astrophysical constraints. Fortunately as we will now see for the considerations of phenomenologists, the mass

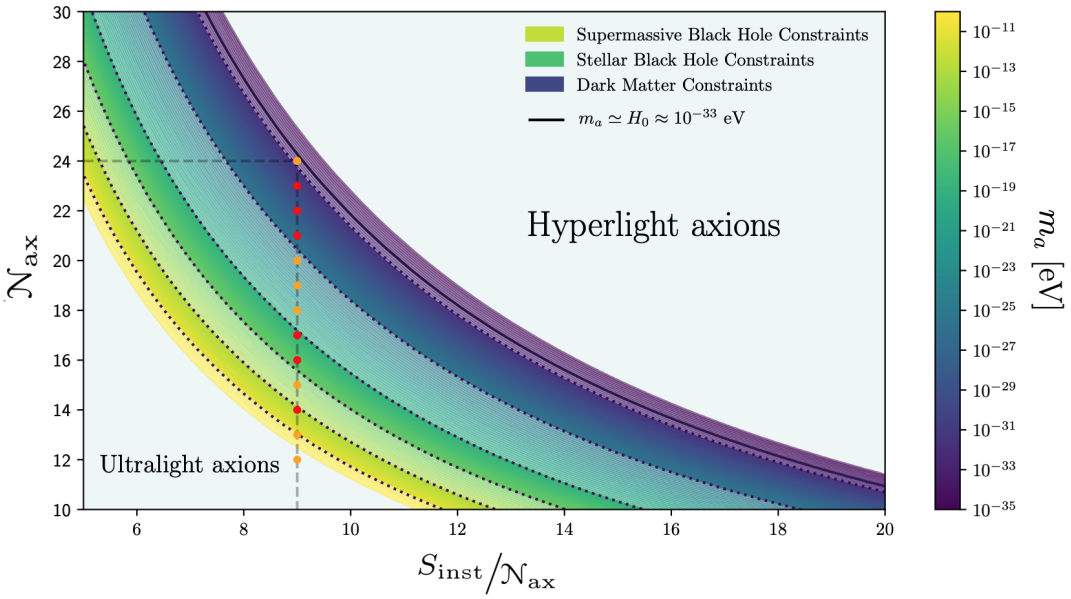


Figure 5.3: Schematic representation of equidistant axion masses used to realise a natural quintessence scenario, where the axion mass eigenstates are generated by the function in Eq. (2.120). As shown in Ref. [765] the axion quintessence field appears as the twenty forth field where in this example, $S_{\rm inst} = 216$. This value falls inside the approximate bounds for the value of the instanton action required to break the field shift symmetry of a single axion with a vacuum energy comparable to present DE density today [1230, 1231]. The previous fields entering the horizon in the ultralight domain could encounter problematic or constrained regions as shown by the *red* points, defined inside the phenomenological contours. Methods would be required to dilute the energy densities of these fields such as decaying to Standard Model fields or higher order corrections to the fields potential or in the case of superradiance constraints, considerations of non-linear effects such as bosenova or bose supernova events. This would ensure the energy density in the coherent field oscillations scale comparable to radiation like components and the superradiance process is shut off to avoid limits placed on the fields mass.

distributions arising from effective RMT models under the considerations of multivariate statistics are indeed generally not log-flat from the Hubble scale to the Planck scale.

5.2.2 The Black Boxes of the Axion Cosmology

5.2.2.1 Utilising the Spectral Theory of Traditional Ensembles

We will now detail a series of models, each of which are loosely related to previous studies in the literature, categorised according to the initial basis we start in and possible perturbations to the mass spectrum using the notations of Lebesgue decomposed measures. Traditionally for sample covariance models, positive-semidefinite constructions generate a point mass at zero, which occurs above the limit of minimum rectangularity for our Y-matrix, i.e. $\beta > 1$. This is of course vital to ensure the invertibility condition, which is required to ensure the mass spectrum is a well defined quantity. To ensure this is absent, unless otherwise stated, we define the minimum and maximum values of the distribution shaping parameter, as found in Eq. (4.83) to be, $\beta_{\text{min}} = 0.05$ and $\beta_{\text{max}} = 1.00$ respectively in any example spectra. For each model presented below we adopt the notation of identifying spiked eigenvalues as separated point mass measure with some absolutely continuous bulk. We can of course always express the bulk as a weighted sum of point masses (e.g. the ESD in Eq. (4.17)), where we choose to separate the treatment of the spikes to detail the features of the model. As such the results below can be considered as indicative of a single realised draw in the large $\mathcal{N}$ limit, where the modelled spikes are more generally subject to some absolutely continuous spectrum for their statistical fluctuations. We also only focus on the simplest case of spiked ensembles containing a singular spike with a singular linear statistic and is therefore not a general study of spiked statistics. We leave the case of linear spectral statistics (LSS) at its associated CLTs for large dimensional random matrices as a natural extension to any models covered here.

We will only focus only on models constructed using ensembles possessing group symmetries and real spectra with possible allowances made for correlated entries. Each of these are initially defined according to either the null or alternative hypothesis of the Wishart-Laguerre ensemble, as covered in Section 4.2.2. The axion

mass matrix is represented by a sample covariance matrix, which depending on the coordinate transformations of the canonical fields will be perturbed both through normalisation of the field basis and some initial assumption made on possible data correlations from higher order stochastic processes.

5.2.2.2 Augmenting the Unknown

Strictly speaking data augmentation consists of latent or unavailable data represented as parameters requiring estimation [820, 1244, 1245]. Instrumental in the pioneering works of Nicholas Metropolis [941] and Wilfred Keith Hastings [675], laying the groundwork for Markov chain Monte Carlo (MCMC) methods and algorithm classes applied to the analysis of complex systems. Our realisation of the string axiverse is formed using probability techniques based on heuristics and analytical statistics, our field parameter values populated via pre-determined priors, with minimal information applied to our models. In this context, these models are used to maintain a high level of simplicity, according to the idea we are lacking a practical way of obtaining the 'complete' information for the effective potential in the lattice/kinetic basis.

This represents a stochastic approach to features of exploring ad hoc models of the axiverse introduced in Ref. [107] such as the possible exponential sensitivity of cycles over the total extra-dimensional compactified manifold. These data vector type models are generally speaking far from explicit physically realistic models, but offer an efficient sampling of a high-dimensional parameter space. In this sense we can associate the resultant parameter spectra very loosely to unimodal functions (plus point mass fluctuations) regulated by statical parameters to greatly reduce the dimension of the model (see Section 5.4). In each of the RMT models presented below we use the notation $\mathcal{M}$ for sample axion mass matrices which have not been perturbed from basis rotations and $\tilde{\mathcal{M}}$ for matrices which have been perturbed before sampling. Many of the models below are inspired by those which have initially been

considered in the context of multi-field inflationary models, these dynamics we now reproduce in the ultralight sector of axion cosmology.

5.2.3 I. Models With Degenerate Mass States

Diagonalised Mass-Eigenstate Basis

5.2.3.1 Degenerate Scalings

Originally defined in the context of models of *N-flation* [457], representing an axion generalisation of models of assisted inflation [859], the kinetic matrix and axion mass matrix are represented by scalar matrices, initially aligned in their spectral decomposition basis,

$$\mathcal{K}_{ij} = \delta_{ij}\tilde{k}_{jk}, \quad \mathcal{M}_{ij} = \delta_{ij}\tilde{m}_{jk} \ . \tag{5.35}$$

The quantities, $\tilde{k}_{jk}$ and $\tilde{m}_{jk}$ are matrices, with each element fixed to a single scalar variable, defined by the two scalar quantities $\bar{f}_a$ and $\bar{\Lambda}_{m_a}$. Each value is fixed to some generic scale for either PQ symmetry breaking or the non-perturbative physics responsible for breaking the axion shift symmetries, i.e. $\bar{f}_a \approx M_{\rm GUT}$ and $\bar{m}_a \approx M_{\rm FDM}$ (see Section 2.8.3). Each matrix has a degenerate spectrum represented by the point mass measure functions,

$$\mu_{f_a^2} \equiv \mu^{\rm pm}_{\bar{f}_a^2}, \quad \mu_{m_a^2} \equiv \mu^{\rm pm}_{\tilde{\Lambda}_{m_a^2}} \ , \tag{5.36}$$

where $\tilde{\Lambda}_{m_a^2}$ now represents the canonical mass scale of the theory. This defines the maximum invariant field range which is parametrically scaled as, $\sqrt{\mathcal{N}_{\rm ax}}\bar{f}_a$ (see Fig. 5.2). The canonical fields are distributed according to a rescaled uniform prior on the unit circle,

$$\phi \in \mathcal{U}\left[-\bar{f}_a\pi; \bar{f}_a\pi\right] \ . \tag{5.37}$$

5.2.3.2 Non-Trivial Metric with a Degenerate Mass Spectrum

The spectrum of the matrices in the initial basis is now defined to be non-degenerate. The kinetic and mass matrices are both defined as isotropic Y-matrices which possess the following alignment relation,

$$\mathcal{K}_{ij} = \mathcal{M}_{ij} = \mathcal{P}^{-1}\mathbb{X}\mathbb{I}\mathbb{X}^{\mathrm{T}} \ , \tag{5.38}$$

where each matrix is fully normalised. Each matrix is initially aligned in such a basis that performing a singular $GL(\mathcal{N}, \mathbb{R})$ transformation simultaneously puts each matrix in its eigendecomposition basis where the kinetic and mass matrices in the Lagrangian are,

$$\mathcal{K}_{ij} = \mathbb{U}\mathrm{diag}\left(f_a^2\right)\mathbb{U}^{\mathrm{T}}, \quad \mathcal{M}_{ij} = \mathbb{V}\mathrm{diag}\left(m_a^2\right)\mathbb{V}^{\mathrm{T}} \ , \tag{5.39}$$

with the eigenvector proportionality relationship defining, $\mathbb{U} \propto \mathbb{V}$. In the large $\mathcal{N}$ limit in the initial basis $f_{a,i} \propto m_{a,i}$. In this model, the kinetic terms initially begin with the canonical normalisation factor of $1/2$ present, where $\mathcal{K}_{ij}$ and $\mathcal{M}_{ij}$ are distributed so that after full canonical normalisation the degenerate perturbed mass spectrum is,

$$\tilde{\mathcal{M}}_{ij} = \delta_{ij}\Lambda_{m_a}^2 \ , \tag{5.40}$$

where $\Lambda_{m_a}^2$ represents a general squared mass scale of the theory from non-perturbative physics. This model is a generalisation of the original N-flation model [457] with non-degenerate metric eigenvalues whilst retaining the trivial degenerate spectrum of mass eigenstates. The maximum invariant field range is parametrically suppressed compared to the previous model. The axion decay constant spectrum is realised as the Marčhenko-Pastur distribution with a degenerate mass spectrum weighted at the mass scale of the theory, defining the two parameter measures,

$$\mu_{f_a^2} \equiv \mu_{\mathrm{bulk}}^{\mathrm{ac}} = \mu_{\mathrm{MP}}^{\mathrm{ac}}, \quad \mu_{m_a^2} = \mu_{\tilde{\Lambda}_{m_a^2}}^{\mathrm{pm}} \ . \tag{5.41}$$

We consider this an atypical configuration of the general isotropic approach presented in Section 5.2.5. The canonical fields are distributed according to the measure,

$$\phi_i = \mathbb{R}_{ij}\theta_j \ , \tag{5.42}$$

$$\mathbb{R}_{ij} = \mathbb{U}_{ik}\mathbb{U}_{kj}\text{diag}(f_a) \ . \tag{5.43}$$

5.2.4 II. Models With Random Matrix Mass States

Canonically Normalised Kinetic Basis

When we define our model in the canonically normalised kinetic basis, the axion decay constants are generally defined as a vector of degenerate scalings used to determine the nature of the canonical fields. Unlike the models in Section 5.2.3 the mass spectrum is now non-trivial, where the resulting mass distribution depends entirely on how we define the axion mass matrix before diagonalisation.

5.2.4.1 The Marčhenko-Pastur Isotropic Model

The initial axion mass matrix is defined under the null formalism, $\mathcal{H}_0$, absent of any external perturbation or basis rotation before sampling the mass eigenstate sample space basis. The total theoretical uncertainty of the model parameters are contained in a single isotropic Y-matrix:

- We assume no covariance between the elements of the data vectors of the masses, in the large $\mathcal{N}$ limit. The mass matrix population covariance matrix is defined as $\Sigma_{\mathcal{P}} = \mathbb{I}$. The empirical sample covariance mass matrix is defined as $\mathcal{M} = \mathcal{P}^{-1}\mathbb{X}\mathbb{X}^{\text{T}}$, where $\mathbb{X}_{ij} \in \mathcal{N}(0,1)$.

- There is no redefinition of the the sampled eigenspace via the absence of any canonical normalisation perturbation, $\mathbb{P}_{\mathcal{N}} = \mathbb{I}$, before the mass eigenstates are sampled. The LSDs of this model follow the historical universal limits for

uncorrelated Wishart matrices.

Formulated from the work of Richard Easther and Liam McAllister to describe the inflationary dynamics of assisted multi-field axion models [499], the theoretical uncertainty of the Type IIB models superpotential is encoded entirely in the universal nature of a symmetric random matrix, used to determine the axion mass terms. In their work this matrix form is extracted from the universal features of the KKLT compactification treatment for the complete superpotential in Type IIB theories. Their approach is detailed in Appendix I. If we begin in the canonically normalised kinetic basis then we define the model parameters to be,

$$\mathcal{K}_{ij} = \delta_{ij}, \quad \mathcal{M}_{ij} = \mathcal{P}^{-1}\mathbb{X}\mathbb{I}\mathbb{X}^{\mathrm{T}} = \mathbb{V}\mathrm{diag}\left(m_a^2\right)\mathbb{V}^{\mathrm{T}} \ , \tag{5.44}$$

where the axion mass matrix is an isotropic Wishart matrix with trivial covariance. In their model the distribution shaping parameter is defined using the ratio of the number of axions to the total dimension of the moduli space, shown in Eq. (5.45), defined by the Hodge numbers, $h^{1,1}$ and $h^{2,1}$. Using the fit shown in the *left panel* of Fig. 3.3 we can assign a prior to this parameter,

$$\beta_{\mathcal{M}} = \frac{h^{1,1}}{h^{1,1} + h^{2,1} + 1} \in \mathcal{N}\left(0.5, 0.125^2\right) \ , \tag{5.45}$$

as an indication of the typical values this could take.

The universal mass spectrum is an absolutely continuous measure defined by the limiting Marčhenko-Pastur distribution of Eq. (4.67), unperturbed from canonical normalisation for the square singular values of the individual axion mass scales,

$$\mu_{m_a^2} \equiv \mu^{\mathrm{ac}}_{\mathrm{bulk}} = \mu^{\mathrm{ac}}_{\mathrm{MP}} \ . \tag{5.46}$$

The normalisation of Eq. (5.46) is fixed to some phenomenological defining scale, through the spectrums standard deviation, $\sigma^2_{\mathrm{MP}} \equiv \bar{\Lambda}^2_{m_a}$. Example normalised spectra are displayed in both the *left* and *right panels* of Fig. 5.4 for a range of values of the

distribution shaping parameter, $\beta_{\mathcal{M}}$, using both linear and logarithmic scales. The axion decay constants are introduced as a degenerate spectrum of point masses, i.e. $\mu_{f_a^2} = \mu^{\rm pm}_{\bar{f}_a^2}$, defined by a scalar value fixed to some fundamental scale of the theory, i.e. $\bar{f}_a \approx M_{\rm GUT}$. The fields are displaced by a scaling of equal magnitude so that the canonical fields are distributed according to a rescaled uniform prior on the unit circle as in Eq. (5.37), like the previous original models of N-flation in Section 5.2.3. Depending on our choice of formalities, we could choose to retroactively introduce non-degeneracy for the axion field metric which is a non-trivial imposing of the canonical normalisation of the field metric in order to define a spectrum of decay constants. In this case and following Ref. [499] the simplified mass spectrum is formalised as an approximation of the full superpotential (see Appendix I) in the canonically normalised kinetic basis such that,

$$\lim_{\mathcal{N}\to\infty} \frac{1}{\sigma^2_{m_a}} \text{eig}\left(\mathcal{K}_{ij}\right) = \lim_{\mathcal{N}\to\infty} \frac{1}{\sigma^2_{f_a}} \text{eig}\left(\mathcal{M}_{ij}\right), \tag{5.47}$$

where $\sigma^2_{f_a}/\sigma^2_{m_a}$ represents the natural hierarchy between PQ symmetry breaking and shift symmetry breaking non-perturbative energy scales. In this model the canonical fields are defined by the matrix product,

$$\phi_i = \mathbb{R}_{ij}\theta_j \ , \tag{5.48}$$

$$\mathbb{R}_{ij} = \mathbb{U}_{ik}\text{diag}(f_a)_{kj} \ . \tag{5.49}$$

5.2.4.2 Finite Rank Spiked N-flation Mass Matrix

The axion mass matrix is defined under the alternative formalism, $\mathcal{H}_A$, with a finite rank deformation from the population covariance matrix, absent of any external perturbation or basis rotation before sampling the mass eigenstates.

- The initially defined sample eigenspace for the axion mass matrix contains both signal and noise from possible strong correlations between random variables.

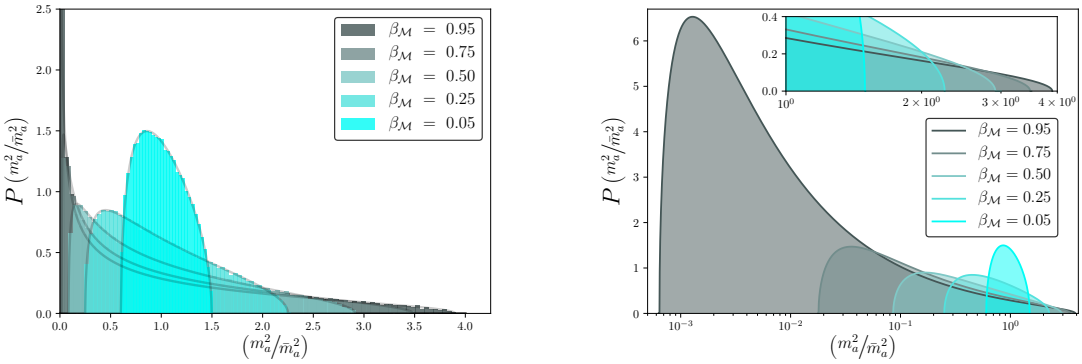


Figure 5.4: Normalised eigenvalue spectra for the Marčhenko-Pastur RMT model, along with associated probability density functions for the squared axion masses, m_a^2, presented with both linear and logarithmic scales in the *left* and *right panels* respectively. Each panel shows five selected values of the spectrum shaping parameter $\beta_{\mathcal{M}}$, approximately covering its defining interval $\beta_{\mathcal{M}} \in (0, 1]$. *Left panel*: The mass distribution converges to the Marčhenko-Pastur limiting law as $\mathcal{N}_{\rm ax} \to \infty$. Asymptotically the largest eigenvalue, which can fluctuate outside its defined compact interval, is determined by the Tracy-Widom law in Eq. (D.4). *Right panel*: Probability density functions for each of the associated distributions in the *left panel* displayed on a logarithmic mass scale. Inset: As $\beta_{\mathcal{M}}$ increases,1 the positive logarithmic displacement of the upper bound is limited compared to the negative displacement of the lower bound of the distribution.

The sample covariance mass matrix $\mathcal{M}_{ij}$, is initially perturbed by a singular or finite rank perturbation to the identity population covariance matrix used in the model in Section 5.2.4.1, where $\Sigma_{\mathcal{P}} \not\propto \mathbb{I}$.

- The axion mass matrix is defined using the general form found in Eq. (4.109) with σ some positive real number and $\mathbb{P}$ a linear transformation vector for the population covariance matrix eigenvalues. The limiting spectrum is defined by both a bulk probability measure with a finite number of *spiked* outliers, which are subject to Gaussian fluctuations, like the measure form in Eq. (4.84).

- The mass spectrum probability measure is takes the decomposed form,

$$\mu_{\mathcal{M}} \equiv \mu_{\rm MP}^{\rm ac} + \sum_{i=1}^{\mathcal{R}} \mu_{\rm spike}^{\rm pm} \ , \tag{5.50}$$

where $\mu_{\rm MP}^{\rm ac}$ converges almost surely to the absolutely continuous measure under the *null* formalism. The summation component represents a series of separated point mass measures forming the model spikes, representing statistical fluctuations of extremal eigenvalues separated from the upper support of the bulk measure. The value of $\mathcal{R}$ represents the rank of the perturbation to the population covariance matrix minus the total number of population eigenvalues with a degeneracy greater than unity plus the number of groups of degenerate values associated to the weight of the point masses.

The spectrum adopts the formalities of the original random matrix N-flation model discussed in Section 5.2.4.1 from Ref. [499] and as detailed in Appendix I, with the possibility of allowing for strong correlations between model parameters which generate sharp transitions in the fields mass eigenspectrum. Discrimination between the null hypothesis of Section 4.3.1 and the finite rank alternative assumption, is strictly concerned with the asymptotics of extremal eigenvalues and their perturbatively in the limit of critically. Finite rank perturbations to the mass spectrum generate a mass hierarchy between the spectrum bulk and a finite number or outliers. In this model the kinetic metric is still assumed to be trivial where we only perturb the limiting spectrum of the model in Section 5.2.4.1. In the canonically normalised kinetic basis we define our model according to Eq. (5.44) where the mass matrix is formed by drawing the matrix elements from a distribution with non-centred mean, $\Omega = (\emptyset, \Sigma)$, i.e. we break the moment requirements of Eq. (4.80). This generates a mass hierarchy in the form of a bulk measure and a singular perturbed spike for the largest mass. These models are analogous to the rank-one spiked models covered in Section 4.3.2.2. They represent the presence of an enforced *non-centrality spike*, as apposed to the complimenting case of defining finite spiked covariance. This process relates to a specific case of non-central Wishart matrices [76, 746, 1017] with rank-one non-centrality parameters. The axion mass matrix is formally defined by the ensemble,

$$\mathcal{M}_{ij} \sim \mathcal{W}(\mathcal{P}, \mathbb{I}, \Theta) \ , \tag{5.51}$$

where $\mathbb{I}$ is the identity scale matrix and Θ is a non-centrality matrix. When Θ is rank one the largest axion mass is non-compactly supported defined in the supercritical regime for the BBP phase transition of Section 4.3.2.2. To do this we relax the use of Gaussian entries and draw each element of the mass matrix from a log-uniform prior distribution,

$$\log_{10} \mathbb{X}_{ij} \in [m_{\rm min}, m_{\rm max}]. \tag{5.52}$$

The mass spectrum is now parameterised by two upper and lower distribution parameters, $m_{\rm min}$ and $m_{\rm max}$. The ratio, $^{m_{\rm min}}/_{m_{\rm max}}$ determines the region of criticality the BBP phase transition susceptible eigenvalue and highest axion mass falls into, which if separated from the bulk, also controls the magnitude of the rank one separated point mass. An example limiting mass spectrum for this model is displayed in the *left panel* of Fig. 5.5, showing both the rank one perturbation and the limiting bulk spectrum defined by the Marčhenko-Pastur measure. If we suspect strong correlations in multiple model parameters then the sharp transitions may have a finite rank greater than unity, where several field masses will escape the spectral limits of the Marčhenko-Pastur bulk. This can be modelled simply with a diagonal population covariance where the prior placed on the diagonal elements possesses a sharp enough tail to generate sufficient $\mathcal{O}(1)$ population covariance eigenvalues, ensuring a finite number of elements fall inside the sub-critical regime. Various explicit forms of the LSD are know for the case of rank one spiked models, in either the case of spiked covariance or non-central ensembles [2, 434, 999, 1017, 1322],

$$\frac{\mathcal{C}_{\mathcal{N}}[l]}{2\pi i} \oint_C l(z) \prod_{1 \leq j \leq k \leq \mathcal{N}} (x_k - x_j)^2 \prod_{j=1}^{\mathcal{N}} \frac{x_j^{\mathcal{P}-\mathcal{N}} e^{-x_j}}{z - x_j} dz \ , \tag{5.53}$$

which represents a contour integral representation of the joint eigenvalue density for the complete set of eigenvalues, x_k, where,

$$l(z) = \begin{cases} e^{\left(\frac{\delta}{1+\delta} z\right)} \ , & \text{Spiked covariance} \ , \\ {}_0F_1 \left(\mathcal{P} - \mathcal{N} + 1, \mathcal{N}\nu z\right) \ , & \text{Non} - \text{centred ensemble} \ , \end{cases} \tag{5.54}$$

with ${}_0F_1$ a confluent hypergeometric function and the function, $\mathcal{C}_{\mathrm{N}}[l]$ a normalisation constant and $l(z)$ encapsulates the behaviour of the singular spiked eigenvalue. We include this simply to highlight a neat example demonstrating the complicated nature of defining an explicit spectral form when finite rank perturbations are present in the model.

In a phenomenological context a simple example we could consider would be a toy model, where $\bar{\Lambda}^2_{\mathrm{DE}}$ represents the defining mass scale which controls the non-perturbative breaking of the field shift symmetries for a collection of quintessence fields. These present as idiosyncratic noise in the total axion mass spectrum, collectively providing sufficient late time DE. Assuming a large enough hierarchy between the matrix bulk and isolated eigenvalues, directly related to the correlation strength between model variables, a single axion mass could break from the bulk distribution and fall into the mass ranges required for oscillating DM fields. If the correlation strength is strong enough, driven by the features of the model then this could avoid constraints between late-time ultralight DM fields today, such as those considered in Ref. [710], whilst supplying a sizeable contribution to the total required DM content. We will assume these models represent localised mass hierarchies so the unknown underlying physics is the same, i.e. $\sigma^2_{\mathcal{M}} = \bar{\Lambda}^2_{\mathrm{DE}}$, from the possible tower of states, where fields with substantially large masses have been integrated out from the effective theory. For mass hierarchies coming from different sectors of the axion phenomenological landscape see the discussions in Section 5.2.6.

5.2.4.3 Full Rank Perturbed N-flation Mass Matrix

The axion mass matrix is defined under the alternative formalism, $\mathcal{H}_A$, with a full rank deformation from the population covariance matrix, absent of any external perturbation or basis rotation before sampling the mass eigenstates.

- The sample mass eigenspace is defined by a probability measure formed from the multiplicative free convolution of the limiting eigenspaces for the initial

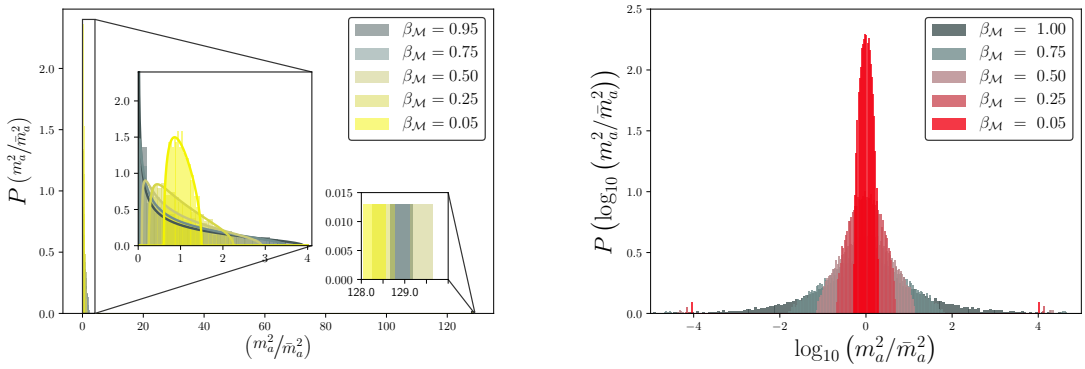


Figure 5.5: Normalised eigenvalue spectra for the axion mass matrix defined with spikes from eigenvalues defined in the supercritical regime of the BBP phase transition. *Left panel*: Example mass spectra for the model presented in Section 5.2.4.2 for a range of values of the distribution shaping parameter $\beta_{\mathcal{M}}$. The spiked eigenvalues, $\mu^{\rm pm}_{\rm spike}$, repulsed from the bulk of the spectrum are enhanced by $\mathcal{O}(\mathcal{N}_{\rm ax})$ (*right inset*). The bulk of the spectrum, $\mu^{ac}_{\rm MP}$, is defined by the Marčhenko-Pastur limiting laws (*left inset*). *Right panel*: Example mass spectra for the model presented in Section 5.2.5.2.3 for a range of values of the distribution shaping parameter $\beta_{\mathcal{M}}$. The bulk of the perturbed mass spectrum is defined as $\mu^{\rm ac}_{\rm F}$ found in Eq. (4.101) inheriting two spiked values defined from both the kinetic and mass matrices. In the limit $\beta_{\mathcal{K},\mathcal{M}} = 1$ the total distribution measure becomes an absolutely continuous function with each of the spiked point masses absolved into the bulk support.

> data vectors and the population covariance matrix which converges almost surely to,
>
> $$\mu_{\mathcal{M}} \equiv \mu^{\rm ac}_{\boxtimes} = \mu^{\rm ac}_{\rm MP} \boxtimes \mu^{\rm ac}_{\Sigma_{\mathcal{P}}} , \tag{5.55}$$
>
> for an isotropic Y-matrix and the limiting spectral measure of a well defined population covariance matrix.

We may also wish to allow for correlations between the random variable vectors in the form of a prior placed on the population covariance matrix. This is a full rank perturbation to the isotropic model discussed in Section. 5.2.4.1. Much like the entries of the sample matrix itself, given the absence of specific information about the true covariance matrix, we require restricted attention to a general class of covariance estimators which we will generalise to a discussion of examples based

on imposing both conjugate on non-conjugate priors. It is often problematic to assume a *pure noise* approach to stochastic processes, where a general relaxation of this assumption requires a definition of suitable population covariance estimators.

5.2.4.3.1 Conjugate Priors

Taking the '*default*' approach for covariance estimation for isotropic Y-matrices, makes use of the conjugate prior on the covariance matrix, $\Sigma_{\mathcal{P}}$, which is distributed according to a standard inverse-Wishart distribution found in Eq. (4.97). The initial sample eigenspace for the axion mass matrix contains data vector corrections regulated by this conjugate prior of the sample space distribution where the empirical sample covariance mass matrix and kinetic matrix are defined as,

$$\mathcal{K}_{ij} = \delta_{ij}, \quad \mathcal{M}_{ij} \equiv \mathbb{Y}_1 \mathbb{Y}_2 = \mathcal{P}^{-1} \mathbb{X} \Sigma \mathbb{X}^{\mathrm{T}} \ , \tag{5.56}$$

with,

$$\mathbb{X}_{ij} \in \mathcal{N}(0,1); \quad \Sigma \sim \mathcal{W}^{-1}(\mathbb{I}, \nu) \ . \tag{5.57}$$

The entries of the axion mass matrix are drawn according to the Fisher-Snedeco distribution in Eq.(4.98). The limiting spectrum of the F-matrix mass matrix is, $\mu_{m_a^2} \equiv \mu_{\mathrm{bulk}}^{\mathrm{ac}} = \mu_{\mathrm{F}}^{\mathrm{ac}}$, defined by the function found in Eq. (4.101). When $\mathbb{Y}_1 \propto \mathbb{I}$ then we recover the RMT N-flation model of Ref. [499] (see Appendix I). This mass spectrum in this model is equivalent to the model found in Section 5.2.5.1. The absolved decay constant spectra through canonical normalisation takes the form of an inverse-Wishart perturbation due to the rotational invariance of the ensemble. See Fig. 5.6 for example mass spectra and discussions in Section 5.2.5.1 for further details on the form of the spectrum.

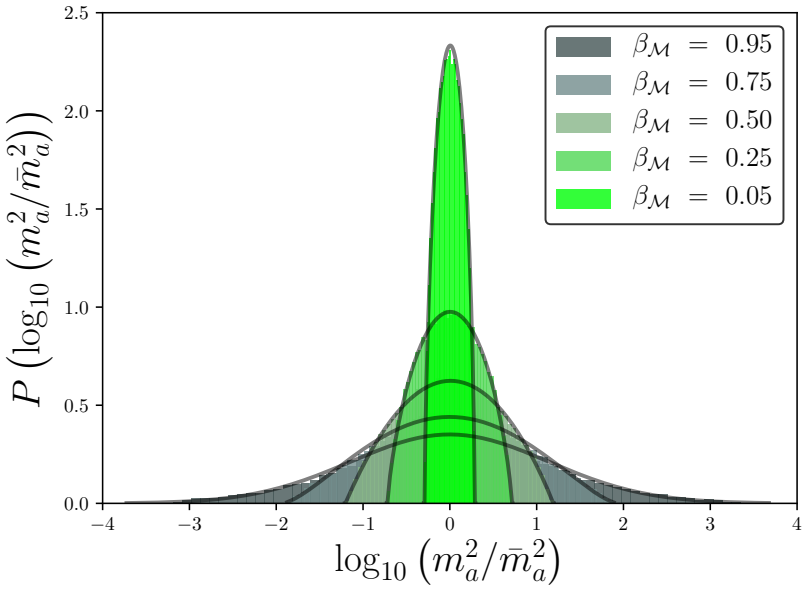


Figure 5.6: Normalised mass spectra for the model presented in Section 5.2.5.1 for a range of values of the distribution shaping parameters $\beta_{\mathcal{K}} = \beta_{\mathcal{M}}$. The multiplicative free convolution of the absolved decay constants with the initial mass matrix causes the sampled spectra to universally converge to a symmetric LSD on logarithmic scales. The mass spectrum measure is defined by the absolutely continuous measure function, $\mu_{\mathrm{F}}^{\mathrm{ac}}$ defined in Eq. (4.101). Each spectra is fitted with a beta distribution function according to the expression found in Eq. (G.6). The $\beta_{\mathcal{M}}$ parameter regulates the limiting distributions kurtosis, acting as a free compression operation, $\boxdot$ (see Section 4.4.2). In the limit $\beta_{\mathcal{M}} \to 0$ the LSD approaches the limiting kurtosis of the infinity divisible bounds for beta distributions, represented by the limit for a semi-circular distribution.

5.2.4.3.2 Non-Conjugate Priors

Following a series of general covariance estimators motivated from models incorporating the separation strategy found in Ref. [66, 161] we can define the following examples for limiting forms of correlated mass spectra:

- *Isometric Y-matrix Population Covariance Matrix*: If the population covariance matrix for the sample covariance mass matrix is also an isometric Wishart matrix then the resulting mass matrix represents a multiplicative free convolution of two independent Wishart matrices. Using the separation strategy

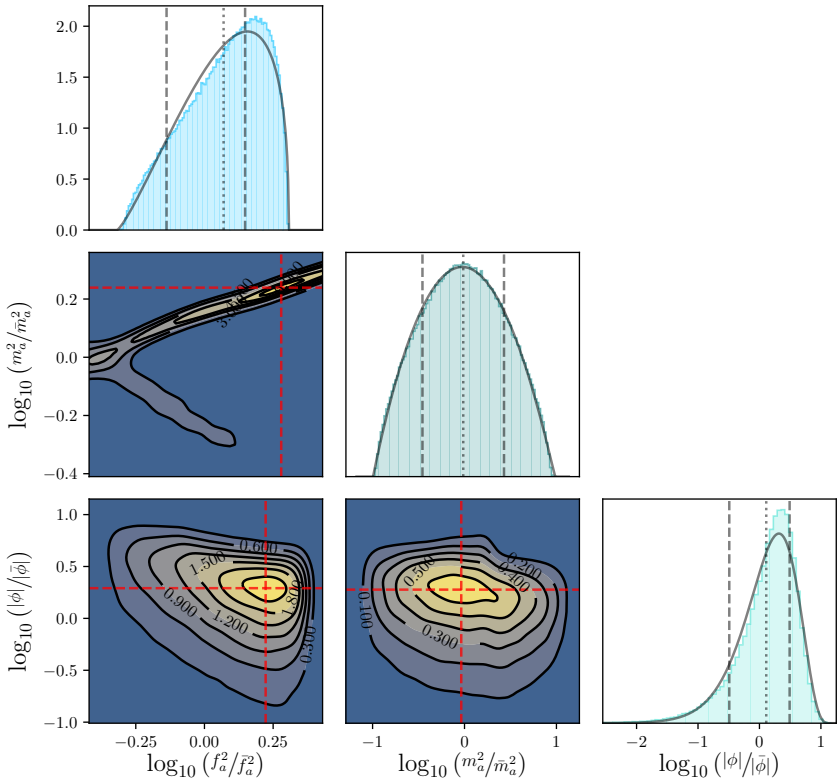


Figure 5.7: Normalised mass, decay constant and canonical field spectra for the model presented in Section 5.2.5.1, for a single equal value of the distribution shaping parameters $\beta_{\mathcal{K}} = \beta_{\mathcal{M}} = 0.5$. The *upper* panels display model spectra, fitted with beta distribution functions according to the expression found in Eq. (G.6). The vertical *dotted* lines represent the spectral mean, where the *dashed* lines represent a 1σ translation from this value. In the *lower left*, *lower middle* and *left central* panels we display the covariance between each of the simple axion cosmology model parameters. The strongest covariance relationship comes from the decay constants which act as a full rank perturbation to the initial mass matrix ensemble in the geometric lattice basis. The reduced dependance between the other parameters comes from the basis rotations moving into the mass eigenstate basis. The *red dashed* lines represent the two-dimensional peak of the contours in each case.

decomposition, this is the equivalent as fixing the model standard deviations to the null scenario, with the Wishart distribution drawing the mass matrix correlations. The LSDs in these models are represented by combinatorial sequences which define the Fuss-Catalan distributions [952, 1047]. The mass

spectrum is defined as, $\mu^{\rm ac}_{m_a^2} \equiv \mu^{\rm FC}_{\rm s=2}$, where $s = 2$ is the second order multiplicative free convolution of Marčhenko-Pastur distribution measures. See discussions in Appendix E for further details, as well as the spectral plots in both the *right panel* of Fig. 5.8 and the *right panel* of Fig. 5.19.

- *Log-Uniform Standard Deviation Priors*: In the case of log-uniform priors placed on the standard deviations by using the separation strategy with identity correlations, this model is analogous to canonically normalising the initial mass spectrum with scale invariant values whilst maintaining the degenerate scalings on the canonical axion fields like the methods found in Section 5.2.4.1. The covariance matrix is assumed to be diagonal, i.e. formed using the separation strategy discussed in Section B.3, with a prior placed directly on the eigenvalues of $\Sigma_{\mathcal{P}}$. If we assume the PQ symmetry breaking scales come from uniformly distributed priors like those in Section 5.1.2 then the covariance eigenvalues hold the equivalence of drawing,

$$\sigma_{\Sigma} \equiv f_a^{-1} \in \mathcal{U}\left[\alpha M_{\rm Pl}^{-1}; \beta M_{\rm Pl}^{-1}\right] \ , \tag{5.58}$$

  where α and β are suppression constants for the WGC and $\alpha \gtrsim \beta$. See the *right panel* of Fig. 5.8 for an example mass spectrum plot in this model.

- *Log-Gaussian Priors*: Motivated by discussions in Ref. [66, 161], in the absence of total scale invariance placed on the standard deviations, a natural substitute is to assume a normal distribution for the logarithms of the entries of the diagonal matrix in the decomposed population covariance matrix. If we assume we also have the presence of correlations then the population covariance mass matrix takes the form of the most general sample covariance matrix, with a scaled inverse Wishart prior as found in Refs. [1008]. The mass matrix takes the form [66],

$$\mathcal{M}_{ij} = \mathcal{P}^{-1}\mathbb{X}\delta Q \delta \mathbb{X}^{\rm T} \ , \tag{5.59}$$

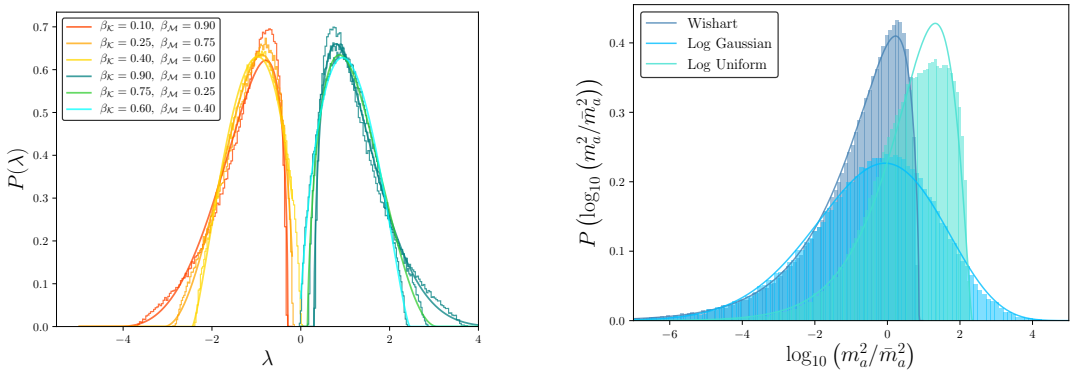


Figure 5.8: *Left panel*: Representation of the skew effect apparent when $\beta_{\mathcal{K}} \neq \beta_{\mathcal{M}}$ for arbitrarily normalised eigenvalues defined from matrices in the model presented in Section 5.2.4.1. We demonstrate this using three examples each when $\beta_{\mathcal{K}} < \beta_{\mathcal{M}}$ (*negative skew*) and $\beta_{\mathcal{K}} > \beta_{\mathcal{M}}$ (*positive skew*). Each example has both binned eigenvalue densities from direct sampling along with an approximated beta function fits defined from Eq. (G.6). *Right panel*: Example normalised mass spectra for the model presented in Section 5.2.4.1 for a range of priors on the population covariance matrix. We demonstrate how some standard example models can be well approximated within the bounds of the Beta distribution function of Eq. (G.6) for skewed spectra. Specifically the case of log-uniform priors on the standard deviations using the separation strategy defined in Eq. (B.6) to define the mass matrix population covariance matrix, shows an example where the need for explicit spectral functions may be required.

where,

$$Q \sim \mathcal{W}^{-1}(\mathbb{I}, \nu) \quad \log(\delta_i) \sim \mathcal{N}(\mu, \sigma) \ , \tag{5.60}$$

as shown in the example plot in found in the *right panel* of Fig. 5.8.

5.2.5 III. Kinetically Aligned Mass Spectra

Geometric Lattice Basis

Beginning in the most general basis means defining our models in the geometric lattice basis. In these models the spectra of both the axion decay constants and masses are non-trivial. The decay constant spectrum depends entirely on how we define the kinetic metric before diagonalisation, whilst the LSD of the masses depends both

on the definition of the initial mass matrix and the initial form of the spiked kinetic metric.

5.2.5.1 The Symmetric Isotropic Case

Both sample eigenspaces are initially defined under the null formalism, $\mathcal{H}_0$, where the axion mass spectrum is perturbed multiplicatively by a full rank perturbation from the canonical normalisation of the fields kinetic terms.

- We assume no covariance between the elements of the data vectors of both the decay constants and masses, in the large $\mathcal{N}$ limit. The kinetic and mass matrix, population covariance matrices are each defined as $\Sigma_{\mathcal{P}} = \mathbb{I}$, i.e. we enforce the equality hypothesis of null covariance. The empirical sample covariance kinetic matrix is defined as $\mathcal{K}_{ij} = \mathcal{P}^{-1}\mathbb{X}\mathbb{X}^{\mathrm{T}}$, where $\mathbb{X}_{ij} \in \mathcal{N}(0,1)$. The decay constant spectra is determined by the measure function, $\mu_{f_a^2} \equiv \mu^{\mathrm{ac}}_{\mathrm{bulk}} = \mu^{\mathrm{ac}}_{\mathrm{MP}}$. The kinetic matrix resides in the Wishart-Lagueue ensemble.

- After basis rotations the sample eigenspace for each parameter is defined by only an absolutely continuous bulk measure component. This model relates to the classical multiplicative perturbation model defined in Section 4.4.2. In the sample basis for the axion masses the empirical sample covariance mass matrix is $\tilde{\mathcal{M}}_{ij} = \mathcal{P}^{-1}\mathbb{P}\mathbb{X}\mathbb{I}\mathbb{X}^{\mathrm{T}}\mathbb{P}$, where $\mathbb{X}_{ij} \in \mathcal{N}(0,1)$ and $\mathbb{P} = \delta_{ij} f_{a,j}$. The mass spectrum defined as $\mu_{m_a^2} \equiv \mu^{\mathrm{ac}}_{\mathrm{bulk}} = \mu^{\mathrm{ac}}_{\mathrm{MP}} \boxtimes \mu^{\mathrm{ac}}_{\mathrm{IW}} = \mu^{\mathrm{ac}}_{\mathrm{F}}$, as shown in Fig. 5.6. The mass matrix resides in the Jacobi ensemble, specifically defined as a Fisher matrix, representing a generalisation of the one-dimensional Fisher ratio.

Inspired by discussions surrounding models of *kinetic alignment* in well aligned models of axion field inflation, we assume the kinetic metric is now non-diagonal when we begin in the geometric lattice basis. This model represents an extension to the models of N-flation in Section 5.2.4.1, where the Y-matrix mass matrix is now combined with a non-degenerate decay constant spectrum, imposing a symmetric isotropic construction, now defining it as an F-matrix. These models are a form of *double*

Wishart model, residing in the general Jacobi ensemble, acting as an extension to the N-flation matrix model where we not induce the non-trivial kinetic metric. The kinetic field space metric is related to the Kähler metric in supergravity theories, where a first order matrix model of random metrics based on considerations of the complex Kähler geometry has been shown to be well approximated by a Wishart matrix [532, 533]. This can also be found in more traditional approximations made on the kinetic field space metric for non-trivial kinetic mixing [128, 131]. In this model the kinetic metric is defined by an Y-matrix where the perturbed mass matrix is well defined using the F-type ratio relation distributed according to a multivariate F-distribution. Both the decay constants and masses have well defined LSDs, found in Eq. (4.67), shown in Fig. 4.3 and Eq. (4.101), shown in Fig. 4.4 respectively. The introduction of a perturbative measure term to the axion mass matrix in the kinetic basis causes the moments of the universal distributions to be well bounded on logarithmic scales. The LSD moments of the resulting mass spectrum are regulated by the ratio of the two dimensional shaping parameters for each matrix. The strength of the correlations between the physical parameters is determined by the nature of the inverse decay constant factors, which take the role of the models population covariance matrix eigenvalues, as displayed in the example ensemble found in Fig. 5.7.

5.2.5.1.1 Unbroken Symmetry ($\beta_{\mathcal{K}} = \beta_{\mathcal{M}}$)

If we assume the ratio of distribution shaping parameters is unity for the decay constants and mass eigenstates in the initial basis, then after the perturbation from canonical normalisation, the mass spectrum universally converges to a distribution well modelled by its first, second and forth centralised moments on logarithmic scales, i.e. it is skew-symmetric. Changing the value of $\beta_k = \beta_m$ alters the kurtosis of the resulting mass distribution where the distribution remains skew symmetric about the normalised mean scale of the spectral masses. See Fig. 5.6 for a range of example probability density plots for different values of $\beta_k = \beta_m$. These distribu-

tions can be well approximated by a three-parameter family of continuous Pearson distributions, which we approximate and fit by a series of Beta distribution functions to the examples in Fig. 5.6.

5.2.5.1.2 Broken Symmetry ($\beta_{\mathcal{K}} \neq \beta_{\mathcal{M}}$)

When $\beta_k \neq \beta_m$ the third centralised moment of the LSD for $\log_{10}(m_a)$ is sufficiently perturbed to induce a non-negligible skew factor to the resulting mass spectrum. When $\beta_k > \beta_m$ the distribution is positively skewed, when $\beta_k < \beta_m$ the resulting distribution is negatively skewed. These distributions can be well approximated by a four-parameter family of continuous distributions. See the *left panel* of Fig. 5.8 for probability density plots for example mass spectra along with beta distribution function fits.

5.2.5.2 Spiked Kinetic Alignment

The sample mass eigenspace is defined either under the null or alternative formalism, $\mathcal{H}_0/\mathcal{H}_{\mathrm{A}}$ *and then perturbed multiplicatively by a full rank perturbation from a kinetic metric formed from either the null or alternative formalism. The resulting mass spectrum measure contains an absolutely continuous measure component plus either finite number of a point mass measures separated above or below the spectrum support or both.*

These matrices are referred to and generalised as spiked Fisher matrices, where the covariance matrix of either one or both of the sample covariance ratio matrices contains a finite perturbation from triviality [155, 331, 332, 435, 666, 751, 1326] and are common place in numerous classical multivariate statistical tests. Once again, much like the general spiked Wishart matrix, explicit representation of these models is a tricky task, where approximated measure decomposition offers the logical approach for model scanning. In the case of rank 1 spiked multivariate F-matrices the join eigenvalue distribution (unordered) can be expressed in various ways such

as zonal polynomials [748] or contour integral representations [1017].

5.2.5.2.1 Spiked Mass Spectrum

If we choose to model the canonically normalised mass spectrum with possible strong correlations then repulsed eigenvalues could have significant effects with model phenomenology. This model initially defines,

$$\mathcal{K}_{ij} = \mathcal{P}^{-1}\mathbb{X}\mathbb{I}\mathbb{X}^{\mathrm{T}}, \quad \mathcal{M}_{ij} = \mathcal{P}^{-1}\mathbb{X}\Sigma_{\mathcal{M}}\mathbb{X}^{\mathrm{T}} \ , \tag{5.61}$$

where, $\Sigma_{\mathcal{M}} \not\propto \mathbb{I}$. In the limit $\mathcal{N} < \mathcal{P}$ the sample eigenspace is defined by a bulk measure with a finite number of point mass measure mass states. In the limit $\mathcal{N} = \mathcal{P}$ the probability measure recovers the multiplicative convoluted measure $\mu_{\tilde{\mathcal{M}}} = \mu_{\mathrm{MP}}^{\mathrm{bulk}} \boxtimes \mu_{\mathbb{P}}^{\mathrm{bulk}} \equiv \mu_{\mathrm{F}}^{\mathrm{ac}}$, with the largest eigenvalues subject to statistical fluctuations about the upper limit of the measure support. When spikes are present the mass spectrum is defined as, $\mu_{\tilde{\mathcal{M}}} \equiv \mu_{\mathrm{F}} + \mu_{\lambda_+}^{\mathrm{pm}}$, which represents a simple perturbation of the model in Section 5.2.4.1. In the *right panel* of Fig. 5.5 we demonstrate the normalised mass spectra for a range of values of $\beta_{\mathcal{M}}$, where the singular repulsed eigenvalues are of the order, $\mathcal{O}(\mathcal{N}_{\mathrm{ax}})$.

5.2.5.2.2 Spiked Decay Spectrum

The eigenvalues of the kinetic mixing matrix fix the effective decay constant scales of the model, where previous models consider the case of field alignment occurring precisely if one of the associated eigenvalues becomes large [297, 367, 773]. This in the context of our RMT models, is emulated when the eigenvalues which define the effective decay constants from the covariance matrix, fall in the BBP supercritical regime. Consider then the following toy model where we first assume the mass spectrum is initially constructed isotropically, allowing for correlations in the decay

constant scales where,

$$\mathcal{K}_{ij} = \mathcal{P}^{-1}\mathbb{X}\Sigma_{\mathcal{K}}\mathbb{X}^{\mathrm{T}}, \quad \mathcal{M}_{ij} = \mathcal{P}^{-1}\mathbb{X}\mathbb{I}\mathbb{X}^{\mathrm{T}} \ . \tag{5.62}$$

We can either fix a prior on $\Sigma_{\mathcal{K}}$ or draw the elements of the sub-matrices, $\mathbb{X}$ for $\mathcal{K}_{ij}$, according to Eq. (5.52) with $\Sigma_{\mathcal{K}} = \mathbb{I}$, where we have a rank 1 perturbation to the null case. This relates to the use of either centred or non-centred Wishart ensembles for the initial data vectors. The mass spectrum is described by a standard Marčhenko-Pastur bulk with a perturbation placed on the smallest field mass in the initial basis. After canonical normalisation this becomes a point mass measure from the initial outlying decay constant. This eigenvalue in the spectrum, is now negatively logarithmically displaced from the bulk, $\mu_{\mathrm{F}}^{\mathrm{ac}}$. Of course depending on statistical fluctuations a point mass decay constant could perturb a mass state eigenvalue which remains inside the bulk supports if the magnitude of the initial perturbation is small.

5.2.5.2.3 Double Spiked Point Mass Spectrum

This is the generalisation of the model in Section 5.2.4.2 which involves a rotation of a spiked mass matrix, perturbed from the canonical normalisation of a spiked decay spectrum. The outlying eigenvalue in each spectrum retains its separation from the spectral bulk where its separation is logarithmically perturbed either positively or negatively with respect to the bulk separated from the change of basis with a non-trivial metric. The spectrum in this model adopts the features of the models in both Section 5.2.5.2.1 and Section 5.2.5.2.2, where the mass matrix takes the general form,

$$\tilde{\mathcal{M}} = \Sigma_1^{1/2}\tilde{\mathbb{Y}}_1\Sigma_1^{1/2}\Sigma_2^{1/2}\tilde{\mathbb{Y}}_2\Sigma_2^{1/2} \ . \tag{5.63}$$

This model can be formulated in two ways, either with the use of a central Wishart ensemble where both $\Sigma_1, \Sigma_2 \not\propto \mathbb{I}$, or assuming the null hypothesis combined with a non-central Wishart ensemble matrix for both $\mathbb{Y}_1$ and $\mathbb{Y}_2$. The resulting mass

spectrum contains at least two point mass measures, $\mu^{\rm pm}_{\rm spike,+}$ and $\mu^{\rm pm}_{\rm spike,-}$, coming from the spiked mass matrix and kinetic metric respectively. The decay constant spectrum is defined in Eq. (5.50), where the mass spectrum is,

$$\mu_{\tilde{\mathcal{M}}} \equiv \mu^{\rm ac}_{\rm F} + \sum_{i=1}^{\mathcal{R}} \mu^{\rm pm}_{\rm spike,+} + \sum_{i=1}^{\mathcal{Q}} \mu^{\rm pm}_{\rm spike,-} \quad . \tag{5.64}$$

The value of $\mathcal{R}$ represents the rank of the perturbation to the population covariance matrix of the mass matrix minus the total number of population eigenvalues with degeneracy greater than unity plus the number of groups of degenerate values. The value of $\mathcal{Q}$ is the same for the spiked eigenvalues of the kinetic metric. In the limit $\beta_{\mathcal{K}} = \beta_{\mathcal{M}} = 1$ the spikes are absolved in the bulk of the spectrum where the spectrum matches the mass spectrum of the model in Section 5.2.5.1. See the *right panel* of Fig. 5.5 for example density plots for the mass spectrum distribution for various values of $\beta_{\mathcal{K}} = \beta_{\mathcal{M}}$.

5.2.5.3 Correlated Kinetic Alignment

The sample decay constant and mass eigenspace are defined under the alternate formalism, $\mathcal{H}_A$, where either one or both of the sample matrices has a full rank, non-trivial population covariance matrix.

- Constructed in a form closely resembling the examples presented in Section 5.2.5.2, we now allow for the definition of a full rank population covariance matrix with all eigenvalues in the supercritical regime of the BBP phase transition for either the kinetic and mass matrices or a combination of both.

- These examples represent the largest spread in the axion mass spectrum due to the possibility of including uncertainty in the initial mass spectrum, the correlations between mass matrix variables, the decay constant spectrum and the correlations between kinetic matrix variables. Like the case of finite rank data correlations, the mass matrix in the kinetic basis is represented by a

general sample covariance matrix of the form found in Eq. (4.93).

In the limit that either of $\mathcal{Q}$ and $\mathcal{R}$ represent a full rank sum in Eq. (5.64), we can define numerous combinations of models which can be constructed in this general way. The mass matrix takes the form of a sample canonical correlation matrix, more relevant for the type of modelling found in canonical correlation analysis (CCA) [671]. Generally the explicit LSD of the joint distribution for the eigenvalues of F-type matrices is only well defined in the Gaussian case. In a more general setting we must fall back on the nature of the universal convergence of the asymptotic results of free probability to draw inferences in these models. Any combination of the population covariances estimators covered in Section 5.2.4.3.2 could be used for either matrix. The LSD of the axion masses in these models represent the general logarithmic '*Gaussianisation*' of the spectrum, under certain configurations, where the number of convolutions causes the spectra to converge towards normality. In the case that both the kinetic matrix and mass matrix are initially defined with full rank data correlations between variables, the decay constant spectrum is defined as the absolutely continuous measure function, $\mu_{\mathcal{K}} = \mu_{\mathrm{MP}} \boxtimes \mu_{\Sigma_{\mathcal{K}}}$. The mass spectrum is also represented by an absolutely continuous measure function defined in the canonically normalised kinetic basis as, $\mu_{\tilde{\mathcal{M}}} = \mu_{\mathrm{MP}} \boxtimes \mu_{\Sigma_{\mathcal{M}}} \boxtimes {}^{1}/_{\mu_{\mathcal{K}}}$. In the case of finite rank spikes, also present in either spectrum, we simply substitute in the additional point mass functions like the models covered in Section 5.2.5.2, where the matrices represent spiked forms of the most general sample covariance matrices.

5.2.6 Multi-Modality for Extended Sectors of Axion Physics

A very natural extension to the models presented above is to introduce a multi-modal axion mass spectrum measure, motivated by the incorporation of distinct sectors of axion physics appearing in the low energy effective theory. Doing so would correspond to performing a decomposition of the axion kinetic and mass matrix to take a block-diagonal form. This situation would elevate the point mass functions

above to be replaced by absolutely continuous measure functions based on physical model considerations. These probability measures are closely related to mixture models of parametric probability density functions [1104, 1394]. Traditionally these appear as weighted sums of Gaussian component densities [1103], which are also well adapted to Bayesian frameworks [838, 1093]. We must then also naively introduce a further level for the hyperparameters, representing extended draws for the mean scales of each sub-matrix appearing in Eq. (5.65). Phenomenologically these types of models would be well suited to exploring the complete ultralight sector of ad hoc models of a string axiverse landscape, possibly addressing solutions to several paradigm issues at once, such as inflation and DM cosmology, which naturally require a very large separation in the order of magnitude of defining parameters for the model scales. The limiting distributions of the axion parameters are well described using free probability theory in the models presented above, where correlations and or perturbations are allowed between or to the entries, whilst still retaining universal spectral forms [1150, 1151]. Suppose we now expand the space such that we have n axionic sectors, an example phenomenological block diagonal mass matrix would be defined by the direct sum,

$$\mathbb{M} = \underbrace{\mathcal{M}_1}_{\text{GUT}} \oplus \overbrace{\mathcal{M}_2}^{\text{DM}} \oplus \cdots \oplus \underbrace{\mathcal{M}_n}_{\text{DE}} , \tag{5.65}$$

where it is always possible to perform a linear transformation to the basis in which the extended diagonal of $\mathbb{M}$ represents the complete axion mass spectrum of the model. Such random block matrices commonly occur in data modelling when considering large data structures in which the number of observables (*axions*) is sufficiently greater than the number of strata (*axionic sectors*) or $\mathcal{N}_{\text{ax}} \gg n$ in Eq. (5.65). The LSD closely related to the previously mentioned mixture models, determining the full eigenstpectrum of some random non-diagonal block matrices falls under the discipline of operator valued free probability theory, which we leave as a topic beyond the scope of the work covered here [1205].

5.2.7 Initial Conditions for the Canonical Fields

5.2.7.1 Effective Axion Decay Constants

The role of the axion decay constants, for our purposes, will be to fix the natural initial field displacements, in order to analyse features such as the axion relic density from vacuum realignment [13, 458, 1073] (see Chapter 7). Expanding the potential to the mass term alone, the dimensionful scales that control the evolution and relic densities are the initial displacements of the canonical fields. In all cases we set our initial conditions on the axion fields as,

$$\phi_i^{\rm ini} = \mathcal{F}_{ij}\vartheta_j \,, \tag{5.66}$$

for some (random) matrix $\mathcal{F}_{ij}$, where ϑ represents a random vector of elements in the range $[0, \pi]$, which is expected for an initially massless field with a discrete shift symmetry and symmetric potential. We set the initial conditions on ϑ_i to uniformly sample the field space in some basis. We do this in the basis where the ϑ_i form a cubic lattice, adhering to the discussions in Section 5.1.1.1. We uniformly sample in this cubic basis, since this is operationally very simple. However, we note as also detailed in Section 5.1.1.1 this is not a uniform sampling of the field space in the '*charge basis*' defined by the charge matrix, $\mathcal{Q}$, an integer matrix whose entries reside in a charge lattice in the more generalised simplified cosine potential,

$$V(\theta) = \sum_{X,i} \Lambda_X \left[1 - \cos\left(\mathcal{Q}_i^X \theta_i\right)\right] \ . \tag{5.67}$$

We leave investigations of this interesting question, which is intimately related to the notions of alignment and charge quantisation for future work. Other discussions of this point, and sampling of initial conditions in general, see Refs. [128, 130, 499, 500, 915].

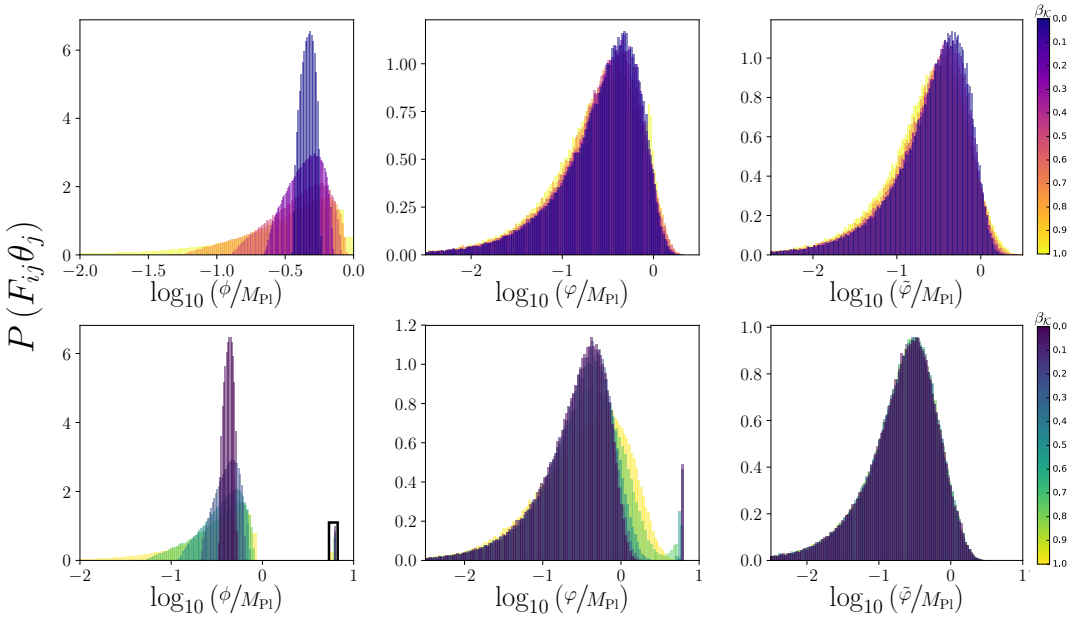


Figure 5.9: Probability density plots for the initial axion field displacements defined in each basis outlined in Eq. (5.14), Eq. (5.69) and Eq. (5.70) for 5000 iterations using $\mathcal{N}_{\rm ax} = 75$. *Upper panels*: Zero centred mean, gaussian distributions used for the elements of the kinetic matrix $\mathcal{K}_{ij}$ (isotropic Y-matrix in Section 5.2.4.1). *Lower panels*: Non-zero centred mean, non-Gaussian distributions are used for the elements of the kinetic matrix $\mathcal{K}_{ij}$ (finite ranked spiked matrix model in Section 5.2.4.2). The highlighted (*black rectangle*) values demonstrate the enhancement of the spectral width in the spiked matrix in the initial basis. As the spectrum is rotated through canonical normalisation the spectra converge to universal forms where the two models eventually harmonise.

5.2.7.2 Sample Basis Scalings

We define the matrix $\mathcal{F}_{ij}$ for two different possibilities for the cubic basis we can initialise our sampling in. These correspond to the geometric lattice and the canonically normalised kinetic basis from Section 5.1.1.2. Consider the set of transformations that turn the initial fields, θ, into the canonically normalised quantities, ϕ, which in index notation defines,

$$\frac{\phi_i}{M_{pl}} = V_{ij}\text{diag}(f_a)_{jk}U_{kl}\theta_l \ . \tag{5.68}$$

In general we should expect that in the cubic basis both $\mathcal{K}_{ij}$ and $\mathcal{M}_{ij}$ are off-diagonal, and so $\vartheta_i = \theta_i$. On the other hand, it could be the case that the cubic

basis is the same basis as the one in which $\mathcal{K}_{ij}$ is diagonal. In that case, it is natural to set $\vartheta_i = U_{ij}\theta_j$. We allow for both possibilities in our numerical explorations, such as those conducted in Chapter 7, as defined relative to each RMT model above. For completeness of discussion, we still seek to define a measure on the initial field displacements that is somewhat equivalent to the usual notion of a 'decay constant'. We define such a measure by the following vector for the most general case of basis rotations,

$$\tilde{\varphi}_i := |V_{ij}\text{diag}(f_a)_{jk}U_{kl}\langle\vartheta\rangle_l| \,, \tag{5.69}$$

where $\langle\vartheta\rangle$ is the vector of $\pi/2$ values representing the average of ϑ. For the case of the cubic basis with diagonal $\mathcal{K}_{ij}$, we define our measure as,

$$\varphi_i = |V_{ij}\text{diag}(f_a)_{jk}\langle\vartheta\rangle_k| \,. \tag{5.70}$$

The overall scale of our initial conditions is set by the eigenvalues of $\mathcal{K}_{ij}$ giving the elements f_a. However, rotations can shift these values on to different canonical fields, allowing for a general *N-flation* type enhancement by the pythagorean sum (see Fig. 5.1 and Fig. 5.2). The initial field conditions defined from f_a for ϕ, $\tilde{\varphi}$ and φ are shown in Fig. 5.9. In the *upper* and *lower left panels* we show the initial field displacements of the general form, $\phi = f_a\theta$, for both example isometric and spiked models where the bulk of the spectrum is initially limited to sub Planck scale values (*upper* and *lower left panels*). The value of ϕ is defined using Eq. (5.66), where $\mathcal{F}_{ij} = \text{diag}(\sqrt{2f_a^2})_{ij}$ such that, $\phi_i = \text{diag}(\sqrt{2}f_a)_{ij}\langle\vartheta\rangle_j$. In the *upper panels* we see that the initial field displacements quickly converge to a negatively skewed distribution on a logarithmic scale, when using an isometric Y-matrix for $\mathcal{K}_{ij}$ (see Section 5.2.4.1). Selecting a new basis identified by a further rotation acting on $\mathcal{F}_{ij}$ does not alter the initial field displacements, where we observe a degeneracy across all values of $\beta_\mathcal{K}$. When a *spiked* Wishart matrix is used for $\mathcal{K}_{ij}$ (see Section 5.2.4.2) the repulsed eigenvalues shown for ϕ, 'enhances' the potential initial field conditions when selecting a new basis for sampling (see discussions in Ref. [750]). Rephrased,

this shows the convergence of the spectra via the unitary rotation perturbations as 'slower' in this model, maintaining features of the initial matrix spectra for $\mathcal{K}_{ij}$. The spectra for each choice of basis is distinct in its output as shown in the *central* and *right lower panels*. In the basis for φ for lower values of $\beta_{\mathcal{K}}$ we maintain the hard edge of the non-rotated spectra (*lower left panel*) with values of $\beta_{\mathcal{K}} \to 1$ providing larger probability densities for field displacement transcending the $M_{\rm Pl}$ limit. The two models universally converge when finally selecting $\tilde{\varphi}$ as the choice of basis.

5.2.8 Random Supergravity and the Superpotential Hessian

5.2.8.1 The Hessian Matrix

It is worth quickly contrasting the RMT models presented above for random axion cosmology, using the effective axion field equations, to the case of scalar parameters drawn from RMT models found in the context of random supergravity and sample vacua from the viewpoint of random Gaussian potentials. The generic final stage of defining the axion states in some general string model, is a minimisation of the superpotential of the form in Eq. (3.28), in order to search for metastable de Sitter vacua. This is an extremely difficult issue when the dimensionality of the problem is large. In previous studies found in the literature there have been excellent attempts to construct models utilising RMT in order to obtain a spectrum of scalar masses coming from a non-supersymmetric vacuum, in a generic four-dimensional $\mathcal{N} = 1$ supergravity theories [873]. These random supergravity theories [125, 127, 290, 909] make use of the ability to map across features of the second order derivates of the superpotential, following the work of Ref. [429], to particular well known random matrix ensembles, in particular the GOE/GUE and LOE/LUE ensembles [909]. Consider a set of critical points, $\mathcal{K}$ which satisfy the critical point equation,

$$\partial_a V|_{\mathcal{K}} = e^K \left(\mathcal{D}_a(F_b)\bar{F}^b - 2F_a\bar{W} \right) = 0 \ , \tag{5.71}$$

defined using the supergravity potential found in Eq. (3.28), where $\mathcal{D}_a$ denotes the appropriate Kähler and geometrical covariant derivative [909]. The superpotential Hessian matrix at these points is defined as [909],

$$\mathcal{H} = \begin{pmatrix} \nabla^2_{a\bar{b}} V & \nabla^2_{ab} V \\ \nabla^2_{\bar{a}\bar{b}} V & \nabla^2_{\bar{a}b} V \end{pmatrix} , \tag{5.72}$$

$$= \begin{pmatrix} Z^{\bar{c}}_a \bar{Z}_{\bar{b}\bar{c}} - F_a \bar{F}_{\bar{b}} - R_{a\bar{b}c\bar{d}} \bar{F}^c F^{\bar{d}} & U_{abc} \bar{F}^c - Z_{ab} \overline{W} \\ \bar{U}_{\bar{a}\bar{b}\bar{c}} F^{\bar{c}} - \bar{Z}_{\bar{a}\bar{b}} W & \bar{Z}^c_{\bar{a}} Z_{bc} - \bar{F}_{\bar{a}} F_b - R_{b\bar{a}c\bar{d}} \bar{F}^c F^{\bar{d}} \end{pmatrix} + \tag{5.73}$$

$$\mathbb{1} \left(F^2 - 2|W|^2 \right) , \tag{5.74}$$

where $Z_{ab} = \mathcal{D}_a F_b$ and $U_{abc} = \mathcal{D}_a \mathcal{D}_b F_c$. For generic compactification models possessing many moduli, the spectrum could approach the limits where it can be suitably defined using classical random matrix ensembles. The eigenvalues of the Hessian matrix in Eq. (5.72) define the squared physical masses of the canonically normalised scalar fields. The general metastability requirement of either Minkowski or de Sitter critical points fixes the ensemble requirement,

$$m^2_{\text{min}} > 0 \ . \tag{5.75}$$

The vacuum statistics which have often had a focus on slow-roll inflation, have been extensively studied with the use of random Gaussian fields [5, 127, 174, 226, 228, 502, 558, 921–924, 1254, 1323, 1372]. The spectrum of example Hessian configurations in Eq. (5.72) have been calculated to various degrees of perturbatively with respect to the GOE/GUE ensemble using the principles of Gaussian random landscapes.

5.2.8.2 An Ensemble Approximation to Random Supergravity

In Ref. [909] both the superpotential and Kähler potential are described by random functions, where the matrix in Eq. (5.72) is constructed using a random matrix model formed from perturbative free convolution operations using a series of matri-

ces residing in the GOE/GUE and LOE/LUE ensembles. See Ref. [290] for discussions where these limits might not hold in explicit flux compactifications. Consider the case of the free convolution Hessian spectrum defined in Ref. [909], defined according to the constituent parts, $\mathcal{H} = \mathcal{H}_{\rm SUSY} + \mathcal{H}_{\rm pure} + \mathcal{H}_{\rm K^{(4)}} + \mathcal{H}_{\rm K^{(3)}} + \mathcal{H}_{\rm Shift}$. It was shown these terms can be well approximated by the free additive convolution, $\mathcal{H} \equiv \text{Wigner} \boxplus \text{Wishart} \boxplus \text{Wishart}$, where the critical points in this ensemble relate to unstable saddle-points. The ensembles found in models of random supergravity often contain a large portion of negative eigenvalues. Metastable de Sitter vacua are therefore generally expected to be a rare occurrence in the use of random potentials, where we must rely on the statistical fluctuations of an atypical system configurations, along with an often complicated assessment of stability. There are however ways in which these spectra can be addressed to relieve these tensions for more general cases of stabilised spectra, i.e. the scale of the F-terms compared to the scale of the supersymmetric masses [909]. In the context of our simplified models for axion cosmology, the mass spectrum of Ref. [909] would most likely require an additional additive free convolution operation of a further Wishart matrix to define the lowest order perturbative model with consistent sampling from some positive definite spectrum. We have of course offered no physical motivates for such a model but use this to highlight the potential structure of models which involve additive convolutions of different ensembles in the invariant sector of RMT, required for positive definite spectra. We leave the fascinating results of random Gaussian landscapes and random supergravity as a topic beyond the scope of any work covered here.

5.3 The M-theory Stochastic Superpotential

Suppose now we wish to model a matrix space, not from the universality of statistical models formed on the grounds of maximised information entropy using classical matrix ensembles, with respect to some weighted polynomial, but from data vectors constructed using theoretical variables directly. Each multivariate model in Sec-

tion 5.2 consisted of a series of statistical parameters assigned to fixing the shape of the models LSD. Now we turn to the case of expanding the superpotential in the M-theory axiverse, introduced in Section 3.3.5 in order to define the form of the axion mass matrix and the properties of the LSD for the fields. As with any approach to the considering a randomised approach to a complex landscape there are a series of general terms which come with theoretical uncertainty we must account for. For the axion fields in the M-theory landscape these are:

- *The superpotential* $W(\Phi_i)$ - This is an arbitrary holomorphic function of superfields that is invariant under the gauge symmetries of the theory with mass dimension *three*. The superpotential describes and encodes non-gauge interactions between chiral multiplets.

- *The Kähler potential* $K(\Phi_i, \tilde{\Phi}^{j*})$ - A supergauge invariant function of the chiral, antichiral and vector superfields with mass dimension *two* which gives rise to chiral kinetic terms and gauge interactions.

- *Gauge kinetic functions* $F_{\alpha\beta}(\Phi_i)$ - A *dimensionless* holomorphic function of chiral superfields which describes kinetic mixing between abelian components of the relevant gauge groups, as well as giving rise to non-renormalisable couplings of the gauge supermultiplets to the chiral supermultiplets.

For general supergravity we need to explore the the non-perturbative superpotential generated by instanton solutions representing our source of how to understand the ultralight scalar sector, which can be expanded to reveal a spectrum of ultralight degrees of freedom forming the string axiverse.

5.3.1 The Random Matrix Axiverse in M-theory

5.3.1.1 M-theory Moduli Stabilisation

Recapping and continuing the discussions in Section 5.2, axions generically arise in large numbers in numerous string compactification models as Kaluza-Klein modes

of antisymmetric tensor fields, often forming a tower of ultra-light scalar states defined by the complicated topology of such theories, which can manifest realistic models of four-dimensional high-energy physics. The shift symmetries stemming from the higher-dimensional gauge invariance of these antisymmetric tensors leave the resulting scalar tower massless to all perturbative orders. We must then turn to specific details of the moduli stabilisation techniques and any possible present non-perturbative instanton solutions, in order to understand the properties of the massive spectrum of ALPs, embedded in testable relativistic supergravity quantum field theories. To do this we will now discuss a random matrix model approach [1221], based on the explicit realisation of the string axiverse found in G_2 compactified M-theory, outlined in detail in Refs. [28, 29, 31], with its low energy theory, described approximated by an effective eleven-dimensional supergravity theory.

It has been shown in the case of M-theory models compactified on manifolds with G_2 holonomy, the moduli can be stabilised in a number of ways. One example consists of models using fluxes of warped geometries to provide suitable moduli sector stabilisation, demonstrating vacua similar to those found in Calabi-Yau flux vacua of type IIA models [21, 26, 117, 186, 401]. Despite the successes of realising a consistent compactified theory, the visible sector phenomenology is generally not of great interest due to the large mass scales fixed by the formalities of the theory, determined by the scale of supersymmetry breaking. This issue can be hierarchically suppressed however if we consider M-theory models compactified with a distinct absence of fluxes, via a non-perturbative superpotential generated by strong gauge dynamics in a hidden sector [25]. In these models, under certain conditions for the hidden sectors, supersymmetry is spontaneously broken in a metastable de Sitter vacuum at significantly lower scales, defining phenomenologies generally more relevant for realistic approaches to embedding supersymmetric GUTs [22, 27, 28, 31, 179].

To look at the resulting spectrum we will begin by reviewing some results for the G_2 Minimal Supersymmetric Standard Model (MSSM), used to define the various relevant potentials highlighted in the beginning of this section, before moving on to

look at how the ultralight spectrum of axionic scalars are stabilised in the theory, resulting in the low energy axiverse scenario. The minimalist approach in the zero-flux sector of the model, which realises a four-dimensional effective theory with $\mathcal{N} = 1$ supersymmetry, is defined by a hidden sector with at least two non-abelian asymptotically free gauge groups, $SU(Q) \times SU(P+1)$, with hidden sector squark superfields fields, Φ and $\tilde{\Phi}$ charged under the $SU(P+1)$ symmetry. In the framework of four-dimensional supergravity, the superpotential is a holomorphic function of the scalar sector of the moduli superfield,

$$z_i = t_i + is_i \ , \tag{5.76}$$

where the real components, t_i denote the axion fields and the imaginary, s_i denote the geometric moduli. The general form of the Kähler potential in Planck units to leading order is [26, 244],

$$K = -3\ln\left(4\pi^{1/3}\mathcal{V}_7\right) + \tilde{K}_{\rm hid}(s_i)\bar{\phi}\phi \ , \tag{5.77}$$

where ϕ represents the scalar component of the squark superfields, $\mathcal{V}_7$ is the volume of the hidden G_2 manifold X and is a homogeneous function of the moduli s_i, of degree $^7/_3$ in units of the eleven-dimensional Planck length, l_{11}, where the positive real numbers of the microscopic parameters specifically follow,

$$\mathcal{V}_7 = \prod_{i=1}^{\mathcal{N}} (s_i)^{\alpha_i} \equiv {}^{\rm Vol(X)}/_{l_{11}^7} \ , \tag{5.78}$$

$$\sum_i \alpha_i = \frac{7}{3} \ . \tag{5.79}$$

The sum in Eq. (5.79) is a constant determined purely by the geometry of the extra spacetime dimensions, which is equal to unity in Calabi-Yau compactifications [33]. The second term in Eq. (5.77) is an adiabatic variant which is generally $\mathcal{O}(1)$ and a homogeneous function of the moduli of degree zero. Defining the axion decay constants by an analysis of the form of the moduli sector, we will for simplicity,

assume that the Kähler potential is dominated only by a single term, taking the generic form,

$$K = -3 \ln \left(\prod_{i=1}^{\mathcal{N}} (s_i)^{\alpha_i} \right) \ . \tag{5.80}$$

The constants of the potential which determine the values of the moduli at the minimum can be determined for specific considerations of G_2 manifold structure. It was shown in Ref. [22] a minimisation of the scalar potential for the moduli can be achieved when all moduli are stabilised with VEVs of the approximate order,

$$\langle s_i \rangle \simeq \frac{M_{\rm Pl}}{10} \ , \tag{5.81}$$

which rectifies the issues surrounding low scale supersymmetry breaking, whilst supplying a sufficiently small cosmological constant. The small cosmological constant determines that the F-terms of the hidden sector meson fields are in general much greater than that of the moduli. The scale of the scalar field masses in the supergravity theory is fixed by the relation,

$$m_{3/2} = \frac{\langle F_\phi \rangle}{\sqrt{3} M_{\rm Pl}} = e^{K/2M_{\rm Pl}} \frac{|W|}{M_{\rm Pl}^2} \ . \tag{5.82}$$

Once supersymmetry has been broken the scale of the gravitino, $m_{3/2}$, is typically used to fix the scales of the scalar sector. At this stage the moduli posses masses such that the lightest modulus field is fixed to the order [34],

$$m_{X_o}^2 = \mathcal{O}(1) m_{3/2}^2 \ . \tag{5.83}$$

In order to replicate successful predictions for standard cosmological thermal histories without spoiling the formalities of Big-Bang Nucleosynthesis, it is expected that the lightest modulus field must have decayed before approximately 10^{-2} seconds after the end of inflation [33, 34]. This fixes a lower bound for the moduli as [519, 780, 1338],

$$m_{X_o}^2 \gtrsim 30 \text{ TeV} \ . \tag{5.84}$$

This requirement that all the moduli must have decayed away before Big-Bang Nucleosynthesis as to avoid excessive matter domination through the energy oscillations of the moduli avoiding the possibility of over closing the Universe is known as the cosmological moduli problem [150, 381, 412]. The standard methods to avoid this issue are achieved with thermal inflation models [884, 961, 1087]. An upper bound can be formed considering the relic abundance of the axions proportional to the gravitino scale required for a suitable DM component. This has been shown to only occur when $m_{3/2} \lesssim 100$ TeV [31] which defines, the phenomenological gravitino mass bound to be,

$$30 \text{ TeV} \lesssim m_{3/2} \lesssim 100\text{TeV} \ . \tag{5.85}$$

An important feature of the Kähler potential is the general assumption it leads to a non-trivial Kähler metric, charactering the spectrum of the low energy sector,

$$\mathcal{K}_{ij} \equiv \frac{\partial^2 K}{\partial z_i \partial \bar{z}_j} \ , \tag{5.86}$$

which in the case of the general effective descriptions already discussed in the previous RMT models in Section 5.2, is directly related to the kinetic mixing matrix, and is a homogeneous function of degree minus two. When we relax the assumption the moduli dependent kinetic terms are defined by complicated functions the simplest form parametrising the non-trivial Kähler metric is,

$$\mathcal{K}_{ij} = \frac{a_{ij}}{s_{ij}} \, , \tag{5.87}$$

where a_i are topological constants and s_i represent the VEVs of the moduli fields as before. We will assume the moduli VEVs can be parameterised by maximal and minimal values we expect the scales of the theory to define, which we denote as $s_{\rm max}$ and $s_{\rm min}$. The results of moduli stabilisation in M-theory show that the moduli VEVs should range between the approximate limits,

$$\langle s_i \rangle \sim (10 \to 100) \ , \tag{5.88}$$

in units of the string scale [22, 28, 29]. It is then natural to assume that our choice of prior should be a uniform distribution,

$$P(s_i) = \mathcal{U}(s_{\min}, s_{\max}) \ , \tag{5.89}$$

where we fix $s_{\min} \approx 10$ and $s_{\max} \approx 100$.

5.3.1.2 Diagonal Kähler Metrics

5.3.1.2.1 A Model for Dark Radiation

Sampling a general metric constructed in the manner of Eq. (5.87), analogous to the techniques found in Section 5.2, does not contain positive real values due to the asymmetry of its elements. When the moduli are randomly assigned between these two limits, analysing the positive real components via the absolute value of the eigenvalue distribution shows this is nothing more than an inverted case of the decay spectrum considered for field alignment in Section 5.2.5.2.2. We will make no assumptions on the topological structure of the manifold, which then fixes the constants,

$$a_i = a_j = 1 \ . \tag{5.90}$$

The non-centred mean of the distributed moduli VEVs defines a susceptibility for a single sharp transition for the smallest eigenvalue to be repulsed far from the bulk spectrum. This is demonstrated for a range of values for the fixed maximum and minimum moduli VEVs in the *right panel* of Fig. 5.10. The alignment of the eigenvalues for the metric in Eq. (5.87) in the eigendecomposition basis, lifts the bulk of the decay constant spectrum scales to values parametrically larger than the mean of the distributed moduli VEVs, the repulsed eigenvalue sitting below the mean scale. It is possible to make a further simplification to the form of the Kähler metric in Eq. (5.87) without any loss of generality in order to derive traceable results and recover the requirement of only real positive eigenvalues for the axion

decay constants. It was shown in Ref. [24] that a large number of axionic degrees of freedom can actually suppress the presence of *dark radiation*, relieving constraints in string axiverse models [87], by shifting the general number dependance of the moduli over to the visible sector couplings, where the dark radiation is now surpassed by Standard Model radiation. Following the discussions of Ref. [24] the general kinetic terms of the moduli theory, with mixing regulated by the Kähler metric, which determines the nature of the visible sector enters the Lagrangian as,

$$\mathcal{L} = \frac{1}{2}\mathcal{K}_{ij}\partial_\mu s^i \partial^\mu s^j + \frac{1}{2}\mathcal{K}_{ij}\partial_\mu t^i \partial^\mu t^j. \tag{5.91}$$

After canonical normalisation of each kinetic term in Eq. (5.91) the Kähler metric is expanded as a function of the moduli fields. The general decay width of the modulus to axionic field channel, $\Gamma(s_i \to t_j t_j)$, using the canonically normalised fields is,

$$\Gamma_{\rm ax} = \frac{1}{32\pi}\sum_{i=1}^{\mathcal{N}}\left(\sum_{j=1}^{\mathcal{N}}\frac{1}{\sqrt{\mathcal{K}_{ii}^{\rm diag}}}\frac{\partial \ln \mathcal{K}_{ii}^{\rm diag}}{\partial s_j}U_{jk}\right)^2 \frac{m_{X_k}^3}{M_{\rm Pl}^2}\ . \tag{5.92}$$

The internal manifold conditions in both Eq. (5.78) and Eq. (5.79) can be translated as conditions placed on the decay width coefficients appearing in Eq. (5.92). The suppression of dark radiation occurs when a non-generic relation between the moduli mass mixing matrix is realised, where the eigenvalues of the Kähler metric satisfy,

$$\sqrt{\mathcal{K}_{ii}^{\rm diag}} \propto U_{ij}\ . \tag{5.93}$$

Here $\mathcal{K}_{ii}^{\rm diag}$ represents the diagonal form of the Kähler metric and U_{ij} is an orthogonal rotation matrix. This suggests it is preferential to initially define the Kähler metric in the form,

$$\mathcal{K}_{ij} \equiv \mathcal{K}_{ii}^{\rm diag} = {\rm diag}\left(\frac{a_i}{s_i}\right) \simeq {\rm diag.}\left(\frac{1}{s_i}\right)\ , \tag{5.94}$$

using the assumptions made on the Kähler metric parameters.

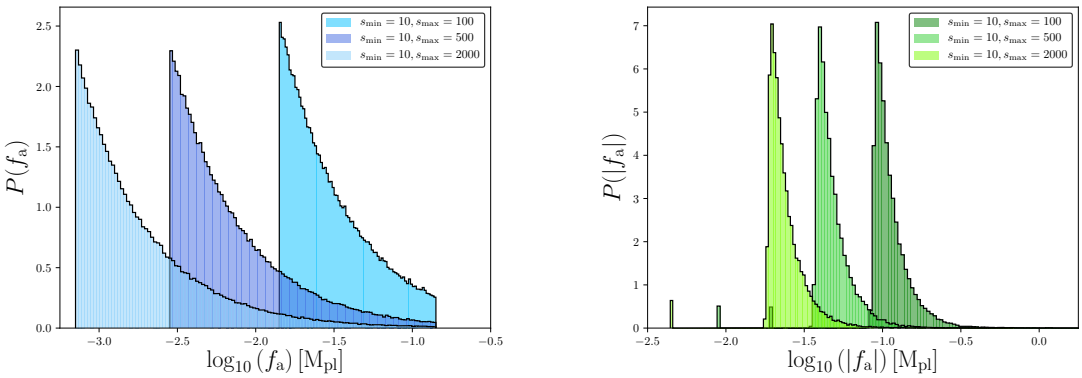


Figure 5.10: *Left panel:* Example axion decay constant spectra defined using the Kähler metric defined in Eq. (5.94) which can be modelled by the prior fit in Eq. (5.96) for various values of the minimum and maximum moduli VEVs parameters, $s_{\min}$ and $s_{\max}$. *Right Panel*: Example spectra of the axion decay constant modulus defined using the non-diagonal Kähler metric in Eq. (5.87) formed with uniform priors for the moduli VEVs. The non-centred mean leads to perturbed eigenvalues from the bulk which give a non-positive spectrum for the squared values of the axion decay constants as the matrix is not defined in the form of a sample covariance matrix.

5.3.1.2.2 The Spectrum of Decay Constants

When the moduli VEVs are distributed between the expected limits from moduli stabilisation, the normalised axion decay constants are now approximately distributed between,

$$f_{a,i} = \sqrt{2}a_i/s_i \sim (10^{-2} - 10^{-1}) \ , \tag{5.95}$$

in units of the string scale. The logarithms of the axion decay constants are modelled by a truncated exponential curve of the form,

$$P\left(f_a\right) = \prod(f_a) \times \mathcal{C}_0 * e^{-(\mathcal{C}_2 * (f_a - \mathcal{C}_1) + \mathcal{C}_3)} \ , \tag{5.96}$$

where the coefficients are fixed by the variance of the moduli VEVs. The truncations are regulated by the boxcar function,

$$\prod(f_a) = \Theta(f_a - f_a^{\min}) - \Theta(f_a - f_a^{\max}) \ , \tag{5.97}$$

where $f_a^{\min} \leq f_a \leq f_a^{\max}$ for $f_a^{\min} \equiv \sqrt{2s_{\min}}$ with $f_a^{\max} \equiv \sqrt{2s_{\max}}$ and $\Theta(x)$ is the Heaviside step function which fully defines the prior on the effective decay constants in the model. In the *left panel* of Fig. (5.10) we display several example spectra under these assumptions for the axion decay constants, drawn from diagonal metrics defined using different value ranges of the $s_{\min}$ and $s_{\max}$ moduli parameters.

5.3.1.3 The M-Theory Random Matrix Mass Spectrum

5.3.1.3.1 Higher Order Instanton Corrections

We can now move on to the sector of the supergravity theory which defines the form of the axion mass matrix. When the model is considered at energies below the confinement scales of the non-abelian asymptotically free gauge groups, the non-perturbative superpotential is defined as,

$$W = M_{\rm Pl}^3 \left(\mathcal{A}\phi^a e^{ib_1 F_1} + \mathcal{B} e^{ib_2 F_2} \right) \ , \tag{5.98}$$

$$a = {}^{2}/_{P_1}; \quad b_{1,2} = {}^{2\pi}/_{P_{1,2}} \ , \tag{5.99}$$

with ϕ the meson superfield of the hidden sector, along with $\mathcal{A}$ and $\mathcal{B}$ representing normalisation constants for a given manifold. The remaining constants come from the dual Coxeter numbers of the hidden sector gauge theory, $P_{1,2} \in \mathrm{Z}^+$, proportional to one loop beta function coefficients of the two gauge groups. The tree-level gauge kinetic functions, F_1 and F_2, are linear combinations of the moduli superfields in Eq. (5.76). These are defined such that the three-cycles for the hidden sector gauge fields are localised to fall inside an identical homology class. This assumption allows for the definition,

$$F_{\rm hid} \equiv F_1 = F_2 = \sum_{i=1}^{\mathcal{N}} N_i z_i = \sum_{i=1}^{\mathcal{N}} N_i \left(t_i + i s_i \right) \ , \tag{5.100}$$

where we have $\mathcal{N}_{\rm ax}$ axion zero-modes formed from the three-form fields of the eleven-dimensional supergravity theory. The integer constants, N_i, are determined from

the topology of the submanifolds which support the hidden sector gauge groups and span the homology class of the three-cycles. The previous components can be used at this point to conduct the laborious task of defining and characterising the full low energy spectrum of the supergravity theory, comprising of both the visible matter and hidden sectors [22, 30]. Instead we will divert and greatly simplify this analysis by using statistical sampling for the defining model parameters, considered as stochastic terms in order to investigate a spectrum of axions. If a series of higher order corrections are added to the superpotential defined in Eq. (5.98), then following Ref. [31] and absolving any previous Planck scale factors the newly defined standard factorised form of the superpotential is,

$$W = \mathcal{A}\phi_1^a e^{ib_1 F_1} + \mathcal{B}e^{ib_2 F_2} + \sum_{k=3}^{\infty} \mathcal{C}_k e^{ib_k F_k} \ , \tag{5.101}$$

where ϕ_1 is a holomorphic composite field made of hidden sector matter fields. The order one constants $\mathcal{C}_k$ are introduced through the high dimensional PQ symmetries. The first two terms come from the same strong gauge dynamics considered in Eq. (5.98), where the equivalent exponent gauge kinetic term factors now represent the process of defining a single linear combination of terms, representing the axion field required to be stabilised in the process of compactification, which occurs at the order defined in Eq. (5.85). The remainder of the axion spectrum is present through the infinite sum generated by higher order instanton effects which define the mass scales to be exponentially suppressed relative to those found in Eq. (5.85), where the spectrum is expected to contain a significant ultralight component. The summation can be truncated at the order of the number of independent axions due to the superfluous non-perturbative sources which can contribute to the Kähler potential, such as membrane instantons or gaugino condensates in order to break the high-dimensional gauge shift symmetries. The higher order $b_{3,4}$ terms in the summation are the instanton integers,

$$b_k = 2\pi I; \quad I \in \mathrm{Z}^+ \ , \tag{5.102}$$

defined under the assumption each of these terms are generated purely by membrane instantons. The associated scales involved in the stabilisation of both the moduli and axions is used to determine the spectrum of ultra-light axions which are free to be stabilised by the sub-leading non-perturbative effects. In the low energy sector of the four-dimensional effective supergravity theory all the moduli superfields possess the required PQ symmetries. Performing an integration over the the moduli and heavy axion combinations determines the spectrum of axions where the relevant effective superpotential takes the form,

$$W_{\rm inst} = \sum_{i=1}^{\mathcal{N}_{\rm inst}} \widetilde{\Lambda}_i^3 e^{ib_i F_i} \, , \tag{5.103}$$

with each term defined by the non-perturbative defining mass scales, $\tilde{\Lambda}_i$. The only terms we need to concern ourselves with are the correctional terms, the membrane instanton integers defined in Eq. (5.102) and the gauge kinetic functions found in Eq. (5.100). Let us reparameterise the generalised volume of the corresponding three-dimensional submanifolds, relevant for the axions, supporting the hidden sector gauge theories required for compactification in eleven-dimensional Planck units,

$$\mathcal{V}_X^i \equiv {\rm Im}(F_k) = \sum_{k=1}^{\mathcal{N}_{\rm ax}} N_i^k s_k = \frac{1}{2\pi} \sum_{k=1}^{\mathcal{N}_{\rm ax}} \widetilde{N}_i^k s_k \, . \tag{5.104}$$

The $\widetilde{N}_i^k$ terms represent the normalised values which regulate the properties of the moduli. The F-term potential in $\mathcal{N} = 1$ supergravity is defined as,

$$V_{\rm F} = e^K \left(\mathcal{K}^{i\bar{j}} \frac{DW}{Dz^i} \frac{D\overline{W}}{D\bar{z}^j} - 3|W|^2 \right) \, , \tag{5.105}$$

where K is the Kähler potential and $\mathcal{K}^{i\bar{j}}$ is the inverse of the Kähler metric defined in Eq. (5.86), where each index runs over the N chiral superfields of the theory. The form of the periodic potentials arise from the interference of the instanton superpotential and the superpotential from other supersymmetry breaking sources, W_0.

5.3.1.3.2 The Expanded Effective Superpotential

Assuming that the scale of supersymmetry breaking is,

$$F \sim \frac{DW_0}{Dz_i}\,, \tag{5.106}$$

this gives rise to the following form of the potential,

$$V \approx F\left(\sum_{i=1}^{\mathcal{N}_{\rm ax}}\frac{\partial}{\partial z_i}\sum_{j=1}^{\mathcal{N}_{\rm inst}}\widetilde{\Lambda}_j^3 e^{ib_jF_j}\right) + \text{c.c.}\ ,$$

which can be re-expressed using the periodic axion instanton potential,

$$V \approx \sum_{i=1}^{\mathcal{N}_{\rm ax}}\sum_{j=1}^{\mathcal{N}_{\rm inst}}\frac{2F\widetilde{\Lambda}_j^3 b_j N_j^i}{M_S}e^{-b_j\sum_k^{\mathcal{N}_{\rm ax}}N_j^k s_k}\cos\left(\sum_{k=1}^{\mathcal{N}_{\rm ax}} b_j N_j^k t_k\right)\ . \tag{5.107}$$

The form of the potential in Eq. (5.107) allows us to present a special type of RMT model motivated by the M-theory axiverse arguments above. As we will see shortly, the matrix structure of the expanded superpotential in the M-theory framework can be constructed in a similar manner to the statistical RMT models, guaranteeing well defined vacua with an absence of tachyonic states for the axion masses. The M-theory axion mass matrix is defined as the quadratic order bare term in the Taylor polynomial of Eq. (5.107),

$$\mathcal{M}_{ij} = \sum_{k=1}^{\mathcal{N}_{\rm ax}}\sum_{r=1}^{\mathcal{N}_{\rm inst}}\frac{4F\widetilde{\Lambda}_r^3 b_r N_r^k}{M_S^3}e^{-b_r\sum_m^{n_{\rm ax}}N_r^m s_m}b_r N_r^i b_r N_r^j\ , \tag{5.108}$$

which takes the factorised form,

$$\mathcal{M}_{ij} = \sum_{r=1}^{\mathcal{N}_{\rm ax}}\frac{4F\widetilde{\Lambda}_r^3 C_r}{M_S^3}e^{-S_r}\widetilde{N}_r^i\widetilde{N}_r^j\,, \tag{5.109}$$

where,

$$\widetilde{N}_i^j = b_i N_i^j\ , \tag{5.110}$$

$$C_r = \sum_k^{\mathcal{N}_{\rm ax}} \widetilde{N}_r^k \ , \tag{5.111}$$

$$S_r = \sum_m^{\mathcal{N}_{\rm ax}} \widetilde{N}_r^m s_m \ , \tag{5.112}$$

and each $\widetilde{N}_i^j$ are rectangular matrices of dimension $\mathcal{N}_{\rm ax} \times \mathcal{N}_{\rm inst}$, purely controlled by the axion population size and the number of instanton terms. The form of the mass matrix in Eq. (5.109) allows us to re-parameterise its structure in the form of a general covariance matrix, represented by a normalised product of two rectangular matrices,

$$\mathcal{M}_{ij} = \frac{1}{\mathcal{N}_{\rm ax}} \mathcal{R}_{ik} \mathcal{R}_{kj} \, , \tag{5.113}$$

with the contracted sub-matrix structure,

$$\mathcal{R}_{ik} = \sqrt{\frac{1}{\mathcal{N}_{\rm ax}}} \left(2 \sqrt{\frac{F \widetilde{\Lambda}_r^3 C_r}{M_S^3}} \right) e^{-S_r/2} \widetilde{N}_r^i \, , \tag{5.114}$$

where each index runs over, $i, j = 1, \ldots, \mathcal{N}_{\rm ax}$ and $k = 1, \ldots, \mathcal{N}_{\rm inst}$. Note that as $\mathcal{R}_{ik}$ is a rectangular matrix of dimension $\mathcal{N}_{\rm ax} \times \mathcal{N}_{\rm inst}$, where the instanton sources defining the higher order correction summation to the superpotential must satisfy $\mathcal{N}_{\rm inst} \geq \mathcal{N}_{\rm ax}$, this implies the traditional distribution shaping parameter, $\beta_{\mathcal{M}}$ must follow $\beta_{\mathcal{M}} \leq 1$. For convenience we normalise the scale of the spectrum by introducing a rescaling of the model parameters so that all the physical model parameters are now considered as dimensionless variables,

$$F \to \frac{F}{M_H^2} \ , \tag{5.115}$$

$$\widetilde{\Lambda}_i \to \frac{\widetilde{\Lambda}_i}{M_S} \ , \tag{5.116}$$

$$\mathcal{M}_{ij} \to \frac{\mathcal{M}_{ij}}{M_H^2} \ , \tag{5.117}$$

$$\tag{5.118}$$

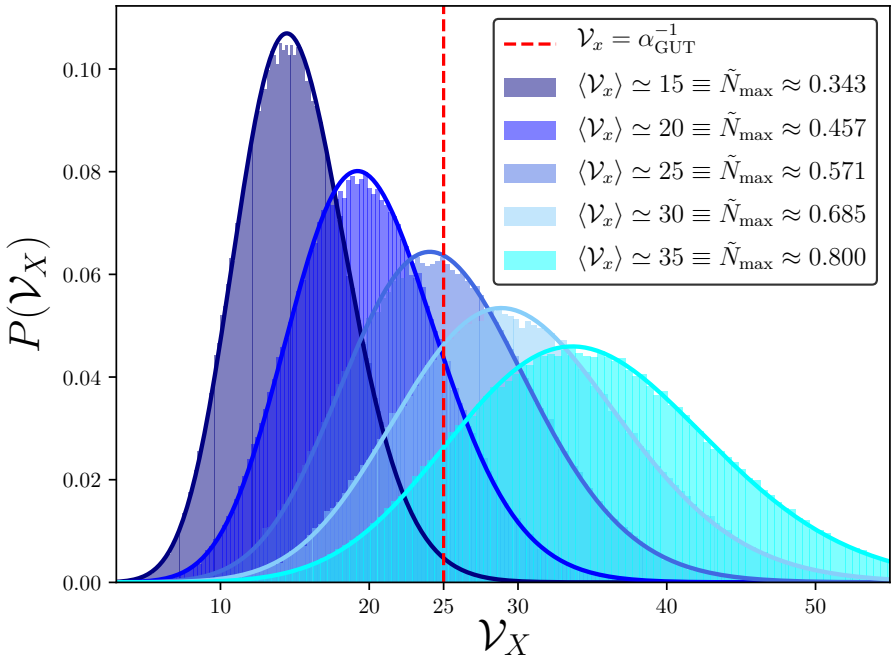


Figure 5.11: Probability density plots for various spectra representing the three-cycle volumes along with Gaussian function fits, each for different values of the average three-cycle volume, $\langle \mathcal{V}_X \rangle$, generated using the corresponding values of $\widetilde{N}_{\rm max} \approx 0.343 \rightarrow 0.8$ with an axion population size, $\mathcal{N}_{\rm ax} = 10$. The moduli VEVs are uniformly distributed between 10 to 100 in units of the string scale, $P(s_i) = \mathcal{U}(10, 100)$. The probability density of retrieving the required GUT unification value, $\mathcal{V}_X \simeq 25$ (*red dashed line*), is enhanced for values of $\widetilde{N}_{\rm max} \approx 0.6$.

where the defining mass scales and coefficients regulating the axion mass matrix are taken as the approximate terms,

$$\widetilde{\Lambda}_i \equiv \Lambda \approx \mathcal{O}(1) \ , \tag{5.119}$$

$$F \simeq 5.4 \times 10^{104} \left(m_{3/2} \text{TeV}^{-1} \right) \ . \tag{5.120}$$

The large value of F is only present and imposed by our choice of units and normalisations. The mass scales in the mass matrix, $\mathcal{M}_{ij}$, are measured in units of M_H for the ultralight scalar sector of cosmology, where the scale of the quantities which define the value of F, come naturally from a general perspective on high energy supersymmetry/string theory physics. These choices are made to account for the

fact that non-perturbative scales are expected to show up around the string scale, possessing a certain element of discretion.

5.3.1.3.3 A Series of Simple Stochastic Variables

The supersymmetry breaking order parameter is approximated using general dimensional analysis to be,

$$F \sim \frac{m_{3/2} M_{\rm Pl}}{M_H^2} \ , \tag{5.121}$$

where the gravitino mass is assumed to at least $\mathcal{O}(1)$ TeV from naturalness arguments, as shown in the arguments of Eq. (5.85). To simplify things in practice, we will use a single variable scale parameter,

$$F\Lambda^3 \sim \mathcal{O}(10^{105}) \ . \tag{5.122}$$

Using Eq. (5.85) and absolving the uncertainly of the non-perturbative physics, which becomes relevant around the string scale, we can define a uniform prior on the theoretical uncertainty,

$$\log_{10}\left(F\Lambda^3\right) \in \mathcal{U}[100;115] \ . \tag{5.123}$$

The final form of the axion mass matrix as a product of stochastic variables is,

$$\mathcal{M}_{ij} = \sum_{r=1}^{N} 4F\widetilde{\Lambda}_r^3 C_r e^{-S_r} \tilde{N}_r^i \tilde{N}_r^j \ , \tag{5.124}$$

where the moduli and axion fields are expressed with respect to the string scale and the membrane instanton integers are now normalised to be fixed to unity ($b_i = 2\pi$). This simplified model of the axiverse mass spectrum is defined using the following variable parameters:

- *Supersymmetry order scale* - $F\Lambda^3$ - Fixed according to the arguments of naturalness and the theoretical freedom found in the phenomenological scales of

Eq. (5.85).

- *Moduli VEVs* - s_i - Uniformly distributed values fixed around the stabilised values of the order found in Eq. (5.81). These are used to fix the scales of decay constants via the simplified form of Kähler metric as demonstrated in the *left panel* of Fig (5.10).

- *Dimensional matrix* - $\tilde{N}^i_j$ - Statistical matrices with random entries which represent a parameterisation of the massless fluctuations of the metric associated to the extra spacetime dimensions. Ideally this should be formulated in order to maximise the probability to reproduce successful grand unification coupling via the required coupling constant found in Eq. (5.127).

A significant factor which must be accounted for in our treatment of a randomised M-theory axiverse, whilst defining the general scales of the theory, is the problematic elements of modulus decay. When the moduli are initially displaced, before they have decayed away, our entire treatment of the axiverse effective theory presented above is not valid, specifically since the Kähler metric in Eq. (5.86) is a dynamical quantity. For our simple treatment to hold, we must consider all axions still in slow-roll in their potential ,after the lightest modulus field X_0 has decayed. This fixes the upper bound on the axion masses as,

$$m_a < \Gamma_{X_0} \approx \mathcal{O}(1)\frac{m^3_{X_0}}{M^2_{\rm Pl}} \ , \tag{5.125}$$

where $m_{X_0} \approx 30$ TeV as defined in Eq. (5.84). This translates to the highest axion mass in the fully stabilised framework limit to be of the order,

$$m_a \simeq 10^{-15} \text{ eV} \ . \tag{5.126}$$

The spectrum of Eq. (5.124) is easy to treat due to the universal nature of the mass eigenstates on logarithmic scales. Analogous to the nature of products of positive random variables, stemming from statistical staples such as the law of large

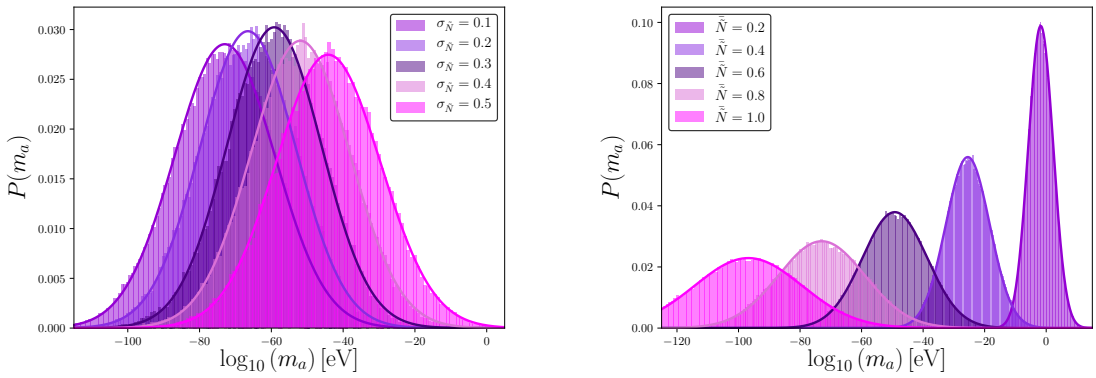


Figure 5.12: *Left panel:* Example M-theory RMT model eigenvalue spectra representing axion masses, m_a constructed using different variance values, $\sigma_{\tilde{N}}$, when using Gaussian priors defined in Eq. (5.129) on the elements of $\tilde{N}^i_j$ along with Gaussian prior fits. Changing the value of $\sigma_{\tilde{N}}$ has the effect of shifting the mean scale of the spectrum across the ultralight sector. *Right panel:* Example M-theory RMT model eigenvalue spectra representing axion masses, m_a constructed using different mean values, $\bar{\tilde{N}}$ when using Gaussian priors defined in Eq. (5.129) on the elements of $\tilde{N}^i_j$ along with Gaussian prior fits. Decreasing the value of $\bar{\tilde{N}}$ has the effect of both reducing the spread of the spectrum whilst increasing the mean value.

numbers, along with numerous other eponymous laws, a Mote-Carlo analysis of the mass matrix shows the limiting spectrum of the M-theory RMT axiverse is approximately log-normally distributed. This is demonstrated in Fig. 5.12, Fig. 5.13, Fig. 5.14 and Fig. 5.15 along with Gaussian fits for each case. Indeed the form of the matrix stricture in Eq. (5.124), representing a Wishart/Gram type matrix ensures we have positive eigenvalues. These converge such that the LSD is well described by the first two centralised moments, which are regulated by both the scales of the model and the theoretical uncertainly placed on the stochastic variables which form Eq. (5.124). The axion mass spectrum is therefore fully defined by considering the theoretical uncertainty placed on the model parameters defined above in the form of statistical priors.

5.3.1.3.4 Simple Physical Considerations for Spectral Moments

Given the form of the universal spectral convergence, we only need to consider the first two centralised moments of the mass spectrum, namely the scale of the mean and the expected degree of spread linked to the variances of the stochastic variables defining Eq. (5.124). Since we are considering M-theory models which represent GUTs in their low energy limits, at least one of the gauge kinetic functions of Eq. (5.104) must give rise to the expected value of the grand unification coupling constant. Supersymmetric theories with gauge coupling unification predict a single visible sector generalised volume to reproduce the required value of $\alpha_{\rm GUT}$ expressed via the relationship,

$$\mathcal{V}_{\rm GUT} \approx \alpha_{\rm GUT}^{-1} \approx 25 \ . \tag{5.127}$$

Drawing inspiration from previous RMT models we can define two example priors on the elements of $\widetilde{N}_i^k$ as,

$$P(\widetilde{N}_i^k) = \mathcal{U}(0, \widetilde{N}_{\rm max}) \, , \tag{5.128}$$

$$P(\widetilde{N}_i^k) = \mathcal{N}(\bar{N}, \sigma_N) \ . \tag{5.129}$$

In the *left* and *right* panels of Fig. 5.12 we demonstrate various example spectra when using the priors defined in Eq. (5.129) to regulate the moduli VEVs. When the distributions are uniform this translates across to fixing a prior directly on the average value of three-cycle volume distribution,

$$\langle \mathcal{V}_X \rangle = \frac{\mathcal{N}_{\rm ax} \widetilde{N}_{\rm max} \langle s \rangle}{4\pi} \ , \tag{5.130}$$

which we can solve given the toy example values of $\mathcal{N}_{\rm ax} = 10$ and $\langle s \rangle = 50$ and using Eq. (5.95), with $\langle \mathcal{V}_X \rangle = 25$ which gives,

$$\widetilde{N}_{\rm max} \simeq 0.57119866428 \ . \tag{5.131}$$

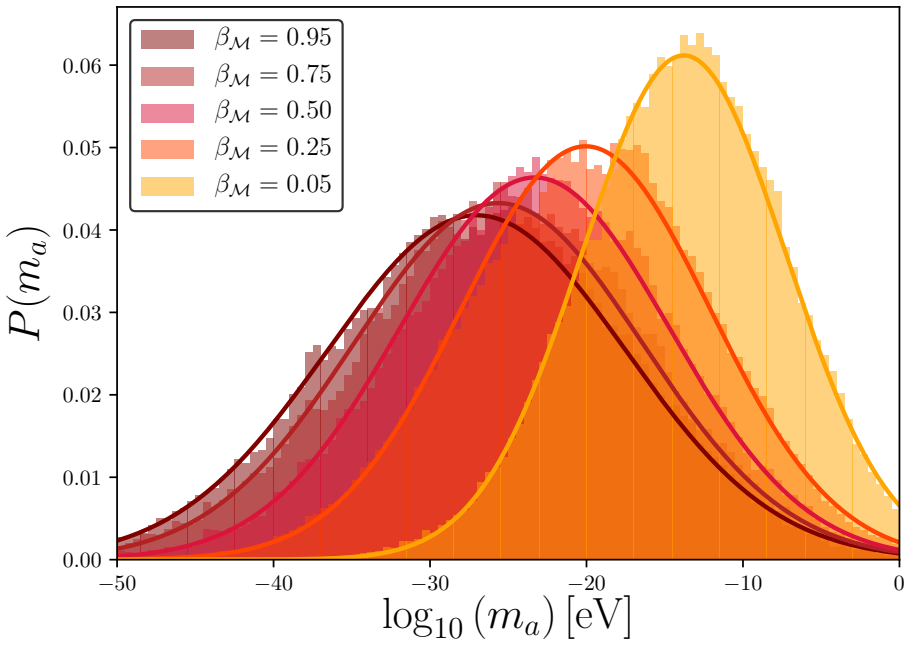


Figure 5.13: M-theory RMT model eigenvalue spectra representing axion masses, m_a for different values of the spectrum shaping parameter $\beta_{\mathcal{M}}$. The mass spectra converge to an approximate log-normal distribution defined by the function in Eq. (5.132) which have been fitted to each example spectrum in the mass eigenstate basis. Each spectrum is constructed using a fixed value of the average three-cycle volume, $\langle \mathcal{V}_X \rangle = 25$ required for GUT scale unification. The spectra are constructed using 10000 iterations in the case of an axion population size, $\mathcal{N}_{\rm ax} = 10$.

In Fig. 5.11 we show the enhanced probability density for retrieving values of $\mathcal{V}_X \approx 25$ when using $\widetilde{N}_{\rm max} \approx 0.6$. Increasing the value of $\widetilde{N}_{\rm max}$ serves to increase the spread of the distributions for $\mathcal{V}_X$, at values centred around $\mathcal{V}_X \gg 25$, which are too high for the requirements of a suitable GUT coupling constant. In each panel in Fig. 5.12 we construct the probability density plots for the axion mass spectrum using 10000 points in the parameter space. In Fig. 5.13 we show the effect of varying $\beta_{\mathcal{M}}$ for fixed values of $\langle \mathcal{V}_X \rangle$ and the effective shift this produces. As $\beta_{\mathcal{M}} \to 0$ it shifts the mass spectrum to be centred around higher mass scales whilst also decreasing the spread of the masses. In these configurations we see axion masses covering many orders of magnitude, which is a key result common in many string axiverse models. Of course these brief examples only give a very simplistic picture of the scales and

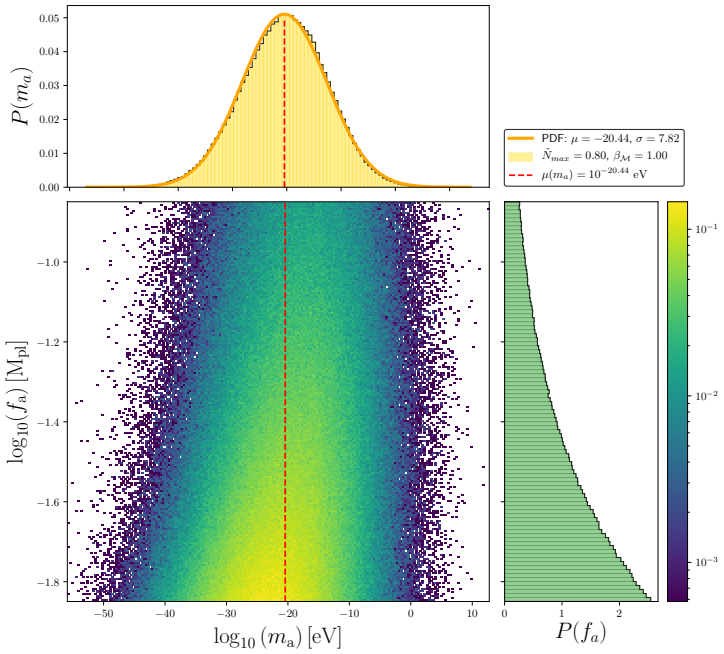


Figure 5.14: Single example mass spectrum and decay constant spectrum for the M-theory RMT model using a fixed value of the spectrum shaping parameter $\beta_{\mathcal{M}} = 1$. *Left panel*: The mass spectrum converges to an approximate log-normal distribution shown by the Gaussian fit on the logarithms of the mass states. The value of $\tilde{N}_{\text{max}}$ is fixed to 0.8 ensuring the mass spectrum is centred close to the phenomenological mass scales of FDM, $\mu(m_a) \approx 10^{-20.5}$ eV. *Right panel*: Example decay constant spectrum using the Kähler construction of Eq. (5.94) with the values $s_{\text{min}} = 10$ and $s_{\text{max}} = 100$. *Central panel*: Density plot normalised to unity, represented by the logarithmic colour bar on the far right, representing the correlation between the axion decay constants and the masses in the M-theory RMT model. Due to the simplified construction of the matrix defining the axion decay constants the correlation is limited, shown by the minor skew about the mean mass scale represented by the *red dashed* line.

form of the spectrum we find using this type of stochastic analysis. The number of model variables leads to a general mass spectrum well understood by the function,

$$P(m_a^2) = \frac{1}{\sqrt{2\pi\sigma^2}} \exp\left[\frac{-\log_{10}(m_a/\bar{m}_a)^2}{2\sigma^2}\right] . \tag{5.132}$$

This is nothing more than a log-normal continuous probability distribution, representing the Gaussian type convergence of the logarithm of the axion masses. The values of $\bar{m}_a$ and σ are fixed according to linear combinations of the parameters

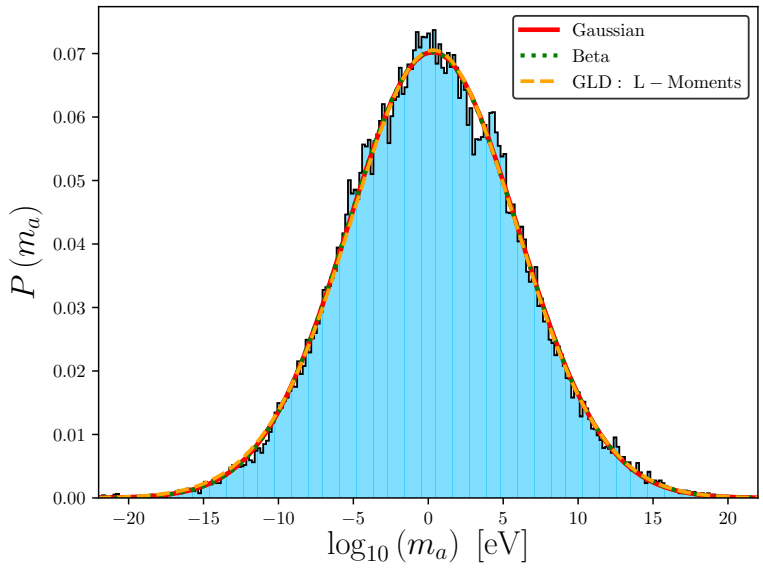


Figure 5.15: Example mass spectra in M-theory RMT axiverse as found in Fig. 5.14 normalised to shift the mean scale to unity. We demonstrate the nature of universal convergence of the mass spectra in this model to be well described by its first two centralised moments. The logarithm of the spectrum is fitted with a Gaussian density fit (Eq. (5.142)), a Beta distribution function (Eq. (G.6)) and GLD distribution using the method of L-moments (Eq. (H.2)). All of these converge when modelling the peak and tails of the distribution, representing a redundancy in using more complicated distribution families which can model the higher moments.

discussed above. We can assume that any theoretical uncertainty of our model is convergent and encoded in this simple two-parameter family prior, which lends itself nicely to generalisations of priors using random matrix models.

5.4 Unimodal Priors for the String Axiverse

5.4.1 Algebraic High-Dimensional Matrices

The main narrative of this work will ultimately not concern itself with a specific detailed treatment of the LSD for each class of matrix model we have introduced. Given the form of each matrix, we can of course derive explicit results for the density functions associated to either the axion mass eigenstates or decay constant spectra.

These generally consist of using more sophisticated techniques such as saddle point analysis [418, 419], for extremal values or algebraic methods to asses the LSD of invariant ensembles [1092]. This is well enforced using the theory of free probability covered in Section 4.4 and our use of rotationally invariant ensembles in the initial basis of the field equations. In particular the polynomial methods in Ref. [1092] make use of the transforms defined in Section 4.1.6.1, as interconnected bivariate polynomials in order to understand a class of algebraic matrices. We have already covered a particular example of this in Chapter 5.2.8, namely the decomposed RMT Hessian found in Ref. [909], demonstrating the ability to effectively implement convolutions incorporating well defined spectral functions, under the manipulation and definition of polynomials via the relevant Stieltjes transforms (Eq. (C.1)) [1092]. For details of the possible complexity of such functions along with alternative methods to define explicit functions and the general ability to define positive density spaces, which highlight the fascinating relationship between combinatorial number sequences and measure densities, see the discussions in Appendix E. A matrix is algebraic if it satisfies the condition that the Stieltjes transform (Eq. (C.1)) of its LSD function is algebraic, whilst also satisfying a bivariate polynomial equation, $L_{mz}(m, z)$ [1092]. If we satisfy the general solution $L_{mz}(m_\mu(z), z) = 0$, then we can define an algebraic random matrix with a limiting measure which falls inside a family of algebraic distribution functions.

Given that all the moments of an algebraic probability distribution exist, then they can be numerated efficiently. Specifically the moments of all order should exist if the distribution is compactly supported. For any of the non-commutative canonical operations introduced in Section 4.4.2, associated to free asymptotics, any algebraic random matrix along with a matrix possessing unitary invariance will always produce a further algebraic random matrix. The most general case of any sample covariance matrices we consider are therefore always algebraically representable. The algebraic densities are associated to the liming deterministic Borel measures in the large $\mathcal{N}$ limit. In Ref. [1092] they associate these operations to produce

algebraic probability distributions which form a semi-group. This semi-group consists of bounded functions which implicitly encode free convolution operations into polynomial functions. Rather nicely though for our simple examples we consider, the limiting moments converge sufficiently when we perform a change of scale to model our variables, from linear to logarithmic, defined in Eq. (5.22), Eq. (5.23) and Eq. (5.24). The discussions above represent powerful tools and vital results in order to form strong statements on the resulting limits of complex systems. These results can however, remain computationally bulky when we wish to apply them to a large region on the parameter space for various phenomenological analyses across multiple models. We can for the purposes of a simple evaluation, using Bayesian type methods, approximate the explicit algebraic LSD a stage further with well known families of statistical distributions controlled by a number of *shaping* parameters. Working with the general Lebesgue decompositional form of the limiting measure function, we assume only the presence of point masses and an absolutely continuous functional bulk for the eigenvalues. We can best approximate where necessary, depending on the model, the form of the statistical fluctuations and positions of the point masses representing model spikes, with the relevant functions, i.e. Tracy-Widom or Gaussian etc. The bulk in each of our models possesses a unique mode, where the LSD is strictly monotonically increasing/decreasing, below/above some singular functional peak. In order to best understand the space we are operating in, at least quantitatively, we can analyse the nature of the distribution moments of the unimodal spectra in Section 5.1.2, Section 5.2 and Section 5.3 in order to asses the degree of asymmetry about the defining physical scales and the nature of any outliers in the distribution tails.

5.4.2 Classification of Spectral Moments

The unimodal models of the RMT axiverse each possess well defined limiting distributions, whose explicit forms can be constructed from many of the successful results

spanning the field of RMT. Specifically for the axion mass spectra, both the Class I and Class III models are well defined by the nature of LSDs. Class I is simply a uniform prior function, under the assumptions to model scale invariance. Class III converges sufficiently quickly to be well modelled by two moments, the phenomenological scale, and spread from the theoretical uncertainty, sufficiently modelled using a Gaussian prior. Class II and the RMT axiverse possess more flexibility in how we configure the initial matrices and subsequently the approximated LSD priors. The CLTs of RMT do however allow us to make rather bold assumptions based on the convergence of moments and the universal forms which arise on logarithmic scales. We are therefore assigning a simplified best fit model to limiting form of μ^{ac} in each of the introduced models. The n^{th} centralised moment about the mean of a continuous univariate distribution is defined as,

$$\mu_n = \mathbb{E}\left[(X - \mathbb{E})^n\right] = \int_{-\infty}^{+\infty} (x - \mu)^n f(x) dx \ . \tag{5.133}$$

In order to render the moments as scale invariant quantities we must consider the standardised moments, where the superscript, n is replaced with a normalisation factor, $n = k = {}^{\mu_k}/_{\sigma_k}$, that ensures the moments are homogeneous functions of degree k. Now defined as dimensionless quantities, these represent the standard approach taken to compare the resulting shapes of distribution functions. By definition the first and second order standardised moments are zero and one respectively. We can also define the higher order moments of the considered function, the third and fourth standardised population moments which are expressed as a measure of the Fisher-Pearson skewness and kurtosis respectively,

$$\sqrt{\beta_1} = \text{Skew}\left[X\right] = \mathbb{E}\left[\left(\frac{X - \mu}{\sigma}\right)^3\right] = \frac{\mu_3}{\sigma^3} = \frac{\mathbb{E}\left[(X - \mathbb{E})^3\right]}{\left(\mathbb{E}\left[(X - \mathbb{E})^2\right]\right)^{3/2}} = \frac{\kappa_3}{\kappa_2^{3/2}} \ , \tag{5.134}$$

$$\beta_2 = \text{Kurt}\left[X\right] = \mathbb{E}\left[\left(\frac{X - \mu}{\sigma}\right)^4\right] = \frac{\mu_4}{\sigma^4} = \frac{\mathbb{E}\left[(X - \mathbb{E})^4\right]}{\left(\mathbb{E}\left[(X - \mathbb{E})^2\right]\right)^2} = \frac{\kappa_4}{\kappa_2^{4/2}} \ , \tag{5.135}$$

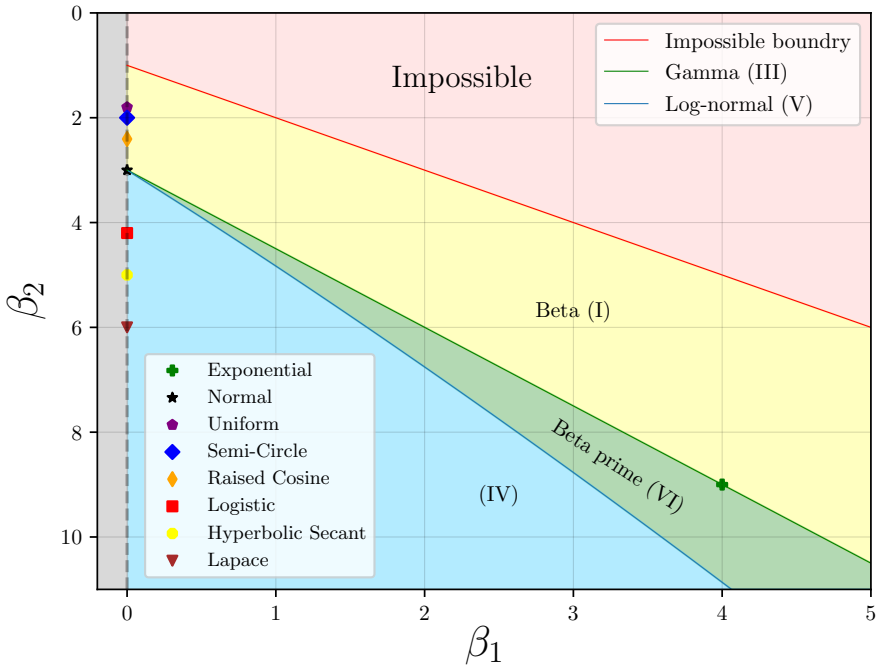


Figure 5.16: Pearson limit curves for the moment ratios for skew and kurtosis define in Eq. (5.134) and Eq. (5.135) respectably. The impossible region is defined by the function line, $\beta_2 = \beta_1^2 - 1 = 0$. Each two parameter distribution family are represented by a data point in the space. We display a series of well defined symmetric distributions defined by two parameters or less which sit on the line, $\beta_1 = 0$. The Pearson family types which require a parameterisation of three variables define a series of contour limits in the space. These limits then define bounded regions in the β_1, β_2 plane corresponding to the four parameter distribution families.

where κ_i are the i^{th} cumulants. The kurtosis is bounded from below by the squared skewness relation,

$$\frac{\mu_4}{\sigma^4} \geq \left(\frac{\mu_3}{\sigma^3}\right)^2 + 1 \ , \tag{5.136}$$

with the lower limits fixed by the Bernoulli distribution and its upper value unbounded. It is common to normalise the kurtosis coefficients by defining the *excess kurtosis*,

$$\beta_2^{\text{exc}} = \beta_2 - 3 \ , \tag{5.137}$$

where the normalisation value of 3 comes from the standard result coming from a Gaussian distribution. The coefficients β_1 and β_2 are often referred to as the Pearson

moment coefficients of skewness and kurtosis respectively. In general the higher order moments are not sufficiently suppressed in order to ignore their presence. Let us consider the model presented in Section 5.2.5 as a toy example. Assuming a non-trivial kinetic matrix and mass matrix, when we impose the symmetric constraint, $\beta_{\mathcal{K}} = \beta_{\mathcal{M}}$ then β_1 becomes a sufficiently negligible parameter, and the distribution of the axion parameter logarithms are well accounted for with the first, second and forth standardised moments. When the symmetry is broken, $\beta_{\mathcal{K}} \neq \beta_{\mathcal{M}}$ then β_1 is sufficiently perturbed from zero and must be accounted for, incorporating standard errors. The decay constant spectra are generally defined by well known limiting distribution laws under some assumption placed on the covariance matrix used for the kinetic matrix, such as isotropy or a particular prior on the data covariance. The mass spectrum is not well defined in such a way. There is normally a form of additive and/or multiplicative convolution of the limiting spectral functions to define the mass eigenstates. When the dimensions of the sub-matrices for the kinetic and mass matrix are equal, the mass spectrum is approximated using a three parameter family of distributions, consisting of predominately platykurtic density functions. The correct measure of kurtosis guides the distribution peak but more importantly enforces the outliers are correctly modelled, which is important given the potential sensitivity field masses can have on the considered phenomenology. In general the empirical fit of most spectra when compared to a convergent function under the assumptions of Gaussianity will break the Dyson-Finucan condition [420], i.e. cross the density function twice in the given interval corresponding to a poor fit for the peak and tails. In the RMT axiverse we will, in general, not expect to realise the simplistic limit where Eq. (5.137) equates to zero, within standard errors, and so more freedom in the prior shape makes sense on these grounds.

5.4.2.1 The Pearson Density System

As the total spectrum or spectral bulk of any of the RMT distributions constitute unimodal continuous probability functions these can then be well understood using

the Pearson classification system for parametric families of distributions. This is appealing as a process of model simplification on the grounds that the choice of priors on the axion space directly effects the centralised moments, which posses a direct correspondence to the distribution (hyper)parameters. Normalising the first and second distribution moments, the limiting distributions can be categorised according to the two moment ratios found in Eq. (5.134) and Eq. (5.135). The systematic basis for this classification depends on the solutions of Eq. (5.138). Although the matching of specific functions is in general somewhat more involved [80, 1031], the classical approach is more than sufficient for a general classification and definition of a suitable function to approximate the models probability measure. Any Pearson density is defined as a solution to the differential equation [1028–1030, 1032],

$$\frac{f'(x)}{f(x)} = \frac{P(x)}{Q(x)} = \frac{x-a}{\mathcal{A}_0 + \mathcal{A}_1 x + \mathcal{A}_2 x^2} \ , \tag{5.138}$$

where the moment-parameter relations are defined as,

$$\mathcal{A}_1 = a = -\frac{\mu_3\left(\mu_4 + 3\mu_2^2\right)}{10\mu_4\mu_2 - 18\mu_2^3 - 12\mu_3^2} = -\frac{\sqrt{\mu}_2\beta_1(\beta_2+3)}{10\beta_2 - 18 - 12\beta_1^2} \ , \tag{5.139}$$

$$\mathcal{A}_0 = -\frac{\mu_2(4\mu_2\mu_4 - 3\mu_3^2)}{10\mu_4\mu_2 - 18\mu_2^3 - 12\mu_3^2} = -\frac{\mu_2(4\beta_2 - 3\beta_1^2)}{10\beta_2 - 18 - 12\beta_1^2} \ , \tag{5.140}$$

$$\mathcal{A}_2 = -\frac{(2\mu_2\mu_4 - 3\mu_3^2 - 6\mu_2^3)}{10\mu_4\mu_2 - 18\mu_2^3 - 12\mu_3^2} = -\frac{(2\beta_2 - 3\beta_1^2 - 6)}{10\beta_2 - 18 - 12\beta_1^2} \ . \tag{5.141}$$

The root solutions of the relevant polynomials classify twelve distinct families of distributions, covering a large region of the two dimensional skew-kurtosis parameter space as shown in Fig. 5.16. In Fig. 5.16 we display this two dimensional moment space along with the limiting values of the two (*point*), three (*line*) and four (*area*) parameter density families familiar in statistical analysis, using the Pearson coordinate system, defining six types of function we could select.

Using the symmetry properties of the 30,108 distinct Hodge pairs from the Kreuzer-Skarke list, for the four-dimensional reflexive polytopes that were briefly covered in Section 3.3.6 as a proxy prior, we can demonstrate the possible behaviour of the

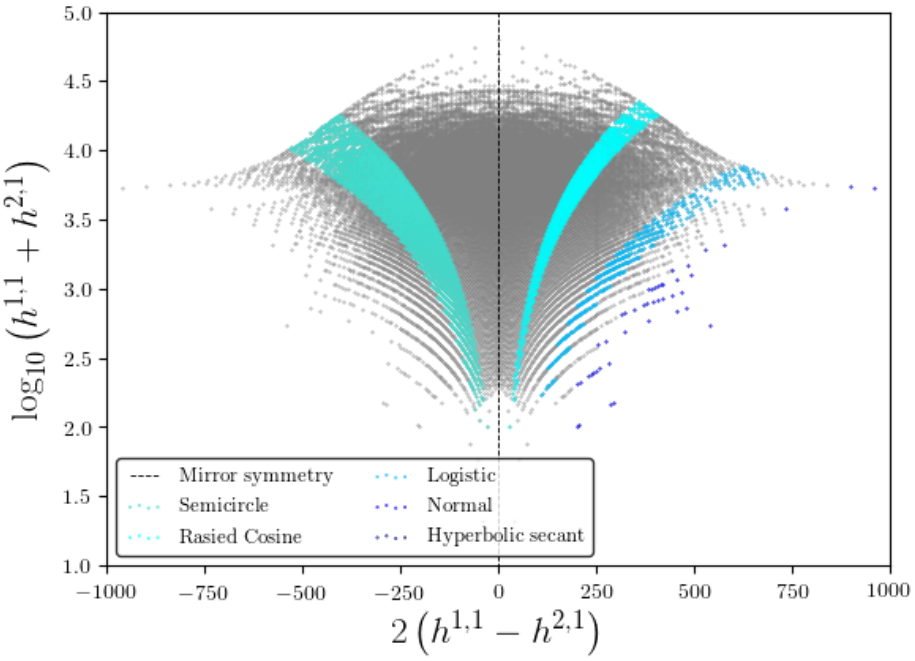


Figure 5.17: Hodge fountain for the distributions of the topological invariant Hodge numbers $h^{1,1}$ and $h^{2,1}$ using the Euler number and additive height. The mirror symmetry is realised at Euler number, $\chi = 0$. Each of the banded segments superimposed denotes the manifest forms of the distributions for the spectra of $\log_{10}(m_a)$ using the model in Section 5.2.5 when the distribution symmetry parameters are defined as equal. The selected distributions represent unimodal bounded for the kurtosis of well defined functions. The sum of the shaded regions approximate the total fraction of the spectra which related to symmetric functions about their mean.

universal convergence of the axion mass spectrum. We do this by plotting moment ratio classification for the standard Pearson families in the limit $\beta_1 \simeq 0$. In Fig. 5.17 we show the approximate fraction of symmetric density functions by plotting the Euler characteristic against the logarithm of the total moduli dimension (minus the dilaton) using a sum of the topological invariants, forming a *Hodge fountain*. Superimposed are various approximated mass distributions we can associate to the model symmetry condition limit, $\beta_{\mathcal{K}} = \beta_{\mathcal{M}}$ which fall within the bounds of certain well defined platykurtic, mesokurtic and leptokurtic density functions defined by two parameters or less, up to standard errors on the kurtosis coefficient. The platykurtic

region crosses well into the positive domain of the Euler number where gaussianity or the mesokurtic region is found around $\beta_{\mathcal{K}} = \beta_{\mathcal{M}} \gtrsim 0.85$. This indicates a majority of the LSD functions will congregate inside the limits requiring $n_{\text{params}} > 2$ for our choice of approximate distribution. This is shown exactly in Fig. (5.18), using the method of moments to approximate the first four moments of ten-thousand spectra datasets for various ratios of ${}^{\beta_{\mathcal{K}}}/_{\beta_{\mathcal{M}}}$. When the magnitude of separation between $\beta_{\mathcal{K}}$ and $\beta_{\mathcal{M}}$ is large the distributions saturate inside the Type I region and converge asymptotically towards a limiting boundary point of a semi-circular distribution. As the ratio approaches unity, the distributions approach the gamma function contour boundary, where we see statistical fluctuations into the Type VI region. As the symmetry property is realised between the two shaping parameters the spectra converges towards the limit $\beta_1 = 0$, between the approximate bounded points representing a logistic and Semi-Circular distribution. In the large $\mathcal{N}$ limit most spectra are well bounded by the log-normal contour, where the finite sampling is generally responsible for data point fluctuations into the Type IV region. It's clear from Fig. (5.18) the RMT axiverse can be well modelled by the family of Beta distributions, where the priors of the distribution functions directly relate to the hyperparameters of the normalised parameter space, a manifestation of the bounded nature of the spectral radii for the eigenvalues. See Appendix G for a formal definition of the Beta function parameterisation and a short summary of the defining features of the general family of Beta functions. Using the standard Beta distribution, Beta(ξ, χ), defined in Eq. (G.4), confined to the limiting normalised support, $\lambda \in [0, 1]$, we can recover the following well-defined function limits which relate to previously discussed specific cases:

1. Beta(1,1) - Uniform distribution $\sim$ Scale invariant prior.
   (a) No points of inflection, $\beta_2^{\text{ex}} = -{}^6/_5$
   (b) Relevant for discussions found in Section 5.1.2.
2. Beta($^3/_2$,$^3/_2$) - Semi-elliptic distribution $\sim$ Wigner semi-circular limit.

   (a) Singular point of inflection, $\beta_2^{\text{ex}} = -1$

   (b) Relevant for discussions found in Section 5.2 for spectral limits where $\beta_{\mathcal{M}\to 0}$.

3. Beta(>2,>2) - Bell shaped distribution $\sim$ Unimodal Pearson Type I function.

   (a) Dual points of inflection, excess kurtosis - $\beta_2^{\text{ex}} \geq -\frac{6}{7}$

   (b) Relevant for discussions found in Section 5.2 relating to the bulk component of the spectral measures. Also when the parameters $\alpha, \beta \gg 1$ the functions converge to the limits of the distributions discussed in Section 5.3.

4. Beta(∞,∞) - Degenerate function $\sim$ Point mass representing a Dirac delta spike at the mean of distribution support.

   (a) Excess kurtosis - $\beta_2^{\text{ex}} \to 0$

   (b) Relevant for discussions found in Section 5.2 for the spiked outliers of correlated spectral eigenvalues.

These functions represent a good first order approximation of the measure probability functions defined from the convolution operations in Section 5.2, associated to perturbed random matrices. Indeed it is sometimes not possible to define the Voiculescu transform in Eq. C.4 explicitly, where the technical analysis can become very tricky. The Beta distributions also share a strong relation to features of free probability such as infinite divisibility (see Appendix F) [195, 672], within the limits defined above, containing the affine transformations of both Wigner's semicircle law and the free Poisson law [672]. To ensure the distributions moments are well accounted for we can compare the spectral fits to a family of distributions well known for its flexibility in modelling the first four distribution moments. The generalised lambda distribution (GLD) family offers an effective way to model functions which could exhibit both heavy-tails and skewness. See Appendix H for a detailed introduction to the GLD family of functions. For both the RMT M-theory model and

the statistical RMT axiverse we show comparisons for the the use of prior function approximations for the model mass spectrum in Fig. 5.15 and Fig. 5.19 respectively. The most extreme case of maximal kurtosis for standard symmetric densities occurs when $\beta_{\mathcal{K}} = \beta_{\mathcal{M}} = 1$. We find the best fit using the method of L-moments for a GLD function and shown in the *left panel* of Fig. 5.19. The closest limiting Pearson distribution which provides a good fit is given by a Hyperbolic secant function, which provides a good account of the spectral peak. The Gaussian function represents an approximate space in the Beta function parameterisation, which offers a fairly sufficient first order approximation of the limiting spectrum. Likewise in the *right panel* of Fig. 5.19, we show how Beta distributions can sufficiently match GLD L-moments modelling, for both the logarithmic spectra of the well defined Marčhenko-Pastur (Eq. (4.67)) and first order Fuss-Catalan (Eq. (E.9)) functions, used to define examples of possible axion decay constant spectra. Finally in Fig. 5.15 we show the CLT type convergence of the stochastic variables spectra, which converges sufficiently so that each of the considered functions are almost indistinguishable for the M-theory mass spectra, when using a L-moments GLD function, Beta function and Gaussian function. With this process we have encoded the minimal information and model uncertainly in the freedom to choose a series of simple distribution shaping parameters, which can account for the first four moments of the models limiting spectrum. For simplicity and a unified approach when accounting for each class of model we propose a further general simplification.

5.4.3 Unifying the Model Classes

We have seen in the previous section that the convergence of the mass spectrum is more generally such that we require a four-parameter family of distributions to model the LSD of the axion masses effectively. If we assume in general the decay constant spectra can be defined using some model with the null hypothesis, or well defined covariance estimations, the functional space is explicit from the limiting laws

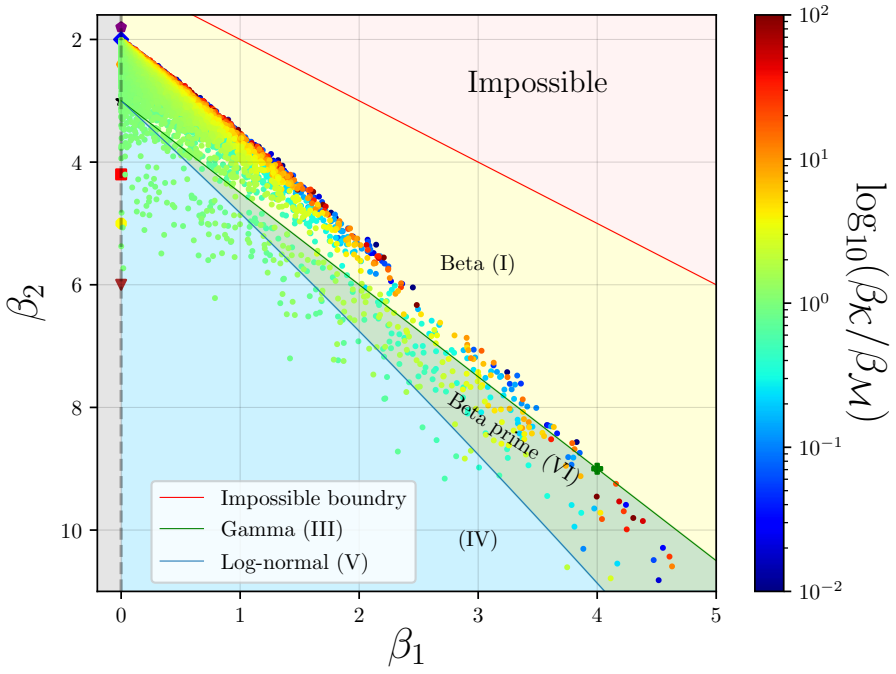


Figure 5.18: Pearson window for valid values of the distribution skew and kurtosis moments. The impossible region is defined by the line function, $\beta_2 = \beta_1^2 - 1 = 0$. Each two parameter distribution family is represented by a fixed data point in the space. The three parameter families define the contour limits, where the four parameter families define the shaded area regions bounded from the three parameter family contours. The overlaid points relate to spectra datasets for different mass spectra found using the model of Section 5.2.5 for various ratios of the distribution shaping parameters, $\beta_\mathcal{K}$ and $\beta_\mathcal{M}$. For most values of this ratio the resulting mass distribution can be well modelled by either a Beta function of the first or second kind.

of RMT. We then only need to make a simplistic approximation for the axion masses in this case. The complexity of the distribution family used to describe the axion mass spectra when considering fixing priors for the axion phenomenology defines the number of hyperparameters of the effective model.

5.4.3.1 Resorting to Normality

The simplest case we can consider, which uses each of the model class frameworks, involves reducing the dimensions of the distribution parameter space to its minimum.

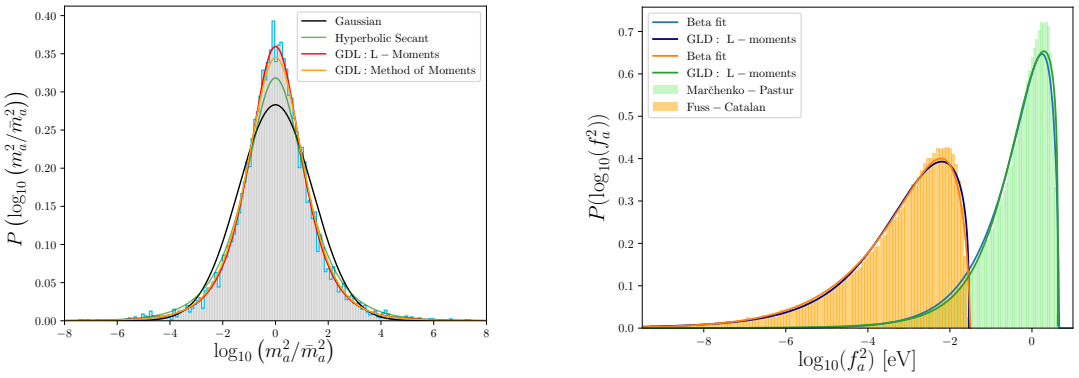


Figure 5.19: Comparative fits for example mass and decay constant spectra using both simplistic priors as well as the GLD determined using various methods. *Left panel*: Normalised mass spectra from the model outlined in Section 5.2.5 for the case where $\beta_{\mathcal{K}} = \beta_{\mathcal{M}} = 1$. The GLD defined by using the method of L-moments (Eq. (H.2)) provides the best fit to the distribution peaks and tails. The worst fit is the Gaussian function (Eq. (5.142)) which provides a good first order approximation but misses several characteristic features of the LSD for the axion masses. *Right panel*: Logarithmic spectra for both the Marčhenko-Pastur density spectra and first order multiplicative convolution of two Marčhenko-Pastur spectra representing the decay constant distributions arbitrarily normalised to two separated scales. Each spectrum is fitted with both a Beta function fit and a GLD function determined by the method of L-moments which to a first order approximation are sufficiently similar.

By isolating our analysis to consider just the mean scale of the spectrum along with its spread or variance, we replace the dependance of the complete model shape parameters with two independent vague proper priors on the location and scale of the distribution. The simplest case in terms of conducting an analysis to model these two features, is with the use of a Gaussian distribution,

$$f(x|\mu,\sigma^2) = \frac{1}{\sqrt{2\pi\sigma^2}} e^{-\frac{(x-\mu)^2}{2\sigma^2}} \quad . \tag{5.142}$$

For the case of the epistemic priors in Section 5.1.2 we can use the nature that the log-flat prior must contain phenomenological upper and lower bounds defining the ULA parameter space. When these are fixed we can assume that as $\sigma \to \infty$ this dilutes the strength of the prior approximating the uninformative scale invariance of the log-

flat prior via a series of *super-weak* priors which extend far beyond the limits of the ultralight sector. For the RMT axiverse, consider specifically the case of a symmetric mass distribution, such as those found in Fig. 5.6, modelled by a Beta function where $\alpha \simeq \beta$ in Eq. (G.4). Specifically complete convergence occurs in the limit $\alpha = \beta \to \infty$ it can be shown that the LSD of the Beta function converges point-wise to the case of a probability density function of a standard normal random variable. Which using Scheffé's theorem for some random variable, determines the distribution converges to the standard normal distribution. Under the general assumption then that $\beta_{\mathcal{K}} \simeq \beta_{\mathcal{M}}$ which may come from defining priors such as those found in the N-flation model and Eq. (5.45), assuming an independence for these variables. If we also factor in the possibility to define priors on the population covariance matrix, we can assume in general the Beta functions we would expect to find, as a fit to our mass spectra, would be of the form Beta$(> 2, > 2)$, for some unimodal function with an absence of a heavy tail. We can then assume a normal distribution would act as a good first order approximation to a large range of mass spectra we would encounter. The M-theory RMT axiverse is trivial, as the logarithm strongly converges to the case of a LSD which closely resembles a normally distributed variable. Using this we can provide a well motivated case for the use of a very simplistic, coherent approach, incorporating each of the discussions of Section 5.1.2, Section 5.2 and Section 5.3 for the spectrum of the axion mass eigenstates. This is a very simplistic assumption in order to capture a quantitive analysis of the large field population limits behaviour by taking the normal distribution limit. This will be the process we adopt in the following chapter, in order to demonstrate the first of our results chapters, detailing constraints on the spectra covered in this chapter by considering the phenomenology of BH superradiance.



Part III

Augmenting the Axiverse

Chapter 6

Black Hole Spin Constraints on the Mass Spectrum and Number of Axion-like Fields

> "*The treatment of the perturbations of the Kerr spacetime in this chapter has been prolixius in its complexity. Perhaps, at a later time, the complexity will be unravelled by deeper insights. But meantime, the analysis has led us into a realm of the rococo: splendorous, joyful, and immensely ornate.*"
>
> The Mathematical Theory of Black Holes
>
> Subrahmanyan Chandrasekhar

6.1 Black Hole Superradiance

6.1.1 Singularities in Spacetime

Given the potential complexity that may arise from the study of model dependant axions or ALPs, when attempting to constrain the overall picture of the parameter space, as ultralight scalars appearing in the low energy sector of GUTs, a valuable

insight and probe of their underlying physics could come from the phenomena known as BH superradiance [106, 107, 286, 317, 810, 1361, 1378]. Note, that in order to conform to the practises found in the superradiance literature, we shall now refer to the axion mass parameter using the standard, $\mu_{\rm ax}$ notation, for the duration of this chapter. Axions with masses spanning the ultra-light sector, especially those approaching the energy scales associated to FDM models ($\mu_{\rm ax} \sim 10^{-15}{\rm eV} - 10^{-20}{\rm eV}$) are very challenging to tackle with lab based searches. The Penrose process [1044] describes how infalling bosonic waves in the presence of a rotating BH, can emerge with additional energy as compared to the energy they possess upon entry of the BHs horizon. This astrophysical process is an exact analogy to other superradiant processes in physics, such as Cherenkov radiation [446, 639, 1149]. The process is powerful as it relies predominantly on the gravitational interactions between the field and the BH, suppressing the need to understand fully, potentially complicated properties such as matter field couplings or the field's cosmological energy density, in order to probe its potential existence in the accessible parameter space. In this way, such a probe for the presence of axion physics can be thought of as model independent, and a vital window into understanding the low energy phenomenology of string theory models with large numbers of ALPs, fundamental to the formulation of their low energy sectors.

If such bosonic fields are confined around a BH by a mirror, then wave amplification can continue indefinitely leading to Press and Teukolsky's "*black hole bomb*" scenario [1076, 1077]. Massive bosonic fields present in the Kerr spacetime form a series of hydrogenic-like bound states, analogous to that represented in Fig. 2. In this case, the potential barrier is provided by the particle mass playing the role of the mirror, leading to a natural realisation of the BH superradiance process for massive bosons in orbits around astrophysical BHs. See Ref. [286] for an extensive review of superradiance and its applications to BHs. There is no doubt, BHs are one of the most fascinating products of the cosmological landscape, offering a powerful theoretical and observational portal into non-perturbative dynamics of complex gravita-

tional physics. They can be understood as classical solutions to relativistic metrics of gravity theories, possessing highly non-trivial properties and solutions which predict very interesting physical characteristics [157, 321, 600, 601, 676–680, 682, 683]. Their complex nature however may, in-fact, lend itself to a conventionally simple approach to probing the landscape of the string axiverse at the perturbative level of their effective theory, covering many orders of magnitude in the cosmological axion parameter space.

The very first initial physical intuition which can be tied to the understanding of BH dynamics covers several centuries, which saw the developing ideas and concepts associated to universal laws of gravitational forces, light and classical bodies in geometrical spaces. It was not until the introduction of Einstein's seminal work on the geometrical significance of space and time and its ties to gravitational physics, that BHs really became defined as familiar objects in the scientific community [511–514]. As an intellectual pursuit, BHs have a copious history in early 20^{th} century physics literature, they were initially conceived as exotic theoretical solutions to vacuum field equations for uncharged spherically-symmetric non-rotating systems. This initial solution to the spacetime geometry, with metric of the generic form $ds^2 = g_{\alpha\beta}dx^\alpha dx^\beta$, from Einstein's newly proposed theory of general relativity, was presented by Karl Schwarzschild in 1916, the so called *Schwarzschild solution* [1164]. The Schwarzschild metric solution, with coordinates (t, r, θ, ϕ) and BH mass M_{BH}, is defined by the element,

$$ds^2_{\text{Schw}} = -\left(1 - \frac{2M_{\text{BH}}}{r}\right)dt^2 + \frac{dr^2}{1 - {}^{2M_{\text{BH}}}/_{r}} + r^2\left(d\theta^2 + \sin^2\theta d\phi^2\right) \ , \tag{6.1}$$

used to describe the gravitational field surrounding massive spherical bodies. These solutions would subsequently be re-addressed and expanded upon in the following year by Johannes Droste [480] as well as in the works of David Hilbert [706] and Hermann Weyl [1349]. Approaching the end of the Great War, Gunnar Nordström showed the previously mentioned understanding held for BHs also held for charged

spherically-symmetric non-rotating systems [990], independently expanding on work conducted in 1916 by Hans Reissner [1099]. It would however take until the 1930's for the defined mathematical constructs of BH physics to be tied precisely to the physical contexts of astrophysical systems. Initial works in the first half of the decade by Lev Davidovich Landau [1] and Subrahmanyan Chandrasekhar [333], theorised BH solutions to be chronological limits to the evolutionary nature of massive stars, collapsing to form spacetime singularities. In these works a limit was placed on the maximum mass of a stable white dwarf star, often referred to as *the Chandrasekhar Limit*, a continuation of previous studies conducted by Wilhelm Anderson [78] and Edmund Clifton Stoner [504, 1056], commencing in 1929 for polytrope models of stars of uniform density in hydrostatic equilibrium. These works introduced the notions of a standardised thinking regarding BHs as physical objects and not just exotic mathematical rigour. A vital piece of literature outlining this change of thought came at the turn of the decade when Oppenheimer and Snyder showed that the spherical gravitational collapse of physical systems would produce a BH [1001].

6.1.1.1 Gravitational Waves and Black Hole Masses

Ever since the seminal works highlighted above, research into the physics of BH systems has flourished, now serving as generic probes to extremal limits of theoretical constructs in UV complete theories of general relativity and quantum mechanics [1042]. One astrophysical mechanism of note is the observational understanding behind gas dynamics and stellar kinematics of galactic nuclei, where there is a firm understanding that galactic structures host SMBHs with masses spanning the approximate range in units of the solar mass $M_{\odot}$,

$$\text{SMBHs} : M_{\text{BH}} \sim 10^{6} M_{\odot} - 10^{9} M_{\odot} \ . \tag{6.2}$$

These seemingly inconceivable galactic engines actually could serve as the smoking gun to scalar physics and DM candidates operating on the smallest scales. The

historic Advanced Laser Interferometry Gravitational-Wave Observatory (LIGO) observations of gravitational waves from the binary coalescence of astrophysical BHs has ushered in a new era of interest in BH physics [8]. The ultraluminous X-ray sources which participated in this detection, constitute stellar objects born in the collapse of massive stars, and can have masses of the order several hundred times that of our sun,

$$\text{Stellar Mass BHs} : M_{\rm BH} \sim M_\odot - 10^2 M_\odot \ . \tag{6.3}$$

The recent observations of such binary BHs dynamics greatly enhanced our understanding of the nature, lifetime and formation of these objects. Gravitational wave data can be used to infer the mass and spin of the two BHs in the binary. LIGO has the prospects to detect the existence of many hundreds of such events, accurately determining the mass and spin distribution of BHs. The future of BH superradiance constraints derived from LIGO, the growing global network of GW observatories, and future space-based missions (e.g. Ref. [68]), are extremely promising to serve as a probe of fundamental physics [110, 167, 287, 317, 670].

Currently to date, stellar mass candidates and SMBHs represent the only two classes of observed BH. The current missing link of BH physics which needs demystifying, corresponds to candidates traversing the two previously defined regimes, so called *intermediate mass* BHs (IMBHs),

$$\text{IMBHs} : M_{\rm BH} \sim 10^2 M_\odot - 10^5 M_\odot \ . \tag{6.4}$$

These BHs are sometimes considered as the seeds for SMBHs under early universe dynamics. They are objects hypothesised to exist in dwarf galaxies and could even wander into more massive galaxy halo structures. The elusive nature of IMBHs comes from the absence of accretion events or traditional dynamical signatures present in these environments. A large portion of the axion superradiance window in Eq. (6.6) corresponds to the physics of these IMBH candidates, which would

act as probes to the approximate limits on the axion mass,

$$1 \times 10^{-16}\ \text{eV} \lesssim \mu_{\text{ax}} \lesssim 7 \times 10^{-14}\ \text{eV}\ . \tag{6.5}$$

The most promising realisation of detecting BHs in this space comes from the proposed space based gravitational wave observatories such as the Laser Interferometer Space Antenna (LISA) [947] (see Fig. 6.2).

6.1.1.2 Black Hole Hair and Spacetime Metrics

One of the critical postulates of BH physics, which generalises the metric solutions found in Table 6.1, is the *No-hair Theorem* for static BH solutions in four spacetime dimensions [325, 742, 743]. This physical conjecture states that any BH solution to the Einstein-Maxwell field equations of general relativity for gravity and electromagnetism are characterised by a three-dimensional externally observable parameter space. This space consists of the BH mass, M_{BH}, electric charge, Q_{BH} and spin angular momentum, J_{BH}. The simplest solutions to the Einstein field equations correspond to the Schwarzschild metric, for a general stationary vacuum, describing a non-rotating BH with zero charge (i.e. $Q_{\text{BH}} = J_{\text{BH}} = 0$). These in general will not correspond to the most realistic situation for modelling astrophysical BHs formed during the evolutionary epochs of large scale structure formation. The relevant processes for formation of observed astrophysical BHs are induced by either a form of gravitational collapse or accretion, ensuring we must consider a non-zero angular momentum component ($J_{\text{BH}} \neq 0$). The generalisation of the non-rotating Schwarzschild solution to a rotating uncharged axially-symmetric BHs with a quasi-spherical event horizon is given by the Kerr metric [783]. The solutions for uncharged BH metrics can be further generalised to the case of non-neutral backgrounds with an existing charge. Kerr-Newman BHs represent the most general case of asymptotically flat solutions in Einstein-Maxwell theories [977]. These solutions are stable for massless perturbations [316, 445]. Finally the Reissner-Nordström solutions provide the

Table 6.1: Simple grid parameterisation of possible BH background metric solutions for various configurations of the quantities used to describe a BH under the assumption of the no-hair theorem. The work conducted in this chapter is only concerned with Neutral-Rotating BHs described using the Kerr spacetime.

Black Hole Background Metrics		
	Neutral ($Q_{\rm BH} = 0$)	**Charged** ($Q_{\rm BH} \neq 0$)
Stationary ($J_{\rm BH} = 0$)	Schwarzschild [1164]	Reissner-Nordström [991]
Rotating ($J_{\rm BH} \neq 0$)	Kerr [783]	Kerr-Newman [977]

required description of gravitational fields for non-rotating, spherically symmetric BHs possessing a charge [991, 1099, 1348].

It is generally expected that the measured charge of a BH we may wish to consider would be small, where the physical interpretation and significance in relation to modelling astrophysical systems is more debatable than the remaining two defining members of the BH parameter space. Examples of this consist of neutralisation of an initial non-vanishing electric charge via highly ionised environments [146], whereby the presence of plasma around an astrophysical BH will often fix the considered effective charge to zero. It is also important to note however, BHs may acquire charges from several different mechanisms. Examples consist of primordial charges from the formation of systems via the collapse of charged compact stars [1095] or stable (Wald) charges acquired from the rotational spin of a BH system in an external magnetic field [1315].

6.1.1.3 Gravitational Engines as Phenomenological Probes

Only recently has the first visual reproduction and fruitful validation of the existence of BHs been produced, constructed from observations made using the very long baseline interferometry array of the Event Horizon Telescope [48–53]. As shown in Fig 6.1, the core of the *Messier 87* galaxy is shown to house a SMBH, M87*, which is surrounded by a transparent emission region. This *dark shadow effect* is revealed using the warping of gravitational light and photon capture at the event horizon. The shadow observed in Fig. 6.1 is consistent with those expected from Kerr BH



Figure 6.1: M87* SMBH at the centre of the Messier 87 galaxy as imaged by the Event Horizon Telescope [48–53]. The BH presents a dark shadow (central spot), which is larger than the BH event horizon, caused by the gravitational warping of light and photon capture at the event horizon. Image credit: Event Horizon Telescope, `https://www.eso.org/public/images/eso1907a/`.

solutions. We shall review the potentially interesting consequences of obtaining detailed measurements for M87* and what conclusions this could lead to for models of the axiverse and DM physics in Section 6.4.7.

For the individual axion field *stellar* and *SMBHs* are able to probe axions physics in the field mass range,

$$10^{-20}\ \text{eV} \lesssim \mu_{\text{ax}} \lesssim 10^{-10}\ \text{eV}\ , \tag{6.6}$$

which constitutes a significantly large portion of the ultralight sector mass space. These approximate limits come from the current smallest/largest observed measurements of astrophysical BH systems and/or the theoretical gravitational bounds on such structures. If BH measurements increase in accuracy over the coming years, then strong exclusions placed on this window would provide a very interesting inference on the tuning required for the underlying geometries of the string landscape,

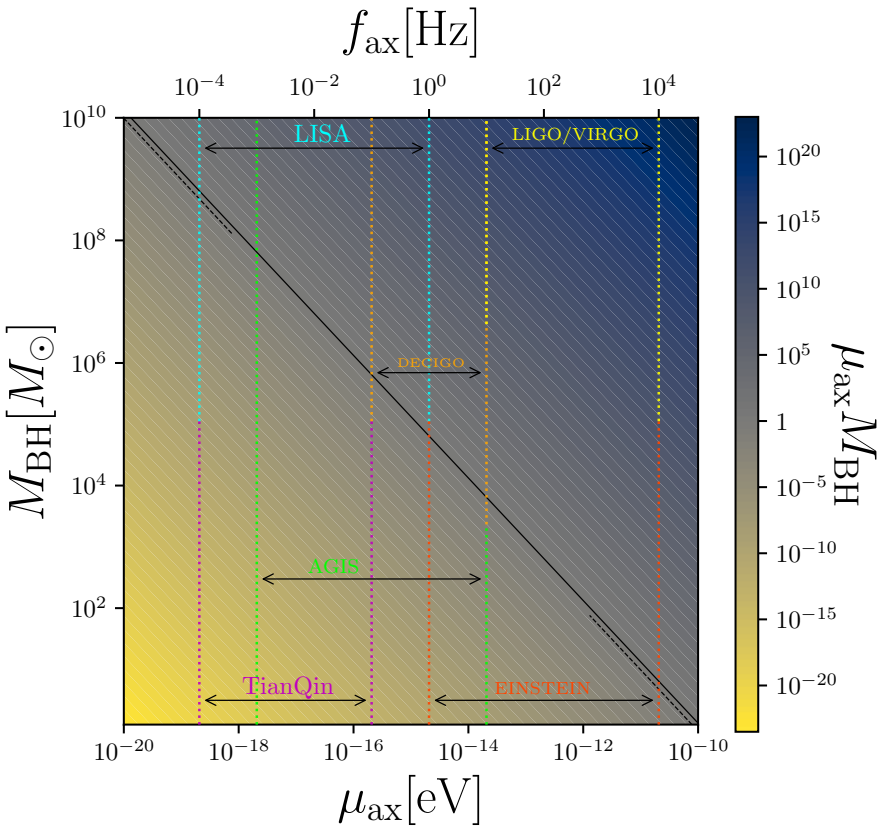


Figure 6.2: The BH-scalar condensate coupling, $\alpha = \mu_{\rm ax} M_{\rm BH}$. The solid black line represents the unity limit for non-relativistic and relativistic regimes. The dashed line corresponds to $\alpha = 0.5$, the approximate limit in which the analytical approximation for the instability rate is valid. Dotted lines correspond to frequency ranges for monochromatic gravitational wave emission from the scalar cloud accessible to current and future GW observatories [4, 68, 69, 456, 523, 879, 1147].

or the properties the full multi-field potential may require in order to describe observational signatures in the low energy sector.

Considering the points above we can suitably adopt the formalities of considering an uncharged rotating BH, utilising the Kerr metric as our description of the axion fields background geometry. The ability to constrain ultralight bosonic fields from BH-scalar condensate systems come in the form of two phenomena. It may be possible to identify the presence of scalar clouds in the vicinity of BHs as emission sources of monochromatic gravitational waves (GWs). The signal frequency, $f_{\rm ax} \sim {}^{\mu_{\rm ax}}/_{\pi}$, with boson mass, $\mu_{\rm ax}$, could be detected by either ground or space-

based GW observatories and proposes to be an exciting methodology to enhance constraints on the mass bounds for bosonic fields. This subject has been extensively discussed in Refs. [106, 168, 178, 288]. The second phenomenon of interest, and the primary subject of the work presented in this chapter, is the spin down of astrophysical BHs. If the superradiance rate is faster than any other astrophysical process affecting the BH mass, $M_{\rm BH}$, and dimensionless spin, a_*, then the BH superradiance process can efficiently reduce these quantities. This occurs when the boson Compton wavelength is of the order of the gravitational radius of the BH. Thus, if a massive boson exists, then astrophysical BHs possessing particular values in the $(M_{\rm BH}, a_*)$ *Regge plane* (which, according to the no-hair theorems, gives a complete description of spinning BHs) should be absent in future experimental observations. The Regge plane shall be introduced in Section 6.2.3. The masses and spins of a large number of astrophysical BHs have been measured, often incorporating either X-ray reflection spectroscopy or continuum-fitting methods (see Table 6.2 and Table 6.3 for BH parameter measurements and corresponding references). These measurements can be used to probe the possible existence of massive bosons [284, 1379]. Constraints from BH superradiance also apply to a wide range of particle physics models, including a possible mass for the photon or the graviton [283, 1012] (and indeed to the photon plasma mass near the BH), as well as to exotic particles, such as massive vector (Proca) fields [167], massive spin-two fields [809] along with ALPs and other massive scalars [106–108].

These represent powerful and generic exclusions, which currently leave many axion models of interest unconstrained. Stellar BHs are too heavy to place constraints on the QCD axion [1036, 1335, 1353], possessing a decay constant far below the Planck scale [108]. FDM of the order $\mu_{\rm ax} \approx 10^{-22}$ eV [722, 728, 914, 1078, 1152], with its novel effects on the formation of galaxies, is too light to make predictions about the spin distribution of SMBHs with $M_{\rm BH} \lesssim 10^9 M_\odot$, that inhabit the centres of galaxies. Finally, the axion mass scale associated to GUTs in M-theory ($\mu_{\rm ax} \approx 10^{-15}$ eV [31]) sit inside the *desert* of IMBHs probes. There is hope, however, since each of these

models is only a small logarithmic distance from the BH superradiance constrained regions, while as we have covered, axion models typically have a spectrum spanning many orders of magnitude [107, 1221]. All previous studies of BH superradiance constraints on bosons have focused on the range of excluded masses assuming the existence of a single new bosonic field. In this chapter we will explore, for the first time, what constraints can be drawn on the properties of axion mass distributions from BH superradiance. To do this we must begin with the properties of the spacetime surrounding BHs susceptible to axion induced scalar field instabilities.

6.1.2 The Kerr Black Hole Spacetime

6.1.2.1 The Rotating Invariant Line Element

One of the most remarkable features of BH superradiance is the realisation that it is not required to formulate a fastidious understanding of the intricate and complex nature of the Kerr geometry, in order to probe the phenomenological consequences of axion field perturbations at the horizon and how these ultimately effect the evolutionary dynamics of a rotating BH system. For any rotating spacetime there is no realisation of the famous *Birkhoff theorem* for spherically symmetric solutions of the vacuum field equations for a neutral, non-rotating system. A rotating BH does however possess a series of very powerful uniqueness theorems which directly tie the physical significance of the Kerr solutions to unique exact solutions for stationary rotating BHs. The Kerr solution is the asymptotic metric used to describe systems which have settled from their initial dynamical production. Therefore formally, the spectroscopy of the superradiant system is defined using the Kerr metric for a neutrally charged astrophysical system with a non-zero angular momentum component. There are several choices of coordinate systems used to represent the invariant line element of the Kerr geometry. The most convenient are the *Boyer-Lindquist* coordinates, typically used to minimise the number of off-diagonal elements in the metric. Asymptotically ($r \to \infty$) the form of the metric approaches the form in Eq. (6.1),

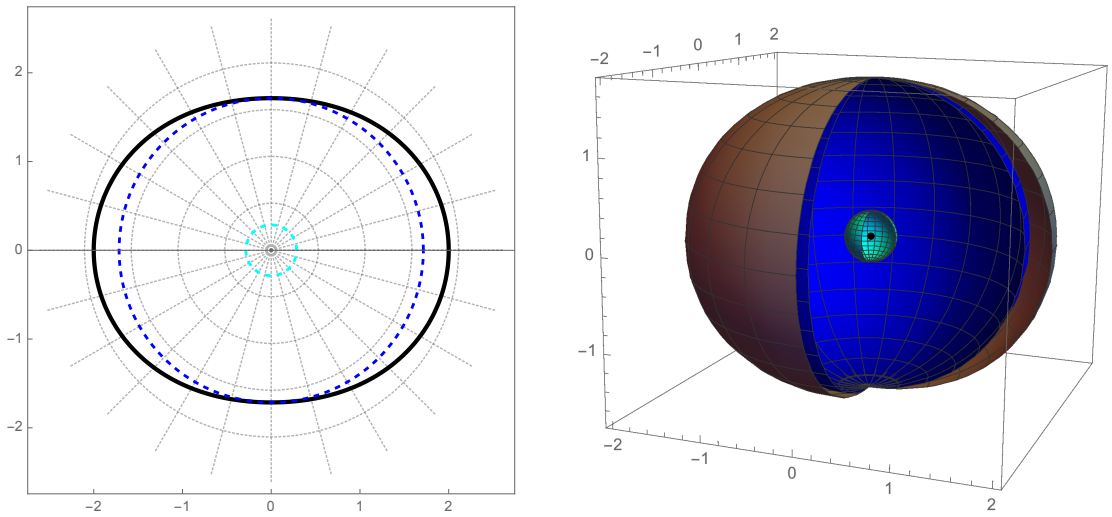


Figure 6.3: Behaviour of a Kerr BH horizons in three-dimensional and two-dimensional Cartesian Kerr-Schild coordinates, for fixed values of the dimensionless spin parameter, a_* approaching the limit for a non-rotating BH. The solid black line represents the ergoregion defined using Eq. (6.12), which is minimally perturbed in the non-relativistic spin limit, $a_* < 1$, where these two regions approach the Schwarzschild solution limit. The dashed blue and cyan lines represent the outer and inner horizons respectively defined using Eq. (6.10). The two hypersurfaces of the event horizon and the ergosphere meet at the co-latitude pole of 0 degrees. The x-axis is the radial distance from the black hole in polar coordinates.

whereby if the BH rotational parameter, a, is taken to its zero limit then we fully reproduce the standardised Schwarzschild curvature coordinates. This is represented visually in Fig. 6.3, which displays the relevant topologically spherical horizons for a non-relativistic rotating BH in two-dimensional and three-dimensional polar coordinates. The real geometrical property of interest in Fig. 6.3 and a new conceptual property of rotating BHs is the *ergosphere*, represented by the *black* line/surface. Before we define the distinctive properties of this region of the BH spacetime, let us formally define the invariant line element and positional coordinates of the geometrical horizons. The (3+1)-dimensional spacetime region outside the horizon of a rotating Kerr BH is described by the invariant line element for a stationary spacetime, which using the standard Boyer-Lindquist coordinates (t, r, θ, ϕ) and metric

signature $[-,+,+,+]$, takes the form,

$$ds^2_{\rm Kerr} = -\left(1 - \frac{2M_{\rm BH}r}{\Sigma} -\right) dt^2 - \frac{4M_{\rm BH}ar\sin^2\theta}{\Sigma}dtd\phi + \frac{\Sigma}{\Delta}dr^2 + \Sigma d\theta^2 + \frac{(r^2+a^2)^2 - a^2\Delta\sin^2\theta}{\Sigma}\sin^2\theta d\phi^2 \,, \tag{6.7}$$

with $M_{\rm BH}$ the mass of the BH and $a = {}^{J_{\rm BH}}/_{M_{\rm BH}}$, the angular momentum per unit mass ($J_{\rm BH}$). The metric possesses the following metric functions,

$$\Sigma = r^2 + a^2\cos^2\theta \ , \tag{6.8}$$

$$\Delta = r^2 + a^2 - 2M_{\rm BH}r \ , \tag{6.9}$$

$$r_\pm = M_{\rm BH} \pm \sqrt{M^2_{\rm BH} - a^2} \ . \tag{6.10}$$

The zero solutions of Eq. (6.9) correspond to the singularities of the metric components which define two horizons, an inner *Cauchy horizon* at r_-, with the larger root at r_+ defining the outer physical *event horizon*. The interior of the BH is defined by the region, $r < r_+$. The area of the horizon is, $A_+ = 8\pi M_{\rm BH}r_+$, which when differentiated as a function of the angular momentum, produces an expression for the angular velocity of the horizon for an observer at spacial infinity with respect to the BH,

$$\Omega_{\rm H} = \frac{a}{2M_{\rm BH}r_+} \ . \tag{6.11}$$

6.1.2.2 The Ergoregion of the Black Hole Spacetime

The defining property of Kerr BHs, and the previously expressed region of interest is defined by the surface external to the outer horizon, known as the *ergosurface*. The ergosurface is defined by the static limit roots (i.e. no static observer is allowed beyond this limit), $g_{tt} = 0$, with the radius coordinates,

$$r_{\rm ergo} = M_{\rm BH} + \sqrt{M^2_{\rm BH} - a^2\cos^2\theta} \ . \tag{6.12}$$

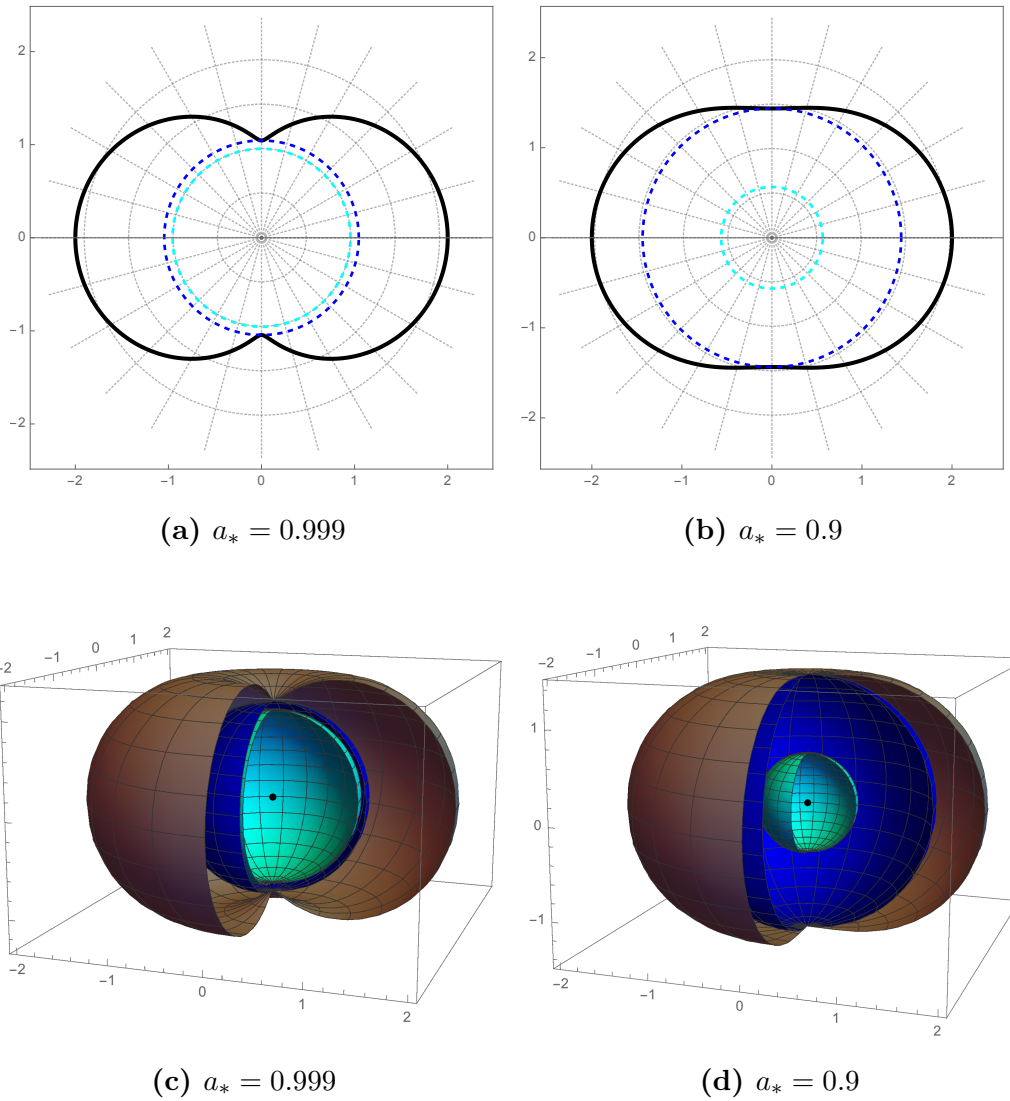
The region defined between the event horizon and ergosurface is the *ergoregion*. The geometrical invariant properties of this region correspond to the region of spacetime in which the time-translation Killing vector, $\xi = \partial_t$ or $\xi^\mu = (1, 0, 0, 0)$, becomes spacelike. Any stationary axisymmetric spacetime which processes a timelike killing vector external to this region, undergoes a transition to spacelike behaviour inside the ergoregion of the BH. This is understood as an observer contained inside being forced to co-rotate with the BH, due to this spacelike nature. The local light cones in this region observe a tilt, transforming the timelike vectors such that they obtain rotational components, forbidding any stationary physical trajectories inside the ergosphere.

The characteristic limits of each BH horizon as a function of the dimensionless spin are displayed in the panels of Fig. 6.4. As the spin of the BH approaches the extremal limit, $a_* = 1$, the inner and outer horizons coincide. As the BH spin approaches the static Schwarzschild solution, $a_* \to 0$, the ergosurface and outer horizon coincide. The region between the outer horizon and ergosurface defines the ergoregion. Inside the ergoregion the vector ξ^μ, in the time coordinate basis becomes spacelike, $\xi^\mu \xi^\nu g_{\mu\nu} = g_{tt} > 0$. This property allows for a Killing energy in the presence of a BH to be negative inside the ergoregion, leading to the superradiant amplification of the infalling waves associated to the bosonic field.

6.1.3 Axions as Perturbative Catalysts for Superradiant Instabilities

6.1.3.1 A Separable Solution

The presence of the axion field on the Kerr spacetime solution outside the BHs event horizon can be considered as a perturbation problem for the stability of the BH evolution. These perturbations can be described by a single *master equation*, incorporating a spin-weight parameter, representing scalar ($s = 0$), neutrino ($s =$



(a) $a_* = 0.999$ **(b)** $a_* = 0.9$

(c) $a_* = 0.999$ **(d)** $a_* = 0.9$

Figure 6.4: Behaviour of a Kerr BHs defining horizons in three-dimensional space and in the xz-plane for fixed values of the dimensionless spin parameter, a_*, approaching the limit for an extremal BH. The solid *black* line/surface represents the ergoregion defined using Eq. (6.12), the dashed *blue* and *cyan* lines/surfaces represent the outer and inner horizons respectively defined using Eq. (6.10). In the limit that the BH is extreme ($a_* = 1$) the inner and outer horizons coincide. The two hypersurfaces of the event horizon and the ergosphere meet at the co-latitude pole of zero degrees. In the non-relativistic spin region these two regions approach each other in the Schwarzschild limit. The x-axis is the radial distance from the BH in polar coordinates.

½), electromagnetic ($s = 1$) and gravitational ($s = 2$) perturbations [1256, 1257],

$$\left[\frac{(r^2+a^2)^2}{\Delta} - a^2\sin^2\theta\right]\frac{\partial^2\psi}{\partial t^2} + \frac{4M_{\rm BH}ar}{\Delta}\frac{\partial^2\psi}{\partial t\partial\phi} + \left[\frac{a^2}{\Delta} - \frac{1}{\sin^2\theta}\right]\frac{\partial^2\psi}{\partial\phi^2} - \Delta^{-s}\frac{\partial}{\partial r}\left(\Delta^{s+1}\frac{\partial\psi}{\partial r}\right) - \frac{1}{\sin\theta}\frac{\partial}{\partial\theta}\left(\sin\theta\frac{\partial\psi}{\partial\theta}\right) - 2s\left[\frac{a\,(r-M_{\rm BH})}{\Delta} + \frac{i\cos\theta}{\sin^2\theta}\right]\frac{\partial\psi}{\partial\phi} - 2s\left[\frac{M_{\rm BH}\,(r^2-a^2)}{\Delta} - r - ia\cos\theta\right]\frac{\partial\psi}{\partial t} + \left(s^2\cot^2\theta - s\right)\psi = 4\pi\Sigma T\ . \quad (6.13)$$

This equation for ψ represents a perturbing field with source term, T. For the scalar axion case, consider the example vacuum formed by fixing, $s = 0$ and $T = 0$, with a test linearised massive spin-0 scalar field, $\psi = \Psi_0$. The dynamics of an axion field in the vicinity of the Kerr spacetime obey the general Klein-Gordon wave equation,

$$(g^{\mu\nu}\nabla_\mu\nabla_\nu - \mu_{\rm ax}^2)\Psi_0(t,\mathbf{r}) = 0\ , \quad (6.14)$$

with Kerr metric $g^{\mu\nu}$, and associated covariant derivatives, ∇_μ. It has been shown linearised perturbations to the Kerr spacetime described under the formalism of a master equation in Eq. (6.13), reduces to the form of the metric in Eq. (6.7), for the case of spin-0 test scalar field. Although the phenomenon of such instabilities can be studied for bosons of various spins, i.e. massive vectors [168, 498, 569], the procedure does fortunately significantly simplify somewhat in the case of axionic fields. This is due to the properties of Eq. (6.14), which for massive spin-0 fields, exhibit well known separable solutions in Boyer-Lindquist coordinates [282, 324], suppling a satisfactory level of analytical tractability to these perturbative solutions. The background spacetime is assumed to be stationary, allowing for a Fourier domain analysis of the test scalar which can be expressed using the separable ansatz,

$$\Psi_0 = \sum_{l,m} e^{-i\omega t + im\psi} S_{lm}(\theta) R_{lm}(r) + h.c.\ , \quad (6.15)$$

with a frequency ω. The values of l and m are defined in Section 6.2.1.2. For the perturbation function, rather conveniently the Klein-Gordon wave equation fol-

lows a separation of variables via spheroidal harmonics, and can be expressed by two coupled ordinary differential equations (ODEs), with an infinite discrete set of complex eigenfrequencies ω_{lmn}, of the form in Eq. (6.77). Using the Teukolsky formalism [1256] the separated ODEs for the radial and angular components, $R_{lm}(r)$ and $S_{lm}(\theta)$ respectively are defined as,

$$\frac{1}{\sin(\theta)}\frac{d}{d\theta}\left(\sin(\theta)\frac{dS}{d\theta}\right)\left[a^2(\omega^2-\mu_{\rm ax}^2)\cos^2(\theta)-\frac{m^2}{\sin^2(\theta)}+\Lambda_{lm}\right]S_{lm}(\theta)=0\ , \tag{6.16}$$

$$\Delta\partial_r(\partial_r R)+(\omega^2(r^2+a^2)^2-4ar_g rm\omega+a^2m^2-\Delta(\mu_{\rm ax}r^2a^2\omega^2+l(l+1))R(r)=0\ . \tag{6.17}$$

The first ODE in Eq. (6.16) is the oblate spheroidal angular wave equation which determines the angular component, $S_{lm}(\theta)$ of the scalar eigenfunction. The angular solutions of Eq. (6.16), S_{lm}, are the spin-weighted spheroidal harmonics, $e^{im\psi}S \equiv S_{lm}(a\omega,\theta,\psi)$, which generalise spheroidal wave functions for spin-0 fields, where the θ dependance is understood via the spheroidal functions,

$$S_{lm}=S_l^m\left(\cos(\theta),aM_{\rm BH}^2\sqrt{\omega^2-\mu_{\rm ax}^2}\right)\ . \tag{6.18}$$

In the non-rotating or non-relativistic limit the spheroidal harmonics reduce to the spherical harmonics, $S_{lm}\rightarrow Y_{lm}$. These are required to be regular at the pole boundaries, $\theta=0$ and $\theta=\pi$, which is expressed via the orthonormality condition,

$$\int_0^\pi |S^2|\sin\theta d\theta=1\ . \tag{6.19}$$

These boundary conditions single out a discrete family, $\{K_{lm}\}$, of angular eigenvalues defining the *coupling* or *separation* constant, which characterises the details of the massive scalar. The angular eigenvalues can either be found using an expansion in the limit that for spin-weighted spherical harmonics, $a\omega$ and $a\mu_{\rm ax}\rightarrow 0$, where the

expansion of K_{lm} is described by the linearised sum,

$$\Lambda_{lm} = l(l+1) + \sum_{k=1}^{\infty} c_k [a^2(\mu_{\rm ax}^2 - \omega^2)]^k \,, \tag{6.20}$$

with expansion coefficients c_k. The exact solutions of which can be found in Ref. [208]. The function inside the sum defines the so called *spheroidicity*, where in the non-rotating limit we can define the truncated angular separation constant as,

$$\Lambda_{lm} \to l(l+1) + \mathcal{O}(a^2\omega^2) \ . \tag{6.21}$$

Generic spin considerations and higher orders of k require numerical solutions. These angular eigenvalues can also be found via methods such as Leavers' continued fraction method [840] or Hughes' spectral decomposition method [727]. A rescaling of the radial function whilst introducing the function,

$$\psi_{lm} = \sqrt{r^2 + a^2} R_{lm} \ , \tag{6.22}$$

along with a definition of the Regge-Wheeler tortoise coordinate, which maps the interval (r_+, ∞) to $(-\infty, \infty)$,

$$dr^* = \frac{(r^2 + a^2)}{\Delta} dr \,, \tag{6.23}$$

with Δ defined in Eq. (6.9) and,

$$r^* = r + \frac{2M}{r_+ - r_-} \left(r_+ \ln \left| \frac{r - r+}{2M} \right| - r_- \ln \left| \frac{r - r-}{2M} \right| \right) \ , \tag{6.24}$$

allowing for a redefinition of the radial Teukolsky equation in Eq. (6.17). A separation of the angular dependance for field modes of the form,

$$\psi = R(r) e^{-i\omega t} \ , \tag{6.25}$$

now define a series of equations expressed in the form of a *Schrödinger* like wave equation,

$$\frac{d^2\psi_{lm}}{dr^{*2}} = \left[\omega^2 - V(r,\omega)\right]\psi_{lm}\,, \tag{6.26}$$

with the effective potential defined as,

$$V(r,\omega) = \frac{4r_g r a m\omega - a^2m^2}{(r^2+a^2)^2} + \frac{\Delta}{(r^2+a^2)}(\mu_{\rm ax} + \frac{l(l+1)+(\mu_{\rm ax}+\omega^2)a^2}{r^2+a^2} + \frac{3r^2-4r_g r+a^2}{(r^2+a^2)^2} - \frac{3\Delta r^2}{(r^2+a^2)^3})\,. \tag{6.27}$$

The value of r_g represent the gravitation radius and is defined in Eq. (6.74).

6.1.3.2 The Weak-Field Analytical Approximation for Scalar Induced Superradiance

We require solutions to Eq. (6.17), with boundary conditions defining an outgoing solution tending to zero at spacial infinity and purely incoming waves at the event horizon. Formally these solutions to the radial equation, which are required to characterise the nature of the axion induced instability can be found in three distinct regimes. Each of these are defined by the nature of the interaction of the test scalar and the Kerr geometry, which is regulated by the gravitational coupling of the scalar-BH system. This is expressed by the ratio of the axion field mass and BH mass, $\mu_{\rm ax}M_{\rm BH}$. The three regimes correspond to nature of this ratio with respect to unity,

$$\text{I} : \mu_{\rm ax}M_{\rm BH} \ll 1\,, \tag{6.28}$$

$$\text{II} : \mu_{\rm ax}M_{\rm BH} \sim 1\,, \tag{6.29}$$

$$\text{III} : \mu_{\rm ax}M_{\rm BH} \gg 1\,. \tag{6.30}$$

The limits in Eq. (6.28) and Eq. (6.30) are susceptible to analytic methods, via matched asymptotic expansions and WBK methods respectively. When $\mu_{\rm ax}M_{\rm BH}$ approaches the maximal superradiance limit of unity, it is required to solve the

radial mode function ODE's eigenvalue problem using numerical techniques. At the horizon, non-singular solutions of the radial equation satisfy the boundary conditions for an incoming wave as well as an outgoing wave at spacial infinity. These boundary conditions correspond to the modifications to the radial solutions in the defined limits,

$$\lim_{r^*\to-\infty} \to R_{lm}(r) \sim e^{-ik_+ r^*} \,, \tag{6.31}$$

$$\lim_{r^*\to\infty} \to R_{lm}(r) \sim \frac{1}{r} e^{i\sqrt{(\omega^2-\mu_{\rm ax}^2)}r^*} \,, \tag{6.32}$$

where $k_+ \equiv \omega - m\Omega_{\rm H}$. The wave is therefore confined around the BH in the bounds,

$$0 < \omega < \mu_{\rm ax} \,, \tag{6.33}$$

representing the understanding that massive scalar fields can naturally provide the mirror required to realise the superradiance process in an astrophysical context.

In the low energy limit, defined in Eq. (6.28), the radial equation is amenable to the method of matched asymptotics. This stems from the nature that for significantly small values of the scalar coupling, which indicate the scalars Compton wavelength is much shorter than the BHs Schwarzschild radius, we obtain solutions comparable to the radial wave function of the Schrödinger equation with an r^{-1} potential. These analytic solutions for small values of the coupling can be found using approximate solutions at large and small radii in terms of hypergeometric functions, where matching techniques are used at an intermediate radius to obtain the superradiance rates to leading order in α (Eq. (6.85)) [433]. In this limit analytical methods utilise the fact that the radial mode functions, $R_{lm}(r)$, can be approximated in asymptotic regimes by known analytical functions. For each region the equations can be reduced to the form of a confluent hypergeometric function. Considering regions far from the BH outer horizon adhering to $r \gg r_g$, whilst also ensuring we are in the

$\mu_{\rm ax} M_{\rm BH} \ll 1$ regime, allow the ODE in Eq. (6.17) to be approximated as,

$$\frac{d^2}{dr^2}(rR) + \left[\omega^2 - \mu_{\rm ax}^2 + \frac{2M_{\rm BH}\mu_{\rm ax}^2}{r} - \frac{l(l+1)}{r^2}\right] rR(r) = 0 \ , \tag{6.34}$$

where the axion momentum is given by,

$$k^2 \equiv \mu_{\rm ax}^2 - \omega^2 \ . \tag{6.35}$$

Solutions can then be extracted by defining,

$$\nu \equiv \frac{\mu_{\rm ax}^2 M_{\rm BH}}{k} = n + l + 1 + \delta\nu \ , \tag{6.36}$$

where the value of $\delta\nu$ represents a small complex number which describes the deviation away from the pure hydrogenic spectrum. When the axion momentum satisfies $k^2 > 0$, we are presented with a series of quasi-bound state solutions. This equation is the same form of the Schrödinger equation which governs the electron in the hydrogen atom (see Fig. 2). The solution to Eq. (6.34) can be expressed as,

$$R(r) = (2kr)^l e^{-kr} U\left(l + 1 - \frac{\alpha}{r_g k}, 2(l+1), 2kr\right) \ , \tag{6.37}$$

where $U(a, b, z)$ is the confluent hypergeometric function of the second kind and α is defined in Eq. (6.85). In the region where $r \ll r_g$, Eq. (6.17) is solved analytically and takes the approximate solution,

$$z(z+1)\frac{d}{dz}\left[z(z+1)\frac{dR}{dz}\right] + \left[P^2 - l(l+1)z(z+1)\right] R(r) = 0 \ , \tag{6.38}$$

with the defined parameter values,

$$z = \frac{r - r_+}{r_+ - r_-} \ , \tag{6.39}$$

$$P = \frac{2r_+(\omega - m\omega_+)}{r_+ - r_-} \ . \tag{6.40}$$

The form of the equation in Eq. (6.38) presents a solution infalling at the horizon,

$$R(r) = \left(\frac{r - r_+}{r - r_-}\right)^{-iP} {}_2F_1\left(-l, l+1, 1+2iP, \left(\frac{r - r_-}{r_+ - r_-}\right)\right) \ , \tag{6.41}$$

where ${}_2F_1$ is the Gauss hypergeometric function. Enforcing the condition that $\mu_{\rm ax} M_{\rm BH} \ll 1$ the two approximate solutions in Eq. (6.37) and Eq. (6.41) have an overlap in their respective regions of validity. Matching the lowest terms for r in Eq. (6.37) with the asymptotic form of Eq. (6.41), determines solutions for the imaginary component of the frequency encapsulating the superradiance rate, defined as the small imaginary component of the energy of the free field solution on the Kerr background. The nature of these scalar instability rates are well researched covering both the frequency [433, 467, 1396] and time domains [468]. Comparing the large r behaviour of the near-region solution, with the small r behaviour of the far-region solution yields the allowed values of the small imaginary component of the frequency, denoted as ω_I. The instability rate in the or $\mu_{\rm ax} M_{\rm BH} \ll 1$ limit or *small mass* approximation is found to be [433],

$$\Gamma_{nlm} = 2\mu_{\rm ax} r_+ \left(m\Omega_{\rm H} - \mu_{\rm ax}\right) \left(\mu_{\rm ax} M_{\rm BH}\right)^{4l+4} \mathcal{C}_{nlm} \ , \tag{6.42}$$

where,

$$\mathcal{C}_{nlm} = \frac{2^{4l+2}(2l+n+1)!}{n!(n+l+1)^{2l+4}} \left[\frac{l!}{(2l+1)!(2l)!}\right]^2 \times \prod_{j=1}^{l} \left[j^2\left(1 - \frac{a^2}{M_{\rm BH}^2}\right) + 4r_+^2\left(\mu_{\rm ax} - m\Omega_{\rm H}\right)^2\right] \ . \tag{6.43}$$

For the fundamental mode, the rate can be approximated as,

$$M_{\rm BH}\Gamma_{011} = {}^1\!/_{48}\left({}^a\!/_{M_{\rm BH}} - 2\mu_{\rm ax} r_+\right)\left(M_{\rm BH}\mu_{\rm ax}\right)^9 \ . \tag{6.44}$$

Making use of Eq. (6.42), the superradiance rates for scalar fields scale according to

the approximate proportionality relationship,

$$\Gamma_{nlm} \propto \alpha^{4l+4} \mu_{\rm ax} \ , \tag{6.45}$$

which is maximised close to the superradiance boundary. The approximate limits for the analytical superradiance rates have been shown to span the region,

$$M_{\rm BH}\omega_I \sim \left(10^{-14} - 10^{-7}\right) \ . \tag{6.46}$$

The key features of a superradiant instabilities are represented by wave function solutions, peaked far outside of the ergoregion, with a small complex component defining the BH spin-down rate, which must satisfy the superradiance condition to indicate the presence of an instability. The fastest growing mode occurs for Γ_{011}, i.e. a nodeless mode with principle quantum number, $\bar{n} = 2$, with the superradiance rates significantly suppressed as the orbital mode number, l is increased, and linearly suppressed for non-fundamental nodes. The maximum superradiance rates are found for the maximised, L_z, momentum mode, which occurs when the values of l and m reproduce the condition, $l = m$, where m determines whether the superradiance condition in Eq. (6.71) is satisfied. The hierarchies in the time scales of the considered modes is approximated as [286],

$$\frac{\Gamma_{n,l+1,m+1}}{\Gamma_{n,l,m}} \sim \left(M_{\rm BH}\mu_{\rm ax}\right)^4 \ . \tag{6.47}$$

In Fig. 6.5 we show the superradiance rates for a range of modes and spins as a function of the axion-BH coupling, $\mu_{\rm ax}M_{\rm BH}$, derived using Eq. (6.42). The heavy suppression of rates when $m < l$ by potentially many orders of magnitude is displayed in the superradiance rate solutions found in Fig. 6.6. The value of Γ_{nlm} has a limited dependance on the overtone mode, n. When the BH possesses significant spin, higher order overtone modes for larger values of $l = m$ can present greater superradiance rates as compared to the fundamental overtone mode. Analytically

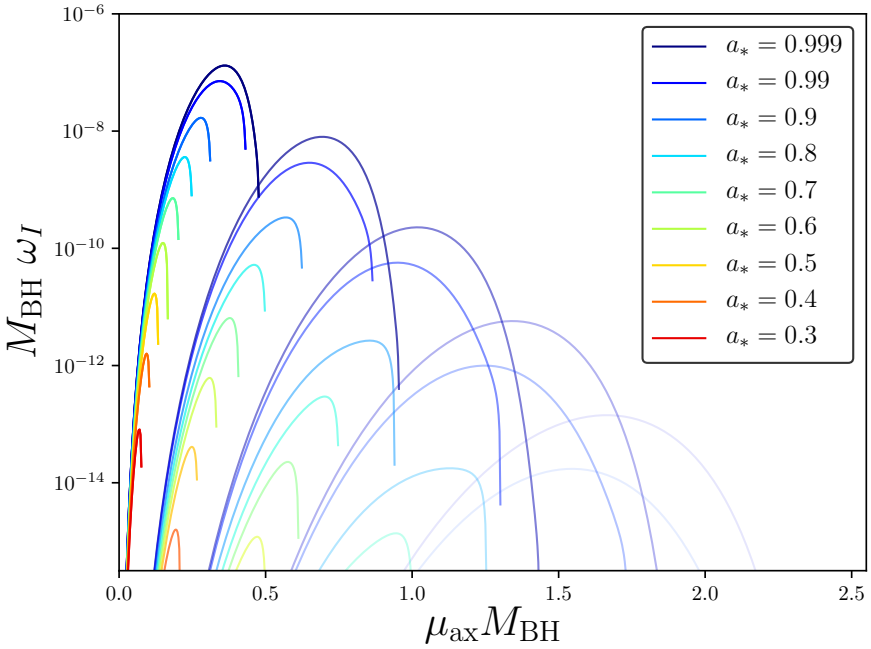


Figure 6.5: Imaginary component of the bound-state frequency, $M_{\rm BH}\omega_I$, representing the superradiance instability rate, $\Gamma_{\rm nlm}$, as a function of the dimensionless coupling, $\alpha = \mu_{\rm ax} M_{\rm BH}$. The superradiance rates presented are for each of the orbital/azimuthal quantum numbers, $l = m = 1$ to 5 for various values of the dimensionless BH spin, a_*, approaching the extremal relativistic limit ($a_* = 1$). The functions presented were determined using the weak-field analytical approximations found in Eq. (6.42).

this is apparent for $l = m = 4$ (see the *inset* of Fig. 6.6) where it has also been shown to occur for $l = m = 3$ when considering numerical solutions [1381]. We shall assume from now on any discussions will focus on the limiting case for mode solutions which only satisfy $l = m$. We now have the ability to understand the evolution of the axion field which is defined by the characteristic eigenfrequencies corresponding to the instability timescales for the unstable modes of the system.

6.1.3.3 Numerical Solution in the Strong-Coupling Regime

When analysing the region of the parameter space where $\alpha \sim 1$, solutions for the unstable modes can be found using a numerical analysis of the wave equation [315, 467, 578]. In particular see Refs. [467, 840] for details on the stages quoted below.

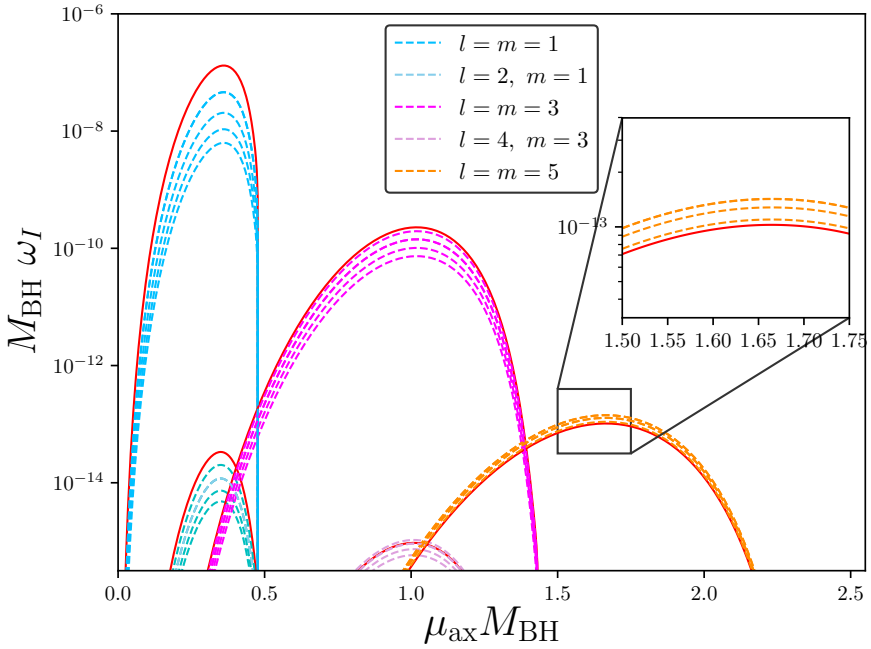


Figure 6.6: Imaginary component of the bound-state frequency, $M_{\rm BH}\omega_I$ representing the superradiance instability rate, $\Gamma_{\rm nlm}$, as a function of the dimensionless coupling, $\alpha = \mu_{\rm ax} M_{\rm BH}$. The superradiance rates presented are for the fundamental and higher order overtone modes $n = 0$ to 4 for various configurations satisfying either $l = m$ or $l > m$. The red lines correspond to the fundamental overtone modes, $n = 0$ which become subdominant for values of $l = m \geq 4$ (see *inset*). The functions presented were determined using the weak-field analytical approximations found in Eq. (6.42).

The radial function $R(r)$ is now assumed to take the following form of the infinite series,

$$R(r) = (r - r_+)^{-i\sigma}(r - r_-)^{i\sigma+\chi-1} e^{qr} \sum_{n=0}^{\infty} a_n \left(\frac{r - r_+}{r - r_-}\right)^n , \tag{6.48}$$

where,

$$\sigma = \frac{2r_+(\omega - \omega_c)}{r_+ - r_-} , \tag{6.49}$$

$$q = \pm\sqrt{\mu^2 - \omega^2} , \tag{6.50}$$

$$\chi = \frac{\mu - 2\omega^2}{q} . \tag{6.51}$$

A substitution of Eq. (6.48) into Eq. (6.17) obtains the three term relation for the expansion coefficients a_n for $n > 0, n \in \mathbb{N}$,

$$\alpha_0 a_1 + \beta_0 a_0 = 0\,, \tag{6.52}$$

$$\alpha_n a_{n+1} + \beta_n a_n + \gamma_n a_{n-1} = 0\,, \tag{6.53}$$

where,

$$\alpha_n = n^2 + (c_0 + 1)n + c_0\,, \tag{6.54}$$

$$\beta_n = -2n^2 + (c_1 + 2)n + c_3\,, \tag{6.55}$$

$$\gamma_n = n^2 + (c_2 - 3)n + c_4\,. \tag{6.56}$$

The values of the constants c_1, c_2, c_3 and c_4 are expressed as functions dependant on the parameters, ω, σ, m as well as the angular eigenvalues, Λ_{lm} (Eq. (6.20)), where,

$$c_0 = 1 - 2i\omega - \frac{2i}{b}\left(\omega - \frac{am}{2}\right)\,, \tag{6.57}$$

$$c_1 = -4 + 4i\left(\omega - iq(1+b)\right) + \frac{4i}{b}\left(\omega - \frac{am}{2}\right) - \frac{2(\omega^2 + q^2)}{q}\,, \tag{6.58}$$

$$c_2 = 3 - 2i\omega - \frac{2(q^2 - \omega^2)}{q} - \frac{2i}{b}\left(\omega - \frac{am}{2}\right)\,, \tag{6.59}$$

$$c_3 = \frac{2i(\omega - iq)^3}{q} + 2(\omega - iq)^2 b + q^2 a^2 + 2iqam - \Lambda_{lm} - 1 - \frac{(\omega - iq)^2}{q} 2qb \tag{6.60}$$

$$+ \frac{2i}{b}\left(\frac{(\omega - iq)^2}{q} + 1\right)\left(\omega - \frac{am}{2}\right)\,, \tag{6.61}$$

$$c_4 = \frac{(\omega - iq)^4}{q^2} + \frac{2i\omega\,(\omega - iq)^2}{q} - \frac{2i\,(\omega - iq)^2}{bq}\left(\omega - \frac{am}{2}\right)\,. \tag{6.62}$$

with,

$$b = \sqrt{1 - a^2}\,. \tag{6.63}$$

The three factor recurrence relation can be solved in terms of a continued fraction if we take the assumption that the factor, $a_{n+1}/a_n \to 0$ as $n \to \infty$, obtaining the

relation,

$$\frac{(a_{n+1})}{(a_n)} = -\frac{(\gamma_{n+1})}{(\beta_{n+1}) + (\alpha_{n+1})\left(\frac{\alpha_{n+2}}{\alpha_{n+1}}\right)} = -\frac{(\gamma_{n+1})}{(\beta_{n+1}-)}\frac{(\alpha_{n+1})\,(\gamma_{n+2})}{(\beta_{n+2}-)}\frac{(\alpha_{n+2})\,(\gamma_{n+3})}{(\beta_{n+3}-)}\ \cdots\ . \tag{6.64}$$

Rearranging Eq. (6.52) and noting,

$$\frac{a_1}{a_0} = \frac{-\beta_0}{\alpha_0}\,, \tag{6.65}$$

whilst substituting $n = 0$ into Eq. (6.64) gives the condition for the eigenvalue equation of the bound state eigenfrequencies which take the form found in Eq. (6.77),

$$\beta_0 - \frac{\alpha_0\gamma_1}{\beta_1-}\frac{\alpha_1\gamma_2}{\beta_2-}\frac{\alpha_2\gamma_3}{\beta_3-}\ldots = 0\ . \tag{6.66}$$

This represents the discrete set of complex values, solved using numerical method techniques to find the exact solutions for the spectrum of complex eigenfrequencies of the scalar field. When α surpasses unity, WKB methods are formulated to evaluate the rate, presenting an exponential suppression proportional to α where the approximate rate proportionality is $\Gamma_{nlm} \propto e^{-3.7\alpha}$ [106, 1396]. See Refs. [315, 578] for an initial study incorporating Leaver's continued fraction method for numerical calculations and Dolan's work [467], for an extensive study of the expanded parameter space, providing numerical solutions using a three-term recurrence relation and the continued fraction method.

6.2 The Dynamics of Black Hole Superradiance

We explored in the previous section how in the limit $\omega m \ll 1$ and $\mu_{\rm ax} m \ll 1$, Eq. (6.17) is susceptible to analytic methods. For a particular axion bound state, when the superradiance condition is satisfied, then providing the instability rate dominates over relevant astrophysical timescales, wave modes will extract energy and angular momentum from the BH. The generic effective action for $\mathcal{N}_{\rm ax}$ real scalar

fields Ψ_i with masses $\mu_{\mathrm{ax},i}$ takes the form,

$$S_{\mathrm{eff}} = \int d^4x\sqrt{-g}\sum_{i=1}^{\mathcal{N}_{\mathrm{ax}}}\left(-\frac{1}{2}\nabla_\mu\Psi_i\nabla^\mu\Psi_i - \frac{1}{2}\mu_{\mathrm{ax},i}^2\Psi_i^2\right), \tag{6.67}$$

where ∇_μ is the covariant derivative on the spacetime determined by the metric g. As we have discussed for astrophysical spinning BHs the metric, g is assumed to be the Kerr metric, which we take as the background field geometry. The superradiant process leads to a time dependence in the BH mass and spin, but the structure of the metric does not change due to backreaction. It is known for single field superradiance processes that the backreaction of the scalar condensate on the Kerr geometry is small [285]. This is because, although the cloud can obtain a large mass, it is distributed over a large volume compared to the BH, (see discussions below surrounding Eq. (6.91)) leading to a low scalar energy density (and thus a low source of curvature) in the cloud. Concerns that backreaction is a more severe problem with large numbers of fields as opposed to the single field solution can be alleviated by considering the properties of the scalar cloud itself. The gravitational backreaction is a function of $M_{\mathrm{Cloud}}/M_{\mathrm{BH}}$, where M_{Cloud} is the total mass in the scalar cloud. There is a maximum value of M_{Cloud} independent of the number of axion fields, which is determined by the BH mass, initial spin, $M_{\mathrm{BH}}(a_*)$, and irreducible mass after all possible spin has been extracted in a superradiant cycle, $M_{\mathrm{BH}}(a_* = 0)$. For $\mathcal{N}_{\mathrm{ax}}$ fields, there cannot be an extraction of any more total mass than if only a single field was present, and for resonant modes the cloud size is of the same order of magnitude for all the fields, therefore gravitational backreaction is not enhanced to a greater severity than the single field case. Non-linearities coming from axion interactions, on the other hand, can increase with the number of fields, which we shall discuss in Section 6.3. Neglecting the presence of self-interactions, each field Ψ_i evolves independently on the fixed background. In this separable limit, the total

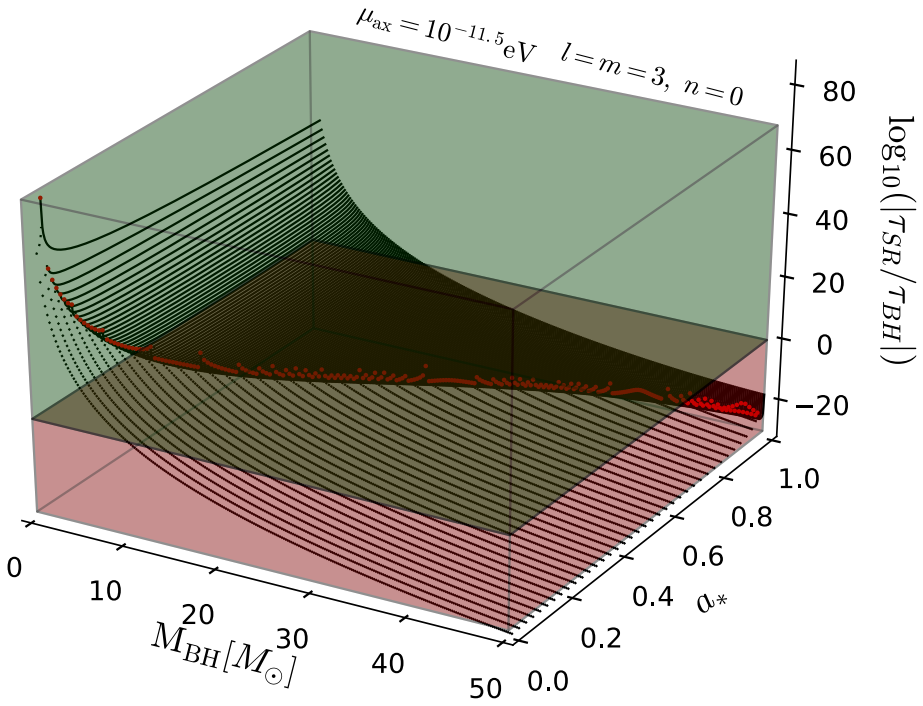


Figure 6.7: Timescale ratios for the superradiance rates determined for an axion with a mass $\mu_{\rm ax} = 10^{-11.5}$ eV. These rates are compared with a typical BH astrophysical timescale, here taken to be $\tau_{\rm Salpeter}$ (Eq. (6.108)). Each cusp represents the analytical limit beyond which Eq. (6.71) is satisfied. The limit to the right of the cusp (soldid line) represents the ratio defining the nature of the timescales where superradiance is apparent. The red volume defines the limit in the two dimensional BH mass-spin parameter space where superradiance occurs within the defined astrophysical timescale used to map the Regge plane isocontour limits, such as those found in Fig. 6.8.

rate of the superradiant process is given simply by the sum of the single field rates,

$$\Gamma^{\rm Tot}_{nlm} = \sum_{i=1}^{\mathcal{N}_{\rm ax}} \Gamma^{i}_{nlm}\,, \tag{6.68}$$

which simplifies the combinatorics of the superradiance phenomenon for multiple bosonic fields and the process of deriving constraints from BH spin measurements.

6.2.1 The Astrophysics of Black Hole Superradiance

6.2.1.1 The Gravitational Atom

Astrophysical BHs with a mass, $M_{\rm BH}$ and spin $J_{\rm BH} = aM_{\rm BH}$, are susceptible to the previously discussed superradiant instabilities, whereby they undergo an extraction of energy and angular momentum [106, 286], being spun down to form very large gravitationally bound states comprising of a scalar cloud consisting of exponentially large axion population numbers. Axions states bound in this way are understood as a *gravitational atom*, where superradiant instabilities are strongest when the Compton wavelength of the field, $\lambda_{\rm ax} = \bar{h}/\mu_{\rm ax}c$, is comparable to the Schwarzschild radius of the BH, $r_{\rm s} = 2G_{\rm N}M_{\rm BH}/c^2$. For stellar mass BHs ($r_s^{\odot}$) and SMBHs ($r_s^{10^6\odot}$) this approximates to the bounds,

$$\lambda_{\rm ax} \simeq \left(\frac{10^{-10}\ {\rm eV}}{\mu_{\rm ax}}\right)\left(\frac{M_{\rm BH}}{M_{\odot}}\right) r_s^{\odot}\ , \tag{6.69}$$

$$\lambda_{\rm ax} \simeq \left(\frac{10^{-16}\ {\rm eV}}{\mu_{\rm ax}}\right)\left(\frac{M_{\rm BH}}{10^6 M_{\odot}}\right) r_s^{10^6\odot}\ , \tag{6.70}$$

respectively, the effects of which non-linearly deviate as the field mass deters from these values. The general condition for mode amplification of the scalar field requires the angular velocity of the BH horizon to exceed the angular phase velocity of the wave mode, in turn defining the superradiance condition,

$$\frac{\omega}{m} < \Omega_{\rm H}\,, \tag{6.71}$$

where m is the spherical harmonic quantum number. An example of this is shown in Fig. 6.7 for a singular mode and fixed axion mass. The cusp (denoted by a *red* point) of each calculated curve defines the limit where the superradiance condition fails to hold in the dimensionless spin plane for a fixed BH mass. Tracing the cusps through the BH mass dimension yields the Regge Plane boundaries for the selected mode, used to generate field constraints based on BH spin measurements, which

will be discussed in Section 6.2.3. The *green* and *red* separated volumes define the region in which superradiance occurs within relevant timescales (i.e. Eq. (6.110)). The effective angular velocity of the BH as a function of the dimensionless rotation spin parameter is,

$$\Omega_{\rm H} = \frac{a_*}{2r_g(1+\sqrt{1-a_*^2})}\,, \tag{6.72}$$

where the BHs dimensionless spin is defined as,

$$a_* = \frac{a}{r_g} \equiv \frac{J_{\rm BH}}{G_{\rm N} M_{\rm BH}^2}\,, \tag{6.73}$$

which is limited by the bounds, $0 \leq |a_*| < 1$, in Boyer-Lindquist coordinates. The gravitational radius of the BH is,

$$r_g \equiv G_{\rm N} M_{\rm BH}\,. \tag{6.74}$$

The volume of the axion cloud is considered to be constant, simulating the evolution of the density means simulating the evolution of the number density of axions.

6.2.1.2 The Kinematical Evolution of the Scalar Cloud

The growth rate of the system depends on details of the scalar field binding. The kinematic equations for the occupation numbers for different levels N_i, is [106],

$$\frac{dN_i}{dt} = \Gamma_{ij} N_j + \Gamma_{ijk} N_j N_k ...\,, \tag{6.75}$$

where $\Gamma_{ij} = \delta_{ij}\Gamma_i$. In the case where the superradiance condition is met and maximised, superradiance sets in and the number of axions, N, in the scalar condensate close to the BH is exponentially amplified via the dominant mode, $l = m = 1$, which in the linearised limit is represented by the growth rate,

$$\frac{dN}{dt} = \Gamma_{\rm SR} N\,. \tag{6.76}$$

From this point forward we shall assume a normalisation for our units, such that we are working in Planck units, $c = \hbar = G_{\rm N} = 1$, defining the equivalence relation, $r_g \equiv M_{\rm BH}$. The Kerr-Klein-Gordon system discussed in Section 6.1.3 admits quasi-bound states with complex eigenfrequencies,

$$\omega_{nlm} = \omega_R + i\omega_I \ , \tag{6.77}$$

where $\{\omega_R, \omega_I\} \in \mathbb{R}$. Using Eq. (6.71) Kerr BHs present a critical frequency for superradiant scattering,

$$\omega_c \equiv m\Omega_{\rm H} \ , \tag{6.78}$$

which defines the stability thresholds for the scalar modes,

$$\omega_{nlm} > m\Omega_{\rm H} \ \rightarrow \ \text{Stable} \ , \tag{6.79}$$

$$\omega_{nlm} < m\Omega_{\rm H} \ \rightarrow \ \text{Unstable} \ . \tag{6.80}$$

For values of ω_{nlm} satisfying $0 < \omega_{nlm} < \omega_c$, the imaginary component can be either negative or positive defining the superradiant regime representing either the spinning up or down of the BH respectively. Scalar modes in the presence of the Kerr BH spacetime with a scalar mass $\mu_{\rm ax}$, contain a natural confinement mechanism, expressed in Eq. (6.33), bounded from escaping via their potential which is detailed in Eq. (6.27). Modes satisfying these conditions will grow exponentially in time according to a rate equation, identifying the presence of a time-dependant instability in the Kerr spacetime. When $\omega_{nlm} = \omega_c$, the imaginary component of the frequency drops out allowing for the formation of bound states representing scalar clouds acting as an effective quasi-stable hair solution.

Aside from regions within a significant proximity to the BH, the gravitational potential is well approximated by the function proportionality, $\propto r^{-1}$, where the spherically symmetric properties of the potential to leading order allow for a separation of variables of the field evolution in the background, reproducing a Schrödinger

type wave-equation (as discussed in Section 6.1.3). The equation for the separated radial wave function (Eq. (6.17)) is the equivalent of that of the Scalar Coulomb, thereby presenting hydrogenic wavefunctions. To leading order the energy levels for the bound states are well approximated by the spectrum of the hydrogen atom in the non-relativistic limit. When the superradiance condition is saturated the eigenfrequencies take the approximate form,

$$\omega_{nlm} \equiv \omega_R \simeq \mu_{\rm ax}\left(1 - \frac{\alpha^2}{2(n+l+1)^2} + \delta\omega_{nlm}\right) \approx \mu_{\rm ax}\ , \tag{6.81}$$

where $\delta\omega_{nlm}$ represents higher order correctional terms [209], which can be found expressed up to fifth order in Ref. [178],

$$\delta\omega_{nlm} \simeq \left(-\frac{\alpha^4}{8\bar{n}^4} + \frac{(2l-3\bar{n}+1)\,\alpha^4}{\bar{n}\,(l+1/2)} + \frac{2a_*m\alpha^5}{\bar{n}l\,(l+1/2)\,(l+1)}\right)\ . \tag{6.82}$$

The orbitals and quasi-bound state solutions are indexed by the overtone (n), orbital multi-pole (l) and azimutal (m) quantum numbers, which in general satisfy $l \leq \bar{n}-1$ and $|m| \leq l$, forming the discrete sets, $\{n, l, m\}$, used to quantise the superradiant behaviour. The principle quantum number present in the denominators of the leading order correctional terms in Eq. (6.81) is defined by,

$$\bar{n} = n + l + 1\ . \tag{6.83}$$

Before the superradiance condition is saturated the superradiance rate for the exponential growth of the field is,

$$\Gamma_{nlm} = \tau_{\rm SR}^{-1} \equiv {\rm Im}(\omega_{nlm})\ . \tag{6.84}$$

We will only consider solutions using the non-relativistic approximation for Γ_{nlm}, which are determined using Eq. (6.42). Superradiance requires evolving modes to co-rotate with the BH which satisfy, $m > 0$. The previously introduced dimensionless coupling or *gravitational fine structure constant* of the gravitational BH-scalar

condensate system is,

$$\alpha = r_g \mu_{\rm ax} \equiv \mu_{\rm ax} M_{\rm BH} \ , \tag{6.85}$$

in Planck units. As the superradiance process is maximally efficient when the Compton wavelength of the axion is just below that which is required to saturate Eq. (6.71), this suggests an approximate maximal scalar coupling of,

$$\frac{r_+}{\lambda_{\rm ax}} \simeq \frac{\alpha}{l} \simeq \frac{1}{2} \ . \tag{6.86}$$

This limit is shown by the delimited *dotted line* boundary in Fig. 6.2 as a function of the axion parameter space, which also details potential regions of the axion mass parameter space open to investigation for BH masses spanning the stellar and supermassive limits. In the non-relativistic regime the BH-scalar coupling can be approximated to [286],

$$\alpha \simeq 0.02 \left(\frac{M_{\rm BH}}{3 M_\odot} \right) \left(\frac{\mu_{\rm ax}}{10^{-12} \ {\rm eV}} \right) \ . \tag{6.87}$$

The depletion of the spin of the BH with minimum mass valid for exclusion defines superradiance is sufficiently quick to form a maximally filled scalar-cloud in the defined BH characteristic timescale,

$$\Gamma_{nlm} \tau_{\rm BH} \geq \log N_{\rm max} \ . \tag{6.88}$$

The value of $N_{\rm max}$ represents the final occupation number of the axion cloud after the BH spins down by an $\mathcal{O}(1)$ fractional shift, Δa_* [109],

$$N_{\rm max} \simeq \frac{G_N M_{\rm BH}^2 \Delta a_*}{m} \ . \tag{6.89}$$

The axion cloud which forms after it has completed a full superradiant cycle, powered by the rotational energy of the BH, has a radial profile with eigenfunctions which

peak at the approximate average distance [106],

$$r_{c,\bar{n}} \simeq \left(\frac{\bar{n}^2}{\alpha^2}\right) r_g \ . \tag{6.90}$$

For the maximally efficient $2p$-axion cloud state, the topology of the cloud is well approximated by a toroidal structure, its radii expressed via the *Bohr radius* (r_0) of the cloud [1118]. Specifically the major radius is expressed as,

$$\langle r \rangle = 5r_0 = \frac{5}{\mu_{\rm ax}\alpha} \simeq 330 \left(\frac{\alpha}{0.03}\right)^{-1} \left(\frac{\mu_{\rm ax}}{10^{-5}\ {\rm eV}}\right)\ {\rm cm}\ , \tag{6.91}$$

with an outer minor radius,

$$\Delta r \simeq \sqrt{5} r_0 \equiv \frac{\langle r \rangle}{\sqrt{5}}\ . \tag{6.92}$$

Comparing this with event horizon defined in Eq. (6.10) shows that in the $\alpha \ll 1$ limit the condensate cloud is localised in a region far from the horizons of the BH, where it is accepted that curvature effects can be removed from consideration when looking at the evolution of the system. The evolution of the BH system is therefore well approximated in the quasi-linear regime, which can generalised trivially to the case of multiple axions due to their independent evolution on the Kerr spacetime.

6.2.2 Multi-Field Superradiant Evolution in the Quasi-Linear Regime

6.2.2.1 Dissipative Energy Channels

Sequential to the formational phase of a BH, superradiant evolution can begin via quantum fluctuations of the vacuum, where each of the quantised superradiant levels begins to grow exponentially with their corresponding superradiance rates. The standard approach to quantifying this evolution through observational spin signatures is understood through the so called *Regge Plane* formed using BH mass-spin

measurements. The fastest-growing level which satisfies the superradiance condition always dominates the initial superradiant evolution, until it has extracted enough spin so that the superradiance condition is no longer satisfied. The BH energy loss through mass reduction is minimal compared to the shift in angular momentum due to the extent of the scalar cloud. This can be approximated using Eq. (6.89) as [109, 286],

$$\Delta M_{\rm BH} \simeq \mu_{\rm ax} N_{\rm max} \simeq \frac{\alpha M_{\rm BH} \Delta a_*}{m} \ . \tag{6.93}$$

Once the growth of the dominant level has stopped the BH can spend a significant portion of its lifetime on a Regge trajectory (dashed lines in Fig. 6.8, defined in Section 6.2.3), separating higher mode instability bounds [109]. The rate at this stage is dominated by two-axion to one-graviton annihilations [106],

$$\tau_{\rm reg} \simeq \frac{\left|\Gamma_{\rm SR}^{l-1}/\Gamma_{\rm SR}^{l+1}\right|^{1/2}}{(N_{\rm Bose}\Gamma_a)} \ , \tag{6.94}$$

where $N_{\rm Bose}$ is defined in Eq (6.121) and Γ_a is the annihilation rate for a single pair of axions defined as [109],

$$\Gamma_a \simeq 10^{-10} \left\{ \left(\frac{\alpha/l}{0.5} \right)^p + \mathcal{O}\left(\frac{\alpha/l}{0.5} \right)^{p+1} \right\} \frac{G_{\rm N}}{r_g^3} \ . \tag{6.95}$$

The exponent factors are $p = 17$ for $l = 1$ and $p = 4 + 11$ for $l \geq 2$. Axions do not carry any conserved charge and therefore allow for gravitational wave emission processes that do not conserve axion number. Kinematically the one-graviton annihilation of two axions is naturally forbidden in flat space due to energy and momentum conservation concerns. The leading order process in flat space would indeed be a more familiar process of two-axions annihilating to two-gravitons, with an amplitude proportional to $M_{\rm Pl}^{-2}$. However, by taking into account the properties of the Kerr metric where the BH spacetime breaks translational invariance, leads to one-graviton annihilations, a process which can occur at the same order of perturbation

theory as axion traditions between different states in the surrounding cloud[1] (amplitude proportional to $M_{\rm Pl}^{-1}$). A key observational feature of this unusual process is that the wavelength of emitted radiation is not parametrically longer than the size of the emitting source. This renders the standard quadrupole approximation as invalid when searching for signatures. For more details see Refs. [106, 107, 109, 111, 1379]. In particular see the discussion in Section 3.1 of Ref. [106].

The trajectory of the BH on the Regge plane can be understood from the basic intuition that as the higher modes of the BH begin to spin down the BH, it is perturbed from the Regge trajectory where the negative component of the eigenfrequency for the previous mode dominates the evolution, spinning up the BH. This process is apparent until a significant portion of the scalar density in the cloud is reduced from the previously dominant level. At this point the BH traverses the Regge plane towards the successive superradiant boundary, repeating the process until the timescales considered are too large for superradiance to occur.

If non-linearities are taken into account level mixing can increase the time spent on the superradiance condition boundary via perturbations of the gravitational potential around the BH. There are numerous dissipative channels which can occur in the scalar cloud, such as processes involving the annihilation of axions into gravitons or unbound axions [106, 108]. These features form the general umbrella of features probable via GW detections. The potential to probe these signatures and the sensitivities of various leading experiments is detailed in Fig. 6.2. The scalar cloud will generally become maximally occupied before annihilation processes begin in the non-relativistic limit for the case of string axions with $f_a \gtrsim f_a^{\rm GUT}$. In the non-linear sector further complications to the evolutionary trajectory of the BH can come from the *bosenova* phenomena, introducing intermediate stages comprising of bursts of GWs stemming from the partial collapse of the axion cloud, with phases spinning down the BH before the superradiance condition is finally saturated. We

[1] As pointed out in Ref. [106] a close analogue in physics is the one-photon annihilation of a positron with an atomic electron [531].

will discuss these concerns in Section 6.3.

6.2.2.2 Evolution of the Scalar Cloud in the Quasi-Linear Regime

Given the hierarchy of timescales between the superradiant instability and the GW emission from non-linearities when compared to the dynamical time scale of the BH, it is possible to study the systems evolution in the *quasi-adiabatic* approximation under certain conditions, which we now generalise for the case of $\mathcal{N}_{\rm ax}$ fields [285, 286, 288] using the real and imaginary factors of the complex eigenfrequencies in Eq. (6.77). The total scalar energy flux from the superradiance process through the horizon is [285],

$$\dot{E} = 2M_{\rm Cloud} \sum_{g=1}^{\mathcal{N}_{\rm ax}} \omega_{I,g} \,, \tag{6.96}$$

where $M_{\rm Cloud}$ represents the total mass of the scalar cloud. With a disregard for accretion the evolution of the system is described by the following set of equations,

$$-\dot{E}_{\rm Cloud} = \dot{M}_{\rm BH} \,, \tag{6.97}$$

$$-\dot{E} = \dot{M}_{\rm BH} + \dot{M}_{\rm Cloud} \,, \tag{6.98}$$

$$-m\dot{E}_{\rm Cloud}/\sum_{g=1}^{\mathcal{N}_{\rm ax}} \omega_{R,g} = \dot{J}_{\rm BH} \,, \tag{6.99}$$

$$-m\dot{E}/\sum_{g=1}^{\mathcal{N}_{\rm ax}} \omega_{R,g} = \dot{J}_{\rm BH} + \dot{J}_{\rm Cloud} \,, \tag{6.100}$$

where $E_{\rm Cloud}$ is the total energy of the scalar cloud with angular momentum, $J_{\rm Cloud}$. The scalar cloud extracts mass and spin until reaching a saturation point. The final angular momentum of the BH is defined as,

$$J_{\rm BH,F} = \frac{4mM_{\rm BH,F}^3 \sum_{g=1}^{\mathcal{N}_{\rm ax}} \omega_{R,g}}{m^2 + 4M_{\rm BH,F}^2 \sum_{g=1}^{\mathcal{N}_{\rm ax}} \omega_{R,g}^2} \,. \tag{6.101}$$

The final mass of the BH after the phase of superradiant evolution is defined by Eq. (6.99), where the variations in the defining BH parameters are related by,

$$\delta J_{\rm BH} = \frac{m}{\sum_{g=1}^{\mathcal{N}_{\rm ax}} \omega_{R,g}} \delta M_{\rm BH} \ . \tag{6.102}$$

This defines the final mass of the BH as,

$$M_{\rm BH,F} = M_{\rm BH,I} - \frac{\sum_{g=1}^{\mathcal{N}_{\rm ax}} \omega_{R,g}}{m} (J_{\rm BH,I} - J_{\rm BH,F}) \ , \tag{6.103}$$

the subscripts I and F denoting the initial and final states respectively. The true evolution of the full system is of course a vastly complicated picture, where non-linearities must be accounted for and the detailed properties of each BH system adopted suitably. In particular for SMBHs their mass is generally accumulated via accretion which requires very significant perturbations in order to match the evolutionary traits of their stellar counterparts. In the quasi-linear regime above we can still derive strong conclusions of the properties of ultralight scalars in the presence of astrophysical BHs, via measurements of their spin in order to produce conservative constraints. The universal understanding that BHs with spin close to the extremal limit will lose angular momentum on scales vastly shorter than standard astrophysical timescales, leads to model independent constraints on the parameter space of ALPs. In future endeavours this will be improved by the possibility of observing many BHs with parameter measurements corresponding to their expected traversal over the mass-spin Regge plane.

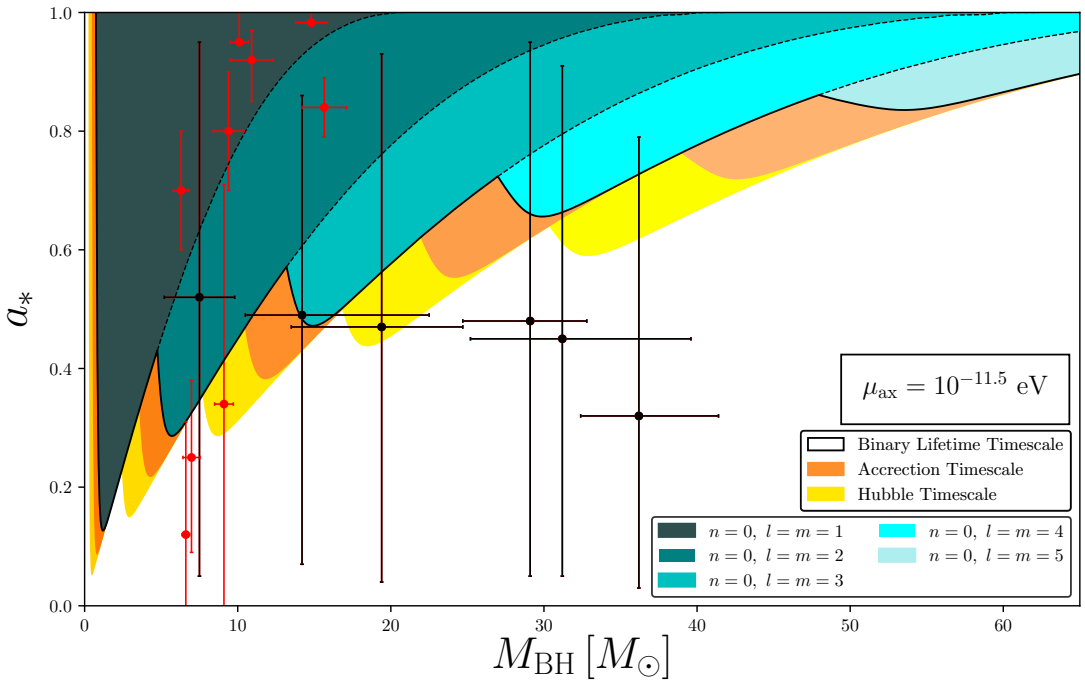


Figure 6.8: Isocontour exclusion bounds in the BH mass-spin Regge plane for an axion mass, $\mu_{\rm ax} = 10^{-11.5}$ eV, probing the stellar BH parameter space. The limits (*black* outline) for the instability threshold are obtained by fixing the superradiant instability time scales for each value of the orbital/azimuthal quantum numbers, $l = m = 1$ to 5 equal to the timescale of a typical BBH system shown in Eq. (6.106). The extended limits come from considering superradiant instability timescales shorter than $\tau_{\rm Salpeter}$ (*orange*, Eq. (6.108)) and $\tau_{\rm Hubble}$ (*yellow*, Eq. (6.107)). The *red*/*black* data points denote mass and spin estimates of the stellar BHs from X-ray/BBH sources presented in Tabel 6.2.

6.2.3 The Black Hole Mass-Spin Regge Plane

6.2.3.1 Axion Constraints from Astrophysical Black Hole Spin Measurements

A fundamental prediction stemming from the generic understanding of superradiant instabilities for bosonic fields is the existence of exclusion thresholds in the BH Regge, or two-dimensional BH mass-spin plane. Estimates of the instability time scale, $\tau_{\rm SR}$, partnered with reliable spin measurements for BHs, can be used to impose stringent constraints on the allowed masses of ultralight bosons. These bounds on the parameters of the fields follow from the requirement that in principle as-

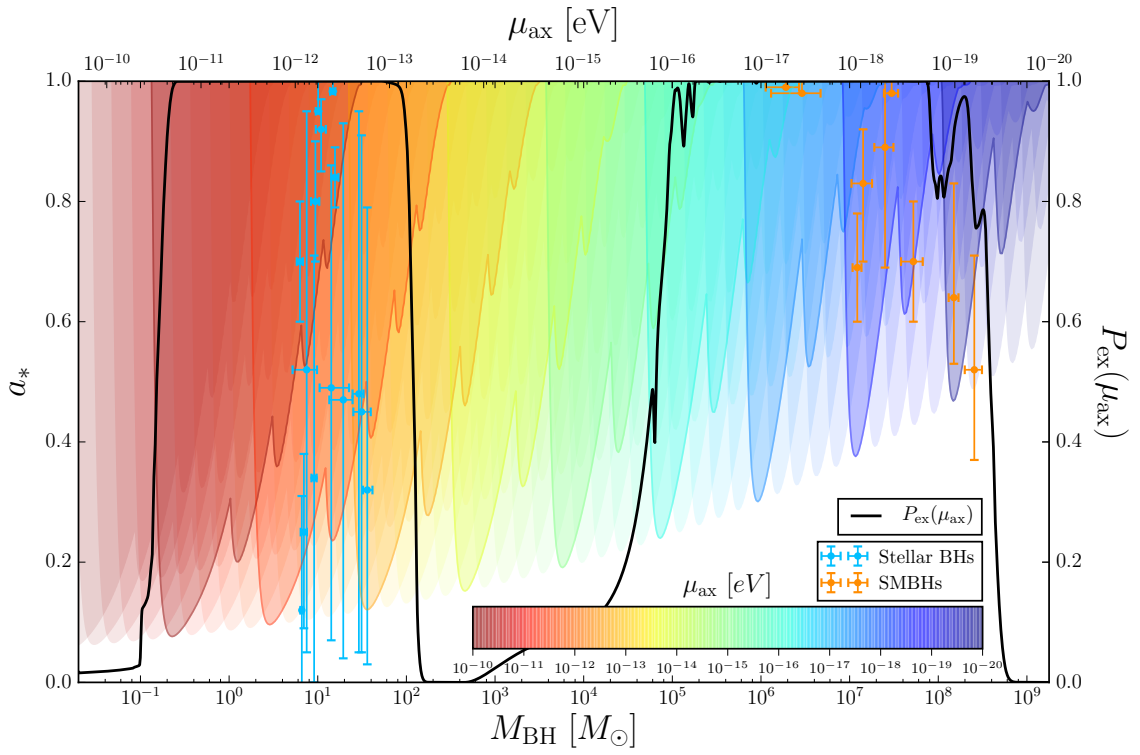


Figure 6.9: Isocontour exclusion bounds and calculated total exclusion probabilities in the BH mass-spin Regge plane from superradiant instabilities with a single axion field with a mass, $\mu_{\rm ax}$, spanning the limits in Eq. (6.105). The shaded regions represent instability thresholds shorter than the time scale $\tau_{\rm Salpeter}$ in Eq. (6.108), for each value of the dominant orbital/azimuthal quantum numbers, $l = m = 1$ to 5. The *blue* data points are mass-spin estimates of stellar X-ray and BBH systems. The *orange* points correspond to mass-spin estimates of SMBHs from X-ray reflection spectroscopy. The exclusion probability function (*black* line) is calculated using the statistical model in Appendix J using the BHs compiled in both Table 6.2 and Table 6.3, which is given as a function of the axion mass spanning both the stellar and supermassive regimes.

trophysical spinning BHs should on average remain stable over their cosmological lifetimes. A superradiant instability time scale which acts faster than core system processes such as accretion, form observational bounds on the expected regions of the two-dimensional parameter space measurement data should fall within. Following the process of superradiant evolution, a large number of BH observations should trace out the superradiance condition boundaries, mapping the Regge trajectories given the existence, of the as yet unidentified fields. For axions the shape of the gaps in the Regge plane are extremely sensitive to variations in the superradiant

growth rate with the scalar mass. This is demonstrated with the non-linear evolution of the isocontour instability bounds in Fig. 6.9. A BH must be absent from observational measurements given the existence of an ultralight boson if its spin is measured above the relevant level curves for different orbital states of the quantised modes for the field. The bounds for bosonic fields with spin are wider than those for ALPs, so the potentially large systematic errors in BH spin measurements could act as a current restriction on using these methods when considering the case of spin-0 fields. The accessible axion mass window we can consider is fixed by the heaviest SMBH with accurate recorded spin measurements, the lower bound defined by the lightest measured stellar mass BH, some $\mathcal{O}(1)$ multiplicity of the Chandrasekhar mass. The current lower and upper bounds on BH masses from X-ray spectroscopy and emission data span the approximate region,

$$5M_{\odot} \lesssim M_{\rm BH} \lesssim 5 \times 10^{8} M_{\odot} \ , \tag{6.104}$$

which defines the relevant approximate axion mass window as,

$$10^{-20} \text{ eV} \lesssim \mu_{\rm ax} \lesssim 10^{-10} \text{ eV} \ . \tag{6.105}$$

The isocontours defining the exclusion bounds are a function of the instability timescale and the boson mass. As the axion mass decreases the instability exclusion contours reduce in size. This corresponds to tighter instability regions which require larger spins for more massive BHs.

6.2.3.2 Characteristic Timescales of Black Hole Evolution

Taking into account accretion and GW emissions can also slightly reduce the bounds in the Regge plane [285]. The timescales associated to the astrophysical processes of relevance alter when considering different compact object systems. For rapidly spinning BH candidates in X-ray binary systems or binary BH (BBH) mergers,

identified as detectable GW sources by LIGO, the strongest constraints can be imposed when considering the typical timescales associated to a binary systems lifetime as other astrophysical processes such as accretion are generally sub-leading. A typical cosmological lower bound approximation for the lifetime of a binary system is,

$$\tau_{\rm BH} \sim 10^6 \text{ yrs} \, . \tag{6.106}$$

The most conservative limits come from exclusion regions constructed using the Hubble time,

$$\tau_{\rm Hub} \sim 10^{10} \text{ yrs} \, . \tag{6.107}$$

As opposed to stellar binary objects, the relevant superradiance timescales for AGN, to maximally grow the scalar cloud for each quantised level come from accretion models. Therefore a statistical analysis of the exclusion limits over the whole BH mass region defined in Eq. (6.104) requires us to use a characteristic timescale derived from accretion considerations. The time scale for mass growth increases exponentially with an e-folding time given by a fraction, $f_{\rm Edd}^{-1}$, of the Salpeter time scale, where $f_{\rm Edd}$ is the Eddington ratio for mass accretion. The accretion time scale is estimated using the Salpeter time for a BH radiating at its Eddington limit,

$$\tau_{\rm Salpeter} = \frac{\sigma_{\rm T}}{4\pi m_{\rm p}} \sim 4.5 \times 10^7 \text{ yrs} \, , \tag{6.108}$$

where $\sigma_{\rm T}$ represents the Thompson cross section and $m_{\rm p}$ the proton mass [1177]. In order to regulate and model the accretion time, the following parameters are introduced [288],

$$\tau_{\rm Salpeter} = 4.5 \times 10^8 \text{ yrs} \frac{\eta}{f_{\rm Edd}(1-\eta)} \, , \tag{6.109}$$

where η, the thin-disk radiative efficiency, is a function of the spin related to a specific energy at the innermost stable circular orbit (ISCO). The value of $f_{\rm Edd}$ represents the Eddington ratio for mass accretion. We select a typical value for the efficiency, $\eta = 0.1$, and the most conservative value of $f_{\rm Edd} = 1$, modelling the effects

of accretion. This fixes the fiducial superradiant instability timescale as,

$$\tau_{\rm SR} = 45{\rm Myrs} \ . \tag{6.110}$$

Other possibilities include increasing the bounds on $f_{\rm Edd}$, where $\tau_{\rm BH} \sim 0.1\tau_{\rm Salpeter}$, in order to account for the possibility of *super-Eddington* accretion [168, 407]. Some astrophysical observations suggest the timescales could be much longer such as recent results for M87* which give, $\dot{M}_{\rm BH}/\dot{M}_{\rm Edd} \sim 2.0 \times 10^{-5}$ [52], implying $\tau_{\rm BH}$ is much larger than the value in Eq. (6.110). A redefinition of $f_{\rm Edd}$ is equivalent to considering a subpopulation of degenerate mass fields (see Section. 6.4.4) or considering different astrophysical processes to define the characteristic timescale of the BH. Such considerations are a limitation in the heuristic *logistics* of encapsulating the behaviour of the total BH spectrum and as such we follow the most conservative limit defined above in Eq. (6.110).

An individual treatment of the instability timescales, derived from the properties of the accretion disc stability for each BH candidate, can be used to tighten constraints on the fields mass exclusion bounds [317]. As the timescale limits for the superradiant instability are increased the limits for each mode, $l = m$ will begin to saturate to the limits set by the boundaries of the superradiance condition. This effect is most prominent for higher order modes in the spin axis of the Regge plane, allowing for enhancements in the possibility to constrain ultralight bosons using observations of BHs with spins a substantial fraction of the extremal limit. In Fig. 6.8 this is shown in the example exclusion window for a fixed axion mass of $\mu_{\rm ax} = 10^{-11.5}$ eV, in the stellar mass BH parameter space for each of the instability timescales defined in Eq. (6.106), Eq. (6.107) and Eq. (6.108). As the considered timescale increases, the saturation of the mode bounds following the limit of the superradiance condition in Eq. (6.71) sees the greatest enhancement for $l = m = 5$. The *red* data points represent the X-ray binary system BHs in Table 6.2. The *black* data points are the *primary* and *secondary* sources involved in the BBH coalescence events (GW150914,

GW151226 and GW170104) over several LIGO detection runs searching for GWs. Extremal BHs such as *NGC 4051* impose constraints on each of the $l = m = 1, 2$ and 3 modes, demonstrating how accurately measured rapidly spinning BHs can be used to constrain significant portions of the axion mass parameter space. The case of a singular axion with a mass, $\mu_{\rm ax} \approx 10^{-11.5}$ eV is tightly constrained by known X-ray binary sources as detailed in Fig. 6.8, with the poor measurements from LIGO data open to a far greater uncertainty if treated separately. Fig. 6.9 details the exclusion bounds we will subsequently define in the next section for the treatment of a single axion covering the full region of the axion mass window in Eq. (6.105), along with the full stellar BH and SMBH data collected in Table 6.2 and Table 6.3. The *primary* axis presents the Regge exclusion bounds for an instability time scale $\tau_{\rm SR} = 45$Myrs, as a function of the axion mass, $\mu_{\rm ax}$. The *blue/orange* data points are the stellar/SM BHs in Table 6.2. The *secondary* axis displays the probability exclusion function formulated from the statistical model in Appendix J and will be used to formulated results in the case of multiple fields as discussed in Section 6.4. The exclusion functions '*well*' corresponds to the absence of any well defined IMBH candidates. Well defined mass and spin measurements for BHs covering the approximate region defined in Eq. (6.4), could fill the currently inaccessible portion of the parameter space required to unify the limits from the stellar and supermassive sectors, providing very strong constraints on the full ultralight sector of axions. This region is also relevant to probe fundamental masses for axions, associated to GUT and supersymmetric models in string/M- theory.

6.2.4 Spin Measurements of Binary Systems and Active Galactic Nuclei

6.2.4.1 Astrophysical Measurements of Black Hole Systems

The identification of compact systems has undergone a steady increase over the past several decades with a number of X-ray binary sources and active galactic nuclei (AGN) now providing well defined, reinforced measurements for the masses and spins of these systems. Currently the main sources of error for catalogued BHs come from the systematic errors when modelling the emissions of the accreting disc for the system. Both stellar BH and SMBH measurements come from analysing the X-ray spectrum of the accretion disk for identified compact sources. Assuming that general relativity holds true as a valid description of the spacetime region outside the BH horizon and the ISCO of the accretion disk possesses a monotonic function potential, then estimates on the spin of BHs can be made. In principle most BH candidates with well defined parameter estimates come from either thermal continuum fitting of the inner accretion disk or inner disk reflection modelling in order to determine the size of the ISCO. Further to this BH spin data has recently been collected via the observations made in several BBH mergers by LIGO [10, 12, 522], as part of the first detections of GWs. Currently such observations, generally contain large errors on both the mass and spin of the BHs when compared to existing X-ray binary system records. The resultant BHs formed from such astrophysical events cannot be included in considerations made when constraining the masses of ultralight bosons, given their observational timescale is less than typical instability timescales by definition in their identification. Generally though future generation ground based detectors are still expected to produce large error measurements on BHs identified in this way and so impose a strong limitation on the accuracy of measurements used for constraints. Improvements in observatory sensitivity with space operated missions such as LISA [801], will open up the potential for a large catalogue of accurate BH measurements capable of probing a large portion of the

cosmologically significant sector for axion-like fields. A large exclusion in the fully accessible space could also lead to tight constraints on how the total axion population or sub-populations may be distributed when seeking realisations of desirable effective models in the context of cosmology.

6.2.4.2 A Data Set of Black Hole Candidates

We consider a generous sample set of BHs, consisting of only those with detailed mass and spin errors available, using comparable measurement methodologies. Each BH chosen in our analysis has both upper and lower bounds on their mass and spin, each with well defined quoted uncertainties in order for us to suitably approximate their errors as multivariate functions, as detailed in Appendix J. In both Table 6.2 and Table 6.3 we present all the stellar BH and SMBH candidates, which form the dataset used to derive constrains on the mass spectrum and number of axion-like fields in Section 6.4 from well known BH sources, along with associated references. For a review of compiled stellar BH data see Refs. [933, 943, 1289] and for SMBHs see Refs. [280, 1101, 1102, 1289]. We currently exclude M87*, the SMBH pictured in Fig. 6.1 in the formation of our data set due to uncertainties in the current analysis of its parameters [52]. We don't expect this will effect the quantitate picture for the constraints placed on multi-field models but we will present some initial results in Section 6.4.7 using fiducial mass-spin priors.

6.3 The $\mathcal{N}$-Radiance Regime

6.3.1 Axion Self-Interactions and the Bose Supernova Phenomenon

In order to fix the region of validity for any constraints, we shall first quickly focus on the non-linearities of the superradiance process. As the axion cloud continues to

Table 6.2: Stellar BHs used to apply constraints on axion masses and values of $\mathcal{N}_{\rm ax}$ for various model mass spectra. Stellar BHs are selected with reliable mass and spin measurements and associated errors are quoted with their CIs and their corresponding references. Stellar BH measurements are sourced from both X-ray binary systems via X-ray continuum-fitting methods and BBH mergers from detected coalescence events at LIGO. Where two methods have been stated we use averaged posterior values for each. For review material and collections of stellar BHs see Refs. [943, 948, 1289].

Stellar object	**Method**	**Mass**	**Spin**	**C.L**	**C.L**	**Ref.**
GW150914 (Primary)	EOBNR+IMRPhenom	$36.2^{+5.2}_{-3.8}$	$0.32^{+0.47}_{-0.29}$	90%	90%	[10]
GW150914 (Secondary)	EOBNR+IMRPhenom	$29.1^{+3.7}_{-4.4}$	$0.48^{+0.47}_{-0.43}$	90%	90%	[10]
GW151226 (Primary)	EOBNR+IMRPhenom	$14.2^{+8.3}_{-3.7}$	$0.49^{+0.37}_{-0.42}$	90%	90%	[10]
GW151226 (Secondary)	EOBNR+IMRPhenom	$7.5^{+2.3}_{-2.3}$	$0.52^{+0.43}_{-0.47}$	90%	90%	[10]
GW170104 (Primary)	Eff+Full precession	$31.2^{+8.4}_{-6.0}$	$0.45^{+0.46}_{-0.40}$	90%	90%	[11]
GW170104 (Secondary)	Eff+Full precession	$19.4^{+5.3}_{-5.9}$	$0.47^{+0.46}_{-0.43}$	90%	90%	[11]
Cygnus X-1	Continuum (KERRBB2)	$14.8^{+1.0}_{-1.0}$	≥ 0.983	1σ	3σ	[1002]/[619]
XTE J1550-564	Continuum (KERRBB2)	$9.10^{+0.61}_{-0.61}$	$0.34^{+0.37}_{-0.34}$	1σ	90%	[1003]/[1216]
A 0620-00	Continuum (KERRBB2)	$6.61^{+0.25}_{-0.25}$	$0.12^{+0.19}_{-0.19}$	1σ	1σ	[310]/[618]
4U 1543-475	Continuum (KERRBB)	$9.4^{+1.0}_{-1.0}$	$0.8^{+0.1}_{-0.1}$	1σ	1σ	[744]/[1176]
GRO J1655-40	Continuum (KERRBB)	$6.30^{+0.50}_{-0.50}$	$0.7^{+0.10}_{-0.10}$	95%	1σ	[1175]/[630]
GRS 1915+105	Continuum (KERRBB2)	$10.1^{+0.6}_{-0.6}$	≥ 0.95	1σ	1σ	[1213]/[932]
LMC X-1	Continuum (KERRBB2)	$10.91^{+1.41}_{-1.41}$	$0.92^{+0.05}_{-0.07}$	1σ	1σ	[1006]/[617]
LMC X-3	Continuum (KERRBB2)	$6.98^{+0.56}_{-0.56}$	$0.25^{+0.13}_{-0.16}$	1σ	1σ	[1004]/[1217]
M33 X-7	Continuum (KERRBB2)	$15.65^{+1.45}_{-1.45}$	$0.84^{+0.05}_{-0.05}$	1σ	1σ	[1005]/[871]

grow the self-interactions amongst the bosons become relevant, where the process enters the non-linear regime. In the non-linear regime the effective action of the axion field is traditionally described using the Sine-Gordon potential description, as apposed to the generic case of the expanded action in Eq. (6.67),

$$S_{\rm eff} = \int d^4x \left[-\frac{1}{2}\partial_\mu\phi\partial^\mu\phi - \mu_{\rm ax}^2 f_a^2 \left(1 - \cos\left(\frac{\phi}{f_a}\right)\right)\right] \ . \tag{6.111}$$

When the expectation value of the axion field is small we recover the effective description of Eq. (6.67), where we need only consider the leading order mass term present. As the field amplitude increases to the point where it satisfies the the field amplitude condition $|\phi| \sim f_a$, non-trivial self-interactions become more pronounced. When the fields attractive self-interactions supersede the gravitational binding energy, the superradiant cloud collapses [106, 810, 955, 1378–1381], before it can extract sufficient amounts of angular momentum akin to a *bosenova* event in

Table 6.3: Selected SMBH system candidates used to apply constraints on axion masses and values of $\mathcal{N}_{\rm ax}$ for various model mass spectra. SMBHs are selected with reliable mass and spin measurements along with associated errors are quoted with their both their CIs and corresponding references. SMBH systems all are observed AGN using X-ray reflection spectroscopy. Where two methods have been stated we have used averaged posterior values for each. For review material and collections of compiled AGN data see Refs. [280, 1100–1102, 1289].

Supermassive object	**Method**	**Mass**	**Spin**	**C.L**	**C.L**	**Ref.**
Mrk 335	Reflection (Suzaku)	$14.20^{+3.70}_{-3.70}$	$0.83^{+0.09}_{-0.13}$	1σ	90%	[1054]/[1318]
Fairall 9	Reflection (Suzaku)	$255.0^{+56.0}_{-56.0}$	$0.52^{+0.19}_{-0.15}$	1σ	90%	[1054]/[872]
Mrk 79	Reflection (Suzaku)	$52.40^{+14.40}_{-14.40}$	$0.70^{+0.1}_{-0.1}$	1σ	90%	[1054]/[583]
NGC 3783	Reflection (Suzaku)	$29.80^{+5.40}_{-5.40}$	≥ 0.98	1σ	90%	[1054]/[280]
MCG-6-30-15	Reflection (Suzaku)	$2.90^{+1.80}_{-1.60}$	≥ 0.98	1σ	90%	[936]/[279]
NGC 7469	Reflection (Suzaku)	$12.20^{+1.40}_{-1.40}$	$0.69^{+0.09}_{-0.09}$	1σ	90%	[1054]/[1019]
Ark 120	Reflection (Suzaku)	$150.0^{+19.0}_{-19.0}$	$0.64^{+0.19}_{-0.11}$	1σ	90%	[1054]/[1318]
Mrk 110	Reflection (Suzaku)	$25.10^{+6.10}_{-6.10}$	≥ 0.89	1σ	90%	[1054]/[1318]
NGC 4051	Reflection (Suzaku)	$1.91^{+0.78}_{-0.78}$	≥ 0.99	1σ	90%	[1054]/[1020]

Bose-Einstein condensates due to Feshbach resonances [472].

6.3.1.1 Additional Dissipative Kinematics

In this regime we can incorporate the axion self-interactions as an effective dissipative factor contribution to the growth rate of Eq. (6.76),

$$\frac{dN}{dt} = \Gamma_{\rm SR} N - \Gamma_{\rm NL} N \ . \tag{6.112}$$

where $\Gamma_{\rm NL} N$ represents an approximation of all initial contributions to non-linear channels i.e. axion-graviton annihilations etc. The growth rate of the superradiant cloud continues to dominate, perturbing the spherical harmonic solutions significantly enough to enter further into the nonlinear regime. As this growth continues the self-organised criticality [955] of the dynamical system is reached, where the stability of the cloud breaks down. At this stage the hydrogenic wave function solutions are no longer valid, resulting in a *bosenova*. This occurs when the gradient *quantum pressure* of the axion cloud fails to withstand the attractive forces from the increased self-interactions in the cloud. In the quasi-linear regime where the

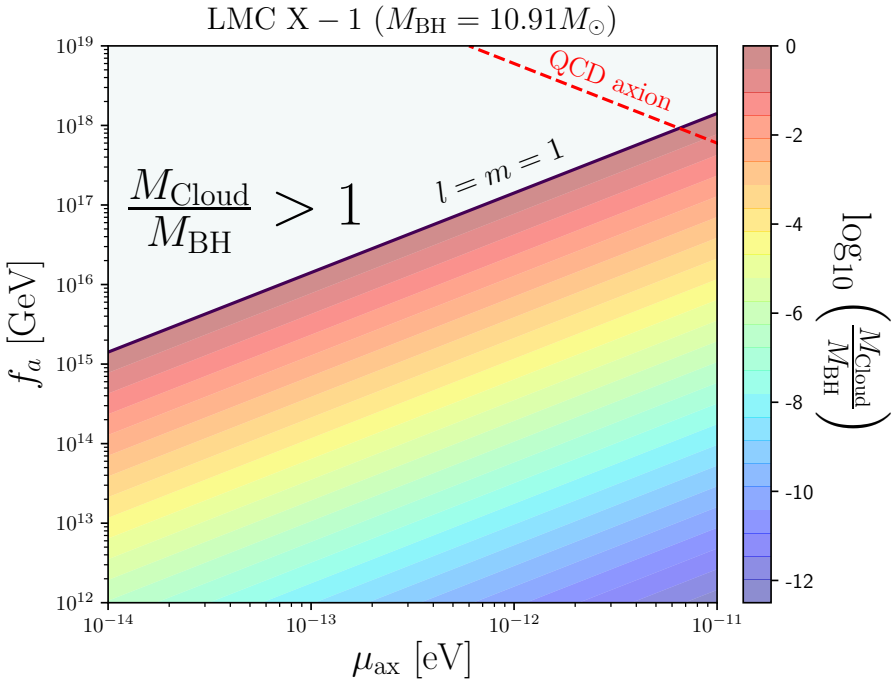


Figure 6.10: Contour bounds for the analytical approximations representing the requirements to account for the non-linear regime for the fundamental mode of the axion cloud system with the BH candidate LMC X-1 in the axion mass and decay constant parameter plane. The *orange* contour bounds represent the possibility of highly non-linear effects occurring when using the approximations defined in Eq. (6.122). The QCD axion approximation (*red* dashed line) is determined using Eq. (6.147).

non-linearities can be treated perturbatively, the factorised total rate equation is,

$$\frac{dN}{dt} = \Gamma_{\rm SR} N - \Gamma_{\lambda^4} N - \Gamma_{\rm Nova} N \ , \tag{6.113}$$

where we have introduced a fictitious dominate rate, $\Gamma_{\rm Nova}$, which represents the dominant self-interaction terms which approximate the presence of a bosenova. We have factorised out the highly suppressed subdominant non-linear channels inside, Γ_{λ^4}. The approximate shutdown of the superradiant instability occurs when the scattering processes realises,

$$\Gamma_{\rm SR} N \simeq \Gamma_{\lambda^4} N + \Gamma_{\rm Nova} N \ , \tag{6.114}$$

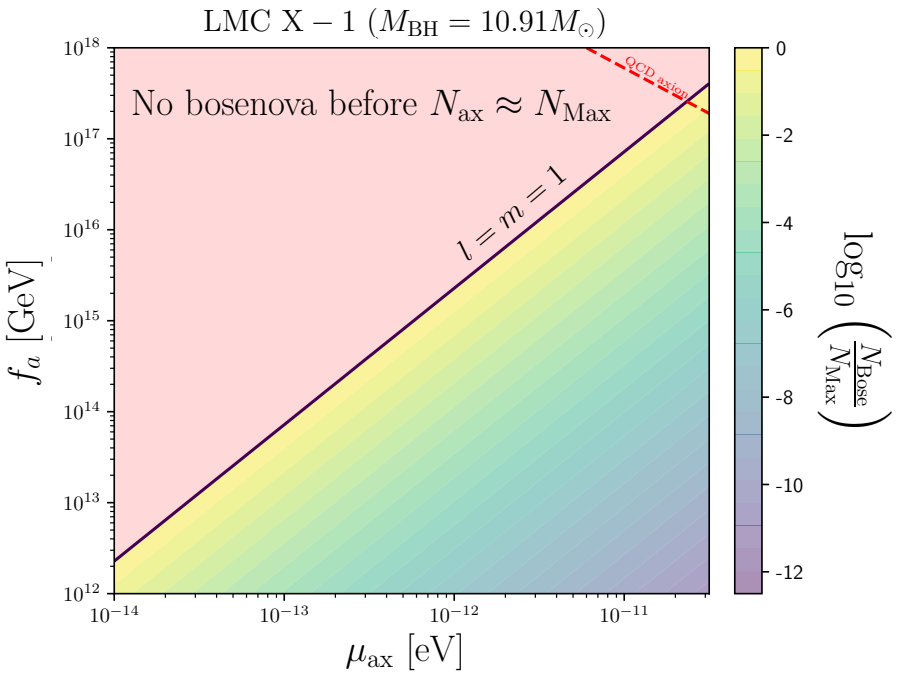


Figure 6.11: Contour bounds on the fractional suppression factor of Eq. (6.124) as a function of the axion mass and decay constant highlighting when a bosenova event occurs before the fundamental superradiant mode has extracted the total allowed spin forming a maximally occupied scalar cloud for the case of the stellar mass BH candidate LMC X-1. The QCD axion approximation (*red* dashed line) is determined using Eq. (6.147).

which for our example we can approximate to,

$$\Gamma_{\rm SR} N \approx \Gamma_{\rm Nova} N \ . \tag{6.115}$$

We can approximate the region of validity for negligible self-interaction processes by using the field description in the non-relativistic limit, where the axion field is expressed as a waveform function ansatz of a slowly varying variable ψ,

$$\phi = \frac{1}{\sqrt{2\mu_{\rm ax}}} \left(e^{-i\mu_{\rm ax} t} \psi + e^{i\mu_{\rm ax} t} \psi^* \right) \ . \tag{6.116}$$

Placing Eq. (6.116) into the action in Eq. (6.111) and considering only the quartic interaction as the leading term for axion self-interactions gives the effective action,

$$S_{\rm eff} = \int d^4x \left(i\psi^* \partial_t \psi - \frac{1}{2\mu_{\rm ax}} \partial_i \psi \partial_i \psi^* - \frac{\alpha}{r} \psi^* \psi + \frac{(\psi^* \psi)^2}{16 f_a^2} \right) \ , \tag{6.117}$$

where αr^{-1} is the Newtonian gravitational potential of the BH. The self-interaction regime becomes apparent when the final terms for the self-interaction and potential energy become comparable [106],

$$\frac{\alpha}{r} \simeq \frac{\psi^* \psi}{8 f_a^2} \ . \tag{6.118}$$

As detailed in Ref. [106], performing an integration over Eq. (6.118) allows the non-linear regime to be defined in terms of the mass of the axion scalar cloud,

$$\frac{M_{\rm Cloud}}{M_{\rm BH}} \gtrsim \frac{2l^4}{\alpha^2} \frac{f_a^2}{M_{\rm Pl}^2} \ . \tag{6.119}$$

Analytically this has been shown to occur for values of the axion decay constant which satisfy [109],

$$f_a \lesssim 2 \times 10^{16} \ {\rm Gev} \frac{1}{\sqrt{\bar{n}}} \left(\frac{\alpha}{0.4\bar{n}} \right)^{\frac{3}{2}} \left(\frac{\Delta a_*}{0.1} \right)^{\frac{1}{2}} \left(\frac{5}{c_0} \right)^{\frac{1}{2}} \ , \tag{6.120}$$

where, Δa_* represents the shift of the BH spin from the superradiant spin-down and the numerical constant c_0, is determined by numerical simulations [810, 1381]. This limit corresponds to a critical value for the number density of the axions in the cloud defined as [109],

$$N_{\rm Bose} \approx 10^{78} c_0 \left(\frac{\bar{n}^4}{\alpha^3} \right) \left(\frac{M_{\rm BH}}{10 M_\odot} \right)^2 \left(\frac{f_a}{M_{\rm PL}} \right)^2 . \tag{6.121}$$

Given the high non-linearity of these systems, they are in general best understood using numerical simulations. In these simulations the critical bosenova occupation number is parameterised by a dimensionless fraction, which has been shown to occur

when [1381],

$$\epsilon \equiv \frac{M_{\rm Cloud}}{M_{\rm BH}} \simeq 10^{-4} \ . \tag{6.122}$$

The maximal occupation number of the number of bosons in the cloud, defined in Eq. (6.89) can be approximated as,

$$N_{\rm Max} \approx 10^{76} \left(\frac{\Delta a_*}{0.1}\right) \left(\frac{M_{\rm BH}}{10 M_\odot}\right)^2 \ , \tag{6.123}$$

which defines the fractional suppression factor on the superradiance rate used to approximate the value of $\Gamma_{\rm Nova}$ in Eq. (6.113),

$$N_{\rm Nova} = \left(\frac{N_{\rm Bose}}{N_{\rm Max}}\right) \approx 10^2 c_0 \left(\frac{0.1}{\Delta a_*}\right) \left(\frac{f_a}{M_{\rm PL}}\right)^2 \left(\frac{n^4}{\alpha^3}\right) \ . \tag{6.124}$$

Taking into account both the number densities in Eq. (6.123) and Eq. (6.124) the superradiant evolution equation defined in Eq. (6.88) is modified to include the analytically derived approximation for the shutdown of the BH spin down phase, due to the non-linear features of the system. This means we now evaluate the rate equation [109],

$$\Gamma_{\rm SR} \tau_{\rm bh} N_{\rm Nova} \geq \log N_{\rm Bose} \ , \tag{6.125}$$

where the suppression factor, $N_{\rm Nova}$ represents how an increase in the self-coupling strength generates an increase in the effective overall time it takes the cloud to extract spin as it experiences a series of bosenova cycles.

6.3.1.2 LMC X-1: A Specific Example

To explore the limits of when this phenomena becomes relevant we will calculate the approximate non-linear regime occurrence for the isolated stellar BH candidate LMC X-1 below. We formulate this example as a toy model to define the two dimensional space in which non-linear effects become important, as shown in the contour bounds of Fig. 6.10. Using Eq. (6.122) as a baseline, the non-linear regime can be determined

using decay constants of the approximate order $\sim \mathcal{O}(10^{16})$ GeV for the heaviest axions susceptible to superradiance. Lower axion masses have relaxed constraints on the scale of the decay constants whilst undergoing a complete superradiant cycle, allowing for a total disregard of non-linearities to first order.

In terms of a possible bosenova, we recover a similar picture exploring the limits in which we find a total absence of any bosenova. This is displayed in Fig. 6.11 showing the fractional suppression factor of Eq. (6.124) as a function of the axion mass and decay constant where a bosenova occurs before the fundamental mode has extracted the total allowed spin. Again the highest probable axion masses show the potential occurrence of a bosenova around, $f_a \sim 10^{16}$ GeV and lowest masses have associated decay scales of the order $f_a \sim 10^{14}$ GeV. Superradiance can also be shut off by other complex non-linear effects such as level mixing, or perturbed by axion emission due to annihilations [106, 108, 1379]. Returning to the linearised description, the interaction tensor can used to calculate these rates, e.g. for axion emission via the general $\phi\phi\phi \to \phi$ process. The inclusion of axion self-interactions which play an important role in BH superradiance, in principle can be understood, by expanding the instanton potential to higher orders using the RMT effective model for the axiverse which could lead to some well defined distribution for the quartic interaction tensor,

$$\mathcal{L}_{\rm int} = \lambda_{ijkl}\phi_i\phi_j\phi_k\phi_l \ . \tag{6.126}$$

We are unaware of any study of the distribution of λ_{ijkl} in RMT, and thus the treatment of interactions is beyond the scope of the present constraints detailed in Section 6.4. For sparse charge matrices the flavour changing, non-diagonal, entries in λ_{ijkl} will be rare. The level-mixing will be enhanced if the λ_{ijkl} are non-diagonal and allow for the scattering of axions of different flavours. Decays from one flavour into another will have a similar effect of additional cooling of the cloud, such as the axion photon coupling considered in Ref. [106]. The bosenova critical size $N_{\rm Bose}$, could also decrease in such a case due to the increased phase space for the scattering.

How these and other non-linear effects compete with the basic increase of the BH superradiance rate and increased probability of mass outliers at large $\mathcal{N}_{\rm ax}$ is unclear.

6.3.1.3 The Weakly Self-Interacting Regime

Using the single instanton, dilute gas potential, as a description of a single field, it can be shown that the ratio of emission via the quartic interaction compared to graviton emission due to annihilations is given by [106],

$$\frac{P_\lambda}{P_{\rm Grav}} \approx 10^{-2}\alpha^4 \frac{M_{\rm Cloud}}{M_{\rm BH}} \left(\frac{M_{\rm Pl}}{f_a}\right)^4 . \tag{6.127}$$

The overall strength of the interactions, and their importance relative to gravity, are controlled solely by the axion decay constants, f_a. The decay constant distributions for multiple fields were derived using the RMT axiverse in Chapter 5. Distributions with a high probability of small decay constants will have non-linearities dominated by self-interactions, while for a high probability of large decay constants the pure-gravity results can be applied. Since we consider BH superradiance dominated by gravity, our results should be understood as applicable strictly with the use of distributions dominated by large f_a, which is often predicted in string models.

Taking the single-field results of Ref. [108] as a guide, along with the intuition gained from the simplified analysis shown in Fig. 6.10 and Fig. 6.11, we define the linearised $\mathcal{N}$-*Radiance* regime with negligible non-linear features and suppressed superradiance rate mode mixings to be valid when our model conforms to the approximate bounds,

$$f_a \gtrsim 10^{14-16}\ \text{GeV} . \tag{6.128}$$

In the context of string models, the results presented in Section 6.4 should apply well to small volume compactifications [758], whereas self-interactions will be expected to play an important role in the Large Volume Scenario [364]. Any constraints we present in the following sections will hold for the general case of ultralight spin-0

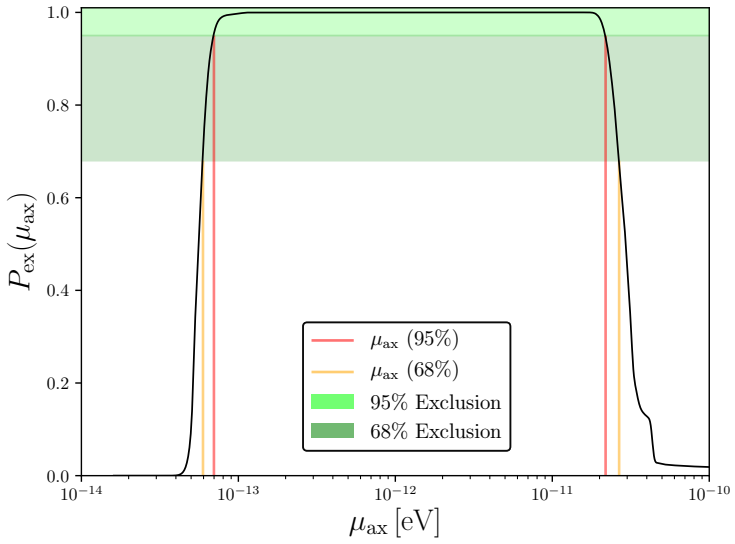


Figure 6.12: Constraints on the masses of ULAs, $\mu_{\rm ax}$, for singular fields determined by the total probability of exclusion calculated using the methodology in Appendix J via Eq. (J.1). Exclusion bounds are presented in the 68% and 95% CIs as a function of $\mu_{\rm ax}$ with *orange*/*red* lines representing the upper and lower limits of the 68%/95% intervals. These probability limit functions are determined using the BH data given in Table 6.2.

string ALPs with masses inside the limits of Eq. (6.105) and decay constants above the approximate super-GUT scale bounds of Eq. (6.128).

6.4 Superradiance Constraints on Axion-Like Particles

6.4.1 A Single Axion-Like Field

We will begin the presentation of our results by computing the single field limits to validate the consistency of the statistical methodology found in Appendix J, when approaching the multi-field case by comparing with previous results found in the literature. We will also see the single-field case well approximates the factorised limits of the multi-field setup. The statistical methods used in order to derive constraints on the axion parameter space using recorded BH spin measurements are covered in

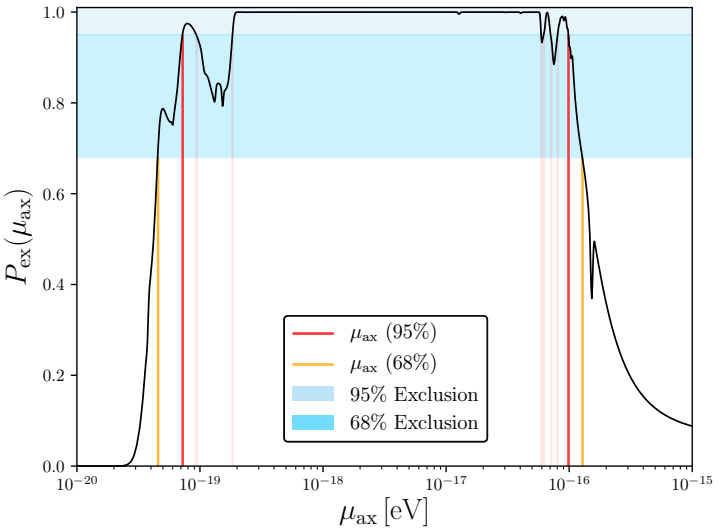


Figure 6.13: Constraints on the masses of ULAs, $\mu_{\rm ax}$, for singular fields determined by the total probability of exclusion calculated using the methodology in Appendix J via Eq. (J.1). Exclusion bounds are presented in the 68% and 95% CIs as a function of $\mu_{\rm ax}$ with *orange*/*red* lines representing the upper and lower limits of the 68%/95% interval. These probability limit functions are determined using the SMBH data given in Table 6.3.

detail in Appendix J, where we demonstrate an example calculation of the exclusion probability function, $P_{\rm ex}(\mu_{\rm ax})$. Using the model in Appendix J and treating the axion mass as a free parameter allows us to determine $P_{\rm ex}(\mu_{\rm ax})$ over the approximate bounds of Eq. (6.104). The exclusion bounds for a single axion field using the full data in Table 6.2 and Table 6.3 are presented in Fig. 6.9, superimposed over the fully accessible Regge plane susceptible to axion instabilities with the associated BH data points used. The instability bounds are found when superradiance is effective over the characteristic accretion timescale defined in Eq. (6.110). We are in fact perfectly consistent when treating the stellar BH and SMBH limits in Fig. 6.9 as individual data sets, where we can factorise the results for a single axion field with mass $\mu_{\rm ax}$, into results for the two distinct BH mass regimes. In the combined data set the exclusion probability continues to remain finite over a range of intermediate axion masses due to the large mass errors on the lightest SMBHs considered. The distinct absence of any IMBH data measurements to date, determines the regions

of the mass parameter space where the $P_{\rm ex}(\mu_{\rm ax}) > 0.68$ (1σ *exclusion*) limits do not overlap between the two datasets, allowing for their separability.

6.4.2 Constraints on Axion Masses from Stellar Mass Black Holes

The exclusion probability function for the stellar mass BH data set of Table 6.2 is shown in more detail in Fig. 6.12, determining both the 68% and 95% CI bounds. The high quality of the measurements of X-ray binary sources, and the larger quantity on candidates, lead to a smoother exclusion function. At the 95% CI the stellar BHs exclude axions with masses,

$$7.0 \times 10^{-14}\ \text{eV} \lesssim \mu_{\rm ax} \lesssim 2.2 \times 10^{-11}\ \text{eV}\ , \tag{6.129}$$

and at the 68% CI exclude,

$$6.0 \times 10^{-14}\ \text{eV} \lesssim \mu_{\rm ax} \lesssim 2.7 \times 10^{-11}\ \text{eV}\ . \tag{6.130}$$

6.4.3 Constraints on Axion Masses from Supermassive Black Holes

For SMBHs the exclusion probability derived from the data is shown in Fig. 6.13, again shown with derived 68% and 95% CI bounds. The data is generally of poorer quality than the stellar data, with certain systems containing significantly larger errors on mass estimates. It is also much sparser, with fewer SMBHs in the considered data set. The sparseness of the data leads to oscillatory features in the exclusion probability, driven by the shape of the BH superradiance contours found for each of the radial modes of the axion cloud, with the exclusion functions oscillations driven by the logarithmic separation of individual BH points. This causes the probabil-

ity exclusion function to oscillate between the 95% CI when transitioning between certain BHs, particularly prominent for the constraints coming from *ARK 120* and *Fairall 9*. This uncertainly is represented by the faded red lines in Fig. 6.13, where we expect increased accuracy in data measurements and identification of further SMBH candidates would dissolve these limits and ensure consistency in the total bound. In particular the largest considered candidate, *Fairall 9*, drives the non-monotonic nature of the function at low axion masses. The large mass errors lead to a non-zero exclusion probability extending to large axion masses. Taking the outer edge of the 95% CI region, the SMBHs exclude axions with masses in the range,

$$7.2 \times 10^{-20}\ \text{eV} \lesssim \mu_{\text{ax}} \lesssim 1.0 \times 10^{-16}\ \text{eV}\ , \tag{6.131}$$

with the outer 68% limits,

$$4.6 \times 10^{-20}\ \text{eV} \lesssim \mu_{\text{ax}} \lesssim 1.3 \times 10^{-16}\ \text{eV}\ . \tag{6.132}$$

Our exclusions for the stellar BH and SMBH datasets are consistent with previous results for axion mass constraints found in Refs. [108, 317], after accounting for the differences in the data sets and methodology used. In particular comparing to Ref. [108], our choice to include BBH coalescence events with large masses when partnered with their large uncertainties push the constraints to incorporate lower masses, increasing the current lower bound on the axion mass exclusion limits, which could be tightened with future improvements to observational measurements. Finally to ensure consistency with the $\mathcal{N}$-*Radiance* regime defined in Section 6.3, we expand the single field constraints into the two-dimensional axion mass, decay constant plane implementing the statistical procedure in Appendix J for the case of the toy model BH LMC X-1, considered in Section 6.3.1.2. These constraints are found by deriving bounds using Eq. (6.125) instead of Eq. (6.88) used for the single field limits placed on just the axion mass, where we find results consistent with those found in Ref. [109]. The LMC X-1 constraints on the two-dimensional axion

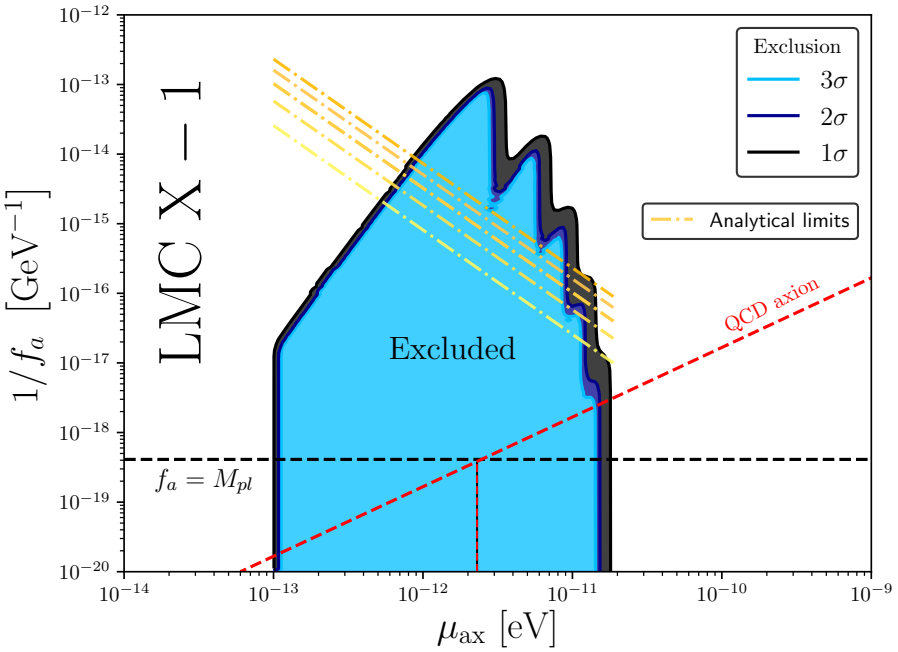


Figure 6.14: Example constraints in the axion decay constant, f_a, and axion mass, $\mu_{\rm ax}$, plane from BH candidate LMC X-1. The contour bounds representing the constrained region in the two-dimensional plane are presented with 1σ, 2σ and 3σ limits. The bounds are calculated using Eq. (6.125) with superradiance timescales defined according to the limit in Eq. (6.110). The *yellow* and *orange* dot-dashed lines represent the analytical limits determined using Eq. (6.120). The *red* dashed line represents the approximate mass of the QCD axion using the chiral potential (Eq. (6.147)), which intercepts the Planckian limit for the lowest axion mass which can be constrained when considering the WGC.

parameter space from spin measurements are shown in Fig 6.14. The analytical limits represent the bounds formed using Eq. (6.120) which are not sensitive to the functional shape of the radial mode contours.

6.4.4 A Degenerate Axion Mass Population

We can now begin our considerations of models with multiple axion fields present, using the simplest case. The degenerate case, such as those found in the models detailed in Section (5.2.3), is trivial to treat for any value of $\mathcal{N}_{\rm ax}$, as by definition

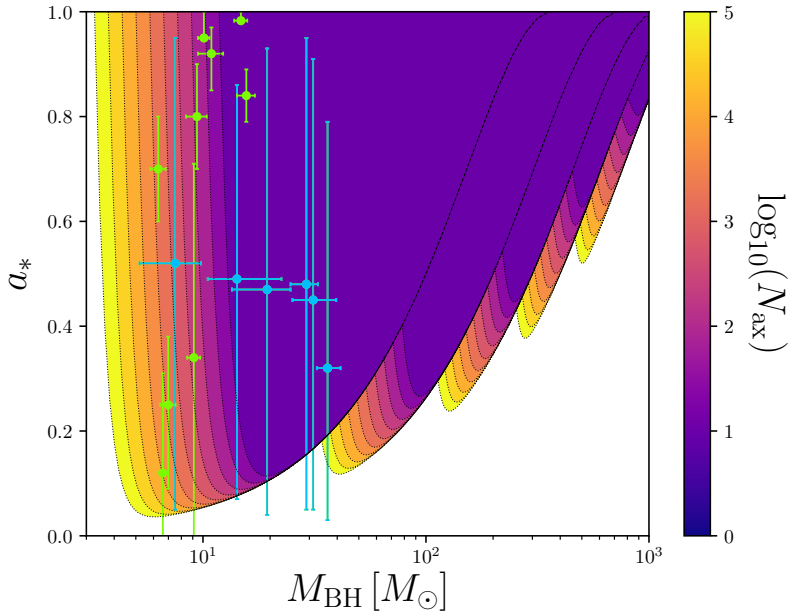


Figure 6.15: Isocontour exclusion regions for degenerate mass axion populations with $\mathcal{N}_{\rm ax} = \mathcal{O}(10^0 \to 10^5)$ in the stellar BH parameter-space. The limits for the instability threshold are obtained by fixing the superradiant instability time scales for each value of the orbital/azimuthal quantum numbers, $l = m = 1$ to 5 equal to $\tau_{\rm Salpeter}$ defined in Eq. (6.108) using a fixed axion mass of $\mu_{\rm ax} = 10^{-12.75}$eV. Large values of $\mathcal{N}_{\rm ax}$ effectively correspond to greater superradiance instability timescales considering a single field. The *green* data points are mass-spin estimates of X-ray binary stellar BH candidates. The *blue* data points are primary and secondary sources from BBH coalescence detections at LIGO.

each axion has an identical mass, $\mu_{\rm ax}$, and thus superradiance dynamics. Since the rate is additive in $\mathcal{N}_{\rm ax}$, when the fields follow the limits in Eq. (6.128), we can define the degenerate total superradiance rate as,

$$\Gamma_{\rm SR}^{\rm Tot} = \mathcal{N}_{\rm ax}\Gamma_{\rm SR} \ . \tag{6.133}$$

Using the relation, $\tau_{\rm BH}\Gamma_{\rm SR}^{\rm Tot} = 1$ is equivalent to observing the single field case with a characteristic timescale rescaled as,

$$\tau_{\mathcal{N}_{\rm ax}} = \mathcal{N}_{\rm ax}\tau_{\rm BH} \ . \tag{6.134}$$

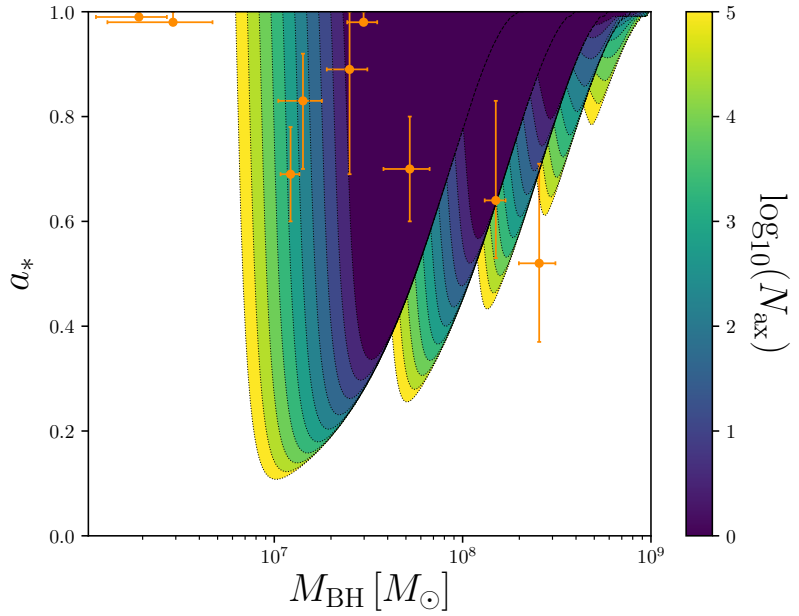


Figure 6.16: Isocontour exclusion regions for degenerate mass axion populations with $\mathcal{N}_{\rm ax} = \mathcal{O}(10^0 \to 10^5)$ in the stellar BH parameter-space Regge plane. The limits for the instability threshold are obtained by fixing the superradiant instability time scales for each value of the orbital/azimuthal quantum numbers, $l = m = 1$ to 5 equal to $\tau_{\rm Salpeter}$ defined in Eq. (6.108) using a fixed axion mass of $\mu_{\rm ax} = 10^{-18.5}$eV. The *orange* data points are the mass-spin estimates of AGN SMBH candidates detailed in Table 6.3.

Thus, for the degenerate case the exclusion probabilities are trivial to compute for any value of $\mathcal{N}_{\rm ax}$, where the contour bounds simply expand as the number of degenerate fields, $\mathcal{N}_{\rm ax}$ increases. The rescaling of Eq. (6.88) pushes each of the radial mode contours towards the saturation point, $a_* = 0$. This effect is shown in both BH mass regimes in Fig. 6.15 and Fig. 6.16 on the Regge plane windows with a degenerate population of axions with masses for various orders of the axion population size, $\mathcal{N}_{\rm ax} = \mathcal{O}(1 \to 10000)$.

6.4.5 Constraints on a Degenerate Population

For the case of stellar BHs we fix the axion mass to be, $\mu_{\rm ax} = 10^{-12.75}$ eV, and for SMBHs, $\mu_{\rm ax} = 10^{-18.5}$ eV. It is clear from each example that an increase in $\mathcal{N}_{\rm ax}$

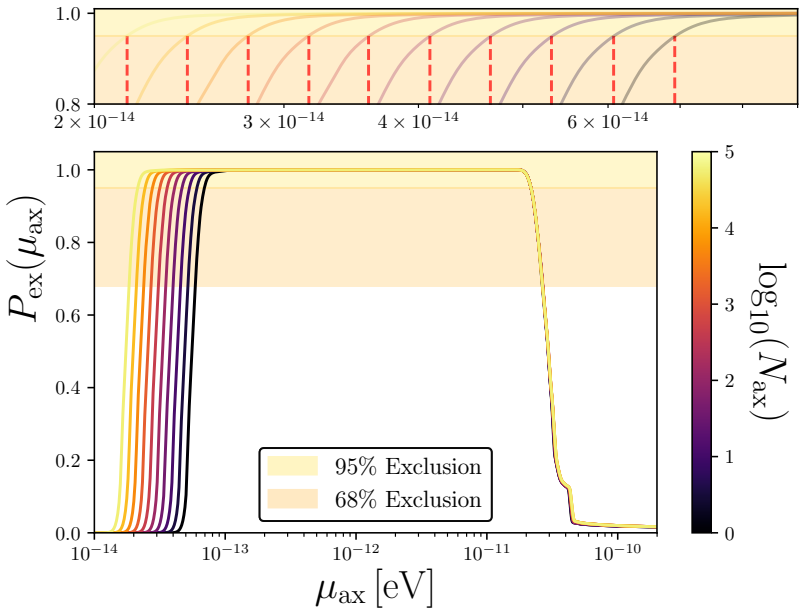


Figure 6.17: Constraints on masses of ULAs, $\mu_{\rm ax}$, via the total exclusion probability in the 68% and 95% CIs for large numbers, $\mathcal{N}_{\rm ax}$, of degenerate fields. *Upper panels:* Dashed red lines represent the shift of the lower bounds in the 95% CI, which decreases as $\mathcal{N}_{\rm ax}$ increases. The exclusion probability functions showing the $\mathcal{N}_{\rm ax}$ type enhancement for the stellar BH data set are calculated using Eq. (6.133).

can lead to an exclusion on $\mu_{\rm ax}$ where there was not one in the case of a single field (*purple* limits). As the instability thresholds sweep through the Regge plane, as a function of the axion mass, the wider instability limits possess the ability to *catch* lighter BHs in their exclusion bounds. It is also possible to find an exclusion from BHs with lower spins, which may have avoided all radial mode contours, where it takes $\mathcal{N}_{\rm ax} \gtrsim \mathcal{O}(10^5)$ to shift the dominant $l = m = 1$ mode $\Delta a_* \approx \mathcal{O}(0.1)$. Higher modes experience a greater enhancement from the presence of multiple fields. The $l = m = 5$ mode in the stellar example presented in Fig. 6.15, shifts $\Delta a_* \approx 0.3$ for $\mathcal{N}_{\rm ax} \gtrsim \mathcal{O}(10^5)$. This difference is suppressed for SMBHs as the axion mass decreases. Both the $l = m = 1$ and $l = m = 5$ modes receiving an approximate contour shift $\Delta a_* \approx 0.25$ for $\mathcal{N}_{\rm ax} \gtrsim \mathcal{O}(10^5)$, as shown in Fig. 6.16.

To quantify the effect these enhancements have on the field constraints we present the exclusion probabilities $P_{\rm ex}(\mu_{\rm ax})$, for various values of $\log_{10}(\mathcal{N}_{\rm ax})$ for each BH mass

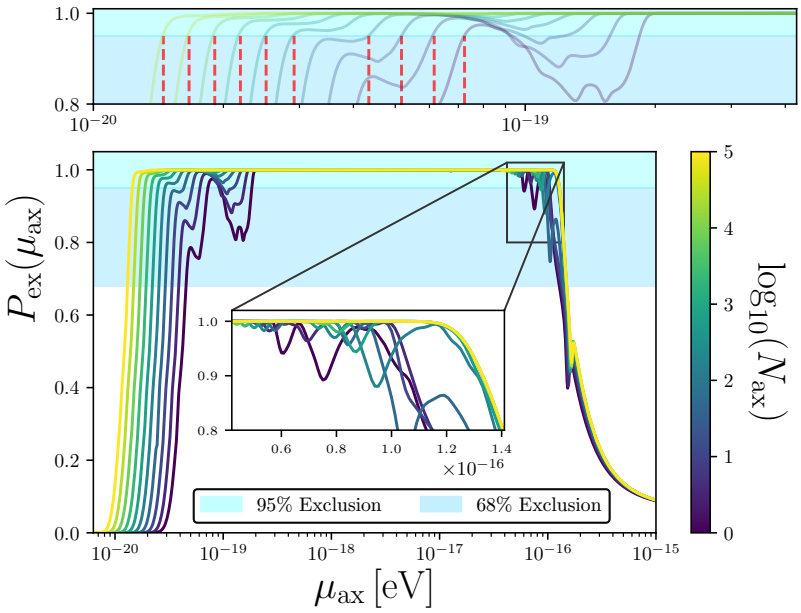


Figure 6.18: Constraints on masses of ULAs, $\mu_{\rm ax}$, via the total exclusion probability in the 68% and 95% CIs for large numbers, $\mathcal{N}_{\rm ax}$, of degenerate fields. *Upper panels:* Dashed red lines represent the shift of the lower bounds in the 95% CI, which decreases as $\mathcal{N}_{\rm ax}$ increases. The exclusion probability functions showing the $\mathcal{N}_{\rm ax}$ type enhancement for the SMBH data set are calculated using Eq. (6.133). *Inset:* Oscillatory behaviour of the exclusion probability due to higher values of the orbital/azimuthal quantum numbers passing over low mass SMBHs.

regime, repeating the procedure used to generate both Fig. 6.12 and Fig. 6.13, which are displayed in Fig. 6.17 and Fig. 6.18 respectively. The example contours in both Fig. 6.15 and Fig. 6.16 always increase in the direction of smaller values of $M_{\rm BH}$, with an effective "*lag*", and so the constraints detailed in both Fig. 6.17 and Fig. 6.18 only broaden relative to the single field case for smaller axion masses. For SMBHs, where the higher harmonics play a role in the exclusion, the oscillations in the exclusion probability at high mass in the absence of sufficient BH data point densities, are also mildly affected. This is shown in the *inset* of the *left panel* of Fig. 6.18. Extremely large values of $\mathcal{N}_{\rm ax}$ quench the oscillations from the instability bounds of the higher order modes, saturating the upper bounds on the constraints. In general we find that the 95% excluded regions for $\mu_{\rm ax}$, for the case of a degenerate population of axions change by less than an order of magnitude compared to the results for a

single field when $\mathcal{N}_{\rm ax} \lesssim 10^5$. This shows that any increase in the superradiance rate for multiple fields, i.e. the rate sum found in Eq. (6.68), can be virtually neglected to leading order when computing the multi-field exclusion probability bounds for sufficiently non-interacting fields, even in the most extreme cases presenting a very large population of degenerate mass superradiant fields. Given the extreme number of axions, along with the singular nature of the mass spectrum required for any significant effect, we can assume from now on that superradiance rate mixing and multi-field effects defining modifications to the contour bounds in the Regge plane offer highly suppressed contributions.

6.4.6 A Non-degenerate Axion Mass Population

For a non-degenerate population with masses defined from a models matrix eigenvalues, spectral correlations must be accounted for. In the following section we detail the considerations which must be made in this case and the simplifications we make to our mass distribution prior.

6.4.6.1 Correlated Eigenstates

Individual eigenvalue statistics naturally stem from our understanding of gap probabilities, providing insight into the fine structure of the spectrum of study [46, 505, 754, 939]. The following points are important for the analysis conducted and the results presented in the following section (Section 6.4.6 and specifically the results displayed in Fig. 6.25). The features of RMT covered in both Section 4.1 and Section 4.3.1 allow us a nice picture of the limiting density functions we may wish to use when assigning priors to parameters in our models. In the context of random ensemble modelling there are two types of correlation we must account for however. The first concerns density correlation functions which can be approached on either global or local scales. The second, and those relevant to the discussions here, are the correlations involving individual eigenvalue statistics. These are often represented

using spectral features such as their distribution or spacing. A common approach to evaluating these features of local correlations are gap probabilities, that is the investigation that a certain interval is void of any eigenvalues. Consider a general joint probability density function for $\mathcal{N}$ eigenvalues,

$$\int_{\lambda_-}^{\lambda_+} d\lambda_1 \ldots \int_{\lambda_-}^{\lambda_+} d\lambda_{\mathcal{N}} P(\lambda) = 1 \ , \tag{6.135}$$

for some choice of random matrix ensemble we may wish to consider to model the axion parameter space. The values of λ_+ and λ_- represent the eigenvalue supremum and infimum supports which determine the domain of the eigenvalues whilst fixing the limits of integration.

As we have covered, the results of classical RMT and the nature of the matrix eigenvalues understood through methods such as the log gas formalism incorporate the Vandermonde determinant. This term represents the probabilistic nature it is unlikely to find two eigenvalues in close vicinity of each other. Let us also define the eigenvalue hierarchy, $\lambda_- \leq \lambda_\alpha \leq \lambda_\beta \leq \lambda_+$ for two eigenvalues, sitting inside the eigenvalue domain. For particular spectral statistics (individual eigenvalue probabilities or correlations etc.) it is common practise to study these characteristics through the case that all eigenvalues fall inside the domain $[\lambda_\alpha, \lambda_\beta]$ (denoted $\acute{P}$), which is understood as [827],

$$\acute{P}(\lambda_\alpha, \lambda_\beta) = \int_{\lambda_\alpha}^{\lambda_\beta} d\lambda_1 \ldots \int_{\lambda_\alpha}^{\lambda_\beta} d\lambda_{\mathcal{N}} P(\lambda) \ . \tag{6.136}$$

The alternative consideration of the problem is therefore the gap probability associated to a *gap* of eigenvalues (denoted $\grave{P}$) in the equivalent domain,

$$\grave{P}(\lambda_\alpha, \lambda_\beta) = \int\limits_{(\lambda_-, \lambda_\alpha) \cup (\lambda_\beta, \lambda_+)} d\lambda_1 \ldots \int\limits_{(\lambda_-, \lambda_\alpha) \cup (\lambda_\beta, \lambda_+)} d\lambda_{\mathcal{N}} P(\lambda) \ . \tag{6.137}$$

Eigenvalue correlations determine that the relationship between these two expressions is non-trivial in the case of a spectrum. The point that must be stressed here

is that,

$$\grave{P}(\lambda_\alpha, \lambda_\beta) \neq 1 - \acute{P}(\lambda_\alpha, \lambda_\beta) \ , \tag{6.138}$$

when $\mathcal{N} > 1$. Using Eq. (6.138) we can at best make the approximation, $\grave{P}(\lambda_\alpha, \lambda_\beta) \approx 1 - \acute{P}(\lambda_\alpha, \lambda_\beta)$ when $\mathcal{N}$ is of the order of a '*few*'. Such correlations are defined to be local objects. Considering eigenvalues which present a global separation as suitably screened we can make the rough approximation of a small sample as uncorrelated. As $\mathcal{N}$ increases the local statistics become ever more significant in our evaluation of the join density function in Eq. (6.135). Beyond such an approximation the highly correlated eigenvalues must certainly be accounted for when utilising a RMT model directly with a large number of fields.

The probability of selecting individual eigenvalues in RMT models utilising a LSD as a prior is therefore heavily dependant this correction. The study of gap probabilities is central to the topic of extreme eigenvalues (i.e. λ_+ or λ_-) where the distribution of a particular eigenvalue (say $P(\lambda_+)$) follows by differentiation of $\grave{P}(\lambda_+)$. We have touched on these topics and example studies in Section 4.1.6.1 and Appendix D. Gap probabilities have been tackled with several established techniques, such as Fredholm eigenfunctions [590, 940], linear differential equations [505] and Painlevé transcendental equations [1266]. Indeed once we have an understanding of the spectral correlations (point correlation function in Eq. (4.14) and Eq. (4.16)) often represented in terms of a kernel (Eq. (4.12)) generated by (skew)-orthogonal polynomials (Eq. (4.10)) we can in principle define the gap probabilities (see Section 4.1.4.1). A calculation of these of gap probabilities then lead us to distributions for individual eigenvalues or spacings as required. Once dealing with the first gap probability a common step is to then focus on the gap probability generating function for all subsequent gaps [380, 423–425].

Results have been obtained for the statistical probabilities concerning multiple eigenvalues using Wishart-Laguerre matrices such as the examples (lowest eigenvalue to second order and higher) found in Ref. [395]. Results regarding the spectral density

of eigenvalues and gap probabilities in the Wishart-Laguerre ensembles relevant to the models discussed in Chapter 5 can be found in the following. See Ref. [827] for explicit results in both the correlated and uncorrelated cases (alternative and null cases in our definitions respectivly). See also Refs. [47, 1355, 1356, 1358, 1359] and Ref. [506] for results for gap probabilities in the correlated and uncorrelated real Wishart-Laguerre ensemble with various considerations for the kernels involved. The specific details of these calculations will depend on our choice of $\tilde{\beta}$, with real ensembles often proving to be more technically challenging in specific regards. This is certainly true when correlations among the matrix elements are introduced [552, 1357].

Given these technical challenges presented by correlated ensembles with real entries we will relax any consideration of local correlations and gap probabilities in the following section. It must be stated this type of assumption that the eigenvalues of some random matrix model can be selected by independent draws using the ensembles LSD for a non-trivial value of $\mathcal{N}_{\rm ax}$ is in principle incorrect. To simplify our analysis however we will adopt the assumption that our prior on the axion masses follows the approximation discussed in Section 5.4.3 and that our draws for multiple fields are uncorrelated. We are therefore placing constraints only on modal functions representative of the types of liming spectra we could find in RMT models (analogous to Poissonian type spectra) which asymptotes toward the type of prior motivated in Ref. [107], with an assumption of statistical independence between the axion masses. The following constraints should therefore be interpreted as not representative of direct constraints to be placed on the number of fields determined from the eigenstates of some random matrix ensemble model of the axiverse.

The effect of the ensemble local spectral correlation functions on the exclusion bounds would be an interesting extension in future work and is not represented in the integrals calculated below. A basic consideration of the local eigenvalue repulsion could have the effect of probabilistically pushing a subsequent mass eigenstate either in or out of the excluded regions of interest. This may therefore lead to different exclusion bounds when conducting a direct analysis of RMT models and the number of

fields they would typically exclude. The general results for anti-correlation between gap-probabilities [939] could give interesting results in this regard. Our masses are assumed to be represented by a sequence of real points determined by some fully factorised function rather than those which emerge from RMT calculations directly, offering a simple first order approximation of such an analysis.

6.4.6.2 Simplified Factorised Probabilities

There are two effects which regulate BH superradiance constraints when dealing with an axion mass distribution. The first is the effect of rate addition, and the second is the effect of an overlap between the mass distribution and the exclusion probability. The results of the previous section have detailed how that even for the extreme case of degenerate masses, this effect is virtually negligible in the exclusion probability for $\mu_{\rm ax}$, in the limits we are operating in. Rate addition will be even more negligible for non-singular mass distributions of finite width, where off-resonant superradiance rates are non-linearly suppressed. This leaves the probability overlap as the dominant effect when considering a mass distribution of finite width.

With the effect of rate addition neglected, the exclusion probability for a mass distribution is trivial to construct from the exclusion probability for a single mass from the overlap integral. We use the probability that a model is allowed ($P_{\rm al}$), since this trivially accounts for the combinatorics, and the excluded probability ($P_{\rm ex}$) is in turn found trivially from this. Let the expression,

$$P_{\rm al}(\mu_{\rm ax}|\mathcal{N}_{\rm ax}=1) = 1 - P_{\rm ex}(\mu_{\rm ax}|\mathcal{N}_{\rm ax}=1)\ , \tag{6.139}$$

be the probability that a given axion mass is allowed, assuming just one axion field. We then have that in a given model $\mathcal{M}$, with one axion, the probability that some parameters θ are allowed is,

$$P_{\rm al}(\theta, \mathcal{N}_{\rm ax}=1|\mathcal{M}) = \int {\rm d}\mu_{\rm ax} p(\mu_{\rm ax}|\theta,\mathcal{M}) P_{\rm al}(\mu_{\rm ax}|\mathcal{N}_{\rm ax}=1)\,, \tag{6.140}$$

where $\mathrm{d}\mu_{\rm ax} p(\mu_{\rm ax}|\theta, \mathcal{M})$ is the probability distribution for the field mass $\mu_{\rm ax}$ in the model. The allowed regions for a single axion were evaluated numerically in Section 6.4.1, where the integral in Eq. (6.140) can be evaluated numerically given $p(\mu_{\rm ax}|\theta, \mathcal{M})$. The above trivially generalises to the case of $\mathcal{N}_{\rm ax}$ fields via the exponentiation,

$$P_{\rm al}(\theta, \mathcal{N}_{\rm ax}|\mathcal{M}) = \left[\int \mathrm{d}\mu_{\rm ax}\ p(\mu_{\rm ax}|\theta, \mathcal{M}) P_{\rm al}(\mu_{\rm ax}|\mathcal{N}_{\rm ax} = 1)\right]^{\mathcal{N}_{\rm ax}} . \tag{6.141}$$

The exclusion probability for a non-degenerate population of axion fields in a given model is then found via the simple relationship,

$$P_{\rm ex}(\theta, \mathcal{N}_{\rm ax}|\mathcal{M}) = 1 - P_{\rm al}(\theta, \mathcal{N}_{\rm ax}|\mathcal{M}) \ . \tag{6.142}$$

Given the previously derived exclusion functions, we now only need to define the nature of the mass spectrum via the universality of the effective models previously introduced, in order to constrain the number of fields we could expect in the ultralight sector.

6.4.6.3 The M-theory Axiverse: the QCD Axion, GUTs, and FDM

We can reduce the dimensionality of the parameter space, and simply the nature of the priors placed on the LSD function of the axion mass matrix by considering the unified approach for the three model classes defined in Chapter 5, using the methods detailed in Section 5.4.3. The log-normal distribution (Eq. (5.132)), centred on a particular mean mass scale $\bar{\mu}_{\rm ax}$, with some variance σ^2, provides a useful benchmark, covering each different type of model. For small σ, recall it resembles a degenerate spectrum, like the models in Section 5.2.3. For large σ the spectra are approximately log-flat, representing the epistemic priors of Section 5.1.2, given the limiting nature of the upper and lower bounds which define the ultralight sector. Finally any intermediate values of σ are statistically similar to eigenvalue distribu-

tions found in both the RMT axiverse (Section 5.2) and M-theory random matrix model (Section 5.3). Therefore by adopting the combined approach introduced in Section 5.4.3, we now parameterise our constraints in terms of a distribution fully determined by its first two centralised moments, its limiting shape now fully logarithmically symmetric about some phenomenologically characterising mean scale. In Fig. 6.25 we present the 95% CI excluded region defined in the $(\sigma, \mathcal{N}_{\rm ax})$ model hyperplane, using the log-normal distribution across a range of central values. For low-energy concerns we will focus on the case of reproducing the three previously covered phenomenological scenarios of interest which we recall here for convenience, realised approximately from this simple model for the random matrix and M-theory axiverse.

As we have previously covered, the M-theory formulation of the low energy axiverse with successful GUT scale unification predicts the existence of an axion with an associated mass scale,

$$\mu_{\rm ax,GUT} \approx 10^{-15}\ {\rm eV}\,, \tag{6.143}$$

which arises from fixing a single modulus to give the correct GUT scale coupling, $\alpha_{\rm GUT} \simeq 1/25$, associated to a three-cycle with a volume, $\mathcal{V}_X \simeq 25$ in string units. We explore this possibility by fixing the log-normal spectral mean to,

$$\log_{10} \bar{\mu}_{\rm ax}^{\rm GUT} = -15\ . \tag{6.144}$$

The FDM model [722, 728, 914, 1078, 1152] covered in Section 2.8.3 posits that DM composed of axions with mass,

$$\mu_{\rm ax,FDM} \approx 10^{-22}\ {\rm eV}\,, \tag{6.145}$$

and possesses certain desirable properties that could lead to it being favoured over standard cold DM by observations of galactic structure. This scale is the lower bound on standard FDM models currently not probed by superradiance effects (see

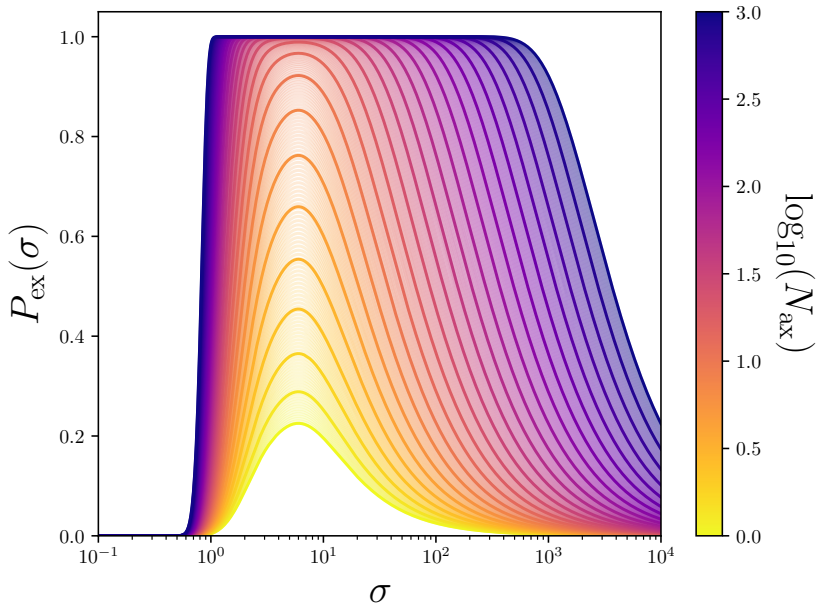


Figure 6.19: Probability of exclusion represented as a function of the dimensionless variance, σ, defining the mass spectra in the RMT axiverse for $\mathcal{N}_{\rm ax} = (10^0 \to 10^3)$. These constraints are for the scenario in which the mean of the mass spectra is fixed according to Eq. (6.145) in order to maximise the probability of drawing a desired axion mass associated to models of FDM, as detailed in Section 6.4.6.3. In the limit $\sigma \gg 1$ the total probability for $\mathcal{N}_{\rm ax} = 1 \to \infty$ converges to zero as the spread crosses the bounds probable by BH spin measurements. The behaviour in the limit $\sigma \ll 1$ is determined by the accuracy of the available BH mass-spin measurements.

discussions in Section 6.4.7). We model this by fixing the log-normal spectral mean to,

$$\log_{10} \bar{\mu}_{\rm ax}^{\rm FDM} = -22 \ . \tag{6.146}$$

The QCD axion [1036, 1335, 1353] mass is given by,

$$\mu_{\rm ax,QCD} \approx 6 \times 10^{-10} \text{ eV} \left(\frac{10^{16} \text{ GeV}}{f_a} \right) . \tag{6.147}$$

In order to realise the QCD axion in M-theory, some light eigenstate in the "*pure M-theory*" spectrum should receive its mass dominantly from QCD instantons. Furthermore, the VEV of this field should be not far displaced from $\theta = 0$, to provide a valid solution to the strong-CP problem. These two conditions together require

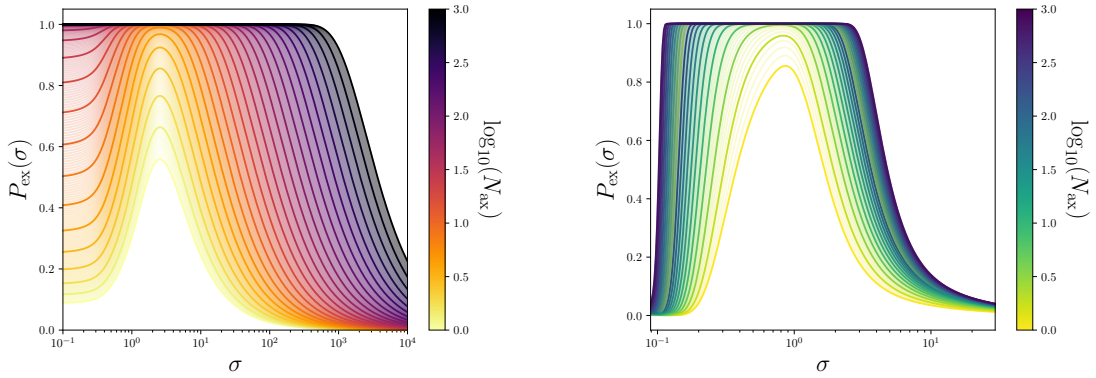


Figure 6.20: Probability of exclusion as a function of the dimensionless variance, σ defining the mass spectra in the M-theory axiverse for $\mathcal{N}_{\rm ax} = (10^0 \to 10^3)$. *Left panel*: These constraints represent the scenario in which the mean of the mass spectra is fixed according to Eq. (6.143) in order to maximise the probability of drawing a desired axion mass associated to models of GUT in the M-theory axiverse. *Right panel*: These constraints represent the scenario in which the mean of the mass spectra is fixed using Eq. (6.149) in order to maximise the probability of drawing a desired axion mass associated to models of the QCD axion of the Standard Model. In the limit $\sigma \gg 1$ the total probability for $\mathcal{N}_{\rm ax} = 1 \to \infty$ converges to zero as the spread crosses the bounds probable by BH spin measurements. The behaviour in the limit $\sigma \ll 1$ is determined by the accuracy of the available BH mass-spin measurements.

that there is at least one eigenstate in the pure M-theory spectrum with [31],

$$\mu_{\rm ax} \lesssim \mu_{\rm ax,low} \approx 10^{-14}\ {\rm eV}\,, \tag{6.148}$$

where $\mu_{\rm ax,low}$ represents an upper bound mass scale fixed by the theory. We model this by fixing $\bar{\mu}_{\rm ax}$ and σ such that $\mu_{\rm ax,low}$ is within 95% of the probability at the lower end of the distribution after $\mathcal{N}_{\rm ax}$ draws. This fixes $\bar{\mu}_{\rm ax}(\sigma, \mathcal{N}_{\rm ax})$ in terms of the standard error functions (erfc),

$$\mathcal{N}_{\rm ax}{\rm erfc}\left[-\frac{\log_{10}(\mu_{\rm ax,low}/\bar{\mu}_{\rm ax})}{\sqrt{2\sigma^2}}\right] = 0.1\ . \tag{6.149}$$

Using the intuition above, one linear combination of axions receives its mass from QCD instantons. We therefore must remove one axion from the M-theory distribu-

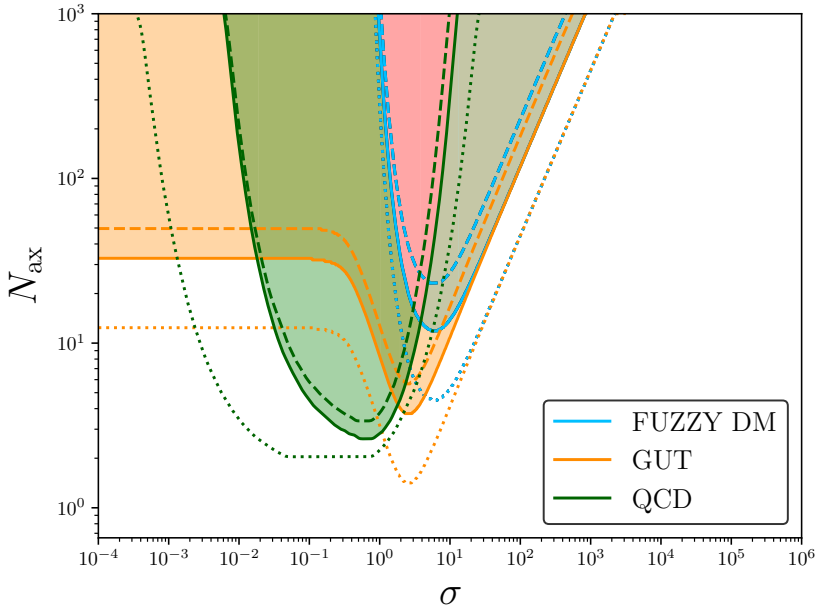


Figure 6.21: Exclusion bounds for the allowed number of fields, $\mathcal{N}_{\rm ax}$, as a function of the distribution width, σ, represented by 68% (*dotted* line), 95% (*solid* line) and 99.7% (*dashed* line) limits. Each example represents the phenomenological models defined by Eq. (6.143) (GUT), Eq. (6.145) (FDM), and Eq. (6.149) (QCD). Regions above the contours are excluded. The *red* region represents the intersection of the 95% exclusion bounds which excludes $\mathcal{N}_{\rm ax} \gtrsim \mathcal{O}(30)$ for $\sigma \sim \mathcal{O}(1)$ for each of the three examples.

tion and replace it with the QCD axion. The total probability that the QCD axion in the M-theory random matrix axiverse is allowed based on BH superradiance data is thus,

$$P_{\rm al}(\sigma, \mathcal{N}_{\rm ax}) = \mathcal{P}\left\{\int \mathrm{d}\mu_{\rm ax}\; p[\mu_{\rm ax}|\sigma, \bar{\mu}_{\rm ax}(\sigma, \mathcal{N}_{\rm ax})] P_{\rm al}(\mu_{\rm ax}|\mathcal{N}_{\rm ax}=1)\right\}^{\mathcal{N}_{\rm ax}-1}, \quad (6.150)$$

where,

$$\mathcal{P} = P_{\rm al}(\mu_{\rm ax,QCD}|\mathcal{N}_{\rm ax}=1)\ . \quad (6.151)$$

Constraints on the distribution parameters of each of these benchmark models are displayed in Fig 6.19, the *left panel* of Fig 6.20 and *right panel* of Fig 6.20 for the FDM, GUT and QCD scenarios respectively. While none of these models are ruled out for a single axion, in all cases the exclusion probability starts to become signif-

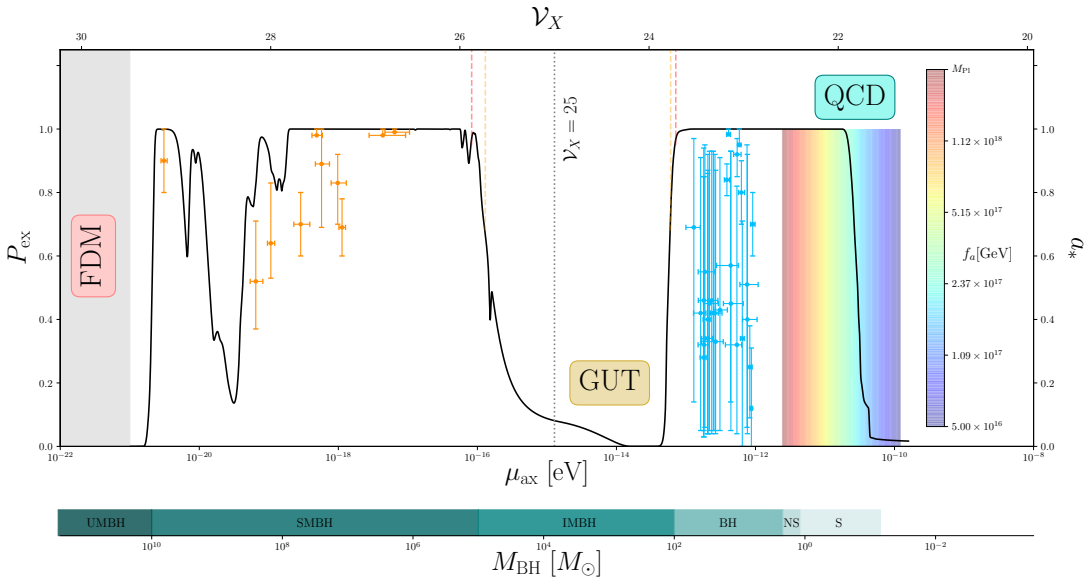


Figure 6.22: Constraints on the masses of ULAs in the bounds of Eq. (6.105) plus the additional limits from M87* approaching the FDM domain using Eq. (6.155) and Eq. (6.156). The singular field bounds are determined by the total probability of exclusion calculated using the methodology in Appendix J via Eq. (J.1), as in Fig. 6.9. The external lower axis represents the approximate mass bounds of known BHs plus UMBHs, neutron stars (NS) and stellar (S) objects, used to probe specific bosonic field mass bounds. The upper axis represents the generalised volume of the corresponding three-dimensional submanifolds in eleven-dimensional Planck units defined in Eq. (5.104), related to the geometrical axion mass scales of M-theory in the lower axis. The *black dotted* line defines the geometrical axion mass scale and generalised volume associated to gauge coupling unification and the visible sector. Finally the *inset colourbar* represents the associated axion decay constant scale for the QCD axion determined by the relationship to its mass defined in Eq. (6.147).

icant for non-zero distribution widths and for large numbers of fields. In all cases, a clustering or multi-component structure to the effective singular phenomenological field shows the maximum allowed value of $\mathcal{N}_{\rm ax}$ increases only for very large σ. For large σ the distribution is effectively log-flat over the ultralight sector of axion cosmology, with respect to the data exclusions, where increasing the width simply reduces the probability of producing an overlap.

The GUT model has a small exclusion probability at zero width due to the large mass errors on the lightest SMBHs (*NGC 4051* and *MCG-6-30-15*). The GUT model is excluded at better than 95% CI for all widths, $\sigma < \mathcal{O}(100)$, for $\mathcal{N}_{\rm ax} \gtrsim 100$.

The FDM model is excluded at better than 95% CI for all widths $1 \lesssim \sigma \lesssim 10^3$ if $\mathcal{N}_{\rm ax} \gtrsim 100$. The QCD axion model is the least constrained by the data. The mass of the QCD axion with $f_a \gtrsim 10^{17}$ GeV is not excluded itself by BH superradiance, nor is the light mass $\mu_{\rm ax,low}$, required from the M-theory part of the spectrum. There is a small range of intermediate widths where the distribution does overlap the excluded region, excluding $0.2 \lesssim \sigma \lesssim 4$ if $\mathcal{N}_{\rm ax} \gtrsim 10^2$ at 95% CI while $\sigma \gtrsim 4$ is allowed for all $\mathcal{N}_{\rm ax} < 10^3$ considered. A combined picture of these the bounds representing the 68%, 95% and 99.7% CIs is shown in Fig. 6.21 in the $(\sigma, \mathcal{N}_{\rm ax})$ plane. The *red* bounded region represents the intersection of the 95% exclusion bounds for the each of the scales in Eq. (6.143), Eq. (6.145), and Eq. (6.149). For $\mathcal{O}(1)$ values of the distribution spread, fixed by σ, each of these phenomenological models is excluded for spectra consisting of $\mathcal{N}_{\rm ax} \gtrsim \mathcal{O}(30)$.

In Fig. 6.22 we display each of these phenomenological models in the context of the full constrains on ULAs. The lower limit on the bounds stops at the boundary of ultramassive BHs (UMBHs) with masses $\gtrsim 10^{10}\ M_\odot$. The upper bound on the constraints enters the domain of the QCD axion as represented by the colourbar spectrum for sub-Plankian decay constants and masses determined by the relationship in Eq. (6.147). We should proceed with caution however when considering the constraints on the lightest possible QCD axion masses as these are associated to astrophysical mass scales of neutron stars and stellar mass objects. Using the statistical methodology in Appendix J we find the approximate upper bound on the phenomenological QCD axion decay constant at the 68% CI as,

$$f_a^{\rm QCD} \lesssim 3 \times 10^{17}\ \text{GeV}\ . \tag{6.152}$$

Finally when considering the M-theory models presented in Section 5.3, the ultralight bosonic masses stemming from the real components of the moduli superfields and the extra-dimensional compactification process are proportional to the generalised volumes of the corresponding three-dimensional submanifolds. Using the mod-

els detailed in Refs. [28, 29, 31] we can place approximate bounds on the volumes of the threecycles which may be motivated in these phenomenological supersymmetric models. Using the bounds displayed in Fig 6.22 we can roughly exclude volumes in the ranges $23.75 \gtrsim \mathcal{V}_X \gtrsim 21.85$ and $29.25 \gtrsim \mathcal{V}_X \gtrsim 25.75$ related to the field mass bounds defined in Eq. (6.132) and Eq. (6.130) respectively. Using the missing constraints which stem from absent IMBH measurements we can place bounds on the volume of the three-dimensional submanifold which supports the visible sector and therefore ultimately bounds on the grand unification coupling constant in these models (see Eq. (5.127)) as distinguished by the orange and red dashed lines for the 68% and 95% exclusion limits respectively. These are loosely constrained at the 68% CI to the bounds,

$$23.75 \lesssim \mathcal{V}_X \lesssim 25.75 \,, \tag{6.153}$$

$$\frac{1}{23.75} \lesssim \alpha_{\rm GUT} \lesssim \frac{1}{25.75} \,, \tag{6.154}$$

representing a possible realisation of the G_2-MSSM unification coupling window.

6.4.7 FDM Probes Via Superradiant Instabilities of M87*

6.4.7.1 The Event Horizon Telescope and 21cm Observations

Returning full circle to the illustrious efforts to capture the first image of a BH, displayed in Fig. (6.1), also provides an interesting insight into the possible future of BH observational data on axion models. The analysis below is a small extension to the work found in Ref. [1219]. Our analysis in the previous sections chose to include well defined SMBH data from Suzaku reflection fitting techniques. Recents attempts have been made to place bounds on the non-dimensional spin parameter of M87*, which can be partnered with the detailed mass bound placed on the BH

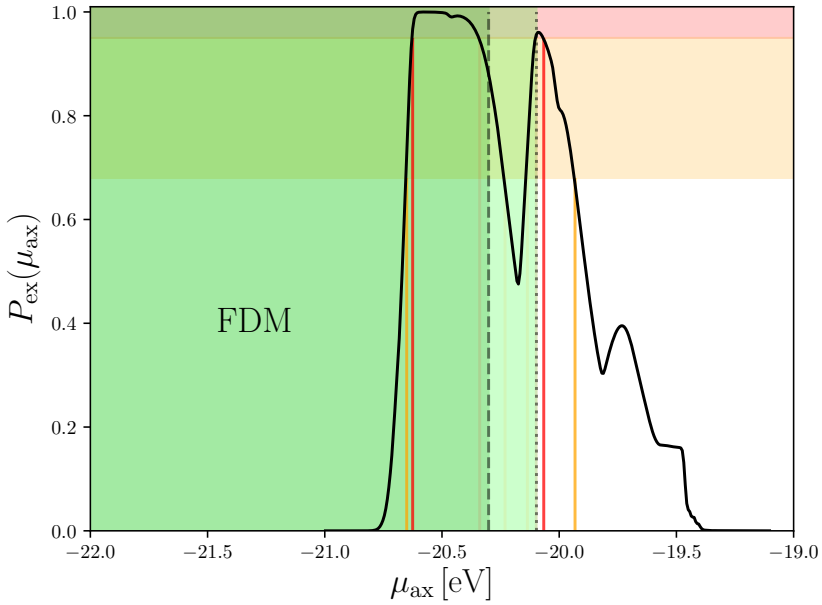


Figure 6.23: Constraints on the masses of ultralight FDM axions, $\mu_{\rm ax}^{\rm FDM}$, for singular fields determined by the total probability of exclusion calculated using the methodology in Appendix J via Eq. (J.1). Exclusion bounds are presented in the 68% and 95% CIs as a function of $\mu_{\rm ax}$ with *orange*/*red* lines representing the upper and lower limits of the 68%/95% intervals. These probability limit functions are determined using the single BH M87* (Fig. 6.1), with the mass and spin of the BH defined using Eq. (6.155) and Eq. (6.156) respectively. The shaded green regions represent example FDM bounds from global 21cm signal observations, defined by the upper (*dotted* line) and lower (*dashed* line) limits of Eq. (6.157).

during the imaging process. The current mass bound on M87* is [52],

$$M_{\rm BH}^{\rm M87^*} = (6.5 \pm 0.7) \times 10^9 M_\odot \ , \tag{6.155}$$

with other previous efforts producing similar bounds [591, 994, 1317]. Recently it has shown through considerations of the warped spacetime region surrounding the BH and its observed twisted light suggest the spin of M87* is,

$$a_*^{\rm M87^*} = 0.9 \pm 0.1 \ , \tag{6.156}$$

This is also in agreement with other independent analyses which have found the spin

to be bounded or closely following these limits [147, 463, 464, 529, 969, 988, 1241]. In particular the recent analysis conducted by the Event Horizon Telescope, partnering the mass measurements in Eq. (6.155) has currently concluded an approximate estimate of $|a_*^{\mathrm{M87}^*}| \gtrsim 0.5$ [52, 976] for the spin of the BH. Constraining the spin from the imaging process is difficult, as the the radius of the measured photon ring in Fig. 6.1 is not dependent on the value of the spin, apart from in the case of an extremal BH. The initial assessments of the nature of the spin of M87* do however, suggest it appears to possess sufficient spin in order to potentially produce interesting constraints on ultralight axionic DM.

Recently it has been claimed that the global 21cm signal [263], which represents strong evidence that the Universe was undergoing reionisation at redshift $z_{\mathrm{re}} \approx 17$, places a lower bound on the FDM mass [861, 1155],

$$\mu_{\mathrm{ax,FDM}} \gtrsim (5 - 8) \times 10^{-21}\ \mathrm{eV}\ . \tag{6.157}$$

Likewise Ref. [912] shows how a dynamical analysis of a central star cluster in the formation of Eridanus-II could constrain the FDM axion mass to values as high as,

$$\mu_{\mathrm{ax,FDM}} \gtrsim (0.6 - 1.0) \times 10^{-19}\ \mathrm{eV}\ , \tag{6.158}$$

with the complete window falling between $10^{-21}\ \mathrm{eV} \lesssim \mu_{\mathrm{ax}} \lesssim 10^{-20}\ \mathrm{eV}$, which is generally affected by narrow band resonances. These result are extremely interesting since, if they are to place confidence in their accuracy, it significantly shrinks the gap between FDM bounds from BH superradiance and structure formation. In the context of the present work, if FDM is realised from a mass distribution, then respecting the reionisation bound and BH superradiance demands an extremely narrow distribution with a small number of light fields. If the gap between FDM constraints from BH superradiance and reionisation is closed, either by the measurement of spins of the most massive SMBHs, or improvements on the lower limit to z_{re}, then FDM with no self-interactions will be completely excluded. Rescuing FDM from

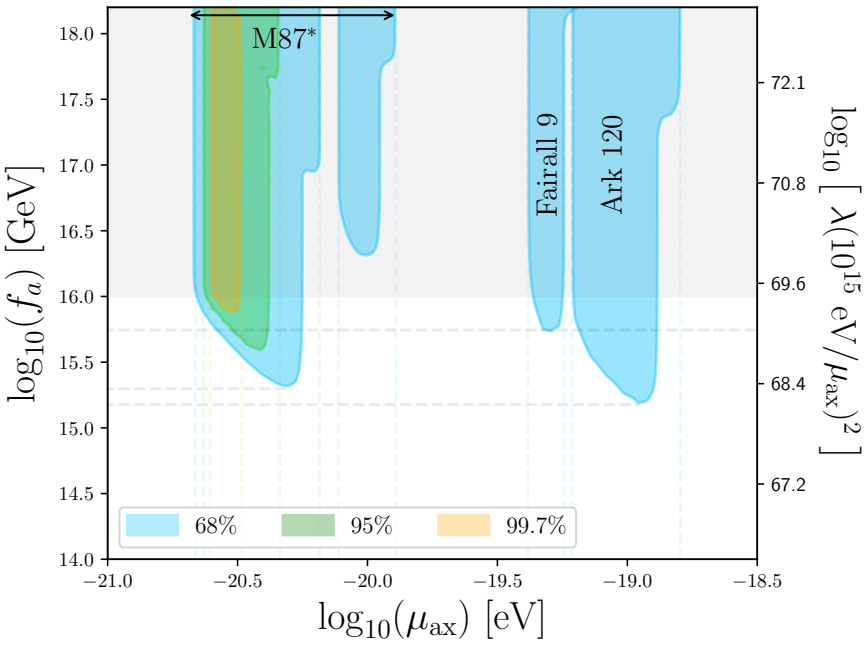


Figure 6.24: Constraints on the masses and decay constants (self-coupling) of ultralight FDM axions, $\mu_{\rm ax}^{\rm FDM}$, for singular fields determined by the total probability of exclusion calculated using the methodology in Section 6.3.1.1 and Section 6.3.1.2. The shaded *blue* bounds represent the 68% exclusion bounds, with the *green* and *orange* regions representing the 95% and 99.7% limits respectively for the three heaviest BHs, *Ark 120*, *Fairall 9* and *M87**. The *right axis* represents the limits on the quartic coupling of ULAs, $\lambda \equiv \mu_{\rm ax}^2/f_a^2$. The bounds stop for lower values of f_a where the axion cloud undergoes a bosenova before extracting sufficient spin from the BH.

BH superradiance constraints in such a case would require self interaction strengths corresponding to decay constants $f_a \lesssim 10^{16}$ GeV. Low decay constants open the door to new FDM phenomenology [431, 699, 850], but this may become increasingly hard to realise in small-volume string compactifications.

6.4.7.2 Constraints on Fuzzy Dark Matter

As an initial analysis of how accurate measurements of M87* could place strong bounds on the mass of a FDM particle, we use the methods of Appendix J and the same approach taken in Section 6.4.1 to calculate the bounds on the axion mass from superradiance and M87* in the weakly interacting limit. Using the fiducial

prior on the spin defined in Eq. (6.156) and the mass measurements from the Event Horizon Telescope in Eq. (6.155), the calculated constraints are shown for the case of a single field in Fig. 6.23. The structure of the exclusion function comes from the lobes of each $l = m$ mode, with only the $l = m = 1$ and $l = m = 2$ modes placing bounds above the 95% CI. The shaded *green* regions represent the limits on FDM defined in Eq. (6.157). The magnitude of the mass of M87* is significant compared to the heaviest BHs considered in our data set for the previously derived results. This generates a mass hierarchy where the single field constraints also dip below the 68% CI like in the case of stellar BHs and SMBHs. The full probability exclusion function calculated using the SMBHs detailed in Table 6.3 along with M87* is shown in Fig. 6.22. Using the results from M87* we can loosely place bounds on FDM, disregarding the function dip between the $l = m = 1$ and $l = m = 2$ mode bounds,

$$2.0 \times 10^{-21}\ \text{eV} \lesssim \mu_{\text{ax}} \lesssim 1.3 \times 10^{-20}\ \text{eV}\ , \tag{6.159}$$

in the 68% CI and,

$$2.5 \times 10^{-21}\ \text{eV} \lesssim \mu_{\text{ax}} \lesssim 8.0 \times 10^{-21}\ \text{eV}\ , \tag{6.160}$$

in the 95% CI. In Fig. 6.24 we present the bounds from M87* in the interacting limit for the decay constants and field masses using the bosenova limits and the methods detailed in Section 6.3.1.1 and Section 6.3.1.2. The lower bound on the axion decay constant is defined when the bosonic self-coupling is strong enough to cause a bosenova, which occurs around, $f_a \sim 10^{15}$ GeV for the heaviest BHs we consider. This relates to a quartic coupling exclusion of,

$$10^{68} \lesssim \lambda(10^{15}\ \text{eV}/\mu_{\text{ax}})^2 \lesssim 10^{73}\ . \tag{6.161}$$

The example bounds in Fig 6.24 from Ark 120 are,

$$\text{Ark 120} \begin{cases} 6.1 \times 10^{-20}\ \text{eV} \lesssim \mu_{\text{ax}} \lesssim 1.6 \times 10^{-19}\ \text{eV}\ , \\ 1.5 \times 10^{15}\ \text{GeV} \lesssim f_a \lesssim M_{\text{Pl}}\ , \end{cases}$$

and from Fairall 9 are,

$$\text{Fairall 9} \begin{cases} 4.1 \times 10^{-20}\ \text{eV} \lesssim \mu_{\text{ax}} \lesssim 5.7 \times 10^{-20}\ \text{eV}\ , \\ 5.6 \times 10^{15}\ \text{GeV} \lesssim f_a \lesssim M_{\text{Pl}}\ . \end{cases}$$

The FDM self-coupling bounds, which are partnered with the bounds in Eq. (6.159), from M87* are,

$$2.0 \times 10^{15}\ \text{GeV} \lesssim f_a \lesssim M_{\text{Pl}}\ . \tag{6.162}$$

Increased accuracy in the measurements of M87* along with an identification of further SMBHs with masses of the same order or higher offers an intriguing future prospect for constraints on FDM models.

6.5 Discussion and Conclusions on Black Hole Superradiance

We have shown in this chapter how BH superradiance can place strong constraints on the possible existence of light bosonic fields with small self-interactions, and in particular on the number of axion-like fields present in effective models of the axiverse. Many authors have considered these constraints for the case of a single new light field. The excluded ranges of the axion mass from our analysis are,

$$7 \times 10^{-14}\ \text{eV} \lesssim \mu_{\text{ax}} \lesssim 2 \times 10^{-11}\ \text{eV}\ ,$$

$$7 \times 10^{-20}\ \text{eV} \lesssim \mu_{\text{ax}} \lesssim 1 \times 10^{-16}\ \text{eV}\ ,$$

$$2 \times 10^{-21}\ \text{eV} \lesssim \mu_{\text{ax}} \lesssim 1 \times 10^{-20}\ \text{eV}\ .$$

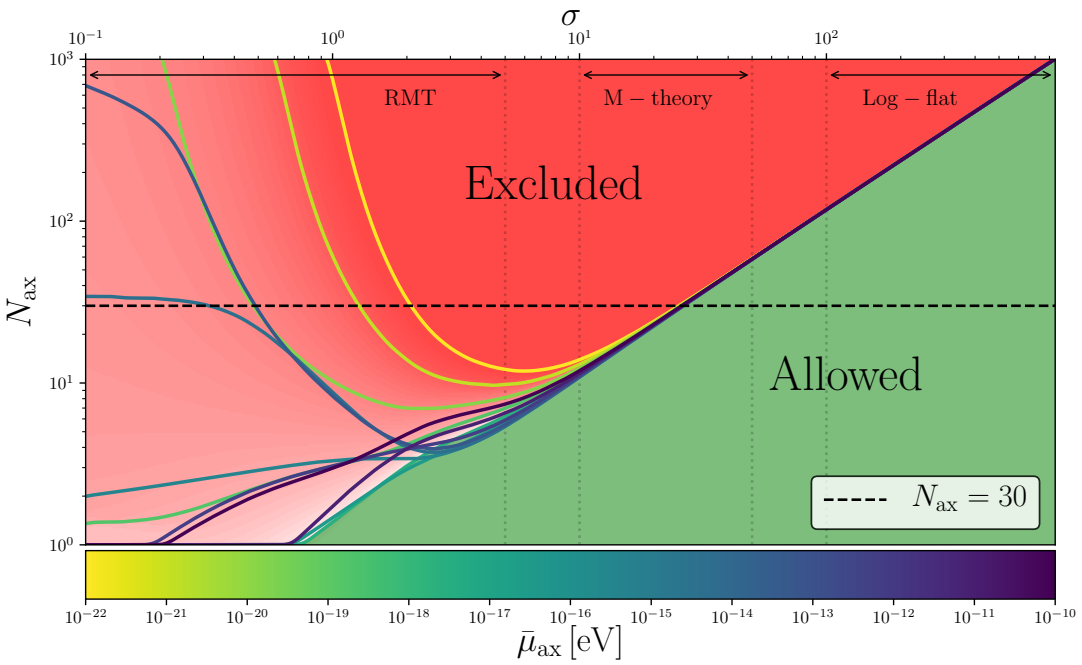


Figure 6.25: Summary of results displaying contours for the 95% exclusion regions using a log-normal axion mass distribution, as a function of the width, σ, and number of fields, $\mathcal{N}_{\rm ax}$, for various central mass mean scales, $\bar{\mu}_{\rm ax}$. Regions above the contours are excluded. Certain ranges of σ correspond closely to RMT and M-theory mass spectra, and can also be used to approximate the log-flat or degenerate spectrum. For $1 \lesssim \sigma \lesssim 20$, $\mathcal{N}_{\rm ax} \gtrsim 30$ is excluded for an extremely wide range of central masses. Constraints neglect axion self-interactions and apply approximately in the limit of large decay constants, $f_a \gtrsim 10^{14}$ GeV.

A model with multiple axions is excluded if just one field lies in the above ranges. We have studied this possibility, and used BH superradiance to exclude certain distributions of axion masses, representing both finite width spectra which are logarithmically symmetric and non-symmetric about the mean distributions scale. The constraints quickly become more severe with larger numbers of axion-like fields due to the increased probability of drawing an outlying field with a mass susceptible to superradiance constraints. This allows us to place constraints on the number of axion-like fields, $\mathcal{N}_{\rm ax}$ we could expect to see in the ultralight sector of cosmology.

Models for axions coming from string theory and M-theory typically involve many axion-like fields. These fields have their masses determined by microscopic quantities related to the geometry of the compact space. Their masses, however, are expected

to follow particular statistical distributions independently of the microscopic details. We have considered different distributions ranging from log-flat to log-normal, using BH superradiance to bound both the parameters of the distribution, and more significantly, the number of light axions within those distributions.

Constraints on $\mathcal{N}_{\rm ax}$ from a process such as BH superradiance, which relies only on the existence of the vacuum fluctuations of the given field, are extremely powerful and could potentially be used in this context to bound the dimensionality of phenomenologically consistent moduli spaces in string/M- theory. Only a small number of fields should obtain masses anywhere in the BH superradiance region from 10^{-10} eV $\lesssim \mu_{\rm ax} \lesssim 10^{-20}$ eV, which can be accommodated with a single very wide distribution $\sigma \gtrsim 30$, or bimodal distributions containing only very light or relatively heavy axions, forming the natural occurrence of mass hierarchies. Our analysis has neglected axion self-interactions and complications from non-linearities, which can shut off or significantly suppress the BH superradiance process if they are strong. We also have not considered partnering these limits with other constraints, for example those coming from the allowed relic abundance as discussed in the following chapter. The present work in this chapter is more model-independent, since it does not rely on any cosmological assumptions, and applies to any model for light scalars with sufficiently small self-interactions, allowing for the formation of a maximally occupied axion-scalar cloud.

Chapter 7

The Spectrum of the Axion Dark Sector

"I have seen the dark universe yawning Where the black planets roll without aim, Where they roll in their horror unheeded, Without knowledge, or lustre, or name."

Nemesis

Howard Phillips Lovecraft

7.1 The Dark Universe

In this chapter we present a stochastic analysis using both frequentist sampling and Bayesian methods to assess axion field evolution under the assumption their defining cosmological parameter scales are determined by a selection of the models introduced in Chapter 5. We will address their potential to provide multi-field solutions to the two defining paradigms of the dark sector of the standard cosmology. We shall then, refer liberally to the *dark sector* of axion cosmology as axion contributions to the approximate 95% of the total energy density of the Universe we have no direct observational or leading theoretical framework for. This could be either as an effective DM fluid component or an effective quintessence like field,

each contributing either a minor fraction or $\mathcal{O}(1)$ contribution to their respective dark sectors. Specifically we will look at calculating the background cosmological (*quasi-*)observables when these models contain a large number of fields. Each of the cosmological (quasi-)observables we need to consider relate to the particular cosmology we wish to realise via the relic density of a collective population of fields. In order to introduce an effective dark fluid component comprised of $n_{\rm ax}$ fields we can define two principle types of cosmology to explore. From this point on throughout this chapter we shall refer to the number of axion fields using the lower-case notation, $n_{\rm ax}$, as a reference to the number of fields we sample in our model.

7.1.1 Axion Cosmologies

Each cosmological realisation is defined via the fixed contributions found in Section 1.4.2 to the total energy density at the present time:

- $\mathcal{N}$-*ULA DM Cosmology* - We denote the effective DM fluid density as $\Omega_{\rm DM}$, coming from a population of axions in the low energy phenomenology. The total matter density parameter is defined by the summation,

$$\Omega_m = \Omega_b + \Omega_{\rm DM} \ , \tag{7.1}$$

  where we decompose the total energy density of the universe into four components,

$$\Omega = \Omega_b + \Omega_{\rm DM} + \Omega_\Lambda + \Omega_r \ . \tag{7.2}$$

  In order to realise standard models of concordance cosmology discussed in Chapter 1, in Section 7.2 we initially look for values of $\Omega_{\rm DM}$ falling inside the the rough observationally suggested bounds,

$$0.2 \lesssim \Omega_{\rm DM} \lesssim 0.4 \ , \tag{7.3}$$

in order to probe the statistical nature of our effective models. We will then address proper constraints via observables subsequently in Section 7.3.

- $\mathcal{N}$-*Quintessence Cosmology* - We denote the effective DE density as $\Omega_{\rm DE}$ coming from the vacuum energy of a collective population of axions. In this setting we fix $\Omega_\Lambda = 0$, decomposing the total density of the universe into the three components,

$$\Omega = \Omega_{\rm DE} + \Omega_m + \Omega_r \ . \tag{7.4}$$

Just as before, to probe our statistical models we look for values of $\Omega_{\rm DE}$ falling in the the rough experimentally suggested bounds,

$$0.6 \lesssim \Omega_{\rm DE} \lesssim 0.8 \ , \tag{7.5}$$

required to reproduce valid effective cosmic acceleration at the current time.

The general field of axion phenomenology possesses a wide range of methodologies used to constrain many orders of magnitude for the field scalings defining the effective field theory, a substantial portion we explored via superradiance in Chapter 6. Perhaps one of the most significant results for ultralight phenomenologies considers the total fraction, axions in the dark sector can contribute to the present cosmological energy density as their masses approach the Hubble scale today. In Ref. [710] it was shown that axion fields in the spectrum are heavily constrained in the approximate mass bound,

$$10^{-32}\ \text{eV} \lesssim m_a \lesssim\ 10^{-25.5}\ \text{eV} \ . \tag{7.6}$$

Defining the ULA dark sector density as $\Omega_{\rm ULA}$ and the total dark sector density as $\Omega_{\rm DS}$, then considering the mass region in Eq. (7.6), the maximum allowed axion contributions are limited at the 95% CI to [710],

$$\frac{\Omega_{\rm ULA}}{\Omega_{\rm DS}} \leq 0.05 \ , \tag{7.7}$$

$$\Omega_{\rm ULA} h^2 \leq 0.006 \ . \tag{7.8}$$

These constrains come from probing axionic contributions to the dark sector via the construction of an eight-dimensional observable parameter space used to explore model degeneracies via CMB and LSS data. We shall use the observable constrains to factorise each of the cosmologies we are considering above to abide by the following approximate mass bounds for fields present in the spectrum. Under these considerations if axions are to account for the total DM, the axions entering the cosmic horizon should have field oscillations onset in the epoch of radiation domination. This requires at least one axion with a mass larger than the Hubble rate at matter-radiation equality which fixes the following empirical spectrum mass limit,

$$m_a \gtrsim 10^{-27} \text{ eV} \ . \tag{7.9}$$

The energy-density of fields above this limit, given the standard instanton form for the potential, will scale as non-relativistic matter throughout the matter dominated era, fixing each field in the spectrum as a potential plausible DM candidate. The observational bounds in Eq. (7.6) fix axions in our empirical models behaving as DE to be limited to masses defined by the upper bound,

$$m_a \lesssim 10^{-32} \text{ eV} \ . \tag{7.10}$$

7.1.2 Late Time Evolution and Initial Model Conditions

We will focus mainly on the case of late time effective cosmic acceleration and disregard the nuances behind fine tuning and models of early DE. In order to output dark sector densities for our defined effective random matrix models, we numerically solve the equations of motion, defined in Eq. (2.89), for $n_{\rm ax}$ axion fields with fixed initial conditions, evolving the solutions forward in time using a time stepped numerical procedure. The field equations considering the standard cosmology can

be found throughout Chapter 1. We rescale each of the canonical fields in Planck units where our cosmic time, t, is the independent variable measured in units of the present day Hubble constant,

$$M_H = \frac{H_0}{h} = 2.13 \times 10^{-33} \text{ eV} = 100 \text{ Km s}^{-1} \text{ Mpc}^{-1} \, . \tag{7.11}$$

This scale naturally sets the normalisation scale for axion masses in our stochastic spectra, each parameterised in units of M_H. It also fixes the scales for the remaining cosmological density parameters, X_i appearing in the Friedmann constraint in Eq. (2.87) which are expressed in terms of their density today as $\Omega_{X_i} h^2$. The initial and final conditions for our cosmological evolution are fixed using the photon temperature as a cosmic clock. The total energy density for the full relativistic degrees of freedom, ρ_r is,

$$\rho_r = \frac{\pi^2}{30} g_\star(T) T^4 \, , \tag{7.12}$$

where $g_\star(T)$, defined in Eq. (1.74), counts the total relativistic degrees of freedom (e.g. Ref. [818]). We fix the point in which we sample the constituent density components from the CMB temperature [541],

$$T_{\rm CMB} = 2.725 \text{ K} \, . \tag{7.13}$$

This normalises the cosmic scale factor to,

$$a(T_{\rm CMB}) \equiv a(t_{\rm Today}) = 1 \, , \tag{7.14}$$

found by integration of the Friedmann constraint. Any analysis of the density components is simplified by considering the scales where we can treat the total relativistic degrees of freedom as a constant. To account for this the axion field equation solutions must begin after neutrino decoupling. The fits in Ref. [1329] determined by Eq. (1.73) and Eq. (1.74), suggest this occurs at the approximate initial value for

the temperature,

$$T_i \approx 23 \text{ keV} \ , \tag{7.15}$$

as shown in Fig. 1.4. This corresponds to the approximate initial value of the comic scale factor,

$$a(t_i) \approx 10^{-8} \ . \tag{7.16}$$

After this time, the radiation energy density evolves as,

$$\rho_r(a) = 3M_H^2 M_{\rm Pl}^2 \frac{\Omega_r h^2}{a^4} \ , \tag{7.17}$$

where at the current time we have,

$$\Omega_r h^2 = \rho_r(T_{\rm CMB})/(3M_H^2 M_{\rm Pl}^2) = 4.16 \times 10^{-5} \ . \tag{7.18}$$

Assuming radiation domination at T_i this fixes the initial physical time as,

$$t_i = (a_i^2/2)(\Omega_r h^2)^{-0.5} \ . \tag{7.19}$$

The effective cosmological constant is set with the fixed initial physical density $\Omega_\Lambda h^2$. The total baryonic and DM density evolves as,

$$\rho_{\rm m}(a) = 3M_H^2 M_{\rm Pl}^2 \frac{\Omega_{\rm m} h^2}{a^3} \ , \tag{7.20}$$

where the minimum value for $\Omega_{\rm m} h^2$ is defined by the physical baryon density [37],

$$\Omega_b h^2 = 0.022 \ . \tag{7.21}$$

Recalling that in the homogeneous limit, the energy-momentum tensor for the axions is described by a perfect fluid with the components $T_0^0 = -\rho$ and $T_j^i = P\delta_j^i$, each expressed in Eq. (2.94) and Eq. (2.95). The pressure of the matter, radiation, and cosmological constant terms in our system of equations are determined by the

equations of state, $P_i = w_i \rho_i$, using the fixed values $w_r = 1/3$, $w_m = 0$ and $w_\Lambda = -1$ for each of the relevant components. The total pressure is then used to fix the nature of expansion at the current time, appearing in the acceleration equation,

$$\dot{H} + H^2 = \frac{\ddot{a}}{a} = -\frac{1}{3}\sum_i (\rho_i + 3P_i) \ , \tag{7.22}$$

with an *accelerating* universe required to satisfy the condition $\ddot{a} > 0$. We determine if a realisation of the axiverse allows for an accelerating universe via the summation in Eq. (7.22). For each individual axion mass satisfying the oscillatory condition, $H \gtrsim m_a$ the axion field velocity remains negligible via Hubble friction. In the limit the field mass can be entirely neglected, the attractor solution is $\dot{\phi} = 0$, fixing the initial conditions for the fields.

7.1.3 Bounds on the Axion Masses

This assumption also sets an upper limit for the axion masses that we can consider for consistency at any given initial temperature. Demanding that each of our initial masses follow the bound, $m_a < 3H(T_i)$, fixed by neutrino decoupling, we find the approximate upper limit for the largest axion mass in the spectrum as,

$$m_a \lesssim 4 \times 10^{-19} \text{ eV} \ . \tag{7.23}$$

The upper bound on the axion mass is also closely related to the baryon Jeans scale, and considerations regarding cosmological structure formation and reionisation. If we were to extend our initial starting point to higher temperatures, and thus incorporate higher axion masses into the spectrum, we are required to model the evolution of $g_\star$ above neutrino decoupling (Fig. 1.4). We shall exclude this possibility for a number of reasons. The exact content of the particle bath is not known beyond scales surpassing orders a few TeV where above $\approx O(1)$ MeV (BBN), the Universe need not have been radiation dominated, and there is currently no observational

necessity to assume this is the case. In string/M- theory models, we also generally expect a non-thermal cosmology at early times, dominated by the energy density of moduli coherently displaced by vacuum fluctuations during inflation. The matter dominated phase is known to alter the relic densities of axions that begin oscillating during that period [31, 149].

Furthermore, the period of moduli displacement, before the moduli have decayed, breaks down our treatment of the axiverse where our effective theory is not a valid description, since the Kähler metric and therefore effective kinetic matrix is dynamical. For simplified effective field theories to hold, as a valid approach to axiverse cosmology, we must consider each axion in the spectrum to still be in slow-roll after the lightest modulus field X_0 has decayed. This defines the ultralight domain for axions in the dark sector,

$$n_{\rm ax}^{-1}\ 2.13\times10^{-33}\ {\rm eV}\lesssim m_a\lesssim 4\times10^{-19}\ {\rm eV}\ , \tag{7.24}$$

where $n_{\rm ax}^{-1}$ is a suppression factor determining the nature of ultralight and irrelevant hyperlight fields in $\mathcal{N}$-quintessence models. Axions which violate the bounds in Eq. (7.24) are removed from the spectrum for a consistent treatment of the ultra-light axiverse dark sector. Numerically, we locate axions in the spectrum violating these bounds, and ensure our initial conditions set the realignment energy density of these fields to remain at zero. Theoretically this form of analysis can be realised assuming a large quantity of entropy production and/or a short period of inflation caused by the modulus-dominated epoch prior to BBN. This will dilute the population of heavy axions that begun oscillating prior to BBN. Such scenarios are relatively natural in the context of a string/M- theory cosmology with many moduli [31, 557, 770, 839].

A more problematic, but theoretically motivated realisation to this issue comes from any heavier axions decaying rapidly prior to BBN, where they contribute to fixing the correct radiation content and baryon density. Axion decays through the canonical two photon coupling are comparatively slow (see e.g. Ref. [946]), and

decays before BBN require $m_a \gtrsim 1$ keV. For axions respecting our bounds to decay, we would require much larger than expected couplings and rapid decay channels and so this should be seen as a potential but unlikely channel to consider the ultralight sector only. Alternatively, we could assume a gapped spectrum with any axions violating our bounds taken to have their masses lifted to a much higher scale to allow for decays through standard channels. Another mechanism to remove any heavy axions which we have previously discussed and demonstrated in Fig. 2.4 is a regulation of the density dissipation via a multi-instanton potential [765] which causes the misalignment population to redshift faster than standard a^{-3} scalings due to the non-quadratic potential minimum. Whether or not the appearance of such a multi-instanton potential occurs naturally in string/M- theory models is not clear, operating currently as an interesting effective analytical device for field evolution. The upper bound in Eq. (7.24) far exceeds any axion masses probed by our simple DM constraints and the hyperparameters for each class of model we consider, thus our model of the defined Universe sits above a few keV, not requiring a full treatment for heavy axions. We only make use of a constant value for the relativistic degrees of freedom, $g_\star$, which does not affect our results.

Despite the construction of the axion mass matrix guaranteeing positive definiteness mathematically, and thus mass eigenstates satisfying $m_a^2 > 0$, the huge spread in the elements of the mass matrix in the M-theory random matrix model can lead to numerical precision errors. These errors represent the existence of *tachyonic* states in our model, $m_a^2 < 0$. We have not been able to overcome this issue of numerical precision within the confines of our code so we remove these tachyonic states from the spectrum just as we remove the heavy states, where they do not contribute to the energy density in the effective model. Fortunately, the negative eigenvalues are guaranteed to be those for which the true values are smallest in absolute value. Since the true eigenvalue is $m_a \ll H_0$ and the field displacements $\phi_i^{\rm ini} \sim \mathcal{O}(M_{\rm Pl})$, even with the correct (positive) eigenvalue these states would not contribute significantly to the spectrum, and so removing them also does not affect our results.

7.1.4 Axion Field Oscillations

In our analysis each realisation of the Universe begins to evolve once we define each of our initial conditions for the fields, where cosmic expansion causes the value of H to decrease monotonically. When any individual field from our initial sampled spectrum satisfies the condition $m_a \gtrsim H$, the field begins to roll towards its potential minimum defining the initialisation of coherent oscillations for the system. These solutions satisfy,

$$\phi(a > a_{\rm osc}) = \phi(a_{\rm osc}) \left(\frac{a}{a_{\rm osc}}\right)^{-3/2} \cos(m_a t)\,, \tag{7.25}$$

where $a_{\rm osc}$, the cosmic scale factor when the field begins to oscillate, occurs at approximately $H(a_{\rm osc}) \approx m_a$. As H decreases further, the time scale of the oscillation induces very small time steps in our numerical integrator of the order ($\sim m_a^{-1}$), much smaller than the dynamical evolutionary time, $t_{\rm dyn} \approx H$. This is computationally prohibitive to integrate directly given the logarithmic hierarchical nature of the axion mass distribution. Although the axion field oscillates, the energy density does not, and therefore obeys the simple scaling solution,

$$\rho_a(a > a_{\rm osc}) = \rho(a_{\rm osc}) \left(\frac{a_{\rm osc}}{a}\right)^3 . \tag{7.26}$$

The pressure of the field oscillates with a frequency $P \sim \cos(2m_a t)$, which leaves us with a time-averaged equation of state $\langle w_a \rangle = 0$, and so we can safely neglect this for our purposes. See Refs. [82, 229, 785, 1070] for non-trivial concerns over these pressure terms. The dynamical time scale in our integration is fixed to be of the order the Hubble scale today, M_H (Eq. (7.11)). In order to be able to integrate models with $m_a \gg M_H$, we approximate the axion evolution for time scales $t > t_{\rm osc}$. The method we choose is simply to set $w_a(t > t_{\rm osc}) = 0$, where the energy density for heavy axions evolve and scale exactly as a^{-3}, at late times. An example alternative method uses a change of co-ordinates in the axion phase space, detailed

and implemented in Ref. [1283]. We define $t_{\rm osc}$ by allowing the equation of state in the full solution to oscillate (cross zero) a fixed number of times denoted by the parameter, $n_{\rm cross}$. We then define $t_{\rm osc}$ using $n_{\rm cross}$. This is an accuracy parameter in our numerical procedure, with larger values of $n_{\rm cross}$ leading to more accurate, but considerably slower, numerical computations. We find our results for derived quasi-observables converge above $n_{\rm cross} = 3$, so we fix $n_{\rm cross} = 5$ in the examples and constraints discussed in this chapter. Care must be taken, however, as using sufficiently large values of $n_{\rm cross}$, while improving the numerical integration accuracy, this can incorrectly assign DM axions to the DE density for the quasi-observables. Fig. 7.1 shows the effect of this procedure for the collective equation of state for example multi-field evolutions involving $n_{\rm ax} = 10$ axions, both for DM and DE cosmologies in different RMT models. The dashed and dotted lines detail our approximations, where we show the effect on the collective equation of state for the axion population when we restrict the individual equations of state for each field to a fixed number of oscillatory crossings. The amplitude of the total equation of state is damped from the oscillatory effects for multiple fields, with non-degenerate scalings in the population, oscillating between the values of ≤ 1 and ≥ -1. In the limit $n_{\rm ax} = 1$ the equation of state amplitude maximises, continuing to oscillate between -1 and 1.

7.1.5 Computing the Model Quasi-Observables

Our quasi-observables are defined using the parameter vector,

$$\bar{\chi} = (\Omega_m, z_{\rm eq}, \ddot{a}, h) \ . \tag{7.27}$$

We compute in physical time, t, up to some final maximum time $t_{\rm f} \approx \mathcal{O}(10)$ and output a fixed number of log-spaced time steps. We then begin by locating $z = 0$ in the output variables. If $z = 0$ has not been reached in ten Hubble times (which may occur for extreme cosmologies) our analysis outputs default quasi-observables

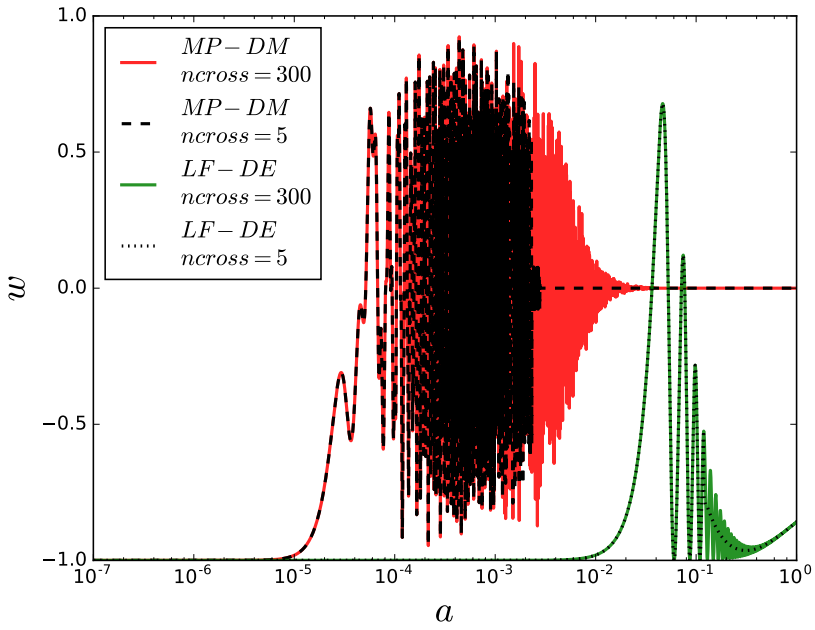


Figure 7.1: Evolution of the collective axion equation of state, ω_a, as a function of the cosmic scale factor, $a(t)$, for axions behaving as either the total DM or total DE densities in selected different RMT models. MP-DM refers to the model presented in Section 5.2.4.1 and LF-DE the model presented in Section 5.2.5.2.3. Each example shows the full evolution along with the restricted evolution where the value of $n_{\rm cross}$ represents the numerical precision of the field evolution considered, where the fields are fixed to their time averaged equation of state after a fixed number of crossings.

which lead to very low likelihoods (in particular, failing the acceleration cut). This is equivalent to a cut on the valid age of the Universe. Having located $z = 0$, computing h is trivial as it is given by the Friedmann constraint evaluated at $z = 0$. Computing the other variables relies on the separation of axions into fields behaving as DM or DE-like based on $n_{\rm cross}$. The split at $z = 0$ trivially gives the total matter density, $\Omega_m = \Omega_b + \Omega_{\rm DM}$. The acceleration is computed from the total pressure and density using,

$$\ddot{a} = -\frac{a}{3}\sum_i (\rho_i + 3P_i) \ , \tag{7.28}$$

where the index i runs over both the axions and the ordinary cosmological components. The pressure for the axions with a number of crossings less than $n_{\rm cross}$ are computed directly from the fields using Eq. (2.95), while for those with crossings

greater than $n_{\rm cross}$ we fix $P_i = 0$. We then finally compute the value of $z_{\rm eq}$. At all values of z the axions are split into the energy density components, $\rho_{\rm DM}$ and $\rho_{\rm DE}$, by selecting fields that have and have not passed the $n_{\rm cross}$ criterion. We are also in possession of the radiation energy density $\rho_r(z)$ and baryon energy density $\rho_b(z)$ at every value of the cosmic redshift. We locate $z_{\rm eq}$ by simply finding numerically the point where the condition $\rho_{\rm DM} + \rho_b = \rho_r$ is satisfied. The value of $\rho_{\rm DE}$ is truncated in the definition of equality. We also find equality using the list of output times, rather than using interpolative functions. The location of equality depends on the number accuracy of the output times used. In our numerical examples we consider 1000 equidistant log-spaced times steps between $t_{\rm ini} = 8 \times 10^{-15}$ and $t_{\rm f}$.

7.1.6 Epistemic priors on the Dark Axiverse

We begin our results by considering the analytical statistical straw-man model, following the *epistemology* of the axiverse. This model was discussed in Section 5.1.2 and serves as a baseline which to compare our physically motivated models moving forward. The epistemic priors on the parameter space are defined by beginning in the mass eigenstate basis where both $\mathcal{K}_{ij}$ and $\mathcal{M}_{ij}$ are diagonal, where we only need to define the priors on the eigenvalues directly, enforcing statistical independence. The parameter space, represented by a $\mathcal{N}$-dimensional hypercube, is fixed by the scale limit parameters, $k_{\rm min}$, $k_{\rm max}$, $m_{\rm min}$ and $m_{\rm max}$ which are used to define each phenomenology. In a Bayesian sense these could also be associated with a corresponding hyperprior used to regulate the physics of scale cut-offs, i.e. heavy tail priors to suppress values of $k_{\rm max}$ reproducing trans-Planckian decay constants. We don't consider this possibility here and fix the scale limits by hand at the level of the hyperparameters.

The fixed bounds $k_{\rm min}$ and $k_{\rm max}$ in Eq. (5.27) are associated to lower and upper bounds on general symmetry breaking scales. The upper and lower bounds, $m_{\rm min}$ and $m_{\rm max}$ represent the fraction of the ULA mass window suited for extracting fields

Table 7.1: The full range of parameters used in the study in this chapter, including the cosmological input parameters along with the model dependant RMT parameters and theoretical M-theory stochastic variable parameters. Our cosmological density and parameter data comes from the *Planck 2015 TT+lowP* likelihood's found in Ref. [37] with our CMB temperature defined using COBE data in Ref. [541].

Parameter	Definition	Prior/Value	Eq./Ref.
$n_{\rm ax}$	Number of axion fields	$\mathcal{O}(1-100)$	-
f_a	Axion decay constant	$\mathcal{O}(10^{-4}M_{\rm Pl} - M_{\rm Pl})$	Eq. (2.83)
m_a	Axion mass	$\mathcal{O}(10^{-35}{\rm eV} - 10^{-15}{\rm eV})$	Eq. (7.24)
θ_i	Initial field misalignment	$\mathcal{U}[0,\pi]$	Eq. (5.29)
ϕ_i	Initial axion field conditions	$\mathcal{F}_{ij}\theta_j$	Eq. (5.66)
$\dot{\phi}_i$	Initial field derivative	0	Eq. (2.99)
$\mathcal{F}_{ij}$	Decay constant matrix	Model dependent	Eq. (5.66)
a	Cosmic scale factor	$[10^{-8} \rightarrow 1]$	-
H_0	Present day Hubble rate	hM_H	Eq. (1.86)
M_H	Hubble mass scale, 100 km s$-$1 Mpc^{-1}	2.13×10^{-33} eV	Eq. (2.87)
$M_{\rm Pl}$	Reduced Planck mass, $1/\sqrt{8\pi G}$	2.435×10^{27} eV	-
$\Omega_{\rm DM}$	Axion DM density parameter	$[0,1]$	-
$\Omega_{\rm DE}$	Axion DE density parameter	$[0,1]$	-
	***Planck 2015 TT+lowP* Parameters**		
	Used as quasi-observable data		
h	Present day Hubble rate	0.6731 ± 0.0096	Ref. [37]
Ω_m	Total matter fraction	0.315 ± 0.013	Ref. [37]
z_{eq}	Redshift of matter-radiation equality	3393 ± 49	Ref. [37]
	Fixed in a given model		
$\Omega_b h^2$	Physical baryon density (all)	0.022	Ref. [37]
$\Omega_c h^2$	Physical DM density (DE models)	0.12	Ref. [37]
$\Omega_\Lambda h^2$	Physical DE density (DM models)	0.31	Ref. [37]
$T_{\rm CMB}$	CMB temperature (COBE, all)	2.725 K	Ref. [541]
	RMT Models		
$\sigma^2_{\mathcal{K}}$	Kinetic matrix distribution scale	$[10^{-4}M_{\rm Pl}, M_{\rm Pl}]$	Eq. (7.36)/Eq. (7.44)
$\sigma^2_{\mathcal{M}}$	Mass matrix distribution scale	$[10^{-2}M_H, 10^{17}M_H]$	Eq. (7.37)/Eq. (7.45)
$\beta_{\mathcal{K},\mathcal{M}}$	Sub-matrix dimension parameter	$[0.01, 1.00]$	Eq. (7.38)
$\bar{f}$	MP RMT model equal field condition scale	$[10^{-9}M_{\rm Pl}, 5M_{\rm Pl}]$	Eq. (7.80)/Eq. (7.77)
$k_{\rm min}$	Non-central spiked RMT model kinetic matrix element lower bound	-5.0	Eq. (7.56)
$k_{\rm max}$	Non-central spiked RMT model kinetic matrix element upper bound	$[-3.0, 0.0]$	Eq. (7.62)
$m_{\rm min}$	Non-central spiked RMT model mass matrix element lower bound	-5.0 (DE), 4.0 (DM)	Eq. (7.66)/Eq. (7.58)
$m_{\rm max}$	Non-central spiked RMT model mass matrix element upper bound	$[-1.0, 8.5]$	Eq. (7.63)/Eq. (7.53)
	M-theory Model		
$F/(M_H^2)$	SUSY order parameter, $m_{3/2}M_{\rm Pl}$	$5.4 \times 10^{104}(m_{3/2}/1$ TeV)	Eq. (5.120)
$m_{3/2}$	Gravitino mass	$\mathcal{O}(10)$ TeV	Eq. (5.85)
Λ	Instanton Mass scale, string units	$[10^{-5},1]$	Eq. (5.116)
s	Averaged value for Moduli VEVs, string units	$\mathcal{U}[10,100]/\mathcal{N}(\bar{s},\sigma_s)$	Eq. (5.88)/(5.129)
$\widetilde{N}_{\rm max}$	Instanton Index Parameter	[0.6,1.6]	Eq. (5.128)
a_0	Axion decay constant scale	1	Eq. (5.90)

behaving as either type of our defined cosmologies, stemming from non-perturbative physics considerations. In Fig. 7.2 we show kernel density estimations (KDEs) for the probability densities retrieved using $\mathcal{N}$-quintessence models defined by epistemic priors with the following baselines,

$$n_{\rm ax} = \mathcal{O}(1 \rightarrow 100) \ , \tag{7.29}$$

$$\log_{10}\left({\rm eig}(\mathcal{K}_{ij})/M_{\rm Pl}\right) \in \mathcal{U}[-4.0, -0.5] \ , \tag{7.30}$$

$$\log_{10}\left({\rm eig}(\mathcal{M}_{ij})/M_H\right) \in \mathcal{U}[-2.0, 2.0] \ . \tag{7.31}$$

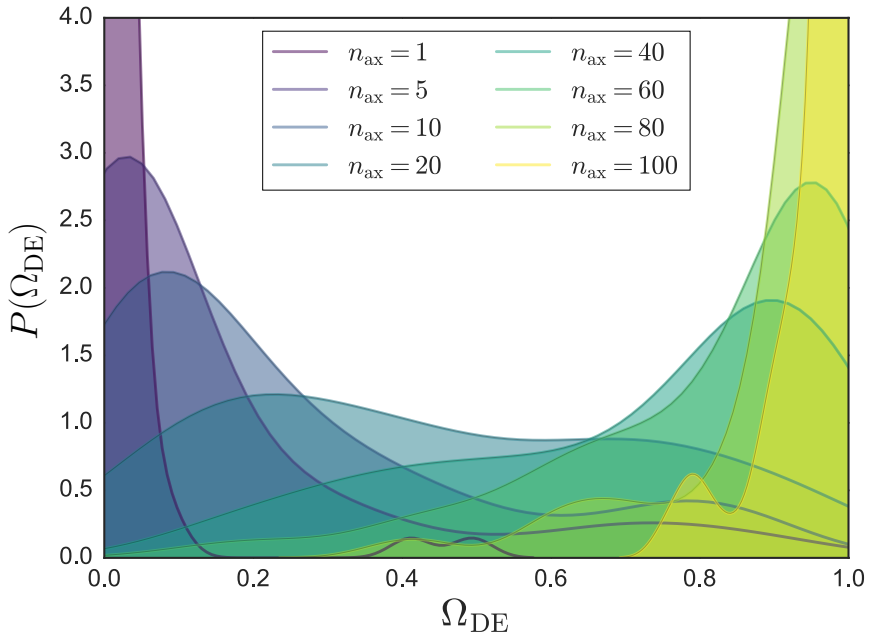


Figure 7.2: KDE plot for the axion DE density parameter, $\Omega_{\rm DE}$, with $n_{\rm ax} = \mathcal{O}(1 \to 100)$ with log-flat priors on both the axion scale parameters, m_a^2 and f_a^2, sampled in the window detailed in Eq. (7.29), Eq. (7.30) and Eq. (7.31). Using the approach of least information with epistemic priors typically requires a large number of fields, $n_{\rm ax} \simeq \mathcal{O}(50)$, to reach the energy densities required for accelerated expansion today, defined by the approximate bounds in Eq. (7.5).

Correspondingly, Fig. 7.3 shows the KDEs for various numbers of axions acting as multi-component DM using the fixed baselines,

$$n_{\rm ax} = \mathcal{O}(1 \to 10) \ , \tag{7.32}$$

$$\log_{10}\left({}^{\rm eig(\mathcal{K}_{ij})}/_{M_{\rm Pl}}\right) \in \mathcal{U}[-4.0, -0.5] \ , \tag{7.33}$$

$$\log_{10}\left({}^{\rm eig(\mathcal{M}_{ij})}/_{M_H}\right) \in \mathcal{U}[6.0, 16.0] \ . \tag{7.34}$$

The results presented in Fig. 7.2 are representative of the general idea a large number of fields should contribute to the vacuum energy to obtain the required quintessence field density we observe today, where in the absence of alignment, each field is deemed '*safe*' in regards to initial displacements and weakest force considerations. We find the recovery of realistic cosmologies for axion population sizes with at least $n_{\rm ax} \approx \mathcal{O}(10)$, in order to return values of $\Omega_{\rm DE}$ sitting in the rough window defined

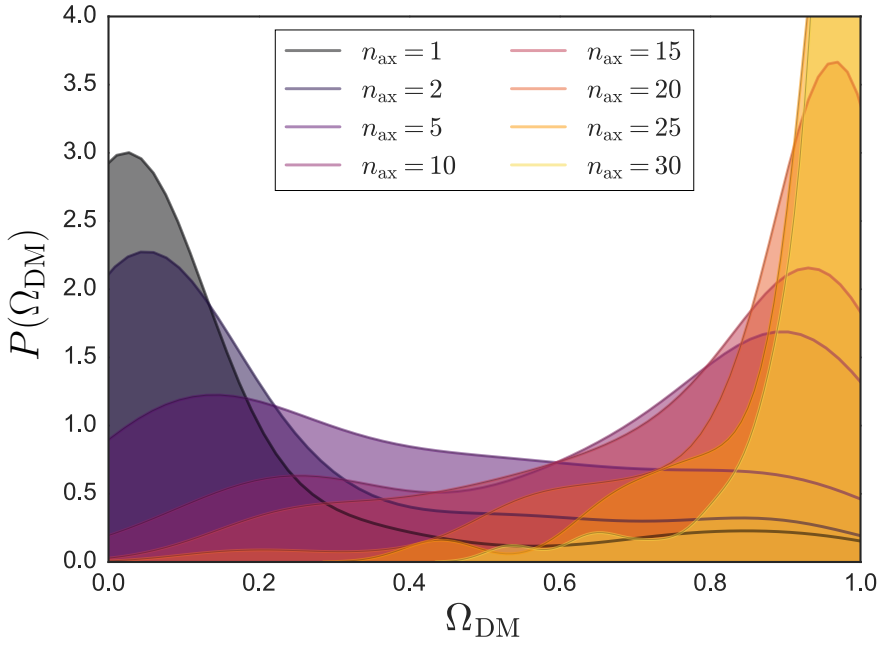


Figure 7.3: KDE plot for the axion DM density parameter, $\Omega_{\rm DM}$ with $n_{\rm ax} = \mathcal{O}(1 \to 10)$ with log-flat priors on both the axion scale parameters, m_a^2 and f_a^2 sampled in the window detailed in Eq. (7.32), Eq. (7.33) and Eq. (7.34). Using too many fields quickly comes to dominate the energy density today. Using the approach of least information with epistemic priors typically requires a smaller number of fields, $n_{\rm ax} \simeq \mathcal{O}(5)$, to peak the probability of returning the energy densities required for the correct DM density, defined by the approximate bounds in Eq. (7.3).

in Eq. (7.5). The probability to reproduce a particular contribution saturates to approximately uniform around $\mathcal{O}(20-40)$ fields, this value regulated by the highest and lowest mass we allow in the spectrum. We therefore expect that late time acceleration will statistically be driven by at least $n_{\rm ax} \gtrsim \mathcal{O}(10)$ fields in the spectrum.

For axion DM, Fig. 7.3 shows us how a minor increase in the field population size can quickly lead to a domination of matter density at the current time. The initial statistical drawing of more field displacements allows for a chance to realise a period of inflationary evolution (see Fig. K.1) when utilising a mass window in which the highest possible mass is allow to exceed the bound in Eq. (7.23). We find that for $n_{\rm ax} = 5$ the density peaks closest to the limits outlined in Eq. (7.3). Interestingly the single field case for both examples demonstrates how an approach of least information on the field scalings, limits the probability of realising each of the dark sector

requirements. In the DE case no realisations reproduced the required density for an accelerating universe, indicating the requirements for specific tunings or further physics. In the DM case, the profile peaks at values $\Omega_{\rm DM} \lesssim \mathcal{O}(0.1)$ with a limited number of realisations contributing an $\mathcal{O}(1)$ contribution to the total DM density we expect.

The information presented in both Fig. 7.2 and Fig. 7.3 gives an indication of how a population of multiple axions could statistically enhance our ability to generate the required values of $\Omega_{\rm DM}$ and $\Omega_{\rm DE}$. In general our RMT models we consider are representative of localised scale windows, fixed by the bounded nature of the spectrum, its limits determined by convolution operations of positive definite probability density spaces in the sample basis for the mass eigenstates. This can be seen as a N-flation type spectrum of fields, clustered together enhancing the density in either type of evolution, their physics determined separately to other sectors of axion physics/phenomenologies. We fix the approximate population size to sample our models with to $n_{\rm ax} \simeq \mathcal{O}(10)$, serving as a good common ground between both types of cosmology which we now explore further.

7.2 Constraints on the Random Matrix Axiverse

In this first results section, we present a snapshot investigation of a population of axions in the dark sector who's mass eigenstates are controlled by either an isometric, finite rank perturbed or full rank perturbed Y-matrix, in the mass eigenstate basis. When we preserve mass isometry after the basis rotations the axion decay constants are approximated as degenerate scalings. In the case of perturbed mass matrix models we impose symmetric construction conditions, where the decay constants are defined by either an isometric (model in Section 5.2.5.1) or rank-one perturbed (model in Section 5.2.5.2.3) kinetic matrix as well as the associated mass matrix. We also explore the case of the M-theory random matrix axiverse model introduced in Section 5.3. The examples explored and presented in the figures found

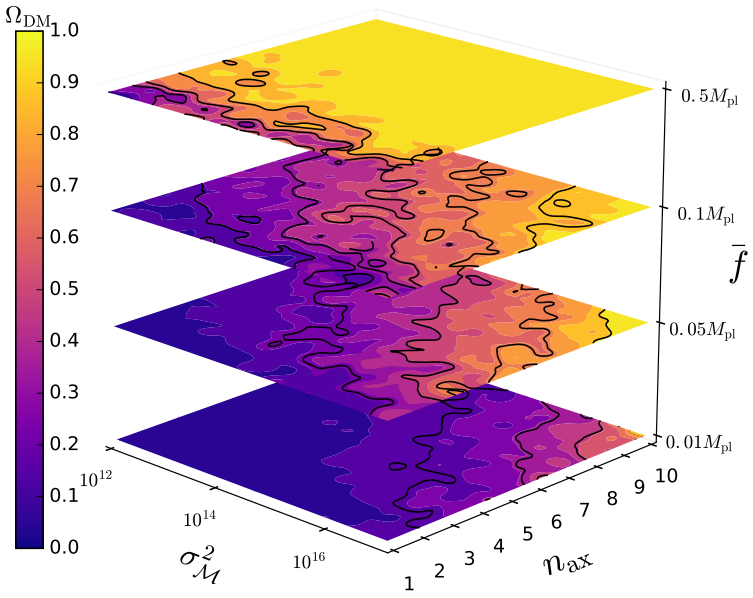


Figure 7.4: Contour density plots for the axion DM density parameter, $\Omega_{\rm DM}$ in the $\sigma^2_{\mathcal{M}}$, $n_{\rm ax} = \mathcal{O}(1 \to 10)$ plane, demonstrated for different discrete fixed values of the initial field displacement scaling parameter, $\bar{f}$. High scalings of $\bar{f}$ generally produce too much DM when using a small number of fields in the ultralight sector. When this scale is lowered we generate contour degeneracies in this plane reproducing the approximate required values defined in Eq. (7.3). For example when $\bar{f} = 0.05M_{\rm Pl}$ we have the approximate relationship, $17 - \log_{10}(\sigma^2_{\mathcal{M}}) \simeq {}^{n_{ax}}/_{2}$ using the presented bounds. For ultralight fields the DM density quickly fades off as the scale of $\bar{f}$ approaches the GUT scale.

in Section 7.2.1, Section 7.2.2 and Section 7.2.3 (Fig. 7.5 through 7.10), each contain data for 2500 example realisations representing randomised axiverse cosmology. Our contour density plots are constructed using 50×50 gridded scans in the multidimensional parameter space, with gaussian filtering and cubic spline interpolation. The M-theory examples in Section 7.2.4 use 10×10 (Fig. 7.12 and Fig. 7.14) and 20×20 (Fig. 7.13) gridded scans with cubic spline interpolation, consisting of 10 samples at each point, giving a total of 1000 and 4000 cosmologies respectively.

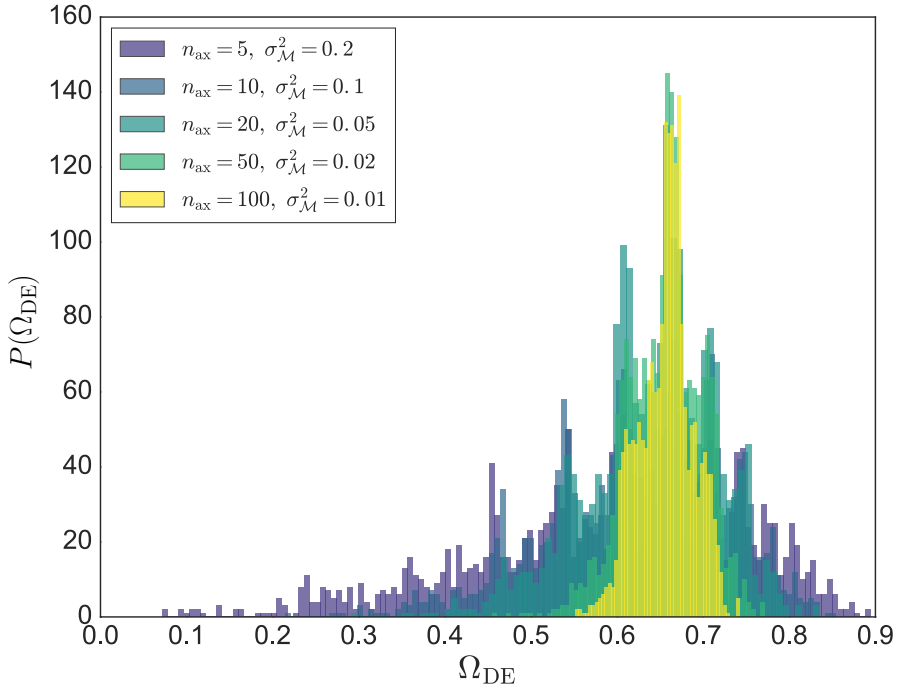


Figure 7.5: Probability density plots for $n_{\text{ax}} = \mathcal{O}(1 \to 100)$ with fixed values of $\sigma^2_{\mathcal{M}}$ according to the approximation in Eq. (7.35). In each example we use the fixed parameter values $\beta_{\mathcal{M}} = 0.5$ and $\bar{f} = 1$. The statistical convergence of the models eigenvalues generates an approximate degenerate contribution from each field. When the value of n_{ax} converges to the large $\mathcal{N}$ limit we recover the approximate relationship $\sigma^2_{\mathcal{M}} n_{\text{ax}} \equiv M_H$ where the dominate source the the statistical fluctuations comes from the initial values for the field displacement.

7.2.1 Isometric Y-Matrix Model

In Fig. 7.4 , Fig. 7.5 and Fig. 7.6 we present our first example cosmologies using the RMT model of the axiverse with the minimal parameterisation, for both DE and DM realisations. We assume the symmetry breaking scales of the fields are degenerate, at some fixed scale, $\bar{f}$ representative of some fundamental scale of the theory, where the field masses are encoded in a random isometric Y-matrix. The axion cosmology is defined by the model outlined in Section 7.1. The axion matrix eigenvalues have a bounded spectral width governed by the Marčhenko-Pastur distribution law. When the sub-matrix dimensions are suitably rectangular, i.e. $\beta_{\mathcal{K}} = \beta_{\mathcal{M}} \lesssim 0.5$, this generates a configuration where the fields provide almost degenerate contributions to the total energy density up to variations in both the initial fields misalignment and

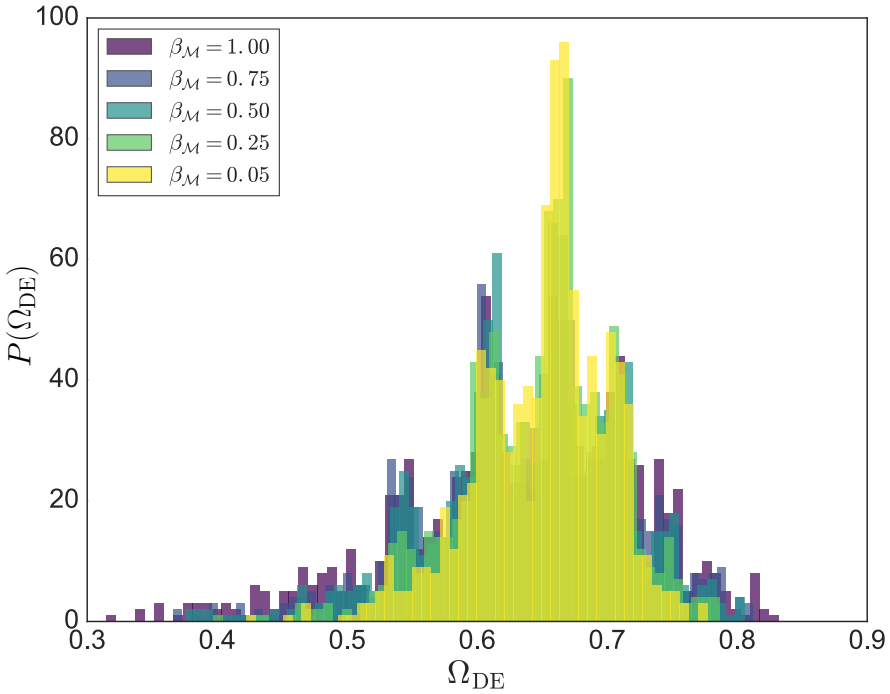


Figure 7.6: Approximate degeneracy for values of $\beta_{\mathcal{M}} \in (0, 1]$ for the axion DE density parameter $\Omega_{\rm DE}$ using $n_{\rm ax} = 20$ axions. We also use the fixed parameter values $\sigma^2_{\mathcal{M}} = 0.05$ and $\bar{f} = 1$ for each example. When the number of fields is limited, the effect of the spectrum approaching degeneracy ($\beta_{\mathcal{M}} \to 0$) only has a limited effect of enhancing the probability of producing values in the approximate limits of Eq. (7.5).

statistical fluctuations from our choice of basis, due to the absence of any treatment required when dealing with a non-trivial distribution for $\mathcal{K}_{ij}$. The normalised scale of the mass distribution, defining the nature of the fields, fixed by the first raw moment $\sigma^2_{\mathcal{M}}$, acts as a free scaling parameter to switch between each type of dark sector cosmology defined in Section 7.1.1.

7.2.1.1 Isometric Y-Matrix Dark Matter

In Fig. 7.4 we display contour density planes for different mass distribution scales, against the axion population size discretised over several values for the initial field condition scaling. We demonstrate the emergence of axion DM density domination at the present time with large initial field displacement scalings, $\bar{f} \approx M_{\rm Pl}$, when the

field population is $n_{\rm ax} \gtrsim 1$. See Appendix K for a visual example of the evolution of the cosmological densities in these configurations. In each of our RMT models the form of the mass matrix is such that a population of axions behaving as the total DM requires initial field oscillations onset, at a scale where requirements on the heaviest axion mass in the population set the order of the total mass scale, $\sigma^2_{\mathcal{M}} \gg M_H$. This is regulated by the fluctuations of extremal eigenvalues defining the spectral radii, which follow universal laws, such as those discussed Appendix D. The equal field scale conditions $\bar{f}$, along with the uniform sampling of θ, restrict the total number of axions $n_{\rm ax}$ allowed in the population at any given mass scale. Only when we set $n_{\rm ax} \approx 1$, do we recover the potential to find values of $\Omega_{\rm DM}$ consistent with expectations presenting an approximate degeneracy along the total mass scale interval we consider. Larger population numbers feel both the linear sum of field density contributions along with the convergence of the initial misalignments in our prior sampling to their averaged value $\langle\theta\rangle \approx \pi/2$, showing a large region of parameter space returning values of $\Omega_{\rm DM} \gtrsim 0.8$.

We find a significant increase in the possibility of larger population sizes returning values in the limits of Eq. (7.3) by relaxing the scaling of the initial field displacements to $\bar{f} = \mathcal{O}(0.1 M_{\rm Pl})$, as demonstrated in the lower panels. The degeneracy relationship between the number of fields allowed in the population and the mass distribution scale becomes more apparent in the second and third panels. As expected larger values of $n_{\rm ax}$ quickly return values of Ω_{DM} far in excess of what is required, as the mass distribution scale is increased. Our simple example highlights this when $\bar{f} = 0.1 M_{\rm Pl}$, where mass distributions with $\sigma^2_{\mathcal{M}} \approx 10^{12}$ require a population size, $n_{\rm ax} \approx 10$. Distributions with $\sigma^2_{\mathcal{M}} \approx 10^{17}$ generally require $n_{\rm ax} \approx 1$. The lower panels show a shift in the preferred values of $\sigma^2_{\mathcal{M}}$ as we reduce the scaling for the initial field displacements.

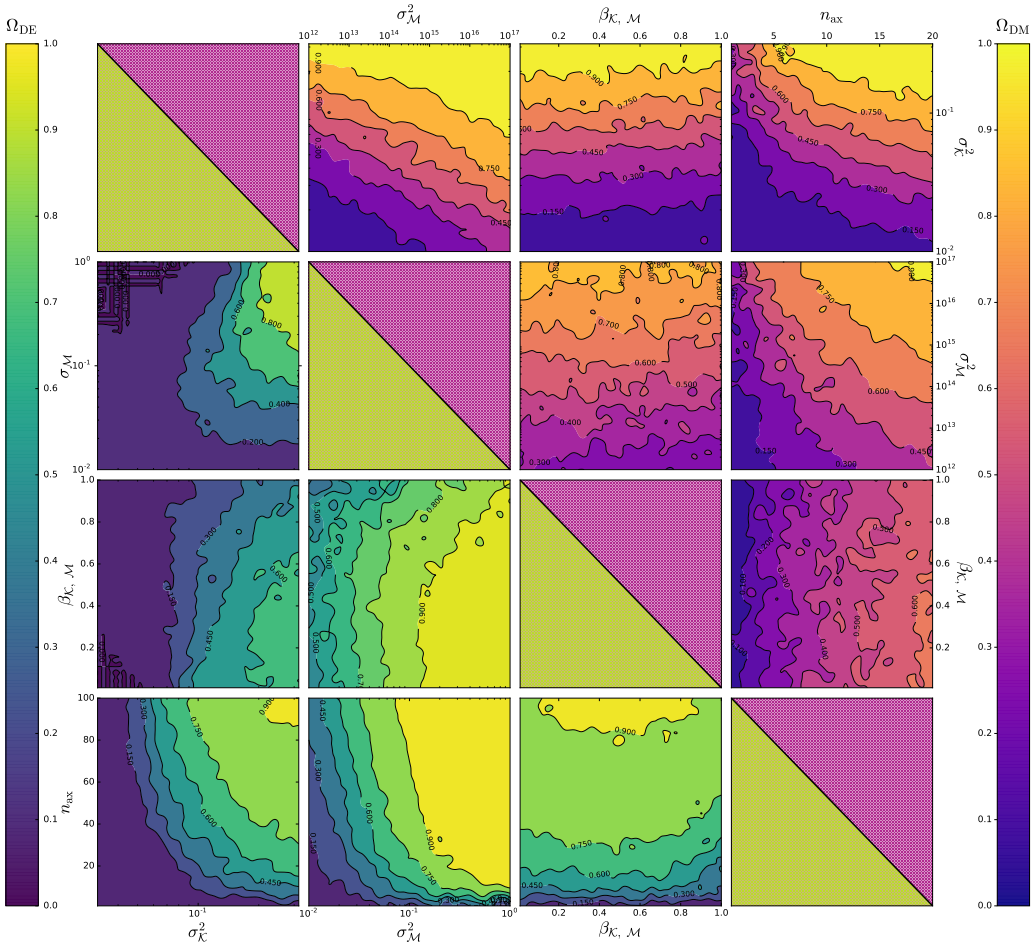


Figure 7.7: Contour density plots for two-dimensional slices of the model parameter space for each parameter in the correlated F-matrix model of Section 5.2.5.1. The mass spectrum is determined explicitly using Eq. (4.101). *Upper-triangle panels*: Example contours for excluded regions of parameter space for the axion DM density parameter, $\Omega_{\rm DM}$ using the intervals outlined in Eq. (7.36), Eq. (7.37) and Eq. (7.38) along with the fixed values found in Eq. (7.40), Eq. (7.41), Eq. (7.42) and Eq. (7.43). *Lower-triangle panels*: Example contours for excluded regions of parameter space for the axion DE density parameter, $\Omega_{\rm DE}$ using the intervals outlined in Eq. (7.44), Eq. (7.45) and Eq. (7.46) along with the fixed values found in Eq. (7.48). Eq. (7.49), Eq. (7.50) and Eq. (7.51).

7.2.1.2 Isometric Y-Matrix Dark Energy

It is easy to find parameters of the simplified Y-matrix model that give rise to sufficient DE as the requirements more trivial to handle. Our Y-matrix DE cosmologies

begin with the approximation that the mass scale at which axion field oscillation begins follow the simple limiting constraint, $\langle m_a^2 \rangle \lesssim M_H^2$. We allow for a maximisation of the initial field displacements by fixing $\bar{f} = M_{\rm Pl}$ as well as constraining the shape of the distribution by setting $\beta_{\mathcal{M}} = 0.5$. When searching for a population of non-oscillating fields about the Hubble scale today we approximate the value of the first raw moment of the distribution $\sigma_{\mathcal{M}}^2$, with a large number of fields driving a phase of acceleration via the simplified fraction,

$$\sigma_{\mathcal{M}}^2 \approx \frac{\sigma_{M_H}^2}{n_{\rm ax}} \approx \frac{1}{(5 \rightarrow 100)} \approx (0.2 \rightarrow 0.01) \ . \tag{7.35}$$

The value of $\sigma_{M_H}^2$ represents a mean scale for the distribution fixed at the scale found in Eq. (7.11). In Fig. 7.5 we display the probability densities for $n_{\rm ax} = \mathcal{O}(1 \rightarrow 100)$, for corresponding values of $\sigma_{\mathcal{M}}^2$ determined by Eq. (7.35). Seemingly larger values of $n_{\rm ax}$ tailor the potential for desirable values of $\Omega_{\rm DE}$, suppressing the uncertainty coming from the uniform prior on the initial misalignment the fields can be drawn with. A population size of $n_{\rm ax} = 100$ returns a high probability of reproducing cosmologies with values of $\Omega_{\rm DE}$ contained in the window of Eq. (7.5). As $n_{\rm ax} \rightarrow \mathcal{O}(100)$, once again the initial field misalignments in the population converge to their averaged value $\langle \theta \rangle$, where the linear combination of the field density contributions cause the probability density of the DE density parameter to converge towards the modal value. Decreasing the value of $n_{\rm ax}$ increases the chance of returning cosmologies failing the acceleration criterion, $\ddot{a} > 0$ at $z = 0$ used in Section 7.3.2, an N-flation type statistical enhancement very simple to quantify in this case.

Using the relationship in Eq. (7.35) we address the role of the final parameter in this model, $\beta_{\mathcal{M}}$, regulating the shape of the distribution. The density plots in Fig. 7.6 show the spread of $\Omega_{\rm DE}$ values for fixed values of $\beta_{\mathcal{M}}$, distributed about $\sigma_{M_H}^2 n_{\rm ax}^{-1} = 20^{-1}$. We highlight the approximate degeneracy across our five fixed values of $\beta_{\mathcal{M}}$. We could take the statistical sampling of $\beta_{\mathcal{M}}$ to be controlled by different functional forms, i.e. uniform distribution or Gaussian sampling motivated by the previously

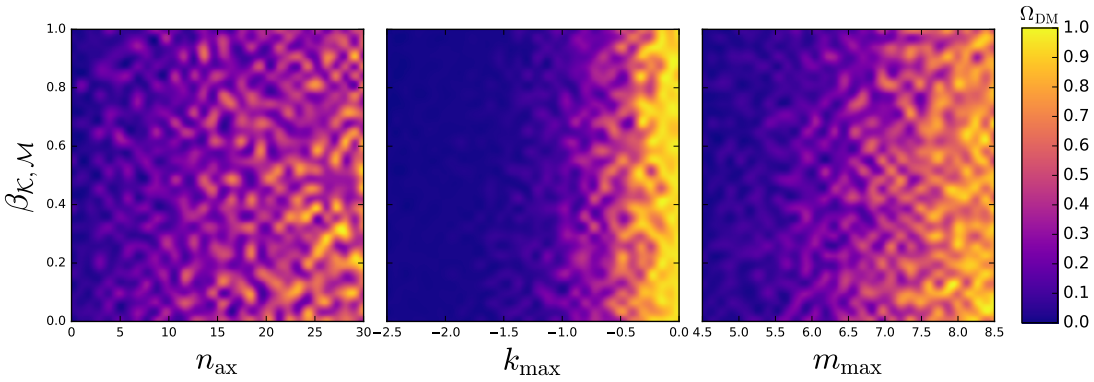


Figure 7.8: Density heat maps for the axion DM density parameter, $\Omega_{\rm DM}$ for values of $\beta_{\mathcal{K},\mathcal{M}} \in (0, 1]$ as a function of the remaining model parameters, $n_{\rm ax}$, $k_{\rm max}$ and $m_{\rm max}$. We limit the values of the number of fields in the population to be, $n_{\rm ax} = [1 - 30]$ axions, along with varied limits on both the decay constants parameterised by $k_{\rm max}$ and the masses parameterised by $m_{\rm max}$. Restricting our examples to the case of high decay constants quickly saturates the Universe with DM (*middle* panel). Likewise a spectrum of almost degenerate mass states quickly dominates as DM when the mass scale in increased (*right* panel). We also find a general degeneracy across all mass spectra shapes.

mentioned Type IIB dimensionality [499] (*left panel* of Fig. 3.3). Only extremal values representing outliers or values close to the boundary for any of these priors will induce limited variations to the spread of $\Omega_{\rm DE}$ as compared to the benchmark case of $\beta_{\mathcal{M}} = 0.5$. Each value retains a mean value of $\Omega_{\rm DE} \approx 0.65$. It appears in a simplified sense that randomised figurations require statistical enhancements from a large number of fields, if the fields are to sit below the Hubble scale. The shape of the distribution and priors placed on them generates a limiting effect when a large number of fields are included. We should expect the dimension of the axion mass matrix using random matrix methods for DE sectors to be in general much larger than for DM sectors in order to produce sufficient vacuum energy today.

7.2.2 Full Rank Perturbed *F*-Matrix Model

We now focus on the case of logarithmically symmetric mass spectra models ($\beta_{\mathcal{K}} = \beta_{\mathcal{M}}$), generated from perturbations stemming from basis normalisation, along with non-trivial scalings on the field decay constants. These models have equal limiting probabilities to draw outlying fields, both positive and negatively logarithmically displaced from the distribution mean. In Fig. 7.7 we display contour density plots for intervals of the two-dimensional parameter space, representing two-dimensional hyperplane slices of the parameter hypercube required to scan over all parameter configurations.

7.2.2.1 Perturbed *F*-Matrix Dark Matter

For DM cosmologies, the model parameters we allow to run are scanned over the following intervals,

$$\log_{10}(\sigma_{\mathcal{K}}^2) \in [-4.0, -1.0] \,, \tag{7.36}$$

$$\log_{10}(\sigma_{\mathcal{M}}^2) \in [12.00, 17.0] \,, \tag{7.37}$$

$$\beta_{\mathcal{K},\mathcal{M}} \in [0.01, 1.00] \,, \tag{7.38}$$

$$n_{\rm ax} \in [1, 20] \,. \tag{7.39}$$

When we fix parameter dimensions to define a hyperplane we use the following fixed values for the parameter static baselines,

$$\log_{10}(\sigma_{\mathcal{K}}^2) = -2.60 \,, \tag{7.40}$$

$$\log_{10}(\sigma_{\mathcal{M}}^2) = 5.70 \,, \tag{7.41}$$

$$\beta_{\mathcal{K},\mathcal{M}} = 0.5 \,, \tag{7.42}$$

$$n_{\rm ax} = 20 \,. \tag{7.43}$$

The top row of parameter hyperplanes detail the banding effects of the DM density whilst increasing the first raw moment distribution scale of our kinetic matrix, $\sigma^2_{\mathcal{K}}$. As seen in the upper left hyperplane the probability density of axion DM domination widens as the distribution scale of the initial mass matrix, $\sigma^2_{\mathcal{M}}$, leaves the lower DM mass limit. Indeed it is expected that the limited spectral width in these models is such that we should not expect large amounts of freedom to reposition ourselves in the parameter space before traversing into the bounds of the contours with non-desirable quantities of DM. The limited width of the *purple* and *mauve* bands indicate the freedom we have to centre the decay constant spectra with fixed mass matrix scales. The gradient of the bands corresponds to the fact that in general we should not expect far-in excess the quantities of DM required when considering axion populations at the mass scale limit detailed in Eq. (7.23), unless we compensate the construction of the distribution scales for $\mathcal{K}_{ij}$. In order to realise multi-component DM with $n_{\rm ax} \gtrsim \mathcal{O}(10)$, the decay constants should be fixed to sub-GUT scales. For string like axions with GUT or trans-GUT decay constants, the contour bands convergence, producing values of $\Omega_{\rm DM} \lesssim 0.9$ for $n_{\rm ax} \lesssim 5$, as shown in the upper right hyperplane. Correspondingly the hyperplane below details the convergence in the same regard as the scale of the non-perturbative physics responsible for fixing the first raw moment of the mass matrix. The bands widen when considering a larger number of fields $n_{\rm ax} \approx \mathcal{O}(10)$, at lower mass scales in the approximate regions (*purple* and *mauve*) for fixed $\sigma^2_{\mathcal{K}}$. Likewise at lower values of $\sigma^2_{\mathcal{K}}$ we see a widening in the regions when $n_{\rm ax} \approx \mathcal{O}(10)$. The simplicity of the matrix structure we use will provide very comparable results between the isometric and perturbed models. These approximate comparisons can be visualised in the middle right hand hyperplanes of Fig. 7.7 and the hyperplane second from top in Fig. 7.4. This is expected, as averaging the field contributions with $n_{\rm ax} \gtrsim \mathcal{O}(10)$ gives comparable results when using the equal initial field conditions for the field VEVs in the N-flation type model of Section 5.2.4.1 which is also partnered with the random scanning from rotations and sampling for the misalignments.

7.2.2.2 Perturbed *F*-Matrix Dark Energy

The DE configurations reside in the lower left triangle of hyperplanes in Fig. 7.7. Unlike models of DM cosmology the requirement to generate fields still fixed from Hubble friction, understood by the lower limiting mass bound in Eq. (7.24), once again defines the approximate scale of the mass scaling parameter $\sigma_{\mathcal{M}}^2 \approx M_H$. This time however quintessence like fields have a susceptibility to draw non-maximised decay constants. The DM parameters allowed to run are scanned over the following intervals,

$$\log_{10}(\sigma_{\mathcal{K}}^2) \in [-2.0, 0.0] \,, \tag{7.44}$$

$$\log_{10}(\sigma_{\mathcal{M}}^2) \in [-2.0, 1.0] \,, \tag{7.45}$$

$$\beta_{\mathcal{K},\mathcal{M}} \in [0.01, 1.00] \,, \tag{7.46}$$

$$n_{\rm ax} \in [1, 100] \,, \tag{7.47}$$

Once again we fix parameter dimensions to define a hyperplane by using the following fixed parameter values for the static baselines,

$$\log_{10}(\sigma_{\mathcal{K}}^2) = -0.60 \,, \tag{7.48}$$

$$\log_{10}(\sigma_{\mathcal{M}}^2) = -1.65 \,, \tag{7.49}$$

$$\beta_{\mathcal{K},\mathcal{M}} = 0.5 \,, \tag{7.50}$$

$$n_{\rm ax} = 20 \,. \tag{7.51}$$

In the *upper left*, *lower left* and *lower central* hyperplanes we show the relationship between the axion population size and the scale of each matrix argument in the effective Lagrangian found in Eq. (5.12). In general we do require scaling parameters of the order, $\sigma_{\mathcal{K}}^2 \approx M_{\rm Pl}$ and $\sigma_{\mathcal{M}}^2 \approx M_H$ (*upper left* panel), with the regions of parameter space with either $\sigma_{\mathcal{K}}^2 \lesssim 0.1 M_{\rm Pl}$ or $\sigma_{\mathcal{M}}^2 \lesssim 0.1 M_H$ quickly suppressing the total DE density unless the population size is increased to $n_{\rm ax} \approx 40$ to compensate, representing the lowest number of axions required in order to linearly scale the

solutions (*lower left* and *central* panels). The *upper* and *left central* hyperplanes show the preference for the incorporation of the full tail of the distributions corresponding to values of $\beta_{\mathcal{K},\mathcal{M}} \to 1$, as the defining decay and mass scales of the distributions are increased. The increased chance of drawing outliers enhanced to select preferred scales.

The reduction of the spectral width for the decay constants and mass eigenstates generates a degeneracy in the contours for values of $\beta_{\mathcal{K},\mathcal{M}} \lesssim 0.5$ for fixed parameter scales, prominently shown in the *upper central* panel. The preferential defining shape of the sub-matrices is dependant on the distribution scales, where the model maximises the potential to draw suitable quintessence fields. In the *left central* panel we see the recovery of a full degeneracy across all spectra shapes when the initial field displacement conditions are insufficient for any form of significant axionic DE presence at the current time. Finally, the *lower right* hyperplane shows the relationship between the shape of the distribution and the axion population size. Fixed population sizes present a degeneracy with distribution shape parameters, $\beta_{\mathcal{K},\mathcal{M}} \lesssim 0.5$. The contour curvature as $n_{\rm ax} \to \mathcal{O}(100)$ corresponds to a spreading of the mass spectrum, increasing the probability density of lighter fields. It could however also correspond to the inclusion of heavier oscillating late time DM like fields at $z = 0$, as the tails of the distributions are sampled for large $n_{\rm ax}$.

7.2.3 Full Rank Perturbed $\boldsymbol{F}$-Matrix with Rank One Noise Model

Contour density plots for the axion DM density parameter, $\Omega_{\rm DM}$ in the $\sigma^2_{\mathcal{M}}$, $n_{\rm ax} = \mathcal{O}(1 \to 10)$ plane, demonstrated for different discrete fixed values of the initial field displacement scaling parameter, $\bar{f}$.

High scalings of $\bar{f}$ generally produce too much DM when using a small number of fields in the ultralight sector. When this scale is lowered we generate contour degeneracies in this plane, reproducing the approximate required values defined in

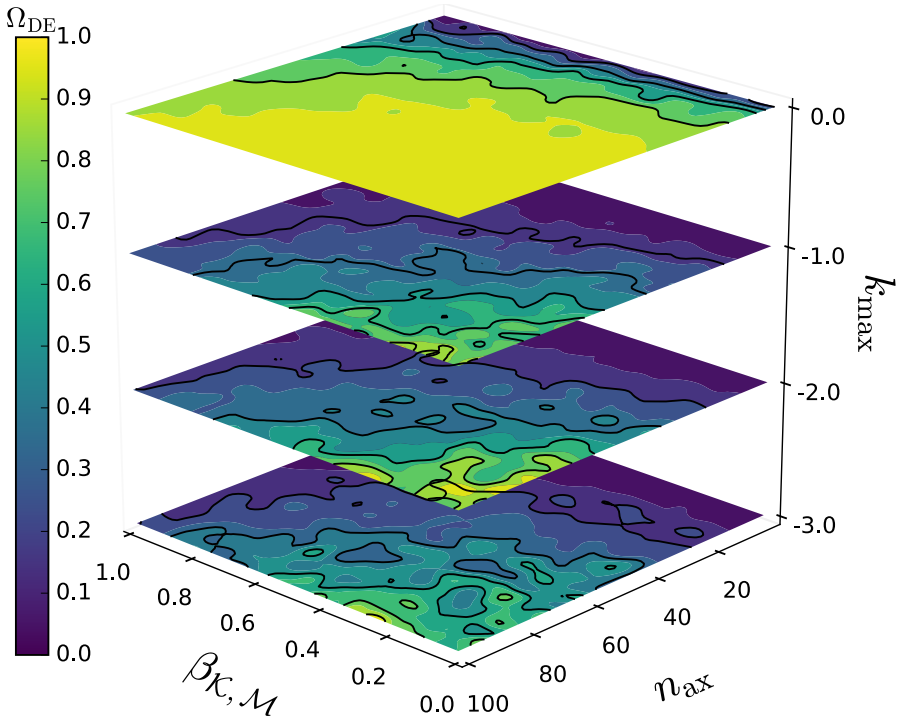


Figure 7.9: Contour density plots for the axion DE density parameter, $\Omega_{\rm DE}$ in the $\beta_{\mathcal{K},\mathcal{M}}$, $n_{\rm ax} = \mathcal{O}(1 \to 100)$ plane, demonstrated for different discrete fixed values regulating the upper bound on the axion decay constants, $k_{\rm max}$. High scalings from larger values of $k_{\rm max}$ generally furnish these models with sufficient DE in the bounds defined in Eq. (7.5). When $\beta_{\mathcal{M}}$ approaches the rectangularisation limit of unity a larger number of fields are preferred to counteract the statistical spread of the distribution as shown in *top* panel.

Eq. (7.3). For example when $\bar{f} = 0.05 M_{\rm Pl}$ we have the approximate relationship, $17 - \log_{10}(\sigma^2_{\mathcal{M}}) \simeq {}^{n_{ax}}/_{2}$ using the presented bounds. For ultralight fields the DM density quickly fades off as the scale of $\bar{f}$ approaches the GUT scale.

The full rank perturbed F-Matrix with rank one noise model examples, introduced in Section 5.2.5.2.3, can be used to investigate potential differences in our example cosmology outputs from the $\mathcal{O}(n_{\rm ax})$ enhanced eigenvalues present in each of our physical quantities in this model when compared to the limiting eigenvalues of the previous models. It is worth noting by construction our examples will see very little variation compared to the full rank perturbed Y-matrix models due to an absence of extended large correlated signals, coming from the order of magnitude of our axion population numbers we select and our choice to use spectral signal generated from

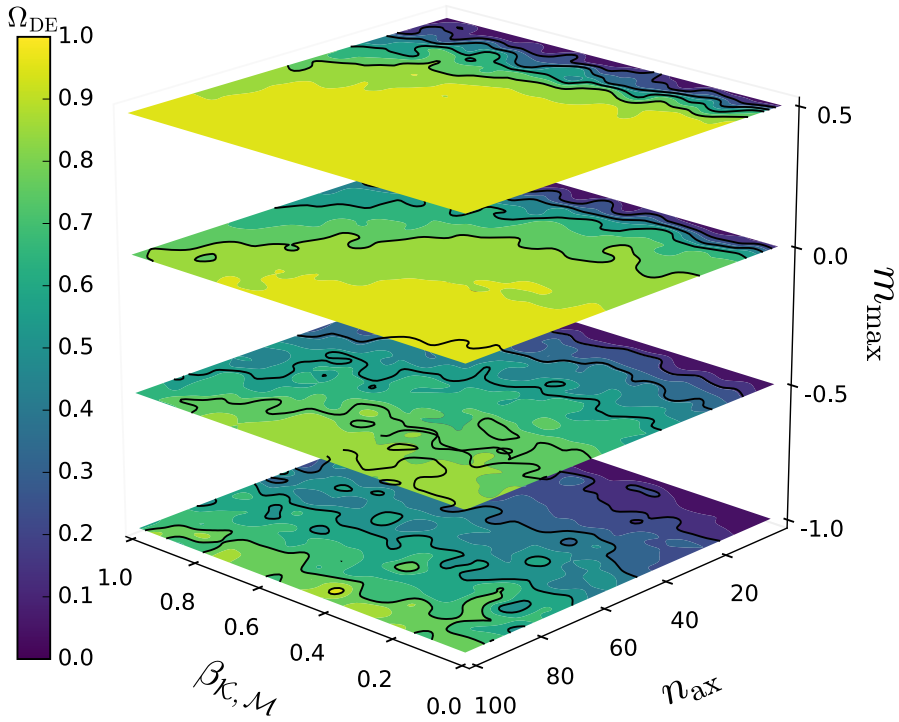


Figure 7.10: Contour density plots for the axion DE density parameter, $\Omega_{\rm DE}$ in the $\beta_{\mathcal{K},\mathcal{M}}$, $n_{\rm ax} = \mathcal{O}(1 \to 100)$ plane, demonstrated for different discrete fixed values regulating the upper bound on the axion mass states, $m_{\rm max}$. Axion masses surpassing the limit of M_H quick provide too much DE. When the spectrum sit around or just below this scale once again a larger number are preferred when $\beta_{\mathcal{M}}$ approaches the rectangularisation limit of unity. This is shown in the two *middle* panels sufficiently reproducing values of $\Omega_{\rm DE}$ falling in the bounds of Eq. 7.5.

non-central Wishart ensembles. These models do ensure the presence of outlying eigenvalues with every realisation. We leave the study of large population numbers where our largest eigenvalues could obtain significant enhancements in the form of both large singular decay constants and a widening of the spectral width, through enhanced data correlations of the mass distribution to future study. We limit the number of parameters we consider in our examples in this model by fixing the values of our lower bounds on our distributions, controlled by the baselines $k_{\rm min}$ and $m_{\rm min}$ throughout. The values of $\langle f_a \rangle$ and $\langle m_a \rangle$ are scaled by changing the values of $k_{\rm max}$ and $m_{\rm max}$ accordingly.

7.2.3.1 Full Rank Perturbed *F*-Matrix with Rank One Noise Dark Matter

We are interested in the role of a spectrum of large decay constants in the low mass axion window for DM cosmologies, which we explore using the possible effects of enhanced correlated eigenvalues in both spectra. Our parameter intervals are defined as,

$$k_{\rm max} \in [-2.5, 0.0] \ , \tag{7.52}$$

$$m_{\rm max} \in [4.5, 8.5] \ , \tag{7.53}$$

$$\beta_{\mathcal{K},\mathcal{M}} \in [0.01, 1.00] \ , \tag{7.54}$$

$$n_{\rm ax} \in [1, 30] \ , \tag{7.55}$$

with the following static baselines,

$$k_{\rm min} = -5.0 \ , \tag{7.56}$$

$$k_{\rm max} = -1.0 \ , \tag{7.57}$$

$$m_{\rm min} = 4.0 \ , \tag{7.58}$$

$$m_{\rm max} = 6.0 \ , \tag{7.59}$$

$$n_{\rm ax} = 20 \ , \tag{7.60}$$

$$\beta_{\mathcal{K},\mathcal{M}} = 0.5 \ . \tag{7.61}$$

The values in Eq. (7.56) are chosen to fix the lowest scale of $\langle f_a \rangle$ fixing the bulk of the spectrum to sub-GUT values when $k_{\rm max}$ is at its lowest value. The upper limit of $k_{\rm max}$ corresponds to the decay constant scale, $\langle f_a \rangle = \mathcal{O}(0.1 M_{\rm Pl})$. Our lower limit on $m_{\rm min}$ in Eq. (7.58) is to ensure we have fields oscillating with masses $m_a \gtrsim 10^6 M_H$. The maximum fixed value of $m_{\rm max}$ corresponds to fields drawn from a mass distribution centred around $\langle m_a \rangle \approx \mathcal{O}(10^7 M_H)$, with the upper limit $m_{\rm max}$ giving a mass distribution scale, $\langle m_a \rangle \approx \mathcal{O}(10^9 M_H)$.

In Fig. 7.8 we display heat density maps representing the two-dimensional parameter space for each model parameter against values of $\beta_{\mathcal{K},\mathcal{M}}$, defined in the interval in Eq. (7.54). In each of the panels we find a reproduction of the approximate degeneracy across all values of $\beta_{\mathcal{K},\mathcal{M}}$, mimicking the results presented in the panels in Fig. 7.7. It is clear that this model can offer little deviation from models without significantly strong correlated signal eigenvalues for DM cosmologies, given we need in general a low number of fields at the mass scales we are considering. In the middle panel we see the clustered heat density reproduced for large values of $\Omega_{\rm DM}$ as we scale the distribution of f_a towards $M_{\rm Pl}$, once again indicating a preference to incorporate values of $f_a \approx M_{\rm Pl}$ in the model. The left hand panel shows a measure of the likelihood, at fixed physical parameter scales, to find acceptable quantities of DM as the population size increase via the *speckled* nature of the probability densities.

7.2.3.2 Full Rank Perturbed *F*-Matrix with Rank One Noise Dark Energy

In both Fig. 7.9 and Fig. 7.10 we introduce a small step into the three-dimensional parameter space for $\Omega_{\rm DE}$ contour densities. We initially focus on the configuration where the scales of our dimensional quantities are determined by the relationship, $m_{\rm min} = k_{\rm min}$ and $m_{\rm max} = k_{\rm max}$. This ensures that our rotated mass spectrum is centred about, $\langle m_a \rangle = M_H$ with a spectral width determined by the value we fix for $k_{\rm max}$. Our parameters which we allow to run are scanned over the following intervals,

$$k_{\rm max} \in [-3.0, 0.0] \ , \tag{7.62}$$

$$m_{\rm max} \in [-1.0, 0.5] \ , \tag{7.63}$$

$$\beta_{\mathcal{K},\mathcal{M}} \in [0.01, 1.00] \ , \tag{7.64}$$

$$n_{\rm ax} \in [1, 100] \ , \tag{7.65}$$

with the following parameter values for the models fixed baselines,

$$k_{\min} = m_{\min} = -5.0 \ , \tag{7.66}$$

$$k_{\max} = m_{\max} = 0.0 \ , \tag{7.67}$$

$$n_{\rm ax} = 20 \ , \tag{7.68}$$

$$\beta_{\mathcal{K},\mathcal{M}} = 0.5 \ . \tag{7.69}$$

The panels of Fig. 7.9 display the contour densities for $\beta_{\mathcal{K},\mathcal{M}}$ against $n_{\rm ax}$ for stacked decay constant distribution scales, emphasising the previously determined preference for high scale decay constants to provide sufficient $\Omega_{\rm DE}$, when using mass centred distributions about M_H. Lower vales of $k_{\max}$ slowly recover the degeneracy across all values of $\beta_{\mathcal{K},\mathcal{M}}$ providing little DE density. For $k_{\max} = 0.0$, as the population number $n_{\rm ax}$ increases significantly, a preference is made for the inclusion of the full tail of the mass spectrum where $\beta_{\mathcal{K},\mathcal{M}} \to 1$, maximising the spread of mass values the fields can take. Values of $k_{\max}$ minimally offset from this value require $\beta_{\mathcal{K},\mathcal{M}} \to 0$ to ensure a large population of fields have approximately degenerate and sufficient mass values ($\approx M_H$), in order to furnish our cosmologies with a sufficient DE density.

Correspondingly the panels of Fig. 7.10 present contour density plots for $\beta_{\mathcal{K},\mathcal{M}}$ against $n_{\rm ax}$ for stacked mass distribution scales, offset with respect to the scale $\langle m_a \rangle \approx M_H$ fixed by $m_{\max}$. Each configuration uses a fixed distribution of high scale decay constants (Eq. (7.67)). It is clear in the upper panel that distributions offset towards the upper mass limit in Eq. (7.10) quickly produce high probability densities for cosmologies with axion DE domination. Scales centred about $\langle m_a \rangle \approx M_H$ increase the width of the contour bands with acceptable values of $\Omega_{\rm DE}$ (*green* and *light green*). Large population sizes ($n_{\rm ax} \approx \mathcal{O}(100)$) at this scale make a preference for a wider bulk for the mass distribution with values of $\beta_{\mathcal{K},\mathcal{M}} \to 1$, a feature consistent with the previous models behaviour. Mass scales offset below M_H ($m_{\max} = -0.5$) give a preference for $\beta_{\mathcal{K},\mathcal{M}} \to 0$, whilst also requiring large population sizes. A further increase in the offset below the mass scale of M_H recovers approximate de-

generacies across all values of $\beta_{\mathcal{K},\mathcal{M}}$, with significantly reduced probability densities for the required values of $\Omega_{\rm DE}$.

7.2.4 The M-theory Random Matrix Model

We now turn to investigating cosmologies returning the required values of $\Omega_{\rm DM}$ and $\Omega_{\rm DE}$ drawn from the random matrix M-theory landscape, where we fix the number of fields in our examples to $n_{\rm ax} = 10$ throughout, and focus on the remaining model parameters and their effects on the distribution moments. In order to account for gauge couplings consistent with the known elementary particles we chose to sample average values for the three-cycle volume inside the interval,

$$\langle \mathcal{V}_X \rangle = [25 - 60] \ . \tag{7.70}$$

In Fig. 7.12, Fig. 7.13 and Fig. 7.14 we make use of narrow prior windows incorporating Gaussian distributions in our sampling (see Section 7.2.4.3).

7.2.4.1 M-theory Random Matrix Dark Matter

For our initial look at how axions in the M-theory axiverse model could give rise to DM, we begin by fixing the average value of the three-cycle volume distribution $\langle \mathcal{V}_X \rangle$, to maximise the probability density of retrieving axions with masses in the ultralight DM window within the bounds of Eq. (7.24), which we do by selecting the following values,

$$\langle \mathcal{V}_X \rangle = \{45, 50, 55, 60\} \ . \tag{7.71}$$

The two panels in Fig. 7.11 present the probability density for the axion DM density parameter $\Omega_{\rm DM}$, on both linear and logarithmic scales for each selected average value of $\langle \mathcal{V}_X \rangle$ in Eq. (7.71). In the *upper* panel of Fig. 7.11 we show the high probability of returning values of $\Omega_{\rm DM} \lesssim 0.05$. The *lower* panel of Fig. 7.11 details the spread of these values logarithmically, with a minor peak in the probability density to return

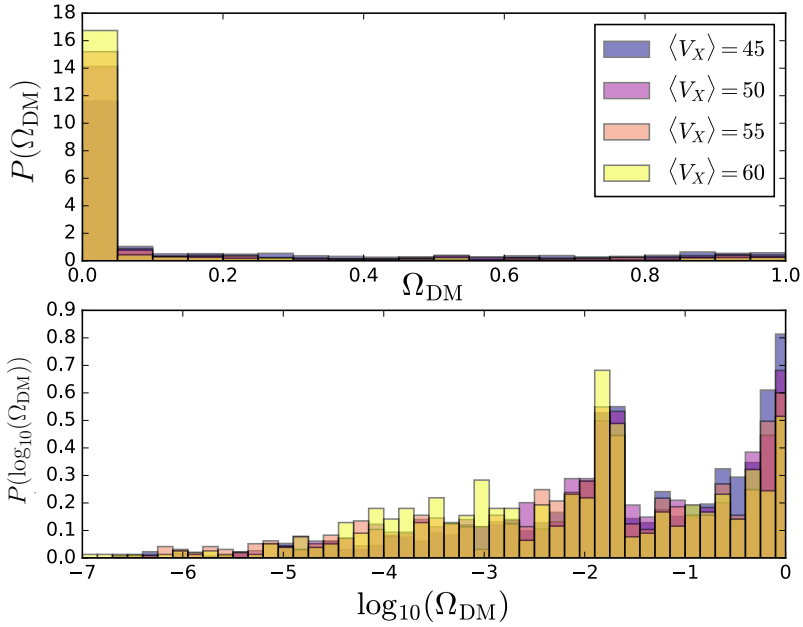


Figure 7.11: Probability densities for the fractional percentage of axion DM recovered, measured with the axion DM density parameter, $\Omega_{\rm DM}$ in the M-theory random matrix model presented in both linear and logarithmic scales.. Each example configuration uses the parameter set $\langle \mathcal{V}_X \rangle = \{45, 50, 55, 60\}$, for the average average values for the three-cycle volume. Generally without the use of very narrow priors on the model variables the model produces negligible quantities of axion DM.

values of $\Omega_{\rm DM} = \mathcal{O}(10^{-2})$. The low quantities of DM arise from the M-theory mass spectrum consistent with axiverse models spanning many decades, naturally giving a significantly lower percentage of cosmologies with values of $\Omega_{\rm DM}$ falling in the window of Eq. (7.3), especially for cosmologically unconstrained masses as compared to the localised scale statistical RMT models of the string axiverse with far more localised bounded spectra. The spread of the axion masses is such that we can tune the moments of the distribution using the average three-cycle volume values, $\langle \mathcal{V}_X \rangle = 45$ and $\langle \mathcal{V}_X \rangle = 60$. For this example we find an increase in the number of cosmologies with values of $\Omega_{\rm DM}$ falling inside the required window, go from $\approx 33^{-1}$ to $\approx 11.75^{-1}$.

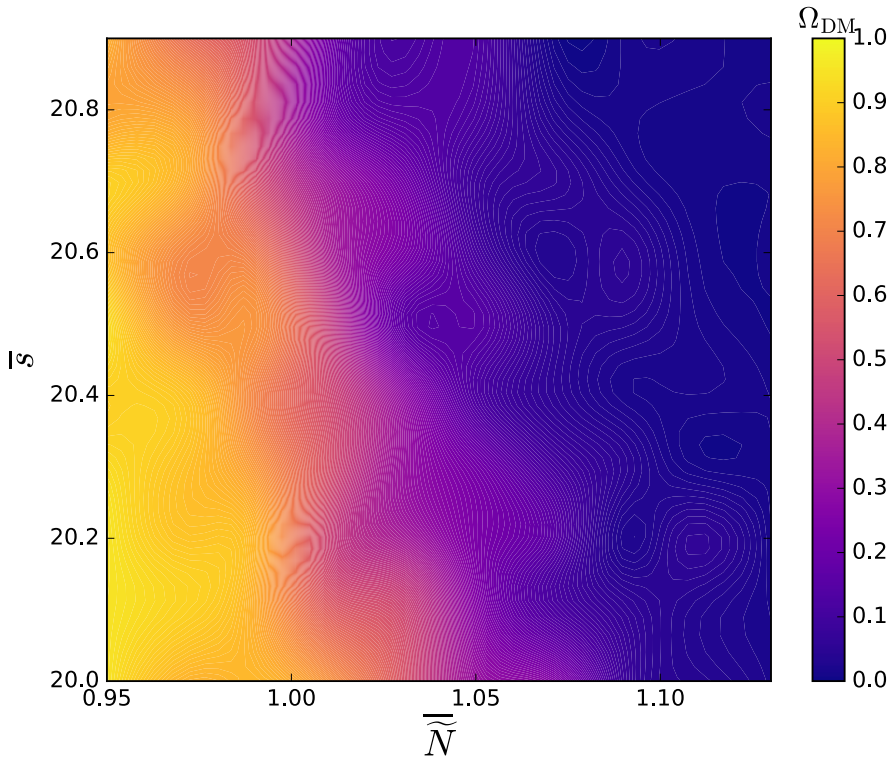


Figure 7.12: Contour density plot for the axion DM density parameter, $\Omega_{\rm DM}$, found by using narrow priors for the moduli VEV, s, and instanton index parameter $\bar{\tilde{N}}$. There is a very minor correlation between the two parameters where inside the transitional region of $\overline{\tilde{N}} \approx 1.02 - 1.06$ which generates DM inside the bound in Eq. (7.3).

7.2.4.2 M-theory Random Matrix Dark Energy

Initial searches for axions with the properties of DE in the M-theory model show that there is no satisfactory mass distribution which returns reasonable probabilities of producing values of the DE density parameter, $\Omega_{\rm DE}$, falling inside the bounds of Eq. (7.5). This feature arises due to the nature of the axion decay constants in the model which are typically too small, $f_a \sim a/s_i \sim 10^{-2} M_{\rm Pl}$, as regulated by the expected values of the moduli VEVs under the conditions of the compactification model. The DE density could be increased significantly by using a much larger number of axions or utilising the alignment mechanism to effectively enhance the decay constants. Our assumptions however, on the diagonal form of the kinetic matrix to reduce tensions from dark radiation constraints in Eq. (5.94) does not allow for the inclusion of any such an alignment mechanism. Therefore, we postpone

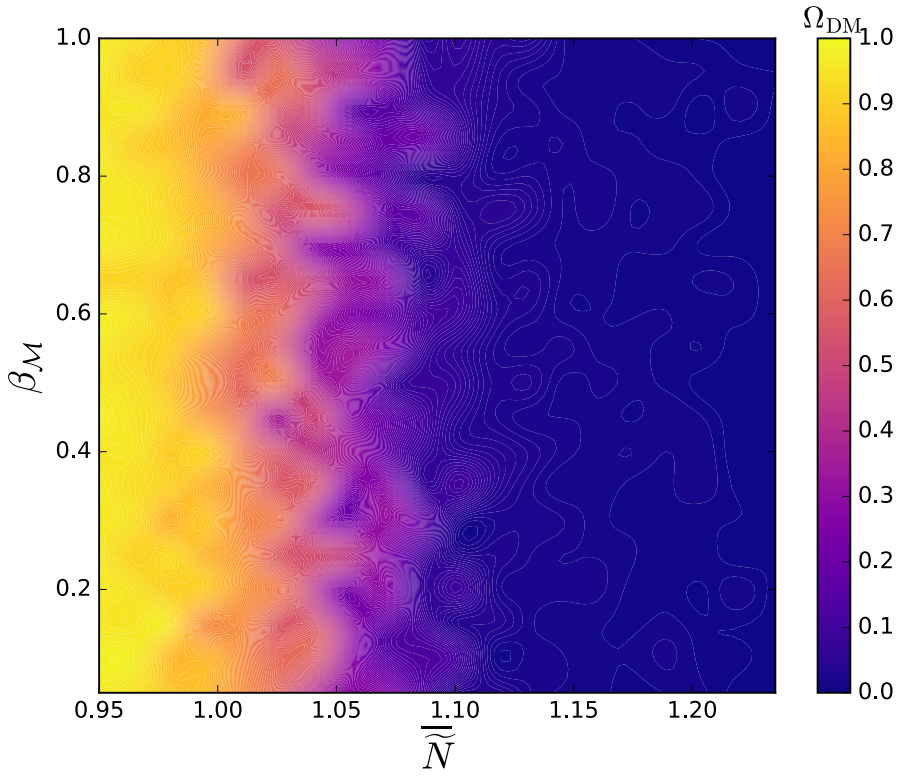


Figure 7.13: Contour density plots for the axion DM parameter, $\Omega_{\rm DM}$ for $\beta_{\mathcal{M}}$ found by using narrow priors on the instanton index parameter $\bar{\widetilde{N}}$. The correlation between these parameters is extremely small, with statical fluctuations in the approximate transitional region, $\overline{\widetilde{N}} \approx 1.00 - 1.08$, generating DM which falls inside the bounds of Eq. (7.3).

an enhanced look into the possibility of sampling the M-theory axiverse models for DE as a topic of interest for future work, utilising a more detailed investigation of the properties of the Kähler metric in these models.

7.2.4.3 A Finely Tuned M-theory Random Matrix Toy Model

In order to paint a better picture of the potential of the dark sector in the current incarnation of the M-theory random matrix model, despite the previously highlighted issues, we now consider a toy model with narrow prior probability densities placed on the associated hyperparameters. In particular, if the priors on the moduli VEV, s, and the instanton index parameter, $\widetilde{N}_i^j$, which control the volume function are narrow, our M-theory mass distributions will generically only spread over a few or-

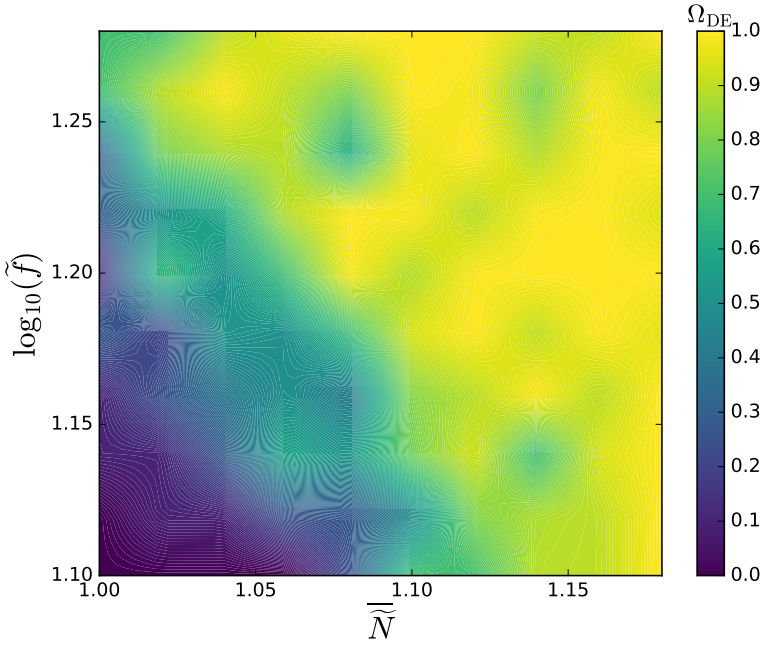


Figure 7.14: Contour density plot for the axion DE parameter, $\Omega_{\rm DE}$, found by using narrow priors for $\widetilde{N}$ along with an enhancement factor on decay constant, f_a. The parameters are generally well correlated with small regions displaying flections reproducing DE inside the bounds in Eq. (7.5). The axion decay constants are generally required to be enhanced by $\mathcal{O}(10)$ in these limits to produce sufficient DE.

ders of magnitude instead of the many decades of the axiverse we would typically expect when incorporating the full theoretical uncertainty of the stochastic model parameters. As a result, the axion dark sector density parameters, $\Omega_{\rm DM}$ and $\Omega_{\rm DE}$ will also be concentrated around particular values. This configuration allows us to study correlations between mean values of the M-theory model parameters in a relatively simple manner. We restrict the sampling of the parameters by fixing the prior distributions for s and $\widetilde{N}_i^j$ to be drawn from Gaussian distributions, $\mathcal{N}(\mu, \sigma)$. We limit the width of the prior sampling by fixing the distribution standard deviation for s and $\widetilde{N}$ to,

$$\sigma_s = 1 \ , \tag{7.72}$$

$$\sigma_{\widetilde{N}} = 0.01 \ , \tag{7.73}$$

respectively. For the case of DM cosmologies, we simulate cosmologies for a range of mean values of s and $\widetilde{N}_i^j$ as shown in the contours of Fig. 7.12. The contour density plot shows a trend of hyperbolic constraint as expected, from the relation $\overline{\mathcal{V}}_X \sim \overline{s} \times \overline{N}$. We find a minor correlation for $\overline{\widetilde{N}} \approx 1.02-1.06$ and the values of $\bar{s}$ considered, which reproduce the correct DM content. Our example cosmologies where we allow for variations in $\beta_{\mathcal{M}}$, are given in Fig. 7.13. We see a general degeneracy across the distribution shaping parameter and the values of $\overline{\widetilde{N}}$. The transitional region is approximately, $\overline{\widetilde{N}} \approx 1.00-1.08$ where the DM relic abundance statistically fluctuates across this region, generating the weaving effect in the contours. The model is very sensitive to the value of $\overline{\widetilde{N}}$ for DM, a widening of the prior on this parameter representing the statistical suppression of correctly generating DM in the M-theory random matrix axiverse.

Finally when considering the DE cosmology case, consider a toy model which gives us an insight on how much enhancement the decay constants could require in the M-theory model. We study this effect by parametrising the decay constant enhancement factor as,

$$\widetilde{f} = \frac{f_a'}{f_a} \,, \tag{7.74}$$

where f_a' represents an enhanced decay constant scale. In Fig. 7.14 we explore the correlations between the values of this enhancement and $\overline{\widetilde{N}}$. There is a fairly strong correlation between the two parameters, reproducing a very minor band of cosmologies producing the correct DE density. The value of $\overline{\widetilde{N}}$ can only be reduced when the decay constants are largely enhanced. We find that we would require an enhancement factor potential related to field alignment, necessary to accomplish the observed DE, is of the order $f_a \sim [10 - 100]$. For both toy models reproducing DM and DE we find a narrow banding of valid parameters from the moduli sector indicating the requirement for significant fine tuning to produce acceptable cosmologies.

7.3 A Bayesian Hierarchical Network of the Axion Dark Sector

7.3.1 The Structure of the Network

The second section of our dark sector results consist of several brief examples treating the string axiverse as a *hierarchical Bayesian network*, as detailed in Appendix B.2, following previous examples and similar methods used to address issues in inflation [1080], Type Ia supernovae data analysis [896, 897, 902, 1127], spatially localised features in the CMB [527] and details surrounding cosmic shear [62] etc. A generic example Bayesian network for axion cosmology is shown in Fig. 7.15, a generalisation of the generic structure shown in Fig. B.1, with various levels for the observables, parameters and hyperparameters of the model. We implement the Bayesian network using MCMC techniques. For this purpose we use the affine-invariant ensemble sampler [616] implemented in EMCEE [549]. The resultant cosmological parameters of interest are defined by the parameter vector,

$$\vec{p} = (\Omega_r h^2, \Omega_{\rm mat} h^2, \Omega_\Lambda h^2) \ . \tag{7.75}$$

In principle the cosmological parameters are determined stochastically from the hyperparameters of a higher level distribution, though in practice here we take these as fixed Dirac delta distributions, determined by the model under consideration. The standard matter density $\Omega_{\rm mat} = \Omega_b + \Omega_c$, contains ordinary CDM and baryons, and the total matter density includes in addition the contribution from axions that have begun oscillations,

$$\Omega_m = \Omega_{\rm mat} + \Omega_a^{\rm osc} \ . \tag{7.76}$$

The axion model parameters fixed by the theory are $\{m_i\}$ and $\{\phi_i\}$. Given the complete set of model parameters the quasi-observables are found deterministically by solving the equations of motion for the system of axions.

The *level 1* (L1) theory hyperparameters stochastically determine the model parameters $\{\phi_i\}$ and $\{m_i\}$. The model selection (theory L2) fixes the model, the number of axions, and the prior distributions for the L1 hyperparameters. The theoretical modelling from L1 to the model parameters accounts for treating the axion potential as a pure mass matrix, and the fixing the moduli. Theoretical modelling and cuts going from L1 to the quasi-observables includes a cut on the maximum field mass m_a, and the choice of cosmological model. The quasi-observables are the fractional densities in each part of the dark sector, the Hubble parameter, the redshift of matter-radiation equality, and the acceleration of the cosmic scale factor. In principle we could consider also the evolution of the background quantities with redshift. For simplicity we apply Gaussian likelihoods to Ω_m, h, and $z_{\rm eq}$, assuming the *Planck* (2015) TT+lowP results [37] presented in Table 7.1. We assign axions to the total matter or effective quintessence density according to whether the fields equation of state has begun oscillating or not. We also apply a cut demanding our Universe should be accelerating, where $\ddot{a} > 0$.

Our treatment of the quasi-observables should be considered only as giving approximate constraints on the considered models. Our models can have non-trivial effects on the equation of state for DE, $w(z)$, and for ultralight DM axions, also on structure formation and the CMB power spectrum [710], which we do not account for in constraints placed on simplified quasi-observables with Gaussian likelihoods. In ordinary ΛCDM, Ω_m, $z_{\rm eq}$, and h are not independent. However, in axion models a change in the equation of state at late times can alter these relationships by the creation of additional matter-like axion density after $z_{\rm eq}$. Our use of $z_{\rm eq}$ as an independent quasi-observable from the matter density and h, serves as an approximation of the constraints found in Ref. [710], which disfavour large energy densities of ULAs that begin oscillating after equality. We ignore covariance between the quasi-observables for the same reason that dependences are not the same in axion models as in ΛCDM. Our quasi-observables we present are a simplified example. A more advanced compression of the CMB, BOA and growth data appropriate for DE

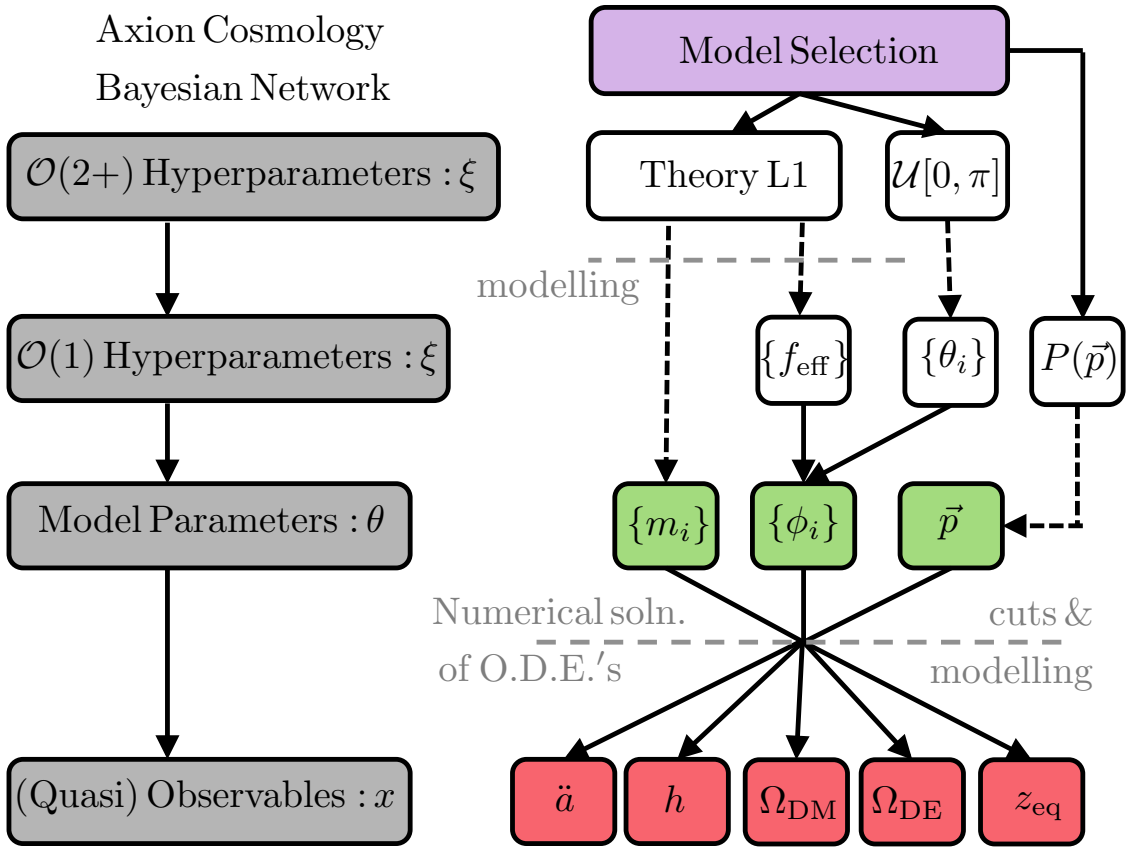


Figure 7.15: A Generic Bayesian Network for Axion Cosmology detailing the schematic relationship between the model parameters and hyperparameters. The arrows indicate the direction of dependence, with dashed arrows indicating stochastic dependence, and solid arrows indicating deterministic dependence. The *red* nodes represent the quasi-observables, *green* nodes the model parameters and *white* nodes the higher order level hyperparameters.

models is given by the treatments in Refs. [121, 1388]. In these, the CMB data are compressed into a vector of measurements for the matter densities, matter power spectrum amplitude, and the angular size of the sound horizon, including covariance considerations.

7.3.2 Constraints on the String Axiverse

All the constraints shown in the following configurations hold the number of axions in the population fixed at $n_{\rm ax} = 20$. Numerical accuracy settings are defined according to the discussions in Section 7.1. All EMCEE walkers are initialised from the priors,

where the chains are ran in order to converge according to the spectral method of Ref. [485].

7.3.2.1 Bayesian Isometric Y-Matrix Constraints

7.3.2.1.1 Bayesian Isometric Y-Matrix Dark Energy

The first set of example constraints we show make use of the simplest random matrix model both in construction and in numerical computational terms, the isotropic Y-Matrix model of Section 5.2.4.1, which we initially tailor to provide DE. We fix the matter density to $\Omega_{\rm mat}h^2 = 0.148$, including dust-like CDM and baryons. The L1 hyperparameters have the following priors (fixed L2 parameters),

$$\bar{f} \in \mathcal{U}[0.0, 5.0] \ , \tag{7.77}$$

$$\sigma_{\mathcal{M}} \in \mathcal{U}[0.0, 10.0] \ , \tag{7.78}$$

$$\beta_{\mathcal{M}} \in \mathcal{U}[0.01, 1.00] \ . \tag{7.79}$$

After applying Gaussian likelihoods to h, $z_{\rm eq}$ and Ω_m, and a cut for $\ddot{a} > 0$, we determine the constraints shown in Fig. 7.17. The mass parameter and $\bar{f}$ are constrained to values consistent with those previously explored and required for sufficient DE density. The cut on acceleration with the requirement $\Lambda = 0$ leads to a maximum allowed value of distributions first raw moment, $\sigma_{\mathcal{M}}$. This model shows no preference on the shape of the distribution through $\beta_{\mathcal{M}}$. With a linear prior on $\sigma_{\mathcal{M}}$, near M_H, the width of the mass distribution is not important. The degeneracies of this model are demonstrated in Fig. 7.16. We show random samples drawn with different values of $(\bar{f}, \sigma_{\mathcal{M}})$ with the distribution shape fixed, $\beta_{\mathcal{M}} = 0.5$ and demonstrate how the quasi-observable distributions shift. The models moving along the degeneracy direction give accelerated expansion and consistent values of $\Omega_{\rm DE}$, which change relatively little. Perpendicular to this direction, the DE density is too low if the mass is too large (oscillations begin before $z = 0$) or the decay constant is too low

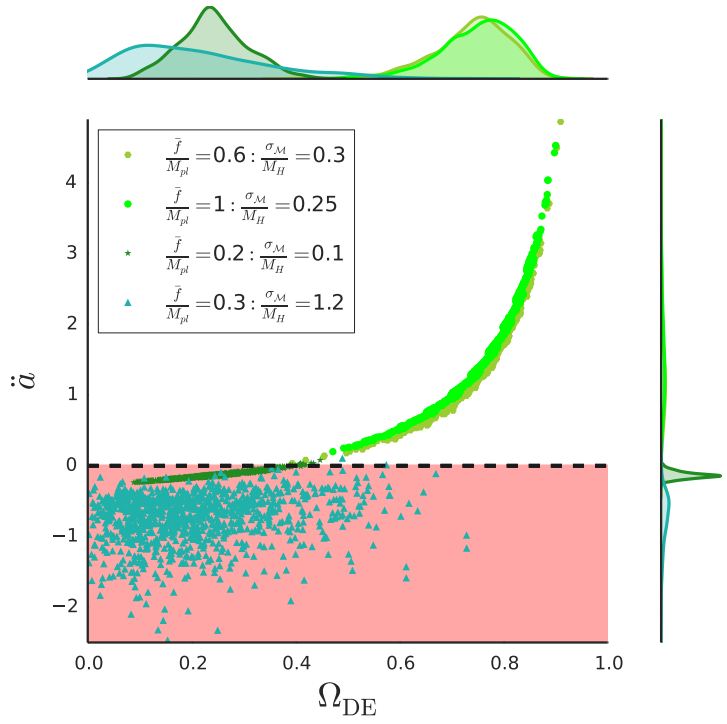


Figure 7.16: Degeneracies in the Y-matrix RMT model for DE. We show random samples form four locations in the $(\bar{f}, \sigma_{\mathcal{M}})$ plane at fixed $\beta_{\mathcal{M}} = 0.5$, marked in Fig. 7.17. Along the degeneracy direction the quasi-observable distributions do not change much. Across this direction, models are disfavoured, with the quasi-observables distributions moving in opposite directions on either side.

(field displacement too small). This has a knock-effect of making the acceleration parameter negative in these models.

7.3.2.1.2 Bayesian Isometric *Y*-Matrix Dark Matter

Next, we consider the computationally more challenging but physically more interesting case of the Marčhenko-Pastur model assigned to DM. The model is more computationally challenging than the DE model due to the required switch in the equations of motion and tracking of any axion field oscillations before the switch (an average run of our numerical code for this model takes $\mathcal{O}(20\text{s})$ in wall-clock time). We fix the (non-axion) matter density to the baryon density, $\Omega_b h^2 = 0.022$, and we fix the physical cosmological constant density to $\Omega_\Lambda h^2 = 0.31$ (this gives the central

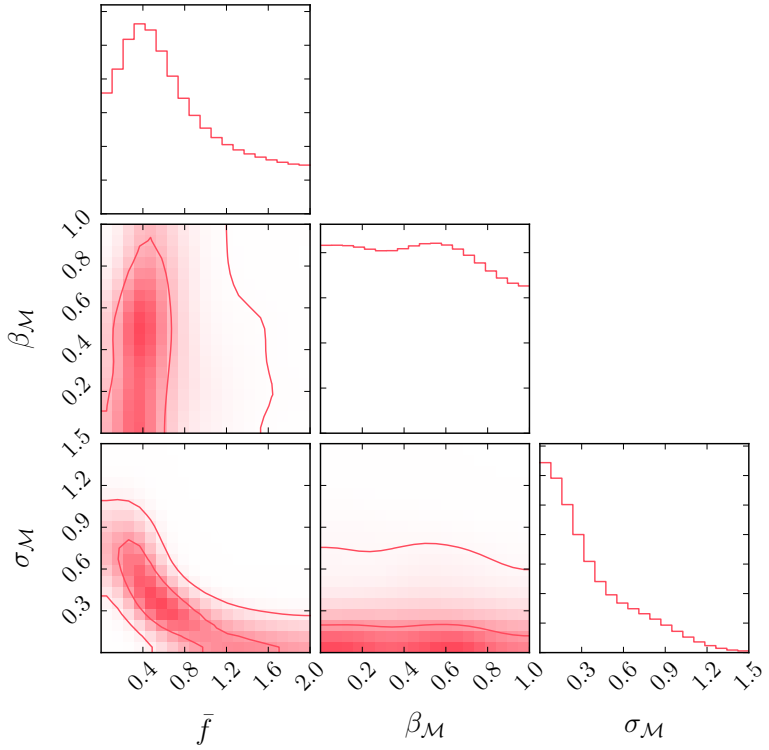


Figure 7.17: Constraints on the isotropic Y-matrix model parameters for DE cosmologies. The contours represent 1σ and 2σ in the posterior distribution after imposing likelihoods and cuts on the quasi-observables. Demanding acceleration with $\Lambda = 0$ gives the bound $\sigma_{\mathcal{M}} < 0.9$ and $M_H = 1.9 \times 10^{-33}$ eV (95% C.L.) from requiring the total equation of state $w < -1/3$ with the fields in slow roll at $z = 0$.

Planck value for $\Omega_\Lambda = 1 - \Omega_m$ when $h = 0.673$). The L1 hyperparameters have fixed priors,

$$\log_{10} \bar{f} \in \mathcal{U}[-9.0, -1.0] \ , \tag{7.80}$$

$$\log_{10} \sigma_{\mathcal{M}} \in \mathcal{U}[0.0, 8.0] \ , \tag{7.81}$$

$$\beta_{\mathcal{M}} \in \mathcal{U}[0.01, 1.00] \ . \tag{7.82}$$

The posterior distributions for these priors are shown in Fig. 7.18. The constraint on the matter density parameter, Ω_m, fixes a direction in the two-dimensional $(\bar{f}, \sigma_{\mathcal{M}})$ space. The constraint on $z_{\rm eq}$ leads to a minimum allowed value of $\sigma_{\mathcal{M}}$. Interestingly, this model shows a mild preference for $\beta_{\mathcal{M}} = 0.5$. The preference for $\beta_{\mathcal{M}} = 0.5$ is possibly driven by the preference for a *not-too-wide* mass distribution. Preventing

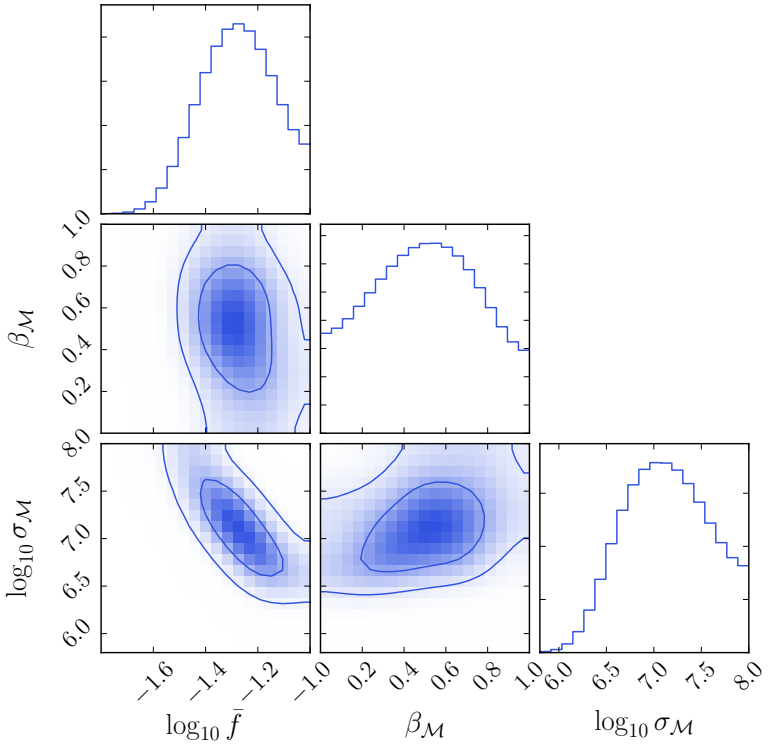


Figure 7.18: Constraints on the isotropic Y-matrix model parameters for DM cosmologies. The contours represent 1σ and 2σ in the posterior distribution after imposing likelihoods and cuts on the quasi-observables. Fixing $z_{\rm eq}$ with only baryons as additional matter leads to the constraint $\log_{10}\sigma_{\mathcal{M}} > 6.6 \Rightarrow \sigma_{\mathcal{M}} > 4\times10^{-27}$ eV (95% C.L.) from requiring the fields to be oscillating with $w = 0$ prior to this epoch. We find a mild preference for $\beta = 0.5$, as shown in the *lower* middle and *upper left* middle panels.

the occurrence of axions with $m_a < H(z_{\rm eq})$ selects against $\beta_{\mathcal{M}} = 1$ and a wide distribution. There is no strongly preferred mass for DM above this scale, and so $\beta_{\mathcal{M}} \to 0$ is disfavoured to keep the distribution from becoming singular. The minimum value of $\bar{f}$ depends on the maximum value of $\sigma_{\mathcal{M}}$, fixed by obtaining the relic density.

In both the above considered Marčhenko-Pastur models we observe a constraint on the characteristic axion mass and decay constant. The location of the constraint on the mass is fixed by the quasi-observables, and the problem under consideration, either by the condition on $\ddot{a}$ for $h \approx 0.7$ for axion DE, or by the conditions on $z_{\rm eq}$ and Ω_m for axion DM. The modal value of $\bar{f}$ in the Marčhenko-Pastur model is

determined by the required energy density of the axions, and is thus dependent on our *fixed* parameter $n_{\rm ax} = 20$. In the DE example, the modal value (after binning on the linear prior) is $\bar{f} = 0.3 M_{\rm Pl}$, reduced from the naive extremal value $\bar{f} = M_{\rm Pl}$ in a single axion model by the 'N-flation' type enhancement $1/\sqrt{n_{\rm ax}}$ effect (for constraints on axions as quintessence see Ref. [1198]). There is a similar effect in the DM example, where $\bar{f}$ is lowered from the value expected for single field ultralight DM with a simple $m^2\phi^2$ model for the DM relic density (e.g. Ref. [911]). A model with varying $n_{\rm ax}$ would display a degeneracy in the two-dimensional $(\bar{f}, n_{\rm ax})$ plane.

7.3.2.2 Bayesian Dark Matter from the M-theory Random Matrix Axiverse

The M-theory axiverse, with it's suppressed higher order distribution moments and approximate log-normal mass distribution (Section 5.3) which in general possesses a very wide spread, means that the constraints must be read carefully (in a preliminary investigation, we found the same considerations apply to the case of strong finite correlations and spiked matrix models.). The constraints on the the M-theory model parameters for the case of a uniform distribution placed on s and $\tilde{N}$ are shown in Fig. 7.19. The constraints on the M-theory model primarily derive from not over-producing DM. With decay constants typically of order the GUT scale, axions with masses $m_a \gtrsim 10^{-18}$ eV typically provide too much DM density ('*anthropically constrained*' [107]). This leads to minimum values of $s_{\rm min}$ and $s_{\rm max}$, with large moduli giving large instanton actions, low axion masses, and correspondingly lower relic densities. There is also a lower bound on $\tilde{N}$, which sets the scale of the instanton charges, and also leads to lower axion masses. The vast majority of the M-theory DM models within the 2σ allowed region in Fig. 7.19 produce a cosmology with quasi-observables,

$$(h, \Omega_m, z_{\rm eq}) \approx (0.57, 0.06, 520) \ , \tag{7.83}$$

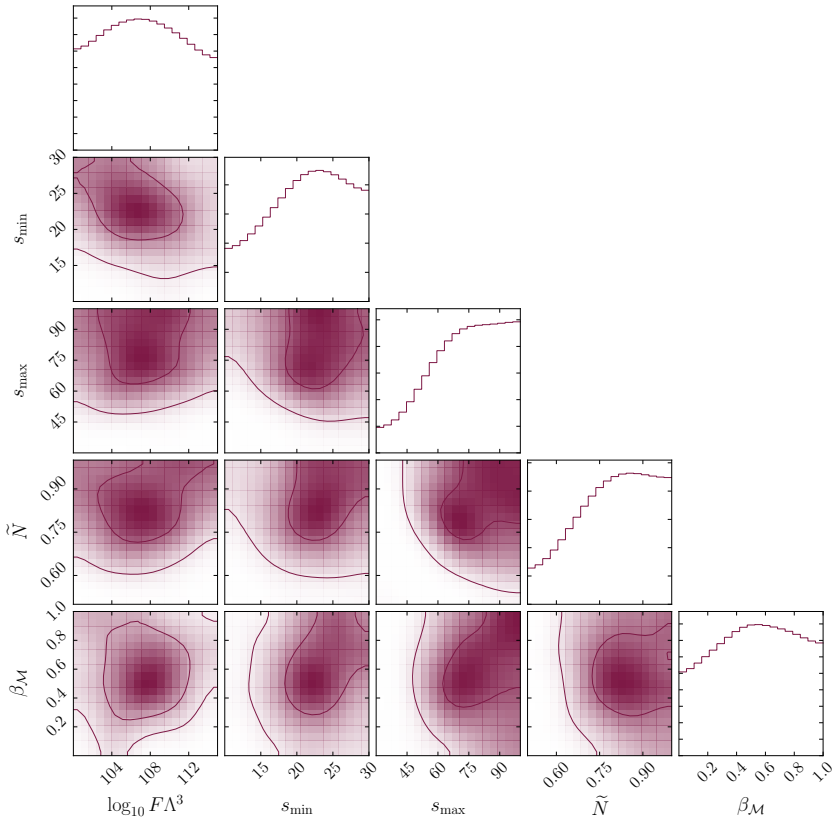


Figure 7.19: Constraints on M-theory random matrix model for DM cosmologies with represented by 1σ and 2σ contours in the posterior distribution after imposing likelihoods and cuts on the quasi-observables. One sided constraints on parameters are driven by the simultaneous requirements of not overproducing DM and maintaining an accelerating Universe at $z = 0$. The constraints are one-sided due to the best-fit region being very narrow, with a plateau in the likelihood away from this region where the axion density drops to zero. The value of $z_{\rm eq}$ is fixed by the baryons alone, and acceleration is guaranteed by the inclusion of a cosmological constant.

with $\ddot{a} > 0$ provided by the cosmological constant, and the matter density provided by the baryons. While this is a bad fit to the data, it is a better fit than a model with, for example, total DM domination at $z = 0$, $\ddot{a} < 0$, and $z_{\rm eq} \approx 10^5$, which results if heavy axions *overclose* the Universe by providing too much DM. This is not to say that there are not examples of M-theory models that do provide a good fit to the data. For example, it is easy to find a model in our chains with hyperparameters,

$$(\log_{10} F\Lambda^3, s_{\rm min}, s_{\rm max}, \tilde{N}, \beta_{\mathcal{M}}) \approx (105, 26, 54, 0.7, 0.9) \ , \tag{7.84}$$

and quasi-observables,

$$(h, \Omega_m, z_{\rm eq}) \approx (0.7, 0.3, 3000) \ . \tag{7.85}$$

We have checked that this general trend also applies in the alternative Gaussian priors on s and $\tilde{N}$, and also using the alternative quasi-observable $\Omega_d h^2$, for the axion DM instead of the total matter content including baryons.

This one-sided behaviour in the constraints, and with many samples being poor fits, can be understood by considering the results of grid-based sampling in a simplified model. We took the Gaussian priors model for s and $\tilde{N}$, holding $\sigma_s = 1$ and $\sigma_N = 0.01$ fixed whilst varying $\bar{s} \in [20, 21]$ and $\bar{N} \in [0.5, 0.55]$, with $n_{\rm ax} = 20$. We sampled each point in parameter space ten times, and interpolated the average quasi-observables on a linear grid. Fig. 7.20 shows the results of this sampling. The contours show the location of $\bar{x} \pm 2\sigma_x$ for quasi-observable x, and the location of $\ddot{a} > 0$. We see that there is only a very narrow region of parameter space where the quasi-observables all have values near the means, complimentary to the behaviour explored in Section 7.2.4.3. For small $\bar{N}$ the likelihood goes to zero due to the cut on $\ddot{a}$. On the other hand, for large $\bar{N}$ the likelihood plateaus. As the axion DM density drops to zero, the baryon contribution leads to minimum values of $z_{\rm eq}$ and h. Thus the whole region of parameter space with large $\bar{N}$ is equally disfavoured, and has large prior volume. This leads to a one-sided constraint on parameters driven by $\ddot{a} > 0$, which is in turn driven by the requirement of not overproducing DM and having $z_{\rm eq}$ too large. These observations highlight some limitations of our methodology when applied to a model with high-dimensional parameter space and a very small prior volume in the best-fit region. It also highlights how our use of quasi-observables does not equally disfavour all possibilities away from the best-fit.

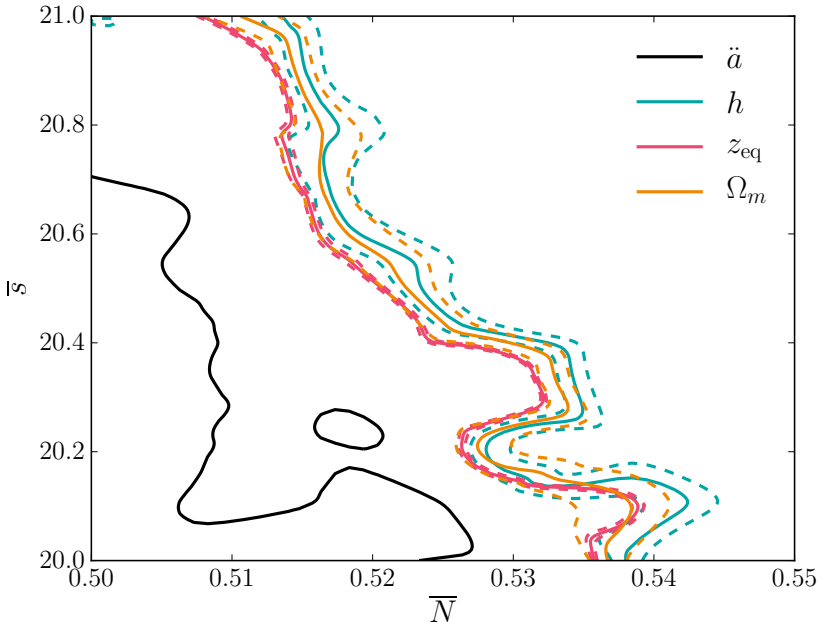


Figure 7.20: Grid sampling details for the M-theory RMT model for the DM example. Solid (dashed) contours show the mean ($\pm 2\sigma$) values of the quasi-observables on a grid based sampling of $(\bar{N}, \bar{s})$ for $n_{\rm ax} = 20$. For small $\bar{N}$, $\ddot{a} < 0$ leading to zero likelihood (cut), while for large $\bar{N}$, $\ddot{a} > 0$. For large $\bar{N}$ the axion density goes to zero, but the likelihood plateaus due to the inclusion of the baryons and the cosmological constant.

7.4 Discussion and Conclusions on the Axion Dark Sector

The *existence* of a *dark sector* of particles largely decoupled from the Standard Model is necessary to explain the phenomenon of DM, and could also play a role in the accelerated expansion of the Universe as DE. String theory and M-theory predict the existence of a complex, multi-component dark sector containing (among other things) many axion fields. Making definite predictions in such a landscape of possibilities seems at present an almost impossible task. However, statistical tools have enabled us to explore these possibilities. Already we have discussed and briefly explored in the context of inflationary theory, the successes of random matrix models as useful simplifications, owing to the nature of universality, applied to the study of

BH superradiance.

In this chapter we have investigated random matrix models for the axion dark sector, with sampled axion masses and initial field values, the quantities which determine the resulting energy densities contributions to the effective DM and DE. By treating these as a series of quasi-observables we have been able to constrain the parameters of the several random matrix model approaches to the string axiverse. This is to date, the first use of random multi-field models applied to the problem of dark sector cosmology, where we have incorporated the adaptable framework of Bayesian networks to perform a Monte Carlo investigation of this scenario.

We have chosen to investigate axion models for DM and DE as factorised sectors. A model for axion DM *and* DE *together* requires a mass splitting at least of $\mathcal{O}(H(z_{\rm eq})/M_H) \sim 10^6$ so as not to generate too much energy density from light states [710]. Such a hierarchy cannot be generated in the models we have considered easily. The structure of the matrices we have assumed is that all the stable axions acquire their masses from similar sources. That is, the elements of the matrices are all drawn from the same distributions. There are no separate sectors, which would occur for matrices with mixed distributions and for block-diagonal matrices such as those discussed in Section 5.2.6. In our models, the only effect that can lead to hierarchies in the mass spectrum is the existence of large eigenvalues, typically from strong correlations, and we have not found this to be sufficient to allow axions to simultaneously provide DM and DE without extensive fine tuning. The strength and circumstances surrounding the required data correlations to realise both sectors could be an interesting direction for future investigation. A further similar interesting extension of our work would be to consider a *hierarchical* model, constraining the $\{m_i\}$ and $\{\phi_i\}$ distributions separately for DM and DE. With this information one could design block-diagonal random matrix models for an entirely axionic dark sector, spanning a much larger mass range. In a high energy physics context, such a model could be realised if part of the axion sector was protected from the leading order instanton effects and received masses only at some higher order.

Hierarchies can also be generated in multi-axion models with non-trivial potentials [394], where isocurvature perturbations (see below) can also be suppressed. This highlights another major simplification and limitation of our work, the use of only the mass term in the potential. While it is technically trivial to replace the mass term with some general function (such as the instanton expansion), computationally it is more challenging. Firstly, by this simplification it is necessary to impose after oscillations (for a non-quadratic minimum, one cannot use $w_a = 0$), and secondly by the possibility of meta-stable minima leading to dynamics on widely separated timescales.

We have found, in the case of DM models, data-driven lower bounds on axion mass distributions set by the matter density and $z_{\rm eq}$. Low mass scales for axions find theoretical and phenomenological motivation also. Theoretically, as discussed, the mass scale $m_a \approx 10^{-15}$ eV, emerges from fixing the GUT scale unified gauge coupling, $\alpha_{\rm GUT} \approx 1/25$, in the M-theory compactifications [31], with a similar approximate relation in string models [728]. Generation of ultralight masses has been discussed extensively recently, in string theory and supersymmetry [659], in QCD-related theories [408], and through use of discrete symmetries [796]. Constraints on the axion parameter space in the context of Peccei-Quinn symmetry breaking scales for ULA CDM, in both standard and non-standard cosmologies has been explored in Ref. [1302] and Ref. [1303] respectively. Ultralight DM has distinctive effects on cosmic structure formation that allow it to be distinguished from CDM, and it represents a frontier of DM research [728, 911]. The 'anthropic window' of the axion parameter space for ultralight masses constituting the total DM has been analysed in Ref. [1301]. The idea of "catastrophic boundaries" [261] in the multiverse may lead to a preference for universes '*on the edge*' of such a frontier.

Phenomenologically, axion masses in the range we have constrained [approximately $H_0 \lesssim m_a \lesssim H(z_{\rm eq})$], and up to 10^{-23} eV, are probed by the CMB power spectrum and large scale structure [710, 711, 1283]. Higher masses in the range 10^{-22} eV $\lesssim m_a \lesssim 10^{-20}$ eV are motivated by their interesting effects on galaxy formation [728,

911, 914, 1152, 1160], and are probed by high redshift galaxy formation [267, 377, 1144, 1153] and the Lyman-alpha forest flux power spectrum [104, 741]. Still more massive axions in the range 10^{-20} eV $\lesssim m_a \lesssim 10^{-18}$ eV can be probed purely gravitationally by the 21cm power spectrum [910]. Constraints from quasi-observables cannot make contact to such detailed constraints as discussed above. To even begin such a task would require the perturbation theory of multi-axion models. While technically trivial, this is a computationally challenging task that we have not currently investigated. As well as axion mass distributions, we have computed the distributions of decay constants, f_a, from the eigenvalues of the kinetic matrix. The WGC [100] can be used to place bounds on combinations of axion decay constants and masses, and broadly speaking can be said to constrain the existence of trans-Planckian values for f_a (without the alignment mechanism). Overcoming this apparent constraint is a prime motivation for the introduction of multi-field models of axion inflation, and has in part motivated this work exploring the case of DM and DE.

We have held $n_{\rm ax}$ fixed in our example Bayesian Network constraints. It would be interesting to explore in a future work how imposing the (weak or strong forms of the) WGC as a prior could lead to a lower bound on the value of $n_{\rm ax}$ required, by providing the correct energy densities in a given DM or DE model. In the case of N-flation (and related models), the necessary minimum number of fields has been argued to be in conflict with entropy bounds in de Sitter space [365], and a similar conclusion for axion DE or DM could have profound implications. Our random matrix approach provides a more versatile, and realistic, approach to the distributions. Our Bayesian forward model is able to quantify and extend the estimates outlined in Ref. [765] for the mass and decay constant distributions. Ref. [520] consider the observables for DE models more thoroughly, such as the angular diameter distance to the CMB, and improvements from future BOA measurements by the Square Kilometre Array. It would be interesting to include these in our methods incorporating Bayesian methodologies.

The only concrete axiverse construction we have used to inform our random matrix models has been the M-theory model of Ref. [31]. An explicit axiverse model has also been realised in Type IIB [351] as covered in Section 3.3.4, where the models for N-flation and N-quintessence have also been constructed [353], and our methodology could easily be applied to these models also. We note however, that in the case where these models can have a low string scale, $M_s \sim 10^{12}$ GeV, the DM abundance from vacuum realignment of light axions will be hard to achieve. Our discussions in this chapter have been set entirely in the late Universe, in particular during radiation domination post-BBN and we have made no explicit connection between our models and inflationary theory. This neglects the very important constraints on axion DM coming from isocurvature perturbations (e.g. Ref. [557, 1304]). High scale inflation, in particular with observably large tensor-to-scalar ratio, typically generates large amplitude number density perturbations in axions, which contribute to the CMB power spectrum acoustic peaks such as to shift their phase, inconsistent with observations [819, 1061]. The Hubble scale during inflation is constrained, for the QCD axion with typical f_a, to be $H_I \lesssim 10^8$ GeV.

The requirements on H_I are significantly loosened for ULAs, with isocurvature perturbations becoming negligible for $m_a \lesssim 10^{-26}$ eV [916, 917]. The constraints become multiplicatively worse, however, in the case of multiple axion fields [887]. In Ref. [31] it was shown that the M-theory axiverse requires $H_I \lesssim 10^{10}$ GeV. The adaptability of the Bayesian networks approach means that including the isocurvature amplitude as a quasi-observable and H_I as a model parameter is another easily tackled problem. Such an investigation would clarify the prior dependence in the results of Ref. [887]. The study of random matrix multi-axion models has been popular for some time in inflationary theory. While inflation is well-motivated by cosmological observations, it is unlikely to be possible to determine the theory precisely due to the limited information available. The study of DM, on the other hand, offers far greater prospects for precision measurement [711], and so by studying multi-axion models in the late Universe, we might discover more about physics

beyond the Standard Model. In this chapter we have been able to present the first exploration of a random matrix multi-axion models for DM and DE, using statistical methods to place bounds on the axion mass and decay constant distributions determined from selected models in the random matrix axiverse.

Overall Conclusions and Future Directions

Sic Parvis Magna.

The motto of Sir Francis Drake

Time and Space

In this thesis we have addressed selected issues surrounding the statistical treatment of models incorporating a simplified effective field theory of ALPs [107, 1231], motivated from the landscape of string theory [184, 235, 387, 461, 625, 629, 800, 1063–1065, 1262, 1344, 1366, 1399]. Superstring theories currently offer the most likely approach to realising a successful quantum theory of gravity, capable of reproducing a complete treatment of each fundamental force of nature. The scale of this landscape [112, 260, 428] offers many fascinating solutions to theoretical tensions and traditional, currently unexplained paradigms, through the vast nature of well defined four-dimensional solutions. These frameworks currently offer our bests hopes of traversing from the mathematical curiosity of a ten/eleven-dimensional spacetime to the physical universe we observe [25, 129, 308, 417, 427, 429, 475, 481, 625, 642, 659, 660, 758, 873, 874, 893, 909, 1013, 1222, 1364]. One of the most important and diverse features of string models is the nature of their moduli [26, 33, 150, 381, 412] and the possible extensive sector of ultralight scalars which may be apparent in the four-dimensional limit of these theories. The scope of this thesis in regards to these

factors was two-fold. The first was to address the issues of modelling the statistical spaces associated to the treatment of a large number of fields in a simplified manner. This was done through the use of universality in the landscape using RMT [138, 641, 939, 1279] and the limiting results of well known classical ensembles [901]. The second was to use these tools to determine inferences from phenomenological features in the four-dimensional theory, stemming from the unique roles axion fields may play due to their symmetry properties and defining scales. A focus was then placed on these in the case of multiple fields using the simplified results determined from a RMT [128, 131, 499] approach to the effective field equations [1219, 1221]. In particular the key points we covered in each chapter are now detailed here below.

In Part I we introduced the foundational basis of the Standard Model of Concordance Cosmology, which forms our theoretical playbook for a simplified probing the Universe and its evolution over cosmic scales. Indeed, the introduced FLRW metric [846, 1114–1116, 1316], representing a homogenous and isotropic universe allows for the ability to incorporate the addition of test fields in a palatable manner. After reviewing the standard assumptions of zero curvature we detailed how Einstein's field equations from his general theory of relativity [513] for such a universe, lead to a specific form of the Friedmann expressions applicable to the constituent energy components of the Universe. We covered all relevant parameters for a simple effective description of an expanding universe, incorporating matter, radiation and a cosmological constant, noting specific features such as invariant distance, redshift at matter-radiation equality and the relevant equations of state, a common dimensionless parameterisation of the diagonal components of the stress-energy tensor when using a perfect fluid approximation. Of particular note in the description of the cosmic expansion is the Raychaudhuri equation, which using the aforementioned parameters, allows us to define the temporal evolution of the cosmic fluid components. To conclude the chapter we covered the problematic paradigms which plague the standard model of concordance cosmology today. Large scale structural issues such as the flatness problem, horizon problem, primordial fluctuations associated

to large scale structure and magnetic monopoles turn to significant epochal modifications in the very early Universe, such as cosmic inflation. Most striking maybe from the outside perspective to our current view of cosmology is the inability to define approximately 95% of the energy density of the observable universe. This unified enigma defines an erroneous dark universe, incompatible with the current theoretical abilities of well defined particle physics solutions to shed light on both the mysterious gravitationally observed DM and DE.

Turning to Chapter 2 we continued to review a further standard approach to modelling fundamental physics, this time the theoretical pillar of the Standard Model of particle physics [15, 958, 1052]. We reviewed the form of the Standard Model Lagrangian, the matter constituents, gauge group representations and several of the large enigmas which don't possess satisfactory solutions within the specific gauge group representation of the strong, weak and electromagnetic interactions. The most relevant to the bulk of the work covered in this thesis, is the strong CP problem, stemming from the $U(1)_{\mathrm{A}}$ axial problem. Reviewing the leading solution to this issue, typically introduces an extended symmetry, used to dynamically relax the problematic QCD θ parameter to a CP conserving minimum, through the introduction of the QCD axion field. Historically this Peccei-Quinn solution [1034, 1035] offered an array of possible realisations through minimal extensions to the Standard Model, where we covered the primary forms categorised as, visible (PQWW) [1035, 1036, 1335, 1353] and invisible (KSVZ and DFSZ) [438, 789, 1182] models of the axion. The effective field theory of the invisible axion models sparked a great interest in the study of axions in the cosmological setting due to the field's stability over cosmic timescales and the form of its non-perturbative potential, defining the field's dimensionful scales. The dilute instanton gas approximation founded the ability to provide a minimal analytical treatment using a solution of a massive pseudoscalar boson, apparent in the low energy spectrum. It had previously been shown this instanton potential is always minimised at the CP conserving limit [1288]. We continued to introduce the features of this possible ultralight component

which we referred to as the cosmological axion. Considering non-thermal production mechanisms, specifically vacuum realignment, axions sitting in certain regions of the parameter space can contribute an $\mathcal{O}(1)$ fraction of the required DM density today. If symmetry breaking occurs before or during the end of the inflationary epoch, the field is homogenised over our Hubble volume, defining the axion phenomenology as dependent to first order on a simple, three-dimensional parameter space (Eq. (2.85)). Combining this with the discussions of the previous chapter we showed how these fields evolve in an expanding FLRW universe, determined by the fields mass, where the field initially remains fixed due to Hubble friction. The homogeneous energy-density of these ultralight fields evolves through the coherent oscillatory nature of the field's equations, which are described via those of a damped harmonic oscillator, offering the exciting possibility to act both as an effective DM and/or DE component. Finally we drew attention to the specific roles these diverse phenomenological utilities offer in terms of solutions to the cosmological paradigms of inflation [647], DM and DE. The closing remarks of this chapter consisted of brief points regarding the issues, details and methods behind the detection of these fields through various compelling probes on both cosmic and laboratory scales.

The final chapter of Part I concerned itself with elements of superstring theory, a focus placed on particular compactification scenarios which lead to the plethoric phenomenological sector known as the string axiverse. Initially we covered the historical factors which excite many theorists to consider this framework as a front-running model of quantum gravity. We detailed a simple understanding of how these theories bring forward generic complexities, in the form of extra dimensions required to ensure consistency in the removal of quantum anomalies, along with ever-present moduli which must be stabilised. To connect these models to our four-dimensional landscape requires compactification, the general geometrical process of reducing a topological space into a compact space. This potentially brings with it critical phenomenological consequences. This was demonstrated using a simple example of KK reduction [763, 802, 803], utilising the five-dimensional action of a real massless

scalar. Expanding upon these concepts we moved to the process of ten-dimensional compactification required for the critical dimension of the superstring. In particular a focus was placed on Type IIB theories [144, 369], showing the forms of the generic Kähler potential, superpotential and effective supergravity action which come about from this perturbative sector of the superstring theory space (Fig 3.2). To account for the stabilisation of the Kähler moduli we briefly discussed two methodologies, namely the KKLT and LVS models. The LVS framework offers an attractive solution by demonstrating an ability to explicitly reproduce the string axiverse when the flux compactification process generates states which are parametrically lighter in the low energy spectrum than the field corresponding to the del Pezzo divisor modulus [351]. Next we introduced the overarching picture of the string axiverse and the nature of its spectrum in the low energy sector, through the general presence of p-form gauge fields [657, 911] and the topological diversity of complex extra-dimensional manifolds. Concluding the discussions in this chapter, we highlighted and contrasted the key aspects, forms, features and phenomenological potential of several explicit axiverse constructions, namely M-theory [31], Type IIB [351] and the geometrical landscape of the Kreuzer-Skarke axiverse [427], formulated using the list of categorised Calabi-Yau threefolds and associated four-dimensional reflexive polytopes [825]. We also discussed issues regarding the realisation of light axions and subsequently an axiverse in regards to supersymmetric AdS vacua and tachyonic moduli [364].

Part II of this thesis was focused on the statistical principles of universality, encapsulated in the mathematical field of RMT. We began with the introduction of the paradigm universality and spectral statistics of LSDs and probability measure spaces associated to classical matrix ensembles. We very loosely associated these models to the conjecture of the string axiverse and the effective field equations for multiple scalar fields [5, 125, 127, 127, 174, 226, 228, 290, 429, 502, 558, 873, 909, 921–924, 1254, 1323, 1372]. To tackle these issues we introduced the Bayesian methodologies [1080, 1221, 1270] relevant for hierarchical modelling and to define a (hy-

per)parameterisation of our models for the axiverse. In order to model the physical parameters of the axion fields, loosely related to the notions of minimal information [1178], we introduced key elements of canonical RMT, focusing on the use of rotationally invariant ensembles. Next we moved onto the specific case of high-dimensional random data matrices with positive (semi)definite spectra, namely those residing in the Wishart-Laguerre ensemble. To do this we looked at the standard forms of sample covariance matrices under both the null and alternative hypothesis, introducing the limiting features defined in numerous historical results in the field, such as the Marčhenko-Pastur bulk measure density [901] and universality of the spectral edge statistics of the infimum and supremum eigenvalues [1268, 1269]. Under the alternative hypothesis [754], these statistics are subject to perturbative formalisms, where we covered a seminal result, the BBP phase transition phenomena [142], defining the nature of so called spiked models [232, 233, 954, 1321]. These finite rank operations were generalised to the case of full rank perturbations to draw traceable results via the use of well defined limits concerning correlated or non-isotropic Wishart matrices [76, 746, 1017, 1037]. Firstly we drew attention to the Fisher sample covariance matrix [856, 920, 1165], the standard form of covariance estimation for isotropic Wishart type matrices via the use of a conjugate prior on the population covariance matrix. Secondly we focused on how to generalise these models to the case of full rank perturbations [313]. To do this we looked at classical ensembles via the non-commutative generalisation of measure spaces via the principle of asymptotic freeness [1204, 1308, 1310], ensuring the incorporation of traditional invariant ensembles. Free convolution operations were introduced to model particular configurations, where specific requirements on the parameters of classically perturbed models would ensure the fields mass spectrum is both non-tachyonic and non-singular.

Motivated by the focus of defining results in these potentially vastly complex spaces, we adopted the CLTs of canonical matrix ensembles. These we presented in the previous chapter, where sufficiently complex systems can obey universal laws that do

not depend significantly on the underlying microscopic mechanisms of that system [138, 493–495, 497, 497, 641, 939, 1279, 1351, 1352, 1360]. This allowed us to traverse from the apparent vast and intricate landscape of explicit compactified string models to a significantly simplified description, using the paradigm of effective field theory. We used the assumption that we can operate at the level of the effective multi-field action, for classes of periodic potentials in arbitrary dimensions, representing a minimal addition to the traditional Standard Model components. Our arguments considered the case of using the simplest approach to the multi-field potential, so called well-aligned theories [128, 131], in which the effective description allows for an expansion around the potential minimum, generating a Lagrangian described to first order by two non-explicit matrix arguments [1221]. We adopted this description from the enigmatic theories of the string axiverse by using sample covariance matrices to model these two arguments, used to define the positive parameters of the effective theory, in order to sample the space representing the axion cosmology. These methods are already well established in the context of inflationary theory [128, 131, 499], where random matrix models have proven to be a useful simplification, owing to the universality of the models LSD. We then used these to attempt to drive inferences which may constrain string theoretic considerations from the structure of the low-energy theory. We introduced three different classes of model to approach this, based on simplistic statistical models and priors on the axion decay constants and masses. The first class, epistemic priors on the parameter space, motivated in principle by the original conjecture of the string axiverse. The second made use of high-dimensional forms for the statistical uncertainty, using assumptions made on the initial basis we began our analysis. Each model we considered made some assumption on the form of the axion field kinetic metric and mass matrix in the initial basis we started in. We then detailed the forms of the possible spectra in terms of Lebesgue decomposed measures [190] and convolution operations [191, 219, 1204, 1311, 1313], for each possible model. In terms of the axion mass spectrum these consisted of isotopic models, finite rank perturbed spiked models and

full rank perturbed correlated models. Each of these were shown to have traceable results and clearly defined probability measures which could be used to model the axion parameter space. The final class of model we investigated was a special case of using a random matrix approach to the M-theory axiverse, where we replaced the statistical approach from the previous classes with matrix entries formulated from stochastic parameters associated to the model's variables, the priors on these related to theoretical uncertainty in the model. Performing an analysis using a diagonal approximation of the models Kähler metric, with the mass matrix defined from the expanded superpotential structured in the form of a sample covariance matrix, we found the mass spectrum converged to normally distributed variables over logarithmic scales. Finally we applied a simplistic fit to each of these models using Pearson density functions [1028–1030, 1032], specifically Beta density functions, focusing on approximations for the first four distribution moments. We rounded off discussions by suggesting a simplification to incorporate the approximate features of each class of model. This was done by only considering the universal forms of perturbed mass spectra, sufficiently described by two moments relating to some fixed mean scale and distributional spread. We then applied this approach in the first of our results chapters.

The concluding part of this thesis compiled together two chapters which made use of the RMT effective models in Chapter 5, in order to explore possible inferences or constraints on the axion parameter space via two distinct phenomenological sectors. The first of these [1219] considered BH superradiance [106, 107, 286, 317, 810, 1361, 1378], used to determine constraints on the field's parameter space through the Penrose process [1044]. We began by introducing this process in the context of the rotating Kerr BH spacetime [783], where axions can act as perturbative catalysis for superradiant instabilities when partnered with both stellar and supermassive astrophysical BHs. We covered the specific regimes in which results have been derived in the literature, where we focused in particular on the weak-field or non-relativistic approximation [433], in order to ensure computational simplicity in the analytical expressions

determining the superradiance rates. Beginning with the case of a single field, we found that in the limit of sufficiently suppressed interactions, defined by ensuring axion decay constants of the order, $f_a \gtrsim M_{\rm GUT}$, BH spin measurements can be used to define two factorised exclusion regions from the Regge mass-spin plane [106]. Using a generous data set of known BH spins and masses [10, 12, 280, 522, 943, 948, 1100–1102, 1289, 1289] we were able to constrain the axion mass in the case of a single field to,

$$7 \times 10^{-14}\ \text{eV} \lesssim m_a \lesssim 2 \times 10^{-11}\ \text{eV}\ , \tag{7.86}$$

from stellar mass BH observational measurements, and,

$$7 \times 10^{-20}\ \text{eV} \lesssim m_a \lesssim 1 \times 10^{-16}\ \text{eV}\ , \tag{7.87}$$

$$2 \times 10^{-21}\ \text{eV} \lesssim m_a \lesssim 1 \times 10^{-20}\ \text{eV}\ , \tag{7.88}$$

from supermassive BH observational measurements. We also showed various phenomenological inspired constraints such as $2.0 \times 10^{15}\ \text{GeV} \lesssim f_a \lesssim M_{\rm Pl}$ for the self-coupling of ultralight DM, $f_a \lesssim 3 \times 10^{17}\ \text{GeV}$ for the QCD axion and $23.75 \lesssim \alpha_{\rm GUT}^{-1} \lesssim 25.75$ for the grand unification coupling constant in M-theory models. We also detailed in the limit of weak self-interaction, in the case of an atypical degenerate spectrum of fields, even large numbers of fields did not perturb the single field constraints significantly. Using this we adopted the single field methodologies to trivially generalise our constraints to the case of a population of fields. A model incorporating possible large numbers of axions is excluded if just a single field lies in one of the constrained ranges in Eq. (7.86), Eq. (7.88) and Eq. (7.88)[108, 317]. Using the ability to factorise the stellar and supermassive sectors we defined our constraints via an integral over the probability products of drawing a field from a given effective field theory model and the probability that a given mass is constrained by the BH superradiance process.

We considered the possibility of using these BH superradiance constraints to exclude certain examples of simplified spectra representative of the previously discussed ax-

iverse distributions for the axion masses. This under the assumption of statistical independence in our model for the masses. The constraints become more severe with larger numbers of axion-like fields due to the increased probability of drawing an outlier. We adopted the approach of using the first two distribution moments through the unified approach detailed in Chapter 5, to show that only a small number of fields should be allowed to obtain masses surrounding the BH superradiance susceptible region. Constraints on the ultralight sector were shown to generally vanish in the limit of very large distribution variances. Constraints in these models on the allowed values of $\mathcal{N}_{\rm ax}$ from processes such as BH superradiance, which rely only on the existence of field vacuum fluctuations, are in principle extremely powerful. Interesting extensions in the future would be to see how these could possibly shape the bounds on the dimensionality or geometric features of phenomenologically consistent moduli spaces in string/M- theory. We have seen from this simple analysis that the benchmark value of,

$$\mathcal{N}_{\rm ax} \gtrsim 30 \ , \tag{7.89}$$

is generally excluded with our simplified priors fixed to some scale in the ultralight sector of axion cosmology. Comparing and contrasting these constraints with possible limits on the hodge numbers using explicit values from minimised potentials in the Kreuzer-Skarke axiverse would offer a fascinating future extension. Also the analysis we demonstrated made a distinct neglect of the possible effects of axion self-interactions, which can shut down the BH superradiance process via highly non-linear phenomena, such as level mixing or bosenova events [106, 810, 1381]. An obvious extension in future work would be to expand this analysis into the two-dimensional parameter space for both the axion decay constants and masses. Axion mixing in the form of scattering events may also offer interesting observational signatures in future gravitational wave based experiments. Along with these options using the superradiance constraints in conjunction with other phenomenological considerations could help shape the constrained regions of the axion parameter space. It would be interesting in this regard to combine this work with the analysis in

the following chapter to combine calculations for the axion masses, the axion decay constants, relic density, and self-interaction potential etc. The work covered in this chapter was generally more model-independent, with a limited focus placed on cosmological assumptions, detailing a general model of light scalars with sufficiently small self-interactions.

The second results chapter looked at the dark sector of axion physics [1221], focusing on the possible existence of a largely decoupled sector of ultralight scalars which may explain the nature of DM and/or DE. This multi-component dark sector could contain many fields, whereby using the simple effective RMT models, we were able to compute a spectrum of axion masses and initial field values in order to determine the resulting energy densities of axionic DM and DE. As making distinct and definite predictions in such a vast landscape of possibilities is a tricky task [318, 319, 363, 390, 657, 662, 687, 688, 1131], often utilising numerous cosmological parameters, we have made use of statistical tools in order to make first footings into constraints on this space. We started by introducing the relevant cosmological model framework in order to evolve the axion fields over time, detailing simplifications to help with the numerical practicalities. By using a few selected simple quasi-observables [40] we have been able to constrain the parameters of the random matrix models. In particular we split the analysis via two different methods. The first, a snapshot indicating the general results in each of the model classes and their potential to reproduce satisfactory DM or DE cosmologies. The second made use of the the adaptable framework of Bayesian networks to perform a Monte Carlo investigation of these scenarios. We generally found in the scenarios for DM models, data-driven lower bounds on axion mass distributions set by the matter density and $z_{\rm eq}$. We also found motivations for low mass scales for a population of axions through phenomenological results. Generally speaking future considerations for our constraints from quasi-observables should include extended considerations such as perturbation theory. We also considered the implications of the introduced spectrum of axion decay constants. General considerations of the WGC can place bounds on

combinations of axion decay constants and masses, which broadly speaking, can provide inferences on the ability to constrain the existence of super-Planckian values (excluding aligned potentials). Overcoming this apparent constraint is a prime motivation for the introduction of multi-field models of axion inflation, which is a strong motivation as to why we investigated modelling multi-component DM and DE. Our examples ensured the number of fields remained fixed in the presented results. Future Bayesian network constraints could incorporate a possible extension through the removal of this limitation. We argued a random matrix approach to the effective field equations provided a more versatile and realistic approach to modelling the required parameter distributions. The discussions in this chapter were all considered under the assumption of an analysis entirely in the late Universe, in particular during the epoch of radiation domination, post-BBN, where we had an explicit disconnection in these models to inflationary theory. We presented here the first simplified results using a random matrix approach to multi-axion models, in order to probe the possible DM and DE relic densities from a population of fields, fixed to some spectrum defining scale, using statistical methods to constrain specific axion mass and decay constant distributions. In order to extend this work it would be interesting to explore the nature of field alignment along with the use of non-canonical multi-instanton potentials [774, 1071], to facilitate the decay of problematic heavy axion fields that otherwise provide energy densities which are too large. Along with this, an extension to the Bayesian network space through the addition of extended model (hyper)parameters associated to observables such as the angular diameter distance to the CMB or BOA measurements would give a more detailed analysis. Other considerations could also be made to model variables such as the supersymmetry breaking scale or the Hubble scale during inflation which could provide interesting results when incorporating multiple fields. There is no doubt, a vast amount of work must be done, in numerous areas surrounding these subjects, in order to best define where in the landscape our best hopes lie in the initial identification of either the axion or an ALP. The inauguration of these fields into the particle



Figure 7.21: The Vision of the Empyrean: The Empyrean Heaven, representative in the study of ancient cosmogony as the highest heaven occupied by the aether. Classically regarded as a place of divinity, observed in notable works such as Dante's *Paradiso*, the conceptual metaphysical origins used to define the highest heaven translate to our modern understanding and cosmological endeavours regarding the aspiration to quantify the higher dimensions of spacetime. For the theoretical particle cosmologist the metaphorical '*Empyrean*' of UV-completion currently seems to be hidden amongst a colossal phenomenological, geometrical and mathematical landscape. Image credit: Taken from `https://fineartamerica.com/featured/the-vision-of-the-empyrean-gustave-dore.html`.

landscape could represent the first steps in the formal theoretical synergy between the Standard Model of particle physics and its much needed extensions, breaking the current theoretical and experimental impasse. It would also represent an indication of the presence of extra-dimensional physics, a vital mathematical formality in our current best approaches to defining the true quantum nature of the Universe. The defining scales for these fields can significantly alter their role in the cosmic puzzle, constraining these parameters a logical first task in providing direction to a minor fraction of the arduous process of piecing together the nature of the true theory of quantum gravity. A very general and first order approach, such as the ones conducted here in this thesis, is the analysis of the universal forms the spectra for these parameters. We have introduced spectra under the general model framework of the *random matrix axiverse*, utilising several of the key seminal results of RMT to greatly simplify statistical priors and ultimately our results. Axion physics offers a hugely rewarding framework, related to both physics on the smallest scales and as possible solutions to the most grandiose cosmological paradigms. Using this simplified framework we have been able to make initial footings into various possible features of multi-axion cosmology. An explicit understanding of the role of axions naturally arises from a complete categorisation of the true nature of spacetime and its foundational components,

> "Now that the very name '*space*' seemed a blasphemous libel for this *empyrean* ocean of radiance in which they swam. He could not call it 'dead'; he felt *life* pouring in at every moment."
>
> Out of the Silent Planet
>
> C.S. Lewis

potentially hidden in one of the numerous beautiful mathematical amalgamations representing theories currently seeking to unify everything we have ever questioned on the frontier of particle physics and cosmology. The identity, scale and nature of the true fundamental integrants, the most pressing of open questions, *what and where are they*?



Appendix A

The Expanded Standard Model Lagrangian

A.1 The Equation

The complete expanded form of the Standard Model Lagrangian representing a local, completely renormalisable, quantum field theory obeying Lorentz and gauge invariance is,

$$
\begin{aligned}
\mathcal{L}_{\mathrm{SM}} = & -\frac{1}{2}\partial_\nu g^a_\mu \partial_\nu g^a_\mu - g_s f^{abc}\partial_\mu g^a_\nu g^b_\mu g^c_\nu - \frac{1}{4}g_s^2 f^{abc} f^{ade} g^b_\mu g^c_\nu g^d_\mu g^e_\nu + \frac{1}{2} i g_s^2 (\bar{q}^\sigma_i \gamma^\mu q^\sigma_j) g^a_\mu \\
& + \bar{G}^a \partial^2 G^a + g_s f^{abc}\partial_\mu \bar{G}^a G^b g^c_\mu - \partial_\nu W^+_\mu \partial_\nu W^-_\mu - M^2 W^+_\mu W^-_\mu - \frac{1}{2}\partial_\nu Z^0_\mu \partial_\nu Z^0_\mu \\
& - \frac{1}{2c_w^2} M^2 Z^0_\mu Z^0_\mu - \frac{1}{2}\partial_\mu A_\nu \partial_\mu A_\nu - \frac{1}{2}\partial_\mu H \partial_\mu H - \frac{1}{2} m_h^2 H^2 - \partial_\mu \phi^+ \partial_\mu \phi^- - M^2 \phi^+ \phi^- \\
& - \frac{1}{2}\partial_\mu \phi^0 \partial_\mu \phi^0 - \frac{1}{2c_w^2} M \phi^0 \phi^0 - \beta_h [\frac{2M^2}{g^2} + \frac{2M}{g} H + \frac{1}{2}(H^2 + \phi^0 \phi^0 + 2\phi^+ \phi^-)] \\
& + \frac{2M^4}{g^2}\alpha_h - igc_w [\partial_\nu Z^0_\mu (W^+_\mu W^-_\nu - W^+_\nu W^-_\mu) - Z^0_\nu (W^+_\mu \partial_\nu W^-_\mu - W^-_\mu \partial_\nu W^+_\mu) \\
& + Z^0_\mu (W^+_\nu \partial_\nu W^-_\mu - W^-_\nu \partial_\nu W^+_\mu)] - igs_w [\partial_\nu A_\mu (W^+_\mu W^-_\nu - W^+_\nu W^-_\mu) \\
& - A_\nu (W^+_\mu \partial_\nu W^-_\mu - W^-_\mu \partial_\nu W^+_\mu) + A_\mu (W^+_\nu \partial_\nu W^-_\mu - W^-_\nu \partial_\nu W^+_\mu)] - \frac{1}{2} g^2 W^+_\mu W^-_\mu W^+_\nu W^-_\nu \\
& + \frac{1}{2} g^2 W^+_\mu W^-_\nu W^+_\mu W^-_\nu + g^2 c_w^2 (Z^0_\mu W^+_\mu Z^0_\nu W^-_\nu - Z^0_\mu Z^0_\mu W^+_\nu W^-_\nu)
\end{aligned}
$$

$$
\begin{aligned}
&+ g^2 s_w^2 (A_\mu W_\mu^+ A_\nu W_\nu^- - A_\mu A_\mu W_\nu^+ W_\nu^-) + g^2 s_w c_w [A_\mu Z_\nu^0 (W_\mu^+ W_\nu^- - W_\nu^+ W_\mu^-) \\
&- 2 A_\mu Z_\mu^0 W_\nu^+ W_\nu^-] - g\alpha [H^3 + H\phi^0\phi^0 + 2H\phi^+\phi^-] - \frac{1}{8} g^2 \alpha_h [H^4 + (\phi^0)^4 + 4(\phi^+\phi^-)^2 \\
&+ 4(\phi^0)^2 \phi^+\phi^- + 4H^2\phi^+\phi^- + 2(\phi^0)^2 H^2] - gMW_\mu^+ W_\mu^- H - \frac{1}{2} g \frac{M}{c_w^2} Z_\mu^0 Z_\mu^0 H \\
&- \frac{1}{2} ig [W_\mu^+ (\phi^0 \partial_\mu \phi^- - \phi^- \partial_\mu \phi^0) - W_\mu^- (\phi^0 \partial_\mu \phi^+ - \phi^+ \partial_\mu \phi^0)] \\
&+ \frac{1}{2} g [W_\mu^+ (H \partial_\mu \phi^- - \phi^- \partial_\mu H) - W_\mu^- (H \partial_\mu \phi^+ - \phi^+ \partial_\mu H)] \\
&+ \frac{1}{2} g \frac{1}{c_w} (Z_\mu^0 (H \partial_\mu \phi^0 - \phi^0 \partial_\mu H) - ig \frac{s_w^2}{c_w} M Z_\mu^0 (W_\mu^+ \phi^- - W_\mu^- \phi^+) \\
&+ igs_w M A_\mu (W_\mu^+ \phi^- - W_\mu^- \phi^+) - ig \frac{1 - 2c_w^2}{2c_w} Z_\mu^0 (\phi^+ \partial_\mu \phi^- - \phi^- \partial_\mu \phi^+) \\
&+ igs_w A_\mu (\phi^+ \partial_\mu \phi^- - \phi^- \partial_\mu \phi^+) - \frac{1}{4} g^2 W_\mu^+ W_\mu^- [H^2 + (\phi^0)^2 + 2\phi^+\phi^-] \\
&- \frac{1}{4} g^2 \frac{1}{c_w^2} Z_\mu^0 Z_\mu^0 [H^2 + (\phi^0)^2 + 2(2s_w^2 - 1)^2 \phi^+\phi^-] - \frac{1}{2} g^2 \frac{s_w^2}{c_w} Z_\mu^0 \phi^0 (W_\mu^+ \phi^- + W_\mu^- \phi^+) \\
&- \frac{1}{2} ig^2 \frac{s_w^2}{c_w} Z_\mu^0 H (W_\mu^+ \phi^- - W_\mu^- \phi^+) + \frac{1}{2} g^2 s_w A_\mu \phi^0 (W_\mu^+ \phi^- + W_\mu^- \phi^+) \qquad \text{(A.1)} \\
&+ \frac{1}{2} ig^2 s_w A_\mu H (W_\mu^+ \phi^- - W_\mu^- \phi^+) - g^2 \frac{s_w}{c_w} (2c_w^2 - 1) Z_\mu^0 A_\mu \phi^+ \phi^- \\
&- g^1 s_w^2 A_\mu A_\mu \phi^+ \phi^- - \bar{e}^\lambda (\gamma \partial + m_e^\lambda) e^\lambda - \bar{\nu}^\lambda \gamma \partial \nu^\lambda - \bar{u}_j^\lambda (\gamma \partial + m_u^\lambda) u_j^\lambda \\
&- \bar{d}_j^\lambda (\gamma \partial + m_d^\lambda) d_j^\lambda + igs_w A_\mu [-(\bar{e}^\lambda \gamma^\mu e^\lambda) + \frac{2}{3} (\bar{u}_j^\lambda \gamma^\mu u_j^\lambda) - \frac{1}{3} (\bar{d}_j^\lambda \gamma^\mu d_j^\lambda)] \\
&+ \frac{ig}{4c_w} Z_\mu^0 [(\bar{\nu}^\lambda \gamma^\mu (1 + \gamma^5) \nu^\lambda) + (\bar{e}^\lambda \gamma^\mu (4s_w^2 - 1 - \gamma^5) e^\lambda) + (\bar{u}_j^\lambda \gamma^\mu (\frac{4}{3} s_w^2 - 1 - \gamma^5) u_j^\lambda) \\
&+ (\bar{d}_j^\lambda \gamma^\mu (1 - \frac{8}{3} s_w^2 - \gamma^5) d_j^\lambda)] + \frac{ig}{2\sqrt{2}} W_\mu^+ [(\bar{\nu}^\lambda \gamma^\mu (1 + \gamma^5) e^\lambda) + (\bar{u}_j^\lambda \gamma^\mu (1 + \gamma^5) C_{\lambda\kappa} d_j^\kappa)] \\
&+ \frac{ig}{2\sqrt{2}} W_\mu^- [(\bar{e}^\lambda \gamma^\mu (1 + \gamma^5) \nu^\lambda) + (\bar{d}_j^\kappa C_{\lambda\kappa}^\dagger \gamma^\mu (1 + \gamma^5) u_j^\lambda)] + \frac{ig}{2\sqrt{2}} \frac{m_e^\lambda}{M} [-\phi^+ (\bar{\nu}^\lambda (1 - \gamma^5) e^\lambda) \\
&+ \phi^- (\bar{e}^\lambda (1 + \gamma^5) \nu^\lambda)] - \frac{g}{2} \frac{m_e^\lambda}{M} [H (\bar{e}^\lambda e^\lambda) + i\phi^0 (\bar{e}^\lambda \gamma^5 e^\lambda)] \\
&+ \frac{ig}{2M\sqrt{2}} \phi^+ [-m_d^\kappa (\bar{u}_j^\lambda C_{\lambda\kappa} (1 - \gamma^5) d_j^\kappa) + m_u^\lambda (\bar{u}_j^\lambda C_{\lambda\kappa} (1 + \gamma^5) d_j^\kappa] \\
&+ \frac{ig}{2M\sqrt{2}} \phi^- [m_d^\lambda (\bar{d}_j^\lambda C_{\lambda\kappa}^\dagger (1 + \gamma^5) u_j^\kappa) - m_u^\kappa (\bar{d}_j^\lambda C_{\lambda\kappa}^\dagger (1 - \gamma^5) u_j^\kappa] - \frac{g}{2} \frac{m_u^\lambda}{M} H (\bar{u}_j^\lambda u_j^\lambda) \\
&- \frac{g}{2} \frac{m_d^\lambda}{M} H (\bar{d}_j^\lambda d_j^\lambda) + \frac{ig}{2} \frac{m_u^\lambda}{M} \phi^0 (\bar{u}_j^\lambda \gamma^5 u_j^\lambda) - \frac{ig}{2} \frac{m_d^\lambda}{M} \phi^0 (\bar{d}_j^\lambda \gamma^5 d_j^\lambda) + \bar{X}^+ (\partial^2 - M^2) X^+ \\
&+ \bar{X}^- (\partial^2 - M^2) X^- + \bar{X}^0 (\partial^2 - \frac{M^2}{c_w^2}) X^0 + \bar{Y} \partial^2 Y + igc_w W_\mu^+ (\partial_\mu \bar{X}^0 X^- - \partial_\mu \bar{X}^+ X^0) \\
&+ igs_w W_\mu^+ (\partial_\mu \bar{Y} X^- - \partial_\mu \bar{X}^+ Y) + igc_w W_\mu^- (\partial_\mu \bar{X}^- X^0 - \partial_\mu \bar{X}^0 X^+) \\
&+ igs_w W_\mu^- (\partial_\mu \bar{X}^- Y - \partial_\mu \bar{Y} X^+) + igc_w Z_\mu^0 (\partial_\mu \bar{X}^+ X^+ - \partial_\mu \bar{X}^- X^-) \\
&+ igs_w A_\mu (\partial_\mu \bar{X}^+ X^+ - \partial_\mu \bar{X}^- X^-) - \frac{1}{2} gM [\bar{X}^+ X^+ H + \bar{X}^- X^- H + \frac{1}{c_w^2} \bar{X}^0 X^0 H]
\end{aligned}
$$

$$+\frac{1-2c_w^2}{2c_w}igM[\bar{X}^+X^0\phi^+ - \bar{X}^-X^0\phi^-] + \frac{1}{2c_w}igM[\bar{X}^0X^-\phi^+ - \bar{X}^0X^+\phi^-]$$
$$+igMs_w[\bar{X}^0X^-\phi^+ - \bar{X}^0X^+\phi^-] + \frac{1}{2}igM[\bar{X}^+X^+\phi^0 - \bar{X}^-X^-\phi^0] \ .$$

The equation above can be roughly factorised into sections concerned with gluon interactions, bosonic interactions, weak force interactions, ghosts associated to the Higgs sector and Faddeev-Popov ghosts. For specific definitions and a good overview of the parameters in Eq. (A.1) see Ref. [160]. See also Refs.[582, 1052, 1161, 1243] for discussions surrounding the Standard Model parameters and their interactions.

Appendix B

Bayesian Statistical Modelling

B.1 Bayes Theorem

Here we discuss the basic context of high dimensional graphical models and associated measure spaces susceptible to hyper-parameterisation or hyperparameter optimisation. There are traditionally speaking considered to be two opposing schools of statistical reasoning forming the historical umbrellas of frequentist or Bayesian approaches. The Bayesian school of thought [1270] is the naturally adopted framework in a cosmological setting, where we are forced to accept and account for the obvious consideration that both the true underlying theory is vastly complex and uncertain. Observationally we are also plagued to only have a single reference frame, as observers, our personal realisation of the Universe we find ourselves in, explicitly a one time deal.

In order to evaluate the probability associated to a given model, described by a series of parameters $\vec{\theta}$, whilst assuming we possess some suitable sampled data D, we define the following values of interest. The probability of the theory, $P(\vec{\theta})$ is referred to as the statistical *prior*. The probability of the data given the theory is the *likelihood*. Finally the probability of the data, $P(D)$ is a normalisation factor found by marginalisation. The relationship between all of these quantities is defined

by Bayes' theorem,

$$P\left(\vec{\theta}|D\right) = \frac{P\left(D|\vec{\theta}\right)P\left(\vec{\theta}\right)}{P\left(D\right)} \ . \tag{B.1}$$

The marginal normalisation or evidence term is often defined as a a simple integral normalisation term or partition function,

$$P\left(D\right) = \int d\theta P(D|\theta)P(\theta) \ . \tag{B.2}$$

A joint probability distribution in this setting is defined as,

$$P(\vec{\theta}, D) = P(D, \vec{\theta})P(\vec{\theta}) \ . \tag{B.3}$$

Our primary inputs to define are the likelihood process and prior distribution function. The prior is our main focus represented by the properties of the measure space for the eigenvalues of our matrix ensembles. The true distributional structure of some compactification model residing in the string landscape is a potentially a Goliath task, often combined with very specific model features. Independent concerns may deviate from how we formulate a more general and simplified understanding. Generating a consistent formalism for adaptable but self-consistent prior functions is something that is of particular interest when dealing with available cosmological data and what inferences that could be found in order to lead how we may shape more specific models. This shaping comes from incorporating Bayes' theorem in a special type of high dimensional graphical model adopting the statistical language above, known as a *Bayesian hierarchical network* [295]. These probabilistic graphical models rely on a global factorisation of the joint probability distribution for a set of random variables into a product of local conditional probability distributions.

B.2 Hierarchical Modeling

Consider a model $\mathcal{M}$, where the hyperparameters of $\mathcal{M}$ represent the parameters of the relevant prior distributions of the model, the hyperpriors are therefore a natural extension using the singular values of the models hyperparameters. These models are often constructed as high dimensional probabilistic models, visualised using an acyclic graph with a fixed number of nodes which represent the model parameters. The graphs edges correspond to the systems stochastic or deterministic dependencies (see discussions in Section 7.3.1 and Fig. 7.15). Typically speaking at each node sits an assigned random variable, surrounded by a plate, which indicates the number of variables, each defined using the same hyperparameters. When the data is of variable size the plate must be repeated. A simple example of this is visually represented in Fig. (B.1) which concerns the conditional probability,

$$P(x, \alpha, \beta, \gamma) = P(x|\alpha, \beta, \gamma) \cdot P(\alpha, \beta, \gamma) \ . \tag{B.4}$$

These types of models represent a flow of information where we initially formulate nested sets of conditional dependencies between model parameters. We allow for the treatment of each parameter and hyperparameter as a random variable in the network. When the network is initialised we truncate the network at the highest order of the hyperparameters and fix singular terms in order to define the networks dependancies in order to generate data for the lowest level of the model parameters.

The standard prior taken on the grounds of an uninformative analysis using Bayesian methods is the Jeffery's prior, represented by the proportionality relationship with the Fisher information matrix,

$$P(\vec{\theta}) = \sqrt{\det \mathcal{I}(\vec{\theta})} \ . \tag{B.5}$$

String models suggest such natural priors can arise through physical motivations

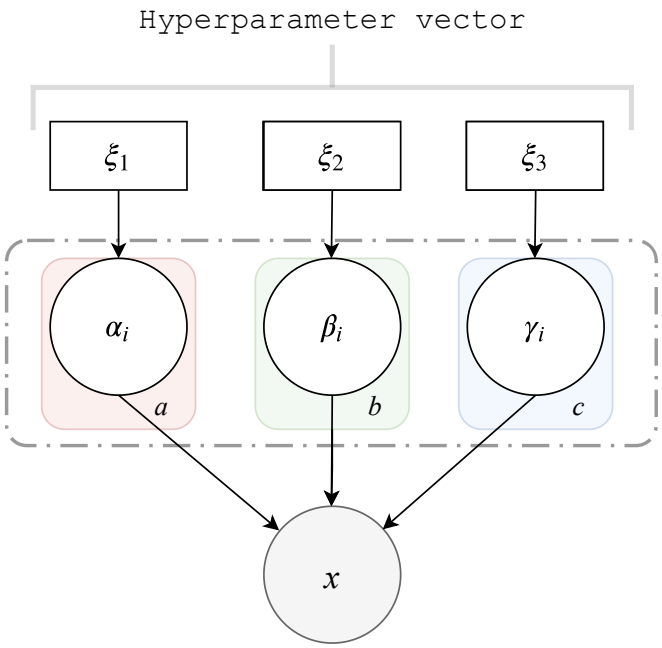


Figure B.1: Graphical representation of a generic model detailing the standard relevant layers. The hyperparameter vector defines the values of the hyperparameters which determine the nature of the model variables α_i, β_i and γ_i, which can represent either initial conditions or a series of stochastic variables which appear in the model Lagrangian. The *dashed dotted* box represents the stage of data compression using functional encoders. Each of these have a, b and c IID variables, where the surrounding plates represent a repetition or sampling process. Finally x represents a deterministic variable or observable we wish to draw conclusions on.

and could be useful given several scale invariant aspects of the landscape. Although not strictly a Jeffery prior, on the grounds of ensuring the correct normalisation, we have discussed these epistemic priors on axion parameter spaces in Section 5.1.2. We have argued however modality is a more naturally arising prior for randomised high-dimensional arguments present in the effective field theory.

Currently the full use of Bayesian networks are heavily constrained in a practical sense to focus their analysis on a very small number of fields, or more commonly, the case of the addition of a singular field [444]. The process of tracking the flow of information in models is a very tricky procedure when models have a large number of free parameters. The development and processing of future algorithms will allow for simplified models to draw stronger conclusions on the relations between these

parameters in terms of dependencies and the ability to integrate out nodes which the information content shows are safe to avoid. This is also vital on the grounds of including multiple fields, which gives an $\mathcal{N}_{\rm ax}$ factor enhancement to scale of the problem. See Refs. [318, 319, 363, 390, 657, 662, 687, 688, 1131] and references therein for relevant discussions. It is best then currently, to focus on methodologies which are useful in scenarios where multiple fields are present. Although these methods offer a much more simplified and uninformed approach, we can still draw interesting conclusions from these models. In this thesis we will focus on the case of a large number of fields and so we will assume we sit at the effective global minimum of the information we pass into our system of equations, disregarding any tracking of the nature of where and how that information my have been lost. In the context of generating consistent and traceable priors these methods are particularly adaptable, where we can turn to the mathematics of random matrices and numerous relevant associated universal properties.

B.3 General Approaches to Variances and Correlations

The choice of prior placed on the covariance matrix is a ubiquitous issue prevalent in modern statistics. Usually driven by the covariance estimation of multivariate random vectors, the formalities are particularly challenging in the high dimensional regime. We can still take inspiration on how to understand model formulation from Bayesian methods of matrix estimation and shrinkage priors based on reference prior models. There is a general consensus in the literature that the covariance matrix estimator should be understood under some form of decomposition, instead of the classical approach taken in Eq. (4.97). The preference on the decomposition structure is less clear, often incorporating factors of the standard deviations or variances, the prior placed on these a further level of hesitancy in the problem.

There are a number of ways of accounting for the problems detailed above found in the literature. These consist of, but are far from limited to, non-conjugate reference priors such as scaled inverse Wishart [778, 970, 1008], hierarchical half-t [723], Wishart [350], Cholesky-factor [1200], shrinkage priors [1324], reference priors [1373], matrix logarithms [718] and separation-formalism priors [161, 595, 723]. A common general approach which is most relevant to our discussions when dealing with this issue prevalent in extensions incorporating a Bayesian type analysis, is a decomposition of the variance components, known as the separation strategy or variance-correlation strategy [161]. The primary motivations for the use of the separation strategy is a flexibility and directness in modelling information in terms of standard deviations and correlations between data rather than a spectral decomposition of the full covariance matrix, Σ.

B.3.1 The Separation Strategy

A general argument is that it is often hard to deal with an unknown covariance matrix because the number of parameters increases very quickly as the dimension of the matrix increases. These parameters are also constrained by the complicated condition that the covariance matrix must be non-negative definite. The decomposed form of the covariance matrix in Eq. (4.59) using these methods is,

$$\Sigma = \Xi \mathcal{Q} \Xi \ , \tag{B.6}$$

where, $\Xi = \text{diag}(\delta_i)$. We can associate this type of model in equivalent to perturbative models of isometric matrices in various limits such as,

$$\mathbb{Y} = \sqrt{\mathbb{P}} \mathbb{X} \Sigma \mathbb{X}^{\text{T}} \sqrt{\mathbb{P}} \quad \text{where} \quad \Sigma \equiv \Xi \mathcal{Q} \Xi \propto \mathbb{I} \ , \tag{B.7}$$

$$\mathbb{Y} \equiv \sqrt{\mathbb{P}} \mathbb{X} \Xi \mathcal{Q} \Xi \mathbb{X}^{\text{T}} \sqrt{\mathbb{P}} \quad \text{where} \quad \sqrt{\mathbb{P}} \propto \mathbb{I} \ , \tag{B.8}$$

assuming equivalent prior dependancies. We need not restrict $\mathfrak{Q}$ to be a correlation matrix (see Ref. [1008]) but only that it is strictly positive definite, if we wish to not over-parameterise the model.

B.4 Probability and Measurable Spaces

In particular a remarkable olive branch in mathematics ensures well defined points representing measures on a statistical manifold formed from non-commutative operations, gives us a safe space to operate in, a striking contrast from classical statistical analogues, which was the focus of Section 4.4. We quote now, without derivation, a series of points beyond the scope of this thesis, tied into the concepts of measure theory, which provide interesting context to how the statistical spaces we will coverer in the following chapter could be understood in a wider picture. Information geometry [981] represents the interdisciplinary field that formulates an amalgamation of various methods of differential geometry and probability theory. Usually its applications are more relevant to machine learning [444], in order to study the spaces where each point is a hypothesis about some state or model. A statistical model [934] is a family $\mathcal{M}$, of probability measures on a measurable space Ω. The hyperparameters we initialise our model with are mapped to the probability density functions priors on the measurable space via $\mathcal{M}$. Consider a statistical manifold space, $\mathfrak{X}$ which defines a measure, $(\mathfrak{X}, \mathfrak{S}, \mu)$ on $\mathfrak{X}$. We can also define a suitable classical probability space, $(\Omega, \mathcal{B}, P)$, which represents a probability space on $\Omega = \mathfrak{X}$ with sigma-algebra[1] representing the set of events, $\mathcal{B} = \mathfrak{S}$ and probability $P = \mu$, on the measurable space $(\Omega, \mathcal{B})$. The map $P : \mathcal{B} \to [0, 1]$ is the probability function. When $\mu(\Omega) = 1$ we define a probability measure. If we fix the sigma-algebra we define the general infinite-dimensional statistical manifold, $\mathcal{S}(\mathfrak{X})$ each point representing a Borel measurable function[2] from Ω to $\mathfrak{X}$. The Borel sigma-algebra $\mathcal{B}$ on a

[1] A sigma-algebra or σ-algebra in the context of this work represents a definition of the measurable sets relevant to valid priors in our modelling.

[2] Formally we will reference the LSD functions for our choice of ensembles as Borel probability measures, again the technicalities beyond the scope of this thesis but quoted to reference specific

topological space is the smallest sigma-algebra containing all open sets. It is then often common practise to work in a finite dimensional setting defined by considering a limited set of probability distributions related by some continuously varying parameter. This parameter selects the relevant measures. Although beyond the scope of this thesis, these principles will be relevant for how we understand the limiting distributions for eigenvalues in the context of RMT.

mathematical features they represent in the study of free probability, e.g. see Refs. [190, 750, 1206].

Appendix C

Matrix Operations

C.1 Matrix Transforms

One example of the potential these models have comes with the understanding of how the LSD behaves for a class of general high-dimensional Wishart matrices, forming one of the defining cornerstones of RMT analysis. Specifically the origins of which are found in the seminal work of Vladimir Marčhenko and Leonid Pastur in 1967 [901] which we will address in Section 4.3.1.1, detailing how the limiting probability measure on the eigenspace of large random matrices is convergent and minimally dependant of the choice of the distribution of choice for the matrix entries. We are actually concerned with conditional factors placed on the distribution moments rather than the specificity of the distribution used for the undefined degrees of freedom encoded in the random matrix. Let us introduce some of the defining matrix transformations which will prove vital in understanding and defining the nature of the LSD away from classical constructions. See Refs. [138, 939, 1279] for details and formal definitions of any of the operations quoted below. First the Cauchy transform and respectively its functional inverse of the LSD, μ on $\mathbb{R}^+$ which

is defined as the limiting analytic self-map,

$$G_\mu(z) = \int_{\mathbb{R}} \frac{1}{z-x} d\mu(x) \quad z \in \mathbb{C}^+ \ , \tag{C.1}$$

$$F_\mu(z) = \frac{1}{G_\mu(z)} \ . \tag{C.2}$$

The negative definition of Eq. (C.1) defines the *Stieltjes transform*, $m_\mu(z) \equiv -G_\mu(z)$. The η-transform for any positive measure on the positive real line is,

$$\eta_\mu(z) = \frac{m_\mu(-1/z)}{z} \ , \tag{C.3}$$

defining a strictly monotonically decreasing function. The Voiculescu transform is [202],

$$\phi_\mu(z) = F_\mu^{-1}(z) - z \ . \tag{C.4}$$

The R-transform is the free analog of the log-moment generating function in classical probability theory, used for its additive properties, defined in the domain, $\mathbb{C}^+$ and is related to the Stieltjes transform [193],

$$R_\mu(z) = m_\mu^{-1}(-z) - \frac{1}{z} \ . \tag{C.5}$$

The S-transform is the free analog of the Mellin transform in classical probability theory, used for its multiplicative properties and is defined in terms of the η-transform,

$$S_\mu(z) = -\frac{z+1}{z}\eta_\mu^{-1}(z+1) \ . \tag{C.6}$$

The relevance of these transformations [1280] will become clear, as they provide a vital combinatorial description when assessing the distributions of the product or additions of free random variables in Section 4.4. They represent the ability to explicitly define a measure function given a particular model realisation. For example the famous Marčhenko-Pastur law we will introduce in Section 4.3.1.1 in Eq. (4.67), has a well defined S-transform $S_{\mu_{\rm MP}}(z) = 1/1+\beta z$.

Appendix D

The Tracy-Widom Limiting Laws

D.1 Extremal Spectral Functions

One of primary results from the literature states that for any sample covariance matrix constructed under the null covariance assumption, the largest eigenvalue converges almost surely to a limiting distribution. These limiting distributions are the *Tracy-Widom* laws, dependant on the invariance of the ensemble. Generally we have for a *white*-Wishart matrix, $\mathbb{W}$, when $\mathcal{N}, \mathcal{P} \to \infty$,

$$\frac{\lambda_{\max}(\mathbb{W}) - \mu_{\mathcal{N},\mathcal{P}}}{\sigma_{\mathcal{N},\mathcal{P}}} \to F_{\tilde{\beta}} \ , \tag{D.1}$$

where $F_{\tilde{\beta}}$ represents a family of different Tracy-Widom cumulative distribution functions parameterised under the standard $\tilde{\beta}$ ensembles of the *threefold way* in RMT. The Tracy-Widom functions are formulated in terms of solutions to the nonlinear second-order ordinary Painlevë II differential equation. This behaviour was first shown for the GUE by Kurt Johansson in Ref. [753] and again by Iain Johnstone for the GOE in Ref. [754]. Each of these distributions relates the statistical properties of the largest normalised eigenvalues of a given random Hermitian matrix. It was shown under a $\mathcal{N}^{2/3}$ scaling that for each of the GOE ($\tilde{\beta} = 1$) [1269], GUE ($\tilde{\beta} = 2$)

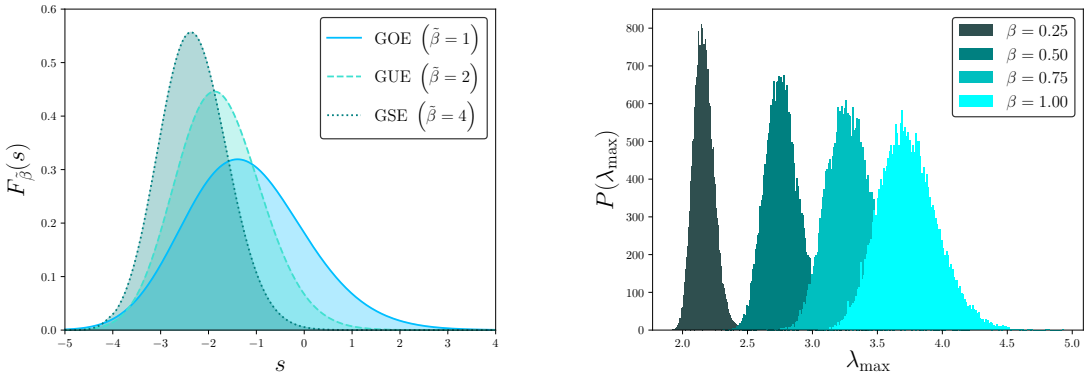


Figure D.1: *Left panel:* Tracy-Widom limiting probability measures defined in Eq. (D.3), Eq. (D.4) and Eq. (D.5) for the normalised singular eigenvalues defining the spectral supremum of each possible choice of real, complex, or quaternion matrix entries for the classical Gaussian ensembles. *Right panel:* Example sample spectra for the largest eigenvalues from 25000 matrix simulations from the GOE ensemble for various values of the dimensionality parameter, β.

[1268] and GSE ($\tilde{\beta} = 4$) the general edge universality follows,

$$F_{\tilde{\beta}}(s) = \lim_{\mathcal{N}\to\infty} F_{\mathcal{N},\tilde{\beta}}(2\sigma\sqrt{\mathcal{N}} + \sigma\mathcal{N}^{-1/6}s) \ , \tag{D.2}$$

where the family of functions are explicitly defined as,

$$F_2(s) = \exp\left(-\int_s^\infty (x-s)q^2(x)dx\right) \ , \tag{D.3}$$

$$F_1(s) = \exp\left(-\frac{1}{2}\int_s^\infty q(x)dx\right)[F_2(s)]^{1/2} \ , \tag{D.4}$$

$$F_4(2^{-2/3}s) = \cosh\left(-\frac{1}{2}\int_s^\infty q(x)dx\right)[F_2(s)]^{1/2} \ . \tag{D.5}$$

The value of $q(s)$ represents the unique solution of the Painlevë II differential equation,

$$q''(s) = sq(s) + 2q(s)^3 + \alpha \ , \tag{D.6}$$

assuming the following boundary conditions,

$$q(s) \sim Ai(s), \quad s \to +\infty \ , \tag{D.7}$$

with the Airy special function, $Ai(s)$. The *left panel* of Fig. D.1 shows the limiting laws of order $1, 2$ and 4 for each of the largest eigenvalues of the GOE, GUE and GSE ensembles respectively. The *right panel* shows examples of numerical simulations for the eigenvalues defining the spectral radii of the GOE ensemble for various ratios of shaping parameter, β.

Appendix E

Combinatorial Sequences and the Fuss-Catalan Distributions

E.1 The Fuss-Catalan Numbers

A subject with very close ties to free probability theory, the construction of matrix ensembles and the asymptotic characteristics of positive density spaces is the study of combinatorial moment sequences. In order to briefly highlight the potential complications of modelling the explicit asymptotical level density functions for perturbed systems we quickly review the explicit formulation of some specific compact measures supported on, $\mathbb{R}^+$. Sequences can often be formed as an approach to generalising the famous limiting laws for classical ensembles. For example a generalised set of matrix ensembles for positive definite hermitian matrices comes from the free multiplicative powers/roots of the Marčhenko-Pastur distribution, know as the Fuss-Catalan distributions [148, 1047].

These distributions have a range of associations to quantum systems and the modelling of quantum states in areas such as entanglement and multi-particle systems [952, 1400]. The asymptotic behaviour of the squared singular values for the fixed set of probability measures have moments associated to the Fuss-Catalan numbers

[105, 951] to a given order, s. The combinatorics of the Fuss-Catalan numbers are linked to the binomial coefficients and serve as a representation of the legal-permutations for the arrangement of a series of values or objects. The Fuss-Catalan numbers are generated by the sequence of terms,

$$FC_s(n) = \frac{1}{sn+1}\begin{pmatrix} sn+n \\ n \end{pmatrix} . \tag{E.1}$$

To an arbitrary order, s, the LSD functions can be found as follows. For each index s it is possible to show that the following equation can be satisfied [1047],

$$\int_0^{K_s} x^n \mu_s^{\mathrm{FC}}(x)dx = FC_s(n) , \tag{E.2}$$

for all,

$$K_s = \frac{(s+1)^{s+1}}{s^s} . \tag{E.3}$$

The function $\mu_s^{\mathrm{FC}}(x)$ is representative of the positive probability measure density function for the eigenvalues of matrix products of the form,

$$\mathbb{X}_{ij(s)} = \left(\mathbb{Y}_{kj(1)}\mathbb{Y}_{kj(2)}...\mathbb{Y}_{kj(s)}\right)^\dagger \left(\mathbb{Y}_{ik(1)}\mathbb{Y}_{kl(2)}...\mathbb{Y}_{yz(s)}\right) . \tag{E.4}$$

Performing an inverse Mellin transform on the function, $\mu_s^{\mathrm{FC}}(x)$ and incorporating Euler's gamma function via the Gauss-Legendre formula we arrive at a form for the density which contains products of gamma functions with shifted arguments [1047]. The nuance here, in this formulation, is that the form of this function actually allows for the Mellin transform to undergo a further representation in terms of a Meijer G-function,

$$\mu_s^{\mathrm{FC}}(x) = \frac{1}{\sqrt{2\pi}}\frac{s^{\left(s-\frac{3}{2}\right)}}{(s+1)^{\left(s+\frac{1}{2}\right)}} G^{s,0}_{s,s}\left(z \,\middle|\, \begin{matrix} \alpha_1, \ldots, \alpha_p \\ \beta_1, \ldots, \beta_q \end{matrix} \right) . \tag{E.5}$$

The form of the Meijer G-function defines the function parameters,

$$\alpha_j = \frac{1+j-s}{s} \ , \tag{E.6}$$

$$\beta_j = \frac{j-1-s}{s+1} \ . \tag{E.7}$$

This generalisation of the positive density spaces generated by the standard LSDs of isotropic Wishart matrices detailed in Section 4.3.1 asymptotically defines the combinatorial *Fuss-Catalan* probability distributions,

$$\mu_s^{\mathrm{FC}}(x) = \left[\mu_1^{\mathrm{MP}}(x)\right]^{\boxtimes s} \ , \tag{E.8}$$

defined in the context of free convolution operations. The function $\mu_1^{\mathrm{MP}}(x)$ is the standard Marčhenko-Pastur probability measure function found in Eq. (4.67). The explicit form of the second order free convolution measure is [870, 1046, 1047],

$$\mu_{s=2}^{\mathrm{FC}}(x) = \frac{\sqrt[3]{2}\sqrt{3}}{12\pi} \frac{\sqrt[3]{2}\left(27+3\sqrt{81-12x}\right)^{2/3} - 6\sqrt[3]{x}}{x^{2/3}\sqrt[3]{\left(27+3\sqrt{81-12x}\right)}} \ . \tag{E.9}$$

Simplifying Eq. (E.5) the Fuss-Catalan distributions to arbitrary order are defined as [1047],

$$\mu_s^{\mathrm{FC}}(x) = \sum_{k=1}^{s} \Lambda_{k,s} x^{\frac{k}{s+1}-1} \ {}_sF_{s-1}\left(\left[\{\alpha\}_{j=1}^{s}\right], \left[\{\beta\}_{j=1}^{k-1}, \{\gamma\}_{j=k+1}^{s}\right]; \frac{s^s}{(s+1)^{s+1}}x\right) \ , \tag{E.10}$$

$$\alpha = 1 - \frac{1+j}{s} + \frac{k}{s+1}; \beta = 1 + \frac{k-j}{s+1}; \gamma = 1 + \frac{k-j}{s+1} \ , \tag{E.11}$$

where ${}_sF_{s-1}$ is a hypergeometric function and x represents the space of eigenvalues bounded by the upper and lower spectral limits for the model parameters. The values of $\Lambda_{k,s}$ represent the model coefficients,

$$\Lambda_{k,s} = s^{-\frac{3}{2}}\sqrt{\frac{(s+1)}{2\pi}}\left(\frac{s^{\frac{s}{(s+1)}}}{(s+1)}\right)^k \frac{\left[\Gamma_{j=1}^{k-1}\gamma\left(\frac{j-k}{s+1}\right)\right]\left[\gamma_{j=k+1}^{s}\gamma\left(\frac{j-k}{s+1}\right)\right]}{\left[\Gamma_{j=1}^{s}\gamma\left(\frac{j+1}{s}-\frac{k}{s+1}\right)\right]} \ . \tag{E.12}$$

The Fuss-Catalan numbers are actually a special limit of a larger family of combinatorial sequences.

E.2 The Raney Numbers

This space of positive measures can be expanded in a more general setting using the Raney lemma [1047, 1090], where the number of the Raney sequences of order $\mathcal{P}$ and fixed length $\mathcal{P}n+1$, is defined by the Fuss-Catalan numbers in Eq. (E.1). These Raney numbers are defined as,

$$R_{\mathcal{P},\mathcal{R}}(n) = \frac{\mathcal{R}}{(\mathcal{P}n+\mathcal{R})}\begin{pmatrix}\mathcal{P}n+\mathcal{R}\\ n\end{pmatrix} \tag{E.13}$$

with the relation, $FC_{p-1}(n) = R_{\mathcal{P},1}(n)$. These sequences have been shown to describe the moments of probability measure functions, $\mu^{\mathrm{R}}_{\mathcal{R},\mathcal{P}}$ with compact support on the positive real interval [951]. These are related to the previously defined Fuss-Catalan densities when $\mathcal{R}=1$, where $\mu^{\mathrm{R}}_{s+1,1} \equiv \mu^{\mathrm{FC}}_{s}$. This complete set of positive density measures are parameterised by the inequality, $0 < \mathcal{R} \leq \mathcal{P}$, as displayed in Fig. E.1. Repeating the general treatment above for the definition of the Fuss-Catalan functions, it is possible to form a generalisation of Eq. (E.5), i.e. applying an inverse Mellin transformation for specific parameters defines a representation of the Raney distributions in terms of the hypergeometric functions, which is expressed as the rather cumbersome summation [1047],

$$\mu^{\mathrm{R}}_{\mathcal{P},\mathcal{R}}(\chi) = \sum_{\mathcal{J}=1}^{\mathcal{P}} \Omega(\mathcal{P},\mathcal{R};\mathcal{J})\,\chi^{\left(\frac{(\mathcal{R}-1+\mathcal{J})}{\mathcal{P}}-1\right)}{}_{\mathcal{P}}F_{\mathcal{P}-1}\left(\gamma_1,\gamma_2;\frac{(\mathcal{P}-1)^{\mathcal{P}-1}}{\mathcal{P}^{\mathcal{P}}}\chi\right)\ , \tag{E.14}$$

$$\gamma_1 = \left[1+\beta_{\mathcal{J}},\{1+\beta_{\mathcal{J}}-\alpha_{\mathcal{I}}\}_{\mathcal{I}=2}^{\mathcal{P}}\right]\ , \tag{E.15}$$

$$\gamma_2 = \left[\left\{1+\frac{\mathcal{J}-\mathcal{I}_2}{\mathcal{P}}\right\}_{\mathcal{I}_2=1}^{\mathcal{J}-1},\left\{1+\frac{\mathcal{J}-\mathcal{I}_3}{\mathcal{P}}\right\}_{\mathcal{I}_3=\mathcal{J}+1}^{\mathcal{P}}\right]\ , \tag{E.16}$$

$$\alpha_1 = 0 \quad ; \quad \alpha_{\mathcal{I}} = \left(\frac{\mathcal{R} - \mathcal{P} - 1 + \mathcal{J}}{\mathcal{P}} \right) \quad \text{for} \;\; \mathcal{I} = 2, \ldots, \mathcal{P} \; , \tag{E.17}$$

$$\beta_{\mathcal{J}} = \frac{(\mathcal{R} - \mathcal{P} + \mathcal{I})}{(\mathcal{P} - 1)} \quad \text{for} \;\; \mathcal{J} = 1, \ldots, \mathcal{P} \; , \tag{E.18}$$

$$\Omega\left(\mathcal{P}, \mathcal{R}; \mathcal{J}\right) = \frac{\mathcal{R}}{\sqrt{2\pi}} \frac{\mathcal{P}^{\left(\mathcal{R}-\mathcal{P}-\frac{1}{2}\right)}}{(\mathcal{P}-1)^{\left(\mathcal{R}-\mathcal{P}+\frac{3}{2}\right)}} \left(\frac{(\mathcal{P}-1)^{(\mathcal{P}-1)}}{\mathcal{P}^{\mathcal{P}}} \right)^{\frac{(\mathcal{R}-\mathcal{P}-1+\mathcal{J})}{\mathcal{P}}} \frac{1}{\Gamma\left(\frac{(\mathcal{P}-\mathcal{R}+1-\mathcal{J})}{\mathcal{P}}\right)} \frac{[\mathcal{C}_1]\,[\mathcal{C}_2]}{[\mathcal{C}_3]} \; , \tag{E.19}$$

$$\mathcal{C}_1 = \prod_{\mathcal{I}_1=1}^{\mathcal{J}-1} \Gamma\left(\frac{\mathcal{I}_{\mathcal{I}} - \mathcal{J}}{\mathcal{P}} \right) ; \; \mathcal{C}_2 = \prod_{\mathcal{I}_2=1}^{\mathcal{P}-\mathcal{J}} \Gamma\left(\frac{\mathcal{I}_2}{\mathcal{P}} \right) \; , \tag{E.20}$$

$$\mathcal{C}_3 = \prod_{\mathcal{I}_3=2}^{\mathcal{P}} \Gamma\left(\frac{(\mathcal{R} - \mathcal{P} + \mathcal{I}_3)}{\mathcal{P}-1} - \frac{(\mathcal{R} - \mathcal{P} - 1 + \mathcal{J})}{\mathcal{P}} \right) \; , \tag{E.21}$$

where we can associate χ to either a positive space of mass-eigenstates or decay constants, defined in the interval,

$$\mu^{\mathrm{R}}_{\mathcal{P},\mathcal{R}} \in \left[0, \mathcal{P}^{\mathcal{P}} / (\mathcal{P}-1)^{\mathcal{P}-1}\right] \; . \tag{E.22}$$

The functional support is determined by the convergence of the hypergeometric series, ${}_{\mathcal{P}}F_{\mathcal{P}-1}$. Particular combinations of $\mathcal{P}$ and $\mathcal{R}$ reduce to well known ensemble limits, as detailed in Fig. E.1. Using these relations we have the intriguing possibility to define specific relations between these limits by a translation of the defining parameters, which can be used to single out a specific models. For example the semi-circle distribution $\left(\mu^{\mathrm{R}}_{2,2}\right)$ is related to the Marčhenko-Pastur function, $\left(\mu^{\mathrm{FC}}_{1}\right)$, as defined by the general relation [1047],

$$\mu^{\mathrm{R}}_{\mathcal{P},\mathcal{R}}(x) = x\mu^{\mathrm{R}}_{\mathcal{P},1}(x) = x\mu^{\mathrm{FC}}_{p-1}(x) \; . \tag{E.23}$$

These general densities represent quantities often too complex to generate and scan in a more Bayesian sense for phenomenological models, where we need to fall back on simpler more general characterisations of distribution moments as discussed in Section 5.4. These functions do however represent a fascinating relationship between various model spectra and act as a powerful demonstration of universality amongst

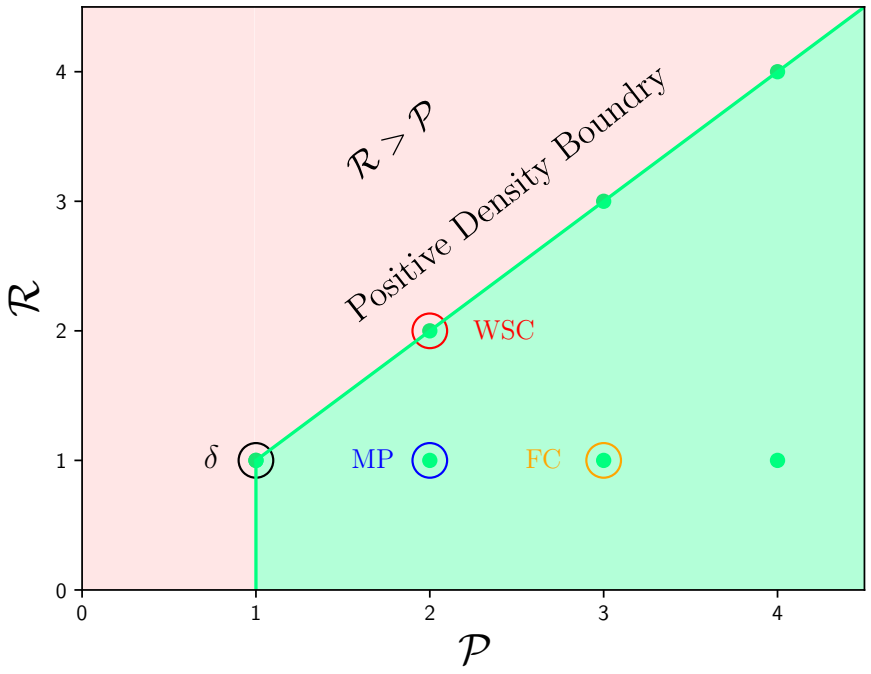


Figure E.1: Raney density function space defined by Eq. (E.13), with specific limiting density functions generated at the coordinates $(\mathcal{P}, \mathcal{R})$ used to define the Raney numbers in Eq. (E.14). The *green* shaded region relates to the set of non-negative probability measures. The boundary defines the generalisations of the semi-circular distribution. The delta function positioned at $(1, 1)$ (*black* circle) corresponds to the mass distribution in Section 5.2.3 which under the translation $\mathcal{P} + 1$ generates the mass spectrum in Section 5.2.4.1 (*blue* circle). The *orange* circle relates to discussions in Section 5.2.4.3.2. Finally the *red* circle could relate to spectral forms associated to shifted distributions of the superpotential Hessian as discussed in Section 5.2.8. Reproduced from Refs. [952, 1047].

numerous non-trivial examples of ensembles found in perturbative constructions. Specifically in our general form of model construction we are concerned with the free convolution relationships [951, 1047],

$$\mu^{\mathrm{R}}_{\mathcal{P}+\mathcal{R}\mathcal{Q},\mathcal{R}} = \mu^{\mathrm{R}}_{\mathcal{P},\mathcal{R}} \boxtimes \mu^{\mathrm{R}}_{1+\mathcal{Q},1} \ , \tag{E.24}$$

$$\left[\mu^{\mathrm{R}}_{1+\mathcal{P},1}\right]^{\boxtimes s} = \mu^{\mathrm{R}}_{1+s\mathcal{P},1} \ , \tag{E.25}$$

for all $\mathcal{R}, \mathcal{Q}, \mathcal{P} > 0$, which define the ability to place priors on model components associated to well defined limits of the Raney space shown in Fig. E.1.

Appendix F

Elements of Measure Spaces

F.1 Free Operations

Further free operations related to the discussions found in Section 4.4 are defined as,

- $\boxminus$ - *Additive free deconvolution*: For the case of a unique probability measure μ, we can define the additive free convolution operation as $\mu = \xi \boxminus \nu$, where ξ represents the resultant measure from the additive free convolution defined above [94, 1133, 1134].

- $\boxslash$ - *Multiplicative free deconvolution*: For the case of a unique probability measure μ, we can define the multiplicative free convolution operation as $\mu = \xi \boxslash \nu$, where ξ represents the resultant measure from the multiplicative free convolution defined above [94, 1133, 1134].

- $\boxdot$ - *Free compression*: As discussed in Ref. [996], the compressive convolution represents the operation $\mu_{\mathbb{X}} \to \frac{\mathcal{N}}{\mathcal{P}} \boxdot \mu$ for a measure, μ for the weakly converging distribution of a matrix, $\mathbb{A}$. Introducing the parameter, $\alpha \in (0, 1]$ defines the R-transform, $R_{\alpha \boxdot \mu}(z) = R_{\mu}(\alpha z)$ and inverse Cauchy transformation, $G^{-1}_{\alpha \boxdot \mu}(y) = G^{-1}_{\mu}(\alpha y) + {}^{1}/_{y} - {}^{1}/_{\alpha y}$.

In the following section we detail a few features of measure spaces related to these operations which indicates the ability to associate any measure we could produce (given specific symmetry restrictions etc.) as a parametrisable and well defined function residing in a measure or distribution family [673], with suitable features such as regularity and modality. Just as a Gaussian distribution distribution may appear as a specific limit in a wider family, the limiting laws of RMT could belong or be closely represented by a family formed from convoluted measures.

F.2 Infinite Divisibility

Any probability measure defined on $\mathbb{R}$, the analytical subordination for free convolution powers defines the freely infinitely divisibility of a measure, for all $n \in \mathbb{Z}^+$, if there is a well defined probability measure which satisfies,

$$\mu = \mu_n^{\boxplus n} \equiv \mu_n \boxplus \cdots \boxplus \mu_n \ , \tag{F.1}$$

under the repetition on n free additive convolutions and $\mu_n^{\boxplus n}$ defines a class of free infinitely divisible measure functions. These are analogous to classical cases it is possible to define free Levy processes and free infinite divisibility [195, 1049] with respect to free convolution operations. This is a powerful relation, especially when considerations of the bijection it represents between classically and freely infinitely divisible probability measures are considered, the so called Bercovici-Pata bijection [203]. This is the CLT relation between free random variables and classical counterparts, i.e. Wigner's semicircle law is the free analogue relation to the Gaussian law and the Marčhenko-Pastur distribution the free analogue of the Poisson limit theorem, which possesses an interesting relation to kurtosis [93], and as bijection preserves cumulants provides a direct relation between moments. A stronger criterion from free infinite divisibility is free regularity. Any measure on $\mathbb{R}$ is free regular when its free convolution power $\mu_n^{\boxplus n}$ is fully analytic on $[0, \infty)$. Other key aspects

represent the unimodality of the resulting measures.

For any symmetric probability measure function, we can say it is infinity divisible for any integer, $n \in \mathbb{Z}^+$ where again a further measure, μ_n defines the convoluted sum,

$$\mu = \mu_n \boxplus_\beta \mu_n \boxplus_\beta \cdots \boxplus_\beta \mu_n \ . \tag{F.2}$$

For the information plus noise model other more traditional free operations, such as free multiplicative convolution have been used to construct measure spaces [1091]. It is typically considered the operand measure is the Marčhenko-Pastur distribution, with the perturbing function a discrete measure density [833]. Perhaps more interestingly operations using free deconvolution were discussed in Refs. [1132, 1133] providing insight into the fascinating ability to backtrace results from non-commutative operations, also allowing for further definitions of noise profiles such as coloured noise.

F.3 Spectral Noise

Ensuring that the matrix $\mathbb{X}$ in the information plus noise model converges almost surely to a compactly supported probability measure $\mu_{\mathbb{X}}$, then we can define,

$$\mu_{\mathbb{M}} \boxdot \mu_{\mathrm{MP}} = (\mu_{\mathbb{X}} \boxdot \mu_{\mathrm{MP}}) \boxplus \mu_{\sigma^2 I} \ , \tag{F.3}$$

where μ_{MP} is the Marčhenko-Pastur measure defined in Eq. (4.67) and $\mu_{\sigma^2 I}$ is the atomic measure of additional noise, which typically reproduces Gaussian fluctuations. It is then possible to deconvolve Eq. (F.3) in order to express the measure of the final matrix,

$$\mu_{\mathbb{M}} = ((\mu_{\mathbb{X}} \boxdot \mu_{\mathrm{MP}}) \boxplus \mu_{\sigma^2 I}) \boxtimes \mu_{\mathrm{MP}} \ , \tag{F.4}$$

whilst also defining a measure for the isolated information,

$$\mu_{\mathbb{X}} = ((\mu_{\mathbb{M}} \boxtimes \mu_{\mathrm{MP}}) \boxplus \mu_{\sigma^2 I}) \boxtimes \mu_{\mathrm{MP}} \ . \tag{F.5}$$

The fluctuations of eigenvalues in the isolated measure components representing the presence of spikes is primarily regulated by the choice made for the matrix ensemble. See Ref. [313] for details regarding the IID case and frameworks outside of free probability. The support of the resultant measure also corresponds to the characteristics of the perturbing measure where we can assume a traceable safety in the nature of the new support when the support of ν has a finite union of closed disjoint intervals [312, 313]. The nature of the measure at the hard and soft edges has also be shown to be a continuous density function for each respective model [218, 476, 1189].

Appendix G

Beta Distribution Functions

G.1 Family Parameterisations

The Beta family of distributions can be defined by the parameterisation,

$$\text{FBeta}(x;\gamma,\kappa,\xi,\chi) = \frac{x^{\xi-1}(1-(1-\kappa)(x/\gamma))^{\xi-1}}{\gamma^{\xi}\beta(\xi,\chi)(1+\kappa(x/\gamma))^{\xi+\chi}} \ , \tag{G.1}$$

where, $0 < x < b/(1-c)$ and,

$$\beta(\xi,\chi) = \frac{\Gamma(\xi)\Gamma(\chi)}{\Gamma(\xi+\chi)} \ , \tag{G.2}$$

using the Gamma function, Γ. This represents a special limit of the extremely versatile generalised Beta distribution [57],

$$\text{FBeta}\left(y;\gamma,\kappa,\xi,\chi\right) = \text{GBeta}\left(y;\alpha=1,\gamma,\kappa,\xi,\chi\right) \ . \tag{G.3}$$

The beta and inverted beta distributions or beta distributions of the first and second kind are defined by the functions,

$$\text{Beta}(x) = \frac{x^{\xi-1}(1-x)^{\chi-1}}{\beta(\xi,\chi)} \ , \tag{G.4}$$

$$\text{Beta}'(x) = \frac{x^{\xi-1}(1+x)^{-\xi-\chi}}{\beta(\xi,\chi)} \ , \tag{G.5}$$

which are recovered in the limit of $\kappa = 0$ and $\kappa = 1$ for the FBeta function in Eq. (G.1) respectively. The standard normalised Beta distribution is defined by the support, $x \in [0,1]$. When the mean and variance are not normalised the function must adopt two further parameters defining the four-parameter Beta function family or collection of Type I Pearson distributions,

$$\text{Beta}(x) = \frac{(x-\xi)^{\xi-1}(\chi-x)^{\chi-1}}{\beta(\xi,\chi)(\chi-\xi)^{\xi+\chi-1}} \ . \tag{G.6}$$

The values of ξ and χ will correspond to the upper and lower limits of the largest and smallest eigenvalues, which translate across to the standard location and scale parameters of the function, parameterised by ξ and $\chi - \xi$ respectively. The skewness of the Beta distribution is defined as,

$$\sqrt{\beta_1} = \frac{2\,(\chi-\xi)\,\sqrt{\xi+\chi+1}}{(\xi+\chi+2)\ \sqrt{\xi\chi}} \ , \tag{G.7}$$

and the excess kurtosis is,

$$\beta_2^{\text{ex}} = \frac{6\left[(\xi-\chi)^2\,(\xi+\chi+1) - \xi\chi\,(\xi+\chi+2)\right]}{\left[\xi\chi\,(\xi+\chi+2)\,(\xi+\chi+3)\right]} \ . \tag{G.8}$$

The geometry of the distribution function relates to the parameter of the RMT models, regulated by both ξ and χ. In the limit, $\xi = \chi$ the distribution is symmetric about the mean where we can define the linearity relationship,

$$\beta_{\mathcal{K}} \equiv \mathcal{C}_1 \xi \ , \tag{G.9}$$

$$\beta_{\mathcal{M}} \equiv \mathcal{C}_2 \chi \ . \tag{G.10}$$

The constants $\mathcal{C}_1$ and $\mathcal{C}_2$ represent a proportionality scaling factor relating to distribution shaping parameter to the Beta distribution parameters. When the distribu-

tion is symmetric the constants equate.

Appendix H

Generalised Lambda Distributions

H.1 A Flexible Framework for Spectral Moments

A very flexible and commonly used distribution framework for modelling logarithmic asymmetric random variables due to the possible presence of significant heavy-tails or skewness is the family of GLDs [378, 563, 776, 1085]. This family of distributions is an extension of the Tukey lambda distribution family [674, 1277]. The GLD is a four parameter family with a focus placed on its extreme flexibility and ability to model the moments of a statistical distribution. There are a wide range of generalised flexible distribution families (normal inverse Gaussian [163], generalised hyperbolic distribution [162], Johnson translation [1211, 1232] etc), most of which possessing properties of infinite divisibility. The GLD is defined by a quantile function such that its parameters can be estimated even when its moments do not exist. This feature of the GLD family gives a specific flexibility to accurately represent various shapes of defined density functions, where particularly they are capable of mapping unimodal, monotone, U-shape and S-shape functions to a high degree of accuracy. The general efficiency of these spectra is determined by how to categorise, determine and fit the relevant empirical moments to their theoretical counterparts (i.e. L-moments [716], maximum likelihood functions [989] etc). Although certain limits of the mass

distributions will correspond to well known distributions, particularly well known point limits residing in the family of Pearson Types discussed in Section 5.4, the general modelling of most spectra will correspond to an (*excess*) kurtosis and skew approximated to increased accuracy by the use of a series of continuous functions in this space.

H.2 The Freimer-Kollia-Mudholkar-Lin Parameterisation

Under the Freimer-Kollia-Mudholkar-Lin (FKML) parameterisation [563], the parameters of interest of the GLD are defined by the quantile function which is the given inverse of its cumulative distribution function (CDF),

$$F^{-1}(p|\lambda_1, \lambda_2, \lambda_3, \lambda_4) = \lambda_1 + \frac{1}{\lambda_2}\left[\frac{p^{\lambda_3} - 1}{\lambda_3} - \frac{(1-p)^{\lambda_4} - 1}{\lambda_4}\right] , \tag{H.1}$$

where p represents a probability weight, $p \in [0, 1]$. The GLD probability function is then defined as,

$$f_\lambda(F^{-1}(p|\lambda_1, \lambda_2, \lambda_3, \lambda_4)) = \frac{\lambda_2}{p^{(\lambda_3-1)} + (1-p)^{(\lambda_4-1)}} . \tag{H.2}$$

The empirical moments can be found using the following relationships to the λ parameters which define the probability density of the GLD,

$$\mu = \nu_1 , \tag{H.3}$$

$$\sigma^2 = \frac{\nu_2 - \nu_1^2}{\lambda_2^2} , \tag{H.4}$$

$$\sqrt{\beta_1} = \frac{\nu_3 - 3\nu_1\nu_2 + 2\nu_1^3}{(\nu_2 - \nu_1^2)^{3/2}} , \tag{H.5}$$

$$\beta_2 = \frac{\nu_4 - 4\nu_1\nu_3 + 6\nu_1^2\nu_2 - 3\nu_1^4}{(\nu_2 - \nu_1^2)^2} , \tag{H.6}$$

where the ν functions are functions of the shaping parameters for the higher moments of the distribution,

$$\nu_1 = \frac{1}{(1+\lambda_3)\lambda_3} - \frac{1}{(1+\lambda_4)\lambda_4} \ , \tag{H.7}$$

$$\nu_2 = \frac{1}{(1+2\lambda_3)\lambda_3^2} + \frac{1}{(1+2\lambda_4)\lambda_4^2} - \frac{2\zeta(1+\lambda_3, 1+\lambda_4)}{\lambda_3\lambda_4} \ , \tag{H.8}$$

$$\nu_3 = \frac{1}{(1+3\lambda_3)\lambda_3^3} - \frac{1}{(1+3\lambda_4)\lambda_4^3} - \frac{3\zeta(1+2\lambda_3, 1+\lambda_4)}{\lambda_3^2\lambda_4} + \frac{3\zeta(1+\lambda_3, 1+2\lambda_4)}{\lambda_3\lambda_4^2} \ , \tag{H.9}$$

$$\nu_4 = \frac{1}{(1+4\lambda_3)\lambda_3^4} + \frac{1}{(1+4\lambda_4)\lambda_4^4} - \frac{4\zeta(1+3\lambda_3, 1+\lambda_4)}{\lambda_3^3\lambda_4} \tag{H.10}$$

$$+ \frac{6\zeta(1+2\lambda_3, 1+2\lambda_4)}{\lambda_3^2\lambda_4^2} - \frac{4\zeta(1+\lambda_3, 1+3\lambda_4)}{\lambda_3\lambda_4^3} \ , \tag{H.11}$$

where the function, ζ is,

$$\zeta(x, y) = \int_0^1 \Gamma^{(x-1)}(1-\Gamma)^{(y-1)} d\Gamma \ , \tag{H.12}$$

representing a standard Euler integral of the first kind.

Appendix I

The Random Matrix Type IIB Superpotential

I.1 The N-flation Matrix Model

In this Appendix we briefly review the original arguments of Ref. [499], which provide a solid context as to how universal spectral forms arise in specific models of flux compactification, as discussed in Section 3.3.4. Here we detail the context behind the appearance of the Marčhenko-Pastur models in KKLT [758] compactifications of Type-IIB string theory. The unique parameter, $\beta_{\mathcal{M}}$ in this model is the total dimension of the moduli space, defined in Eq. (5.45). As previously highlighted the original model for N-flation explored the required trans-Planckian displacements for axion inflation models by considering $\mathcal{N}_{\rm ax} \gg 1$ decoupled fields each with identical masses that served to drive a period of inflation through the assisted inflation mechanism [457, 859]. The fields have periodic potentials, as expressed in Eq. (5.9), where the scales Λ_n can be significantly lower that the UV cutoff scale of the theory due to dimensional transmutation. The fields with identical masses undergo a common initial displacement ϕ' as they continue to roll in unison, providing an effective single field displacement of the order $\sqrt{\mathcal{N}_{\rm ax}}\phi'$.

Further expanding on these concepts the work of Ref. [499] incorporated the principles of RMT in a more general framework where the axion masses are now defined using a distinct spectral measure. In their framework the form of the matrix used to determine a spectrum of axion masses is only dependant on the basic structure the matrix possesses, which can be understood using the supergravity potential found in Eq. (3.28).

I.2 A Simplified Superpotential

The KKLT superpotential from non-perturbative effects which are generated from the associated moduli and axions is,

$$W_i = \widetilde{\Lambda}_i e^{-2\pi\rho_i} e^{2\pi i\phi_i} \equiv C_i e^{2\pi i\phi_i} \ , \tag{I.1}$$

where C_i are constants when the moduli are fixed at their minimum. A Taylor expansion about the origin at $\phi_i = 0$, along with the F-flatness conditions $D_A W|_{\phi_i=0} = 0$, defines the mass matrix from the quadratic order terms of the Lagrangian,

$$\mathcal{M}_{ij} = (2\pi)^2 e^K \left(K^{AB} D_A C_i D_B C_j - 3 C_i C_j \right) \ , \tag{I.2}$$

where the simplified potential is now represented in the form,

$$V(\phi) = \phi^i \mathcal{M}_{ij} \phi^j \ . \tag{I.3}$$

Note that $i, j = 1, \ldots, N$ run over the Kähler moduli, where the terms $A, B = 1, \ldots, N + L$ run over the dilaton, complex moduli and Kähler moduli. After the kinetic terms are bought into their canonical form (see Section 5.1.1), the mass matrix is then expressed as,

$$\widetilde{\mathcal{M}}_{ij} = (2\pi)^2 \frac{e^K}{f_i f_j} U_i^k \left(K^{AB} D_A C_k D_B C_l - 3 C_i C_j \right) U_j^l \ . \tag{I.4}$$

Despite the complex form of $\widetilde{\mathcal{M}}_{ij}$ in Eq. (I.4), it can be shown that the characteristics of the N-flation model can be extracted simply from the eigenvalues of a general random matrix with IID entries, which under the arguments of universality are assumed to be Gaussian in nature. Numerically and semi-analytically it was shown that regardless of the input distributions for K, f_i, U_i^k, C_i, $D_A C_i$, and K^{AB}, the complicated structural form of the mass matrix above can be simplified by assuming that the leading contribution to $\widetilde{\mathcal{M}}_{ij}$ takes the general following form,

$$\bar{\mathcal{M}}_{ij} = B_{iA} B_{Aj} \ , \tag{I.5}$$

where the contracted sub-matrix B_{iA} is defined as,

$$B_{iA} = 2\pi \frac{e^{k/2}}{f_i} U_i^K \mathcal{Z}_{Ak} \ , \tag{I.6}$$

with $\mathcal{Z}_{Ak}$ a matrix constructed of Kähler covariant derivatives. The approximation made in Eq. (I.5) is subject to the arguments that the matrix B_{iA} should be a $N \times (N + L)$ dimensional isotropic matrix constructed solely from statistical IID variables with zero mean and unitary variance. The spectral properties of a matrix of this form are well known from the Marčhenko-Pastur limiting law of RMT as discussed in Section 5.2.4.1.

Appendix J

Superradiance Statistical Model

J.1 Black Hole Mass-Spin Data Coordinates

We model any BH data using the collected candidates in Table 6.2 and Table 6.3 via two-dimensional multivariate gaussian distributions, where $x = M_{\rm BH}$ and $y = a_*$. There are N_d data points d_i comprising the data set $\{d_i\}$. For each point in the data set the values of $M_{\rm BH}$ and a_* and their associated errors form centred data values $(\bar{x}, \bar{y})$ with errors (σ_x, σ_y). We are interested in the probability that a given model, $\mathcal{M}$, is excluded given the data, $\{d_i\}$: $P_{\rm ex}(\mathcal{M}|\{d_i\})$. Since a single data point in the disallowed region would exclude the model, $P_{\rm ex}(\mathcal{M}|\{d_i\})$ is given by the probability that any single data point is above the BH superradiance isocontour boundaries for each value of l. For a large number of data points, this is a relatively tricky combinatorial problem. However, the probability is normalised such that,

$$P_{\rm ex}(\mathcal{M}|\{d_i\}) = 1 - P_{\rm allowed}(\mathcal{M}|\{d_i\}) \ . \tag{J.1}$$

Now we can simply use the binomial theorem (or a simple probability tree) to highlight that $P_{\rm allowed}(\mathcal{M}|\{d_i\})$ is simply the cumulative probability that all data

points simultaneously fluctuate below the isocontour boundary limits,

$$P_{\text{allowed}}(\mathcal{M}|\{d_i\}) = \prod_i P_{\text{allowed}}(\mathcal{M}|d_i) \ , \tag{J.2}$$

where $P_{\text{allowed}}(\mathcal{M}|d_i)$ is simply the volume of the bivariate Gaussian function contained outside the isocontour boundary denoted by the function $y = f(x)$. In order to evaluate $P_{\text{allowed}}(\mathcal{M}|d_i)$ in a numerically efficient manner, we introduce two simplifying assumptions. Firstly, we assume each point is modelled under the null formalism where there is zero covariance between x and y, i.e. the covariance matrix of the error bounds is isotropic. Secondly, the error on the two-dimensional data can be evaluated using an effective one dimensional error [886, 913]. These two simplifications allow us to use the standard Gaussian error function to evaluate $P_{\text{allowed}}(\mathcal{M}|d_i)$, rather than the more numerically expensive integral under the curve. The shape of the BH superradiance isocontours $y = f(x)$, which only have support over finite x, requires this procedure to be evaluated in two separate regimes.

J.2 Effective One-Dimensional Errors

When the contour is defined, we fix the contour as $y = f(x)$ and evaluate the effective one dimensional error in y, Σ_y, as,

$$\Sigma_y^2 = \sigma_y^2 + f'(\bar{x})^2 \sigma_x^2 \ . \tag{J.3}$$

When the contour is not defined for a given value of x, we must instead use the inverse function $x = g(y)$ and evaluate the effective error in x, Σ_x, as,

$$\Sigma_x^2 = \sigma_x^2 + g'(\bar{y})^2 \sigma_y^2 \ . \tag{J.4}$$

This procedure for the effective errors is represented visually with example BHs in Fig. J.1. Since any defined functions are given numerically, the inverse function and

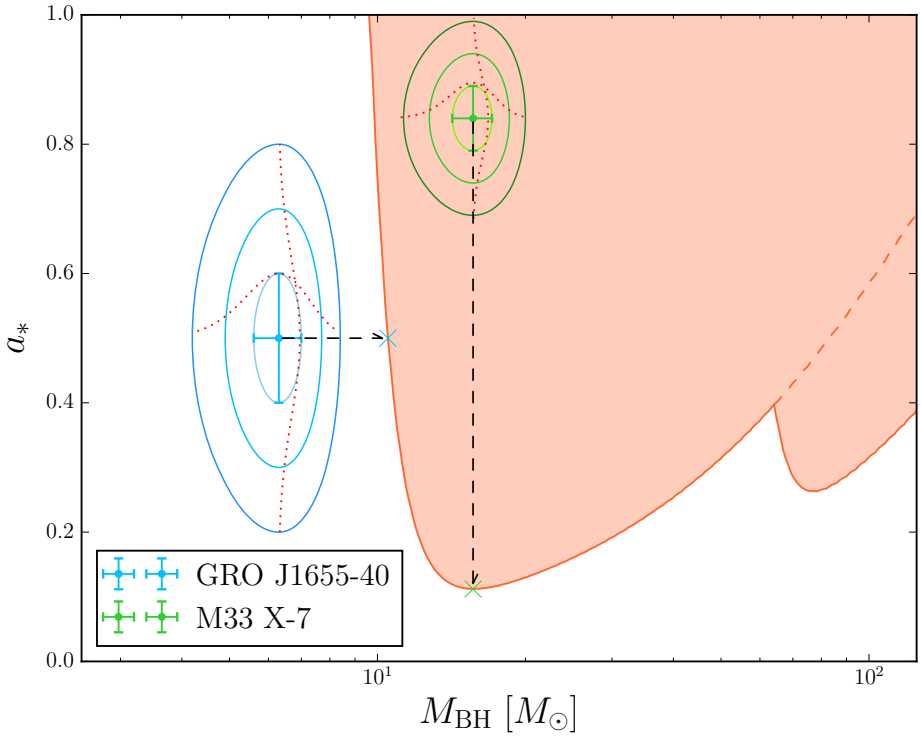


Figure J.1: Visual representation of the statistical model methodology using two example stellar BHs, GRO J1655-40 and M33 X-7 (see Table 6.2) with instability bound function for an axion mass, $\mu_{\rm ax} = 10^{-12.75}$ eV. Each data point is shown with 1σ, 2σ and 3σ error contour levels. Effective errors are calculated by projection onto either the x or y axis (crossed points) depending on whether the BH falls inside the instability bounds where $f(x)$ is defined.

its derivative are trivial to evaluate given the original function. A complication does arise since $g(y)$ is multivalued, taking two possible values g_1 and g_2 for a single y. We choose to evaluate the derivative $g'(\bar{y})$ at the nearest part of the contour (i.e. the value g_i which minimises $\bar{x} - g(\bar{y})$), and evaluate the error function between the two values g_1 and g_2. This approximation only affects $P_{\rm allowed}(\mathcal{M}|d_i)$ for values close to unity, while $P_{\rm ex}(\mathcal{M}|\{d_i\})$ is dominated by the smallest values of $P_{\rm allowed}(\mathcal{M}|d_i)$ contained well within the contours where $f(x)$ has support and is single valued.

The use of the effective errors in, Eq. (J.3) and Eq. (J.4), assumes that, for a given data point, the functions $f(x)$ and $g(y)$ are smooth at the mean value over the range of the chosen errors. When a BH data point with large errors sits close to

a cusp in the contours the exclusion probability computed from the effective error is smaller than the true answer. Cusps in the total contour are caused by the meeting of individual contours with different $l = m$ mode values, each of which are smooth. A more exact procedure would thus be to compute the probability individually for each $l = m$ contour, and then compute the cumulative probability using a product over each value of $l = m$. This would increase the number of likelihood evaluations by $l_{\max} \times N_d$, and for speed of computation we do not perform this more accurate calculation. The more accurate calculation would give larger exclusion probabilities (reducing the overall effective size of BH errors), and so the approximate computation is more conservative in the sense that it does not give overly strong exclusions.

Appendix K

Outlying Cosmologies

K.1 Axionic Cosmic Densities

In this appendix we provide a picture of the evolution of the cosmological densities in the context of example cosmologies which would not pass the cuts outlined in Section 7.3. In Fig. K.1 we show the cosmological evolution for three example configurations using the isometric Y-matrix model for a population of axions behaving as DM. We allow the equal field condition scaling parameter $\bar{f}$ to approach the upper bound, $\bar{f} \to M_{\rm Pl}$ (*blue* line). The large value for $\bar{f}$ causes the population of axions to collectively "*inflate*" the Universe for a period ($10^{-4} \lesssim a \lesssim 10^{-1}$) with the collective energy density overshooting the expected value of $z_{\rm eq}$ before it has entered the scaling regime behaving as non-relativistic matter. The evolution of the collective axion field density as DM begins to scale accordingly at an approximate time of $z \approx 0$ with a value of $z_{\rm eq}$ far too early in the cosmic history. Such cosmologies return axion DM domination with $\Omega_{\rm DM} \approx 0.9999$ at the current time.

Decreasing the scale of $\bar{f}$ to $0.1 M_{\rm Pl}$ (*cyan* line) causes the axions to account for the correct total DM density at the current time where $\Omega_{\rm DM} = 0.2528$. The reduced initial field conditions cause the axions to enter the correct scaling regime with a significantly reduced redshift. The inset of Fig. K.1 shows the value of $z_{\rm eq}$ falling

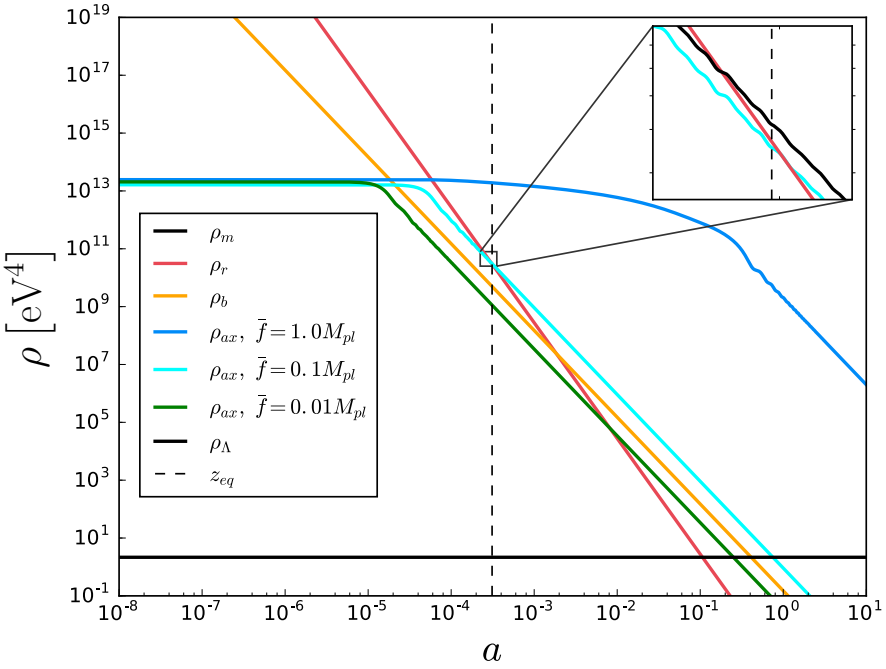


Figure K.1: Evolution of the collective axion density, $\rho_{\rm ax}$, using $n_{\rm ax} = 20$, where the mass eigenstates are drawn from the isometric Y-matrix model. We highlight the effect of using different initial field condition scales set by $\bar{f}$ where values of $\bar{f} \to 1$ returning cosmologies which don't fulfil the criterion for acceptable values of $z_{\rm eq}$ by collectively "*inflating*" the universe. In this particular example when $\bar{f} = 0.1\ M_{\rm Pl}$, the total matter density scales in order to provide the correct value of $z_{\rm eq}$ as shown in the *inset*, the oscillatory nature of the function from the oscillating fields with lighter masses.

within acceptable bounds (crossing of black ($\rho_b + \rho_{\rm ax}$) and red (ρ_r) lines). Further decreasing $\bar{f} = 0.01 M_{\rm Pl}$ (*green* line) corresponds to an example configuration in which the total matter density is insufficient for the Universe to reach redshift zero within ten Hubble times according to our numerical configurations. The lowest value of z reached corresponded to an axion DM density parameter value of $\Omega_{\rm DM} = 0.0119$.

In Fig. K.2 we show potential configurations which do not pass the acceleration criterion, $\ddot{a} > 0$ or give dominant contributions to the critical density at $z = 0$ for isometric Y-matrix model cosmologies. The axion density is set by the initial field displacement and axion mass, $m_a^2\phi^2$. Without a sufficient scaling of the initial

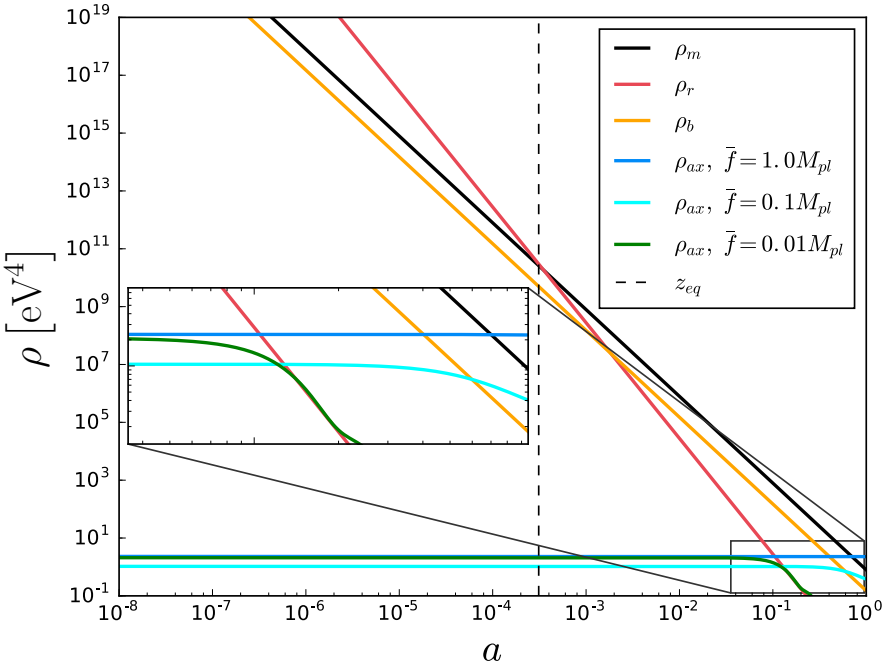


Figure K.2: Evolution of the collective axion density, $\rho_{\rm ax}$, for $n_{\rm ax} = 20$ fields reproducing example DE cosmologies with mass eigenstates drawn from the isometric Y-matrix model. We highlight the effect of using different scales for $\bar{f}$, where insufficient values of $\bar{f}$ lead to outlying cosmologies which do not satisfy the acceleration criterion, $\ddot{a} > 0$. This is shown in the *inset* where the quintessence fields begin to scale as matter components for values of the cosmic scale factor too small to provide sufficient DE at $a(t) \simeq 1$.

field displacements (*light blue* and *green* line), the axion masses need to be higher to account for the acceptable amount of DE density. However, this generally causes the axion to start oscillating earlier following the condition $m_a \leq H$, which returns smaller values of $\Omega_{\rm DE}$. Increasing the value of the scaling $\bar{f}$ in this configuration would satisfy an accelerating universe with sufficient DE density. The increased value of $\bar{f} = 0.1M_{\rm Pl}$ enhances the final DE density at $z = 0$ returning a value of $\Omega_{\rm DE} = 0.1979$. Finally the configuration (*blue* line) with $\bar{f} = 1.0M_{\rm Pl}$ is sufficient for an effective DE cosmology returning a value of $\Omega_{\rm DE} = 0.7732$.

Bibliography

[1] 8 - on the theory of stars. pages 60 – 62, 1965. doi: https://doi.org/10.1016/B978-0-08-010586-4.50013-4. URL http://www.sciencedirect.com/science/article/pii/B9780080105864500134.

[2] *Communications on Pure and Applied Mathematics*, 65(11):1528–1638, 2012. doi: 10.1002/cpa.21415. URL https://onlinelibrary.wiley.com/doi/abs/10.1002/cpa.21415.

[3] G. Aad et al. Observation of a new particle in the search for the Standard Model Higgs boson with the ATLAS detector at the LHC. *Phys. Lett.*, B716: 1–29, 2012. doi: 10.1016/j.physletb.2012.08.020.

[4] J. Aasi et al. Advanced LIGO. *Class. Quant. Grav.*, 32:074001, 2015. doi: 10.1088/0264-9381/32/7/074001.

[5] A. Aazami and R. Easther. Cosmology from random multifield potentials. *JCAP*, 0603:013, 2006. doi: 10.1088/1475-7516/2006/03/013.

[6] S. Abachi et al. Search for high mass top quark production in $p\overline{p}$ collisions at $\sqrt{s} =$ 1.8 tev. *Phys. Rev. Lett.*, 74:2422–2426, Mar 1995. doi: 10.1103/PhysRevLett.74.2422. URL https://link.aps.org/doi/10.1103/PhysRevLett.74.2422.

[7] K. N. Abazajian et al. Light Sterile Neutrinos: A White Paper. 2012.

[8] B. P. Abbott, R. Abbott, T. D. Abbott, M. R. Abernathy, F. Acernese, K. Ackley, C. Adams, T. Adams, P. Addesso, R. X. Adhikari, and et al. Ob-

servation of Gravitational Waves from a Binary Black Hole Merger. *Physical Review Letters*, 116(6):061102, Feb. 2016. doi: 10.1103/PhysRevLett.116.061102.

[9] B. P. Abbott et al. Observation of Gravitational Waves from a Binary Black Hole Merger. *Phys. Rev. Lett.*, 116(6):061102, 2016. doi: 10.1103/PhysRevLett.116.061102.

[10] B. P. Abbott et al. Binary Black Hole Mergers in the first Advanced LIGO Observing Run. *Phys. Rev.*, X6(4):041015, 2016. doi: 10.1103/PhysRevX.6.041015.

[11] B. P. Abbott et al. GW170104: Observation of a 50-Solar-Mass Binary Black Hole Coalescence at Redshift 0.2. *Phys. Rev. Lett.*, 118(22):221101, 2017. doi: 10.1103/PhysRevLett.118.221101.

[12] B. P. e. a. Abbott. Gw170814: A three-detector observation of gravitational waves from a binary black hole coalescence. *Phys. Rev. Lett.*, 119:141101, Oct 2017. doi: 10.1103/PhysRevLett.119.141101. URL `https://link.aps.org/doi/10.1103/PhysRevLett.119.141101`.

[13] L. F. Abbott and P. Sikivie. A Cosmological Bound on the Invisible Axion. *Phys. Lett.*, B120:133–136, 1983. doi: 10.1016/0370-2693(83)90638-X. [,URL(1982)].

[14] F. Abe et al. Observation of top quark production in $\overline{p}p$ collisions with the collider detector at fermilab. *Phys. Rev. Lett.*, 74:2626–2631, Apr 1995. doi: 10.1103/PhysRevLett.74.2626. URL `https://link.aps.org/doi/10.1103/PhysRevLett.74.2626`.

[15] E. Abers and B. Lee. Gauge theories. *Phys. Rep.*, 9:1–2, Nov. 1973. doi: 10.1016/0370-1573(73)90027-6.

[16] A. Y. Abul-Magd. Non-extensive random matrix theory − a bridge connect-

ing chaotic and regular dynamics. *Physics Letters A*, 333:16–22, Nov. 2004. doi: 10.1016/j.physleta.2004.09.082.

[17] A. Y. Abul-Magd. Non-extensive random matrix theory approach to mixed regular-chaotic dynamics. *Phys. Rev. E*, 71(6):066207, Jun 2005. doi: 10.1103/PhysRevE.71.066207.

[18] A. Y. Abul-Magd. Nonextensive and superstatistical generalizations of random-matrix theory. *The European Physical Journal B*, 70(1):39–48, Jul 2009. ISSN 1434-6036. doi: 10.1140/epjb/e2009-00153-0. URL `https://doi.org/10.1140/epjb/e2009-00153-0`.

[19] A. Y. Abul-Magd, G. Akemann, and P. Vivo. Superstatistical generalisations of Wishart-Laguerre ensembles of random matrices. *arXiv e-prints*, art. arXiv:0811.1992, Nov 2008.

[20] B. S. Acharya. On Realizing N=1 superYang-Mills in M theory. 2000.

[21] B. S. Acharya. A Moduli fixing mechanism in M theory. 2002.

[22] B. S. Acharya and K. Bobkov. Kahler Independence of the G(2)-MSSM. *JHEP*, 09:001, 2010. doi: 10.1007/JHEP09(2010)001.

[23] B. S. Acharya and S. Gukov. M theory and singularities of exceptional holonomy manifolds. *Phys. Rept.*, 392:121–189, 2004. doi: 10.1016/j.physrep.2003.10.017.

[24] B. S. Acharya and C. Pongkitivanichkul. The Axiverse induced Dark Radiation Problem. *JHEP*, 04:009, 2016. doi: 10.1007/JHEP04(2016)009.

[25] B. S. Acharya and E. Witten. Chiral fermions from manifolds of G(2) holonomy. 2001.

[26] B. S. Acharya, F. Denef, and R. Valandro. Statistics of M theory vacua. *JHEP*, 06:056, 2005. doi: 10.1088/1126-6708/2005/06/056.

[27] B. S. Acharya, K. Bobkov, G. Kane, P. Kumar, and D. Vaman. An M theory

Solution to the Hierarchy Problem. *Phys. Rev. Lett.*, 97:191601, 2006. doi: 10.1103/PhysRevLett.97.191601.

[28] B. S. Acharya, K. Bobkov, G. L. Kane, P. Kumar, and J. Shao. Explaining the Electroweak Scale and Stabilizing Moduli in M Theory. *Phys. Rev.*, D76: 126010, 2007. doi: 10.1103/PhysRevD.76.126010.

[29] B. S. Acharya, K. Bobkov, G. L. Kane, J. Shao, and P. Kumar. The G(2)-MSSM: An M Theory motivated model of Particle Physics. *Phys. Rev.*, D78: 065038, 2008. doi: 10.1103/PhysRevD.78.065038.

[30] B. S. Acharya, P. Kumar, K. Bobkov, G. Kane, J. Shao, and S. Watson. Non-thermal Dark Matter and the Moduli Problem in String Frameworks. *JHEP*, 06:064, 2008. doi: 10.1088/1126-6708/2008/06/064.

[31] B. S. Acharya, K. Bobkov, and P. Kumar. An M Theory Solution to the Strong CP Problem and Constraints on the Axiverse. *JHEP*, 11:105, 2010. doi: 10.1007/JHEP11(2010)105.

[32] B. S. Acharya, G. Kane, E. Kuflik, and R. Lu. Theory and Phenomenology of μ in M theory. *JHEP*, 05:033, 2011. doi: 10.1007/JHEP05(2011)033.

[33] B. S. Acharya, G. Kane, and P. Kumar. Compactified String Theories – Generic Predictions for Particle Physics. *Int. J. Mod. Phys.*, A27:1230012, 2012. doi: 10.1142/S0217751X12300128.

[34] B. S. Acharya, G. Kane, and E. Kuflik. Bounds on scalar masses in theories of moduli stabilization. *Int. J. Mod. Phys.*, A29:1450073, 2014. doi: 10.1142/S0217751X14500730.

[35] B. S. Acharya, K. Bo?ek, M. Crispim Romo, S. F. King, and C. Pongkitivanichkul. SO(10) Grand Unification in M theory on a G2 manifold. *Phys. Rev.*, D92(5):055011, 2015. doi: 10.1103/PhysRevD.92.055011.

[36] B. S. Acharya, K. Bo?ek, M. Crispim Romo, S. F. King, and C. Pongkiti-

vanichkul. Neutrino mass from M Theory SO(10). *JHEP*, 11:173, 2016. doi: 10.1007/JHEP11(2016)173.

[37] P. A. R. Ade et al. Planck 2015 results. XIII. Cosmological parameters. *Astron. Astrophys.*, 594:A13, 2016. doi: 10.1051/0004-6361/201525830.

[38] S. L. Adler. Axial-vector vertex in spinor electrodynamics. *Phys. Rev.*, 177: 2426–2438, Jan 1969. doi: 10.1103/PhysRev.177.2426. URL `https://link.aps.org/doi/10.1103/PhysRev.177.2426`.

[39] S. L. Adler, J. Gamboa, F. Mendez, and J. Lopez-Sarrion. Axions and 'Light Shining Through a Wall': A Detailed Theoretical Analysis. *Annals Phys.*, 323:2851–2872, 2008. doi: 10.1016/j.aop.2008.02.001.

[40] N. Aghanim et al. Planck 2018 results. VI. Cosmological parameters. 2018.

[41] P. Agrawal, G. Marques-Tavares, and W. Xue. Opening up the QCD axion window. *JHEP*, 03:049, 2018. doi: 10.1007/JHEP03(2018)049.

[42] J. M. Aguirregabiria, L. P. Chimento, and R. Lazkoz. Quintessence as k-essence. *Phys. Lett.*, B631:93–99, 2005. doi: 10.1016/j.physletb.2005.10.011.

[43] K.-J. Ahn and P. R. Shapiro. Formation and evolution of the self-interacting dark matter halos. *Mon. Not. Roy. Astron. Soc.*, 363:1092–1124, 2005. doi: 10.1111/j.1365-2966.2005.09492.x.

[44] G. Akemann and E. Kanzieper. Integrable Structure of Ginibre's Ensemble of Real Random Matrices and a Pfaffian Integration Theorem. *J. Statist. Phys.*, 129:1159–1231, 2007. doi: 10.1007/s10955-007-9381-2.

[45] G. Akemann and L. Shifrin. A generalization of dyson's integration theorem for determinants. *Journal of Physics A: Mathematical and Theoretical*, 40 (32):F785–F791, jul 2007. doi: 10.1088/1751-8113/40/32/f01. URL `https://doi.org/10.1088%2F1751-8113%2F40%2F32%2Ff01`.

[46] G. Akemann, J. Baik, and P. Di Francesco. *The Ox-*

ford Handbook of Random Matrix Theory. Oxford Handbooks in Mathematics. Oxford University Press, 2011. ISBN 9780199574001. URL https://global.oup.com/academic/product/the-oxford-handbook-of-random-matrix-theory-9780199574001?cc=us&lang=en&.

[47] G. Akemann, T. Guhr, M. Kieburg, R. Wegner, and T. Wirtz. Completing the picture for the smallest eigenvalue of real wishart matrices. *Phys. Rev. Lett.*, 113:250201, Dec 2014. doi: 10.1103/PhysRevLett.113.250201. URL https://link.aps.org/doi/10.1103/PhysRevLett.113.250201.

[48] K. Akiyama et al. First M87 Event Horizon Telescope Results. IV. Imaging the Central Supermassive Black Hole. *Astrophys. J.*, 875(1):L4, 2019. doi: 10.3847/2041-8213/ab0e85.

[49] K. Akiyama et al. First M87 Event Horizon Telescope Results. II. Array and Instrumentation. *Astrophys. J.*, 875(1):L2, 2019. doi: 10.3847/2041-8213/ab0c96.

[50] K. Akiyama et al. First M87 Event Horizon Telescope Results. I. The Shadow of the Supermassive Black Hole. *Astrophys. J.*, 875(1):L1, 2019. doi: 10.3847/2041-8213/ab0ec7.

[51] K. Akiyama et al. First M87 Event Horizon Telescope Results. VI. The Shadow and Mass of the Central Black Hole. *Astrophys. J.*, 875(1):L6, 2019. doi: 10.3847/2041-8213/ab1141.

[52] K. Akiyama et al. First M87 Event Horizon Telescope Results. V. Physical Origin of the Asymmetric Ring. *Astrophys. J.*, 875(1):L5, 2019. doi: 10.3847/2041-8213/ab0f43.

[53] K. Akiyama et al. First M87 Event Horizon Telescope Results. III. Data Processing and Calibration. *Astrophys. J.*, 875(1):L3, 2019. doi: 10.3847/2041-8213/ab0c57.

[54] S. Alam et al. The clustering of galaxies in the completed SDSS-III Baryon Oscillation Spectroscopic Survey: cosmological analysis of the DR12 galaxy sample. *Mon. Not. Roy. Astron. Soc.*, 470(3):2617–2652, 2017. doi: 10.1093/mnras/stx721.

[55] A. Albrecht and P. J. Steinhardt. Cosmology for grand unified theories with radiatively induced symmetry breaking. *Phys. Rev. Lett.*, 48:1220–1223, Apr 1982. doi: 10.1103/PhysRevLett.48.1220. URL `https://link.aps.org/doi/10.1103/PhysRevLett.48.1220`.

[56] C. Alcock et al. The MACHO project: Microlensing results from 5.7 years of LMC observations. *Astrophys. J.*, 542:281–307, 2000. doi: 10.1086/309512.

[57] C. Alexander, G. M. Cordeiro, E. M. Ortega, and J. M. Sarabia. Generalized beta-generated distributions. *Computational Statistics & Data Analysis*, 56(6):1880 – 1897, 2012. ISSN 0167-9473. doi: https://doi.org/10.1016/j.csda.2011.11.015. URL `http://www.sciencedirect.com/science/article/pii/S0167947311004129`.

[58] Y. Alhassid. The statistical theory of quantum dots. *Rev. Mod. Phys.*, 72:895–968, Oct 2000. doi: 10.1103/RevModPhys.72.895. URL `https://link.aps.org/doi/10.1103/RevModPhys.72.895`.

[59] S. W. Allen, A. E. Evrard, and A. B. Mantz. Cosmological Parameters from Observations of Galaxy Clusters. *ARA&A*, 49(1):409–470, Sep 2011. doi: 10.1146/annurev-astro-081710-102514.

[60] R. A. Alpher and R. Herman. Evolution of the Universe. *Nature*, 162:774–775, Nov. 1948. doi: 10.1038/162774b0.

[61] R. A. Alpher, H. Bethe, and G. Gamow. The origin of chemical elements. *Phys. Rev.*, 73:803–804, Apr 1948. doi: 10.1103/PhysRev.73.803. URL `https://link.aps.org/doi/10.1103/PhysRev.73.803`.

[62] J. Alsing, A. Heavens, A. H. Jaffe, A. Kiessling, B. Wandelt, and T. Hoff-

mann. Hierarchical Cosmic Shear Power Spectrum Inference. *Mon. Not. Roy. Astron. Soc.*, 455(4):4452–4466, 2016. doi: 10.1093/mnras/stv2501.

[63] A. Altland and M. R. Zirnbauer. Nonstandard symmetry classes in mesoscopic normal-superconducting hybrid structures. *Phys. Rev. B*, 55(2):1142–1161, Jan 1997. doi: 10.1103/PhysRevB.55.1142.

[64] R. Altman, J. Gray, Y.-H. He, V. Jejjala, and B. D. Nelson. A Calabi-Yau Database: Threefolds Constructed from the Kreuzer-Skarke List. *JHEP*, 02: 158, 2015. doi: 10.1007/JHEP02(2015)158.

[65] E. Alvarez, L. Alvarez-Gaume, and Y. Lozano. An Introduction to T duality in string theory. *Nucl. Phys. Proc. Suppl.*, 41:1–20, 1995. doi: 10.1016/0920-5632(95)00429-D.

[66] I. Alvarez, J. Niemi, and M. Simpson. Bayesian inference for a covariance matrix. *arXiv e-prints*, art. arXiv:1408.4050, Aug 2014.

[67] L. Alvarez-Gaume and E. Witten. Gravitational Anomalies. *Nucl. Phys.*, B234:269, 1984. doi: 10.1016/0550-3213(84)90066-X. [,269(1983)].

[68] P. Amaro-Seoane et al. Low-frequency gravitational-wave science with eLISA/NGO. *Class. Quant. Grav.*, 29:124016, 2012. doi: 10.1088/0264-9381/29/12/124016.

[69] P. Amaro-Seoane et al. eLISA/NGO: Astrophysics and cosmology in the gravitational-wave millihertz regime. *GW Notes*, 6:4–110, 2013.

[70] L. Amendola and R. Barbieri. Dark matter from an ultra-light pseudo-Goldsone-boson. *Phys. Lett.*, B642:192–196, 2006. doi: 10.1016/j.physletb.2006.08.069.

[71] P. Anastasopoulos, T. P. T. Dijkstra, E. Kiritsis, and A. N. Schellekens. Orientifolds, hypercharge embeddings and the Standard Model. *Nucl. Phys.*, B759:83–146, 2006. doi: 10.1016/j.nuclphysb.2006.10.013.

[72] L. B. Anderson, J. Gray, Y.-H. He, and A. Lukas. Exploring Positive Monad Bundles And A New Heterotic Standard Model. *JHEP*, 02:054, 2010. doi: 10.1007/JHEP02(2010)054.

[73] L. B. Anderson, J. Gray, A. Lukas, and E. Palti. Two Hundred Heterotic Standard Models on Smooth Calabi-Yau Threefolds. *Phys. Rev.*, D84:106005, 2011. doi: 10.1103/PhysRevD.84.106005.

[74] L. B. Anderson, J. Gray, A. Lukas, and E. Palti. Heterotic Line Bundle Standard Models. *JHEP*, 06:113, 2012. doi: 10.1007/JHEP06(2012)113.

[75] L. B. Anderson, A. Constantin, J. Gray, A. Lukas, and E. Palti. A Comprehensive Scan for Heterotic SU(5) GUT models. *JHEP*, 01:047, 2014. doi: 10.1007/JHEP01(2014)047.

[76] T. W. Anderson. The non-central wishart distribution and certain problems of multivariate statistics. *Ann. Math. Statist.*, 17(4):409–431, 12 1946. doi: 10.1214/aoms/1177730882. URL `https://doi.org/10.1214/aoms/1177730882`.

[77] T. W. Anderson. Asymptotic theory for principal component analysis. *Ann. Math. Statist.*, 34(1):122–148, 03 1963. doi: 10.1214/aoms/1177704248. URL `https://doi.org/10.1214/aoms/1177704248`.

[78] W. Anderson. Über die grenzdichte der materie und der energie. *Zeitschrift für Physik*, 56(11):851–856, Nov 1929. ISSN 0044-3328. doi: 10.1007/BF01340146. URL `https://doi.org/10.1007/BF01340146`.

[79] B. Andreas and G. Curio. Extension Bundles and the Standard Model. *JHEP*, 07:053, 2007. doi: 10.1088/1126-6708/2007/07/053.

[80] A. Andreev, A. Kanto, and P. Malo. Simple approach for distribution selection in the pearson system. WorkingPaper W-388, Helsingin kauppakorkeakoulu, 2005.

[81] I. Antoniadis, C. P. Bachas, and C. Kounnas. Four-Dimensional Superstrings. *Nucl. Phys.*, B289:87, 1987. doi: 10.1016/0550-3213(87)90372-5.

[82] A. Aoki and J. Soda. Detecting ultralight axion dark matter wind with laser interferometers. 2016.

[83] T. Aoyama, M. Hayakawa, T. Kinoshita, and M. Nio. Tenth-Order QED Contribution to the Electron g-2 and an Improved Value of the Fine Structure Constant. *Phys. Rev. Lett.*, 109:111807, 2012. doi: 10.1103/PhysRevLett.109.111807.

[84] T. Aoyama, M. Hayakawa, T. Kinoshita, and M. Nio. Tenth-order electron anomalous magnetic moment: Contribution of diagrams without closed lepton loops. *Phys. Rev. D*, 91(3):033006, Feb. 2015. doi: 10.1103/PhysRevD.91.033006.

[85] T. Aoyama, T. Kinoshita, and M. Nio. Revised and Improved Value of the QED Tenth-Order Electron Anomalous Magnetic Moment. *Phys. Rev.*, D97 (3):036001, 2018. doi: 10.1103/PhysRevD.97.036001.

[86] P. APIAN. volume 18th ed. Antverpiae, Apud Ioannem VVithagium, 1564. URL `http://catalog.hathitrust.org/api/volumes/oclc/781861973.html`.

[87] M. Archidiacono, E. Giusarma, S. Hannestad, and O. Mena. Cosmic dark radiation and neutrinos. *Adv. High Energy Phys.*, 2013:191047, 2013. doi: 10.1155/2013/191047.

[88] M. Archidiacono, S. Hannestad, A. Mirizzi, G. Raffelt, and Y. Y. Y. Wong. Axion hot dark matter bounds after Planck. *JCAP*, 1310:020, 2013. doi: 10.1088/1475-7516/2013/10/020.

[89] P. Arias, J. Jaeckel, J. Redondo, and A. Ringwald. Optimizing Light-Shining-through-a-Wall Experiments for Axion and other WISP Searches. *Phys. Rev.*, D82:115018, 2010. doi: 10.1103/PhysRevD.82.115018.

[90] P. Arias, D. Cadamuro, M. Goodsell, J. Jaeckel, J. Redondo, and A. Ringwald. WISPy Cold Dark Matter. *JCAP*, 1206:013, 2012. doi: 10.1088/1475-7516/2012/06/013.

[91] F. Arias-Aragon and L. Merlo. The Minimal Flavour Violating Axion. *JHEP*, 10:168, 2017. doi: 10.1007/JHEP10(2017)168.

[92] Aristotle. *Metaphysics*. The Internet Classics Archive, 350BCE. URL `http://classics.mit.edu/Aristotle/metaphysics.html`.

[93] O. Arizmendi and V. Prez Abreu. On the non-classical infinite divisibility of power semicircle distributions. *Communications on Stochastic Analysis*, 4, 06 2010. doi: 10.31390/cosa.4.2.03.

[94] O. Arizmendi, P. Tarrago, and C. Vargas. Subordination methods for free deconvolution. *arXiv e-prints*, art. arXiv:1711.08871, Nov 2017.

[95] N. Arkani-Hamed, A. G. Cohen, and H. Georgi. Electroweak symmetry breaking from dimensional deconstruction. *Phys. Lett.*, B513:232–240, 2001. doi: 10.1016/S0370-2693(01)00741-9.

[96] N. Arkani-Hamed, A. G. Cohen, E. Katz, and A. E. Nelson. The Littlest Higgs. *JHEP*, 07:034, 2002. doi: 10.1088/1126-6708/2002/07/034.

[97] N. Arkani-Hamed, A. G. Cohen, E. Katz, A. E. Nelson, T. Gregoire, and J. G. Wacker. The Minimal moose for a little Higgs. *JHEP*, 08:021, 2002. doi: 10.1088/1126-6708/2002/08/021.

[98] N. Arkani-Hamed, H.-C. Cheng, P. Creminelli, and L. Randall. Extra natural inflation. *Phys. Rev. Lett.*, 90:221302, 2003. doi: 10.1103/PhysRevLett.90.221302.

[99] N. Arkani-Hamed, H.-C. Cheng, M. A. Luty, and S. Mukohyama. Ghost condensation and a consistent infrared modification of gravity. *JHEP*, 05:074, 2004. doi: 10.1088/1126-6708/2004/05/074.

[100] N. Arkani-Hamed, L. Motl, A. Nicolis, and C. Vafa. The String landscape, black holes and gravity as the weakest force. *JHEP*, 06:060, 2007. doi: 10.1088/1126-6708/2007/06/060.

[101] C. Armendariz-Picon. Could dark energy be vector-like? *JCAP*, 0407:007, 2004. doi: 10.1088/1475-7516/2004/07/007.

[102] C. Armendariz-Picon, V. F. Mukhanov, and P. J. Steinhardt. Essentials of k essence. *Phys. Rev.*, D63:103510, 2001. doi: 10.1103/PhysRevD.63.103510.

[103] E. Armengaud et al. Axion searches with the EDELWEISS-II experiment. *JCAP*, 1311:067, 2013. doi: 10.1088/1475-7516/2013/11/067.

[104] E. Armengaud et al. Constraining the mass of light bosonic dark matter using SDSS Lyman-α forest. 2017.

[105] D. Armstrong. Generalized Noncrossing Partitions and Combinatorics of Coxeter Groups. *arXiv Mathematics e-prints*, art. math/0611106, Nov 2006.

[106] A. Arvanitaki and S. Dubovsky. Exploring the String Axiverse with Precision Black Hole Physics. *Phys. Rev.*, D83:044026, 2011. doi: 10.1103/PhysRevD.83.044026.

[107] A. Arvanitaki, S. Dimopoulos, S. Dubovsky, N. Kaloper, and J. March-Russell. String Axiverse. *Phys. Rev.*, D81:123530, 2010. doi: 10.1103/PhysRevD.81.123530.

[108] A. Arvanitaki, M. Baryakhtar, and X. Huang. Discovering the QCD axion with black holes and gravitational waves. *Phys. Rev. D*, 91(8):084011, Apr. 2015. doi: 10.1103/PhysRevD.91.084011.

[109] A. Arvanitaki, M. Baryakhtar, and X. Huang. Discovering the QCD Axion with Black Holes and Gravitational Waves. *Phys. Rev.*, D91(8):084011, 2015. doi: 10.1103/PhysRevD.91.084011.

[110] A. Arvanitaki, M. Baryakhtar, S. Dimopoulos, S. Dubovsky, and R. Lasenby.

Black hole mergers and the QCD axion at Advanced LIGO. *Phys. Rev. D*, 95(4):043001, Feb. 2017. doi: 10.1103/PhysRevD.95.043001.

[111] A. Arvanitaki, M. Baryakhtar, S. Dimopoulos, S. Dubovsky, and R. Lasenby. Black Hole Mergers and the QCD Axion at Advanced LIGO. *Phys. Rev.*, D95(4):043001, 2017. doi: 10.1103/PhysRevD.95.043001.

[112] S. Ashok and M. R. Douglas. Counting flux vacua. *JHEP*, 01:060, 2004. doi: 10.1088/1126-6708/2004/01/060.

[113] A. Ashoorioon, H. Firouzjahi, and M. M. Sheikh-Jabbari. M-flation: Inflation From Matrix Valued Scalar Fields. *JCAP*, 0906:018, 2009. doi: 10.1088/1475-7516/2009/06/018.

[114] A. Ashoorioon, H. Firouzjahi, and M. M. Sheikh-Jabbari. Matrix Inflation and the Landscape of its Potential. *JCAP*, 1005:002, 2010. doi: 10.1088/1475-7516/2010/05/002.

[115] A. Ashtekar and J. Lewandowski. Quantum theory of geometry. 1: Area operators. *Class. Quant. Grav.*, 14:A55–A82, 1997. doi: 10.1088/0264-9381/14/1A/006.

[116] A. Ashtekar and J. Lewandowski. Background independent quantum gravity: A Status report. *Class. Quant. Grav.*, 21:R53, 2004. doi: 10.1088/0264-9381/21/15/R01.

[117] P. S. Aspinwall and R. Kallosh. Fixing all moduli for M-theory on K3xK3. *JHEP*, 10:001, 2005. doi: 10.1088/1126-6708/2005/10/001.

[118] S. J. Asztalos et al. Squid-based microwave cavity search for dark-matter axions. *Phys. Rev. Lett.*, 104:041301, Jan 2010. doi: 10.1103/PhysRevLett.104.041301. URL `https://link.aps.org/doi/10.1103/PhysRevLett.104.041301`.

[119] M. Atiyah and E. Witten. M theory dynamics on a manifold of G(2) holon-

omy. *Adv. Theor. Math. Phys.*, 6:1–106, 2003. doi: 10.4310/ATMP.2002.v6.n1.a1.

[120] J. J. Aubert, U. Becker, P. J. Biggs, J. Burger, M. Chen, G. Everhart, P. Goldhagen, J. Leong, T. McCorriston, T. G. Rhoades, M. Rohde, S. C. C. Ting, S. L. Wu, and Y. Y. Lee. Experimental observation of a heavy particle j. *Phys. Rev. Lett.*, 33:1404–1406, Dec 1974. doi: 10.1103/PhysRevLett.33.1404. URL `https://link.aps.org/doi/10.1103/PhysRevLett.33.1404`.

[121] É. Aubourg et al. Cosmological implications of baryon acoustic oscillation measurements. *Phys. Rev. D*, 92(12):123516, Dec. 2015. doi: 10.1103/PhysRevD.92.123516.

[122] J. E. Augustin et al. Discovery of a narrow resonance in e^+e^- annihilation. *Phys. Rev. Lett.*, 33:1406–1408, Dec 1974. doi: 10.1103/PhysRevLett.33.1406. URL `https://link.aps.org/doi/10.1103/PhysRevLett.33.1406`.

[123] F. T. Avignone, III et al. Experimental search for solar axions via coherent Primakoff conversion in a germanium spectrometer. *Phys. Rev. Lett.*, 81:5068–5071, 1998. doi: 10.1103/PhysRevLett.81.5068.

[124] C. Baccigalupi, S. Matarrese, and F. Perrotta. Tracking extended quintessence. *Phys. Rev.*, D62:123510, 2000. doi: 10.1103/PhysRevD.62.123510.

[125] T. C. Bachlechner. On Gaussian Random Supergravity. *JHEP*, 04:054, 2014. doi: 10.1007/JHEP04(2014)054.

[126] T. C. Bachlechner. Axionic Band Structure of the Cosmological Constant. *Phys. Rev.*, D93(2):023522, 2016. doi: 10.1103/PhysRevD.93.023522.

[127] T. C. Bachlechner, D. Marsh, L. McAllister, and T. Wrase. Supersymmetric Vacua in Random Supergravity. *JHEP*, 01:136, 2013. doi: 10.1007/JHEP01(2013)136.

[128] T. C. Bachlechner, M. Dias, J. Frazer, and L. McAllister. Chaotic inflation with kinetic alignment of axion fields. *Phys. Rev.*, D91(2):023520, 2015. doi: 10.1103/PhysRevD.91.023520.

[129] T. C. Bachlechner, C. Long, and L. McAllister. Planckian Axions in String Theory. *JHEP*, 12:042, 2015. doi: 10.1007/JHEP12(2015)042.

[130] T. C. Bachlechner, C. Long, and L. McAllister. Planckian Axions and the Weak Gravity Conjecture. *JHEP*, 01:091, 2016. doi: 10.1007/JHEP01(2016)091.

[131] T. C. Bachlechner, K. Eckerle, O. Janssen, and M. Kleban. Systematics of Aligned Axions. *JHEP*, 11:036, 2017. doi: 10.1007/JHEP11(2017)036.

[132] T. C. Bachlechner, K. Eckerle, O. Janssen, and M. Kleban. Multiple-axion framework. *Phys. Rev.*, D98(6):061301, 2018. doi: 10.1103/PhysRevD.98.061301.

[133] T. C. Bachlechner, K. Eckerle, O. Janssen, and M. Kleban. Axion Landscape Cosmology. 2018.

[134] T. C. Bachlechner, K. Eckerle, O. Janssen, and M. Kleban. The Axidental Universe. 2019.

[135] H. Baer, K.-Y. Choi, J. E. Kim, and L. Roszkowski. Dark matter production in the early Universe: beyond the thermal WIMP paradigm. *Phys. Rept.*, 555:1–60, 2015. doi: 10.1016/j.physrep.2014.10.002.

[136] R. Bähre et al. Any light particle search II ?Technical Design Report. *JINST*, 8:T09001, 2013. doi: 10.1088/1748-0221/8/09/T09001.

[137] J. Bai and S. Shi. Estimating High Dimensional Covariance Matrices and its Applications. *Annals of Economics and Finance*, 12(2):199–215, November 2011. URL `https://ideas.repec.org/a/cuf/journl/y2011v12i2p199-215.html`.

[138] J. W. BAI, Z. & SILVERSTEIN. volume 3rd ed. New York, Springer., 2010. URL http://public.eblib.com/choice/publicfullrecord.aspx?p=510460.

[139] Z. D. Bai and J. W. Silverstein. Clt for linear spectral statistics of large-dimensional sample covariance matrices. *Ann. Probab.*, 32(1A):553–605, 01 2004. doi: 10.1214/aop/1078415845. URL https://doi.org/10.1214/aop/1078415845.

[140] Z. D. Bai and Y. Q. Yin. Convergence to the semicircle law. *Ann. Probab.*, 16(2):863–875, 04 1988. doi: 10.1214/aop/1176991792. URL https://doi.org/10.1214/aop/1176991792.

[141] Z. D. Bai and Y. Q. Yin. Limit of the smallest eigenvalue of a large dimensional sample covariance matrix. *Ann. Probab.*, 21(3):1275–1294, 07 1993. doi: 10.1214/aop/1176989118. URL https://doi.org/10.1214/aop/1176989118.

[142] J. Baik, G. Ben Arous, and S. Peche. Phase transition of the largest eigenvalue for non-null complex sample covariance matrices. *arXiv Mathematics e-prints*, Mar. 2004.

[143] C. A. Baker et al. An Improved experimental limit on the electric dipole moment of the neutron. *Phys. Rev. Lett.*, 97:131801, 2006. doi: 10.1103/PhysRevLett.97.131801.

[144] V. Balasubramanian, P. Berglund, J. P. Conlon, and F. Quevedo. Systematics of moduli stabilisation in calabi-yau flux compactifications. *JHEP*, page 007, 2005.

[145] R. Balian. Random matrices and information theory. *Il Nuovo Cimento B (1965-1970)*, 57(1):183–193, Sep 1968. ISSN 1826-9877. doi: 10.1007/BF02710326. URL https://doi.org/10.1007/BF02710326.

[146] C. Bambi, A. D. Dolgov, and A. A. Petrov. Black holes as antimatter factories. *JCAP*, 0909:013, 2009. doi: 10.1088/1475-7516/2009/09/013.

[147] C. Bambi, K. Freese, S. Vagnozzi, and L. Visinelli. Testing the rotational nature of the supermassive object M87* from the circularity and size of its first image. *Phys. Rev.*, D100(4):044057, 2019. doi: 10.1103/PhysRevD.100.044057.

[148] T. Banica, S. Belinschi, M. Capitaine, and B. Collins. Free Bessel laws. *arXiv e-prints*, art. arXiv:0710.5931, Oct 2007.

[149] T. Banks and M. Dine. The Cosmology of string theoretic axions. *Nucl. Phys.*, B505:445–460, 1997. doi: 10.1016/S0550-3213(97)00413-6.

[150] T. Banks, D. B. Kaplan, and A. E. Nelson. Cosmological implications of dynamical supersymmetry breaking. *Phys. Rev.*, D49:779–787, 1994. doi: 10.1103/PhysRevD.49.779.

[151] T. Banks, M. Berkooz, S. H. Shenker, G. Moore, and P. J. Steinhardt. Modular cosmology. *Phys. Rev. D*, 52:3548–3562, Sep 1995. doi: 10.1103/PhysRevD.52.3548. URL `https://link.aps.org/doi/10.1103/PhysRevD.52.3548`.

[152] T. Banks, W. Fischler, S. H. Shenker, and L. Susskind. M theory as a matrix model: A Conjecture. *Phys. Rev.*, D55:5112–5128, 1997. doi: 10.1103/PhysRevD.55.5112. [,435(1996)].

[153] T. Banks, W. Fischler, I. R. Klebanov, and L. Susskind. Schwarzschild black holes from matrix theory. *Phys. Rev. Lett.*, 80:226–229, 1998. doi: 10.1103/PhysRevLett.80.226.

[154] T. Banks, M. Dine, P. J. Fox, and E. Gorbatov. On the possibility of large axion decay constants. *JCAP*, 0306:001, 2003. doi: 10.1088/1475-7516/2003/06/001.

[155] Z. Bao, J. Hu, G. Pan, and W. Zhou. Canonical correlation coefficients of high-dimensional Gaussian vectors: finite rank case. *arXiv e-prints*, art. arXiv:1704.02408, Apr 2017.

[156] J. Barbour. Shape Dynamics: An Introduction. In *Proceedings, Quantum Field Theory and Gravity: Conceptual and Mathematical Advances in the Search for a Unified Framework: Regensburg, Germany, September 28-October 1, 2010*, pages 257–297, 2012. doi: 10.1007/978-3-0348-0043-3_13.

[157] J. M. Bardeen, B. Carter, and S. W. Hawking. The Four laws of black hole mechanics. *Commun. Math. Phys.*, 31:161–170, 1973. doi: 10.1007/BF01645742.

[158] W. A. Bardeen. Anomalous currents in gauge field theories. *Nuclear Physics B*, 75(2):246 – 258, 1974. ISSN 0550-3213. doi: https://doi.org/10.1016/0550-3213(74)90546-X. URL `http://www.sciencedirect.com/science/article/pii/055032137490546X`.

[159] W. A. Bardeen and S.-H. H. Tye. Current algebra applied to properties of the light Higgs boson. *Physics Letters B*, 74:229–232, Apr. 1978. doi: 10.1016/0370-2693(78)90560-9.

[160] D. Y. Bardin. Field theory and the standard model. 1999.

[161] J. Barnard, R. McCulloch, and X. Meng. Modeling covariance matrices in terms of standard deviations and correlations, with application to shrinkage. *Statistica Sinica*, 10(4):1281–1311, 10 2000. ISSN 1017-0405.

[162] O. Barndorff-Nielsen and C. Halgreen. Infinite divisibility of the hyperbolic and generalized inverse gaussian distributions. *Zeitschrift für Wahrscheinlichkeitstheorie und Verwandte Gebiete*, 38(4):309–311, Dec 1977. ISSN 1432-2064. doi: 10.1007/BF00533162. URL `https://doi.org/10.1007/BF00533162`.

[163] O. E. Barndorff-Nielsen. Normal inverse gaussian distributions and stochastic

volatility modelling. *Scandinavian Journal of Statistics*, 24(1):1–13, 1997. doi: 10.1111/1467-9469.00045. URL `https://onlinelibrary.wiley.com/doi/abs/10.1111/1467-9469.00045`.

[164] S. M. Barr. A Natural Class of Nonpeccei-quinn Models. *Phys. Rev.*, D30: 1805, 1984. doi: 10.1103/PhysRevD.30.1805.

[165] S. M. Barr. Solving the Strong CP Problem Without the Peccei-Quinn Symmetry. *Phys. Rev. Lett.*, 53:329, 1984. doi: 10.1103/PhysRevLett.53.329.

[166] T. Barreiro, E. J. Copeland, and N. J. Nunes. Quintessence arising from exponential potentials. *Phys. Rev.*, D61:127301, 2000. doi: 10.1103/PhysRevD.61.127301.

[167] M. Baryakhtar, R. Lasenby, and M. Teo. Black hole superradiance signatures of ultralight vectors. *Phys. Rev. D*, 96(3):035019, Aug. 2017. doi: 10.1103/PhysRevD.96.035019.

[168] M. Baryakhtar, R. Lasenby, and M. Teo. Black Hole Superradiance Signatures of Ultralight Vectors. *Phys. Rev.*, D96(3):035019, 2017. doi: 10.1103/PhysRevD.96.035019.

[169] B. A. Bassett and R. Hlozek. Baryon Acoustic Oscillations. 2009.

[170] B. A. Bassett, S. Tsujikawa, and D. Wands. Inflation dynamics and reheating. *Rev. Mod. Phys.*, 78:537–589, 2006. doi: 10.1103/RevModPhys.78.537.

[171] E. Battaner and E. Florido. The Rotation curve of spiral galaxies and its cosmological implications. *Fund. Cosmic Phys.*, 21:1–154, 2000.

[172] D. Battefeld and T. Battefeld. Non-Gaussianities in N-flation. *JCAP*, 0705: 012, 2007. doi: 10.1088/1475-7516/2007/05/012.

[173] D. Battefeld and S. Kawai. Preheating after N-flation. *Phys. Rev.*, D77: 123507, 2008. doi: 10.1103/PhysRevD.77.123507.

[174] D. Battefeld, T. Battefeld, and S. Schulz. On the Unlikeliness of Multi-Field

Inflation: Bounded Random Potentials and our Vacuum. *JCAP*, 1206:034, 2012. doi: 10.1088/1475-7516/2012/06/034.

[175] M. Bauer, M. Neubert, and A. Thamm. LHC as an Axion Factory: Probing an Axion Explanation for $(g-2)_\mu$ with Exotic Higgs Decays. *Phys. Rev. Lett.*, 119(3):031802, 2017. doi: 10.1103/PhysRevLett.119.031802.

[176] D. Baumann and L. McAllister. *Inflation and String Theory*. Cambridge Monographs on Mathematical Physics. Cambridge University Press, 2015. ISBN 9781107089693, 9781316237182. doi: 10.1017/CBO9781316105733. URL `http://www.cambridge.org/mw/academic/subjects/physics/theoretical-physics-and-mathematical-physics/inflation-and-string-theory?format=HB`.

[177] D. Baumann, A. Dymarsky, I. R. Klebanov, and L. McAllister. Towards an Explicit Model of D-brane Inflation. *JCAP*, 0801:024, 2008. doi: 10.1088/1475-7516/2008/01/024.

[178] D. Baumann, H. S. Chia, and R. A. Porto. Probing Ultralight Bosons with Binary Black Holes. *Phys. Rev.*, D99(4):044001, 2019. doi: 10.1103/PhysRevD.99.044001.

[179] C. Beasley and E. Witten. A Note on fluxes and superpotentials in M theory compactifications on manifolds of G(2) holonomy. *JHEP*, 07:046, 2002. doi: 10.1088/1126-6708/2002/07/046.

[180] C. Beasley, J. J. Heckman, and C. Vafa. GUTs and Exceptional Branes in F-theory - I. *JHEP*, 01:058, 2009. doi: 10.1088/1126-6708/2009/01/058.

[181] C. Beasley, J. J. Heckman, and C. Vafa. GUTs and Exceptional Branes in F-theory - II: Experimental Predictions. *JHEP*, 01:059, 2009. doi: 10.1088/1126-6708/2009/01/059.

[182] A. C. Becker et al. The SuperMACHO Microlensing Survey. *IAU Symp.*, 225:357, 2005. doi: 10.1017/S1743921305002164.

[183] K. Becker, M. Becker, J.-X. Fu, L.-S. Tseng, and S.-T. Yau. Anomaly cancellation and smooth non-Kahler solutions in heterotic string theory. *Nucl. Phys.*, B751:108–128, 2006. doi: 10.1016/j.nuclphysb.2006.05.034.

[184] K. Becker, M. Becker, and J. H. Schwarz. *String Theory and M-Theory: A Modern Introduction*. Cambridge University Press, 2006. doi: 10.1017/CBO9780511816086.

[185] C. W. J. Beenakker. Applications of random matrix theory to condensed matter and optical physics. *arXiv e-prints*, art. arXiv:0904.1432, Apr 2009.

[186] K. Behrndt, M. Cvetic, and T. Liu. Classification of supersymmetric flux vacua in M theory. *Nucl. Phys.*, B749:25–68, 2006. doi: 10.1016/j.nuclphysb.2006.04.018.

[187] J. D. Bekenstein. Relativistic gravitation theory for the MOND paradigm. *Phys. Rev.*, D70:083509, 2004. doi: 10.1103/PhysRevD.70.083509,10.1103/PhysRevD.71.069901. [Erratum: Phys. Rev.D71,069901(2005)].

[188] A. A. Belavin, A. M. Polyakov, A. S. Schwartz, and Yu. S. Tyupkin. Pseudoparticle Solutions of the Yang-Mills Equations. *Phys. Lett.*, B59:85–87, 1975. doi: 10.1016/0370-2693(75)90163-X. [,350(1975)].

[189] S. Belinschi, F. Benaych-Georges, and A. Guionnet. Regularization by free additive convolution, square and rectangular cases. *arXiv e-prints*, art. arXiv:0706.1419, Jun 2007.

[190] S. T. Belinschi. The lebesgue decomposition of the free additive convolution of two probability distributions. *Probability Theory and Related Fields*, 142 (1):125–150, Sep 2008. ISSN 1432-2064. doi: 10.1007/s00440-007-0100-3. URL `https://doi.org/10.1007/s00440-007-0100-3`.

[191] S. T. Belinschi and H. Bercovici. A new approach to subordination results in free probability. *Journal d'Analyse Mathématique*, 101(1):357–365, Mar

2007. ISSN 1565-8538. doi: 10.1007/s11854-007-0013-1. URL https://doi.org/10.1007/s11854-007-0013-1.

[192] K. Benakli, Y. Chen, E. Dudas, and Y. Mambrini. Minimal model of gravitino dark matter. *Phys. Rev.*, D95(9):095002, 2017. doi: 10.1103/PhysRevD.95.095002.

[193] F. Benaych-Georges. Taylor expansions of R-transforms, application to supports and moments. *arXiv Mathematics e-prints*, art. math/0410459, Oct 2004.

[194] F. Benaych-Georges. Rectangular random matrices. Related convolution. *arXiv Mathematics e-prints*, art. math/0507336, Jul 2005.

[195] F. Benaych-Georges. Classical and free infinitely divisible distributions and random matrices. *Ann. Probab.*, 33(3):1134–1170, 05 2005. doi: 10.1214/009117904000000982. URL https://doi.org/10.1214/009117904000000982.

[196] F. Benaych-Georges. Infinitely divisible distributions for rectangular free convolution: classification and matricial interpretation. *Probability Theory and Related Fields*, 139(1):143–189, Sep 2007. ISSN 1432-2064. doi: 10.1007/s00440-006-0042-1. URL https://doi.org/10.1007/s00440-006-0042-1.

[197] F. Benaych-Georges. On a surprising relation between the Marchenko-Pastur law, rectangular and square free convolutions. *arXiv e-prints*, art. arXiv:0808.3938, Aug 2008.

[198] F. Benaych-Georges and R. Rao Nadakuditi. The eigenvalues and eigenvectors of finite, low rank perturbations of large random matrices. *arXiv e-prints*, art. arXiv:0910.2120, Oct 2009.

[199] F. Benaych-Georges and R. Rao Nadakuditi. The singular values and vectors of low rank perturbations of large rectangular random matrices. *arXiv e-prints*, art. arXiv:1103.2221, Mar 2011.

[200] M. C. Bento, O. Bertolami, and A. A. Sen. Generalized chaplygin gas, accelerated expansion, and dark-energy-matter unification. *Phys. Rev. D*, 66:043507, Aug 2002. doi: 10.1103/PhysRevD.66.043507. URL `https://link.aps.org/doi/10.1103/PhysRevD.66.043507`.

[201] M. C. Bento, O. Bertolami, and A. A. Sen. Generalized Chaplygin gas model: Dark energy - dark matter unification and CMBR constraints. *Gen. Rel. Grav.*, 35:2063–2069, 2003. doi: 10.1023/A:1026207312105.

[202] H. Bercovici and D. Voiculescu. Free convolution of measures with unbounded support. *Indiana University Mathematics Journal*, 42(3):733–773, 1993. ISSN 00222518, 19435258. URL `http://www.jstor.org/stable/24897118`.

[203] H. Bercovici, V. Pata, and P. Biane. Stable laws and domains of attraction in free probability theory. *Annals of Mathematics*, 149(3):1023–1060, 1999. ISSN 0003486X. URL `http://www.jstor.org/stable/121080`.

[204] Z. Berezhiani. Mirror world and its cosmological consequences. *Int. J. Mod. Phys.*, A19:3775–3806, 2004. doi: 10.1142/S0217751X04020075.

[205] V. Berezinsky and J. W. F. Valle. The KeV majoron as a dark matter particle. *Phys. Lett.*, B318:360–366, 1993. doi: 10.1016/0370-2693(93)90140-D.

[206] M. Berg, E. Pajer, and S. Sjors. Dante's Inferno. *Phys. Rev.*, D81:103535, 2010. doi: 10.1103/PhysRevD.81.103535.

[207] J. L. Bernal, L. Verde, and A. G. Riess. The trouble withh0. *Journal of Cosmology and Astroparticle Physics*, 2016(10):019?019, Oct 2016. ISSN 1475-7516. doi: 10.1088/1475-7516/2016/10/019. URL `http://dx.doi.org/10.1088/1475-7516/2016/10/019`.

[208] E. Berti, V. Cardoso, and M. Casals. Eigenvalues and eigenfunctions of spin-weighted spheroidal harmonics in four and higher dimensions. *Phys. Rev.*, D73:024013, 2006. doi: 10.1103/PhysRevD.73.109902,10.1103/PhysRevD.73.024013. [Erratum: Phys. Rev.D73,109902(2006)].

[209] E. Berti, R. Brito, C. F. B. Macedo, G. Raposo, and J. L. Rosa. Ultralight boson cloud depletion in binary systems. *Phys. Rev.*, D99(10):104039, 2019. doi: 10.1103/PhysRevD.99.104039.

[210] O. Bertolami. Time Dependant Cosmological Term. *Nuovo Cim.*, B93:36–42, 1986. doi: 10.1007/BF02728301.

[211] O. Bertolami. Brans-dicke Cosmology With a Scalar Field Dependent Cosmological Term. *Fortsch. Phys.*, 34:829–833, 1986. doi: 10.1002/prop.19860341204.

[212] G. Bertone and D. Hooper. History of dark matter. *Rev. Mod. Phys.*, 90(4): 045002, 2018. doi: 10.1103/RevModPhys.90.045002.

[213] A. C. Bertuola, O. Bohigas, and M. P. Pato. Family of generalized random matrix ensembles. *Phys. Rev. E*, 70:065102, Dec 2004. doi: 10.1103/PhysRevE.70.065102. URL `https://link.aps.org/doi/10.1103/PhysRevE.70.065102`.

[214] D. Bessis. A new method in the combinatorics of the topological expansion. *Comm. Math. Phys.*, 69(2):147–163, 1979. URL `https://projecteuclid.org:443/euclid.cmp/1103905449`.

[215] M. Betz, F. Caspers, M. Gasior, M. Thumm, and S. W. Rieger. First results of the CERN Resonant Weakly Interacting sub-eV Particle Search (CROWS). *Phys. Rev. D*, 88(7):075014, Oct. 2013. doi: 10.1103/PhysRevD.88.075014.

[216] F. L. Bezrukov and M. Shaposhnikov. The Standard Model Higgs boson as the inflaton. *Phys. Lett.*, B659:703–706, 2008. doi: 10.1016/j.physletb.2007.11.072.

[217] P. Bianchi, M. Debbah, M. Maida, and J. Najim. Performance of statistical tests for single-source detection using random matrix theory. *IEEE Transactions on Information Theory*, 57(4):2400–2419, April 2011. ISSN 0018-9448. doi: 10.1109/TIT.2011.2111710.

[218] P. Biane. On the free convolution with a semi-circular distribution. *Indiana University Mathematics Journal*, 46(3):705–718, 1997. ISSN 00222518, 19435258. URL http://www.jstor.org/stable/24899639.

[219] P. Biane. Processes with free increments. *Mathematische Zeitschrift*, 227 (1):143–174, Jan 1998. ISSN 1432-1823. doi: 10.1007/PL00004363. URL https://doi.org/10.1007/PL00004363.

[220] N. Bilic, G. B. Tupper, and R. D. Viollier. Unification of dark matter and dark energy: The Inhomogeneous Chaplygin gas. *Phys. Lett.*, B535:17–21, 2002. doi: 10.1016/S0370-2693(02)01716-1.

[221] N. Bilic, R. J. Lindebaum, G. B. Tupper, and R. D. Viollier. Nonlinear evolution of dark matter and dark energy in the Chaplygin-gas cosmology. *JCAP*, 0411:008, 2004. doi: 10.1088/1475-7516/2004/11/008.

[222] P. Binetruy and G. R. Dvali. D term inflation. *Phys. Lett.*, B388:241–246, 1996. doi: 10.1016/S0370-2693(96)01083-0.

[223] P. Binétruy and M. K. Gaillard. Candidates for the inflaton field in superstring models. *Phys. Rev. D*, 34:3069–3083, Nov 1986. doi: 10.1103/PhysRevD.34.3069. URL https://link.aps.org/doi/10.1103/PhysRevD.34.3069.

[224] S. Birrer et al. H0LiCOW - IX. Cosmographic analysis of the doubly imaged quasar SDSS 1206+4332 and a new measurement of the Hubble constant. *Mon. Not. Roy. Astron. Soc.*, 484:4726, 2019. doi: 10.1093/mnras/stz200.

[225] A. N. Bishop, P. Del Moral, and A. Niclas. An Introduction to Wishart Matrix Moments. *arXiv e-prints*, art. arXiv:1710.10864, Oct 2017.

[226] T. Bjorkmo and M. C. D. Marsh. Manyfield Inflation in Random Potentials. *JCAP*, 1802(02):037, 2018. doi: 10.1088/1475-7516/2018/02/037.

[227] J. J. Blanco-Pillado, C. P. Burgess, J. M. Cline, C. Escoda, M. Gomez-Reino,

R. Kallosh, A. D. Linde, and F. Quevedo. Racetrack inflation. *JHEP*, 11: 063, 2004. doi: 10.1088/1126-6708/2004/11/063.

[228] J. J. Blanco-Pillado, A. Vilenkin, and M. Yamada. Inflation in Random Landscapes with two energy scales. *JHEP*, 02:130, 2018. doi: 10.1007/JHEP02(2018)130.

[229] D. Blas, D. L. Nacir, and S. Sibiryakov. Ultra-Light Dark Matter Resonates with Binary Pulsars. 2016.

[230] M. Blaszczyk, S. Groot Nibbelink, M. Ratz, F. Ruehle, M. Trapletti, and P. K. S. Vaudrevange. A Z2xZ2 standard model. *Phys. Lett.*, B683:340–348, 2010. doi: 10.1016/j.physletb.2009.12.036.

[231] P. M. Bleher. Lectures on random matrix models. The Riemann-Hilbert approach. *arXiv e-prints*, art. arXiv:0801.1858, Jan. 2008.

[232] A. Bloemendal and B. Virág. Limits of spiked random matrices I. *arXiv e-prints*, Nov. 2010.

[233] A. Bloemendal and B. Virág. Limits of spiked random matrices II. *arXiv e-prints*, Sept. 2011.

[234] R. Blumenhagen, M. Cvetic, P. Langacker, and G. Shiu. Toward realistic intersecting D-brane models. *Ann. Rev. Nucl. Part. Sci.*, 55:71–139, 2005. doi: 10.1146/annurev.nucl.55.090704.151541.

[235] R. Blumenhagen, B. Kors, D. Lust, and S. Stieberger. Four-dimensional String Compactifications with D-Branes, Orientifolds and Fluxes. *Phys. Rept.*, 445:1–193, 2007. doi: 10.1016/j.physrep.2007.04.003.

[236] R. Blumenhagen, M. Cvetic, D. Lust, R. Richter, and T. Weigand. Non-perturbative Yukawa Couplings from String Instantons. *Phys. Rev. Lett.*, 100:061602, 2008. doi: 10.1103/PhysRevLett.100.061602.

[237] R. Blumenhagen, V. Braun, T. W. Grimm, and T. Weigand. GUTs in Type

IIB Orientifold Compactifications. *Nucl. Phys.*, B815:1–94, 2009. doi: 10.1016/j.nuclphysb.2009.02.011.

[238] R. Blumenhagen, M. Cvetic, S. Kachru, and T. Weigand. D-Brane Instantons in Type II Orientifolds. *Ann. Rev. Nucl. Part. Sci.*, 59:269–296, 2009. doi: 10.1146/annurev.nucl.010909.083113.

[239] R. Blumenhagen, T. W. Grimm, B. Jurke, and T. Weigand. F-theory uplifts and GUTs. *JHEP*, 09:053, 2009. doi: 10.1088/1126-6708/2009/09/053.

[240] R. Blumenhagen, T. W. Grimm, B. Jurke, and T. Weigand. Global f-theory guts. *Nuclear Physics B*, 829(1):325 – 369, 2010. ISSN 0550-3213. doi: https://doi.org/10.1016/j.nuclphysb.2009.12.013. URL `http://www.sciencedirect.com/science/article/pii/S0550321309006622`.

[241] P. Bode, J. P. Ostriker, and N. Turok. Halo Formation in Warm Dark Matter Models. *ApJ*, 556:93–107, July 2001. doi: 10.1086/321541.

[242] P. Bode, J. P. Ostriker, and N. Turok. Halo formation in warm dark matter models. *Astrophys. J.*, 556:93–107, 2001. doi: 10.1086/321541.

[243] C. G. Boehmer and T. Harko. Physics of dark energy particles. *Found. Phys.*, 38:216, 2008. doi: 10.1007/s10701-007-9199-4.

[244] K. Bo?ek. *Particle phenomenology from M theory inspired models*. PhD thesis, King's Coll. London, 2018-04. URL `https://kclpure.kcl.ac.uk/portal/en/theses/particle-phenomenology-from-m-theory-inspired-models(f03bc0dc-3bda-4c6d-.html`.

[245] M. Bojowald and H. A. Morales-Tecotl. Cosmological Applications of Loop Quantum Gravity. *Lect. Notes Phys.*, 646:421–462, 2004. doi: 10.1007/978-3-540-40918-2_17.

[246] M. Bolz, A. Brandenburg, and W. Buchmuller. Thermal produc-

tion of gravitinos. *Nucl. Phys.*, B606:518–544, 2001. doi: 10.1016/S0550-3213(01)00132-8,10.1016/j.nuclphysb.2007.09.020. [Erratum: Nucl. Phys.B790,336(2008)].

[247] L. Bombelli, J. Lee, D. Meyer, and R. D. Sorkin. Space-time as a causal set. *Phys. Rev. Lett.*, 59:521–524, Aug 1987. doi: 10.1103/PhysRevLett.59.521. URL https://link.aps.org/doi/10.1103/PhysRevLett.59.521.

[248] V. Bonvin et al. H0LiCOW V. New COSMOGRAIL time delays of HE0435-1223: H_0 to 3.8% precision from strong lensing in a flat ΛCDM model. *Mon. Not. Roy. Astron. Soc.*, 465(4):4914–4930, 2017. doi: 10.1093/mnras/stw3006.

[249] M. Born and P. Jordan. Zur quantenmechanik. *Zeitschrift für Physik*, 34 (1):858–888, Dec 1925. ISSN 0044-3328. doi: 10.1007/BF01328531. URL https://doi.org/10.1007/BF01328531.

[250] M. Born, W. Heisenberg, and P. Jordan. Zur quantenmechanik. ii. *Zeitschrift für Physik*, 35(8):557–615, Aug 1926. ISSN 0044-3328. doi: 10.1007/BF01379806. URL https://doi.org/10.1007/BF01379806.

[251] S. Bose et al. No cores in dark matter-dominated dwarf galaxies with bursty star formation histories. *Mon. Not. Roy. Astron. Soc.*, 486(4):4790–4804, 2019. doi: 10.1093/mnras/stz1168.

[252] A. Bosma. *The distribution and kinematics of neutral hydrogen in spiral galaxies of various morphological types*. PhD thesis, PhD Thesis, Groningen Univ., (1978), 1978.

[253] A. Bosma. 21-cm line studies of spiral galaxies. I - Observations of the galaxies NGC 5033, 3198, 5055, 2841, and 7331. *AJ*, 86:1791–1824, Dec. 1981. doi: 10.1086/113062.

[254] A. Bosma. 21-cm line studies of spiral galaxies. II. The distribution and

kinematics of neutral hydrogen in spiral galaxies of various morphological types. *AJ*, 86:1825–1846, Dec. 1981. doi: 10.1086/113063.

[255] V. Bouchard and R. Donagi. An su(5) heterotic standard model. *Physics Letters B*, 633(6):783 – 791, 2006. ISSN 0370-2693. doi: https://doi.org/10.1016/j.physletb.2005.12.042. URL `http://www.sciencedirect.com/science/article/pii/S0370269305018496`.

[256] V. Bouchard and R. Donagi. An SU(5) heterotic standard model. *Phys. Lett.*, B633:783–791, 2006. doi: 10.1016/j.physletb.2005.12.042.

[257] V. Bouchard, A. Klemm, M. Marino, and S. Pasquetti. Remodeling the B-model. *Commun. Math. Phys.*, 287:117–178, 2009. doi: 10.1007/s00220-008-0620-4.

[258] J. P. Bouchaud and M. Potters. Financial Applications of Random Matrix Theory: a short review. *arXiv e-prints*, art. arXiv:0910.1205, Oct 2009.

[259] P. Bourgade and J. P. Keating. *Quantum Chaos, Random Matrix Theory, and the Riemann ζ-function*, pages 125–168. Springer Basel, Basel, 2013. ISBN 978-3-0348-0697-8. doi: 10.1007/978-3-0348-0697-8_4. URL `https://doi.org/10.1007/978-3-0348-0697-8_4`.

[260] R. Bousso and J. Polchinski. Quantization of four form fluxes and dynamical neutralization of the cosmological constant. *JHEP*, 06:006, 2000. doi: 10.1088/1126-6708/2000/06/006.

[261] R. Bousso, L. J. Hall, and Y. Nomura. Multiverse understanding of cosmological coincidences. *Phys. Rev. D*, 80(6):063510, Sept. 2009. doi: 10.1103/PhysRevD.80.063510.

[262] M. J. Bowick and E. Brézin. Universal scaling of the tail of the density of eigenvalues in random matrix models. *Physics Letters B*, 268(1):21–28, Oct. 1991. doi: 10.1016/0370-2693(91)90916-E.

[263] J. D. Bowman, A. E. E. Rogers, R. A. Monsalve, T. J. Mozdzen, and N. Mahesh. An absorption profile centred at 78 megahertz in the sky-averaged spectrum. *Nature*, 555:67–70, Mar. 2018. doi: 10.1038/nature25792.

[264] A. Boyarsky, O. Ruchayskiy, and M. Shaposhnikov. The Role of sterile neutrinos in cosmology and astrophysics. *Ann. Rev. Nucl. Part. Sci.*, 59:191–214, 2009. doi: 10.1146/annurev.nucl.010909.083654.

[265] M. Boylan-Kolchin, J. S. Bullock, and M. Kaplinghat. Too big to fail? The puzzling darkness of massive Milky Way subhaloes. *MNRAS*, 415(1):L40–L44, Jul 2011. doi: 10.1111/j.1745-3933.2011.01074.x.

[266] M. Boylan-Kolchin, J. S. Bullock, and M. Kaplinghat. The Milky Way's bright satellites as an apparent failure of ΛCDM. *Monthly Notices of the Royal Astronomical Society*, 422(2):1203–1218, 04 2012. ISSN 0035-8711. doi: 10.1111/j.1365-2966.2012.20695.x. URL `https://doi.org/10.1111/j.1365-2966.2012.20695.x`.

[267] B. Bozek, D. J. E. Marsh, J. Silk, and R. F. G. Wyse. Galaxy UV-luminosity function and reionization constraints on axion dark matter. *MNRAS*, 450:209–222, June 2015. doi: 10.1093/mnras/stv624.

[268] J. Braden, L. Kofman, and N. Barnaby. Reheating the Universe After Multi-Field Inflation. *JCAP*, 1007:016, 2010. doi: 10.1088/1475-7516/2010/07/016.

[269] G. C. Branco, P. M. Ferreira, L. Lavoura, M. N. Rebelo, M. Sher, and J. P. Silva. Theory and phenomenology of two-Higgs-doublet models. *Phys. Rept.*, 516:1–102, 2012. doi: 10.1016/j.physrep.2012.02.002.

[270] T. D. Brandt. Constraints on MACHO Dark Matter from Compact Stellar Systems in Ultra-Faint Dwarf Galaxies. *Astrophys. J.*, 824(2):L31, 2016. doi: 10.3847/2041-8205/824/2/L31.

[271] A. P. Braun. Tops as building blocks for G_2 manifolds. *JHEP*, 10:083, 2017. doi: 10.1007/JHEP10(2017)083.

[272] A. P. Braun and M. Del Zotto. Mirror Symmetry for G_2-Manifolds: Twisted Connected Sums and Dual Tops. *JHEP*, 05:080, 2017. doi: 10.1007/JHEP05(2017)080.

[273] A. P. Braun and M. Del Zotto. Towards generalized mirror symmetry for twisted connected sum g_2 manifolds. *Journal of High Energy Physics*, 2018 (3):82, Mar 2018. ISSN 1029-8479. doi: 10.1007/JHEP03(2018)082. URL `https://doi.org/10.1007/JHEP03(2018)082`.

[274] A. P. Braun and S. Schäfer-Nameki. Compact, Singular G_2-Holonomy Manifolds and M/Heterotic/F-Theory Duality. *JHEP*, 04:126, 2018. doi: 10.1007/JHEP04(2018)126.

[275] V. Braun, Y.-H. He, B. A. Ovrut, and T. Pantev. The Exact MSSM spectrum from string theory. *JHEP*, 05:043, 2006. doi: 10.1088/1126-6708/2006/05/043.

[276] P. Brax and J. Martin. Quintessence and supergravity. *Phys. Lett.*, B468: 40–45, 1999. doi: 10.1016/S0370-2693(99)01209-5.

[277] P. Brax, J. Martin, and A. Riazuelo. Exhaustive study of cosmic microwave background anisotropies in quintessential scenarios. *Phys. Rev.*, D62:103505, 2000. doi: 10.1103/PhysRevD.62.103505.

[278] P. Breitenlohner and D. Z. Freedman. Stability in gauged extended supergravity. *Annals of Physics*, 144(2):249 – 281, 1982. ISSN 0003-4916. doi: https://doi.org/10.1016/0003-4916(82)90116-6. URL `http://www.sciencedirect.com/science/article/pii/0003491682901166`.

[279] L. W. Brenneman and C. S. Reynolds. Constraining Black Hole Spin Via X-ray Spectroscopy. *Astrophys. J.*, 652:1028–1043, 2006. doi: 10.1086/508146.

[280] L. W. Brenneman, C. S. Reynolds, M. A. Nowak, R. C. Reis, M. Trippe, A. C. Fabian, K. Iwasawa, J. C. Lee, J. M. Miller, R. F. Mushotzky, K. Nandra,

and M. Volonteri. The Spin of the Supermassive Black Hole in NGC 3783. *ApJ*, 736:103, Aug. 2011. doi: 10.1088/0004-637X/736/2/103.

[281] E. Brézin, C. Itzykson, G. Parisi, and J. B. Zuber. Planar diagrams. *Comm. Math. Phys.*, 59(1):35–51, 1978. URL `https://projecteuclid.org:443/euclid.cmp/1103901558`.

[282] D. R. Brill, P. L. Chrzanowski, C. M. Pereira, E. D. Fackerell, and J. R. Ipser. Solution of the scalar wave equation in a kerr background by separation of variables. *Phys. Rev. D*, 5:1913–1915, Apr 1972. doi: 10.1103/PhysRevD.5.1913. URL `https://link.aps.org/doi/10.1103/PhysRevD.5.1913`.

[283] R. Brito, V. Cardoso, and P. Pani. Massive spin-2 fields on black hole spacetimes: Instability of the Schwarzschild and Kerr solutions and bounds on the graviton mass. *Phys. Rev.*, D88(2):023514, 2013. doi: 10.1103/PhysRevD.88.023514.

[284] R. Brito, V. Cardoso, and P. Pani. Black holes as particle detectors: evolution of superradiant instabilities. *Classical and Quantum Gravity*, 32(13):134001, July 2015. doi: 10.1088/0264-9381/32/13/134001.

[285] R. Brito, V. Cardoso, and P. Pani. Black holes as particle detectors: evolution of superradiant instabilities. *Class. Quant. Grav.*, 32(13):134001, 2015. doi: 10.1088/0264-9381/32/13/134001.

[286] R. Brito, V. Cardoso, and P. Pani. Superradiance. *Lect. Notes Phys.*, 906: pp.1–237, 2015. doi: 10.1007/978-3-319-19000-6.

[287] R. Brito, S. Ghosh, E. Barausse, E. Berti, V. Cardoso, I. Dvorkin, A. Klein, and P. Pani. Gravitational wave searches for ultralight bosons with LIGO and LISA. *Phys. Rev. D*, 96(6):064050, Sept. 2017. doi: 10.1103/PhysRevD.96.064050.

[288] R. Brito, S. Ghosh, E. Barausse, E. Berti, V. Cardoso, I. Dvorkin, A. Klein,

and P. Pani. Gravitational wave searches for ultralight bosons with LIGO and LISA. *Phys. Rev.*, D96(6):064050, 2017. doi: 10.1103/PhysRevD.96.064050.

[289] I. Brivio, M. B. Gavela, L. Merlo, K. Mimasu, J. M. No, R. del Rey, and V. Sanz. ALPs Effective Field Theory and Collider Signatures. *Eur. Phys. J.*, C77(8):572, 2017. doi: 10.1140/epjc/s10052-017-5111-3.

[290] C. Brodie and M. C. D. Marsh. The Spectra of Type IIB Flux Compactifications at Large Complex Structure. *JHEP*, 01:037, 2016. doi: 10.1007/JHEP01(2016)037.

[291] B. V. Bronk. Exponential ensemble for random matrices. *Journal of Mathematical Physics*, 6(2):228–237, 1965. doi: 10.1063/1.1704274. URL `https://doi.org/10.1063/1.1704274`.

[292] R. Brout and F. Englert. Spontaneous symmetry breaking in gauge theories: A Historical survey. In *High-energy physics. Proceedings, International Europhysics Conference, Jerusalem, Israel, August 19-25, 1997*, pages 3–10, 1998.

[293] J. Brown and C. Teitelboim. Dynamical neutralization of the cosmological constant. *Physics Letters B*, 195(2):177 – 182, 1987. ISSN 0370-2693. doi: https://doi.org/10.1016/0370-2693(87)91190-7. URL `http://www.sciencedirect.com/science/article/pii/0370269387911907`.

[294] D. Budker, P. W. Graham, M. Ledbetter, S. Rajendran, and A. O. Sushkov. Proposal for a cosmic axion spin precession experiment (casper). *Phys. Rev. X*, 4:021030, May 2014. doi: 10.1103/PhysRevX.4.021030. URL `https://link.aps.org/doi/10.1103/PhysRevX.4.021030`.

[295] W. L. Buntine. Theory Refinement on Bayesian Networks. *arXiv e-prints*, art. arXiv:1303.5709, Mar 2013.

[296] Z. Burda, R. A. Janik, and B. Waclaw. Spectrum of the product of indepen-

dent random Gaussian matrices. *Phys. Rev. E*, 81(4):041132, Apr 2010. doi: 10.1103/PhysRevE.81.041132.

[297] C. Burgess and D. Roest. Inflation by Alignment. *JCAP*, 1506(06):012, 2015. doi: 10.1088/1475-7516/2015/06/012.

[298] A. Burkert. The Structure of dark matter halos in dwarf galaxies. *IAU Symp.*, 171:175, 1996. doi: 10.1086/309560. [Astrophys. J.447,L25(1995)].

[299] Y.-F. Cai, E. N. Saridakis, M. R. Setare, and J.-Q. Xia. Quintom Cosmology: Theoretical implications and observations. *Phys. Rept.*, 493:1–60, 2010. doi: 10.1016/j.physrep.2010.04.001.

[300] R. R. Caldwell and M. Kamionkowski. The Physics of Cosmic Acceleration. *Ann. Rev. Nucl. Part. Sci.*, 59:397–429, 2009. doi: 10.1146/annurev-nucl-010709-151330.

[301] R. R. Caldwell and E. V. Linder. The Limits of quintessence. *Phys. Rev. Lett.*, 95:141301, 2005. doi: 10.1103/PhysRevLett.95.141301.

[302] R. R. Caldwell, R. Dave, and P. J. Steinhardt. Cosmological imprint of an energy component with general equation of state. *Phys. Rev. Lett.*, 80: 1582–1585, 1998. doi: 10.1103/PhysRevLett.80.1582.

[303] R. R. Caldwell, M. Kamionkowski, and N. N. Weinberg. Phantom energy: Dark energy with $\omega < -1$ causes a cosmic doomsday. *Phys. Rev. Lett.*, 91:071301, Aug 2003. doi: 10.1103/PhysRevLett.91.071301. URL `https://link.aps.org/doi/10.1103/PhysRevLett.91.071301`.

[304] R. R. Caldwell, W. Komp, L. Parker, and D. A. T. Vanzella. Sudden gravitational transition. *Phys. Rev. D*, 73:023513, Jan 2006. doi: 10.1103/PhysRevD.73.023513. URL `https://link.aps.org/doi/10.1103/PhysRevD.73.023513`.

[305] L. Calibbi, F. Goertz, D. Redigolo, R. Ziegler, and J. Zupan. Minimal axion

model from flavor. *Phys. Rev.*, D95(9):095009, 2017. doi: 10.1103/PhysRevD.95.095009.

[306] C. G. Callan, R. Dashen, and D. J. Gross. Toward a theory of the strong interactions. *Phys. Rev. D*, 17:2717–2763, May 1978. doi: 10.1103/PhysRevD.17.2717. URL `https://link.aps.org/doi/10.1103/PhysRevD.17.2717`.

[307] C. G. Callan, R. F. Dashen, and D. J. Gross. A theory of hadronic structure. *Phys. Rev. D*, 19:1826–1855, Mar 1979. doi: 10.1103/PhysRevD.19.1826. URL `https://link.aps.org/doi/10.1103/PhysRevD.19.1826`.

[308] P. Candelas, G. T. Horowitz, A. Strominger, and E. Witten. Vacuum configurations for superstrings. *Nuclear Physics B*, 258:46 – 74, 1985. ISSN 0550-3213. doi: https://doi.org/10.1016/0550-3213(85)90602-9. URL `http://www.sciencedirect.com/science/article/pii/0550321385906029`.

[309] P. Candelas, A. Constantin, and H. Skarke. An Abundance of K3 Fibrations from Polyhedra with Interchangeable Parts. *Commun. Math. Phys.*, 324:937–959, 2013. doi: 10.1007/s00220-013-1802-2.

[310] A. G. Cantrell, C. D. Bailyn, J. A. Orosz, J. E. McClintock, R. A. Remillard, C. S. Froning, J. Neilsen, D. M. Gelino, and L. Gou. The Inclination of the Soft X-Ray Transient A0620-00 and the Mass of its Black Hole. *ApJ*, 710:1127–1141, Feb. 2010. doi: 10.1088/0004-637X/710/2/1127.

[311] F. Capela, M. Pshirkov, and P. Tinyakov. Constraints on primordial black holes as dark matter candidates from capture by neutron stars. *Phys. Rev.*, D87(12):123524, 2013. doi: 10.1103/PhysRevD.87.123524.

[312] M. Capitaine. Exact separation phenomenon for the eigenvalues of large Information-Plus-Noise type matrices. Application to spiked models. *arXiv e-prints*, art. arXiv:1301.3940, Jan 2013.

[313] M. Capitaine and C. Donati-Martin. Spectrum of deformed random matrices and free probability. *arXiv e-prints*, art. arXiv:1607.05560, Jul 2016.

[314] L. Capparelli, G. Cavoto, J. Ferretti, F. Giazotto, A. D. Polosa, and P. Spagnolo. Axion-like particle searches with sub-THz photons. *Phys. Dark Univ.*, 12:37–44, 2016. doi: 10.1016/j.dark.2016.01.003.

[315] V. Cardoso and S. Yoshida. Superradiant instabilities of rotating black branes and strings. *JHEP*, 07:009, 2005. doi: 10.1088/1126-6708/2005/07/009.

[316] V. Cardoso, A. S. Miranda, E. Berti, H. Witek, and V. T. Zanchin. Geodesic stability, Lyapunov exponents and quasinormal modes. *Phys. Rev.*, D79: 064016, 2009. doi: 10.1103/PhysRevD.79.064016.

[317] V. Cardoso, Ó. J. C. Dias, G. S. Hartnett, M. Middleton, P. Pani, and J. E. Santos. Constraining the mass of dark photons and axion-like particles through black-hole superradiance. *JCAP*, 1803(03):043, 2018. doi: 10.1088/1475-7516/2018/03/043.

[318] J. Carifio, J. Halverson, D. Krioukov, and B. D. Nelson. Machine Learning in the String Landscape. *JHEP*, 09:157, 2017. doi: 10.1007/JHEP09(2017)157.

[319] G. Carleo, I. Cirac, K. Cranmer, L. Daudet, M. Schuld, N. Tishby, L. Vogt-Maranto, and L. Zdeborová. Machine learning and the physical sciences. 2019.

[320] B. Carr, F. Kuhnel, and M. Sandstad. Primordial Black Holes as Dark Matter. *Phys. Rev.*, D94(8):083504, 2016. doi: 10.1103/PhysRevD.94.083504.

[321] B. J. Carr and S. W. Hawking. Black holes in the early Universe. *Mon. Not. Roy. Astron. Soc.*, 168:399–415, 1974.

[322] S. M. Carroll. Quintessence and the rest of the world. *Phys. Rev. Lett.*, 81: 3067–3070, 1998. doi: 10.1103/PhysRevLett.81.3067.

[323] S. M. Carroll, W. H. Press, and E. L. Turner. The Cosmological constant. *Ann. Rev. Astron. Astrophys.*, 30:499–542, 1992. doi: 10.1146/annurev.aa.30.090192.002435.

[324] B. Carter. Hamilton-jacobi and schrödinger separable solutions of einstein's equations. *Comm. Math. Phys.*, 10(4):280–310, 1968. URL `https://projecteuclid.org:443/euclid.cmp/1103841118`.

[325] B. Carter. Axisymmetric black hole has only two degrees of freedom. *Phys. Rev. Lett.*, 26:331–333, Feb 1971. doi: 10.1103/PhysRevLett.26.331. URL `https://link.aps.org/doi/10.1103/PhysRevLett.26.331`.

[326] J. A. Casas and C. Munoz. Three Generation SU(3) x SU(2) x U(1)-Y Models from Orbifolds. *Phys. Lett.*, B214:63–69, 1988. doi: 10.1016/0370-2693(88)90452-2.

[327] J. A. Casas, E. K. Katehou, and C. Munoz. U(1) Charges in Orbifolds: Anomaly Cancellation and Phenomenological Consequences. *Nucl. Phys.*, B317:171–186, 1989. doi: 10.1016/0550-3213(89)90566-X.

[328] C. Caviezel, P. Koerber, S. Kors, D. Lust, T. Wrase, and M. Zagermann. On the Cosmology of Type IIA Compactifications on SU(3)-structure Manifolds. *JHEP*, 04:010, 2009. doi: 10.1088/1126-6708/2009/04/010.

[329] S. Cecotti, M. C. N. Cheng, J. J. Heckman, and C. Vafa. Yukawa Couplings in F-theory and Non-Commutative Geometry. 2009.

[330] J. A. R. Cembranos, A. Dobado, and A. L. Maroto. Brane world dark matter. *Phys. Rev. Lett.*, 90:241301, 2003. doi: 10.1103/PhysRevLett.90.241301.

[331] L. D. Chamain, P. Dharmawansa, S. Atapattu, and C. Tellambura. Detection of a Signal in Colored Noise: A Random Matrix Theory Based Analysis. *arXiv e-prints*, art. arXiv:1901.09568, Jan 2019.

[332] L. D. Chamain, P. Dharmawansa, S. Atapattu, and C. Tellambura. Eigenvalue Based Detection of a Signal in Colored Noise: Finite and Asymptotic Analyses. *arXiv e-prints*, art. arXiv:1902.02483, Feb 2019.

[333] S. Chandrasekhar. The Maximum Mass of Ideal White Dwarfs. *ApJ*, 74:81, July 1931. doi: 10.1086/143324.

[334] S. Chandrasekhar. The mathematical theory of black holes. In *Oxford, UK: Clarendon (1992) 646 p., OXFORD, UK: CLARENDON (1985) 646 P.*, 1985.

[335] D. Chang, W.-F. Chang, C.-H. Chou, and W.-Y. Keung. Large two loop contributions to g-2 from a generic pseudoscalar boson. *Phys. Rev.*, D63: 091301, 2001. doi: 10.1103/PhysRevD.63.091301.

[336] S. Chatrchyan et al. Observation of a New Boson at a Mass of 125 GeV with the CMS Experiment at the LHC. *Phys. Lett.*, B716:30–61, 2012. doi: 10.1016/j.physletb.2012.08.021.

[337] M. Chemtob. Threshold corrections in orbifold models and superstring unification of gauge interactions. *Phys. Rev.*, D53:3920–3941, 1996. doi: 10.1103/PhysRevD.53.3920.

[338] H.-C. Cheng, J. L. Feng, and K. T. Matchev. Kaluza-Klein dark matter. *Phys. Rev. Lett.*, 89:211301, 2002. doi: 10.1103/PhysRevLett.89.211301.

[339] S. L. Cheng, C. Q. Geng, and W. T. Ni. Axion - photon couplings in invisible axion models. *Phys. Rev.*, D52:3132–3135, 1995. doi: 10.1103/PhysRevD.52.3132.

[340] M. Chevallier and D. Polarski. Accelerating universes with scaling dark matter. *Int. J. Mod. Phys.*, D10:213–224, 2001. doi: 10.1142/S0218271801000822.

[341] K. Choi and K. S. Jeong. String theoretic QCD axion with stabilized saxion and the pattern of supersymmetry breaking. *JHEP*, 01:103, 2007. doi: 10.1088/1126-6708/2007/01/103.

[342] K. Choi, A. Falkowski, H. P. Nilles, M. Olechowski, and S. Pokorski. Stability

of flux compactifications and the pattern of supersymmetry breaking. *JHEP*, 11:076, 2004. doi: 10.1088/1126-6708/2004/11/076.

[343] K. Choi, A. Falkowski, H. P. Nilles, and M. Olechowski. Soft supersymmetry breaking in KKLT flux compactification. *Nucl. Phys.*, B718:113–133, 2005. doi: 10.1016/j.nuclphysb.2005.04.032.

[344] K.-S. Choi and J. E. Kim. Quarks and leptons from orbifolded superstring. *Lect. Notes Phys.*, 696:1–406, 2006. doi: 10.1007/b11681670.

[345] K.-Y. Choi, J. E. Kim, and L. Roszkowski. Review of axino dark matter. *J. Korean Phys. Soc.*, 63:1685–1695, 2013. doi: 10.3938/jkps.63.1685.

[346] J. H. Christenson, J. W. Cronin, V. L. Fitch, and R. Turlay. Evidence for the 2π decay of the k_2^0 meson. *Phys. Rev. Lett.*, 13:138–140, Jul 1964. doi: 10.1103/PhysRevLett.13.138. URL `https://link.aps.org/doi/10.1103/PhysRevLett.13.138`.

[347] P. Christodoulidis, D. Roest, and R. Rosati. Many-field Inflation: Universality or Prior Dependence? 2019.

[348] D. J. H. Chung, E. W. Kolb, and A. Riotto. Superheavy dark matter. *Phys. Rev.*, D59:023501, 1999. doi: 10.1103/PhysRevD.59.023501.

[349] D. J. H. Chung, E. W. Kolb, and A. Riotto. Production of massive particles during reheating. *Phys. Rev. D*, 60:063504, Aug 1999. doi: 10.1103/PhysRevD.60.063504. URL `https://link.aps.org/doi/10.1103/PhysRevD.60.063504`.

[350] Y. Chung, A. Gelman, S. Rabe-Hesketh, J. Liu, and V. Dorie. Weakly informative prior for point estimation of covariance matrices in hierarchical models. *Journal of Educational and Behavioral Statistics*, 40(2):136–157, 2015. doi: 10.3102/1076998615570945. URL `https://doi.org/10.3102/1076998615570945`.

[351] M. Cicoli, M. Goodsell, and A. Ringwald. The type IIB string axiverse and its low-energy phenomenology. *JHEP*, 10:146, 2012. doi: 10.1007/JHEP10(2012)146.

[352] M. Cicoli, C. Mayrhofer, and R. Valandro. Moduli Stabilisation for Chiral Global Models. *JHEP*, 02:062, 2012. doi: 10.1007/JHEP02(2012)062.

[353] M. Cicoli, K. Dutta, and A. Maharana. N-flation with Hierarchically Light Axions in String Compactifications. *JCAP*, 1408:012, 2014. doi: 10.1088/1475-7516/2014/08/012.

[354] M. Cirelli and A. Strumia. Minimal Dark Matter: Model and results. *New J. Phys.*, 11:105005, 2009. doi: 10.1088/1367-2630/11/10/105005.

[355] M. Cirelli, N. Fornengo, and A. Strumia. Minimal dark matter. *Nucl. Phys.*, B753:178–194, 2006. doi: 10.1016/j.nuclphysb.2006.07.012.

[356] T. Claeys and A. Doeraene. Gaussian perturbations of hard edge random matrix ensembles. *Nonlinearity*, 29(11):3385, Nov 2016. doi: 10.1088/0951-7715/29/11/3385.

[357] B. T. Cleveland, T. Daily, J. Raymond Davis, J. R. Distel, K. Lande, C. K. Lee, P. S. Wildenhain, and J. Ullman. Measurement of the solar electron neutrino flux with the homestake chlorine detector. *The Astrophysical Journal*, 496(1):505–526, mar 1998. doi: 10.1086/305343. URL `https://doi.org/10.1086%2F305343`.

[358] T. Clifton, P. G. Ferreira, A. Padilla, and C. Skordis. Modified Gravity and Cosmology. *Phys. Rept.*, 513:1–189, 2012. doi: 10.1016/j.physrep.2012.01.001.

[359] D. Clowe, M. Bradac, A. H. Gonzalez, M. Markevitch, S. W. Randall, C. Jones, and D. Zaritsky. A direct empirical proof of the existence of dark matter. *Astrophys. J.*, 648:L109–L113, 2006. doi: 10.1086/508162.

[360] I. B. Cohen, A. Whitman, and J. Budenz. *The Principia: Mathematical Principles of Natural Philosophy*. University of California Press, 1 edition, 1999. ISBN 9780520088160. URL http://www.jstor.org/stable/10.1525/j.ctt9qh28z.

[361] S. Cole et al. The 2dF Galaxy Redshift Survey: Power-spectrum analysis of the final dataset and cosmological implications. *Mon. Not. Roy. Astron. Soc.*, 362:505–534, 2005. doi: 10.1111/j.1365-2966.2005.09318.x.

[362] M. Colless et al. The 2dF Galaxy Redshift Survey: Final data release. 2003.

[363] I. M. Comsa, M. Firsching, and T. Fischbacher. SO(8) Supergravity and the Magic of Machine Learning. 2019.

[364] J. P. Conlon. The QCD axion and moduli stabilisation. *JHEP*, 05:078, 2006. doi: 10.1088/1126-6708/2006/05/078.

[365] J. P. Conlon. Quantum Gravity Constraints on Inflation. *JCAP*, 1209:019, 2012. doi: 10.1088/1475-7516/2012/09/019.

[366] J. P. Conlon. Brane-antibrane backreaction in axion monodromy inflation. *Journal of Cosmology and Astroparticle Physics*, 2012(01):033–033, jan 2012. doi: 10.1088/1475-7516/2012/01/033. URL https://doi.org/10.1088%2F1475-7516%2F2012%2F01%2F033.

[367] J. P. Conlon and S. Krippendorf. Axion decay constants away from the lamppost. *JHEP*, 04:085, 2016. doi: 10.1007/JHEP04(2016)085.

[368] J. P. Conlon and E. Palti. Aspects of Flavour and Supersymmetry in F-theory GUTs. *JHEP*, 01:029, 2010. doi: 10.1007/JHEP01(2010)029.

[369] J. P. Conlon, F. Quevedo, and K. Suruliz. Large-volume flux compactifications: Moduli spectrum and D3/D7 soft supersymmetry breaking. *JHEP*, 08:007, 2005. doi: 10.1088/1126-6708/2005/08/007.

[370] T. Conlon, H. J. Ruskin, and M. Crane. Random matrix theory and fund of

funds portfolio optimisation. *Physica A Statistical Mechanics and its Applications*, 382:565–576, Aug 2007. doi: 10.1016/j.physa.2007.04.039.

[371] J. B. Conrey. L-functions and random matrices. *arXiv Mathematics e-prints*, art. math/0005300, May 2000.

[372] A. Constantin. *Heterotic String Models on Smooth Calabi-Yau Threefolds*. PhD thesis, Oxford U., 2018.

[373] A. Cooray and R. K. Sheth. Halo Models of Large Scale Structure. *Phys. Rept.*, 372:1–129, 2002. doi: 10.1016/S0370-1573(02)00276-4.

[374] E. J. Copeland, A. R. Liddle, and D. Wands. Exponential potentials and cosmological scaling solutions. *Phys. Rev.*, D57:4686–4690, 1998. doi: 10.1103/PhysRevD.57.4686.

[375] E. J. Copeland, M. Sami, and S. Tsujikawa. Dynamics of dark energy. *Int. J. Mod. Phys.*, D15:1753–1936, 2006. doi: 10.1142/S021827180600942X.

[376] E. J. Copeland, T. W. B. Kibble, and D. A. Steer. Constraints on string networks with junctions. *Phys. Rev.*, D75:065024, 2007. doi: 10.1103/PhysRevD.75.065024.

[377] P. S. Corasaniti, S. Agarwal, D. J. E. Marsh, and S. Das. Constraints on dark matter scenarios from measurements of the galaxy luminosity function at high redshifts. *ArXiv e-prints*, Nov. 2016.

[378] C. J. Corrado. Option pricing based on the generalized lambda distribution. *Journal of Futures Markets*, 21(3):213–236, 2001. doi: 10.1002/1096-9934(200103)21:3⟨213::AID-FUT2⟩3.0.CO;2-H. URL `https://onlinelibrary.wiley.com/doi/abs/10.1002/1096-9934%28200103%2921%3A3%3C213%3A%3AAID-FUT2%3E3.0.CO%3B2-H`.

[379] A. Corti, M. Haskins, J. Nordström, and T. Pacini. G_2-manifolds and associa-

tive submanifolds via semi-Fano 3-folds. *Duke Math. J.*, 164(10):1971–2092, 2015. doi: 10.1215/00127094-3120743.

[380] O. Costin, P. Deift, and D. Gioev. On the Proof of Universality for Orthogonal and Symplectic Ensembles in Random Matrix Theory. *Journal of Statistical Physics*, 129(5-6):937–948, Dec. 2007. doi: 10.1007/s10955-007-9277-1.

[381] G. Coughlan, R. Holman, P. Ramond, and G. Ross. Supersymmetry and the entropy crisis. *Physics Letters B*, 140(1):44 – 48, 1984. ISSN 0370-2693. doi: https://doi.org/10.1016/0370-2693(84)91043-8. URL `http://www.sciencedirect.com/science/article/pii/0370269384910438`.

[382] L. Covi, J. E. Kim, and L. Roszkowski. Axinos as cold dark matter. *Phys. Rev. Lett.*, 82:4180–4183, 1999. doi: 10.1103/PhysRevLett.82.4180.

[383] L. Covi, H.-B. Kim, J. E. Kim, and L. Roszkowski. Axinos as dark matter. *JHEP*, 05:033, 2001. doi: 10.1088/1126-6708/2001/05/033.

[384] M. W. Craig and M. Davis. The Structure of dark matter halos in an annihilating dark matter model. *New Astron.*, 6:425, 2001. doi: 10.1016/S1384-1076(01)00072-0.

[385] D. Cremades, L. E. Ibanez, and F. Marchesano. Intersecting brane models of particle physics and the Higgs mechanism. *JHEP*, 07:022, 2002. doi: 10.1088/1126-6708/2002/07/022.

[386] D. Cremades, L. E. Ibanez, and F. Marchesano. Standard model at intersecting D5-branes: Lowering the string scale. *Nucl. Phys.*, B643:93–130, 2002. doi: 10.1016/S0550-3213(02)00746-0.

[387] E. Cremmer, B. Julia, and J. Scherk. Supergravity Theory in Eleven-Dimensions. *Phys. Lett.*, B76:409–412, 1978. doi: 10.1016/0370-2693(78)90894-8. [,25(1978)].

[388] E. Cremmer, S. Ferrara, C. Kounnas, and D. Nanopoulos. Naturally vanish-

ing cosmological constant in n=1 supergravity. *Physics Letters B*, 133(1):61 – 66, 1983. ISSN 0370-2693. doi: https://doi.org/10.1016/0370-2693(83)90106-5. URL `http://www.sciencedirect.com/science/article/pii/0370269383901065`.

[389] R. J. Crewther, P. Di Vecchia, G. Veneziano, and E. Witten. Chiral Estimate of the Electric Dipole Moment of the Neutron in Quantum Chromodynamics. *Phys. Lett.*, 88B:123, 1979. doi: 10.1016/0370-2693(80)91025-4,10.1016/0370-2693(79)90128-X. [Erratum: Phys. Lett.91B,487(1980)].

[390] W. J. Cunningham. *High Performance Algorithms for Quantum Gravity and Cosmology*. PhD thesis, Northeastern U., 2018.

[391] M. Cvetic, J. Halverson, and R. Richter. Realistic Yukawa structures from orientifold compactifications. *JHEP*, 12:063, 2009. doi: 10.1088/1126-6708/2009/12/063.

[392] F.-Y. Cyr-Racine, R. de Putter, A. Raccanelli, and K. Sigurdson. Constraints on Large-Scale Dark Acoustic Oscillations from Cosmology. *Phys. Rev.*, D89 (6):063517, 2014. doi: 10.1103/PhysRevD.89.063517.

[393] A. N. D. Voiculescu, K. Dykema. *Free random variables*, volume volume 1. CRM Monograph Series, 1992.

[394] R. Daido, T. Kobayashi, and F. Takahashi. Dark matter in axion landscape. *Physics Letters B*, 765:293–299, Feb. 2017. doi: 10.1016/j.physletb.2016.12.034.

[395] P. H. Damgaard and S. M. Nishigaki. Distribution of the k-th smallest Dirac operator eigenvalue. *Phys. Rev.*, D63:045012, 2001. doi: 10.1103/PhysRevD.63.045012.

[396] G. D'Amico, M. Kamionkowski, and K. Sigurdson. Dark Matter Astrophysics. *arXiv e-prints*, art. arXiv:0907.1912, Jul 2009.

[397] T. Damour and A. Vilenkin. Gravitational wave bursts from cosmic strings. *Phys. Rev. Lett.*, 85:3761–3764, 2000. doi: 10.1103/PhysRevLett.85.3761.

[398] G. Danby, J.-M. Gaillard, K. Goulianos, L. M. Lederman, N. Mistry, M. Schwartz, and J. Steinberger. Observation of high-energy neutrino reactions and the existence of two kinds of neutrinos. *Phys. Rev. Lett.*, 9: 36–44, Jul 1962. doi: 10.1103/PhysRevLett.9.36. URL `https://link.aps.org/doi/10.1103/PhysRevLett.9.36`.

[399] H. E. Daniels. Saddlepoint approximations in statistics. *Ann. Math. Statist.*, 25(4):631–650, 12 1954. doi: 10.1214/aoms/1177728652. URL `https://doi.org/10.1214/aoms/1177728652`.

[400] P. Das Gupta. Dark energy and Chern-Simons like gravity from a dynamical four-form. 2009.

[401] K. Dasgupta, G. Rajesh, and S. Sethi. M theory, orientifolds and G - flux. *JHEP*, 08:023, 1999. doi: 10.1088/1126-6708/1999/08/023.

[402] K. Dasgupta, C. Herdeiro, S. Hirano, and R. Kallosh. D3 / D7 inflationary model and M theory. *Phys. Rev.*, D65:126002, 2002. doi: 10.1103/PhysRevD.65.126002.

[403] K. Dasgupta, J. P. Hsu, R. Kallosh, A. D. Linde, and M. Zagermann. D3/D7 brane inflation and semilocal strings. *JHEP*, 08:030, 2004. doi: 10.1088/1126-6708/2004/08/030.

[404] R. Dave, L. Hernquist, N. Katz, and D. H. Weinberg. The Low redshift Lyman alpha forest in cold dark matter cosmologies. *Astrophys. J.*, 511: 521–545, 1999. doi: 10.1086/306722.

[405] S. Davidson. Axions: Bose Einstein Condensate or Classical Field? *Astropart. Phys.*, 65:101–107, 2015. doi: 10.1016/j.astropartphys.2014.12.007.

[406] R. L. Davis. Cosmic Axions from Cosmic Strings. *Phys. Lett.*, B180:225–230, 1986. doi: 10.1016/0370-2693(86)90300-X.

[407] H. Davoudiasl and P. B. Denton. Ultra Light Boson Dark Matter and Event Horizon Telescope Observations of M87*. 2019.

[408] H. Davoudiasl and C. W. Murphy. Fuzzy Dark Matter from Infrared Confining Dynamics. 2017.

[409] A. P. Dawid. Some matrix-variate distribution theory: Notational considerations and a bayesian application. *Biometrika*, 68(1):265–274, 1981. ISSN 00063444. URL `http://www.jstor.org/stable/2335827`.

[410] K. S. Dawson et al. The Baryon Oscillation Spectroscopic Survey of SDSS-III. *AJ*, 145(1):10, Jan 2013. doi: 10.1088/0004-6256/145/1/10.

[411] L. V. P. R. de Broglie. Recherches sur la théorie des quanta. *Annals Phys.*, 2:22–128, 1925.

[412] B. de Carlos, J. A. Casas, F. Quevedo, and E. Roulet. Model independent properties and cosmological implications of the dilaton and moduli sectors of 4-d strings. *Phys. Lett.*, B318:447–456, 1993. doi: 10.1016/0370-2693(93)91538-X.

[413] A. De Felice and S. Tsujikawa. f(R) theories. *Living Rev. Rel.*, 13:3, 2010. doi: 10.12942/lrr-2010-3.

[414] A. de Oliveira-Costa, M. Tegmark, M. Zaldarriaga, and A. Hamilton. The Significance of the largest scale CMB fluctuations in WMAP. *Phys. Rev.*, D69:063516, 2004. doi: 10.1103/PhysRevD.69.063516.

[415] R. de Putter and E. V. Linder. Kinetic k-essence and Quintessence. *Astropart. Phys.*, 28:263–272, 2007. doi: 10.1016/j.astropartphys.2007.05.011.

[416] A. De Rujula, H. Georgi, and S. L. Glashow. Hadron Masses in a Gauge Theory. *Phys. Rev.*, D12:147–162, 1975. doi: 10.1103/PhysRevD.12.147.

[417] B. de Wit, D. J. Smit, and N. D. Hari Dass. Residual Supersymmetry of Compactified D=10 Supergravity. *Nucl. Phys.*, B283:165, 1987. doi: 10.1016/0550-3213(87)90267-7.

[418] D. S. Dean and S. N. Majumdar. Large deviations of extreme eigenvalues of random matrices. *Phys. Rev. Lett.*, 97:160201, 2006. doi: 10.1103/PhysRevLett.97.160201.

[419] D. S. Dean and S. N. Majumdar. Extreme value statistics of eigenvalues of Gaussian random matrices. *Phys. Rev. E*, 77(4):041108, Apr 2008. doi: 10.1103/PhysRevE.77.041108.

[420] L. T. Decarlo. On the meaning and use of kurtosis. *Psychological Methods*, pages 292–307, 1997.

[421] S. DeDeo. Particle dark energy. *Phys. Rev. D*, 73:043520, Feb 2006. doi: 10.1103/PhysRevD.73.043520. URL `https://link.aps.org/doi/10.1103/PhysRevD.73.043520`.

[422] C. Deffayet, O. Pujolas, I. Sawicki, and A. Vikman. Imperfect Dark Energy from Kinetic Gravity Braiding. *JCAP*, 1010:026, 2010. doi: 10.1088/1475-7516/2010/10/026.

[423] P. Deift. *Orthogonal polynomials and random matrices: A Riemann-Hilbert approach*. New York University, 1999.

[424] P. Deift and D. Gioev. Universality in Random Matrix Theory for orthogonal and symplectic ensembles. *arXiv e-prints*, art. math-ph/0411075, Nov. 2004.

[425] P. Deift, D. Gioev, T. Kriecherbauer, and M. Vanlessen. Universality for Orthogonal and Symplectic Laguerre-Type Ensembles. *Journal of Statistical Physics*, 129(5-6):949–1053, Dec. 2007. doi: 10.1007/s10955-007-9325-x.

[426] A. Del Popolo. Nonbaryonic Dark Matter in Cosmology. *Int. J. Mod. Phys.*, D23:1430005, 2014. doi: 10.1142/S0218271814300055.

[427] M. Demirtas, C. Long, L. McAllister, and M. Stillman. The Kreuzer-Skarke Axiverse. 2018.

[428] F. Denef and M. R. Douglas. Distributions of flux vacua. *JHEP*, 05:072, 2004. doi: 10.1088/1126-6708/2004/05/072.

[429] F. Denef and M. R. Douglas. Distributions of nonsupersymmetric flux vacua. *JHEP*, 03:061, 2005. doi: 10.1088/1126-6708/2005/03/061.

[430] W. DeRocco and A. Hook. Axion interferometry. *Phys. Rev.*, D98(3):035021, 2018. doi: 10.1103/PhysRevD.98.035021.

[431] V. Desjacques, A. Kehagias, and A. Riotto. Impact of ultralight axion self-interactions on the large scale structure of the Universe. *Phys. Rev. D*, 97 (2):023529, Jan. 2018. doi: 10.1103/PhysRevD.97.023529.

[432] H. Dette. Strong approximation of eigenvalues of large dimensional wishart matrices by roots of generalized laguerre polynomials. *Journal of Approximation Theory*, 118(2):290 – 304, 2002. ISSN 0021-9045. doi: https://doi.org/10.1006/jath.2002.3725. URL `http://www.sciencedirect.com/science/article/pii/S0021904502937251`.

[433] S. Detweiler. Klein-gordon equation and rotating black holes. *Phys. Rev. D*, 22:2323–2326, Nov 1980. doi: 10.1103/PhysRevD.22.2323. URL `https://link.aps.org/doi/10.1103/PhysRevD.22.2323`.

[434] P. Dharmawansa. Three Problems Related to the Eigenvalues of Complex Non-central Wishart Matrices with a Rank-1 Mean. *arXiv e-prints*, art. arXiv:1306.6566, Jun 2013.

[435] P. Dharmawansa, I. M. Johnstone, and A. Onatski. Local Asymptotic Normality of the spectrum of high-dimensional spiked F-ratios. *arXiv e-prints*, art. arXiv:1411.3875, Nov 2014.

[436] P. Di Francesco, P. H. Ginsparg, and J. Zinn-Justin. 2-D Gravity and random matrices. *Phys. Rept.*, 254:1–133, 1995. doi: 10.1016/0370-1573(94)00084-G.

[437] L. Di Luzio, F. Mescia, and E. Nardi. Redefining the Axion Window. *Phys. Rev. Lett.*, 118(3):031801, 2017. doi: 10.1103/PhysRevLett.118.031801.

[438] L. Di Luzio, F. Mescia, E. Nardi, P. Panci, and R. Ziegler. Astrophobic Axions. *Phys. Rev. Lett.*, 120(26):261803, 2018. doi: 10.1103/PhysRevLett.120.261803.

[439] E. Di Valentino, S. Gariazzo, E. Giusarma, and O. Mena. Robustness of cosmological axion mass limits. *Phys. Rev.*, D91(12):123505, 2015. doi: 10.1103/PhysRevD.91.123505.

[440] E. Di Valentino, E. Giusarma, M. Lattanzi, O. Mena, A. Melchiorri, and J. Silk. Cosmological Axion and neutrino mass constraints from Planck 2015 temperature and polarization data. *Phys. Lett.*, B752:182–185, 2016. doi: 10.1016/j.physletb.2015.11.025.

[441] P. Di Vecchia and G. Veneziano. Chiral Dynamics in the Large n Limit. *Nucl. Phys.*, B171:253–272, 1980. doi: 10.1016/0550-3213(80)90370-3.

[442] P. Diaconis and S. N. Evans. Linear functionals of eigenvalues of random matrices. *Transactions of the American Mathematical Society*, 353(7):2615–2633, 2001. ISSN 00029947. URL `http://www.jstor.org/stable/221816`.

[443] P. Diaconis and P. J. Forrester. A. Hurwitz and the origins of random matrix theory in mathematics. *arXiv e-prints*, art. arXiv:1512.09229, Dec 2015.

[444] M. Dias, J. Frazer, and A. Westphal. Inflation as an Information Bottleneck - A strategy for identifying universality classes and making robust predictions. *JHEP*, 05:065, 2019. doi: 10.1007/JHEP05(2019)065.

[445] O. J. C. Dias, M. Godazgar, and J. E. Santos. Linear Mode Stability of the

Kerr-Newman Black Hole and Its Quasinormal Modes. *Phys. Rev. Lett.*, 114 (15):151101, 2015. doi: 10.1103/PhysRevLett.114.151101.

[446] R. H. Dicke. Coherence in spontaneous radiation processes. *Phys. Rev.*, 93: 99–110, Jan 1954. doi: 10.1103/PhysRev.93.99. URL `https://link.aps.org/doi/10.1103/PhysRev.93.99`.

[447] R. H. Dicke, P. J. E. Peebles, P. G. Roll, and D. T. Wilkinson. Cosmic Black-Body Radiation. *ApJ*, 142:414–419, July 1965. doi: 10.1086/148306.

[448] D. A. Dicus, E. W. Kolb, V. L. Teplitz, and R. V. Wagoner. Astrophysical Bounds on the Masses of Axions and Higgs Particles. *Phys. Rev.*, D18:1829, 1978. doi: 10.1103/PhysRevD.18.1829.

[449] K. R. Dienes. String theory and the path to unification: A Review of recent developments. *Phys. Rept.*, 287:447–525, 1997. doi: 10.1016/S0370-1573(97)00009-4.

[450] K. R. Dienes and A. E. Faraggi. Gauge coupling unification in realistic free fermionic string models. *Nucl. Phys.*, B457:409–483, 1995. doi: 10.1016/0550-3213(95)00497-1.

[451] K. R. Dienes and A. E. Faraggi. Making ends meet: String unification and low-energy data. *Phys. Rev. Lett.*, 75:2646–2649, 1995. doi: 10.1103/PhysRevLett.75.2646.

[452] K. R. Dienes, A. E. Faraggi, and J. March-Russell. String unification, higher level gauge symmetries, and exotic hypercharge normalizations. *Nucl. Phys.*, B467:44–99, 1996. doi: 10.1016/0550-3213(96)00085-5.

[453] A. Diez-Tejedor and D. J. E. Marsh. Cosmological production of ultralight dark matter axions. 2017.

[454] R. Dijkgraaf and C. Vafa. Matrix models, topological strings, and super-

symmetric gauge theories. *Nucl. Phys.*, B644:3–20, 2002. doi: 10.1016/S0550-3213(02)00766-6.

[455] S. Dimopoulos and H. Georgi. Solution of the gauge hierarchy problem. *Physics Letters B*, 117(5):287 – 290, 1982. ISSN 0370-2693. doi: https://doi.org/10.1016/0370-2693(82)90720-1. URL `http://www.sciencedirect.com/science/article/pii/0370269382907201`.

[456] S. Dimopoulos, P. W. Graham, J. M. Hogan, M. A. Kasevich, and S. Rajendran. An Atomic Gravitational Wave Interferometric Sensor (AGIS). *Phys. Rev.*, D78:122002, 2008. doi: 10.1103/PhysRevD.78.122002.

[457] S. Dimopoulos, S. Kachru, J. McGreevy, and J. G. Wacker. N-flation. *JCAP*, 0808:003, 2008. doi: 10.1088/1475-7516/2008/08/003.

[458] M. Dine and W. Fischler. The Not So Harmless Axion. *Phys. Lett.*, B120:137–141, 1983. doi: 10.1016/0370-2693(83)90639-1. [,URL(1982)].

[459] M. Dine, W. Fischler, and M. Srednicki. A simple solution to the strong CP problem with a harmless axion. *Physics Letters B*, 104:199–202, Aug. 1981. doi: 10.1016/0370-2693(81)90590-6.

[460] M. Dine, G. Festuccia, J. Kehayias, and W. Wu. Axions in the Landscape and String Theory. *JHEP*, 01:012, 2011. doi: 10.1007/JHEP01(2011)012.

[461] L. J. Dixon, J. A. Harvey, C. Vafa, and E. Witten. Strings on Orbifolds. *Nucl. Phys.*, B261:678–686, 1985. doi: 10.1016/0550-3213(85)90593-0. [,678(1985)].

[462] L. J. Dixon, J. A. Harvey, C. Vafa, and E. Witten. Strings on Orbifolds. 2. *Nucl. Phys.*, B274:285–314, 1986. doi: 10.1016/0550-3213(86)90287-7.

[463] S. S. Doeleman, V. L. Fish, D. E. Schenck, C. Beaudoin, R. Blundell, G. C. Bower, A. E. Broderick, R. Chamberlin, R. Freund, P. Friberg, M. A. Gurwell, P. T. P. Ho, M. Honma, M. Inoue, T. P. Krichbaum, J. Lamb, A. Loeb, C. Lonsdale, D. P. Marrone, J. M. Moran, T. Oyama, R. Plambeck, R. A.

Primiani, A. E. E. Rogers, D. L. Smythe, J. SooHoo, P. Strittmatter, R. P. J. Tilanus, M. Titus, J. Weintroub, M. Wright, K. H. Young, and L. M. Ziurys. Jet-Launching Structure Resolved Near the Supermassive Black Hole in M87. *Science*, 338(6105):355, Oct 2012. doi: 10.1126/science.1224768.

[464] V. I. Dokuchaev and N. O. Nazarova. The brightest point in accretion disk and black hole spin: implication to the image of black hole M87*. *Universe*, 5:183, 2019. doi: 10.3390/universe5080183.

[465] L. Dolan and J. T. Liu. Running gauge couplings and thresholds in the type II superstring. *Nucl. Phys.*, B387:86–96, 1992. doi: 10.1016/0550-3213(92)90047-F.

[466] M. J. Dolan, T. Ferber, C. Hearty, F. Kahlhoefer, and K. Schmidt-Hoberg. Revised constraints and Belle II sensitivity for visible and invisible axion-like particles. *JHEP*, 12:094, 2017. doi: 10.1007/JHEP12(2017)094.

[467] S. R. Dolan. Instability of the massive Klein-Gordon field on the Kerr spacetime. *Phys. Rev.*, D76:084001, 2007. doi: 10.1103/PhysRevD.76.084001.

[468] S. R. Dolan. Superradiant instabilities of rotating black holes in the time domain. *Phys. Rev.*, D87(12):124026, 2013. doi: 10.1103/PhysRevD.87.124026.

[469] R. Donagi and M. Wijnholt. Model Building with F-Theory. *Adv. Theor. Math. Phys.*, 15(5):1237–1317, 2011. doi: 10.4310/ATMP.2011.v15.n5.a2.

[470] R. Donagi and M. Wijnholt. Breaking GUT Groups in F-Theory. *Adv. Theor. Math. Phys.*, 15(6):1523–1603, 2011. doi: 10.4310/ATMP.2011.v15.n6.a1.

[471] R. Donagi, Y.-H. He, B. A. Ovrut, and R. Reinbacher. The spectra of heterotic standard model vacua. *Journal of High Energy Physics*, 2005(06):070–070, jun 2005. doi: 10.1088/1126-6708/2005/06/070. URL `https://doi.org/10.1088%2F1126-6708%2F2005%2F06%2F070`.

[472] E. A. Donley, N. R. Claussen, S. L. Cornish, J. L. Roberts, E. A. Cornell,

and C. E. Wieman. Dynamics of collapsing and exploding Bose-Einstein condensates. *Nature*, 412(6844):295–299, Jul 2001. doi: 10.1038/35085500.

[473] T. W. Donnelly, S. J. Freedman, R. S. Lytel, R. D. Peccei, and M. Schwartz. Do axions exist? *Phys. Rev. D*, 18:1607–1620, Sep 1978. doi: 10.1103/PhysRevD.18.1607. URL `https://link.aps.org/doi/10.1103/PhysRevD.18.1607`.

[474] M. Doran and G. Robbers. Early dark energy cosmologies. *JCAP*, 0606:026, 2006. doi: 10.1088/1475-7516/2006/06/026.

[475] M. R. Douglas and S. Kachru. Flux compactification. *Rev. Mod. Phys.*, 79: 733–796, 2007. doi: 10.1103/RevModPhys.79.733.

[476] R. B. Dozier and J. W. Silverstein. Analysis of the limiting spectral distribution of large dimensional information-plus-noise type matrices. *Journal of Multivariate Analysis*, 98(6):1099 – 1122, 2007. ISSN 0047-259X. doi: https://doi.org/10.1016/j.jmva.2006.12.005. URL `http://www.sciencedirect.com/science/article/pii/S0047259X06002119`.

[477] R. B. Dozier and J. W. Silverstein. On the empirical distribution of eigenvalues of large dimensional information-plus-noise-type matrices. *Journal of Multivariate Analysis*, 98(4):678 – 694, 2007. ISSN 0047-259X. doi: https://doi.org/10.1016/j.jmva.2006.09.006. URL `http://www.sciencedirect.com/science/article/pii/S0047259X06001606`.

[478] M. Drewes. The Phenomenology of Right Handed Neutrinos. *Int. J. Mod. Phys.*, E22:1330019, 2013. doi: 10.1142/S0218301313300191.

[479] M. J. Drinkwater et al. The WiggleZ Dark Energy Survey: survey design and first data release. *MNRAS*, 401(3):1429–1452, Jan 2010. doi: 10.1111/j.1365-2966.2009.15754.x.

[480] J. Droste. The field of a single centre in Einstein's theory of gravitation and

the motion of a particle in that field. *KNAW*, Proceedings, 19 I, Amsterdam: pp. 197–215, 1917.

[481] M. J. Duff, B. E. W. Nilsson, and C. N. Pope. Kaluza-Klein Supergravity. *Phys. Rept.*, 130:1–142, 1986. doi: 10.1016/0370-1573(86)90163-8.

[482] L. D. Duffy and K. van Bibber. Axions as dark matter particles. *New Journal of Physics*, 11(10):105008, oct 2009. doi: 10.1088/1367-2630/11/10/105008. URL `https://doi.org/10.1088%2F1367-2630%2F11%2F10%2F105008`.

[483] I. Dumitriu and A. Edelman. Eigenvalues of hermite and laguerre ensembles: large beta asymptotics. *Annales de l'Institut Henri Poincare (B) Probability and Statistics*, 41(6):1083 – 1099, 2005. ISSN 0246-0203. doi: https://doi.org/10.1016/j.anihpb.2004.11.002. URL `http://www.sciencedirect.com/science/article/pii/S0246020305000646`.

[484] I. Dumitriu and A. Edelman. Global spectrum fluctuations for the ?-hermite and ?-laguerre ensembles via matrix models. *Journal of Mathematical Physics*, 47(6):063302, 2006. doi: 10.1063/1.2200144. URL `https://doi.org/10.1063/1.2200144`.

[485] J. Dunkley, M. Bucher, P. G. Ferreira, K. Moodley, and C. Skordis. Fast and reliable Markov chain Monte Carlo technique for cosmological parameter estimation. *MNRAS*, 356:925–936, Jan. 2005. doi: 10.1111/j.1365-2966.2004.08464.x.

[486] R. Durrer and J. Laukenmann. The Oscillating universe: An Alternative to inflation. *Class. Quant. Grav.*, 13:1069–1088, 1996. doi: 10.1088/0264-9381/13/5/021.

[487] G. Dvali and M. S. Turner. Dark energy as a modification of the Friedmann equation. 2003.

[488] G. R. Dvali and S. H. H. Tye. Brane inflation. *Phys. Lett.*, B450:72–82, 1999. doi: 10.1016/S0370-2693(99)00132-X.

[489] G. R. Dvali, A. Melfo, and G. Senjanovic. Is There a monopole problem? *Phys. Rev. Lett.*, 75:4559–4562, 1995. doi: 10.1103/PhysRevLett.75.4559.

[490] G. R. Dvali, G. Gabadadze, and M. Porrati. 4-D gravity on a brane in 5-D Minkowski space. *Phys. Lett.*, B485:208–214, 2000. doi: 10.1016/S0370-2693(00)00669-9.

[491] F. Dyson. A meeting with Enrico Fermi. *Nature*, 427:297, Jan. 2004. doi: 10.1038/427297a.

[492] F. J. Dyson. The Threefold Way. Algebraic Structure of Symmetry Groups and Ensembles in Quantum Mechanics. *Journal of Mathematical Physics*, 3: 1199–1215, Nov. 1962. doi: 10.1063/1.1703863.

[493] F. J. Dyson. Statistical theory of the energy levels of complex systems. i. *Journal of Mathematical Physics*, 3(1):140–156, 1962. doi: 10.1063/1.1703773. URL `https://doi.org/10.1063/1.1703773`.

[494] F. J. Dyson. Statistical theory of the energy levels of complex systems. ii. *Journal of Mathematical Physics*, 3(1):157–165, 1962. doi: 10.1063/1.1703774. URL `https://doi.org/10.1063/1.1703774`.

[495] F. J. Dyson. A brownian?motion model for the eigenvalues of a random matrix. *Journal of Mathematical Physics*, 3(6):1191–1198, 1962. doi: 10.1063/1.1703862. URL `https://doi.org/10.1063/1.1703862`.

[496] F. J. Dyson. Correlations between eigenvalues of a random matrix. *Comm. Math. Phys.*, 19(3):235–250, 1970. URL `https://projecteuclid.org:443/euclid.cmp/1103842703`.

[497] F. J. Dyson and M. L. Mehta. Statistical Theory of the Energy Levels of Complex Systems. IV. *Journal of Mathematical Physics*, 4:701–712, May 1963. doi: 10.1063/1.1704008.

[498] W. E. East and F. Pretorius. Superradiant instability and backreaction of

massive vector fields around kerr black holes. *Phys. Rev. Lett.*, 119:041101, Jul 2017. doi: 10.1103/PhysRevLett.119.041101. URL https://link.aps.org/doi/10.1103/PhysRevLett.119.041101.

[499] R. Easther and L. McAllister. Random matrices and the spectrum of N-flation. *JCAP*, 0605:018, 2006. doi: 10.1088/1475-7516/2006/05/018.

[500] R. Easther and L. C. Price. Initial conditions and sampling for multifield inflation. *JCAP*, 7:027, July 2013. doi: 10.1088/1475-7516/2013/07/027.

[501] R. Easther, J. Frazer, H. V. Peiris, and L. C. Price. Simple predictions from multifield inflationary models. *Phys. Rev. Lett.*, 112:161302, 2014. doi: 10.1103/PhysRevLett.112.161302.

[502] R. Easther, A. H. Guth, and A. Masoumi. Counting Vacua in Random Landscapes. 2016.

[503] J. Eby, M. Leembruggen, P. Suranyi, and L. C. R. Wijewardhana. QCD Axion Star Collapse with the Chiral Potential. *JHEP*, 06:014, 2017. doi: 10.1007/JHEP06(2017)014.

[504] A. S. Eddington and E. C. Stoner. The Minimum Pressure of a Degenerate Electron Gas. *Monthly Notices of the Royal Astronomical Society*, 92(7): 651–661, 05 1932. ISSN 0035-8711. doi: 10.1093/mnras/92.7.651. URL https://dx.doi.org/10.1093/mnras/92.7.651.

[505] A. Edelman. Eigenvalues and condition numbers of random matrices. *SIAM J. Matrix Anal. Appl.*, 9(4):543?560, Dec. 1988. ISSN 0895-4798. doi: 10.1137/0609045. URL https://doi.org/10.1137/0609045.

[506] A. Edelman. The distribution and moments of the smallest eigenvalue of a random matrix of wishart type. *Linear Algebra and its Applications*, 159:55 – 80, 1991. ISSN 0024-3795. doi: https://doi.org/10.1016/0024-3795(91)90076-9. URL http://www.sciencedirect.com/science/article/pii/0024379591900769.

[507] K. Ehret et al. New alps results on hidden-sector lightweights. *Physics Letters B*, 689(4):149 – 155, 2010. ISSN 0370-2693. doi: https://doi.org/10.1016/j.physletb.2010.04.066. URL `http://www.sciencedirect.com/science/article/pii/S0370269310005526`.

[508] J. Einasto. On the Construction of a Composite Model for the Galaxy and on the Determination of the System of Galactic Parameters. *Trudy Astrofizicheskogo Instituta Alma-Ata*, 5:87–100, 1965.

[509] J. Einasto, A. Kaasik, and E. Saar. Dynamic evidence on massive coronas of galaxies. *Nature*, 250:309–310, July 1974. doi: 10.1038/250309a0.

[510] A. Einstein. Ist die trägheit eines körpers von seinem energieinhalt abhängig? *Annalen der Physik*, 323(13):639–641, 1905. doi: 10.1002/andp.19053231314. URL `https://onlinelibrary.wiley.com/doi/abs/10.1002/andp.19053231314`.

[511] A. Einstein. Die Feldgleichungen der Gravitation. *Sitzungsberichte der Königlich Preußischen Akademie der Wissenschaften (Berlin), Seite 844-847.*, 1915.

[512] A. Einstein. On the General Theory of Relativity. *Sitzungsber. Preuss. Akad. Wiss. Berlin (Math. Phys.)*, 1915:778–786, 1915. [Addendum: Sitzungsber. Preuss. Akad. Wiss. Berlin (Math. Phys.)1915,799(1915)].

[513] A. Einstein. The Foundation of the General Theory of Relativity. *Annalen Phys.*, 49(7):769–822, 1916. doi: 10.1002/andp.200590044,10.1002/andp.19163540702. [Annalen Phys.354,no.7,769(1916)].

[514] A. Einstein. Cosmological Considerations in the General Theory of Relativity. *Sitzungsber. Preuss. Akad. Wiss. Berlin (Math. Phys.)*, 1917:142–152, 1917.

[515] N. El Karoui. High-dimensionality effects in the markowitz problem and other quadratic programs with linear constraints: Risk underestimation. *Ann.*

Statist., 38(6):3487–3566, 12 2010. doi: 10.1214/10-AOS795. URL https://doi.org/10.1214/10-AOS795.

[516] J. Ellis. The Future of High-Energy Collider Physics. In *38th International Symposium on Physics in Collision (PIC 2018) Bogotá, Colombia, September 11-15, 2018*, 2018.

[517] J. Ellis, J. Hagelin, D. Nanopoulos, K. Olive, and M. Srednicki. Supersymmetric relics from the big bang. *Nuclear Physics B*, 238(2):453 – 476, 1984. ISSN 0550-3213. doi: https://doi.org/10.1016/0550-3213(84)90461-9. URL http://www.sciencedirect.com/science/article/pii/0550321384904619.

[518] J. Ellis, A. Lahanas, D. Nanopoulos, and K. Tamvakis. No-scale supersymmetric standard model. *Physics Letters B*, 134(6):429 – 435, 1984. ISSN 0370-2693. doi: https://doi.org/10.1016/0370-2693(84)91378-9. URL http://www.sciencedirect.com/science/article/pii/0370269384913789.

[519] J. Ellis, D. Nanopoulos, and M. Quiros. On the axion, dilaton, polonyi, gravitino and shadow matter problems in supergravity and superstring models. *Physics Letters B*, 174(2):176 – 182, 1986. ISSN 0370-2693. doi: https://doi.org/10.1016/0370-2693(86)90736-7. URL http://www.sciencedirect.com/science/article/pii/0370269386907367.

[520] R. Emami, D. Grin, J. Pradler, A. Raccanelli, and M. Kamionkowski. Cosmological tests of an axiverse-inspired quintessence field. *Phys. Rev. D*, 93 (12):123005, June 2016. doi: 10.1103/PhysRevD.93.123005.

[521] F. Englert and R. Brout. Broken symmetry and the mass of gauge vector mesons. *Phys. Rev. Lett.*, 13:321–323, Aug 1964. doi: 10.1103/PhysRevLett.13.321. URL https://link.aps.org/doi/10.1103/PhysRevLett.13.321.

[522] B. P. A. et al, L. S. Collaboration, and V. Collaboration). Gw170608: Observation of a 19 solar-mass binary black hole coalescence. *The Astro-*

physical Journal Letters, 851(2):L35, 2017. URL `http://stacks.iop.org/2041-8205/851/i=2/a=L35`.

[523] S. K. et al. The japanese space gravitational wave antenna; decigo. *Journal of Physics: Conference Series*, 120(3):032004, 2008. URL `http://stacks.iop.org/1742-6596/120/i=3/a=032004`.

[524] B. Eynard and N. Orantin. Computation of Open Gromov-Witten Invariants for Toric Calabi-Yau 3-Folds by Topological Recursion, a Proof of the BKMP Conjecture. *Commun. Math. Phys.*, 337(2):483–567, 2015. doi: 10.1007/s00220-015-2361-5.

[525] B. Eynard, T. Kimura, and S. Ribault. Random matrices. 2015.

[526] J. Faldey and W. Gawronski. On the limit distributions of the zeros of jonqui?re polynomials and generalized classical orthogonal polynomials. *Journal of Approximation Theory*, 81(2):231 – 249, 1995. ISSN 0021-9045. doi: https://doi.org/10.1006/jath.1995.1047. URL `http://www.sciencedirect.com/science/article/pii/S0021904585710477`.

[527] S. M. Feeney, M. C. Johnson, J. D. McEwen, D. J. Mortlock, and H. V. Peiris. Hierarchical Bayesian Detection Algorithm for Early-Universe Relics in the Cosmic Microwave Background. *Phys. Rev.*, D88:043012, 2013. doi: 10.1103/PhysRevD.88.043012.

[528] B. Feng, X.-L. Wang, and X.-M. Zhang. Dark energy constraints from the cosmic age and supernova. *Phys. Lett.*, B607:35–41, 2005. doi: 10.1016/j.physletb.2004.12.071.

[529] J. Feng and Q. Wu. Constraint on the black-hole spin of M87 from the accretion-jet model. *Mon. Not. Roy. Astron. Soc.*, 470:612, 2017. doi: 10.1093/mnras/stx1283.

[530] D. Féral and S. Péché. The largest eigenvalues of sample covariance matrices

for a spiked population: Diagonal case. *Journal of Mathematical Physics*, 50 (7):073302–073302, Jul 2009. doi: 10.1063/1.3155785.

[531] E. Fermi and G. E. Uhlenbeck. On the recombination of electrons and positrons. *Phys. Rev.*, 44:510–511, Sep 1933. doi: 10.1103/PhysRev.44.510.2. URL `https://link.aps.org/doi/10.1103/PhysRev.44.510.2`.

[532] F. Ferrari, S. Klevtsov, and S. Zelditch. Simple Matrix Models for Random Bergman Metrics. *J. Stat. Mech.*, 1204:P04012, 2012. doi: 10.1088/1742-5468/2012/04/P040122012,10.1088/1742-5468/2012/04/P04012.

[533] F. Ferrari, S. Klevtsov, and S. Zelditch. Random Kahler Metrics. *Nucl. Phys.*, B869:89–110, 2013. doi: 10.1016/j.nuclphysb.2012.11.020.

[534] P. G. Ferreira and M. Joyce. Cosmology with a primordial scaling field. *Phys. Rev.*, D58:023503, 1998. doi: 10.1103/PhysRevD.58.023503.

[535] R. P. Feynman. Space-time approach to nonrelativistic quantum mechanics. *Rev. Mod. Phys.*, 20:367–387, 1948. doi: 10.1103/RevModPhys.20.367.

[536] R. P. Feynman. Space-time approach to quantum electrodynamics. *Phys. Rev.*, 76:769–789, Sep 1949. doi: 10.1103/PhysRev.76.769. URL `https://link.aps.org/doi/10.1103/PhysRev.76.769`.

[537] R. P. Feynman. Very high-energy collisions of hadrons. *Phys. Rev. Lett.*, 23: 1415–1417, 1969. doi: 10.1103/PhysRevLett.23.1415. [,494(1969)].

[538] R. P. Feynman and M. Gell-Mann. Theory of Fermi interaction. *Phys. Rev.*, 109:193–198, 1958. doi: 10.1103/PhysRev.109.193. [,417(1958)].

[539] L. Fidkowski, V. Hubeny, M. Kleban, and S. Shenker. The Black hole singularity in AdS / CFT. *JHEP*, 02:014, 2004. doi: 10.1088/1126-6708/2004/02/014.

[540] M. Fierz and W. Pauli. On relativistic wave equations for particles of arbi-

trary spin in an electromagnetic field. *Proc. Roy. Soc. Lond.*, A173:211–232, 1939. doi: 10.1098/rspa.1939.0140.

[541] D. J. Fixsen, E. S. Cheng, J. M. Gales, J. C. Mather, R. A. Shafer, and E. L. Wright. The Cosmic Microwave Background spectrum from the full COBE FIRAS data set. *Astrophys. J.*, 473:576, 1996. doi: 10.1086/178173.

[542] D. J. Fixsen, E. S. Cheng, J. M. Gales, J. C. Mather, R. A. Shafer, and E. L. Wright. The cosmic microwave background spectrum from the FullCOBE-FIRAS data set. *The Astrophysical Journal*, 473(2):576–587, dec 1996. doi: 10.1086/178173. URL `https://doi.org/10.1086%2F178173`.

[543] T. Flacke, C. Frugiuele, E. Fuchs, R. S. Gupta, and G. Perez. Phenomenology of relaxion-Higgs mixing. *JHEP*, 06:050, 2017. doi: 10.1007/JHEP06(2017)050.

[544] R. Flauger, L. McAllister, E. Pajer, A. Westphal, and G. Xu. Oscillations in the CMB from Axion Monodromy Inflation. *JCAP*, 1006:009, 2010. doi: 10.1088/1475-7516/2010/06/009.

[545] R. A. Flores and J. R. Primack. Observational and theoretical constraints on singular dark matter halos. *Astrophys. J.*, 427:L1–4, 1994. doi: 10.1086/187350.

[546] A. Font and L. E. Ibanez. Yukawa Structure from U(1) Fluxes in F-theory Grand Unification. *JHEP*, 02:016, 2009. doi: 10.1088/1126-6708/2009/02/016.

[547] A. Font, L. E. Ibanez, F. Quevedo, and A. Sierra. The Construction of 'Realistic' Four-Dimensional Strings Through Orbifolds. *Nucl. Phys.*, B331:421–474, 1990. doi: 10.1016/0550-3213(90)90215-Y.

[548] R. Foot. Mirror dark matter: Cosmology, galaxy structure and direct detection. *Int. J. Mod. Phys.*, A29:1430013, 2014. doi: 10.1142/S0217751X14300130.

[549] D. Foreman-Mackey, D. W. Hogg, D. Lang, and J. Goodman. emcee: The MCMC Hammer. *PASP*, 125:306–312, Mar. 2013. doi: 10.1086/670067.

[550] P. Forrester. *Log-Gases and Random Matrices (LMS-34)*. Princeton University Press, 2010. ISBN 9780691128290. URL `http://www.jstor.org/stable/j.ctt7t5vq`.

[551] P. J. Forrester. The spectrum edge of random matrix ensembles. *Nucl. Phys.*, B402:709–728, 1993. doi: 10.1016/0550-3213(93)90126-A.

[552] P. J. Forrester. Eigenvalue distributions for some correlated complex sample covariance matrices. *Journal of Physics A: Mathematical and Theoretical*, 40(36):11093–11103, aug 2007. doi: 10.1088/1751-8113/40/36/009. URL `https://doi.org/10.1088%2F1751-8113%2F40%2F36%2F009`.

[553] P. J. Forrester. Probability densities and distributions for spiked and general variance Wishart β-ensembles. *arXiv e-prints*, art. arXiv:1101.2261, Jan 2011.

[554] P. J. Forrester. Eigenvalue statistics for product complex Wishart matrices. *Journal of Physics A Mathematical General*, 47(34):345202, Aug 2014. doi: 10.1088/1751-8113/47/34/345202.

[555] P. J. Forrester, T. Nagao, and G. Honner. Correlations for the orthogonal-unitary and symplectic-unitary transitions at the hard and soft edges. *Nuclear Physics B*, 553(3):601–643, Aug. 1999. doi: 10.1016/S0550-3213(99)00272-2.

[556] P. J. Forrester, N. E. Frankel, and T. M. Garoni. Asymptotic form of the density profile for Gaussian and Laguerre random matrix ensembles with orthogonal and symplectic symmetry. *Journal of Mathematical Physics*, 47 (2):023301, Feb. 2006. doi: 10.1063/1.2165254.

[557] P. Fox, A. Pierce, and S. D. Thomas. Probing a QCD string axion with precision cosmological measurements. 2004.

[558] J. Frazer and A. R. Liddle. Exploring a string-like landscape. *JCAP*, 1102: 026, 2011. doi: 10.1088/1475-7516/2011/02/026.

[559] W. L. Freedman and B. F. Madore. The hubble constant. *Annual Review of Astronomy and Astrophysics*, 48(1):673–710, 2010. doi: 10.1146/annurev-astro-082708-101829. URL `https://doi.org/10.1146/annurev-astro-082708-101829`.

[560] K. C. Freeman. On the Disks of Spiral and S0 Galaxies. *ApJ*, 160:811, June 1970. doi: 10.1086/150474.

[561] K. Freese, J. A. Frieman, and A. V. Olinto. Natural inflation with pseudo - Nambu-Goldstone bosons. *Phys. Rev. Lett.*, 65:3233–3236, 1990. doi: 10.1103/PhysRevLett.65.3233.

[562] K. Freese, J. A. Frieman, and A. V. Olinto. Natural inflation with pseudo nambu-goldstone bosons. *Phys. Rev. Lett.*, 65:3233–3236, Dec 1990. doi: 10.1103/PhysRevLett.65.3233. URL `https://link.aps.org/doi/10.1103/PhysRevLett.65.3233`.

[563] M. Freimer, G. Kollia, G. S. Mudholkar, and C. T. Lin. a study of the generalized tukey lambda family. *Communications in Statistics - Theory and Methods*, 17(10):3547–3567, 1988. doi: 10.1080/03610928808829820. URL `https://doi.org/10.1080/03610928808829820`.

[564] B. Freivogel, R. Gobbetti, E. Pajer, and I.-S. Yang. Inflation on a Slippery Slope. 2016.

[565] A. Friedman. On the Curvature of space. *Z. Phys.*, 10:377–386, 1922. doi: 10.1007/BF01332580. [Gen. Rel. Grav.31,1991(1999)].

[566] J. Frieman, M. Turner, and D. Huterer. Dark Energy and the Accelerating Universe. *Ann. Rev. Astron. Astrophys.*, 46:385–432, 2008. doi: 10.1146/annurev.astro.46.060407.145243.

[567] J. A. Frieman, C. T. Hill, A. Stebbins, and I. Waga. Cosmology with ultralight pseudo Nambu-Goldstone bosons. *Phys. Rev. Lett.*, 75:2077–2080, 1995. doi: 10.1103/PhysRevLett.75.2077.

[568] H. Fritzsch and P. Minkowski. Unified interactions of leptons and hadrons. *Annals of Physics*, 93(1):193 – 266, 1975. ISSN 0003-4916. doi: https://doi.org/10.1016/0003-4916(75)90211-0. URL http://www.sciencedirect.com/science/article/pii/0003491675902110.

[569] V. P. Frolov, P. Krtouš, D. Kubizák, and J. E. Santos. Massive Vector Fields in Rotating Black-Hole Spacetimes: Separability and Quasinormal Modes. *Phys. Rev. Lett.*, 120:231103, 2018. doi: 10.1103/PhysRevLett.120.231103.

[570] G. Frye, C. W. Lee, and L. Susskind. Dual-symmetric theory of hadrons. *Il Nuovo Cimento A (1965-1970)*, 69(3):497–507, Oct 1970. ISSN 1826-9869. doi: 10.1007/BF02726486. URL https://doi.org/10.1007/BF02726486.

[571] J.-X. Fu and S.-T. Yau. The Theory of superstring with flux on non-Kahler manifolds and the complex Monge-Ampere equation. *J. Diff. Geom.*, 78(3): 369–428, 2008.

[572] T. Fugleberg, I. Halperin, and A. Zhitnitsky. Domain walls and theta dependence in qcd with an effective lagrangian approach. *Phys. Rev. D*, 59:074023, Mar 1999. doi: 10.1103/PhysRevD.59.074023. URL https://link.aps.org/doi/10.1103/PhysRevD.59.074023.

[573] M. Fujii and T. Yanagida. Natural gravitino dark matter and thermal leptogenesis in gauge-mediated supersymmetry-breaking models. *Physics Letters B*, 549(3):273 – 283, 2002. ISSN 0370-2693. doi: https://doi.org/10.1016/S0370-2693(02)02958-1. URL http://www.sciencedirect.com/science/article/pii/S0370269302029581.

[574] Y. Fukuda et al. Solar neutrino data covering solar cycle 22. *Phys. Rev.*

Lett., 77:1683–1686, Aug 1996. doi: 10.1103/PhysRevLett.77.1683. URL https://link.aps.org/doi/10.1103/PhysRevLett.77.1683.

[575] Y. Fukuda et al. Evidence for oscillation of atmospheric neutrinos. *Phys. Rev. Lett.*, 81:1562–1567, 1998. doi: 10.1103/PhysRevLett.81.1562.

[576] M. Fukugita and P. J. E. Peebles. The Cosmic energy inventory. *Astrophys. J.*, 616:643–668, 2004. doi: 10.1086/425155.

[577] M. Fukugita, C. J. Hogan, and P. J. E. Peebles. The Cosmic baryon budget. *Astrophys. J.*, 503:518, 1998. doi: 10.1086/306025.

[578] H. Furuhashi and Y. Nambu. Instability of massive scalar fields in Kerr-Newman space-time. *Prog. Theor. Phys.*, 112:983–995, 2004. doi: 10.1143/PTP.112.983.

[579] Y. V. Fyodorov. Introduction to the Random Matrix Theory: Gaussian Unitary Ensemble and Beyond. *arXiv e-prints*, art. math-ph/0412017, Dec. 2004.

[580] G. Gabadadze and M. Shifman. QCD vacuum and axions: What's happening? *Int. J. Mod. Phys.*, A17:3689–3728, 2002. doi: 10.1142/S0217751X02011357. [,521(2002)].

[581] G. Gabadadze and M. A. Shifman. Vacuum structure and the axion walls in gluodynamics and QCD with light quarks. *Phys. Rev.*, D62:114003, 2000. doi: 10.1103/PhysRevD.62.114003.

[582] M. K. Gaillard, P. D. Grannis, and F. J. Sciulli. The standard model of particle physics. *Rev. Mod. Phys.*, 71:S96–S111, Mar 1999. doi: 10.1103/RevModPhys.71.S96. URL https://link.aps.org/doi/10.1103/RevModPhys.71.S96.

[583] L. C. Gallo, G. Miniutti, J. M. Miller, L. W. Brenneman, A. C. Fabian, M. Guainazzi, and C. S. Reynolds. Multi-epoch X-ray observations of the

Seyfert 1.2 galaxy Mrk 79: bulk motion of the illuminating X-ray source. *MNRAS*, 411:607–619, Feb. 2011. doi: 10.1111/j.1365-2966.2010.17705.x.

[584] R. Gambini and J. Pullin. Black holes in loop quantum gravity: The Complete space-time. *Phys. Rev. Lett.*, 101:161301, 2008. doi: 10.1103/PhysRevLett.101.161301.

[585] G. Gamow. Expanding universe and the origin of elements. *Phys. Rev.*, 70: 572–573, Oct 1946. doi: 10.1103/PhysRev.70.572.2. URL `https://link.aps.org/doi/10.1103/PhysRev.70.572.2`.

[586] T. M. Garoni, P. J. Forrester, and N. E. Frankel. Asymptotic corrections to the eigenvalue density of the gue and lue. *Journal of Mathematical Physics*, 46(10):103301, 2005. doi: 10.1063/1.2035028. URL `https://doi.org/10.1063/1.2035028`.

[587] K. Garrett and G. Duda. Dark Matter: A Primer. *Adv. Astron.*, 2011:968283, 2011. doi: 10.1155/2011/968283.

[588] J. Gasser and H. Leutwyler. Quark Masses. *Phys. Rept.*, 87:77–169, 1982. doi: 10.1016/0370-1573(82)90035-7.

[589] M. Gaudin. Sur la loi limite de l'espacement des valeurs propres d'une matrice aléatoire. *Nucl. Phys. A*, 25:447–458, June 1961. doi: 10.1016/0029-5582(61)90176-6.

[590] M. Gaudin. Sur la loi limite de l'espacement des valeurs propres d'une matrice ale?atoire. *Nuclear Physics*, 25:447 – 458, 1961. ISSN 0029-5582. doi: https://doi.org/10.1016/0029-5582(61)90176-6. URL `http://www.sciencedirect.com/science/article/pii/0029558261901766`.

[591] K. Gebhardt, J. Adams, D. Richstone, T. R. Lauer, S. M. Faber, K. Gültekin, J. Murphy, and S. Tremaine. The Black Hole Mass in M87 from Gemini/NIFS Adaptive Optics Observations. *ApJ*, 729(2):119, Mar 2011. doi: 10.1088/0004-637X/729/2/119.

[592] M. Gell-Mann. Symmetries of baryons and mesons. *Phys. Rev.*, 125:1067–1084, 1962. doi: 10.1103/PhysRev.125.1067.

[593] M. Gell-Mann. A Schematic Model of Baryons and Mesons. *Phys. Lett.*, 8: 214–215, 1964. doi: 10.1016/S0031-9163(64)92001-3.

[594] M. Gell-Mann, R. J. Oakes, and B. Renner. Behavior of current divergences under SU(3) x SU(3). *Phys. Rev.*, 175:2195–2199, 1968. doi: 10.1103/PhysRev.175.2195.

[595] A. Gelman. Prior distributions for variance parameters in hierarchical models (comment on article by browne and draper). *Bayesian Anal.*, 1(3):515–534, 09 2006. doi: 10.1214/06-BA117A. URL `https://doi.org/10.1214/06-BA117A`.

[596] A. Gelman, J. B. Carlin, H. S. Stern, and D. B. Rubin. *Bayesian Data Analysis*. Chapman and Hall/CRC, 2nd ed. edition, 2004.

[597] H. Georgi and S. L. Glashow. Unity of all elementary-particle forces. *Phys. Rev. Lett.*, 32:438–441, Feb 1974. doi: 10.1103/PhysRevLett.32.438. URL `https://link.aps.org/doi/10.1103/PhysRevLett.32.438`.

[598] H. Georgi, D. B. Kaplan, and L. Randall. Manifesting the invisible axion at low energies. *Physics Letters B*, 169(1):73 – 78, 1986. ISSN 0370-2693. doi: https://doi.org/10.1016/0370-2693(86)90688-X. URL `http://www.sciencedirect.com/science/article/pii/037026938690688X`.

[599] P. D. F. Gernot Akemann, Jinho Baik. Oxford University Press, USA, 2015. URL `https://www.oxfordhandbooks.com/view/10.1093/oxfordhb/9780198744191.001.0001/oxfordhb-9780198744191`.

[600] G. W. Gibbons and S. W. Hawking. Action Integrals and Partition Functions in Quantum Gravity. *Phys. Rev.*, D15:2752–2756, 1977. doi: 10.1103/PhysRevD.15.2752.

[601] G. W. Gibbons and S. W. Hawking. Cosmological Event Horizons, Thermodynamics, and Particle Creation. *Phys. Rev.*, D15:2738–2751, 1977. doi: 10.1103/PhysRevD.15.2738.

[602] S. B. Giddings, S. Kachru, and J. Polchinski. Hierarchies from fluxes in string compactifications. *Phys. Rev.*, D66:106006, 2002. doi: 10.1103/PhysRevD.66.106006.

[603] G. Giesen, J. Lesgourgues, B. Audren, and Y. Ali-Haimoud. CMB photons shedding light on dark matter. *JCAP*, 1212:008, 2012. doi: 10.1088/1475-7516/2012/12/008.

[604] G. F. Giudice, R. Rattazzi, and A. Strumia. Unificaxion. *Phys. Lett.*, B715:142–148, 2012. doi: 10.1016/j.physletb.2012.07.028.

[605] A. Giveon, M. Porrati, and E. Rabinovici. Target space duality in string theory. *Phys. Rept.*, 244:77–202, 1994. doi: 10.1016/0370-1573(94)90070-1.

[606] S. L. Glashow. Partial Symmetries of Weak Interactions. *Nucl. Phys.*, 22:579–588, 1961. doi: 10.1016/0029-5582(61)90469-2.

[607] S. L. Glashow and S. Weinberg. Breaking chiral symmetry. *Phys. Rev. Lett.*, 20:224–227, 1968. doi: 10.1103/PhysRevLett.20.224.

[608] S. L. Glashow and S. Weinberg. Natural Conservation Laws for Neutral Currents. *Phys. Rev.*, D15:1958, 1977. doi: 10.1103/PhysRevD.15.1958.

[609] F. Gmeiner and G. Honecker. Mapping an Island in the Landscape. *JHEP*, 09:128, 2007. doi: 10.1088/1126-6708/2007/09/128.

[610] F. Gmeiner, R. Blumenhagen, G. Honecker, D. Lust, and T. Weigand. One in a billion: MSSM-like D-brane statistics. *JHEP*, 01:004, 2006. doi: 10.1088/1126-6708/2006/01/004.

[611] H. Goldberg. Constraint on the Photino Mass from Cosmology. *Phys.*

Rev. Lett., 50:1419, 1983. doi: 10.1103/PhysRevLett.103.099905,10.1103/PhysRevLett.50.1419. [,219(1983)].

[612] J. Goldstone, A. Salam, and S. Weinberg. Broken Symmetries. *Phys. Rev.*, 127:965–970, 1962. doi: 10.1103/PhysRev.127.965.

[613] Yu. A. Golfand and E. P. Likhtman. Extension of the Algebra of Poincare Group Generators and Violation of p Invariance. *JETP Lett.*, 13:323–326, 1971. [Pisma Zh. Eksp. Teor. Fiz.13,452(1971)].

[614] E. Gonzalez, G. Kane, K. D. Nguyen, and M. J. Perry. Quark and lepton mass matrices from localization in M-theory on G_2 orbifold. 2020.

[615] J. Goodman. Repulsive dark matter. *New Astron.*, 5:103, 2000. doi: 10.1016/S1384-1076(00)00015-4.

[616] J. Goodman and J. Weare. Ensemble Samplers with Affine Invariance. *Comm. Appl. Math. and Comp. Sci.*, 5:65–80, 2010.

[617] L. Gou, J. E. McClintock, J. Liu, R. Narayan, J. F. Steiner, R. A. Remillard, J. A. Orosz, S. W. Davis, K. Ebisawa, and E. M. Schlegel. A Determination of the Spin of the Black Hole Primary in LMC X-1. *ApJ*, 701:1076–1090, Aug. 2009. doi: 10.1088/0004-637X/701/2/1076.

[618] L. Gou, J. E. McClintock, J. F. Steiner, R. Narayan, A. G. Cantrell, C. D. Bailyn, and J. A. Orosz. The Spin of the Black Hole in the Soft X-ray Transient A0620-00. *ApJLett*, 718:L122–L126, Aug. 2010. doi: 10.1088/2041-8205/718/2/L122.

[619] L. Gou et al. Confirmation Via the Continuum-Fitting Method that the Spin of the Black Hole in Cygnus X-1 is Extreme. *Astrophys. J.*, 790(1):29, 2014. doi: 10.1088/0004-637X/790/1/29.

[620] P. Graf and F. D. Steffen. Thermal axion production in the primordial quark-

gluon plasma. *Phys. Rev.*, D83:075011, 2011. doi: 10.1103/PhysRevD.83.075011.

[621] P. W. Graham and S. Rajendran. New Observables for Direct Detection of Axion Dark Matter. *Phys. Rev.*, D88:035023, 2013. doi: 10.1103/PhysRevD.88.035023.

[622] P. W. Graham, D. E. Kaplan, S. Rajendran, and P. Saraswat. Displaced Supersymmetry. *JHEP*, 07:149, 2012. doi: 10.1007/JHEP07(2012)149.

[623] P. W. Graham, I. G. Irastorza, S. K. Lamoreaux, A. Lindner, and K. A. van Bibber. Experimental Searches for the Axion and Axion-Like Particles. *Ann. Rev. Nucl. Part. Sci.*, 65:485–514, 2015. doi: 10.1146/annurev-nucl-102014-022120.

[624] P. W. Graham, D. E. Kaplan, and S. Rajendran. Cosmological Relaxation of the Electroweak Scale. *Phys. Rev. Lett.*, 115(22):221801, 2015. doi: 10.1103/PhysRevLett.115.221801.

[625] M. Grana. Flux compactifications in string theory: A Comprehensive review. *Phys. Rept.*, 423:91–158, 2006. doi: 10.1016/j.physrep.2005.10.008.

[626] E. Grant. volume 18th ed. Isis, Vol. 78, No. 2., 1987. URL `pp.152-173`.

[627] E. Grant. *De caelo, Commentaries on Aristotle's*, pages 247–251. Springer Netherlands, Dordrecht, 2011. ISBN 978-1-4020-9729-4. doi: 10.1007/978-1-4020-9729-4_138. URL `https://doi.org/10.1007/978-1-4020-9729-4_138`.

[628] M. B. Green and J. H. Schwarz. Anomaly cancellations in supersymmetric d = 10 gauge theory and superstring theory. *Physics Letters B*, 149(1):117 – 122, 1984. ISSN 0370-2693. doi: https://doi.org/10.1016/0370-2693(84)91565-X. URL `http://www.sciencedirect.com/science/article/pii/037026938491565X`.

[629] M. B. Green, J. H. Schwarz, and E. Witten. *Superstring Theory. Volume 2: Loop Amplitudes, Anomalies and Phenomenology.* 1988. ISBN 9780521357531. URL http://www.cambridge.org/us/academic/subjects/physics/theoretical-physics-and-mathematical-physics/superstring-theory-volume-2.

[630] J. Greene, C. D. Bailyn, and J. A. Orosz. Optical and infrared photometry of the micro-quasar gro j1655-40 in quiescence. *Astrophys. J.*, 554:1290, 2001. doi: 10.1086/321411.

[631] G. Grilli di Cortona, E. Hardy, J. Pardo Vega, and G. Villadoro. The QCD axion, precisely. *JHEP*, 01:034, 2016. doi: 10.1007/JHEP01(2016)034.

[632] T. W. Grimm and J. Louis. The Effective action of N = 1 Calabi-Yau orientifolds. *Nucl. Phys.*, B699:387–426, 2004. doi: 10.1016/j.nuclphysb.2004.08.005.

[633] D. Grin, T. L. Smith, and M. Kamionkowski. Axion constraints in non-standard thermal histories. *Phys. Rev.*, D77:085020, 2008. doi: 10.1103/PhysRevD.77.085020.

[634] S. Groot Nibbelink, O. Loukas, and F. Ruehle. (MS)SM-like models on smooth Calabi-Yau manifolds from all three heterotic string theories. *Fortsch. Phys.*, 63:609–632, 2015. doi: 10.1002/prop.201500041.

[635] D. J. Gross, R. D. Pisarski, and L. G. Yaffe. Qcd and instantons at finite temperature. *Rev. Mod. Phys.*, 53:43–80, Jan 1981. doi: 10.1103/RevModPhys.53.43. URL https://link.aps.org/doi/10.1103/RevModPhys.53.43.

[636] D. J. Gross, J. A. Harvey, E. Martinec, and R. Rohm. Heterotic string. *Phys. Rev. Lett.*, 54:502–505, Feb 1985. doi: 10.1103/PhysRevLett.54.502. URL https://link.aps.org/doi/10.1103/PhysRevLett.54.502.

[637] D. J. Gross, J. A. Harvey, E. J. Martinec, and R. Rohm. Heterotic String

Theory. 1. The Free Heterotic String. *Nucl. Phys.*, B256:253, 1985. doi: 10.1016/0550-3213(85)90394-3.

[638] D. J. Gross, J. A. Harvey, E. J. Martinec, and R. Rohm. Heterotic String Theory. 2. The Interacting Heterotic String. *Nucl. Phys.*, B267:75–124, 1986. doi: 10.1016/0550-3213(86)90146-X.

[639] M. Gross and S. Haroche. Superradiance: An essay on the theory of collective spontaneous emission. *Physics Reports*, 93(5):301 – 396, 1982. ISSN 0370-1573. doi: https://doi.org/10.1016/0370-1573(82)90102-8. URL `http://www.sciencedirect.com/science/article/pii/0370157382901028`.

[640] T. Guhr and B. K. lber. A new method to estimate the noise in financial correlation matrices. *Journal of Physics A: Mathematical and General*, 36 (12):3009–3032, mar 2003. doi: 10.1088/0305-4470/36/12/310. URL `https://doi.org/10.1088%2F0305-4470%2F36%2F12%2F310`.

[641] T. Guhr, A. Muller-Groeling, and H. A. Weidenmuller. Random matrix theories in quantum physics: Common concepts. *Phys. Rept.*, 299:189–425, 1998. doi: 10.1016/S0370-1573(97)00088-4.

[642] S. Gukov, C. Vafa, and E. Witten. CFT's from Calabi-Yau four folds. *Nucl. Phys.*, B584:69–108, 2000. doi: 10.1016/S0550-3213(01)00289-9,10.1016/S0550-3213(00)00373-4. [Erratum: Nucl. Phys.B608,477(2001)].

[643] G. S. GURALNIK. The history of the guralnik, hagen and kibble development of the theory of spontaneous symmetry breaking and gauge particles. *International Journal of Modern Physics A*, 24(14):2601–2627, 2009. doi: 10.1142/S0217751X09045431. URL `https://doi.org/10.1142/S0217751X09045431`.

[644] G. S. Guralnik, C. R. Hagen, and T. W. B. Kibble. Global conservation laws and massless particles. *Phys. Rev. Lett.*, 13:585–587, Nov 1964. doi:

10.1103/PhysRevLett.13.585. URL https://link.aps.org/doi/10.1103/PhysRevLett.13.585.

[645] S. Gurrieri, J. Louis, A. Micu, and D. Waldram. Mirror symmetry in generalized Calabi-Yau compactifications. *Nucl. Phys.*, B654:61–113, 2003. doi: 10.1016/S0550-3213(03)00045-2.

[646] F. Gursey, P. Ramond, and P. Sikivie. A Universal Gauge Theory Model Based on E6. *Phys. Lett.*, 60B:177–180, 1976. doi: 10.1016/0370-2693(76)90417-2.

[647] A. H. Guth. Inflationary universe: A possible solution to the horizon and flatness problems. *Phys. Rev. D*, 23:347–356, Jan 1981. doi: 10.1103/PhysRevD.23.347. URL https://link.aps.org/doi/10.1103/PhysRevD.23.347.

[648] A. H. Guth. Eternal inflation and its implications. *J. Phys.*, A40:6811–6826, 2007. doi: 10.1088/1751-8113/40/25/S25.

[649] A. H. Guth. Eternal inflation and its implications. *Journal of Physics A: Mathematical and Theoretical*, 40(25):6811–6826, jun 2007. doi: 10.1088/1751-8113/40/25/s25. URL https://doi.org/10.1088%2F1751-8113%2F40%2F25%2Fs25.

[650] A. H. Guth and S. H. H. Tye. Phase transitions and magnetic monopole production in the very early universe. *Phys. Rev. Lett.*, 44:631–635, Mar 1980. doi: 10.1103/PhysRevLett.44.631. URL https://link.aps.org/doi/10.1103/PhysRevLett.44.631.

[651] F. Haake. *Superanalysis for Random-Matrix Theory*, pages 481–567. Springer Berlin Heidelberg, Berlin, Heidelberg, 2010. ISBN 978-3-642-05428-0. doi: 10.1007/978-3-642-05428-0_11. URL https://doi.org/10.1007/978-3-642-05428-0_11.

[652] W. Hachem, O. Khorunzhiy, P. Loubaton, J. Najim, and L. Pastur. A new

approach for mutual information analysis of large dimensional multi-antenna channels. *IEEE Transactions on Information Theory*, 54:3987–4004, 2008.

[653] J. S. Hagelin, G. L. Kane, and S. Raby. Perhaps Scalar Neutrinos Are the Lightest Supersymmetric Partners. *Nucl. Phys.*, B241:638–652, 1984. doi: 10.1016/0550-3213(84)90064-6.

[654] Z. Haiman, J. J. Mohr, and G. P. Holder. Constraints on quintessence from future galaxy cluster surveys. *Astrophys. J.*, 553:545, 2000. doi: 10.1086/320939.

[655] I. Halperin and A. Zhitnitsky. Anomalous effective lagrangian and θ dependence in qcd at finite N_c. *Phys. Rev. Lett.*, 81:4071–4074, Nov 1998. doi: 10.1103/PhysRevLett.81.4071. URL `https://link.aps.org/doi/10.1103/PhysRevLett.81.4071`.

[656] I. E. Halperin and A. Zhitnitsky. Axion potential, topological defects and CP odd bubbles in QCD. *Phys. Lett.*, B440:77–88, 1998. doi: 10.1016/S0370-2693(98)01085-5.

[657] J. Halverson and P. Langacker. TASI Lectures on Remnants from the String Landscape. *PoS*, TASI2017:019, 2018. doi: 10.22323/1.305.0019.

[658] J. Halverson and D. R. Morrison. On gauge enhancement and singular limits in g2 compactifications of m-theory. *Journal of High Energy Physics*, 2016 (4):100, Apr 2016. ISSN 1029-8479. doi: 10.1007/JHEP04(2016)100. URL `https://doi.org/10.1007/JHEP04(2016)100`.

[659] J. Halverson, C. Long, and P. Nath. Ultralight axion in supersymmetry and strings and cosmology at small scales. *Phys. Rev.*, D96(5):056025, 2017. doi: 10.1103/PhysRevD.96.056025.

[660] J. Halverson, C. Long, and B. Sung. Algorithmic universality in F-theory compactifications. *Phys. Rev.*, D96(12):126006, 2017. doi: 10.1103/PhysRevD.96.126006.

[661] J. Halverson, C. Long, and B. Sung. On the Scarcity of Weak Coupling in the String Landscape. *JHEP*, 02:113, 2018. doi: 10.1007/JHEP02(2018)113.

[662] J. Halverson, B. Nelson, and F. Ruehle. Branes with Brains: Exploring String Vacua with Deep Reinforcement Learning. *JHEP*, 06:003, 2019. doi: 10.1007/JHEP06(2019)003.

[663] W. Hampel et al. Gallex solar neutrino observations: results for gallex iv. *Physics Letters B*, 447(1):127 – 133, 1999. ISSN 0370-2693. doi: https://doi.org/10.1016/S0370-2693(98)01579-2. URL `http://www.sciencedirect.com/science/article/pii/S0370269398015792`.

[664] X. Han, G. M. Pan, and B. Zhang. The Tracy-Widom law for the Largest Eigenvalue of F Type Matrix. *arXiv e-prints*, art. arXiv:1506.00089, May 2015.

[665] X. Han, G. Pan, and Q. Yang. A unified matrix model including both CCA and F matrices in multivariate analysis: the largest eigenvalue and its applications. *arXiv e-prints*, art. arXiv:1606.04417, Jun 2016.

[666] X. Han, G. Pan, and B. Zhang. The tracy?widom law for the largest eigenvalue of f type matrices. *Ann. Statist.*, 44(4):1564–1592, 08 2016. doi: 10.1214/15-AOS1427. URL `https://doi.org/10.1214/15-AOS1427`.

[667] D. Hanneke, S. F. Hoogerheide, and G. Gabrielse. Cavity Control of a Single-Electron Quantum Cyclotron: Measuring the Electron Magnetic Moment. *Phys. Rev.*, A83:052122, 2011. doi: 10.1103/PhysRevA.83.052122.

[668] S. Hannestad and E. Mrtsell. Cosmological constraints on the dark energy equation of state and its evolution. *Journal of Cosmology and Astroparticle Physics*, 2004(09):001–001, sep 2004. doi: 10.1088/1475-7516/2004/09/001. URL `https://doi.org/10.1088%2F1475-7516%2F2004%2F09%2F001`.

[669] S. Hannestad, A. Mirizzi, G. G. Raffelt, and Y. Y. Y. Wong. Neutrino and

axion hot dark matter bounds after WMAP-7. *JCAP*, 1008:001, 2010. doi: 10.1088/1475-7516/2010/08/001.

[670] O. A. Hannuksela, R. Brito, E. Berti, and T. G. F. Li. Probing the existence of ultralight bosons with a single gravitational-wave measurement. 2018.

[671] D. R. Hardoon, S. Szedmak, and J. Shawe-Taylor. Canonical correlation analysis: An overview with application to learning methods. *Neural Computation*, 16(12):2639–2664, 2004. doi: 10.1162/0899766042321814. URL `https://doi.org/10.1162/0899766042321814`.

[672] T. Hasebe. Free infinite divisibility for beta distributions and related ones. *arXiv e-prints*, art. arXiv:1305.0924, May 2013.

[673] T. Hasebe and K. Szpojankowski. On free generalized inverse gaussian distributions. *Complex Analysis and Operator Theory*, Apr 2018. ISSN 1661-8262. doi: 10.1007/s11785-018-0790-9. URL `https://doi.org/10.1007/s11785-018-0790-9`.

[674] C. Hastings, F. Mosteller, J. W. Tukey, and C. P. Winsor. Low moments for small samples: A comparative study of order statistics. *Ann. Math. Statist.*, 18(3):413–426, 09 1947. doi: 10.1214/aoms/1177730388. URL `https://doi.org/10.1214/aoms/1177730388`.

[675] W. K. Hastings. Monte carlo sampling methods using markov chains and their applications. *Biometrika*, 57(1):97–109, 1970. ISSN 00063444. URL `http://www.jstor.org/stable/2334940`.

[676] S. W. Hawking. Gravitational radiation from colliding black holes. *Phys. Rev. Lett.*, 26:1344–1346, 1971. doi: 10.1103/PhysRevLett.26.1344.

[677] S. W. Hawking. Black hole explosions. *Nature*, 248:30–31, 1974. doi: 10.1038/248030a0.

[678] S. W. Hawking. Particle Creation by Black Holes. *Commun. Math. Phys.*, 43: 199–220, 1975. doi: 10.1007/BF02345020,10.1007/BF01608497. [,167(1975)].

[679] S. W. Hawking. Black Holes and Thermodynamics. *Phys. Rev.*, D13:191–197, 1976. doi: 10.1103/PhysRevD.13.191.

[680] S. W. Hawking. Breakdown of Predictability in Gravitational Collapse. *Phys. Rev.*, D14:2460–2473, 1976. doi: 10.1103/PhysRevD.14.2460.

[681] S. W. Hawking and T. Hertog. A Smooth Exit from Eternal Inflation? *JHEP*, 04:147, 2018. doi: 10.1007/JHEP04(2018)147.

[682] S. W. Hawking and D. N. Page. Thermodynamics of Black Holes in anti-De Sitter Space. *Commun. Math. Phys.*, 87:577, 1983. doi: 10.1007/BF01208266.

[683] S. W. Hawking and R. Penrose. The Singularities of gravitational collapse and cosmology. *Proc. Roy. Soc. Lond.*, A314:529–548, 1970. doi: 10.1098/rspa.1970.0021.

[684] S. W. Hawking, T. Hertog, and H. S. Reall. Trace anomaly driven inflation. *Phys. Rev.*, D63:083504, 2001. doi: 10.1103/PhysRevD.63.083504.

[685] H. Hayashi, R. Tatar, Y. Toda, T. Watari, and M. Yamazaki. New aspects of heteroticf-theory duality. *Nuclear Physics B*, 806(1):224 – 299, 2009. ISSN 0550-3213. doi: https://doi.org/10.1016/j.nuclphysb.2008.07.031. URL `http://www.sciencedirect.com/science/article/pii/S0550321308004264`.

[686] H. Hayashi, R. Tatar, Y. Toda, T. Watari, and M. Yamazaki. New Aspects of Heterotic–F Theory Duality. *Nucl. Phys.*, B806:224–299, 2009. doi: 10.1016/j.nuclphysb.2008.07.031.

[687] Y.-H. He. Deep-Learning the Landscape. 2017.

[688] Y.-H. He. The Calabi-Yau Landscape: from Geometry, to Physics, to Machine-Learning. 2018.

[689] Y.-H. He, V. Jejjala, and L. Pontiggia. Patterns in Calabi?Yau Distributions. *Commun. Math. Phys.*, 354(2):477–524, 2017. doi: 10.1007/s00220-017-2907-9.

[690] A. Heavens. Weak lensing: Dark Matter, Dark Energy and Dark Gravity. *Nuclear Physics B Proceedings Supplements*, 194:76–81, Oct 2009. doi: 10.1016/j.nuclphysbps.2009.07.005.

[691] A. Hebecker, S. C. Kraus, D. Lust, S. Steinfurt, and T. Weigand. Fluxbrane Inflation. *Nucl. Phys.*, B854:509–551, 2012. doi: 10.1016/j.nuclphysb.2011.08.025.

[692] J. J. Heckman and C. Vafa. Flavor Hierarchy From F-theory. *Nucl. Phys.*, B837:137–151, 2010. doi: 10.1016/j.nuclphysb.2010.05.009.

[693] B. Heidenreich, C. Long, L. McAllister, T. Rudelius, and J. Stout. Instanton Resummation and the Weak Gravity Conjecture. 2019.

[694] L. Heisenberg and A. Refregier. Cosmology in massive gravity with effective composite metric. *JCAP*, 1609(09):020, 2016. doi: 10.1088/1475-7516/2016/09/020.

[695] W. Heisenberg. Über den anschaulichen inhalt der quantentheoretischen kinematik und mechanik. *Zeitschrift für Physik*, 43(3):172–198, Mar 1927. ISSN 0044-3328. doi: 10.1007/BF01397280. URL `https://doi.org/10.1007/BF01397280`.

[696] W. Heisenberg. On the structure of atomic nuclei. *Z. Phys.*, 77:1–11, 1932. doi: 10.1007/BF01342433.

[697] W. Heisenberg and H. Euler. Consequences of Dirac's theory of positrons. *Z. Phys.*, 98(11-12):714–732, 1936. doi: 10.1007/BF01343663,10.1007/978-3-642-70078-1_9.

[698] A. Heithausen. Molecular hydrogen as baryonic dark matter. *Astrophys. J.*, 606:L13–L16, 2004. doi: 10.1086/421111.

[699] T. Helfer, D. J. E. Marsh, K. Clough, M. Fairbairn, E. A. Lim, and R. Becerril. Black hole formation from axion stars. *JCAP*, 1703(03):055, 2017. doi: 10.1088/1475-7516/2017/03/055.

[700] L. Hernquist, N. Katz, D. H. Weinberg, and J. Miralda-Escudé. The Lyman-Alpha Forest in the Cold Dark Matter Model. *ApJLett*, 457:L51, Feb. 1996. doi: 10.1086/309899.

[701] C. S. Herz. Bessel functions of matrix argument. *Annals of Mathematics*, 61 (3):474–523, 1955. ISSN 0003486X. URL `http://www.jstor.org/stable/1969810`.

[702] T. Higaki and T. Kobayashi. Note on moduli stabilization, supersymmetry breaking and axiverse. *Phys. Rev.*, D84:045021, 2011. doi: 10.1103/PhysRevD.84.045021.

[703] P. W. Higgs. Broken symmetries, massless particles and gauge fields. *Phys. Lett.*, 12:132–133, 1964. doi: 10.1016/0031-9163(64)91136-9.

[704] P. W. Higgs. Broken Symmetries and the Masses of Gauge Bosons. *Phys. Rev. Lett.*, 13:508–509, 1964. doi: 10.1103/PhysRevLett.13.508. [,160(1964)].

[705] P. W. Higgs. Spontaneous Symmetry Breakdown without Massless Bosons. *Phys. Rev.*, 145:1156–1163, 1966. doi: 10.1103/PhysRev.145.1156.

[706] D. Hilbert. The field of a single centre in Einstein's theory of gravitation and the motion of a particle in that field. *Nachr. Ges. Wiss. Gottingen*, Math. Phys. Kl.:53, 1917.

[707] C. T. Hill and G. G. Ross. Models and new phenomenological implications of a class of pseudo-goldstone bosons. *Nuclear Physics B*, 311(2):253 – 297, 1988. ISSN 0550-3213. doi: https://doi.org/10.1016/0550-3213(88)

90062-4. URL http://www.sciencedirect.com/science/article/pii/0550321388900624.

[708] M. B. Hindmarsh and T. W. B. Kibble. Cosmic strings. *Rept. Prog. Phys.*, 58:477–562, 1995. doi: 10.1088/0034-4885/58/5/001.

[709] G. Hinshaw, J. L. Weiland, R. S. Hill, N. Odegard, D. Larson, C. L. Bennett, J. Dunkley, B. Gold, M. R. Greason, N. Jarosik, E. Komatsu, M. R. Nolta, L. Page, D. N. Spergel, E. Wollack, M. Halpern, A. Kogut, M. Limon, S. S. Meyer, G. S. Tucker, and E. L. Wright. FIVE-YEARWILKINSON MICROWAVE ANISOTROPY PROBEOBSERVATIONS: DATA PROCESSING, SKY MAPS, AND BASIC RESULTS. *The Astrophysical Journal Supplement Series*, 180(2):225–245, feb 2009. doi: 10.1088/0067-0049/180/2/225. URL https://doi.org/10.1088%2F0067-0049%2F180%2F2%2F225.

[710] R. Hlozek, D. Grin, D. J. E. Marsh, and P. G. Ferreira. A search for ultralight axions using precision cosmological data. *Phys. Rev.*, D91(10):103512, 2015. doi: 10.1103/PhysRevD.91.103512.

[711] R. Hlozek, D. J. E. Marsh, D. Grin, R. Allison, J. Dunkley, and E. Calabrese. Future CMB tests of dark matter: ultra-light axions and massive neutrinos. 2016.

[712] L. Hollenstein, D. Sapone, R. Crittenden, and B. M. Schäfer. Constraints on early dark energy from CMB lensing and weak lensing tomography. *Journal of Cosmology and Astro-Particle Physics*, 2009(4):012, Apr 2009. doi: 10.1088/1475-7516/2009/04/012.

[713] E. Holmberg. A Study of Double and Multiple Galaxies Together with Inquiries into some General Metagalactic Problems. *Annals of the Observatory of Lund*, 6:1–173, 1937.

[714] M. Honda, A. Oikawa, and H. Otsuka. Axion decay constants at special points in type II string theory. *JHEP*, 01:064, 2017. doi: 10.1007/JHEP01(2017)064.

[715] P. Horava and E. Witten. Eleven-dimensional supergravity on a manifold with boundary. *Nucl. Phys.*, B475:94–114, 1996. doi: 10.1016/0550-3213(96)00308-2.

[716] J. R. M. Hosking. L-moments: Analysis and estimation of distributions using linear combinations of order statistics. *Journal of the Royal Statistical Society. Series B (Methodological)*, 52(1):105–124, 1990. ISSN 00359246. URL http://www.jstor.org/stable/2345653.

[717] F. Hoyle. A New Model for the Expanding Universe. *MNRAS*, 108:372, 1948. doi: 10.1093/mnras/108.5.372.

[718] C.-W. Hsu, M. S. Sinay, and J. S. J. Hsu. Bayesian estimation of a covariance matrix with flexible prior specification. *Annals of the Institute of Statistical Mathematics*, 64(2):319–342, Apr 2012. ISSN 1572-9052. doi: 10.1007/s10463-010-0314-5. URL https://doi.org/10.1007/s10463-010-0314-5.

[719] J. P. Hsu and R. Kallosh. Volume stabilization and the origin of the inflaton shift symmetry in string theory. *JHEP*, 04:042, 2004. doi: 10.1088/1126-6708/2004/04/042.

[720] J. P. Hsu, R. Kallosh, and S. Prokushkin. On brane inflation with volume stabilization. *JCAP*, 0312:009, 2003. doi: 10.1088/1475-7516/2003/12/009.

[721] P. L. HSU. On the distribution of roots of certain determinantal equations. *Annals of Eugenics*, 9(3):250–258, 1939. doi: 10.1111/j.1469-1809.1939.tb02212.x. URL https://onlinelibrary.wiley.com/doi/abs/10.1111/j.1469-1809.1939.tb02212.x.

[722] W. Hu, R. Barkana, and A. Gruzinov. Cold and fuzzy dark matter. *Phys. Rev. Lett.*, 85:1158–1161, 2000. doi: 10.1103/PhysRevLett.85.1158.

[723] A. Huang and M. P. Wand. Simple marginally noninformative prior distributions for covariance matrices. *Bayesian Anal.*, 8(2):439–452, 06 2013. doi: 10.1214/13-BA815. URL https://doi.org/10.1214/13-BA815.

[724] Y.-C. Huang and W. Taylor. Mirror symmetry and elliptic Calabi-Yau manifolds. *JHEP*, 04:083, 2019. doi: 10.1007/JHEP04(2019)083.

[725] E. Hubble. A relation between distance and radial velocity among extragalactic nebulae. *Proceedings of the National Academy of Sciences*, 15(3): 168–173, 1929. ISSN 0027-8424. doi: 10.1073/pnas.15.3.168. URL `https://www.pnas.org/content/15/3/168`.

[726] E. P. Hubble. Extragalactic nebulae. *ApJ*, 64, Dec. 1926. doi: 10.1086/143018.

[727] S. A. Hughes. The Evolution of circular, nonequatorial orbits of Kerr black holes due to gravitational wave emission. *Phys. Rev.*, D61(8):084004, 2000. doi: 10.1103/PhysRevD.65.069902,10.1103/PhysRevD.90.109904,10.1103/PhysRevD.61.084004,10.1103/PhysRevD.63.049902,10.1103/PhysRevD.67.089901. [Erratum: Phys. Rev.D90,no.10,109904(2014)].

[728] L. Hui, J. P. Ostriker, S. Tremaine, and E. Witten. Ultralight scalars as cosmological dark matter. *Phys. Rev.*, D95(4):043541, 2017. doi: 10.1103/PhysRevD.95.043541.

[729] C. M. Hull and P. K. Townsend. Unity of superstring dualities. *Nucl. Phys.*, B438:109–137, 1995. doi: 10.1016/0550-3213(94)00559-W. [,236(1994)].

[730] A. Hurwitz. uber die erzeugung der invarianten durch integration. *Nachrichten von der Gesellschaft der Wissenschaften zu Gottingen, Mathematisch-Physikalische Klasse*, 1897:71–2, 1897. URL `http://eudml.org/doc/58378`.

[731] D. Huterer. Weak lensing, dark matter and dark energy. *General Relativity and Gravitation*, 42(9):2177–2195, Sep 2010. doi: 10.1007/s10714-010-1051-z.

[732] E. Iacopini and E. Zavattini. Experimental method to detect the vacuum birefringence induced by a magnetic field. *Physics Letters B*, 85(1):151 – 154, 1979. ISSN 0370-2693. doi: https://doi.org/10.1016/0370-2693(79)

90797-4. URL http://www.sciencedirect.com/science/article/pii/0370269379907974.

[733] L. E. Ibanez. Gauge coupling unification: Strings versus SUSY GUTs. *Phys. Lett.*, B318:73–76, 1993. doi: 10.1016/0370-2693(93)91786-M.

[734] L. E. Ibanez and A. M. Uranga. *String theory and particle physics: An introduction to string phenomenology*. Cambridge University Press, 2012. ISBN 9780521517522, 9781139227421. URL http://www.cambridge.org/de/knowledge/isbn/item6563092/?site_locale=de_DE.

[735] L. E. Ibanez, J. E. Kim, H. P. Nilles, and F. Quevedo. Orbifold Compactifications with Three Families of SU(3) x SU(2) x U(1)**n. *Phys. Lett.*, B191: 282–286, 1987. doi: 10.1016/0370-2693(87)90255-3.

[736] L. E. Ibanez, F. Marchesano, D. Regalado, and I. Valenzuela. The Intermediate Scale MSSM, the Higgs Mass and F-theory Unification. *JHEP*, 07:195, 2012. doi: 10.1007/JHEP07(2012)195.

[737] L. Ibez. The scalar neutrinos as the lightest supersymmetric particles and cosmology. *Physics Letters B*, 137(3):160 – 164, 1984. ISSN 0370-2693. doi: https://doi.org/10.1016/0370-2693(84)90221-1. URL http://www.sciencedirect.com/science/article/pii/0370269384902211.

[738] L. Ibez, H. Nilles, and F. Quevedo. Orbifolds and wilson lines. *Physics Letters B*, 187(1):25 – 32, 1987. ISSN 0370-2693. doi: https://doi.org/10.1016/0370-2693(87)90066-9. URL http://www.sciencedirect.com/science/article/pii/0370269387900669.

[739] I. G. Irastorza and J. Redondo. New experimental approaches in the search for axion-like particles. *Prog. Part. Nucl. Phys.*, 102:89–159, 2018. doi: 10.1016/j.ppnp.2018.05.003.

[740] I. G. Irastorza et al. Prospects for solar axions searches with crystals via

Bragg scattering. *Nucl. Phys. Proc. Suppl.*, 87:102–104, 2000. doi: 10.1016/S0920-5632(00)00645-9. [,102(1999)].

[741] V. Irsic, M. Viel, M. G. Haehnelt, J. S. Bolton, and G. D. Becker. First constraints on fuzzy dark matter from Lyman-α forest data and hydrodynamical simulations. 2017.

[742] W. Israel. Event horizons in static vacuum space-times. *Phys. Rev.*, 164: 1776–1779, Dec 1967. doi: 10.1103/PhysRev.164.1776. URL `https://link.aps.org/doi/10.1103/PhysRev.164.1776`.

[743] W. Israel. Event horizons in static electrovac space-times. *Communications in Mathematical Physics*, 8(3):245–260, Sep 1968. ISSN 1432-0916. doi: 10.1007/BF01645859. URL `https://doi.org/10.1007/BF01645859`.

[744] A. H. J. A. Orosz, K. van der Hucht and C. E. (Eds.). A Massive Star Odyssey: From Main Sequence to Supernova. *IAU Symposium*, Volume 212: p. 365, 2003.

[745] T. Jacobson, G. Kang, and R. C. Myers. On black hole entropy. *Phys. Rev.*, D49:6587–6598, 1994. doi: 10.1103/PhysRevD.49.6587.

[746] A. T. James. The non-central wishart distribution. *Proceedings of the Royal Society of London. Series A, Mathematical and Physical Sciences*, 229(1178): 364–366, 1955. ISSN 00804630. URL `http://www.jstor.org/stable/99771`.

[747] A. T. James. Zonal polynomials of the real positive definite symmetric matrices. *Annals of Mathematics*, 74(3):456–469, 1961. ISSN 0003486X. URL `http://www.jstor.org/stable/1970291`.

[748] A. T. James. Distributions of matrix variates and latent roots derived from normal samples. *Ann. Math. Statist.*, 35(2):475–501, 06 1964. doi: 10.1214/aoms/1177703550. URL `https://doi.org/10.1214/aoms/1177703550`.

[749] A. T. James. Calculation of zonal polynomial coefficients by use of the laplace-beltrami operator. *Ann. Math. Statist.*, 39(5):1711–1718, 10 1968. doi: 10.1214/aoms/1177698153. URL https://doi.org/10.1214/aoms/1177698153.

[750] H. C. Ji. Properties of free multiplicative convolution. *arXiv e-prints*, art. arXiv:1903.02326, Mar 2019.

[751] D. Jiang, Z. Hou, and Z. Bai. Generalized Four Moment Theorem with an application to the CLT for the spiked eigenvalues of high-dimensional general Fisher-matrices. *arXiv e-prints*, art. arXiv:1904.09236, Apr 2019.

[752] H. Jockers and J. Louis. The Effective action of D7-branes in N = 1 Calabi-Yau orientifolds. *Nucl. Phys.*, B705:167–211, 2005. doi: 10.1016/j.nuclphysb.2004.11.009.

[753] K. Johansson. Shape Fluctuations and Random Matrices. *Communications in Mathematical Physics*, 209:437–476, Jan 2000. doi: 10.1007/s002200050027.

[754] I. M. Johnstone. On the distribution of the largest eigenvalue in principal components analysis. *Ann. Statist.*, 29(2):295–327, 04 2001. doi: 10.1214/aos/1009210544. URL https://doi.org/10.1214/aos/1009210544.

[755] I. M. Johnstone. High Dimensional Statistical Inference and Random Matrices. *arXiv Mathematics e-prints*, art. math/0611589, Nov 2006.

[756] W. Jun, W. Ya-Bo, W. Di, and Y. Wei-Qiang. Extended analysis on new generalized chaplygin gas. *Chinese Physics Letters*, 26(8):089801, aug 2009. doi: 10.1088/0256-307x/26/8/089801. URL https://doi.org/10.1088%2F0256-307x%2F26%2F8%2F089801.

[757] S. Kachru, R. Kallosh, A. D. Linde, J. M. Maldacena, L. P. McAllister, and S. P. Trivedi. Towards inflation in string theory. *JCAP*, 0310:013, 2003. doi: 10.1088/1475-7516/2003/10/013.

[758] S. Kachru, R. Kallosh, A. D. Linde, and S. P. Trivedi. De Sitter vacua in string theory. *Phys. Rev.*, D68(4):046005, Aug. 2003. doi: 10.1103/PhysRevD.68.046005.

[759] Y. Kahn, B. R. Safdi, and J. Thaler. Broadband and Resonant Approaches to Axion Dark Matter Detection. *Phys. Rev. Lett.*, 117(14):141801, 2016. doi: 10.1103/PhysRevLett.117.141801.

[760] R. Kallosh. On inflation in string theory. *Lect. Notes Phys.*, 738:119–156, 2008. doi: 10.1007/978-3-540-74353-8_4.

[761] R. Kallosh, N. Sivanandam, and M. Soroush. Axion Inflation and Gravity Waves in String Theory. *Phys. Rev.*, D77:043501, 2008. doi: 10.1103/PhysRevD.77.043501.

[762] N. Kaloper and L. Sorbo. Of pngb quintessence. *JCAP*, 0604:007, 2006. doi: 10.1088/1475-7516/2006/04/007.

[763] T. Kaluza. Zum Unitätsproblem der Physik. *Sitzungsber. Preuss. Akad. Wiss. Berlin (Math. Phys.)*, 1921:966–972, 1921. doi: 10.1142/S0218271818700017. [Int. J. Mod. Phys.D27,no.14,1870001(2018)].

[764] A. Yu. Kamenshchik, U. Moschella, and V. Pasquier. An Alternative to quintessence. *Phys. Lett.*, B511:265–268, 2001. doi: 10.1016/S0370-2693(01)00571-8.

[765] M. Kamionkowski, J. Pradler, and D. G. E. Walker. Dark energy from the string axiverse. *Phys. Rev. Lett.*, 113(25):251302, 2014. doi: 10.1103/PhysRevLett.113.251302.

[766] G. Kane and M. W. Winkler. Deriving the Inflaton in Compactified M-theory with a De Sitter Vacuum. *Phys. Rev.*, D100(6):066005, 2019. doi: 10.1103/PhysRevD.100.066005.

[767] G. Kane and M. W. Winkler. Baryogenesis from a Modulus Dominated Universe. *JCAP*, 2002(02):019, 2020. doi: 10.1088/1475-7516/2020/02/019.

[768] I. Kant. *Critique of Pure Reason*. The Cambridge Edition of the Works of Immanuel Kant. Cambridge University Press, New York, NY, 1998. Translated by Paul Guyer and Allen W. Wood.

[769] D. B. Kaplan. Opening the Axion Window. *Nucl. Phys.*, B260:215–226, 1985. doi: 10.1016/0550-3213(85)90319-0.

[770] J. Kaplan. Dark matter generation and split supersymmetry. *JHEP*, 10:065, 2006. doi: 10.1088/1126-6708/2006/10/065.

[771] M. Kaplinghat, L. Knox, and M. S. Turner. Annihilating the cold dark matter cusp crisis. *Phys. Rev. Lett.*, 85:3335, 2000. doi: 10.1103/PhysRevLett.85.3335.

[772] V. S. Kaplunovsky. One loop threshold effects in string unification. 1992.

[773] R. Kappl, S. Krippendorf, and H. P. Nilles. Aligned Natural Inflation: Monodromies of two Axions. *Phys. Lett.*, B737:124–128, 2014. doi: 10.1016/j.physletb.2014.08.045.

[774] R. Kappl, H. P. Nilles, and M. W. Winkler. Modulated Natural Inflation. *Phys. Lett.*, B753:653–659, 2016. doi: 10.1016/j.physletb.2015.12.073.

[775] J. C. Kapteyn. No. 230. First attempt at a theory of the arrangement and motion of the sideral system. *Contributions from the Mount Wilson Observatory / Carnegie Institution of Washington*, 230:1–27, 1922.

[776] Z. A. Karian and E. J. Dudewicz. Fitting the generalized lambda distribution to data: a method based on percentiles. *Communications in Statistics - Simulation and Computation*, 28(3):793–819, 1999. doi: 10.1080/03610919908813579. URL `https://doi.org/10.1080/03610919908813579`.

[777] A. Karozas, S. F. King, G. K. Leontaris, and A. Meadowcroft. Discrete

Family Symmetry from F-Theory GUTs. *JHEP*, 09:107, 2014. doi: 10.1007/JHEP09(2014)107.

[778] R. E. Kass and R. Natarajan. A default conjugate prior for variance components in generalized linear mixed models (comment on article by browne and draper). *Bayesian Anal.*, 1(3):535–542, 09 2006. doi: 10.1214/06-BA117B. URL `https://doi.org/10.1214/06-BA117B`.

[779] H. Kawai, D. C. Lewellen, and S.-H. H. Tye. Construction of fermionic string models in four dimensions. *Nuclear Physics B*, 288:1 – 76, 1987. ISSN 0550-3213. doi: https://doi.org/10.1016/0550-3213(87)90208-2. URL `http://www.sciencedirect.com/science/article/pii/0550321387902082`.

[780] M. Kawasaki and T. Moroi. Gravitino production in the inflationary universe and the effects on big bang nucleosynthesis. *Prog. Theor. Phys.*, 93:879–900, 1995. doi: 10.1143/PTP.93.879,10.1143/ptp/93.5.879.

[781] M. Kawasaki and K. Nakayama. Axions: Theory and Cosmological Role. *Ann. Rev. Nucl. Part. Sci.*, 63:69–95, 2013. doi: 10.1146/annurev-nucl-102212-170536.

[782] M. Kawasaki, K. Nakayama, and M. Senami. Cosmological implications of supersymmetric axion models. *JCAP*, 0803:009, 2008. doi: 10.1088/1475-7516/2008/03/009.

[783] R. P. Kerr. Gravitational field of a spinning mass as an example of algebraically special metrics. *Phys. Rev. Lett.*, 11:237–238, 1963. doi: 10.1103/PhysRevLett.11.237.

[784] S. Khalil, A. Moursy, and A. Nassar. Aspects of moduli stabilization in type IIB string theory. *Adv. High Energy Phys.*, 2016:4303752, 2016. doi: 10.1155/2016/4303752.

[785] A. Khmelnitsky and V. Rubakov. Pulsar timing signal from ultralight scalar dark matter. *JCAP*, 2:019, Feb. 2014. doi: 10.1088/1475-7516/2014/02/019.

[786] T. Kibble. Some implications of a cosmological phase transition. *Physics Reports*, 67(1):183 – 199, 1980. ISSN 0370-1573. doi: https://doi.org/10.1016/0370-1573(80)90091-5. URL http://www.sciencedirect.com/science/article/pii/0370157380900915.

[787] T. W. B. Kibble. Topology of cosmic domains and strings. *Journal of Physics A: Mathematical and General*, 9(8):1387–1398, aug 1976. doi: 10.1088/0305-4470/9/8/029. URL https://doi.org/10.1088%2F0305-4470%2F9%2F8%2F029.

[788] J. E. Kim. Weak Interaction Singlet and Strong CP Invariance. *Phys. Rev. Lett.*, 43:103, 1979. doi: 10.1103/PhysRevLett.43.103.

[789] J. E. Kim. Weak-interaction singlet and strong CP invariance. *Phys. Rev. Lett.*, 43:103–107, Jul 1979. doi: 10.1103/PhysRevLett.43.103. URL https://link.aps.org/doi/10.1103/PhysRevLett.43.103.

[790] J. E. Kim. Light pseudoscalars, particle physics and cosmology. *Phys. Rep.*, 150:1–177, 1987. doi: 10.1016/0370-1573(87)90017-2.

[791] J. E. Kim. Light pseudoscalars, particle physics and cosmology. *Physics Reports*, 150(1):1 – 177, 1987. ISSN 0370-1573. doi: https://doi.org/10.1016/0370-1573(87)90017-2. URL http://www.sciencedirect.com/science/article/pii/0370157387900172.

[792] J. E. Kim. Light Pseudoscalars, Particle Physics and Cosmology. *Phys. Rept.*, 150:1–177, 1987. doi: 10.1016/0370-1573(87)90017-2.

[793] J. E. Kim. Constraints on very light axions from cavity experiments. *Phys. Rev.*, D58:055006, 1998. doi: 10.1103/PhysRevD.58.055006.

[794] J. E. Kim. CP-Conservation in QCD and why only 'invisible' Axions work. pages 61–69, 2017. doi: 10.3204/DESY-PROC-2009-03/Kim_JihnE.

[795] J. E. Kim and G. Carosi. Axions and the Strong CP Problem. *Rev. Mod. Phys.*, 82:557–602, 2010. doi: 10.1103/RevModPhys.82.557.

[796] J. E. Kim and D. J. E. Marsh. An ultralight pseudoscalar boson. *Phys. Rev.*, D93(2):025027, 2016. doi: 10.1103/PhysRevD.93.025027.

[797] J. E. Kim and H. P. Nilles. The mu Problem and the Strong CP Problem. *Phys. Lett.*, 138B:150–154, 1984. doi: 10.1016/0370-2693(84)91890-2.

[798] J. E. Kim, H. P. Nilles, and M. Peloso. Completing natural inflation. *JCAP*, 0501:005, 2005. doi: 10.1088/1475-7516/2005/01/005.

[799] S. A. Kim and A. R. Liddle. Nflation: observable predictions from the random matrix mass spectrum. *Phys. Rev.*, D76:063515, 2007. doi: 10.1103/PhysRevD.76.063515.

[800] E. Kiritsis. *String theory in a nutshell.* Princeton University Press, USA, 2019. ISBN 9780691155791, 9780691188966. URL `https://press.princeton.edu/titles/13376.html`.

[801] A. Klein et al. Science with the space-based interferometer eLISA: Supermassive black hole binaries. *Phys. Rev.*, D93(2):024003, 2016. doi: 10.1103/PhysRevD.93.024003.

[802] O. Klein. Quantentheorie und fünfdimensionale relativitätstheorie. *Zeitschrift für Physik*, 37(12):895–906, Dec 1926. ISSN 0044-3328. doi: 10.1007/BF01397481. URL `https://doi.org/10.1007/BF01397481`.

[803] O. Klein. The Atomicity of Electricity as a Quantum Theory Law. *Nature*, 118:516, 1926. doi: 10.1038/118516a0.

[804] A. Klypin, J. Holtzman, J. Primack, and E. Regos. Structure formation with cold plus hot dark matter. *Astrophys. J.*, 416:1–16, 1993. doi: 10.1086/173210.

[805] A. A. Klypin, A. V. Kravtsov, O. Valenzuela, and F. Prada. Where are the

missing Galactic satellites? *Astrophys. J.*, 522:82–92, 1999. doi: 10.1086/307643.

[806] R. A. Knop et al. New Constraints on $\Omega_{\rm M}$, Ω_Λ, and w from an Independent Set of 11 High-Redshift Supernovae Observed with the Hubble Space Telescope. *ApJ*, 598:102–137, Nov. 2003. doi: 10.1086/378560.

[807] T. Kobayashi, M. Yamaguchi, and J. Yokoyama. Inflation driven by the galileon field. *Phys. Rev. Lett.*, 105:231302, Dec 2010. doi: 10.1103/PhysRevLett.105.231302. URL `https://link.aps.org/doi/10.1103/PhysRevLett.105.231302`.

[808] T. Kobayashi, R. Murgia, A. De Simone, V. Irši, and M. Viel. Lyman-α constraints on ultralight scalar dark matter: Implications for the early and late universe. *Phys. Rev.*, D96(12):123514, 2017. doi: 10.1103/PhysRevD.96.123514.

[809] H. Kodama. Superradiance and Instability of Black Holes. *Progress of Theoretical Physics Supplement*, 172:11–20, 2008. doi: 10.1143/PTPS.172.11.

[810] H. Kodama and H. Yoshino. Axiverse and Black Hole. *Int. J. Mod. Phys. Conf. Ser.*, 7:84–115, 2012. doi: 10.1142/S2010194512004199.

[811] W. Koenig. Orthogonal polynomial ensembles in probability theory. *arXiv Mathematics e-prints*, art. math/0403090, Mar. 2004.

[812] L. Kofman, A. D. Linde, and A. A. Starobinsky. Reheating after inflation. *Phys. Rev. Lett.*, 73:3195–3198, 1994. doi: 10.1103/PhysRevLett.73.3195.

[813] L. Kofman, A. D. Linde, and A. A. Starobinsky. Towards the theory of reheating after inflation. *Phys. Rev.*, D56:3258–3295, 1997. doi: 10.1103/PhysRevD.56.3258.

[814] I. I. Kogan. Axions, monopoles and cosmic strings. pages 0481–491, 1993.

[815] T. S. Koivisto and N. J. Nunes. Inflation and dark energy from three-forms.

Phys. Rev. D, 80:103509, Nov 2009. doi: 10.1103/PhysRevD.80.103509. URL https://link.aps.org/doi/10.1103/PhysRevD.80.103509.

[816] E. W. Kolb. First-order inflation. *Physica Scripta*, T36:199–217, jan 1991. doi: 10.1088/0031-8949/1991/t36/021. URL https://doi.org/10.1088%2F0031-8949%2F1991%2Ft36%2F021.

[817] E. W. Kolb and A. J. Long. Superheavy dark matter through Higgs portal operators. *Phys. Rev.*, D96(10):103540, 2017. doi: 10.1103/PhysRevD.96.103540.

[818] E. W. Kolb and M. S. Turner. *The early universe.* Addison-Wesley, 1990.

[819] E. Komatsu, J. Dunkley, M. R. Nolta, C. L. Bennett, B. Gold, G. Hinshaw, N. Jarosik, D. Larson, M. Limon, L. Page, D. N. Spergel, M. Halpern, R. S. Hill, A. Kogut, S. S. Meyer, G. S. Tucker, J. L. Weiland, E. Wollack, and E. L. Wright. Five-Year Wilkinson Microwave Anisotropy Probe Observations: Cosmological Interpretation. *ApJS*, 180:330–376, Feb. 2009. doi: 10.1088/0067-0049/180/2/330.

[820] A. Kong, J. S. Liu, and W. H. Wong. Sequential imputations and bayesian missing data problems. *Journal of the American Statistical Association*, 89 (425):278–288, 1994. ISSN 01621459. URL http://www.jstor.org/stable/2291224.

[821] M. Kontsevich. Intersection theory on the moduli space of curves and the matrix airy function. *Comm. Math. Phys.*, 147(1):1–23, 1992. URL https://projecteuclid.org:443/euclid.cmp/1104250524.

[822] A. Kovalev. Twisted connected sums and special Riemannian holonomy. *arXiv Mathematics e-prints*, art. math/0012189, Dec 2000.

[823] S. V. Krasnikov. New astrophysical constraints on the light-pseudoscalar–photon coupling. *Phys. Rev. Lett.*, 76:2633–2636, Apr 1996. doi: 10.

1103/PhysRevLett.76.2633. URL https://link.aps.org/doi/10.1103/PhysRevLett.76.2633.

[824] K. V. Krasnov. On Quantum statistical mechanics of Schwarzschild black hole. *Gen. Rel. Grav.*, 30:53–68, 1998. doi: 10.1023/A:1018820916342.

[825] M. Kreuzer and H. Skarke. Complete classification of reflexive polyhedra in four-dimensions. *Adv. Theor. Math. Phys.*, 4:1209–1230, 2002. doi: 10.4310/ATMP.2000.v4.n6.a2.

[826] A. Kuijlaars and W. V. Assche. The asymptotic zero distribution of orthogonal polynomials with varying recurrence coefficients. *Journal of Approximation Theory*, 99(1):167 – 197, 1999. ISSN 0021-9045. doi: https://doi.org/10.1006/jath.1999.3316. URL http://www.sciencedirect.com/science/article/pii/S0021904599933166.

[827] S. Kumar. Gap probabilities and densities of extreme eigenvalues of random matrices: Exact results. *arXiv e-prints*, art. arXiv:1507.08830, July 2015.

[828] A. Kusenko and M. E. Shaposhnikov. Supersymmetric Q balls as dark matter. *Phys. Lett.*, B418:46–54, 1998. doi: 10.1016/S0370-2693(97)01375-0.

[829] A. Kusenko, V. Kuzmin, M. Shaposhnikov, and P. G. Tinyakov. Experimental signatures of supersymmetric dark-matter Q-balls. *Phys. Rev. Lett.*, 80:3185–3188, Apr 1998. doi: 10.1103/PhysRevLett.80.3185. URL https://link.aps.org/doi/10.1103/PhysRevLett.80.3185.

[830] A. Kusenko, M. E. Shaposhnikov, and P. G. Tinyakov. Sufficient conditions for the existence of Q balls in gauge theories. *Pisma Zh. Eksp. Teor. Fiz.*, 67:229, 1998. doi: 10.1134/1.567658. [JETP Lett.67,247(1998)].

[831] V. Kuzmin and I. Tkachev. Ultrahigh-energy cosmic rays, superheavy long living particles, and matter creation after inflation. *JETP Lett.*, 68:271–275, 1998. doi: 10.1134/1.567858. [Pisma Zh. Eksp. Teor. Fiz.68,255(1998)].

[832] V. A. Kuzmin, V. A. Rubakov, and M. E. Shaposhnikov. On anomalous electroweak baryon-number non-conservation in the early universe. *Physics Letters B*, 155:36–42, May 1985. doi: 10.1016/0370-2693(85)91028-7.

[833] J. Kwak, J. Oon Lee, and J. Park. Extremal eigenvalues of sample covariance matrices with general population. *arXiv e-prints*, art. arXiv:1908.07444, Aug 2019.

[834] D. La and P. J. Steinhardt. Extended inflationary cosmology. *Phys. Rev. Lett.*, 62:376–378, Jan 1989. doi: 10.1103/PhysRevLett.62.376. URL `https://link.aps.org/doi/10.1103/PhysRevLett.62.376`.

[835] Z. Lalak, G. G. Ross, and S. Sarkar. Racetrack inflation and assisted moduli stabilisation. *Nucl. Phys.*, B766:1–20, 2007. doi: 10.1016/j.nuclphysb.2006.06.041.

[836] L. Laloux, P. Cizeau, J.-P. Bouchaud, and M. Potters. Noise dressing of financial correlation matrices. *Phys. Rev. Lett.*, 83:1467–1470, Aug 1999. doi: 10.1103/PhysRevLett.83.1467. URL `https://link.aps.org/doi/10.1103/PhysRevLett.83.1467`.

[837] P. Langacker. Grand Unified Theories and Proton Decay. *Phys. Rept.*, 72:185, 1981. doi: 10.1016/0370-1573(81)90059-4.

[838] N. Lartillot and H. Philippe. A Bayesian Mixture Model for Across-Site Heterogeneities in the Amino-Acid Replacement Process. *Molecular Biology and Evolution*, 21(6):1095–1109, 06 2004. ISSN 0737-4038. doi: 10.1093/molbev/msh112. URL `https://doi.org/10.1093/molbev/msh112`.

[839] G. Lazarides, R. K. Schaefer, D. Seckel, and Q. Shafi. Dilution of Cosmological Axions by Entropy Production. *Nucl. Phys.*, B346:193–212, 1990. doi: 10.1016/0550-3213(90)90244-8.

[840] E. W. Leaver. An Analytic representation for the quasi normal modes of

Kerr black holes. *Proc. Roy. Soc. Lond.*, A402:285–298, 1985. doi: 10.1098/rspa.1985.0119.

[841] O. Lebedev, H. P. Nilles, S. Raby, S. Ramos-Sanchez, M. Ratz, P. K. S. Vaudrevange, and A. Wingerter. A Mini-landscape of exact MSSM spectra in heterotic orbifolds. *Phys. Lett.*, B645:88–94, 2007. doi: 10.1016/j.physletb.2006.12.012.

[842] O. Lebedev, H. P. Nilles, S. Raby, S. Ramos-Sanchez, M. Ratz, P. K. S. Vaudrevange, and A. Wingerter. The Heterotic Road to the MSSM with R parity. *Phys. Rev.*, D77:046013, 2008. doi: 10.1103/PhysRevD.77.046013.

[843] O. Lebedev, H. P. Nilles, S. Ramos-Sanchez, M. Ratz, and P. K. S. Vaudrevange. Heterotic mini-landscape. (II). Completing the search for MSSM vacua in a Z(6) orbifold. *Phys. Lett.*, B668:331–335, 2008. doi: 10.1016/j.physletb.2008.08.054.

[844] G. Lemaître. Un Univers homogène de masse constante et de rayon croissant rendant compte de la vitesse radiale des nébuleuses extra-galactiques. *Annales de la Société Scientifique de Bruxelles*, 47:49–59, Jan 1927.

[845] G. Lemaitre. A Homogeneous Universe of Constant Mass and Growing Radius Accounting for the Radial Velocity of Extragalactic Nebulae. *Annales Soc. Sci. Bruxelles A*, 47:49–59, 1927. doi: 10.1007/s10714-013-1548-3. [Gen. Rel. Grav.45,no.8,1635(2013)].

[846] G. Lemaitre. The expanding universe. *Gen. Rel. Grav.*, 29:641–680, 1997. doi: 10.1023/A:1018855621348. [Annales Soc. Sci. Bruxelles A53,51(1933)].

[847] G. K. Leontaris and G. G. Ross. Yukawa couplings and fermion mass structure in F-theory GUTs. *JHEP*, 02:108, 2011. doi: 10.1007/JHEP02(2011)108.

[848] W. LERCHE, D. LST, and A. SCHELLEKENS. Chiral four-dimensional heterotic strings from self-dual lattices. In B. SCHELLEKENS, edi-

tor, *Superstring Construction*, volume 4 of *Current PhysicsSources and Comments*, pages 252 – 282. Elsevier, 1989. doi: https://doi.org/10.1016/B978-0-444-87492-4.50024-0. URL http://www.sciencedirect.com/science/article/pii/B9780444874924500240.

[849] H. Leutwyler. The ratios of the light quark masses. *Physics Letters B*, 378(1):313 – 318, 1996. ISSN 0370-2693. doi: https://doi.org/10.1016/0370-2693(96)00386-3. URL http://www.sciencedirect.com/science/article/pii/0370269396003863.

[850] D. G. Levkov, A. G. Panin, and I. I. Tkachev. Relativistic Axions from Collapsing Bose Stars. *Physical Review Letters*, 118(1):011301, Jan. 2017. doi: 10.1103/PhysRevLett.118.011301.

[851] M. Li. A Model of holographic dark energy. *Phys. Lett.*, B603:1, 2004. doi: 10.1016/j.physletb.2004.10.014.

[852] M. Li, X.-D. Li, S. Wang, and Y. Wang. Dark Energy: A Brief Review. *Front. Phys.(Beijing)*, 8:828–846, 2013. doi: 10.1007/s11467-013-0300-5.

[853] M. Li, L. Gao, and J. Wang. The abundance of satellite galaxies in the inner region of ΛCDM Milky Way sized haloes. *Mon. Not. Roy. Astron. Soc.*, 483 (2):2000–2006, 2019. doi: 10.1093/mnras/sty3292.

[854] R. Li, J. Wang, X.-L. Qi, and S.-C. Zhang. Dynamical axion field in topological magnetic insulators. *Nature Physics*, 6(4):284–288, Apr 2010. doi: 10.1038/nphys1534.

[855] R. Li, C. S. Frenk, S. Cole, L. Gao, S. Bose, and W. A. Hellwing. Constraints on the identity of the dark matter from strong gravitational lenses. *Mon. Not. Roy. Astron. Soc.*, 460(1):363–372, 2016. doi: 10.1093/mnras/stw939.

[856] F. Liang, R. Paulo, G. Molina, M. A. Clyde, and J. O. Berger. Mixtures of g priors for bayesian variable selection. *Journal of the American Statistical As-*

sociation, 103(481):410–423, 2008. doi: 10.1198/016214507000001337. URL https://doi.org/10.1198/016214507000001337.

[857] A. R. Liddle and D. H. Lyth. Inflation and mixed dark matter models. *Mon. Not. Roy. Astron. Soc.*, 265:379, 1993. doi: 10.1093/mnras/265.2.379.

[858] A. R. Liddle and R. J. Scherrer. A Classification of scalar field potentials with cosmological scaling solutions. *Phys. Rev.*, D59:023509, 1999. doi: 10.1103/PhysRevD.59.023509.

[859] A. R. Liddle, A. Mazumdar, and F. E. Schunck. Assisted inflation. *Phys. Rev.*, D58:061301, 1998. doi: 10.1103/PhysRevD.58.061301.

[860] A. R. Liddle, A. Mazumdar, and F. E. Schunck. Assisted inflation. *Phys. Rev. D*, 58:061301, Aug 1998. doi: 10.1103/PhysRevD.58.061301. URL https://link.aps.org/doi/10.1103/PhysRevD.58.061301.

[861] A. Lidz and L. Hui. The Implications of a Pre-reionization 21 cm Absorption Signal for Fuzzy Dark Matter. 2018.

[862] A. Linde. Primordial inflation without primodial monopoles. *Physics Letters B*, 132(4):317 – 320, 1983. ISSN 0370-2693. doi: https://doi.org/10.1016/0370-2693(83)90316-7. URL http://www.sciencedirect.com/science/article/pii/0370269383903167.

[863] A. LINDE. Eternal chaotic inflation. *Modern Physics Letters A*, 01(02):81–85, 1986. doi: 10.1142/S0217732386000129. URL https://doi.org/10.1142/S0217732386000129.

[864] A. D. Linde. A New Inflationary Universe Scenario: A Possible Solution of the Horizon, Flatness, Homogeneity, Isotropy and Primordial Monopole Problems. *Phys. Lett.*, 108B:389–393, 1982. doi: 10.1016/0370-2693(82)91219-9. [Adv. Ser. Astrophys. Cosmol.3,149(1987)].

[865] A. D. Linde. Chaotic Inflation. *Phys. Lett.*, 129B:177–181, 1983. doi: 10.1016/0370-2693(83)90837-7.

[866] A. D. Linde. Hybrid inflation. *Phys. Rev.*, D49:748–754, 1994. doi: 10.1103/PhysRevD.49.748.

[867] A. D. Linde. Inflation, quantum cosmology and the anthropic principle. In *Science and ultimate reality: Quantum theory, cosmology, and complexity*, pages 426–458, 2002.

[868] E. V. Linder. Exploring the Expansion History of the Universe. *Physical Review Letters*, 90(9):091301, Mar. 2003. doi: 10.1103/PhysRevLett.90.091301.

[869] A. G. Lisi. An Exceptionally Simple Theory of Everything. 2007.

[870] D.-Z. Liu, C. Song, and Z.-D. Wang. On Explicit Probability Densities Associated with Fuss-Catalan Numbers. *arXiv e-prints*, art. arXiv:1008.0271, Aug 2010.

[871] J. Liu, J. E. McClintock, R. Narayan, S. W. Davis, and J. A. Orosz. Precise measurement of the spin parameter of the stellar-mass black hole m33 x-7. *The Astrophysical Journal Letters*, 679(1):L37, 2008. URL `http://stacks.iop.org/1538-4357/679/i=1/a=L37`.

[872] A. M. Lohfink, C. S. Reynolds, J. M. Miller, L. W. Brenneman, R. F. Mushotzky, M. A. Nowak, and A. C. Fabian. The Black Hole Spin and Soft X-Ray Excess of the Luminous Seyfert Galaxy Fairall 9. *ApJ*, 758:67, Oct. 2012. doi: 10.1088/0004-637X/758/1/67.

[873] C. Long, L. McAllister, and P. McGuirk. Heavy Tails in Calabi-Yau Moduli Spaces. *JHEP*, 10:187, 2014. doi: 10.1007/JHEP10(2014)187.

[874] C. Long, L. McAllister, and J. Stout. Systematics of Axion Inflation in Calabi-Yau Hypersurfaces. *JHEP*, 02:14, Feb. 2017. doi: 10.1007/JHEP02(2017)014.

[875] C. Lovelace. Pomeron form-factors and dual Regge cuts. *Phys. Lett.*, 34B: 500–506, 1971. doi: 10.1016/0370-2693(71)90665-4.

[876] F. Lucchin and S. Matarrese. Power-law inflation. *Phys. Rev. D*, 32:1316–1322, Sep 1985. doi: 10.1103/PhysRevD.32.1316. URL `https://link.aps.org/doi/10.1103/PhysRevD.32.1316`.

[877] K. Lundmark. Über die Bestimmung der Entfernungen, Dimensionen, Massen und Dichtigkeit fur die nächstgelegenen anagalacktischen Sternsysteme. *Meddelanden fran Lunds Astronomiska Observatorium Serie I*, 125: 1–13, 1930.

[878] O. Lunin and S. D. Mathur. AdS / CFT duality and the black hole information paradox. *Nucl. Phys.*, B623:342–394, 2002. doi: 10.1016/S0550-3213(01)00620-4.

[879] J. Luo et al. TianQin: a space-borne gravitational wave detector. *Class. Quant. Grav.*, 33(3):035010, 2016. doi: 10.1088/0264-9381/33/3/035010.

[880] D. Lust. Intersecting brane worlds: A Path to the standard model? *Class. Quant. Grav.*, 21:S1399–1424, 2004. doi: 10.1088/0264-9381/21/10/013.

[881] D. Lynden-Bell and P. P. Eggleton. On the consequences of the gravothermal catastrophe. *Monthly Notices of the Royal Astronomical Society*, 191(3): 483–498, 07 1980. ISSN 0035-8711. doi: 10.1093/mnras/191.3.483. URL `https://doi.org/10.1093/mnras/191.3.483`.

[882] D. H. Lyth. What would we learn by detecting a gravitational wave signal in the cosmic microwave background anisotropy? *Phys. Rev. Lett.*, 78:1861–1863, 1997. doi: 10.1103/PhysRevLett.78.1861.

[883] D. H. Lyth and A. Riotto. Particle physics models of inflation and the cosmological density perturbation. *Phys. Rept.*, 314:1–146, 1999. doi: 10.1016/S0370-1573(98)00128-8.

[884] D. H. Lyth and E. D. Stewart. Thermal inflation and the moduli problem. *Phys. Rev.*, D53:1784–1798, 1996. doi: 10.1103/PhysRevD.53.1784.

[885] D. H. Lyth, K. A. Malik, and M. Sasaki. A General proof of the conservation of the curvature perturbation. *JCAP*, 0505:004, 2005. doi: 10.1088/1475-7516/2005/05/004.

[886] Y.-Z. Ma, G. Hinshaw, and D. Scott. WMAP Observations of Planck ESZ Clusters. *Astrophys. J.*, 771:137, 2013. doi: 10.1088/0004-637X/771/2/137.

[887] K. J. Mack and P. J. Steinhardt. Cosmological Problems with Multiple Axion-like Fields. *JCAP*, 1105:001, 2011. doi: 10.1088/1475-7516/2011/05/001.

[888] K.-i. Maeda. Inflation as a transient attractor in R^2 cosmology. *Phys. Rev. D*, 37:858–862, Feb 1988. doi: 10.1103/PhysRevD.37.858. URL `https://link.aps.org/doi/10.1103/PhysRevD.37.858`.

[889] A. Maharana and E. Palti. Models of Particle Physics from Type IIB String Theory and F-theory: A Review. *Int. J. Mod. Phys.*, A28:1330005, 2013. doi: 10.1142/S0217751X13300056.

[890] L. Maiani, R. Petronzio, and E. Zavattini. Effects of nearly massless, spin-zero particles on light propagation in a magnetic field. *Physics Letters B*, 175(3):359 – 363, 1986. ISSN 0370-2693. doi: https://doi.org/10.1016/0370-2693(86)90869-5. URL `http://www.sciencedirect.com/science/article/pii/0370269386908695`.

[891] Z. Maki, M. Nakagawa, and S. Sakata. Remarks on the unified model of elementary particles. *Prog. Theor. Phys.*, 28:870–880, 1962. doi: 10.1143/PTP.28.870. [,34(1962)].

[892] J. M. Maldacena. *Black holes in string theory*. PhD thesis, Princeton U., 1996. URL `http://wwwlib.umi.com/dissertations/fullcit?p9627605`.

[893] J. M. Maldacena and C. Nunez. Supergravity description of field theories

on curved manifolds and a no go theorem. *Int. J. Mod. Phys.*, A16:822–855, 2001. doi: 10.1142/S0217751X01003935,10.1142/S0217751X01003937. [,182(2000)].

[894] J. M. Maldacena, A. Strominger, and E. Witten. Black hole entropy in M theory. *JHEP*, 12:002, 1997. doi: 10.1088/1126-6708/1997/12/002.

[895] Y. Malevergne and D. Sornette. Collective origin of the coexistence of apparent random matrix theory noise and of factors in large sample correlation matrices. *Physica A Statistical Mechanics and its Applications*, 331:660–668, Jan 2004. doi: 10.1016/j.physa.2003.09.004.

[896] K. S. Mandel, W. M. Wood-Vasey, A. S. Friedman, and R. P. Kirshner. Type Ia Supernova Light-Curve Inference: Hierarchical Bayesian Analysis in the Near-Infrared. *ApJ*, 704(1):629–651, Oct 2009. doi: 10.1088/0004-637X/704/1/629.

[897] K. S. Mandel, R. J. Foley, and R. P. Kirshner. Type Ia Supernova Colors and Ejecta Velocities: Hierarchical Bayesian Regression with Non-Gaussian Distributions. *Astrophys. J.*, 797(2):75, 2014. doi: 10.1088/0004-637X/797/2/75.

[898] G. Mangano, G. Miele, S. Pastor, T. Pinto, O. Pisanti, and P. D. Serpico. Relic neutrino decoupling including flavor oscillations. *Nucl. Phys.*, B729:221–234, 2005. doi: 10.1016/j.nuclphysb.2005.09.041.

[899] M. Mangano. TASI Lectures on Future Colliders. In *Theoretical Advanced Study Institute in Elementary Particle Physics: Theory in an Era of Data (TASI 2018) Boulder, Colorado, USA, June 4-29, 2018*, 2019.

[900] S. Mantry, M. Pitschmann, and M. J. Ramsey-Musolf. Distinguishing axions from generic light scalars using electric dipole moment and fifth-force experiments. *Phys. Rev.*, D90(5):054016, 2014. doi: 10.1103/PhysRevD.90.054016.

[901] V. A. Marčenko and L. A. Pastur. Distribution of eigenvalues for some sets of

random matrices. *Mathematics of the USSR-Sbornik*, 1(4):457–483, apr 1967. doi: 10.1070/sm1967v001n04abeh001994. URL https://doi.org/10.1070%2Fsm1967v001n04abeh001994.

[902] M. C. March, R. Trotta, P. Berkes, G. D. Starkman, and P. M. Vaudrevange. Improved constraints on cosmological parameters from Type Ia supernova data. *MNRAS*, 418(4):2308–2329, Dec 2011. doi: 10.1111/j.1365-2966.2011.19584.x.

[903] F. Marchesano. Progress in D-brane model building. *Fortsch. Phys.*, 55: 491–518, 2007. doi: 10.1002/prop.200610381.

[904] F. Marchesano, G. Shiu, and A. M. Uranga. F-term Axion Monodromy Inflation. *JHEP*, 09:184, 2014. doi: 10.1007/JHEP09(2014)184.

[905] F. Marchesano, D. Regalado, and G. Zoccarato. Yukawa hierarchies at the point of E_8 in F-theory. *JHEP*, 04:179, 2015. doi: 10.1007/JHEP04(2015)179.

[906] W. J. Marciano, A. Masiero, P. Paradisi, and M. Passera. Contributions of axionlike particles to lepton dipole moments. *Phys. Rev.*, D94(11):115033, 2016. doi: 10.1103/PhysRevD.94.115033.

[907] J. Marsano. Hypercharge flux, exotics, and anomaly cancellation in f-theory grand unification. *Phys. Rev. Lett.*, 106:081601, Feb 2011. doi: 10.1103/PhysRevLett.106.081601. URL https://link.aps.org/doi/10.1103/PhysRevLett.106.081601.

[908] J. Marsano, N. Saulina, and S. Schafer-Nameki. Gauge Mediation in F-Theory GUT Models. *Phys. Rev.*, D80:046006, 2009. doi: 10.1103/PhysRevD.80.046006.

[909] D. Marsh, L. McAllister, and T. Wrase. The Wasteland of Random Supergravities. *JHEP*, 03:102, 2012. doi: 10.1007/JHEP03(2012)102.

[910] D. J. E. Marsh. Nonlinear hydrodynamics of axion dark matter: Relative

velocity effects and quantum forces. *Phys. Rev. D*, 91(12):123520, June 2015. doi: 10.1103/PhysRevD.91.123520.

[911] D. J. E. Marsh. Axion Cosmology. *Phys. Rept.*, 643:1–79, 2016. doi: 10.1016/j.physrep.2016.06.005.

[912] D. J. E. Marsh and J. C. Niemeyer. Strong Constraints on Fuzzy Dark Matter from Ultrafaint Dwarf Galaxy Eridanus II. 2018.

[913] D. J. E. Marsh and A.-R. Pop. Axion dark matter, solitons and the cusp?core problem. *Mon. Not. Roy. Astron. Soc.*, 451(3):2479–2492, 2015. doi: 10.1093/mnras/stv1050.

[914] D. J. E. Marsh and J. Silk. A model for halo formation with axion mixed dark matter. *MNRAS*, 437:2652–2663, Jan. 2014. doi: 10.1093/mnras/stt2079.

[915] D. J. E. Marsh, E. R. M. Tarrant, E. J. Copeland, and P. G. Ferreira. Cosmology of axions and moduli: A dynamical systems approach. *Phys. Rev. D*, 86(2):023508, July 2012. doi: 10.1103/PhysRevD.86.023508.

[916] D. J. E. Marsh, D. Grin, R. Hložek, and P. G. Ferreira. Axiverse cosmology and the energy scale of inflation. *Phys. Rev. D*, 87(12):121701, June 2013. doi: 10.1103/PhysRevD.87.121701.

[917] D. J. E. Marsh, D. Grin, R. Hlozek, and P. G. Ferreira. Tensor Interpretation of BICEP2 Results Severely Constrains Axion Dark Matter. *Phys. Rev. Lett.*, 113(1):011801, 2014. doi: 10.1103/PhysRevLett.113.011801.

[918] M. C. D. Marsh, L. McAllister, E. Pajer, and T. Wrase. Charting an Inflationary Landscape with Random Matrix Theory. *JCAP*, 1311:040, 2013. doi: 10.1088/1475-7516/2013/11/040.

[919] S. P. Martin. A Supersymmetry primer. pages 1–98, 1997. doi: 10.1142/9789812839657_0001,10.1142/9789814307505_0001. [Adv. Ser. Direct. High Energy Phys.18,1(1998)].

[920] Y. Maruyama and E. I. George. Fully bayes factors with a generalized g -prior. *Ann. Statist.*, 39(5):2740–2765, 10 2011. doi: 10.1214/11-AOS917. URL `https://doi.org/10.1214/11-AOS917`.

[921] A. Masoumi and A. Vilenkin. Vacuum statistics and stability in axionic landscapes. *JCAP*, 1603(03):054, 2016. doi: 10.1088/1475-7516/2016/03/054.

[922] A. Masoumi, A. Vilenkin, and M. Yamada. Inflation in random Gaussian landscapes. *JCAP*, 1705(05):053, 2017. doi: 10.1088/1475-7516/2017/05/053.

[923] A. Masoumi, A. Vilenkin, and M. Yamada. Initial conditions for slow-roll inflation in a random Gaussian landscape. *JCAP*, 1707(07):003, 2017. doi: 10.1088/1475-7516/2017/07/003.

[924] A. Masoumi, A. Vilenkin, and M. Yamada. Inflation in multi-field random Gaussian landscapes. *JCAP*, 1712(12):035, 2017. doi: 10.1088/1475-7516/2017/12/035.

[925] R. Massey, T. Kitching, and J. Richard. The dark matter of gravitational lensing. *Rept. Prog. Phys.*, 73:086901, 2010. doi: 10.1088/0034-4885/73/8/086901.

[926] E. Masso, F. Rota, and G. Zsembinszki. On axion thermalization in the early universe. *Phys. Rev.*, D66:023004, 2002. doi: 10.1103/PhysRevD.66.023004.

[927] S. D. Mathur. Fuzzballs and the information paradox: A Summary and conjectures. 2008.

[928] P. Mayr and S. Stieberger. Moduli dependence of one loop gauge couplings in (0,2) compactifications. *Phys. Lett.*, B355:107–116, 1995. doi: 10.1016/0370-2693(95)00683-C.

[929] P. Mayr, H. P. Nilles, and S. Stieberger. String unification and threshold corrections. *Phys. Lett.*, B317:53–59, 1993. doi: 10.1016/0370-2693(93)91569-9.

[930] A. Mayukh Sengupta and P. Pratim Mitra. Capacity of multivariate channels with multiplicative noise: I.Random matrix techniques and large-N expansions for full transfer matrices. *arXiv e-prints*, art. physics/0010081, Oct 2000.

[931] L. McAllister, E. Silverstein, and A. Westphal. Gravity Waves and Linear Inflation from Axion Monodromy. *Phys. Rev.*, D82:046003, 2010. doi: 10.1103/PhysRevD.82.046003.

[932] J. E. McClintock, R. Shafee, R. Narayan, R. A. Remillard, S. W. Davis, and L.-X. Li. The Spin of the Near-Extreme Kerr Black Hole GRS 1915+105. *Astrophys. J.*, 652:518–539, 2006. doi: 10.1086/508457.

[933] J. E. McClintock, R. Narayan, and J. F. Steiner. Black Hole Spin via Continuum Fitting and the Role of Spin in Powering Transient Jets. *Space Sci. Rev.*, 183:295–322, 2014. doi: 10.1007/s11214-013-0003-9.

[934] P. McCullagh. What is a statistical model? *Ann. Statist.*, 30(5):1225–1310, 10 2002. doi: 10.1214/aos/1035844977. URL `https://doi.org/10.1214/aos/1035844977`.

[935] S. S. McGaugh. Confrontation of MOND predictions with WMAP first year data. *Astrophys. J.*, 611:26–39, 2004. doi: 10.1086/421895.

[936] I. M. McHardy, K. F. Gunn, P. Uttley, and M. R. Goad. MCG-6-30-15: Long timescale x-ray variability, black hole mass and AGN high states. *Mon. Not. Roy. Astron. Soc.*, 359:1469–1480, 2005. doi: 10.1111/j.1365-2966.2005.08992.x.

[937] C. F. McKee, A. Parravano, and D. J. Hollenbach. Stars, Gas, and Dark Matter in the Solar Neighborhood. *ApJ*, 814(1):13, Nov 2015. doi: 10.1088/0004-637X/814/1/13.

[938] M. Mehta. On the statistical properties of the level-spacings in nuclear spectra. *Nuclear Physics*, 18:395 – 419, 1960. ISSN 0029-5582. doi: https://doi.org/10.1016/0029-5582(60)90413-2. URL http://www.sciencedirect.com/science/article/pii/0029558260904132.

[939] M. L. MEHTA. volume 3rd ed. Amsterdam, Academic Press, 2004. URL http://search.ebscohost.com/login.aspx?direct=true&scope=site&db=nlebk&db=nlabk&AN=189456.

[940] M. L. Mehta and J. des Cloizeaux. THE PROBABILITIES FOR SEVERAL CONSECUTIVE EIGENVALUES OF A RANDOM MATRIX. *Submitted to: Indian J. Pure and Appl. Phys.*, 1970.

[941] N. Metropolis, A. W. Rosenbluth, M. N. Rosenbluth, A. H. Teller, and E. Teller. Equation of State Calculations by Fast Computing Machines. *Journ. Chem. Phys.*, 21:1087–1092, June 1953. doi: 10.1063/1.1699114.

[942] L. Miao, L. Xiao-Dong, L. Chun-Shan, and W. Yi. Holographic gas as dark energy. *Communications in Theoretical Physics*, 51(1):181–186, jan 2009. doi: 10.1088/0253-6102/51/1/35. URL https://doi.org/10.1088%2F0253-6102%2F51%2F1%2F35.

[943] M. Middleton. Black hole spin: theory and observation. pages 99–151, 2016. doi: 10.1007/978-3-662-52859-4_3.

[944] A. A. Migdal. Loop Equations and 1/N Expansion. *Phys. Rept.*, 102:199–290, 1983. doi: 10.1016/0370-1573(83)90076-5.

[945] M. Milgrom. A modification of the Newtonian dynamics as a possible alternative to the hidden mass hypothesis. *ApJ*, 270:365–370, July 1983. doi: 10.1086/161130.

[946] M. Millea, L. Knox, and B. D. Fields. New bounds for axions and axion-like particles with keV-GeV masses. *Phys. Rev. D*, 92(2):023010, July 2015. doi: 10.1103/PhysRevD.92.023010.

[947] M. C. Miller. Intermediate-Mass Black Holes as LISA Sources. *Class. Quant. Grav.*, 26:094031, 2009. doi: 10.1088/0264-9381/26/9/094031.

[948] M. C. Miller and J. M. Miller. The Masses and Spins of Neutron Stars and Stellar-Mass Black Holes. *Phys. Rept.*, 548:1–34, 2014. doi: 10.1016/j.physrep.2014.09.003.

[949] K. Mimasu and V. Sanz. ALPs at Colliders. *JHEP*, 06:173, 2015. doi: 10.1007/JHEP06(2015)173.

[950] S. Mizoguchi and G. Schroder. On discrete U duality in M theory. *Class. Quant. Grav.*, 17:835–870, 2000. doi: 10.1088/0264-9381/17/4/308.

[951] W. Mlotkowski. Fuss-catalan numbers in noncommutative probability. *Documenta Mathematica*, 15:939–955, 2010. URL `http://eudml.org/doc/222801`.

[952] W. Mlotkowski, K. A. Penson, and K. Zyczkowski. Densities of the Raney distributions. *Documenta Mathematica vol.18*, Nov. 2013.

[953] M. Y. Mo. The rank 1 real Wishart spiked model I. Finite N analysis. *ArXiv e-prints*, Nov. 2010.

[954] M. Y. Mo. The rank 1 real Wishart spiked model. *arXiv e-prints*, Jan. 2011.

[955] G. Mocanu and D. Grumiller. Self-organized criticality in boson clouds around black holes. *Phys. Rev.*, D85:105022, 2012. doi: 10.1103/PhysRevD.85.105022.

[956] R. N. Mohapatra, S. Nussinov, and V. L. Teplitz. Mirror matter as selfinteracting dark matter. *Phys. Rev.*, D66:063002, 2002. doi: 10.1103/PhysRevD.66.063002.

[957] P. J. Mohr, D. B. Newell, and B. N. Taylor. Codata recommended values of the fundamental physical constants: 2014. *Rev. Mod. Phys.*, 88:035009, Sep

2016. doi: 10.1103/RevModPhys.88.035009. URL https://link.aps.org/doi/10.1103/RevModPhys.88.035009.

[958] L. Montanet et al. Review of particle properties. *Phys. Rev. D*, 50:1173–1814, Aug 1994. doi: 10.1103/PhysRevD.50.1173. URL https://link.aps.org/doi/10.1103/PhysRevD.50.1173.

[959] B. Moore and J. Silk. Dynamical and observable constraints on RAMBOs: Robust associations of massive baryonic objects. *ApJLett*, 442:L5–L8, Mar. 1995. doi: 10.1086/187802.

[960] B. Moore, F. Governato, T. R. Quinn, J. Stadel, and G. Lake. Resolving the structure of cold dark matter halos. *Astrophys. J.*, 499:L5, 1998. doi: 10.1086/311333.

[961] T. Moroi, H. Murayama, and M. Yamaguchi. Cosmological constraints on the light stable gravitino. *Phys. Lett.*, B303:289–294, 1993. doi: 10.1016/0370-2693(93)91434-O.

[962] D. R. Morrison and C. Vafa. Compactifications of F theory on Calabi-Yau threefolds. 1. *Nucl. Phys.*, B473:74–92, 1996. doi: 10.1016/0550-3213(96)00242-8.

[963] J. Mulder and L. R. Pericchi. The matrix- f prior for estimating and testing covariance matrices. *Bayesian Anal.*, 13(4):1193–1214, 12 2018. doi: 10.1214/17-BA1092. URL https://doi.org/10.1214/17-BA1092.

[964] O. Müller, M. S. Pawlowski, H. Jerjen, and F. Lelli. A whirling plane of satellite galaxies around Centaurus A challenges cold dark matter cosmology. *Science*, 359:534, 2018. doi: 10.1126/science.aao1858.

[965] R. R. Muller. On the asymptotic eigenvalue distribution of concatenated vector-valued fading channels. *IEEE Transactions on Information Theory*, 48 (7):2086–2091, July 2002. ISSN 0018-9448. doi: 10.1109/TIT.2002.1013149.

[966] R. R. Muller. A random matrix model of communication via antenna arrays. *IEEE Transactions on Information Theory*, 48(9):2495–2506, Sep. 2002. ISSN 0018-9448. doi: 10.1109/TIT.2002.801467.

[967] B. Nadler. Nonparametric detection of signals by information theoretic criteria: Performance analysis and an improved estimator. *IEEE Transactions on Signal Processing*, 58(5):2746–2756, May 2010. ISSN 1053-587X. doi: 10.1109/TSP.2010.2042481.

[968] T. Nagao and M. Wadati. Correlation functions of random matrix ensemblesrelated to classical orthogonal polynomials. *Journal of the Physical Society of Japan*, 60(10):3298–3322, 1991. doi: 10.1143/JPSJ.60.3298. URL `https://doi.org/10.1143/JPSJ.60.3298`.

[969] M. Nakamura et al. Parabolic Jets from the Spinning Black Hole in M87. *Astrophys. J.*, 868(2):146, 2018. doi: 10.3847/1538-4357/aaeb2d.

[970] R. Natarajan and R. E. Kass. Reference bayesian methods for generalized linear mixed models. *Journal of the American Statistical Association*, 95 (449):227–237, 2000. ISSN 01621459. URL `http://www.jstor.org/stable/2669540`.

[971] P. Nath and P. Fileviez Perez. Proton stability in grand unified theories, in strings and in branes. *Phys. Rept.*, 441:191–317, 2007. doi: 10.1016/j.physrep.2007.02.010.

[972] J. F. Navarro, C. S. Frenk, and S. D. M. White. The Structure of cold dark matter halos. *Astrophys. J.*, 462:563–575, 1996. doi: 10.1086/177173.

[973] J. F. Navarro, A. Ludlow, V. Springel, J. Wang, M. Vogelsberger, S. D. M. White, A. Jenkins, C. S. Frenk, and A. Helmi. The Diversity and Similarity of Cold Dark Matter Halos. *Mon. Not. Roy. Astron. Soc.*, 402:21, 2010. doi: 10.1111/j.1365-2966.2009.15878.x.

[974] O. Nebrin, R. Ghara, and G. Mellema. Fuzzy Dark Matter at Cosmic Dawn:

New 21-cm Constraints. *JCAP*, 1904(04):051, 2019. doi: 10.1088/1475-7516/2019/04/051.

[975] A. E. Nelson. Naturally Weak CP Violation. *Phys. Lett.*, 136B:387–391, 1984. doi: 10.1016/0370-2693(84)92025-2.

[976] R. Nemmen. The Spin of M87*. *Astrophys. J.*, 880(2):L26, 2019. doi: 10.3847/2041-8213/ab2fd3.

[977] E. T. Newman, E. Couch, K. Chinnapared, A. Exton, A. Prakash, and R. Torrence. Metric of a Rotating, Charged Mass. *Journal of Mathematical Physics*, 6:918–919, June 1965. doi: 10.1063/1.1704351.

[978] I. Newton. *The Mathematical Principles of Natural Philosophy*. Number v. 1 in The Mathematical Principles of Natural Philosophy. B. Motte, 1729. URL `https://books.google.co.uk/books?id=Tm0FAAAAQAAJ`.

[979] F. Nicastro et al. Chandra detection of the first x-ray forest along the line of sight to Mkn 421. *Astrophys. J.*, 629:700–718, 2005. doi: 10.1086/431270.

[980] A. Nicolis, R. Rattazzi, and E. Trincherini. Galileon as a local modification of gravity. *Phys. Rev. D*, 79:064036, Mar 2009. doi: 10.1103/PhysRevD.79.064036. URL `https://link.aps.org/doi/10.1103/PhysRevD.79.064036`.

[981] F. Nielsen. An elementary introduction to information geometry. *arXiv e-prints*, art. arXiv:1808.08271, Aug 2018.

[982] T. M. Nieuwenhuizen, R. E. Schild, and C. H. Gibson. Do micro brown dwarf detections explain the galactic dark matter? *J. Cosmol.*, 15:6017, 2011.

[983] H. Nilles. Supersymmetry, supergravity and particle physics. *Physics Reports*, 110(1):1 – 162, 1984. ISSN 0370-1573. doi: https://doi.org/10.1016/0370-1573(84)90008-5. URL `http://www.sciencedirect.com/science/article/pii/0370157384900085`.

[984] H. P. Nilles and S. Stieberger. How to reach the correct sin**2 theta-w and

alpha-s in string theory. *Phys. Lett.*, B367:126–133, 1996. doi: 10.1016/0370-2693(95)01400-4.

[985] H. P. Nilles and P. K. S. Vaudrevange. Geography of Fields in Extra Dimensions: String Theory Lessons for Particle Physics. *Mod. Phys. Lett.*, A30(10): 1530008, 2015. doi: 10.1142/S0217732315300086.

[986] H. P. Nilles, S. Ramos-Sanchez, M. Ratz, and P. K. S. Vaudrevange. From strings to the MSSM. *Eur. Phys. J.*, C59:249–267, 2009. doi: 10.1140/epjc/s10052-008-0740-1.

[987] S. Nojiri and S. D. Odintsov. Unifying inflation with LambdaCDM epoch in modified f(R) gravity consistent with Solar System tests. *Phys. Lett.*, B657: 238–245, 2007. doi: 10.1016/j.physletb.2007.10.027.

[988] E. E. Nokhrina, L. I. Gurvits, V. S. Beskin, M. Nakamura, K. Asada, and K. Hada. M87 black hole mass and spin estimate through the position of the jet boundary shape break. *Mon. Not. Roy. Astron. Soc.*, 489(1):1197–1205, 2019. doi: 10.1093/mnras/stz2116.

[989] R. H. Norden. A survey of maximum likelihood estimation. *International Statistical Review / Revue Internationale de Statistique*, 40(3):329–354, 1972. ISSN 03067734, 17515823. URL `http://www.jstor.org/stable/1402471`.

[990] G. Nordström. On the Energy of the Gravitation field in Einstein's Theory. *Koninklijke Nederlandse Akademie van Wetenschappen Proceedings Series B Physical Sciences*, 20:1238–1245, 1918.

[991] G. Nordström. On the Energy of the Gravitation field in Einstein's Theory. *Koninklijke Nederlandse Akademie van Wetenschappen Proceedings Series B Physical Sciences*, 20:1238–1245, 1918.

[992] N. A. Obers and B. Pioline. U duality and M theory. *Phys. Rept.*, 318: 113–225, 1999. doi: 10.1016/S0370-1573(99)00004-6.

[993] L. B. Okun. Mirror particles and mirror matter: 50 years of speculations and search. *Phys. Usp.*, 50:380–389, 2007. doi: 10.1070/PU2007v050n04ABEH006227.

[994] L. J. Oldham and M. W. Auger. Galaxy structure from multiple tracers - II. M87 from parsec to megaparsec scales. *MNRAS*, 457(1):421–439, Mar 2016. doi: 10.1093/mnras/stv2982.

[995] K. A. Olive et al. Review of Particle Physics. *Chin. Phys.*, C38:090001, 2014. doi: 10.1088/1674-1137/38/9/090001.

[996] S. Olver and R. Rao Nadakuditi. Numerical computation of convolutions in free probability theory. *arXiv e-prints*, art. arXiv:1203.1958, Mar 2012.

[997] A. Onatski. Determining the number of factors from empirical distribution of eigenvalues. *The Review of Economics and Statistics*, 92(4):1004–1016, 2010. doi: 10.1162/REST_a_00043. URL `https://doi.org/10.1162/REST_a_00043`.

[998] A. Onatski. Asymptotics of the principal components estimator of large factor models with weakly influential factors. *Journal of Econometrics*, 168(2):244–258, 2012. URL `https://EconPapers.repec.org/RePEc:eee:econom:v:168:y:2012:i:2:p:244-258`.

[999] A. Onatski, M. J. Moreira, and M. Hallin. Asymptotic power of sphericity tests for high-dimensional data. *arXiv e-prints*, art. arXiv:1306.4867, Jun 2013.

[1000] J. H. Oort. The force exerted by the stellar system in the direction perpendicular to the galactic plane and some related problems. *Bull. Astron. Inst. Netherlands*, 6:249, Aug. 1932.

[1001] J. R. Oppenheimer and H. Snyder. On continued gravitational contraction. *Phys. Rev.*, 56:455–459, Sep 1939. doi: 10.1103/PhysRev.56.455. URL `https://link.aps.org/doi/10.1103/PhysRev.56.455`.

[1002] J. A. Orosz, J. E. McClintock, J. P. Aufdenberg, R. A. Remillard, M. J. Reid, R. Narayan, and L. Gou. The Mass of the Black Hole in Cygnus X-1. *ApJ*, 742:84, Dec. 2011. doi: 10.1088/0004-637X/742/2/84.

[1003] J. A. Orosz, J. F. Steiner, J. E. McClintock, M. A. P. Torres, R. A. Remillard, C. D. Bailyn, and J. M. Miller. An Improved Dynamical Model for the Microquasar XTE J1550-564. *ApJ*, 730:75, Apr. 2011. doi: 10.1088/0004-637X/730/2/75.

[1004] J. A. Orosz, J. F. Steiner, J. E. McClintock, M. M. Buxton, C. D. Bailyn, D. Steeghs, A. Guberman, and M. A. P. Torres. The Mass of the Black Hole in LMC X-3. *ApJ*, 794:154, Oct. 2014. doi: 10.1088/0004-637X/794/2/154.

[1005] J. A. Orosz et al. A 15.65 solar mass black hole in an eclipsing binary in the nearby spiral galaxy Messier 33. *Nature*, 449:872, 2007. doi: 10.1038/nature06218.

[1006] J. A. Orosz et al. A New Dynamical Model for the Black Hole Binary LMC X-1. *Astrophys. J.*, 697:573–591, 2009. doi: 10.1088/0004-637X/697/1/573.

[1007] J. P. Ostriker, P. J. E. Peebles, and A. Yahil. The size and mass of galaxies, and the mass of the universe. *ApJLett*, 193:L1–L4, Oct. 1974. doi: 10.1086/181617.

[1008] A. J. OMalley and A. M. Zaslavsky. Domain-level covariance analysis for multilevel survey data with structured nonresponse. *Journal of the American Statistical Association*, 103(484):1405–1418, 2008. doi: 10.1198/016214508000000724. URL `https://doi.org/10.1198/016214508000000724`.

[1009] S. Pafka and I. Kondor. Estimated correlation matrices and portfolio optimization. *Physica A: Statistical Mechanics and its Applications*, 343: 623 – 634, 2004. ISSN 0378-4371. doi: https://doi.org/10.1016/j.physa.

2004.05.079. URL http://www.sciencedirect.com/science/article/pii/S0378437104007447.

[1010] E. Pajer and M. Peloso. A review of Axion Inflation in the era of Planck. *Class. Quant. Grav.*, 30:214002, 2013. doi: 10.1088/0264-9381/30/21/214002.

[1011] P. Pani and A. Loeb. Tidal capture of a primordial black hole by a neutron star: implications for constraints on dark matter. *JCAP*, 1406:026, 2014. doi: 10.1088/1475-7516/2014/06/026.

[1012] P. Pani, V. Cardoso, L. Gualtieri, E. Berti, and A. Ishibashi. Black-Hole Bombs and Photon-Mass Bounds. *Phys. Rev. Lett.*, 109(13):131102, Sept. 2012. doi: 10.1103/PhysRevLett.109.131102.

[1013] G. Papadopoulos and P. K. Townsend. Compactification of D = 11 supergravity on spaces of exceptional holonomy. *Phys. Lett.*, B357:300–306, 1995. doi: 10.1016/0370-2693(95)00929-F.

[1014] E. Papastergis and F. Shankar. An assessment of the "too big to fail" problem for field dwarf galaxies in view of baryonic feedback effects. *A&A*, 591:A58, Jun 2016. doi: 10.1051/0004-6361/201527854.

[1015] L. Parker and A. Raval. New quantum aspects of a vacuum-dominated universe. *Phys. Rev. D*, 62:083503, Sep 2000. doi: 10.1103/PhysRevD.62.083503. URL https://link.aps.org/doi/10.1103/PhysRevD.62.083503.

[1016] L. Parker and D. A. T. Vanzella. Acceleration of the universe, vacuum metamorphosis, and the large-time asymptotic form of the heat kernel. *Phys. Rev. D*, 69:104009, May 2004. doi: 10.1103/PhysRevD.69.104009. URL https://link.aps.org/doi/10.1103/PhysRevD.69.104009.

[1017] D. Passemier, M. R. McKay, and Y. Chen. Asymptotic Linear Spectral Statistics for Spiked Hermitian Random Matrices. *Journal of Statistical Physics*, 160(1):120–150, Jul 2015. doi: 10.1007/s10955-015-1233-x.

[1018] L. A. Pastur. On the universality of the level spacing distribution for some ensembles of random matrices. *Letters in Mathematical Physics*, 25(4):259–265, Aug. 1992. doi: 10.1007/BF00398398.

[1019] A. R. Patrick, J. N. Reeves, A. P. Lobban, D. Porquet, and A. G. Markowitz. Assessing black hole spin in deep suzaku observations of seyfert 1 agn. *Monthly Notices of the Royal Astronomical Society*, 416(4):2725–2747, 2011. doi: 10.1111/j.1365-2966.2011.19224.x. URL `http://dx.doi.org/10.1111/j.1365-2966.2011.19224.x`.

[1020] A. R. Patrick, J. N. Reeves, D. Porquet, A. G. Markowitz, V. Braito, and A. P. Lobban. A suzaku survey of fe #x2009;k lines in seyfert 1 active galactic nuclei. *Monthly Notices of the Royal Astronomical Society*, 426(3):2522–2565, Nov 2012. ISSN 0035-8711. doi: 10.1111/j.1365-2966.2012.21868.x.

[1021] C. Patrignani et al. Review of Particle Physics. *Chin. Phys.*, C40(10):100001, 2016. doi: 10.1088/1674-1137/40/10/100001.

[1022] N. Patterson, A. L. Price, and D. Reich. Population structure and eigenanalysis. *PLOS Genetics*, 2(12):1–20, 12 2006. doi: 10.1371/journal.pgen.0020190. URL `https://doi.org/10.1371/journal.pgen.0020190`.

[1023] D. Paul. Asymptotics of sample eigenstructure for a large dimensional spiked covariance model. *Statistica Sinica*, 17(4):1617–1642, 2007. ISSN 10170405, 19968507. URL `http://www.jstor.org/stable/24307692`.

[1024] D. Paul and A. Aue. Random matrix theory in statistics: A review. *Journal of Statistical Planning and Inference*, 150:1 – 29, 2014. ISSN 0378-3758. doi: https://doi.org/10.1016/j.jspi.2013.09.005. URL `http://www.sciencedirect.com/science/article/pii/S0378375813002280`.

[1025] D. Paul and J. W. Silverstein. No eigenvalues outside the support of the limiting empirical spectral distribution of a separable covariance matrix. *Journal of Multivariate Analysis*, 100(1):37 – 57, 2009. ISSN 0047-

259X. doi: https://doi.org/10.1016/j.jmva.2008.03.010. URL http://www.sciencedirect.com/science/article/pii/S0047259X08001024.

[1026] W. Pauli. Über den Einfluß der Geschwindigkeitsabhängigkeit der Elektronenmasse auf den Zeemaneffekt. *Zeitschrift fur Physik*, 31:373–385, Feb. 1925. doi: 10.1007/BF02980592.

[1027] W. Pauli. Über das wasserstoffspektrum vom standpunkt der neuen quantenmechanik. *Zeitschrift für Physik*, 36(5):336–363, May 1926. ISSN 0044-3328. doi: 10.1007/BF01450175. URL https://doi.org/10.1007/BF01450175.

[1028] K. Pearson. Contributions to the mathematical theory of evolution. [abstract]. *Proceedings of the Royal Society of London*, 54:329–333, 1893. ISSN 03701662. URL http://www.jstor.org/stable/115538.

[1029] K. Pearson. Contributions to the mathematical theory of evolution. iii. regression, heredity, and panmixia. [abstract]. *Proceedings of the Royal Society of London*, 59:69–71, 1895. ISSN 03701662. URL http://www.jstor.org/stable/115632.

[1030] K. Pearson. Contributions to the Mathematical Theory of Evolution. II. Skew Variation in Homogeneous Material. *Philosophical Transactions of the Royal Society of London Series A*, 186:343–414, 1895. doi: 10.1098/rsta.1895.0010.

[1031] K. Pearson. Mathematical Contributions to the Theory of Evolution. X. Supplement to a Memoir on Skew Variation. *Philosophical Transactions of the Royal Society of London Series A*, 197:443–459, 1901. doi: 10.1098/rsta.1901.0023.

[1032] K. Pearson. Mathematical contributions to the theory of evolution. xix. second supplement to a memoir on skew variation. *Philosophical Transactions of the Royal Society of London. Series A, Containing Papers of a Mathematical or Physical Character*, 216:429–457, 1916. ISSN 02643952. URL http://www.jstor.org/stable/91092.

[1033] R. D. Peccei. The Strong CP problem and axions. *Lect. Notes Phys.*, 741: 3–17, 2008. doi: 10.1007/978-3-540-73518-2_1. [,3(2006)].

[1034] R. D. Peccei and H. R. Quinn. CP conservation in the presence of pseudoparticles. *Physical Review Letters*, 38:1440–1443, June 1977. doi: 10.1103/PhysRevLett.38.1440.

[1035] R. D. Peccei and H. R. Quinn. Constraints imposed by CP conservation in the presence of pseudoparticles. *Phys. Rev. D*, 16:1791–1797, Sep 1977. doi: 10.1103/PhysRevD.16.1791. URL `https://link.aps.org/doi/10.1103/PhysRevD.16.1791`.

[1036] R. D. Peccei and H. R. Quinn. CP conservation in the presence of pseudoparticles. *Phys. Rev. Lett.*, 38:1440–1443, Jun 1977. doi: 10.1103/PhysRevLett.38.1440. URL `https://link.aps.org/doi/10.1103/PhysRevLett.38.1440`.

[1037] S. Péché. Non-white wishart ensembles. *Journal of Multivariate Analysis*, 97(4):874 – 894, 2006. ISSN 0047-259X. doi: https://doi.org/10.1016/j.jmva.2005.09.001. URL `http://www.sciencedirect.com/science/article/pii/S0047259X05001545`.

[1038] S. Péché. Universality results for the largest eigenvalues of some sample covariance matrix ensembles. *Probability Theory and Related Fields*, 143(3): 481–516, Mar 2009. ISSN 1432-2064. doi: 10.1007/s00440-007-0133-7. URL `https://doi.org/10.1007/s00440-007-0133-7`.

[1039] F. G. Pedro and A. Westphal. Inflation with a graceful exit in a random landscape. *JHEP*, 03:163, 2017. doi: 10.1007/JHEP03(2017)163.

[1040] P. J. E. Peebles. Fluid dark matter. *Astrophys. J.*, 534:L127, 2000. doi: 10.1086/312677.

[1041] P. J. E. Peebles and B. Ratra. The Cosmological constant and dark en-

ergy. *Rev. Mod. Phys.*, 75:559–606, 2003. doi: 10.1103/RevModPhys.75.559. [,592(2002)].

[1042] R. Penrose. Gravitational collapse and space-time singularities. *Phys. Rev. Lett.*, 14:57–59, Jan 1965. doi: 10.1103/PhysRevLett.14.57. URL `https://link.aps.org/doi/10.1103/PhysRevLett.14.57`.

[1043] R. Penrose. Twistor algebra. *Journal of Mathematical Physics*, 8(2):345–366, 1967. doi: 10.1063/1.1705200. URL `https://doi.org/10.1063/1.1705200`.

[1044] R. Penrose. Gravitational Collapse: the Role of General Relativity. *Nuovo Cimento Rivista Serie*, 1:252, 1969.

[1045] R. Penrose and M. A. H. MacCallum. Twistor theory: An Approach to the quantization of fields and space-time. *Phys. Rept.*, 6:241–316, 1972. doi: 10.1016/0370-1573(73)90008-2.

[1046] K. A. Penson and A. I. Solomon. Coherent States from Combinatorial Sequences. In *Quantum Theory and Symmetries*, pages 527–530, Jun 2002. doi: 10.1142/9789812777850_0066.

[1047] K. A. Penson and K. Życzkowski. Product of Ginibre matrices: Fuss-Catalan and Raney distributions. *Phys. Rev. E*, 83(6):061118, Jun 2011. doi: 10.1103/PhysRevE.83.061118.

[1048] A. A. Penzias and R. W. Wilson. A Measurement of Excess Antenna Temperature at 4080 Mc/s. *ApJ*, 142:419–421, July 1965. doi: 10.1086/148307.

[1049] V. Pérez-Abreu and N. Sakuma. Free infinite divisibility of free multiplicative mixtures of the wigner distribution. *Journal of Theoretical Probability*, 25(1): 100–121, Mar 2012. ISSN 1572-9230. doi: 10.1007/s10959-010-0288-5. URL `https://doi.org/10.1007/s10959-010-0288-5`.

[1050] M. L. Perl et al. Evidence for anomalous lepton production in $e^+ - e^-$ annihilation. *Phys. Rev. Lett.*, 35:1489–1492, Dec 1975. doi: 10.

1103/PhysRevLett.35.1489. URL https://link.aps.org/doi/10.1103/PhysRevLett.35.1489.

[1051] S. Perlmutter et al. Measurements of Omega and Lambda from 42 high redshift supernovae. *Astrophys. J.*, 517:565–586, 1999. doi: 10.1086/307221.

[1052] M. E. Peskin and D. V. Schroeder. *An Introduction to quantum field theory*. Addison-Wesley, Reading, USA, 1995. ISBN 9780201503975, 0201503972. URL http://www.slac.stanford.edu/~mpeskin/QFT.html.

[1053] A. H. G. Peter, M. Rocha, J. S. Bullock, and M. Kaplinghat. Cosmological Simulations with Self-Interacting Dark Matter II: Halo Shapes vs. Observations. *Mon. Not. Roy. Astron. Soc.*, 430:105, 2013. doi: 10.1093/mnras/sts535.

[1054] B. M. Peterson et al. Central masses and broad-line region sizes of active galactic nuclei. II. A Homogeneous analysis of a large reverberation-mapping database. *Astrophys. J.*, 613:682–699, 2004. doi: 10.1086/423269.

[1055] D. Pfenniger, F. Combes, and L. Martinet. Is dark matter in spiral galaxies cold gas? I. Observational constraints and dynamical clues about galaxy evolution. *A&A*, 285:79–93, May 1994.

[1056] E. C. S. Ph.D. V. the limiting density in white dwarf stars. *The London, Edinburgh, and Dublin Philosophical Magazine and Journal of Science*, 7(41): 63–70, 1929. doi: 10.1080/14786440108564713. URL https://doi.org/10.1080/14786440108564713.

[1057] N. B. D. phil. I. on the constitution of atoms and molecules. *The London, Edinburgh, and Dublin Philosophical Magazine and Journal of Science*, 26 (151):1–25, 1913. doi: 10.1080/14786441308634955. URL https://doi.org/10.1080/14786441308634955.

[1058] F. Piazza and S. Tsujikawa. Dilatonic ghost condensate as dark energy. *JCAP*, 0407:004, 2004. doi: 10.1088/1475-7516/2004/07/004.

[1059] D. M. Pierce. Threshold corrections and gauge symmetry in twisted superstring models. *Phys. Rev.*, D50:6469–6480, 1994. doi: 10.1103/PhysRevD.50.6469.

[1060] N. S. Pillai and J. Yin. Universality of covariance matrices. *arXiv e-prints*, art. arXiv:1110.2501, Oct 2011.

[1061] Planck Collaboration, P. A. R. Ade, N. Aghanim, M. Arnaud, F. Arroja, M. Ashdown, J. Aumont, C. Baccigalupi, M. Ballardini, A. J. Banday, and et al. Planck 2015 results. XX. Constraints on inflation. *A&A*, 594:A20, Sept. 2016. doi: 10.1051/0004-6361/201525898.

[1062] V. Plerou, P. Gopikrishnan, B. Rosenow, L. A. N. Amaral, T. Guhr, and H. E. Stanley. Random matrix approach to cross correlations in financial data. *Phys. Rev. E*, 65:066126, Jun 2002. doi: 10.1103/PhysRevE.65.066126. URL `https://link.aps.org/doi/10.1103/PhysRevE.65.066126`.

[1063] J. Polchinski. Tasi lectures on D-branes. In *Fields, strings and duality. Proceedings, Summer School, Theoretical Advanced Study Institute in Elementary Particle Physics, TASI'96, Boulder, USA, June 2-28, 1996*, pages 293–356, 1996.

[1064] J. Polchinski. *String theory. Vol. 1: An introduction to the bosonic string.* Cambridge Monographs on Mathematical Physics. Cambridge University Press, 2007. ISBN 9780511252273, 9780521672276, 9780521633031. doi: 10.1017/CBO9780511816079.

[1065] J. Polchinski. *String theory. Vol. 2: Superstring theory and beyond.* Cambridge Monographs on Mathematical Physics. Cambridge University Press, 2007. ISBN 9780511252280, 9780521633048, 9780521672283. doi: 10.1017/CBO9780511618123.

[1066] G. Polhemus. Statistical mechanics of multiply wound D-branes. *Phys. Rev.*, D56:2202–2205, 1997. doi: 10.1103/PhysRevD.56.2202.

[1067] G. Polhemus. Eigenvalue repulsion and matrix black holes. 1999.

[1068] B. Pontecorvo. Mesonium and Antimesonium. *Soviet Journal of Experimental and Theoretical Physics*, 6:429, 1958.

[1069] B. Pontecorvo. Neutrino Experiments and the Problem of Conservation of Leptonic Charge. *Soviet Journal of Experimental and Theoretical Physics*, 26:984, May 1968.

[1070] N. K. Porayko and K. A. Postnov. Constraints on ultralight scalar dark matter from pulsar timing. *Phys. Rev.*, D90(6):062008, 2014. doi: 10.1103/PhysRevD.90.062008.

[1071] V. Poulin, T. L. Smith, D. Grin, T. Karwal, and M. Kamionkowski. Cosmological implications of ultralight axionlike fields. *Phys. Rev.*, D98(8):083525, 2018. doi: 10.1103/PhysRevD.98.083525.

[1072] V. Poulin, T. L. Smith, T. Karwal, and M. Kamionkowski. Early Dark Energy Can Resolve The Hubble Tension. 2018.

[1073] J. Preskill, M. B. Wise, and F. Wilczek. Cosmology of the invisible axion. *Phys. Lett. B*, 120:127–132, Jan. 1983. doi: 10.1016/0370-2693(83)90637-8.

[1074] J. Preskill, M. B. Wise, and F. Wilczek. Cosmology of the invisible axion. *Physics Letters B*, 120(1):127 – 132, 1983. ISSN 0370-2693. doi: https://doi.org/10.1016/0370-2693(83)90637-8. URL `http://www.sciencedirect.com/science/article/pii/0370269383906378`.

[1075] J. P. Preskill. Cosmological production of superheavy magnetic monopoles. *Phys. Rev. Lett.*, 43:1365–1368, Nov 1979. doi: 10.1103/PhysRevLett.43.1365. URL `https://link.aps.org/doi/10.1103/PhysRevLett.43.1365`.

[1076] W. H. Press and S. A. Teukolsky. Floating Orbits, Superradiant Scattering and the Black-hole Bomb. *Nature*, 238:211–212, July 1972. doi: 10.1038/238211a0.

[1077] W. H. Press and S. A. Teukolsky. Perturbations of a Rotating Black Hole. II. Dynamical Stability of the Kerr Metric. *ApJ*, 185:649–674, Oct. 1973. doi: 10.1086/152445.

[1078] W. H. Press, B. S. Ryden, and D. N. Spergel. Single mechanism for generating large-scale structure and providing dark missing matter. *Phys. Rev. Lett.*, 64:1084–1087, Mar 1990. doi: 10.1103/PhysRevLett.64.1084. URL `https://link.aps.org/doi/10.1103/PhysRevLett.64.1084`.

[1079] L. C. Price, J. Frazer, J. Xu, H. V. Peiris, and R. Easther. MultiModeCode: An efficient numerical solver for multifield inflation. *JCAP*, 1503(03):005, 2015. doi: 10.1088/1475-7516/2015/03/005.

[1080] L. C. Price, H. V. Peiris, J. Frazer, and R. Easther. Designing and testing inflationary models with Bayesian networks. *JCAP*, 1602(02):049, 2016. doi: 10.1088/1475-7516/2016/02/049.

[1081] H. Primakoff. Photo-production of neutral mesons in nuclear electric fields and the mean life of the neutral meson. *Phys. Rev.*, 81:899–899, Mar 1951. doi: 10.1103/PhysRev.81.899. URL `https://link.aps.org/doi/10.1103/PhysRev.81.899`.

[1082] O. Pujolas, I. Sawicki, and A. Vikman. The Imperfect Fluid behind Kinetic Gravity Braiding. *JHEP*, 11:156, 2011. doi: 10.1007/JHEP11(2011)156.

[1083] F. Quevedo. Lectures on string/brane cosmology. *Class. Quant. Grav.*, 19: 5721–5779, 2002. doi: 10.1088/0264-9381/19/22/304.

[1084] G. G. Raffelt. Stars as laboratories for fundamental physics. *Chicago, USA: Univ. Pr. (1996) 664 p*, 1996. URL `http://wwwth.mpp.mpg.de/members/raffelt/mypapers/199613.pdf`.

[1085] J. S. Ramberg and B. W. Schmeiser. An approximate method for generating asymmetric random variables. *Commun. ACM*, 17(2):78–82, Feb. 1974. ISSN

0001-0782. doi: 10.1145/360827.360840. URL http://doi.acm.org/10.1145/360827.360840.

[1086] P. Ramond. Exceptional groups and physics. In *Proceedings, 24th International Colloquium on Group Theoretical Methods in Physics (GROUP 24): Paris, France, July 15-20, 2002*, pages 129–138, 2003.

[1087] L. Randall and S. D. Thomas. Solving the cosmological moduli problem with weak scale inflation. *Nucl. Phys.*, B449:229–247, 1995. doi: 10.1016/0550-3213(95)00228-K.

[1088] L. Randall, M. Soljacic, and A. H. Guth. Supernatural inflation: Inflation from supersymmetry with no (very) small parameters. *Nucl. Phys.*, B472:377–408, 1996. doi: 10.1016/0550-3213(96)00174-5.

[1089] S. W. Randall, M. Markevitch, D. Clowe, A. H. Gonzalez, and M. Bradač. Constraints on the Self-Interaction Cross Section of Dark Matter from Numerical Simulations of the Merging Galaxy Cluster 1E 0657-56. *ApJ*, 679:1173–1180, June 2008. doi: 10.1086/587859.

[1090] G. N. Raney. Functional composition patterns and power series reversion. *Transactions of the American Mathematical Society*, 94(3):441–451, 1960. ISSN 00029947. URL http://www.jstor.org/stable/1993433.

[1091] N. R. Rao and A. Edelman. Free probability, sample covariance matrices, and signal processing. 5:V–V, May 2006. ISSN 1520-6149. doi: 10.1109/ICASSP.2006.1661447.

[1092] N. R. Rao and A. Edelman. The polynomial method for random matrices. *arXiv Mathematics e-prints*, art. math/0601389, Jan 2006.

[1093] C. E. Rasmussen. The infinite gaussian mixture model. In S. A. Solla, T. K. Leen, and K. Müller, editors, *Advances in Neural Information Processing Systems 12*, pages 554–560. MIT Press, 2000. URL http://papers.nips.cc/paper/1745-the-infinite-gaussian-mixture-model.pdf.

[1094] B. Ratra and P. J. E. Peebles. Cosmological consequences of a rolling homogeneous scalar field. *Phys. Rev. D*, 37:3406–3427, Jun 1988. doi: 10.1103/PhysRevD.37.3406. URL `https://link.aps.org/doi/10.1103/PhysRevD.37.3406`.

[1095] S. Ray, A. L. Espíndola, M. Malheiro, J. P. Lemos, and V. T. Zanchin. Electrically charged compact stars and formation of charged black holes. *Phys. Rev. D*, 68(8):084004, Oct. 2003. doi: 10.1103/PhysRevD.68.084004.

[1096] J. Redondo and A. Ringwald. Light shining through walls. *Contemp. Phys.*, 52:211–236, 2011. doi: 10.1080/00107514.2011.563516.

[1097] A. Refregier. Weak gravitational lensing by large scale structure. *Ann. Rev. Astron. Astrophys.*, 41:645–668, 2003. doi: 10.1146/annurev.astro.41.111302.102207.

[1098] F. Reines and C. L. Cowan. The neutrino. *Nature*, 178:446–449, 1956. doi: 10.1038/178446a0.

[1099] H. Reissner. ber die eigengravitation des elektrischen feldes nach der einsteinschen theorie. *Annalen der Physik*, 355(9):106–120, 1916. doi: 10.1002/andp.19163550905. URL `https://onlinelibrary.wiley.com/doi/abs/10.1002/andp.19163550905`.

[1100] C. S. Reynolds. The Spin of Supermassive Black Holes. *Class. Quant. Grav.*, 30:244004, 2013. doi: 10.1088/0264-9381/30/24/244004.

[1101] C. S. Reynolds. Measuring Black Hole Spin using X-ray Reflection Spectroscopy. *Space Sci. Rev.*, 183(1-4):277–294, 2014. doi: 10.1007/s11214-013-0006-6.

[1102] C. S. Reynolds. Observing black holes spin. *Nat. Astron.*, 3(1):41–47, 2019. doi: 10.1038/s41550-018-0665-z.

[1103] D. Reynolds. *Gaussian Mixture Models*, pages 827–832. Springer US, Boston,

MA, 2015. ISBN 978-1-4899-7488-4. doi: 10.1007/978-1-4899-7488-4_196. URL https://doi.org/10.1007/978-1-4899-7488-4_196.

[1104] D. A. Reynolds, T. F. Quatieri, and R. B. Dunn. Speaker verification using adapted gaussian mixture models. *Digital Signal Processing*, 10 (1):19 – 41, 2000. ISSN 1051-2004. doi: https://doi.org/10.1006/dspr.1999.0361. URL http://www.sciencedirect.com/science/article/pii/S1051200499903615.

[1105] M. O. Ribas, F. P. Devecchi, and G. M. Kremer. Fermions as sources of accelerated regimes in cosmology. *Phys. Rev. D*, 72:123502, Dec 2005. doi: 10.1103/PhysRevD.72.123502. URL https://link.aps.org/doi/10.1103/PhysRevD.72.123502.

[1106] A. G. Riess. The Expansion of the Universe is Faster than Expected. *Nature Rev. Phys.*, 2(1):10–12, 2019. doi: 10.1038/s42254-019-0137-0.

[1107] A. G. Riess, S. Casertano, W. Yuan, L. M. Macri, and D. Scolnic. Large Magellanic Cloud Cepheid Standards Provide a 1% Foundation for the Determination of the Hubble Constant and Stronger Evidence for Physics Beyond LambdaCDM. *Astrophys. J.*, 876(1):85, 2019. doi: 10.3847/1538-4357/ab1422.

[1108] A. G. Riess et al. Observational evidence from supernovae for an accelerating universe and a cosmological constant. *Astron. J.*, 116:1009–1038, 1998. doi: 10.1086/300499.

[1109] A. G. Riess et al. Type Ia supernova discoveries at z ¿ 1 from the Hubble Space Telescope: Evidence for past deceleration and constraints on dark energy evolution. *Astrophys. J.*, 607:665–687, 2004. doi: 10.1086/383612.

[1110] A. G. Riess et al. A 3% Solution: Determination of the Hubble Constant with the Hubble Space Telescope and Wide Field Camera 3. *ApJ*, 730(2): 119, Apr 2011. doi: 10.1088/0004-637X/730/2/119.

[1111] A. G. Riess et al. A 2.4% Determination of the Local Value of the Hubble Constant. *Astrophys. J.*, 826(1):56, 2016. doi: 10.3847/0004-637X/826/1/56.

[1112] A. G. Riess et al. Milky Way Cepheid Standards for Measuring Cosmic Distances and Application to Gaia DR2: Implications for the Hubble Constant. *Astrophys. J.*, 861(2):126, 2018. doi: 10.3847/1538-4357/aac82e.

[1113] A. Riotto. Inflation and the theory of cosmological perturbations. *ICTP Lect. Notes Ser.*, 14:317–413, 2003.

[1114] H. P. Robertson. Kinematics and World-Structure. *ApJ*, 82:284, Nov. 1935. doi: 10.1086/143681.

[1115] H. P. Robertson. Kinematics and World-Structure II. *ApJ*, 83:187, Apr. 1936. doi: 10.1086/143716.

[1116] H. P. Robertson. Kinematics and World-Structure III. *ApJ*, 83:257, May 1936. doi: 10.1086/143726.

[1117] V. H. Robles, J. S. Bullock, and M. Boylan-Kolchin. Scalar Field Dark Matter: Helping or Hurting Small-Scale Problems in Cosmology? *Mon. Not. Roy. Astron. Soc.*, 483(1):289–298, 2019. doi: 10.1093/mnras/sty3190.

[1118] J. G. Rosa and T. W. Kephart. Stimulated Axion Decay in Superradiant Clouds around Primordial Black Holes. *Phys. Rev. Lett.*, 120(23):231102, 2018. doi: 10.1103/PhysRevLett.120.231102.

[1119] G. G. Ross and S. Sarkar. Successful supersymmetric inflation. *Nucl. Phys.*, B461:597–624, 1996. doi: 10.1016/0550-3213(96)00013-2.

[1120] L. Roszkowski, E. M. Sessolo, and S. Trojanowski. WIMP dark matter candidates and searches?current status and future prospects. *Rept. Prog. Phys.*, 81(6):066201, 2018. doi: 10.1088/1361-6633/aab913.

[1121] C. Rovelli. Black hole entropy from loop quantum gravity. *Phys. Rev. Lett.*, 77:3288–3291, 1996. doi: 10.1103/PhysRevLett.77.3288.

[1122] C. Rovelli. Loop quantum gravity. *Living Reviews in Relativity*, 11(1):5, Jul 2008. ISSN 1433-8351. doi: 10.12942/lrr-2008-5. URL https://doi.org/10.12942/lrr-2008-5.

[1123] C. Rovelli and L. Smolin. Discreteness of area and volume in quantum gravity. *Nucl. Phys.*, B442:593–622, 1995. doi: 10.1016/0550-3213(95)00150-Q,10.1016/0550-3213(95)00550-5. [Erratum: Nucl. Phys.B456,753(1995)].

[1124] N. Roy and N. Banerjee. Quintessence Scalar Field: A Dynamical Systems Study. *Eur. Phys. J. Plus*, 129:162, 2014. doi: 10.1140/epjp/i2014-14162-7.

[1125] S. N. Roy. On a heuristic method of test construction and its use in multivariate analysis. *Ann. Math. Statist.*, 24(2):220–238, 06 1953. doi: 10.1214/aoms/1177729029. URL https://doi.org/10.1214/aoms/1177729029.

[1126] V. A. Rubakov. Grand unification and heavy axion. *JETP Lett.*, 65:621–624, 1997. doi: 10.1134/1.567390.

[1127] D. Rubin et al. Unity: Confronting Supernova Cosmology?s Statistical and Systematic Uncertainties in a Unified Bayesian Framework. *Astrophys. J.*, 813(2):137, 2015. doi: 10.1088/0004-637X/813/2/137.

[1128] V. C. Rubin. Dark matter in spiral galaxies. *Scientific American*, 248(6):96–109, 1983. ISSN 00368733, 19467087. URL http://www.jstor.org/stable/24968923.

[1129] V. C. Rubin and W. K. Ford, Jr. Rotation of the Andromeda Nebula from a Spectroscopic Survey of Emission Regions. *ApJ*, 159:379, Feb. 1970. doi: 10.1086/150317.

[1130] V. C. Rubin, W. K. Ford, Jr., and N. Thonnard. Rotational properties of 21 SC galaxies with a large range of luminosities and radii, from NGC 4605 /R = 4kpc/ to UGC 2885 /R = 122 kpc/. *ApJ*, 238:471–487, June 1980. doi: 10.1086/158003.

[1131] T. Rudelius. Learning to Inflate. *JCAP*, 1902:044, 2019. doi: 10.1088/1475-7516/2019/02/044.

[1132] Ø. Ryan and M. Debbah. Multiplicative free Convolution and Information-Plus-Noise Type Matrices. *arXiv Mathematics e-prints*, art. math/0702342, Feb 2007.

[1133] O. Ryan and M. Debbah. Free deconvolution for signal processing applications. pages 1846–1850, June 2007. ISSN 2157-8095. doi: 10.1109/ISIT.2007.4557490.

[1134] . Ryan and M. Debbah. Channel capacity estimation using free-probability theory. *IEEE Transactions on Signal Processing*, 56(11):5654–5667, Nov 2008. doi: 10.1109/TSP.2008.927074.

[1135] R. K. Sachs and A. M. Wolfe. Perturbations of a Cosmological Model and Angular Variations of the Microwave Background. *ApJ*, 147:73, Jan. 1967. doi: 10.1086/148982.

[1136] M. Sahlen, A. R. Liddle, and D. Parkinson. Quintessence reconstructed: New constraints and tracker viability. *Phys. Rev.*, D75:023502, 2007. doi: 10.1103/PhysRevD.75.023502.

[1137] V. Sahni and A. A. Starobinsky. The Case for a positive cosmological Lambda term. *Int. J. Mod. Phys.*, D9:373–444, 2000. doi: 10.1142/S0218271800000542.

[1138] V. Sahni and L.-M. Wang. A New cosmological model of quintessence and dark matter. *Phys. Rev.*, D62:103517, 2000. doi: 10.1103/PhysRevD.62.103517.

[1139] M. Sakellariadou. Cosmic strings. *Lect. Notes Phys.*, 718:247–288, 2007. doi: 10.1007/3-540-70859-6_10.

[1140] M. Sakellariadou. Cosmic Superstrings. *Phil. Trans. Roy. Soc. Lond.*, A366: 2881–2894, 2008. doi: 10.1098/rsta.2008.0068.

[1141] A. Salam. Weak and Electromagnetic Interactions. *Conf. Proc.*, C680519: 367–377, 1968.

[1142] A. Salam and J. C. Ward. Electromagnetic and weak interactions. *Phys. Lett.*, 13:168–171, 1964. doi: 10.1016/0031-9163(64)90711-5.

[1143] A. Salvio, A. Strumia, and W. Xue. Thermal axion production. *JCAP*, 1401: 011, 2014. doi: 10.1088/1475-7516/2014/01/011.

[1144] A. Sarkar, R. Mondal, S. Das, S. K. Sethi, S. Bharadwaj, and D. J. E. Marsh. The effects of the small-scale DM power on the cosmological neutral hydrogen (HI) distribution at high redshifts. *JCAP*, 4:012, Apr. 2016. doi: 10.1088/1475-7516/2016/04/012.

[1145] M. Sasaki and E. D. Stewart. A General Analytic Formula for the Spectral Index of the Density Perturbations Produced during Inflation. *Progress of Theoretical Physics*, 95(1):71–78, 01 1996. ISSN 0033-068X. doi: 10.1143/PTP.95.71. URL `https://doi.org/10.1143/PTP.95.71`.

[1146] M. Sasaki and T. Tanaka. Superhorizon scale dynamics of multiscalar inflation. *Prog. Theor. Phys.*, 99:763–782, 1998. doi: 10.1143/PTP.99.763.

[1147] B. Sathyaprakash et al. Scientific Objectives of Einstein Telescope. *Class. Quant. Grav.*, 29:124013, 2012. doi: 10.1088/0264-9381/29/12/124013,10.1088/0264-9381/30/7/079501. [Erratum: Class. Quant. Grav.30,079501(2013)].

[1148] K. Sato. Cosmological baryon-number domain structure and the first order phase transition of a vacuum. *Physics Letters B*, 99(1):66 – 70, 1981. ISSN 0370-2693. doi: https://doi.org/10.1016/0370-2693(81)90805-4. URL `http://www.sciencedirect.com/science/article/pii/0370269381908054`.

[1149] M. Scheibner, T. Schmidt, L. Worschech, A. Forchel, G. Bacher, T. Passow, and D. Hommel. Superradiance of quantum dots. *Nature Physics*, 3:106 EP –, 01 2007. URL `https://doi.org/10.1038/nphys494`.

[1150] J. Schenker and H. Schulz-Baldes. Gaussian fluctuations for random matrices with correlated entries. *arXiv Mathematical Physics e-prints*, July 2006.

[1151] J. H. Schenker and H. Schulz-Baldes. Semicircle law and freeness for random matrices with symmetries or correlations. *arXiv e-prints*, art. math-ph/0505003, May 2005.

[1152] H.-Y. Schive, T. Chiueh, and T. Broadhurst. Cosmic Structure as the Quantum Interference of a Coherent Dark Wave. *Nature Phys.*, 10:496–499, 2014. doi: 10.1038/nphys2996.

[1153] H.-Y. Schive, T. Chiueh, T. Broadhurst, and K.-W. Huang. Contrasting Galaxy Formation from Quantum Wave Dark Matter, ψDM, with ΛCDM, using Planck and Hubble Data. *ApJ*, 818:89, Feb. 2016. doi: 10.3847/0004-637X/818/1/89.

[1154] M. Schmaltz and D. Tucker-Smith. Little Higgs review. *Ann. Rev. Nucl. Part. Sci.*, 55:229–270, 2005. doi: 10.1146/annurev.nucl.55.090704.151502.

[1155] A. Schneider. Constraining Non-Cold Dark Matter Models with the Global 21-cm Signal. 2018.

[1156] A. Schneider, R. E. Smith, A. V. Macciò, and B. Moore. Non-linear evolution of cosmological structures in warm dark matter models. *MNRAS*, 424(1): 684–698, Jul 2012. doi: 10.1111/j.1365-2966.2012.21252.x.

[1157] A. Schopenhauer. *Die welt als wille und vorstellung*. BoD–Books on Demand, 2016.

[1158] E. Schrödinger. An undulatory theory of the mechanics of atoms and

molecules. *Phys. Rev.*, 28:1049–1070, Dec 1926. doi: 10.1103/PhysRev.28.1049. URL https://link.aps.org/doi/10.1103/PhysRev.28.1049.

[1159] E. Schrödinger. Quantisierung als eigenwertproblem. *Annalen der Physik*, 384(4):361–376, 1926. doi: 10.1002/andp.19263840404. URL https://onlinelibrary.wiley.com/doi/abs/10.1002/andp.19263840404.

[1160] B. Schwabe, J. C. Niemeyer, and J. F. Engels. Simulations of solitonic core mergers in ultralight axion dark matter cosmologies. *Phys. Rev. D*, 94(4):043513, Aug. 2016. doi: 10.1103/PhysRevD.94.043513.

[1161] M. D. Schwartz. *Quantum Field Theory and the Standard Model*. Cambridge University Press, 2014. ISBN 1107034736, 9781107034730. URL http://www.cambridge.org/us/academic/subjects/physics/theoretical-physics-and-mathematical-physics/quantum-field-theory-and-standard-model.

[1162] J. H. Schwarz. The power of M theory. *Phys. Lett.*, B367:97–103, 1996. doi: 10.1016/0370-2693(95)01429-2. [,390(1995)].

[1163] K. Schwarzschild. On the Gravitational Field of a Mass Point According to Einstein's Theory. *Abh. Konigl. Preuss. Akad. Wissenschaften Jahre 1906,92, Berlin,1907*, 1916, 1916.

[1164] K. Schwarzschild. Ü about the gravitational field of a mass point according to Einstein's theory. *Sessions of the Royal Prussian Academy of Sciences (Berlin), 1916, pages 189-196*, 1916.

[1165] J. G. Scott and J. O. Berger. Bayes and empirical-Bayes multiplicity adjustment in the variable-selection problem. *arXiv e-prints*, art. arXiv:1011.2333, Nov 2010.

[1166] R. Scranton et al. Physical evidence for dark energy. 2003.

[1167] A. Sedrakian. Axion cooling of neutron stars. *Phys. Rev.*, D93(6):065044, 2016. doi: 10.1103/PhysRevD.93.065044.

[1168] A. Sen. Strong - weak coupling duality in three-dimensional string theory. *Nucl. Phys.*, B434:179–209, 1995. doi: 10.1016/0550-3213(94)00461-M.

[1169] A. Sen. F theory and orientifolds. *Nucl. Phys.*, B475:562–578, 1996. doi: 10.1016/0550-3213(96)00347-1.

[1170] A. Sen. Orientifold limit of F theory vacua. *Phys. Rev.*, D55:R7345–R7349, 1997. doi: 10.1103/PhysRevD.55.R7345.

[1171] A. Sen. Developments in superstring theory. In *High-energy physics. Proceedings, 29th International Conference, ICHEP'98, Vancouver, Canada, July 23-29, 1998. Vol. 1, 2*, pages 371–381, 1998.

[1172] V. N. Senoguz and Q. Shafi. New inflation, preinflation, and leptogenesis. *Phys. Lett.*, B596:8–15, 2004. doi: 10.1016/j.physletb.2004.05.077.

[1173] G. Servant and T. M. Tait. Is the lightest kaluzaklein particle a viable dark matter candidate? *Nuclear Physics B*, 650(1):391 – 419, 2003. ISSN 0550-3213. doi: https://doi.org/10.1016/S0550-3213(02)01012-X. URL `http://www.sciencedirect.com/science/article/pii/S055032130201012X`.

[1174] G. Servant and T. M. P. Tait. Elastic scattering and direct detection of kaluza-klein dark matter. *New Journal of Physics*, 4:99–99, dec 2002. doi: 10.1088/1367-2630/4/1/399. URL `https://doi.org/10.1088%2F1367-2630%2F4%2F1%2F399`.

[1175] R. Shafee, J. E. McClintock, R. Narayan, S. W. Davis, L.-X. Li, and R. A. Remillard. Estimating the spin of stellar-mass black holes by spectral fitting of the x-ray continuum. *The Astrophysical Journal Letters*, 636(2):L113, 2006. URL `http://stacks.iop.org/1538-4357/636/i=2/a=L113`.

[1176] R. Shafee, J. E. McClintock, R. Narayan, S. W. Davis, L.-X. Li, and R. A.

Remillard. Estimating the spin of stellar-mass black holes via spectral fitting of the x-ray continuum. *Astrophys. J.*, 636:L113–L116, 2006. doi: 10.1086/498938.

[1177] F. Shankar, D. H. Weinberg, and J. Miralda-Escude. Self-Consistent Models of the AGN and Black Hole Populations: Duty Cycles, Accretion Rates, and the Mean Radiative Efficiency. *Astrophys. J.*, 690:20–41, 2009. doi: 10.1088/0004-637X/690/1/20.

[1178] C. E. Shannon. A mathematical theory of communication. *Bell Syst. Tech. J.*, 27:379–423, 1948. [Bell Syst. Tech. J.27,623(1948)].

[1179] B. D. Sherwin et al. Evidence for Dark Energy from the Cosmic Microwave Background Alone Using the Atacama Cosmology Telescope Lensing Measurements. *Phys. Rev. Lett.*, 107(2):021302, Jul 2011. doi: 10.1103/PhysRevLett.107.021302.

[1180] A. Sheykhi and M. R. Setare. Interacting new agegraphic viscous dark energy with varying g. *International Journal of Theoretical Physics*, 49(11):2777–2785, Nov 2010. ISSN 1572-9575. doi: 10.1007/s10773-010-0469-0. URL `https://doi.org/10.1007/s10773-010-0469-0`.

[1181] M. Shifman, A. Vainshtein, and V. Zakharov. Can confinement ensure natural cp invariance of strong interactions? *Nuclear Physics B*, 166(3):493 – 506, 1980. ISSN 0550-3213. doi: https://doi.org/10.1016/0550-3213(80)90209-6. URL `http://www.sciencedirect.com/science/article/pii/0550321380902096`.

[1182] M. A. Shifman, A. I. Vainshtein, and V. I. Zakharov. Can Confinement Ensure Natural CP Invariance of Strong Interactions? *Nucl. Phys.*, B166:493–506, 1980. doi: 10.1016/0550-3213(80)90209-6.

[1183] P. Sikivie. Of Axions, Domain Walls and the Early Universe. *Phys. Rev. Lett.*, 48:1156–1159, 1982. doi: 10.1103/PhysRevLett.48.1156.

[1184] P. Sikivie. Experimental tests of the "invisible" axion. *Phys. Rev. Lett.*, 51:1415–1417, Oct 1983. doi: 10.1103/PhysRevLett.51.1415. URL https://link.aps.org/doi/10.1103/PhysRevLett.51.1415.

[1185] P. Sikivie and Q. Yang. Bose-Einstein Condensation of Dark Matter Axions. *Phys. Rev. Lett.*, 103:111301, 2009. doi: 10.1103/PhysRevLett.103.111301.

[1186] E. Silverstein and D. Tong. Scalar speed limits and cosmology: Acceleration from D-cceleration. *Phys. Rev.*, D70:103505, 2004. doi: 10.1103/PhysRevD.70.103505.

[1187] E. Silverstein and A. Westphal. Monodromy in the CMB: Gravity Waves and String Inflation. *Phys. Rev.*, D78:106003, 2008. doi: 10.1103/PhysRevD.78.106003.

[1188] J. Silverstein. The limiting eigenvalue distribution of a multivariate f matrix. *SIAM Journal on Mathematical Analysis*, 16(3):641–646, 1985. doi: 10.1137/0516047. URL https://doi.org/10.1137/0516047.

[1189] J. Silverstein and S. Choi. Analysis of the limiting spectral distribution of large dimensional random matrices. *Journal of Multivariate Analysis*, 54 (2):295 – 309, 1995. ISSN 0047-259X. doi: https://doi.org/10.1006/jmva.1995.1058. URL http://www.sciencedirect.com/science/article/pii/S0047259X85710585.

[1190] S.-J. Sin. Late time cosmological phase transition and galactic halo as Bose liquid. *Phys. Rev.*, D50:3650–3654, 1994. doi: 10.1103/PhysRevD.50.3650.

[1191] K. P. Sinha and E. C. G. Sudarshan. The superfluid as a source of all interactions. *Foundations of Physics*, 8(11):823–831, Dec 1978. ISSN 1572-9516. doi: 10.1007/BF00715056. URL https://doi.org/10.1007/BF00715056.

[1192] K. P. Sinha, C. Sivaram, and E. C. G. Sudarshan. The superfluid vacuum state, time-varying cosmological constant, and nonsingular cosmological

models. *Foundations of Physics*, 6(6):717–726, Dec 1976. ISSN 1572-9516. doi: 10.1007/BF00708950. URL https://doi.org/10.1007/BF00708950.

[1193] K. P. Sinha, C. Sivaram, and E. C. G. Sudarshan. Aether as a superfluid state of particle-antiparticle pairs. *Foundations of Physics*, 6(1):65–70, 1976. doi: 10.1007/BF00708664.

[1194] C. Skordis and A. Albrecht. Planck scale quintessence and the physics of structure formation. *Phys. Rev.*, D66:043523, 2002. doi: 10.1103/PhysRevD.66.043523.

[1195] V. M. Slipher. The radial velocity of the Andromeda Nebula. *Lowell Observatory Bulletin*, 1:56–57, Jan 1913.

[1196] V. M. Slipher. The detection of nebular rotation. *Lowell Observatory Bulletin*, 2:66–66, 1914.

[1197] V. M. Slipher. Radial velocity observations of spiral nebulae. *The Observatory*, 40:304–306, Aug 1917.

[1198] V. Smer-Barreto and A. R. Liddle. Planck Satellite Constraints on Pseudo-Nambu–Goldstone Boson Quintessence. *JCAP*, 1701(01):023, 2017. doi: 10.1088/1475-7516/2017/01/023.

[1199] A. Smercina et al. A Lonely Giant: The Sparse Satellite Population of M94 Challenges Galaxy Formation. *ApJ*, 863(2):152, Aug 2018. doi: 10.3847/1538-4357/aad2d6.

[1200] M. Smith and R. Kohn. Parsimonious covariance matrix estimation for longitudinal data. *Journal of the American Statistical Association*, 97(460):1141–1153, 2002. doi: 10.1198/016214502388618942. URL https://doi.org/10.1198/016214502388618942.

[1201] T. L. Smith, V. Poulin, and M. A. Amin. Oscillating scalar fields and the Hubble tension: a resolution with novel signatures. 2019.

[1202] G. F. Smoot et al. Structure in the COBE differential microwave radiometer first-year maps. *ApJLett*, 396:L1–L5, Sept. 1992. doi: 10.1086/186504.

[1203] T. P. Sotiriou and V. Faraoni. f(R) Theories Of Gravity. *Rev. Mod. Phys.*, 82:451–497, 2010. doi: 10.1103/RevModPhys.82.451.

[1204] R. Speicher. Multiplicative functions on the lattice of non-crossing partitions and free convolution. *Mathematische Annalen*, 298(1):611–628, Jan 1994. ISSN 1432-1807. doi: 10.1007/BF01459754. URL `https://doi.org/10.1007/BF01459754`.

[1205] R. Speicher. Free Probability Theory. *arXiv e-prints*, art. arXiv:0911.0087, Oct 2009.

[1206] R. Speicher. Lecture Notes on "Free Probability Theory". *arXiv e-prints*, art. arXiv:1908.08125, Aug 2019.

[1207] D. N. Spergel and P. J. Steinhardt. Observational evidence for selfinteracting cold dark matter. *Phys. Rev. Lett.*, 84:3760–3763, 2000. doi: 10.1103/PhysRevLett.84.3760.

[1208] D. N. Spergel et al. First year Wilkinson Microwave Anisotropy Probe (WMAP) observations: Determination of cosmological parameters. *Astrophys. J. Suppl.*, 148:175–194, 2003. doi: 10.1086/377226.

[1209] V. Springel, C. S. Frenk, and S. D. M. White. The large-scale structure of the Universe. *Nature*, 440:1137, 2006. doi: 10.1038/nature04805.

[1210] M. Srednicki. Axion Couplings to Matter. 1. CP Conserving Parts. *Nucl. Phys.*, B260:689–700, 1985. doi: 10.1016/0550-3213(85)90054-9.

[1211] P. M. Stanfield, J. R. Wilson, G. A. Mirka, N. F. Glasscock, J. P. Psihogios, and J. R. Davis. Multivariate input modeling with johnson distributions. In *Proceedings of the 28th Conference on Winter Simulation*, WSC '96, pages 1457–1464, Washington, DC, USA, 1996. IEEE Computer Society. ISBN

0-7803-3383-7. doi: 10.1145/256562.256990. URL `http://dx.doi.org/10.1145/256562.256990`.

[1212] A. A. Starobinskiĭ. Multicomponent de Sitter (inflationary) stages and the generation of perturbations. *Soviet Journal of Experimental and Theoretical Physics Letters*, 42:152, Aug. 1985.

[1213] D. Steeghs, J. E. McClintock, S. G. Parsons, M. J. Reid, S. Littlefair, and V. S. Dhillon. The not-so-massive black hole in the microquasar GRS1915+105. *Astrophys. J.*, 768:185, 2013. doi: 10.1088/0004-637X/768/2/185.

[1214] F. D. Steffen. Gravitino dark matter and cosmological constraints. *JCAP*, 0609:001, 2006. doi: 10.1088/1475-7516/2006/09/001.

[1215] G. Steigman. Primordial nucleosynthesis: successes and challenges. *Int. J. Mod. Phys.*, E15:1–36, 2006. doi: 10.1142/S0218301306004028.

[1216] J. F. Steiner, R. C. Reis, J. E. McClintock, R. Narayan, R. A. Remillard, J. A. Orosz, L. Gou, A. C. Fabian, and M. A. P. Torres. The spin of the black hole microquasar XTE J1550-564 via the continuum-fitting and Fe-line methods. *MNRAS*, 416:941–958, Sept. 2011. doi: 10.1111/j.1365-2966.2011.19089.x.

[1217] J. F. Steiner, J. E. McClintock, J. A. Orosz, R. A. Remillard, C. D. Bailyn, M. Kolehmainen, and O. Straub. The Low-Spin Black Hole in LMC X-3. *Astrophys. J.*, 793:L29, 2014. doi: 10.1088/2041-8205/793/2/L29.

[1218] P. J. Steinhardt, L.-M. Wang, and I. Zlatev. Cosmological tracking solutions. *Phys. Rev.*, D59:123504, 1999. doi: 10.1103/PhysRevD.59.123504.

[1219] M. J. Stott and D. J. E. Marsh. Black hole spin constraints on the mass spectrum and number of axionlike fields. *Phys. Rev.*, D98(8):083006, 2018. doi: 10.1103/PhysRevD.98.083006.

[1220] M. J. Stott, T. Elghozi, and M. Sakellariadou. Gravitational Wave Bursts

from Cosmic String Cusps and Pseudocusps. *Phys. Rev.*, D96(2):023533, 2017. doi: 10.1103/PhysRevD.96.023533.

[1221] M. J. Stott, D. J. E. Marsh, C. Pongkitivanichkul, L. C. Price, and B. S. Acharya. Spectrum of the axion dark sector. *Phys. Rev.*, D96(8):083510, 2017. doi: 10.1103/PhysRevD.96.083510.

[1222] A. Strominger. Superstrings with torsion. *Nuclear Physics B*, 274(2):253 – 284, 1986. ISSN 0550-3213. doi: https://doi.org/10.1016/0550-3213(86)90286-5. URL `http://www.sciencedirect.com/science/article/pii/0550321386902865`.

[1223] A. Strominger, S.-T. Yau, and E. Zaslow. Mirror symmetry is T duality. *Nucl. Phys.*, B479:243–259, 1996. doi: 10.1016/0550-3213(96)00434-8.

[1224] L. Susskind. Harmonic-oscillator analogy for the veneziano model. *Phys. Rev. Lett.*, 23:545–547, Sep 1969. doi: 10.1103/PhysRevLett.23.545. URL `https://link.aps.org/doi/10.1103/PhysRevLett.23.545`.

[1225] L. Susskind. Dual symmetric theory of hadrons. 1. *Nuovo Cim.*, A69:457–496, 1970. doi: 10.1007/BF02726485.

[1226] L. Susskind. The World as a hologram. *J. Math. Phys.*, 36:6377–6396, 1995. doi: 10.1063/1.531249.

[1227] L. Susskind. Another conjecture about M(atrix) theory. 1997.

[1228] L. Susskind. Matrix theory black holes and the Gross-Witten transition. 1997.

[1229] L. Susskind. The Anthropic landscape of string theory. pages 247–266, 2003.

[1230] P. Svrcek. Cosmological Constant and Axions in String Theory. *Submitted to: JHEP*, 2006.

[1231] P. Svrcek and E. Witten. Axions In String Theory. *JHEP*, 06:051, 2006. doi: 10.1088/1126-6708/2006/06/051.

[1232] J. J. Swain, S. Venkatraman, and J. R. Wilson. Least-squares estimation of distribution functions in johnson's translation system. *Journal of Statistical Computation and Simulation*, 29(4):271–297, 1988. doi: 10.1080/00949658808811068. URL https://doi.org/10.1080/00949658808811068.

[1233] G. 't Hooft. Renormalization of Massless Yang-Mills Fields. *Nucl. Phys.*, B33:173–199, 1971. doi: 10.1016/0550-3213(71)90395-6.

[1234] G. 't Hooft. Renormalizable Lagrangians for Massive Yang-Mills Fields. *Nucl. Phys.*, B35:167–188, 1971. doi: 10.1016/0550-3213(71)90139-8. [,201(1971)].

[1235] G. 't Hooft. Computation of the quantum effects due to a four-dimensional pseudoparticle. *Phys. Rev. D*, 14:3432–3450, Dec 1976. doi: 10.1103/PhysRevD.14.3432. URL https://link.aps.org/doi/10.1103/PhysRevD.14.3432.

[1236] G. 't Hooft. Symmetry breaking through bell-jackiw anomalies. *Phys. Rev. Lett.*, 37:8–11, Jul 1976. doi: 10.1103/PhysRevLett.37.8. URL https://link.aps.org/doi/10.1103/PhysRevLett.37.8.

[1237] G. 't Hooft. Symmetry Breaking Through Bell-Jackiw Anomalies. *Phys. Rev. Lett.*, 37:8–11, 1976. doi: 10.1103/PhysRevLett.37.8. [,226(1976)].

[1238] G. 't Hooft. Dimensional reduction in quantum gravity. *Conf. Proc.*, C930308:284–296, 1993.

[1239] G. 't Hooft and M. J. G. Veltman. Regularization and Renormalization of Gauge Fields. *Nucl. Phys.*, B44:189–213, 1972. doi: 10.1016/0550-3213(72)90279-9.

[1240] G. 't Hooft and M. J. G. Veltman. One loop divergencies in the theory of gravitation. *Ann. Inst. H. Poincare Phys. Theor.*, A20:69–94, 1974.

[1241] K. Takahashi, K. Toma, M. Kino, M. Nakamura, and K. Hada. Fast-spinning

black holes inferred from symmetrically limb-brightened radio jets. *Astrophys. J.*, 868(2):82, 2018. doi: 10.3847/1538-4357/aae832.

[1242] H. Tam and Q. Yang. Production and Detection of Axion-like Particles by Interferometry. *Phys. Lett.*, B716:435–440, 2012. doi: 10.1016/j.physletb.2012.08.050.

[1243] M. Tanabashi et al. Review of Particle Physics. *Phys. Rev.*, D98(3):030001, 2018. doi: 10.1103/PhysRevD.98.030001.

[1244] M. A. Tanner and W. H. Wong. The calculation of posterior distributions by data augmentation. *Journal of the American Statistical Association*, 82 (398):528–540, 1987. ISSN 01621459. URL `http://www.jstor.org/stable/2289457`.

[1245] M. A. Tanner and W. H. Wong. From em to data augmentation: The emergence of mcmc bayesian computation in the 1980s. *Statist. Sci.*, 25(4):506–516, 11 2010. doi: 10.1214/10-STS341. URL `https://doi.org/10.1214/10-STS341`.

[1246] T. Tao and V. Vu. Random covariance matrices: Universality of local statistics of eigenvalues. *arXiv e-prints*, art. arXiv:0912.0966, Dec 2009.

[1247] T. Tao and V. Vu. Random matrices: Universality of local eigenvalue statistics. *Acta Math.*, 206(1):127–204, 2011. doi: 10.1007/s11511-011-0061-3. URL `https://doi.org/10.1007/s11511-011-0061-3`.

[1248] T. Tao and V. Vu. Random matrices: Universality of local spectral statistics of non-Hermitian matrices. *arXiv e-prints*, art. arXiv:1206.1893, Jun 2012.

[1249] R. Tatar, Y. Tsuchiya, and T. Watari. Right-handed Neutrinos in F-theory Compactifications. *Nucl. Phys.*, B823:1–46, 2009. doi: 10.1016/j.nuclphysb.2009.07.020.

[1250] A. N. Taylor, S. Dye, T. J. Broadhurst, N. Benitez, and E. van Kampen.

Gravitational lens magnification and the mass of abell 1689. *The Astrophysical Journal*, 501(2):539–553, jul 1998. doi: 10.1086/305827. URL https://doi.org/10.1086%2F305827.

[1251] W. Taylor. M(atrix) theory: Matrix quantum mechanics as a fundamental theory. *Rev. Mod. Phys.*, 73:419–462, 2001. doi: 10.1103/RevModPhys.73.419.

[1252] W. Taylor and Y.-N. Wang. A Monte Carlo exploration of threefold base geometries for 4d F-theory vacua. *JHEP*, 01:137, 2016. doi: 10.1007/JHEP01(2016)137.

[1253] W. Taylor and Y.-N. Wang. Scanning the skeleton of the 4D F-theory landscape. *JHEP*, 01:111, 2018. doi: 10.1007/JHEP01(2018)111.

[1254] M. Tegmark. What does inflation really predict? *JCAP*, 0504:001, 2005. doi: 10.1088/1475-7516/2005/04/001.

[1255] S. Teodor Belinschi, H. Bercovici, M. Capitaine, and M. Fevrier. Outliers in the spectrum of large deformed unitarily invariant models. *arXiv e-prints*, art. arXiv:1412.4916, Dec 2014.

[1256] S. A. Teukolsky. Rotating black holes: Separable wave equations for gravitational and electromagnetic perturbations. *Phys. Rev. Lett.*, 29:1114–1118, Oct 1972. doi: 10.1103/PhysRevLett.29.1114. URL https://link.aps.org/doi/10.1103/PhysRevLett.29.1114.

[1257] S. A. Teukolsky. Perturbations of a Rotating Black Hole. I. Fundamental Equations for Gravitational, Electromagnetic, and Neutrino-Field Perturbations. *ApJ*, 185:635–648, Oct. 1973. doi: 10.1086/152444.

[1258] T. Thiemann. QSD 5: Quantum gravity as the natural regulator of matter quantum field theories. *Class. Quant. Grav.*, 15:1281–1314, 1998. doi: 10.1088/0264-9381/15/5/012.

[1259] T. Thiemann. Lectures on loop quantum gravity. *Lect. Notes Phys.*, 631: 41–135, 2003. doi: 10.1007/978-3-540-45230-0_3. [,41(2002)].

[1260] P. Tisserand et al. Limits on the Macho Content of the Galactic Halo from the EROS-2 Survey of the Magellanic Clouds. *Astron. Astrophys.*, 469:387–404, 2007. doi: 10.1051/0004-6361:20066017.

[1261] Tokuda, T. and Goodrich, B. and Van Mechelen, I. and Gelman, A. Visualizing distri- butions of covariance matrices. 2011. URL `http://www.stat.columbia.edu/~gelman/research/unpublished/Visualization.pdf`.

[1262] D. Tong. String Theory. 2009.

[1263] F. Toscano, R. O. Vallejos, and C. Tsallis. Random matrix ensembles from nonextensive entropy. *Phys. Rev. E*, 69:066131, Jun 2004. doi: 10.1103/PhysRevE.69.066131. URL `https://link.aps.org/doi/10.1103/PhysRevE.69.066131`.

[1264] P. K. Townsend. The eleven-dimensional supermembrane revisited. *Phys. Lett.*, B350:184–187, 1995. doi: 10.1016/0370-2693(95)00397-4. [,265(1995)].

[1265] C. A. Tracy and H. Widom. Level spacing distributions and the Airy kernel. *Commun. Math. Phys.*, 159:151–174, 1994. doi: 10.1007/BF02100489.

[1266] C. A. Tracy and H. Widom. Fredholm determinants, differential equations and matrix models. *Commun. Math. Phys.*, 163:33–72, 1994. doi: 10.1007/BF02101734.

[1267] C. A. Tracy and H. Widom. Level spacing distributions and the Bessel kernel. *Commun. Math. Phys.*, 161:289–310, 1994. doi: 10.1007/BF02099779.

[1268] C. A. Tracy and H. Widom. Level-spacing distributions and the airy kernel. *Comm. Math. Phys.*, 159(1):151–174, 1994. URL `https://projecteuclid.org:443/euclid.cmp/1104254495`.

[1269] C. A. Tracy and H. Widom. On orthogonal and symplectic matrix ensembles.

Comm. Math. Phys., 177(3):727–754, 1996. URL https://projecteuclid.org:443/euclid.cmp/1104286442.

[1270] R. Trotta. Bayes in the sky: Bayesian inference and model selection in cosmology. *Contemp. Phys.*, 49:71–104, 2008. doi: 10.1080/00107510802066753.

[1271] C. G. Tsagas, A. Challinor, and R. Maartens. Relativistic cosmology and large-scale structure. *Phys. Rept.*, 465:61–147, 2008. doi: 10.1016/j.physrep.2008.03.003.

[1272] C. Tsallis. Possible generalization of boltzmann-gibbs statistics. *Journal of Statistical Physics*, 52(1):479–487, Jul 1988. ISSN 1572-9613. doi: 10.1007/BF01016429. URL https://doi.org/10.1007/BF01016429.

[1273] C. Tsallis, F. Baldovin, R. Cerbino, and P. Pierobon. Introduction to Nonextensive Statistical Mechanics and Thermodynamics. *arXiv e-prints*, art. cond-mat/0309093, Sep 2003.

[1274] S. Tsujikawa. Modified gravity models of dark energy. *Lect. Notes Phys.*, 800:99–145, 2010. doi: 10.1007/978-3-642-10598-2_3.

[1275] S. Tsujikawa. Quintessence: A Review. *Class. Quant. Grav.*, 30:214003, 2013. doi: 10.1088/0264-9381/30/21/214003.

[1276] P. Tsyba, K. Yerzhanov, K. Esmakhanova, I. Kulnazarov, G. Nugmanova, and R. Myrzakulov. Reconstruction of f-essence and fermionic Chaplygin gas models of dark energy. 2011.

[1277] J. W. Tukey. The future of data analysis. *Ann. Math. Statist.*, 33(1):1–67, 03 1962. doi: 10.1214/aoms/1177704711. URL https://doi.org/10.1214/aoms/1177704711.

[1278] S. Tulin and H.-B. Yu. Dark Matter Self-interactions and Small Scale Structure. *Phys. Rept.*, 730:1–57, 2018. doi: 10.1016/j.physrep.2017.11.004.

[1279] A. Tulino and S. Verdú. *Random Matrix Theory and Wireless Communica-*

tions. now, 2004. ISBN 9781933019000. URL https://ieeexplore.ieee.org/document/8187216.

[1280] A. M. Tulino and S. Verd. Random matrix theory and wireless communications. *Foundations and Trends in Communications and Information Theory*, 1(1):1–182, 2004. ISSN 1567-2190. doi: 10.1561/0100000001. URL http://dx.doi.org/10.1561/0100000001.

[1281] M. S. Turner. Cosmic and local mass density of "invisible" axions. *Phys. Rev. D*, 33:889–896, Feb 1986. doi: 10.1103/PhysRevD.33.889. URL https://link.aps.org/doi/10.1103/PhysRevD.33.889.

[1282] M. S. Turner. Early-universe thermal production of not-so-invisible axions. *Phys. Rev. Lett.*, 60:1101–1101, Mar 1988. doi: 10.1103/PhysRevLett.60.1101.3. URL https://link.aps.org/doi/10.1103/PhysRevLett.60.1101.3.

[1283] L. A. Ureña-López and A. X. Gonzalez-Morales. Towards accurate cosmological predictions for rapidly oscillating scalar fields as dark matter. *JCAP*, 1607(07):048, 2016. doi: 10.1088/1475-7516/2016/07/048.

[1284] L. A. Urena-Lopez and T. Matos. A New cosmological tracker solution for quintessence. *Phys. Rev.*, D62:081302, 2000. doi: 10.1103/PhysRevD.62.081302.

[1285] A. Utsugi, K. Ino, and M. Oshikawa. Random matrix theory analysis of cross correlations in financial markets. *Phys. Rev. E*, 70:026110, Aug 2004. doi: 10.1103/PhysRevE.70.026110. URL https://link.aps.org/doi/10.1103/PhysRevE.70.026110.

[1286] T. Vachaspati, L. Pogosian, and D. Steer. Cosmic Strings. *Scholarpedia*, 10 (2):31682, 2015. doi: 10.4249/scholarpedia.31682.

[1287] C. Vafa. Evidence for F theory. *Nucl. Phys.*, B469:403–418, 1996. doi: 10.1016/0550-3213(96)00172-1.

[1288] C. Vafa and E. Witten. Parity conservation in quantum chromodynamics. *Phys. Rev. Lett.*, 53:535–536, Aug 1984. doi: 10.1103/PhysRevLett.53.535. URL `https://link.aps.org/doi/10.1103/PhysRevLett.53.535`.

[1289] R. V. Vasudevan, A. C. Fabian, C. S. Reynolds, J. Aird, T. Dauser, and L. C. Gallo. A selection effect boosting the contribution from rapidly spinning black holes to the Cosmic X-ray Background. *Mon. Not. Roy. Astron. Soc.*, 458 (2):2012–2023, 2016. doi: 10.1093/mnras/stw363.

[1290] G. Veneziano. Construction of a crossing - symmetric, Regge behaved amplitude for linearly rising trajectories. *Nuovo Cim.*, A57:190–197, 1968. doi: 10.1007/BF02824451.

[1291] J. Verbaarschot and T. Wettig. Random matrix theory and chiral symmetry in qcd. *Annual Review of Nuclear and Particle Science*, 50(1):343–410, 2000. doi: 10.1146/annurev.nucl.50.1.343. URL `https://doi.org/10.1146/annurev.nucl.50.1.343`.

[1292] J. J. M. Verbaarschot. The Spectrum of the Dirac operator near zero virtuality for N(c) = 2 and chiral random matrix theory. *Nucl. Phys.*, B426: 559–574, 1994. doi: 10.1016/0550-3213(94)90021-3.

[1293] J. J. M. Verbaarschot. The Spectrum of the QCD Dirac operator and chiral random matrix theory: The Threefold way. *Phys. Rev. Lett.*, 72:2531–2533, 1994. doi: 10.1103/PhysRevLett.72.2531.

[1294] J. J. M. Verbaarschot. Spectrum of the Dirac operator in a QCD instanton liquid: Two versus three colors. *Nucl. Phys.*, B427:534–544, 1994. doi: 10.1016/0550-3213(94)90638-6.

[1295] L. Verde, T. Treu, and A. G. Riess. Tensions between the Early and the Late Universe. In *Nature Astronomy 2019*, 2019. doi: 10.1038/s41550-019-0902-0.

[1296] A. Vilenkin. Birth of inflationary universes. *Phys. Rev. D*, 27:2848–2855, Jun

1983. doi: 10.1103/PhysRevD.27.2848. URL https://link.aps.org/doi/10.1103/PhysRevD.27.2848.

[1297] A. Vilenkin and E. P. S. Shellard. Cosmic Strings and Other Topological Defects. 2000. URL http://www.cambridge.org/mw/academic/subjects/physics/theoretical-physics-and-mathematical-physics/cosmic-strings-and-other-topological-defects?format=PB.

[1298] B. Virag. Operator limits of random matrices. *arXiv e-prints*, art. arXiv:1804.06953, Apr 2018.

[1299] M. A. Virasoro. Alternative constructions of crossing-symmetric amplitudes with regge behavior. *Phys. Rev.*, 177:2309–2311, Jan 1969. doi: 10.1103/PhysRev.177.2309. URL https://link.aps.org/doi/10.1103/PhysRev.177.2309.

[1300] L. Visinelli. Axion-Electromagnetic Waves. *Modern Physics Letters A*, 28 (35):1350162, Oct 2013. doi: 10.1142/S0217732313501629.

[1301] L. Visinelli. Light Axion-Like Dark Matter must have Anthropic Origins. 2017.

[1302] L. Visinelli and P. Gondolo. Dark matter axions revisited. *Phys. Rev. D*, 80 (3):035024, Aug. 2009. doi: 10.1103/PhysRevD.80.035024.

[1303] L. Visinelli and P. Gondolo. Axion cold dark matter in nonstandard cosmologies. *Phys. Rev. D*, 81(6):063508, Mar. 2010. doi: 10.1103/PhysRevD.81.063508.

[1304] L. Visinelli and P. Gondolo. Axion cold dark matter in view of BICEP2 results. *Phys. Rev. Lett.*, 113:011802, 2014. doi: 10.1103/PhysRevLett.113.011802.

[1305] L. Visinelli and H. Terças. A Kinetic Theory of Axions in Magnetized Plasmas: the Axionon. 2018.

[1306] L. Visinelli and S. Vagnozzi. Cosmological window onto the string axiverse and the supersymmetry breaking scale. *Phys. Rev.*, D99(6):063517, 2019. doi: 10.1103/PhysRevD.99.063517.

[1307] D. Voiculescu. Symmetries of some reduced free product c*-algebras. In H. Araki, C. C. Moore, Ş.-V. Stratila, and D.-V. Voiculescu, editors, *Operator Algebras and their Connections with Topology and Ergodic Theory*, pages 556–588, Berlin, Heidelberg, 1985. Springer Berlin Heidelberg. ISBN 978-3-540-39514-0.

[1308] D. Voiculescu. Addition of certain non-commuting random variables. *Journal of Functional Analysis*, 66(3):323 – 346, 1986. ISSN 0022-1236. doi: https://doi.org/10.1016/0022-1236(86)90062-5. URL `http://www.sciencedirect.com/science/article/pii/0022123686900625`.

[1309] D. Voiculescu. Multiplication of certain non-commuting random variables. *Journal of Operator Theory*, 18(2):223–235, 1987. ISSN 03794024, 18417744. URL `http://www.jstor.org/stable/24714784`.

[1310] D. Voiculescu. Limit laws for random matrices and free products. *Inventiones mathematicae*, 104(1):201–220, Dec 1991. ISSN 1432-1297. doi: 10.1007/BF01245072. URL `https://doi.org/10.1007/BF01245072`.

[1311] D. Voiculescu. The analogues of entropy and of fisher's information measure in free probability theory. i. *Comm. Math. Phys.*, 155(1):71–92, 1993. URL `https://projecteuclid.org:443/euclid.cmp/1104253200`.

[1312] D. Voiculescu. Free probability theory: Random matrices and von neumann algebras. In S. D. Chatterji, editor, *Proceedings of the International Congress of Mathematicians*, pages 227–242, Basel, 1995. Birkhäuser Basel. ISBN 978-3-0348-9078-6.

[1313] D. Voiculescu. The coalgebra of the free difference quotient and free probability. *International Mathematics Research Notices*, 2000(2):79–106, 01

2000. ISSN 1073-7928. doi: 10.1155/S1073792800000064. URL https://doi.org/10.1155/S1073792800000064.

[1314] D. V. Volkov and V. P. Akulov. Possible universal neutrino interaction. *JETP Lett.*, 16:438–440, 1972. [Pisma Zh. Eksp. Teor. Fiz.16,621(1972)].

[1315] R. M. Wald. Black hole in a uniform magnetic field. *Phys. Rev. D*, 10:1680–1685, Sep 1974. doi: 10.1103/PhysRevD.10.1680. URL https://link.aps.org/doi/10.1103/PhysRevD.10.1680.

[1316] A. G. Walker. On milne's theory of world-structure*. *Proceedings of the London Mathematical Society*, s2-42(1):90–127, 1937. doi: 10.1112/plms/s2-42.1.90. URL https://londmathsoc.onlinelibrary.wiley.com/doi/abs/10.1112/plms/s2-42.1.90.

[1317] J. L. Walsh, A. J. Barth, L. C. Ho, and M. Sarzi. The M87 Black Hole Mass from Gas-dynamical Models of Space Telescope Imaging Spectrograph Observations. *Astrophys. J.*, 770:86, 2013. doi: 10.1088/0004-637X/770/2/86.

[1318] D. J. Walton, E. Nardini, A. C. Fabian, L. C. Gallo, and R. C. Reis. Suzaku observations of 'bare' active galactic nuclei. *MNRAS*, 428:2901–2920, Feb. 2013. doi: 10.1093/mnras/sts227.

[1319] B. D. Wandelt, R. Dave, G. R. Farrar, P. C. McGuire, D. N. Spergel, and P. J. Steinhardt. Selfinteracting dark matter. In *Sources and detection of dark matter and dark energy in the universe. Proceedings, 4th International Symposium, DM 2000, Marina del Rey, USA, February 23-25, 2000*, pages 263–274, 2000. URL http://www.slac.stanford.edu/spires/find/books/www?cl=QB461:I57:2000.

[1320] D. Wang. The largest sample eigenvalue distribution in the rank 1 quaternionic spiked model of Wishart ensemble. *arXiv e-prints*, art. arXiv:0711.2722, Nov 2007.

[1321] D. Wang. Spiked Models in Wishart Ensemble. Apr 2008.

[1322] D. Wang. The largest eigenvalue of real symmetric, hermitian and hermitian self-dual random matrix models with rank one external source, part i. *Journal of Statistical Physics*, 146(4):719–761, Feb 2012. ISSN 1572-9613. doi: 10.1007/s10955-012-0417-x. URL `https://doi.org/10.1007/s10955-012-0417-x`.

[1323] G. Wang and T. Battefeld. Vacuum Selection on Axionic Landscapes. *JCAP*, 1604(04):025, 2016. doi: 10.1088/1475-7516/2016/04/025.

[1324] H. Wang and N. S. Pillai. On a class of shrinkage priors for covariance matrix estimation. *Journal of Computational and Graphical Statistics*, 22 (3):689–707, 2013. doi: 10.1080/10618600.2013.785732. URL `https://doi.org/10.1080/10618600.2013.785732`.

[1325] L.-M. Wang and P. J. Steinhardt. Cluster abundance constraints on quintessence models. *Astrophys. J.*, 508:483–490, 1998. doi: 10.1086/306436.

[1326] Q. Wang and J. Yao. Extreme eigenvalues of large-dimensional spiked fisher matrices with application. *Ann. Statist.*, 45(1):415–460, 02 2017. doi: 10.1214/16-AOS1463. URL `https://doi.org/10.1214/16-AOS1463`.

[1327] S. Wang, Y. Wang, and M. Li. Holographic Dark Energy. *Phys. Rept.*, 696: 1–57, 2017. doi: 10.1016/j.physrep.2017.06.003.

[1328] Y. Wang. Figure of merit for dark energy constraints from current observational data. *Phys. Rev. D*, 77:123525, Jun 2008. doi: 10.1103/PhysRevD.77.123525. URL `https://link.aps.org/doi/10.1103/PhysRevD.77.123525`.

[1329] O. Wantz and E. P. S. Shellard. Axion Cosmology Revisited. *Phys. Rev.*, D82:123508, 2010. doi: 10.1103/PhysRevD.82.123508.

[1330] T. Weigand. Lectures on F-theory compactifications and model build-

ing. *Class. Quant. Grav.*, 27:214004, 2010. doi: 10.1088/0264-9381/27/21/214004.

[1331] D. H. Weinberg, J. S. Bullock, F. Governato, R. Kuzio de Naray, and A. H. G. Peter. Cold dark matter: controversies on small scales. *Proc. Nat. Acad. Sci.*, 112:12249–12255, 2015. doi: 10.1073/pnas.1308716112.

[1332] S. Weinberg. Pion scattering lengths. *Phys. Rev. Lett.*, 17:616–621, 1966. doi: 10.1103/PhysRevLett.17.616.

[1333] S. Weinberg. A Model of Leptons. *Phys. Rev. Lett.*, 19:1264–1266, 1967. doi: 10.1103/PhysRevLett.19.1264.

[1334] S. Weinberg. The u(1) problem. *Phys. Rev. D*, 11:3583–3593, Jun 1975. doi: 10.1103/PhysRevD.11.3583. URL `https://link.aps.org/doi/10.1103/PhysRevD.11.3583`.

[1335] S. Weinberg. A new light boson? *Phys. Rev. Lett.*, 40:223–226, Jan 1978. doi: 10.1103/PhysRevLett.40.223. URL `https://link.aps.org/doi/10.1103/PhysRevLett.40.223`.

[1336] S. Weinberg. Ultraviolet Divergences In Quantum Theories Of Gravitation. In *General Relativity: An Einstein Centenary Survey*, pages 790–831. 1980.

[1337] S. Weinberg. Supersymmetry at ordinary energies. masses and conservation laws. *Phys. Rev. D*, 26:287–302, Jul 1982. doi: 10.1103/PhysRevD.26.287. URL `https://link.aps.org/doi/10.1103/PhysRevD.26.287`.

[1338] S. Weinberg. Does gravitation resolve the ambiguity among supersymmetric vacua? *Phys. Rev. Lett.*, 48:1776–1779, Jun 1982. doi: 10.1103/PhysRevLett.48.1776. URL `https://link.aps.org/doi/10.1103/PhysRevLett.48.1776`.

[1339] S. Weinberg. Anthropic bound on the cosmological constant. *Phys. Rev.*

Lett., 59:2607–2610, Nov 1987. doi: 10.1103/PhysRevLett.59.2607. URL https://link.aps.org/doi/10.1103/PhysRevLett.59.2607.

[1340] S. Weinberg. *The Quantum theory of fields. Vol. 1: Foundations*. Cambridge University Press, 2005. ISBN 9780521670531, 9780511252044.

[1341] S. Weinberg. *The quantum theory of fields. Vol. 2: Modern applications*. Cambridge University Press, 2013. ISBN 9781139632478, 9780521670548, 9780521550024.

[1342] S. Weinberg. *The quantum theory of fields. Vol. 3: Supersymmetry*. Cambridge University Press, 2013. ISBN 9780521670555, 9781139632638, 9780521670555.

[1343] S. Wen, S. Wang, and X. Luo. Comparing dark energy models with current observational data. *JCAP*, 1807(07):011, 2018. doi: 10.1088/1475-7516/2018/07/011.

[1344] J. Wess and J. Bagger. *Supersymmetry and supergravity*. Princeton University Press, Princeton, NJ, USA, 1992. ISBN 9780691025308.

[1345] J. Wess and B. Zumino. A Lagrangian Model Invariant Under Supergauge Transformations. *Phys. Lett.*, 49B:52, 1974. doi: 10.1016/0370-2693(74)90578-4.

[1346] C. Wetterich. Cosmology and the fate of dilatation symmetry. *Nuclear Physics B*, 302:668–696, June 1988. doi: 10.1016/0550-3213(88)90193-9.

[1347] C. Wetterich. The Cosmon model for an asymptotically vanishing time dependent cosmological 'constant'. *Astron. Astrophys.*, 301:321–328, 1995.

[1348] H. Weyl. Zur gravitationstheorie. *Annalen der Physik*, 359(18):117–145, 1917. doi: 10.1002/andp.19173591804. URL https://onlinelibrary.wiley.com/doi/abs/10.1002/andp.19173591804.

[1349] H. Weyl. The field of a single centre in Einstein's theory of gravitation and the motion of a particle in that field. *Ann. Phys. (Leipzig)*, page 54, 1917.

[1350] J. Y. Widdicombe, T. Helfer, D. J. E. Marsh, and E. A. Lim. Formation of Relativistic Axion Stars. *JCAP*, 1810(10):005, 2018. doi: 10.1088/1475-7516/2018/10/005.

[1351] E. P. Wigner. On the statistical distribution of the widths and spacings of nuclear resonance levels. *Mathematical Proceedings of the Cambridge Philosophical Society*, 47(4):790?798, 1951. doi: 10.1017/S0305004100027237.

[1352] E. P. Wigner. Characteristic vectors of bordered matrices with infinite dimensions. *Annals of Mathematics*, 62(3):548–564, 1955. ISSN 0003486X. URL `http://www.jstor.org/stable/1970079`.

[1353] F. Wilczek. Problem of strong p and t invariance in the presence of instantons. *Phys. Rev. Lett.*, 40:279–282, Jan 1978. doi: 10.1103/PhysRevLett.40.279. URL `https://link.aps.org/doi/10.1103/PhysRevLett.40.279`.

[1354] F. Wilczek. Two applications of axion electrodynamics. *Phys. Rev. Lett.*, 58:1799–1802, May 1987. doi: 10.1103/PhysRevLett.58.1799. URL `https://link.aps.org/doi/10.1103/PhysRevLett.58.1799`.

[1355] T. Wirtz and T. Guhr. Distribution of the smallest eigenvalue in the correlated wishart model. *Phys. Rev. Lett.*, 111:094101, Aug 2013. doi: 10.1103/PhysRevLett.111.094101. URL `https://link.aps.org/doi/10.1103/PhysRevLett.111.094101`.

[1356] T. Wirtz and T. Guhr. Distribution of the smallest eigenvalue in complex and real correlated wishart ensembles. *Journal of Physics A: Mathematical and Theoretical*, 47(7):075004, feb 2014. doi: 10.1088/1751-8113/47/7/075004. URL `https://doi.org/10.1088%2F1751-8113%2F47%2F7%2F075004`.

[1357] T. Wirtz, G. Akemann, T. Guhr, M. Kieburg, and R. Wegner. The smallest eigenvalue distribution in the real Wishart?Laguerre ensemble with even

topology. *J. Phys.*, A48(24):245202, 2015. doi: 10.1088/1751-8113/48/24/245202.

[1358] T. Wirtz, G. Akemann, T. Guhr, M. Kieburg, and R. Wegner. The smallest eigenvalue distribution in the real wishart–laguerre ensemble with even topology. *Journal of Physics A: Mathematical and Theoretical*, 48(24): 245202, may 2015. doi: 10.1088/1751-8113/48/24/245202. URL `https://doi.org/10.1088%2F1751-8113%2F48%2F24%2F245202`.

[1359] T. Wirtz, M. Kieburg, and T. Guhr. Asymptotic coincidence of the statistics for degenerate and non-degenerate correlated real wishart ensembles. *Journal of Physics A: Mathematical and Theoretical*, 50(23):235203, may 2017. doi: 10.1088/1751-8121/aa6a6c. URL `https://doi.org/10.1088%2F1751-8121%2Faa6a6c`.

[1360] J. Wishart. The generalised product moment distribution in samples from a normal multivariate population. *Biometrika*, 20A(1/2):32–52, 1928. ISSN 00063444. URL `http://www.jstor.org/stable/2331939`.

[1361] H. Witek, V. Cardoso, A. Ishibashi, and U. Sperhake. Superradiant instabilities in astrophysical systems. *Phys. Rev.*, D87(4):043513, 2013. doi: 10.1103/PhysRevD.87.043513.

[1362] E. Witten. Large n chiral dynamics. *Annals of Physics*, 128(2):363 – 375, 1980. ISSN 0003-4916. doi: https://doi.org/10.1016/0003-4916(80)90325-5. URL `http://www.sciencedirect.com/science/article/pii/0003491680903255`.

[1363] E. Witten. Some properties of o(32) superstrings. *Physics Letters B*, 149(4):351 – 356, 1984. ISSN 0370-2693. doi: https://doi.org/10.1016/0370-2693(84)90422-2. URL `http://www.sciencedirect.com/science/article/pii/0370269384904222`.

[1364] E. Witten. New issues in manifolds of su(3) holonomy. *Nuclear Physics*

B, 268(1):79 – 112, 1986. ISSN 0550-3213. doi: https://doi.org/10.1016/0550-3213(86)90202-6. URL http://www.sciencedirect.com/science/article/pii/0550321386902026.

[1365] E. Witten. String theory dynamics in various dimensions. *Nucl. Phys.*, B443: 85–126, 1995. doi: 10.1016/0550-3213(95)00158-O. [,333(1995)].

[1366] E. Witten. Bound states of strings and p-branes. *Nucl. Phys.*, B460:335–350, 1996. doi: 10.1016/0550-3213(95)00610-9.

[1367] E. Witten. Strong coupling expansion of Calabi-Yau compactification. *Nucl. Phys.*, B471:135–158, 1996. doi: 10.1016/0550-3213(96)00190-3.

[1368] E. Witten. Deconstruction, G(2) holonomy, and doublet triplet splitting. In *Supersymmetry and unification of fundamental interactions. Proceedings, 10th International Conference, SUSY'02, Hamburg, Germany, June 17-23, 2002*, pages 472–491, 2001. URL http://www-library.desy.de/preparch/desy/proc/proc02-02/Proceedings/susy02/special/hertz_pr.ps.

[1369] C. S. Wu, E. Ambler, R. W. Hayward, D. D. Hoppes, and R. P. Hudson. Experimental test of parity conservation in beta decay. *Phys. Rev.*, 105: 1413–1415, Feb 1957. doi: 10.1103/PhysRev.105.1413. URL https://link.aps.org/doi/10.1103/PhysRev.105.1413.

[1370] U. A. Yajnik. Dark Energy from ferromagnetic condensation of cosmic magninos. 2011.

[1371] M. Yamada and A. Vilenkin. Hessian eigenvalue distribution in a random Gaussian landscape. *Journal of High Energy Physics*, 2018(3):29, Mar 2018. doi: 10.1007/JHEP03(2018)029.

[1372] I.-S. Yang. Probability of Slowroll Inflation in the Multiverse. *Phys. Rev.*, D86:103537, 2012. doi: 10.1103/PhysRevD.86.103537.

[1373] R. Yang and J. O. Berger. Estimation of a covariance matrix using the

reference prior. *Ann. Statist.*, 22(3):1195–1211, 09 1994. doi: 10.1214/aos/1176325625. URL https://doi.org/10.1214/aos/1176325625.

[1374] X. Yang, X. Zheng, J. Chen, and H. Li. Testing High-dimensional Covariance Matrices under the Elliptical Distribution and Beyond. *arXiv e-prints*, art. arXiv:1707.04010, Jul 2017.

[1375] Y. Q. Yin, Z. D. Bai, and P. R. Krishnaiah. On the limit of the largest eigenvalue of the large dimensional sample covariance matrix. *Probability Theory and Related Fields*, 78(4):509–521, Aug 1988. ISSN 1432-2064. doi: 10.1007/BF00353874. URL https://doi.org/10.1007/BF00353874.

[1376] I. Yokota. Exceptional Lie groups. *arXiv e-prints*, art. arXiv:0902.0431, Feb 2009.

[1377] D. G. York et al. The Sloan Digital Sky Survey: Technical Summary. *AJ*, 120:1579–1587, Sept. 2000. doi: 10.1086/301513.

[1378] H. Yoshino and H. Kodama. Bosenova collapse of axion cloud around a rotating black hole. *Prog. Theor. Phys.*, 128:153–190, 2012. doi: 10.1143/PTP.128.153.

[1379] H. Yoshino and H. Kodama. Gravitational radiation from an axion cloud around a black hole: Superradiant phase. *Progress of Theoretical and Experimental Physics*, 2014(4):043E02, Apr. 2014. doi: 10.1093/ptep/ptu029.

[1380] H. Yoshino and H. Kodama. Probing the string axiverse by gravitational waves from Cygnus X-1. *PTEP*, 2015(6):061E01, 2015. doi: 10.1093/ptep/ptv067.

[1381] H. Yoshino and H. Kodama. The bosenova and axiverse. *Class. Quant. Grav.*, 32(21):214001, 2015. doi: 10.1088/0264-9381/32/21/214001.

[1382] H.-R. Yu, T. Lan, H.-Y. Wan, T.-J. Zhang, and B.-Q. Wang. Constraints on smoothness parameter and dark energy using observational H(z) data.

Research in Astronomy and Astrophysics, 11(2):125–136, Feb 2011. doi: 10.1088/1674-4527/11/2/001.

[1383] H. Yukawa. On the Interaction of Elementary Particles I. *Proc. Phys. Math. Soc. Jap.*, 17:48–57, 1935. doi: 10.1143/PTPS.1.1. [Prog. Theor. Phys. Suppl.1,1(1935)].

[1384] E. Zavattini et al. Experimental observation of optical rotation generated in vacuum by a magnetic field. *Phys. Rev. Lett.*, 96:110406, Mar 2006. doi: 10.1103/PhysRevLett.96.110406. URL `https://link.aps.org/doi/10.1103/PhysRevLett.96.110406`.

[1385] Y. B. Zel'Dovich, I. Y. Kobzarev, and L. B. Okun'. Cosmological consequences of a spontaneous breakdown of a discrete symmetry. *Soviet Journal of Experimental and Theoretical Physics*, 40:1, July 1975.

[1386] Ya. B. Zel'dovich, A. Krasinski, and Ya. B. Zeldovich. The Cosmological constant and the theory of elementary particles. *Sov. Phys. Usp.*, 11:381–393, 1968. doi: 10.1007/s10714-008-0624-6,10.1070/PU1968v011n03ABEH003927. [Usp. Fiz. Nauk95,209(1968)].

[1387] A. R. Zentner and A. P. Hearin. Asymmetric Dark Matter May Alter the Evolution of Low-mass Stars and Brown Dwarfs. *Phys. Rev.*, D84:101302, 2011. doi: 10.1103/PhysRevD.84.101302.

[1388] Z. Zhai, M. Blanton, A. Slosar, and J. Tinker. An evaluation of cosmological models from expansion and growth of structure measurements. *ArXiv e-prints*, May 2017.

[1389] X. Zhang. Holographic Ricci dark energy: Current observational constraints, quintom feature, and the reconstruction of scalar-field dark energy. *Phys. Rev.*, D79:103509, 2009. doi: 10.1103/PhysRevD.79.103509.

[1390] X. F. ZHANG. Information uncertainty and stock returns. *The Journal of Finance*, 61(1):105–137, 2006. doi: 10.1111/j.1540-6261.2006.

00831.x. URL https://onlinelibrary.wiley.com/doi/abs/10.1111/j.1540-6261.2006.00831.x.

[1391] S. Zheng. Central limit theorems for linear spectral statistics of large dimensional f-matrices. *Ann. Inst. H. Poincaré Probab. Statist.*, 48(2):444–476, 05 2012. doi: 10.1214/11-AIHP414. URL https://doi.org/10.1214/11-AIHP414.

[1392] A. R. Zhitnitsky. On Possible Suppression of the Axion Hadron Interactions. (In Russian). *Sov. J. Nucl. Phys.*, 31:260, 1980. [Yad. Fiz.31,497(1980)].

[1393] Q. Zhu, F. Marinacci, M. Maji, Y. Li, V. Springel, and L. Hernquist. Baryonic impact on the dark matter distribution in Milky Way-sized galaxies and their satellites. *Mon. Not. Roy. Astron. Soc.*, 458(2):1559–1580, 2016. doi: 10.1093/mnras/stw374.

[1394] Z. Zivkovic. Improved adaptive gaussian mixture model for background subtraction. In *Proceedings of the 17th International Conference on Pattern Recognition, 2004. ICPR 2004.*, volume 2, pages 28–31 Vol.2, Aug 2004. doi: 10.1109/ICPR.2004.1333992.

[1395] I. Zlatev, L. Wang, and P. J. Steinhardt. Quintessence, cosmic coincidence, and the cosmological constant. *Phys. Rev. Lett.*, 82:896–899, Feb 1999. doi: 10.1103/PhysRevLett.82.896. URL https://link.aps.org/doi/10.1103/PhysRevLett.82.896.

[1396] T. J. Zouros and D. M. Eardley. Instabilities of massive scalar perturbations of a rotating black hole. *Annals of Physics*, 118(1):139 – 155, 1979. ISSN 0003-4916. doi: https://doi.org/10.1016/0003-4916(79)90237-9. URL http://www.sciencedirect.com/science/article/pii/0003491679902379.

[1397] F. Zwicky. Die Rotverschiebung von extragalaktischen Nebeln. *Helvetica Physica Acta*, 6:110–127, 1933.

[1398] F. Zwicky. On the Masses of Nebulae and of Clusters of Nebulae. *ApJ*, 86: 217, Oct. 1937. doi: 10.1086/143864.

[1399] B. Zwiebach. *A first course in string theory*. Cambridge University Press, 2006. ISBN 0521831431, 9780521831437, 9780511207570. URL `http://www.cambridge.org/uk/catalogue/catalogue.asp?isbn=0521831431`.

[1400] K. Życzkowski, K. A. Penson, I. Nechita, and B. Collins. Generating random density matrices. *Journal of Mathematical Physics*, 52(6):062201–062201, Jun 2011. doi: 10.1063/1.3595693.